frontiers | Research Topics

Unconventional myosins in motile and contractile functions: Fifty years on the stage

Edited by
Maria Jolanta Redowicz and Manuel H. Taft

Published in
Frontiers in Physiology

ISSN 1664-8714
ISBN 978-2-8325-5058-8
DOI 10.3389/978-2-8325-5058-8

About Frontiers

Frontiers is more than just an open access publisher of scholarly articles: it is a pioneering approach to the world of academia, radically improving the way scholarly research is managed. The grand vision of Frontiers is a world where all people have an equal opportunity to seek, share and generate knowledge. Frontiers provides immediate and permanent online open access to all its publications, but this alone is not enough to realize our grand goals.

Frontiers journal series

The Frontiers journal series is a multi-tier and interdisciplinary set of open-access, online journals, promising a paradigm shift from the current review, selection and dissemination processes in academic publishing. All Frontiers journals are driven by researchers for researchers; therefore, they constitute a service to the scholarly community. At the same time, the *Frontiers journal series* operates on a revolutionary invention, the tiered publishing system, initially addressing specific communities of scholars, and gradually climbing up to broader public understanding, thus serving the interests of the lay society, too.

Dedication to quality

Each Frontiers article is a landmark of the highest quality, thanks to genuinely collaborative interactions between authors and review editors, who include some of the world's best academicians. Research must be certified by peers before entering a stream of knowledge that may eventually reach the public - and shape society; therefore, Frontiers only applies the most rigorous and unbiased reviews. Frontiers revolutionizes research publishing by freely delivering the most outstanding research, evaluated with no bias from both the academic and social point of view. By applying the most advanced information technologies, Frontiers is catapulting scholarly publishing into a new generation.

What are Frontiers Research Topics?

Frontiers Research Topics are very popular trademarks of the *Frontiers journals series*: they are collections of at least ten articles, all centered on a particular subject. With their unique mix of varied contributions from Original Research to Review Articles, Frontiers Research Topics unify the most influential researchers, the latest key findings and historical advances in a hot research area.

Find out more on how to host your own Frontiers Research Topic or contribute to one as an author by contacting the Frontiers editorial office: frontiersin.org/about/contact

Unconventional myosins in motile and contractile functions: Fifty years on the stage

Topic editors

Maria Jolanta Redowicz — Laboratory of Molecular Basis of Cell Motility, Nencki Institute of Experimental Biology, Polish Academy of Sciences, Poland

Manuel H. Taft — Hannover Medical School, Germany

Citation

Redowicz, M. J., Taft, M. H., eds. (2024). *Unconventional myosins in motile and contractile functions: Fifty years on the stage*. Lausanne: Frontiers Media SA. doi: 10.3389/978-2-8325-5058-8

Table of contents

frontiers | Frontiers in Physiology

TYPE Editorial
PUBLISHED 12 June 2024
DOI 10.3389/fphys.2024.1439746

OPEN ACCESS

EDITED AND REVIEWED BY
Ayako Makino,
The Herbert Wertheim UF Scripps Institute for Biomedical Innovation and Technology, United States

*CORRESPONDENCE
Manuel H. Taft,
taft.manuel@mh-hannover.de
Maria Jolanta Redowicz,
j.redowicz@nencki.edu.pl

RECEIVED 28 May 2024
ACCEPTED 03 June 2024
PUBLISHED 12 June 2024

CITATION
Taft MH and Redowicz MJ (2024), Editorial: Unconventional myosins in motile and contractile functions: fifty years on the stage. *Front. Physiol.* 15:1439746. doi: 10.3389/fphys.2024.1439746

Editorial: Unconventional myosins in motile and contractile functions: fifty years on the stage

Manuel H. Taft[1]* and Maria Jolanta Redowicz[2]*

[1]Institute for Biophysical Chemistry, Hannover Medical School, Hannover, Germany, [2]Laboratory of Molecular Basis of Cell Motility, Nencki Institute of Experimental Biology, Polish Academy of Sciences, Warsaw, Poland

KEYWORDS

unconventional myosins, physiology, cytoskeleton, molecular motor, myosin-1, myosin-6, myosin-5, myosin-18

Editorial on the Research Topic
Unconventional myosins in motile and contractile functions: fifty years on the stage

The myosin superfamily of molecular motors can be classified by various means, of which the most classic one is the overall discrimination between "conventional" myosins that power muscle contraction and "unconventional" myosins that encompass all other myosins (Sellers, 2000; Berg et al., 2001; Odronitz and Kollmar 2007). After the first description of a muscle protein extraction termed "myosin" in 1864 (Kühne, 1864), all characterized myosins for more than a century were conventional myosins. Myosins, still generally mainly known for their involvement in muscle contraction, are molecular motors converting energy from ATP hydrolysis into movement along actin filaments. The first report on the isolation of skeletal muscle myosin was published in 1939 and it took several decades to show the presence of myosins in other muscle types and in non-muscle systems (Engelhardt and Liubimova, 1939; Sellers, 2000). A breakthrough in myosin research came in 1973 when Pollard and Korn purified from a protist, *Acanthamoeba castellanii*, one-headed myosin that was able to hydrolyze ATP in an actin-dependent manner but in contrast to muscle myosins was not capable of filament formation (Pollard and Korn, 1973a; Pollard and Korn, 1973b). The authors termed this novel myosin "myosin I" as unlike two-headed muscle myosins ("myosin II") it contained only one head (Pollard and Korn, Front Physiol 2023). This discovery, considered by the journal *Nature* as one of the milestones in cell biology (Le Bot, 2010), opened a new era in studies on myosins. Intensive research, supported by a concomitant development of genetic, molecular biology, biophysical and visualization techniques, allowed for the discovery of a panoply of new myosins, which, similarly to *Acanthamoeba* myosin I, are not able to form filaments and thus have been termed unconventional ones. Arguably, this classification initially appears rather artificial, as it is not clearly based on phylogenetic, structural or functional parameters; yet it provides researchers with an easy organization, which mainly recognizes the historic context.

In this Research Topic, dedicated to celebrate the 50th anniversary of discovery of the first unconventional myosin, we aim to shed light on their known and novel roles and functions as exemplified by research papers and reviews on seven members, namely, myosin I, myosin IIIA, myosin V, myosin VI, myosin VIIA, myosin XVA and myosin XVIII.

As already emphasized by the title of our collection, one focus is on the historical perspective of research on unconventional myosins. We therefore invited Tom Pollard and Ed Korn to contribute their personal view on the discovery of the very first unconventional myosin, *Acanthamoeba* myosin I. The authors gladly followed our invitation and provided their article enlightening the reader about the laborious experimental process of the search for and ultimate discovery of *Acanthamoeba* myosin I (Pollard and Korn, Front Physiol 2023). The initial skepticism of many researchers about the purified novel myosin being a degradation product of a conventional myosin, as well as the presence of a cofactor necessary to establish ATPase activity, later identified as myosin heavy chain kinase (Maruta and Korn, 1977), further illustrates the long way to acceptance of the presence of unconventional myosins. We are sad to say that Ed Korn passed shortly after publishing his last article but we are sure that he and his discoveries will be remembered, not only by the myosin community.

We asked Jim Spudich to provide us with his personal view on the history of the most widely used experimental tools to study the motor function of myosins, the *in vitro* motility assay and the dual-beam single-molecule laser trap assay. In his article, he not only meticulously describes the invention, improvement and refinement of these aforementioned methods, but also acknowledges a large number of researchers who contributed to the success (Spudich, Front Physiol 2024).

The undoubtedly most studied and best-characterized unconventional myosin is myosin V, implemented in intracellular transport processes including organelle trafficking, vesicle and receptor transport and dynamic tethering and positioning of macromolecules, organelles and subcellular structures. The review article by Rüdiger Rudolf summarizes the vast present literature on the role of myosin Va, one of the three mammalian isoforms, in receptor recycling at the nerve-muscle synapse and discusses a concept of myosin V mediated vesicle tethering in active cAMP microdomains (Rudolf, Front Physiol 2024).

The functional diversification of class 5 myosins can further be increased by alternative splicing. In their research article, Carew et al. report the presence and distribution of Myo5a splice variants, produced from six small alternative exons, in rodent pelvic organs (Carew et al., Front Physiol 2024).

Whereas mammalian myosin 5a and 5b have been shown to move processively along actin filaments to enable cargo transport, myosin 5c appears to lack this property and is characterized as a low duty ratio non-processive motor that needs to cluster on the surface of cargo to support its continuous movement. Kengyel et al. found human myosin 5c localizing in pancreatic β–cells and added new insights on the regulation of the purified protein by characterizing the fine-tuning of its enzymatic and motor function by the presence of different cytoplasmic tropomyosin isoforms (Kengyel et al., Front Physiol 2024). In addition, the interaction of calmodulin as well as essential and regulatory light chains with myosin 5c modulating motor function and the small-molecule mediated inhibition by the allosteric class-5 myosin inhibitor, Pentabromopseudilin, are described.

The duty ratio of a myosin, reflecting the relative proportion of strongly actin bound states during its ATPase cycle, is a critical determinant for its mechanical function. Diensthuber et al. (Diensthuber et al., Front Physiol 2024) utilized mutations of a single amino acid (Y/F) in switch-1 of the active site of two *Dictyostelium discoideum* class-1 myosins to show that this position fine-tunes their kinetic signatures to modulate the respective duty ratio.

Myosin VI is the only myosin characterized so far which moves backwards on actin filaments, i.e., towards the minus end of the filament. It is mainly known from its involvement in endocytosis and cytoskeleton organization but besides its cytoplasmic functions has been shown to function within the nucleus (Shahid-Fuente and Toseland, 2023). Herein, Nowak et al. demonstrate that myosin VI is also present within the nucleolus and is involved in the maintenance of nucleolar structure and ribosome organization (Nowak et al., Front Physiol 2024).

The majority of reports on myosin VI comes from rodent and human studies. Behbehani et al. present new data describing two *Caenorhabditis elegans* myosin VI isoforms, SPE-15/HUM-3 and HUM-8. The authors show that while they share similar motor properties, they have distinct developmental and tissue expression patterns (Behbehani et al., Front Physiol 2024).

Class-18 myosins are acknowledged as being the most divergent members of the myosin superfamily. For both mammalian isoforms, Myo18A and Myo18B, neither ATPase activity nor motor function could be shown (Guzik-Lendrum et al., 2013; Taft et al., 2013; Latham et al., 2020); yet, these myosins are found in active contractile structures including muscle sarcomeres and stress fibers. Horsthemke et al. contribute a review article on the current knowledge of myosin-18 function, specifically discussing the role of splice isoform Myo18Aγ and Myo18B in the sarcomere (Horsthemke et al., Front Physiol 2024).

Several unconventional myosins are known to be involved in the inner ear functions as numerous mutations in their genes were found to be associated with deafness. Miyoshi et al. present a review addressing the mechanisms of myosins' trafficking in a stereocilium using their motor function and make correlations between each described myosin variant with a clinical condition including the severity and onset of hearing loss, mode of inheritance and presence of symptoms other than hearing loss (Miyoshi et al., Front Physiol 2024). The authors concentrate on genes encoding unconventional myosins: IIIA, VI, VIIA and XVA, as well as on those encoding two conventional myosins - so called non-muscle myosins IIA (NM2A) and IIC (NM2C).

In summary, our Research Topic highlights recent discoveries on unconventional myosins (five research articles) and presents reviews (five articles) not only on particular myosins but also provides a historic perspective of renowned researchers on the discovery of the first unconventional myosin and the development of methods enabling studies on a single myosin molecule.

Author contributions

MHT: Writing–original draft, Writing–review and editing. MJR: Writing–original draft, Writing–review and editing.

Funding

The author(s) declare that financial support was received for the research, authorship, and/or publication of this article. This work was supported by the statutory funds granted by the Polish Ministry of Science and Higher Education to the Nencki Institute (MJR) and intramural funding of the Institute for Biophysical Chemistry, Hannover Medical School by the State of Lower Saxony, Germany (MHT).

Acknowledgments

The Research Topic Editors cordially thank all authors for their excellent contributions, the reviewers for expert evaluation of the manuscripts and the team of *Frontiers in Physiology* for continuous support and help.

Conflict of interest

The authors declare that the research was conducted in the absence of any commercial or financial relationships that could be construed as a potential conflict of interest.

The author(s) declared that they were an editorial board member of Frontiers, at the time of submission. This had no impact on the peer review process and the final decision.

Publisher's note

References

Berg, J. S., Powell, B. C., and Cheney, R. E. (2001). A millennial myosin census. *Mol. Biol. Cell* 12 (4), 780–794. doi:10.1091/mbc.12.4.780

Engelhardt, W. A., and Liubimova, M. N. (1939). Myosin and adenosine triphosphatase. *Nature* 144, 688. doi:10.1038/144668b0

Guzik-Lendrum, S., Heissler, S. M., Billington, N., Takagi, Y., Yang, Y., Knight, P. J., et al. (2013). Mammalian myosin-18A, a highly divergent myosin. *J. Biol. Chem.* 288 (13), 9532–9548. doi:10.1074/jbc.M112.441238

Kühne, W. (1864) *Untersuchungen über das Protoplasma und die Contractilität*. Leipzig: W. Engelmann.

Latham, S. L., Weiß, N., Schwanke, K., Thiel, C., Croucher, D. R., Zweigerdt, R., et al. (2020). Myosin-18B regulates higher-order organization of the cardiac sarcomere through thin filament cross-linking and thick filament dynamics. *Cell Rep.* 32 (9), 108090. doi:10.1016/j.celrep.2020.108090

Le Bot, N. (2010). The unconventional ones. *Nat. Rev. Mol. Cell Biol.* 9 (Suppl. 1), s11. doi:10.1038/nrm2562

Maruta, H., and Korn, E. D. (1977). Acanthamoeba cofactor protein is a heavy chain kinase required for actin activation of the Mg2+-ATPase activity of Acanthamoeba myosin I. *J. Biol. Chem.* 252 (23), 8329–8332. doi:10.1016/s0021-9258(19)75219-3

Odronitz, F., and Kollmar, M. (2007). Comparative genomic analysis of the arthropod muscle myosin heavy chain genes allows ancestral gene reconstruction and reveals a new type of 'partially' processed pseudogene. *BMC Mol. Biol.* 9, 21. doi:10.1186/1471-2199-9-21

Pollard, T. D., and Korn, E. D. (1973a). Acanthamoeba myosin. *J. Biol. Chem.* 248 (13), 4682–4690. doi:10.1016/s0021-9258(19)43718-6

Pollard, T. D., and Korn, E. D. (1973b). Acanthamoeba myosin. *J. Biol. Chem.* 248 (13), 4691–4697. doi:10.1016/s0021-9258(19)43719-8

Sellers, J. R. (2000). Myosins: a diverse superfamily. *Biochim. Biophys. Acta* 1496 (1), 3–22. doi:10.1016/s0167-4889(00)00005-7

Shahid-Fuente, I. W., and Toseland, C. P. (2023). Myosin in chromosome organisation and gene expression. *Biochem. Soc. Trans.* 51 (3), 1023–1034. doi:10.1042/BST20220939

Taft, M. H., Behrmann, E., Munske-Weidemann, L. C., Thiel, C., Raunser, S., and Manstein, D. J. (2013). Functional characterization of human myosin-18A and its interaction with F-actin and GOLPH3. *J. Biol. Chem.* 288 (42), 30029–30041. doi:10.1074/jbc.M113.497180

frontiers | Frontiers in Physiology

TYPE Review
PUBLISHED 17 November 2023
DOI 10.3389/fphys.2023.1324623

OPEN ACCESS

EDITED BY
Maria Jolanta Redowicz,
Polish Academy of Sciences, Poland

REVIEWED BY
Chris Toseland,
The University of Sheffield,
United Kingdom
Manuel H. Taft,
Hannover Medical School, Germany
Joanna Moraczewska,
Kazimierz Wielki University of Bydgoszcz,
Poland

*CORRESPONDENCE
Thomas D. Pollard,
thomas.pollard@yale.edu
Edward D. Korn,
korned2@yahoo.com

RECEIVED 20 October 2023
ACCEPTED 07 November 2023
PUBLISHED 17 November 2023

CITATION
Pollard TD and Korn ED (2023), Discovery of the first unconventional myosin: *Acanthamoeba* myosin-I.
Front. Physiol. 14:1324623.
doi: 10.3389/fphys.2023.1324623

Discovery of the first unconventional myosin: *Acanthamoeba* myosin-I

Thomas D. Pollard[1,2]* and Edward D. Korn[3]*

[1]Department of Molecular Cellular and Developmental Biology, Yale University, New Haven, CT, United States, [2]Department of Molecular and Cell Biology, University of California, Berkeley, CA, United States, [3]Scientist Emeritus, Laboratory of Cell Biology, National Heart, Lung, and Blood Institute, National Institutes of Health, Bethesda, MD, United States

Having characterized actin from *Acanthamoeba castellanii* (Weihing and Korn, Biochemistry, 1971, 10, 590–600) and knowing that myosin had been isolated from the slime mold *Physarum* (Hatano and Tazawa, Biochim. Biophys. Acta, 1968, 154, 507–519; Adelman and Taylor, Biochemistry, 1969, 8, 4976–4988), we set out in 1969 to find myosin in *Acanthamoeba*. We used K-EDTA-ATPase activity to assay myosin, because it is a unique feature of muscle myosins. After slightly less than 3 years, we purified a K-EDTA ATPase that interacted with actin. Actin filaments stimulated the Mg-ATPase activity of the crude enzyme, but this was lost with further purification. Recombining fractions from the column where this activity was lost revealed a "cofactor" that allowed actin filaments to stimulate the Mg-ATPase of the purified enzyme. The small size of the heavy chain and physical properties of the purified myosin were unprecedented, so many were skeptical, assuming that our myosin was a proteolytic fragment of a larger myosin similar to muscle or *Physarum* myosin. Subsequently our laboratories confirmed that *Acanthamoeba* myosin-I is a novel unconventional myosin that interacts with membrane lipids (Adams and Pollard, Nature, 1989, 340 (6234), 565–568) and that the cofactor is a myosin heavy chain kinase (Maruta and Korn, J. Biol. Chem., 1977, 252, 8329–8332). Phylogenetic analysis (Odronitz and Kollmar, Genome Biology, 2007, 8, R196) later established that class I myosin was the first myosin to appear during the evolution of eukaryotes.

KEYWORDS

actin, myosin, myosin I, unconventional myosin, *Acanthamoeba*

1 Introduction

Today it must be difficult for a person entering scientific research to appreciate how little was known in 1969 about the molecular basis of cellular movements. Furthermore, the tools available to study this fundamental life process were very limited. These were the days before SDS-gel electrophoresis, methods to determine gene sequences, personal computers, the internet, fluorescence microscopy for cell biology and digital cameras. Some investigators were even skeptical that anything could be learned about cellular movements using biochemical methods.

Nevertheless, pioneering work by Sadashi Hatano and Fumio Oosawa (Hatano and Oosawa, 1966; Hatano and Tazawa, 1968) in Japan and Mark Adelman and Edwin Taylor (Adelman and Taylor, 1969b; Adelman and Taylor, 1969b) in Chicago revealed by purification and characterization that the acellular slime mold *Physarum* has proteins similar to muscle actin and myosin. *Physarum* myosin is a large protein with a heavy chain that resembles the muscle myosin heavy chain in size.

Bob Weihing initiated work on motility proteins in the Korn lab at NIH by purifying actin from *Acanthamoeba* (Weihing and Korn, 1971). When Pollard joined the Korn lab in the summer of 1969, he and Weihing showed that the heavy meromyosin fragment of muscle myosin forms arrowhead-shaped complexes on amoeba actin filaments (Pollard et al., 1970), as first described for muscle actin filaments by Hugh Huxley (Huxley, 1963). Pollard and Weihing also used a method described by Hal Ishikawa in Howard Holtzer's lab (Ishikawa et al., 1969) to decorate actin filaments in the cytoplasm of extracted *Acanthamoeba* cells with myosin (Pollard et al., 1970).

1.1 Discovery of *Acanthamoeba* myosin-I

We set out to find myosin in *Acanthamoeba*, fully expecting a large protein like muscle and *Physarum* myosins. On the advice of Evan Eisenberg, a postdoc with Wayne Kielley in our Department, we used an ATPase assay with EDTA and a high concentration of KCl to monitor the purification process. Myosin was the only known ATPase with high activity under these non-physiological conditions. After we made some progress with the purification, we added a parallel assay with actin filaments to stimulate the Mg-ATPase activity, a second novel feature of known myosins.

Over a period of almost 3 years and more than 70 separate experiments, we purified an enzyme with K-EDTA-ATPase activity, but the protein was much smaller than muscle myosin. The crucial step in the purification was discovered accidently, when we tried to purify a crude fraction with K-EDTA-ATPase activity by gel filtration on a Bio-Rad A1.5m gel filtration column in a low ionic strength buffer (Figure 1). Most of the applied protein flowed through the column, but disappointingly, no ATPase activity eluted. In desperation, Pollard eluted the column with a gradient of KCl. Surprisingly, fractions containing protein emerged from the column, cleanly separating highly purified myosin from contaminants. Apparently, this batch of A1.5m had enough charged groups to act as a very weak ion exchange column. (Later batches of Bio-Rad A1.5m did not have this "magical" activity.) Agarose adsorption became the key step in the purification of *Acanthamoeba* myosin, allowing us to isolate about 3 mg from 600 g of cells using anion exchange chromatography, ammonium sulfate precipitation, agarose adsorption chromatography and hydroxyapatite chromatography (Pollard and Korn, 1973a).

Actin filaments stimulated the Mg-ATPase activity of partially pure *Acanthamoeba* myosin, but this activity was lost with further purification. Sulfhydryl oxidation may have a similar effect on muscle myosin, so we assumed that our protein was damaged during purification. Fortunately, Pollard met Edwin Taylor on a trip to the University of Chicago. Taylor made a crucial suggestion: recombine column fractions without ATPase activity with the fraction having K-EDTA-ATPase activity and assay for Mg-ATPase activity with actin filaments. Upon returning to Bethesda, Pollard dialyzed phosphate out of fractions from a hydroxyapatite column where the fractions with K-EDTA ATPase activity lost their actin-activated Mg-ATPase activity. Pollard was delighted to discover other fractions from the column without ATPase activity stimulated the actin-activated Mg-ATPase activity of the myosin (Figure 2). No one else was in the lab on Saturday, so he telephoned Korn at home with the welcome news. We called this activity the "cofactor" protein and partially purified it (Pollard and Korn, 1973b). Subsequently, we learned that agarose adsorption also separated cofactor protein from *Acanthamoeba* myosin (Figure 1).

Purified *Acanthamoeba* myosin consisted of a single heavy chain of about 140 kDa with a single ATPase head and two light chains. It bound to actin filaments in the absence of ATP but not in the presence of ATP. However, it differed fundamentally from myosins purified from muscle, *Physarum* and animal nonmuscle cells. The Stokes' radius was consistent with a globular protein of about 180 kDa. Despite its small size, *Acanthamoeb*a myosin appeared in electron micrographs to crosslink pairs of actin filaments. In contrast, muscle myosin has two ATPase heads and a long tail formed by a coiled-coil of the two 200 kDa

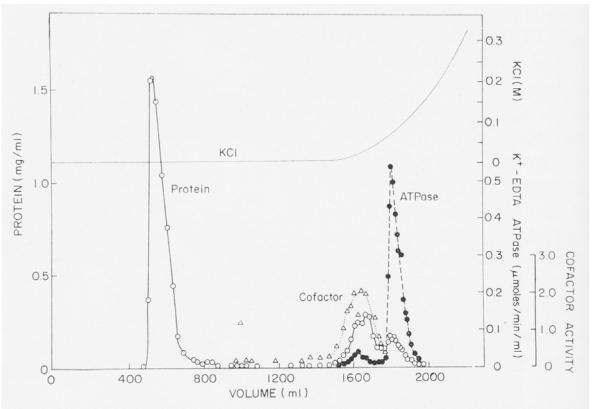

FIGURE 1
Purification of *Acanthamoeba* myosin-I by adsorption to and elution from an agarose gel filtration column. About 40 mL of partially purified myosin-I were applied to a 5 × 75 cm column of Bio-Rad A1.5m (8% agarose) and eluted with 0.2 mM ATP, 1 mM DTT, 2 mM Tris chloride (pH 7.6). No K-EDTA-ATPase activity eluted until the column was eluted with a gradient of KCl Figure 3 in Pollard and Korn (1973b).

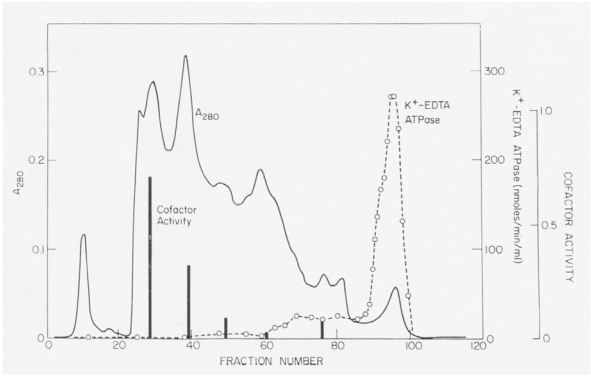

FIGURE 2
Discovery of cofactor protein. Crude *Acanthamoeba* myosin was purified by ion exchange on DEAE-cellulose, fractionation with ammonium sulfate and gel filtration on a column of 8% agarose beads in 500 mM KCl. Crude myosin was run through a column of hydroxyapatite in 500 mM KCl and eluted with a gradient of potassium phosphate. K-EDTA ATPase activity eluted at high phosphate concentrations, but these fractions lacked Mg-ATPase activity stimulated by actin filaments. However, enzymatically inactive fractions that eluted earlier stimulated the actin-activated Mg-ATPase activity of *Acanthamoeba* myosin (black bars). This was the "cofactor" activity Figure 2 in Pollard and Korn (1973b).

heavy chains. *Acanthamoeba* myosin was soluble at low ionic strength, conditions where myosins from skeletal muscle (Huxley, 1963), *Physarum* (Nachmias, 1972), human platelets (Adelstein et al., 1971) and fibroblasts (Adelstein et al., 1972) form bipolar filaments.

These properties led many in the myosin field to conclude that the *Acanthamoeba* myosin was a degradation product of a myosin similar to muscle myosin. In 1864 (yes, 1864), the German physiologist W. Kühne extracted a salt-soluble protein from muscle that he called "myosin" (from the Greek word "mus" for "muscle" (Kühne, 1864). Every myosin isolated from any organism before 1973 resembled muscle myosin, so it was reasonable to suspect that the smaller myosin we isolated from *Acanthamoeba* was a proteolytic fragment of a typical myosin.

Furthermore, *Acanthamoeba* myosin was the first myosin shown to require a cofactor protein for actin-activated ATPase activity. Additional experiments produced fractions enriched in a 97 kDa protein with cofactor activity (Pollard and Korn, 1973b). The Mg-ATPase activity of *Acanthamoeba* myosin depended in a biphasic fashion on the concentrations of actin filaments with a unique peak of activity at low actin concentrations followed by a hyperbolic dependence on higher concentration of actin as seen for other myosins. We suggested that the low actin-activated ATPase activity of purified platelet myosin (Adelstein et al., 1971) might be due to a missing cofactor protein.

1.2 Advances in understanding *Acanthamoeba* myosin-I

Subsequent work by the Korn laboratory found that *Acanthamoeba* contains 3 myosin-I isoforms, (myosin-IA, myosin-IB and myosin-IC) none of which forms filaments (Maruta et al., 1979). Both of our laboratories independently purified from *Acanthamoeba* a myosin similar to muscle myosin (Maruta and Korn, 1977a; Pollard et al., 1978). Electron microscopy showed that this myosin has two ATPase heads, a 90 nm long coiled-coil tail (much shorter than muscle myosin 150 nm) and forms short bipolar filaments (Pollard et al., 1978). John Hammer provided the definitive evidence that the small and large *Acanthamoeba* myosins are different gene products by isolating genomic DNA and sequencing regions of the heavy chains (Hammer et al., 1986a; Hammer et al., 1986b; Jung et al., 1987).

The small amoeba myosins with one heavy chain and one ATPase head became "myosin-I" and the larger myosin with two heavy chains and two ATPase heads became "myosin-II." Myosin-II has long been considered to be "conventional" myosin, and all others, beginning with *Acanthamoeba* myosin-I, are now called "unconventional" myosins. Additional classes of myosin were numbered in order of their discoveries.

Over a period of 20 years, our labs determined the primary structures of the three *Acanthamoeba* myosin-Is and a light chain. The domain structure of myosin-IA (Figure 3) (Lee et al., 1999) is typical of the other two myosin-Is (Brzeska et al., 1988; Lee et al., 1999). The large, N-terminal catalytic domain is homologous to the heads of other myosins. The next domain has binding sites for three light chains. Myosin-IB and myosin-IC have single light chains (Liu et al., 2000). The tail has three "tail homology" domains that fold independently: a basic TH1 domain; a TH2 or GPA-rich (glycine proline alanine) domain; and a TH3/SH3 domain, which is located at the end of the heavy chains of myosin-IA and myosin-IB or in the middle of the TH2 domain in myosin-IC (Liu et al., 2000). The TH1 and TH2 domains bind to each other and bind independently to actin filaments in the presence or absence of ATP (Lee et al., 1999). The hydrodynamic properties of isolated tail domains and their size and shape in reconstructions from electron micrographs (Figure 4) suggest that the TH2/TH3 domains fold back on the TH1 domain (Lee et al., 1999).

Richard Adams discovered that *Acanthamoeba* myosin-I binds membranes (Adams and Pollard, 1989) and transports membrane vesicles along actin filaments (Adams and Pollard, 1986). The TH1 domain in the proximal part of the myosin-I tail binds acidic phosphoglycerides (Doberstein and Pollard, 1992), allowing myosin-I to move actin filaments over the surface of supported lipid bilayers (Zot et al., 1992).

A pre-steady state kinetic analysis by Michael Ostap (Pollard and Ostap, 1996) revealed that the actomyosin ATPase cycle of *Acanthamoeba* myosin-I is similar to muscle myosin with a small duty cycle. Thus, multiple myosin-I molecules must work cooperatively to move a vesicle on an actin filament. The peak of steady state Mg-ATPase activity at low actin filament concentrations was explained by myosin-I crosslinking actin filaments through interactions of the tail with one filament and the cycling head with another filament (Lynch et al., 1986; Brzeska et al., 1988).

Three dimensional reconstructions of *Acanthamoeba* myosin-IB (Jontes et al., 1998) and myosin-IC (Carragher et al., 1998) bound to actin filaments showed that the head binds actin filaments like muscle myosin and a short tail extends from the head.

The physiological functions of *Acanthamoeba* myosin-I's are less well understood than their biochemical properties. However fluorescent antibody localization in fixed cells (Baines et al., 1992; Baines et al., 1995), loading fluorescent antibodies into live cells (Ostap et al., 2003) and transient expression of EGFP-myosin-IC in live cells (Kong and Pollard, 2002) implicated myosin-I isoforms in macropinocytosis, phagocytosis, heterophagy and contractile vacuole function. Transient concentration of myosin-IC around contractile vacuoles required both the head and the SH3 domain

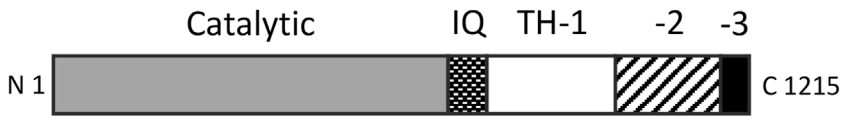

FIGURE 3
Domain organization of *Acanthamoeba* myosin-IA. The catalytic domain has ATPase activity and binds actin filaments in the absence of ATP. The three IQ domains bind light chains. The basic tail homology 1 (TH-1) domain binds acidic membrane lipids and actin filaments. The TH-2 domain binds actin filaments and folds back to interact with the TH-1 domain. TH-3 is an SH3 domain. The organization of myosin-IB is similar, while myosin-IC has the SH3 domain within the TH2 domain. Redrawn from (Lee et al., 1999).

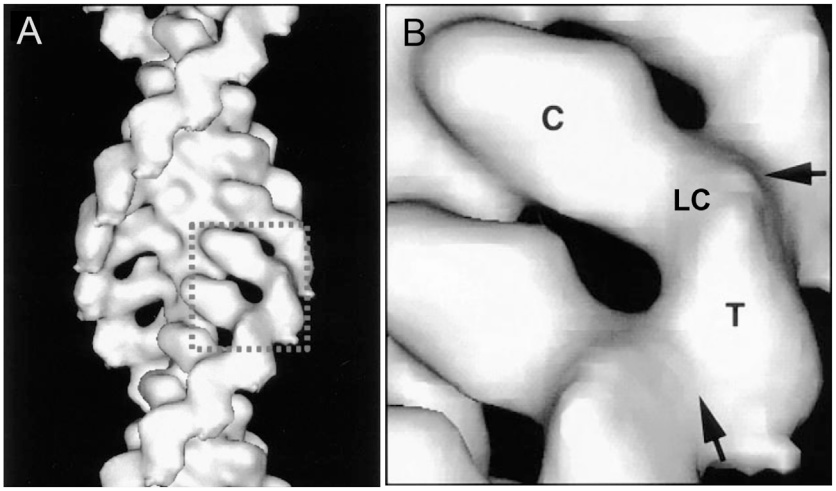

FIGURE 4
Three dimensional reconstruction at 18 Å resolution of cryo-electron micrographs of *Acanthamoeba* myosin-1B bound to actin filaments. **(A)**, overview; **(B)**, detailed view of one molecule. The catalytic domain (C) of one myosin-I is bound to each actin subunit. A narrow region with the single light chain (LC) links the catalytic domain to the tail domains (T). Arrows mark contacts between the tails. Modified from Figure 4 (Jontes et al., 1998).

in the tail (Kong and Pollard, 2002). Loading *Acanthamoeba* cells with inhibitory antibodies to myosin-IC (but not myosin-IB) disrupted contractile vacuole function, and cells swelled and lysed in hypotonic media (Doberstein et al., 1993).

Hiroshi Maruta purified the cofactor protein and discovered that it is a myosin heavy chain kinase (Maruta and Korn, 1977b) that phosphorylates a single serine (Hammer et al., 1983). Extensive additional work in the Korn lab characterized the heavy chain kinase and the phosphorylation sites (Brzeska et al., 1989).

1.3 Expansion of knowledge about myosin-Is

Myosin-I was discovered a second time as the physical link between the bundle of actin filaments inside microvilli of the intestinal brush border and the surrounding plasma membrane. This connection was first recognized in electron micrographs by Mooseker and Tilney (Mooseker and Tilney, 1975). Subsequently the protein was studied biochemically (Matsudaira and Burgess, 1979) and shown to be myosin-I by purification (Collins and Borysenko, 1984). Its primary structure (Hoshimaru and Nakanishi, 1987; Garcia et al., 1989) established that brush border myosin is a myosin-I with three calmodulin light chains and a lipid binding tail.

Dictyostelium amoebae were also found to contain a Class I myosin (Coté et al., 1985), and further work discovered a total of eight Class I myosins (IA-IH) (Falk et al., 2003). Some are homologous with *Acanthamoeba* myosin Is, including domain organization and membrane binding properties.

Research by many laboratories over the past 30 years revealed a remarkably wide range of physiological functions of myosin-I, particularly in animals [reviewed by (McIntosh and Ostap, 2016; Pernier and Schauer, 2022)]. For example, the eight isoforms of human myosin-I have specific functions revealed by combinations of genetic deletion, mRNA depletion, over expression, localization and *in vitro* reconstitution. A pioneering example implicated myosin-IC in the adaptation of sensory hair cells in the ear (Gillespie et al., 1993). Other functions include determining the left-right asymmetry of cells and organisms, delivering vesicles with the glucose carrier GLUT4 to the plasma membrane of muscle and fat cells in response to insulin, organizing cortical actin filaments, generating membrane tension and stabilizing focal adhesions. Decades of additional research are needed to understand how each myosin-I isoform is adapted to its physiological functions.

1.4 Gene sequences of thousands of myosins explain their diversity and evolution

Further research extended the classes of unconventional myosins. Myosin-III was discovered by genetic analysis of mutants affecting photoreceptors in flies (Montell and Rubin, 1988). It has an N-terminal kinase domain, followed by the catalytic domain and a tail that binds calmodulin. Horowitz and Hammer (Horowitz and Hammer, 1990) discovered myosin-IV by cloning the gene from *Acanthamoeba*. The gene encodes a myosin catalytic domain and a tail of 792 residues that differs from all other myosins except for the presence of a C-terminal SH3 domain. The distribution of myosin-IV is limited to *Acanthamoeba* and some unicellular organisms widely separated from amoebae on the phylogenetic tree (Kollmar and Mühlhausen, 2017). Myosin-V was discovered as a cell cycle mutant in budding yeast that encodes a protein required for vesicle transport into the bud (Johnston et al., 1991) and was isolated independently from chicken brain (Espindola et al., 1992). Thus by 1992 (19 years after discovery of the *Acanthamoeba* unconventional myosins) a total of only 14 unconventional myosins were identified forming five different classes of unconventional myosins.

The full extent of the myosin gene family was ultimately revealed by genome sequences of thousands of species spread across the phylogenic tree. By 2017 the inventory included 7,852 myosin genes

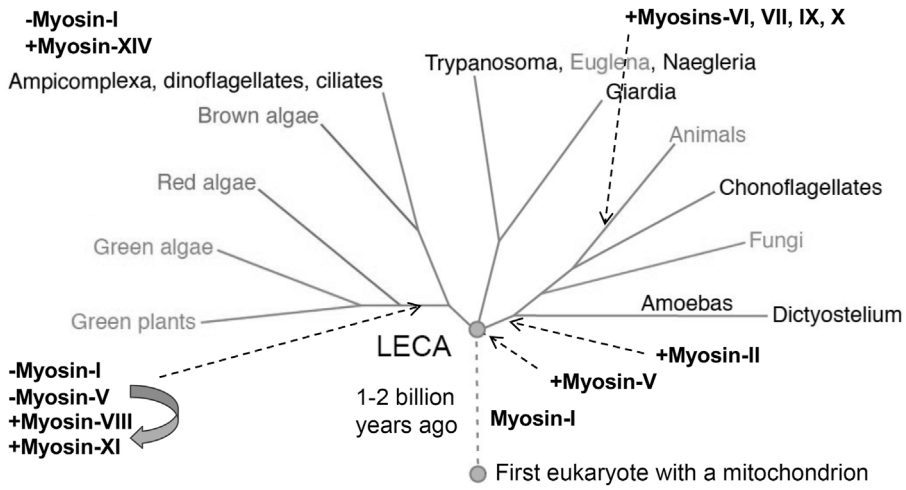

FIGURE 5
Phylogenetic tree showing the evolution of myosin genes beginning with the appearance of myosin-I more than 1 billion years ago between the time of the first eukaryote and the last eukaryotic common ancestor (LECA). Gene duplication closer to the time of LECA produced a second myosin related to myosin-V, which gave rise to all other myosin genes. Eukaryotes branching from LECA inherited these ancient myosin genes, but algae and plants lost the gene for myosin-I and the myosin-V gene evolved into genes for myosins-VIII and XI. Myosin-II appeared in the branch leading to animals, fungi and amoebas. Myosins-VI, VII, IX and X are confined to animals. Myosin-XIV replaced myosin-I in *Ampicomplexa*. [Positions of myosins are based on (Odronitz and Kollmar 2007)].

from 929 organisms, divided into 79 classes (Kollmar and Mühlhausen, 2017).

The first myosin gene to appear during evolution was for a class I myosin (Figure 5). Before the last eukaryotic common ancestor (LECA), the myosin-I gene duplicated and diverged to form a second class of myosin gene that became the precursor for all other classes of myosins. Further gene duplication and divergence produced genes for many new classes of myosin, such as myosin-II in the branch with amoebas, fungi and animals. Myosin genes have been lost many times and a few eukaryotes have none: the red algae *Cyanidioschyzon merolae*, *Porphyridium purpureum* and *Chondrus crispus*; as well as the protozoa *Giardia lamblia*, *Trichomonas vaginalis* and *Spironucleus salmonicida*.

1.5 Myosins and human disease

The discovery of unconventional myosins has had two big impacts. First, as noted by Edwin Taylor when he accepted the E. B. Wilson Medal from the American Society for Cell Biology (Taylor, 2001), it "...was the beginning of the end of the isolation of the muscle community from the rest of cell biology." Second, continued research on unconventional myosins revealed that mutations of myosin genes predispose to many human diseases. A PubMed search for "myosins and human diseases" finds 6,317 papers, many on unconventional myosins. For example, deafness in humans is associated with mutations of heavy chain genes in Classes 1, 2, 3, 6, and 15; hearing and vision loss with mutation of Class 7 heavy chain genes; cardiac myopathies with mutations of Classes 2 and 6 heavy chain genes; platelet anomalies with mutation of Class 2 heavy chain genes; and hypopigmentosis and microvillus inclusion disease with mutation of Class 5 heavy chain genes (reviewed (Coluccio, 2020)). Thus, basic research on cellular movements opened the door for work required to understand human diseases.

Author contributions

TP: Writing–original draft, Writing–review and editing. EK: Writing–original draft, Writing–review and editing.

Funding

The author(s) declare that no financial support was received for the research, authorship, and/or publication of this article.

Acknowledgments

EK thanks all his postdoctoral fellows and Hanna Brzeska, Shi Shu, and Xiong Liu, who spent much of their careers in the EK Lab.; Tom Pollard thanks EK for the opportunity work in his lab to fulfill his military service and all the people, who worked on myosins in his lab over 5 decades. Both authors thank the reviewers for helpful suggestions.

Conflict of interest

The authors declare that the research was conducted in the absence of any commercial or financial relationships that could be construed as a potential conflict of interest.

Publisher's note

References

Adams, R. J., and Pollard, T. D. (1986). Propulsion of organelles isolated from Acanthamoeba along actin filaments by myosin-I. *Nature* 322 (6081), 754–756. doi:10.1038/322754a0

Adams, R. J., and Pollard, T. D. (1989). Binding of myosin I to membrane lipids. *Nature* 340 (6234), 565–568. doi:10.1038/340565a0

Adelman, M. R., and Taylor, E. W. (1969a). Isolation of an actomyosin-like protein complex from slime mold plasmodium and the separation of the complex into actin- and myosin-like fractions. *Biochemistry* 8 (12), 4964–4975. doi:10.1021/bi00840a046

Adelman, M. R., and Taylor, E. W. (1969b). Further purification and characterization of slime mold myosin and slime mold actin. *Biochemistry* 8, 4976–4988. doi:10.1021/bi00840a047

Adelstein, R. S., Conti, M. A., Johnson, G. S., Pastan, I., and Pollard, T. D. (1972). Isolation and characterization of myosin from cloned mouse fibroblasts. *Proc. Natl. Acad. Sci. U. S. A.* 69 (12), 3693–3697. doi:10.1073/pnas.69.12.3693

Adelstein, R. S., Pollard, T. D., and Kuehl, W. M. (1971). Isolation and characterization of myosin and two myosin fragments from human blood platelets. *Proc. Natl. Acad. Sci. U. S. A.* 68 (11), 2703–2707. doi:10.1073/pnas.68.11.2703

Baines, I. C., Brzeska, H., and Korn, E. D. (1992). Differential localization of *Acanthamoeba* myosin I isoforms. *J. Cell. Biol.* 119, 1193–1203. doi:10.1083/jcb.119.5.1193

Baines, I. C., Corigliano-Murphy, A., and Korn, E. D. (1995). Quantification and localization of phosphorylated myosin I isoforms in Acanthamoeba castellanii. *J. Cell. Biol.* 130, 591–603. doi:10.1083/jcb.130.3.591

Brzeska, H., Lynch, T. J., and Korn, E. D. (1988). Localization of the actin-binding sites of Acanthamoeba myosin IB and effect of limited proteolysis on its actin-activated Mg2+-ATPase activity. *J. Biol. Chem.* 263 (1), 427–435. doi:10.1016/s0021-9258(19)57410-5

Brzeska, H., Lynch, T. J., Martin, B., and Korn, E. D. (1989). The localization and sequence of the phosphorylation sites of Acanthamoeba myosins I. *J. Biol. Chem.* 264 (32), 19340–19348. doi:10.1016/s0021-9258(19)47307-9

Carragher, B. O., Cheng, N., Wang, Z. Y., Korn, E. D., Reilein, A., Belnap, D. M., et al. (1998). Structural invariance of constitutively active and inactive mutants of acanthamoeba myosin IC bound to F-actin in the rigor and ADP-bound states. *Proc. Natl. Acad. Sci. U.S.A.* 95, 15206–15211. doi:10.1073/pnas.95.26.15206

Collins, J. H., and Borysenko, C. W. (1984). The 110,000-dalton actin-binding and calmodulin-binding protein from intestinal brush-border is a myosin-like ATPase. *J. Biol. Chem.* 259, 4128–4135.

Coluccio, L. M. (2020). Myosins and disease. *Adv. Exp. Med. Biol.* 1239, 245–316. doi:10.1007/978-3-030-38062-5_12

Coté, G. P., Albanesi, J. P., Uelo, T., Hammer, J. A., III, and Korn, E. D. (1985). Purification from *Dictyostelium discoideum* of a low molecular weight myosin that resembles myosin-I from *Acanthamoeba castellanii*. *J. Biol. Chem.* 260, 4543–4546. doi:10.1016/s0021-9258(18)89100-1

Doberstein, S. K., Baines, I., Weigand, G., Korn, E. D., and Pollard, T. D. (1993). Inhibition of contractile vacuole function *in vivo* by antibodies against myosin-I. *Nature* 365, 841–843. doi:10.1038/365841a0

Doberstein, S. K., and Pollard, T. D. (1992). Localization and specificity of the phospholipid and actin binding sites on the tail of *Acanthamoeba* myosin-IC. *J. Cell. Biol.* 117, 1241–1249. doi:10.1083/jcb.117.6.1241

Espindola, F. S., Espreafico, E. M., Coelho, M. V., Martins, A. R., Costa, F. R. C., Mooseker, M. S., et al. (1992). Biochemical and immunological characterization of p190-calmodulin complex from vertebrate brain: a novel calmodulin-binding myosin. *J. Cell. Biol.* 118, 359–368. doi:10.1083/jcb.118.2.359

Falk, D. L., Wessels, D., Jenkins, L., Pham, T., Kuhl, S., Titus, M. A., et al. (2003). Shared, unique and redundant functions of three members of the class I myosins (MyoA, MyoB and MyoF) in motility and chemotaxis in Dictyostelium. *J. Cell. Sci.* 116, 3985–3999. doi:10.1242/jcs.00696

Garcia, A. E., Coudrier, E., Carboni, J., Anderson, J., Vandekerckhove, M. S., Mooseker, M. S., et al. (1989). Partial deduced sequence ofthe110-kD-calmodulin complex of the avian intestinal microvillus shows that this mechanoenzyme is a member of the myosin-I family. *J. Cell. Biol.* 109, 2895–2903. doi:10.1083/jcb.109.6.2895

Gillespie, P. G., Wagner, M. C., and Hudspeth, A. J. (1993). Identification of a 120 kd hair-bundle myosin located near stereociliary tips. *Neuron* 11, 581–594. doi:10.1016/0896-6273(93)90071-x

Hammer, J. A., III, Albanesi, J. P., and Korn, E. D. (1983). Purification and characterization of a myosin-I heavy-chain kinase from *Acanthamoeba castellanii*. *J. Biol. Chem.* 258, 10168–10175. doi:10.1016/s0021-9258(17)44620-5

Hammer, J. A., III, Jung, G., and Korn, E. D. (1986a). Genetic evidence that *Acanthamoeba* myosin-I is a true myosin. *Proc. Natl. Acad. Sci. U. S. A.* 83, 4655–4659. doi:10.1073/pnas.83.13.4655

Hammer, J. A., III, Korn, E. D., and Paterson, B. M. (1986b). Isolation of a non-muscle myosin heavy chain gene from *Acanthamoeba*. *J. Biol. Chem.* 261 (4), 1949–1956. doi:10.1016/s0021-9258(17)36035-0

Hatano, S., and Oosawa, F. (1966). Isolation and characterization of plasmodium actin. *Biochim. Biophys. Acta* 127, 488–498. doi:10.1016/0304-4165(66)90402-8

Hatano, S., and Tazawa, M. (1968). Isolation, purification and characterization of byosin B from myxomycete plasmodium. *Biochim. Biophys. Acta* 154, 507–519. doi:10.1016/0005-2795(68)90011-1

Horowitz, J. A., and Hammer, J. A., III (1990). A new *Acanthamoeba* myosin heavy chain: cloning of the gene and immunological identification of the polypeptide. *J. Biol. Chem.* 265, 20646–20652. doi:10.1016/s0021-9258(17)30552-5

Hoshimaru, M., and Nakanishi, S. (1987). Identification of a new type of mammalian myosin heavy chain by molecular cloning: overlap of its mRNA with preprotachykinin B mRNA. *J. Biol. Chem.* 262, 14625–14632. doi:10.1016/s0021-9258(18)47842-8

Huxley, H. E. (1963). Electron microscope studies on the structure of natural and synthetic protein filaments from striated muscle. *J. Mol. Biol.* 7, 281–308. doi:10.1016/s0022-2836(63)80008-x

Ishikawa, H., Bischoff, R., and Holtzer, H. (1969). Formation of arrowhead complexes with heavy meromyosin in a variety of cell types. *J. Cell. Biol.* 43, 312–328. doi:10.1083/jcb.43.2.312

Johnston, G. C., Prendergast, J. A., and Singer, R. A. (1991). The *Saccharomyces cerevisiae* MYO2 gene encodes an essential myosin for vectorial transport of vesicles. *J. Cell. Biol.* 113, 539–551. doi:10.1083/jcb.113.3.539

Jontes, J. D., Ostap, E. M., Pollard, T. D., and Milligan, R. A. (1998). Three-dimensional structure of Acanthamoeba castellanii myosin-IB (MIB) determined by cryoelectron microscopy of decorated actin filaments. *J. Cell. Biol.* 141 (1), 155–162. doi:10.1083/jcb.141.1.155

Jung, G., Korn, E. D., and Hammer, J. A., III (1987). The heavy chain of *Acanthamoeba* myosin-IB is a fusion of myosin-like and non-myosin-like sequences. *Proc. Natl. Acad. Sci. U. S. A.* 84, 6720–6724. doi:10.1073/pnas.84.19.6720

Kollmar, M., and Mühlhausen, S. (2017). Myosin repertoire expansion coincides with eukaryotic diversification in the Mesoproterozoic era. *BMC Evol. Biol.* 17, 211. doi:10.1186/s12862-017-1056-2

Kong, H. H., and Pollard, T. D. (2002). Intracellular localization and dynamics of myosin-II and myosin-IC in live Acanthamoeba by transient transfection of EGFP fusion proteins. *J. Cell. Sci.* 115 (Pt 24), 4993–5002. doi:10.1242/jcs.00159

Kühne, W. (1864). *Untersuchungen über das Protoplasma und die Contractilitat*. Leipzig: W. Engelmann.

Lee, W. L., Ostap, E. M., Zot, H. G., and Pollard, T. D. (1999). Organization and ligand binding properties of the tail of Acanthamoeba myosin-IA. Identification of an actin-binding site in the basic (tail homology-1) domain. *J. Biol. Chem.* 274 (49), 35159–35171. doi:10.1074/jbc.274.49.35159

Liu, X., Brzeska, H., and Korn, E. D. (2000). Functional analysis of tail domains of Acanthamoeba myosin IC by characterization of truncation and deletion mutants. *J. Biol. Chem.* 275, 24886–24892. doi:10.1074/jbc.M004287200

Lynch, T. J., Albanesi, J. P., Korn, E. D., Robinson, E. A., Bowers, B., and Fujisaki, H. (1986). ATPase activities and actin-binding properties of subfragments of *Acanthamoeba* myosin-IA. *J. Biol. Chem.* 261, 17156–17162. doi:10.1016/s0021-9258(19)76012-8

Maruta, H., Gadasi, H., Collins, J. H., and Korn, E. D. (1979). Multiple forms of Acanthamoeba myosin I. *J. Biol. Chem.* 254 (9), 3624–3630. doi:10.1016/s0021-9258(18)50807-3

Maruta, H., and Korn, E. D. (1977a). *Acanthamoeba* myosin-II. *J. Biol. Chem.* 252, 6501–6509. doi:10.1016/s0021-9258(17)39986-6

Maruta, H., and Korn, E. D. (1977b). *Acanthamoeba* cofactor protein is a heavy-chain kinase required for actin activation of Mg^{+2}-ATPase activity of *Acanthamoeba* myosin-I. *J. Biol. Chem.* 252, 8329–8332. doi:10.1016/s0021-9258(19)75219-3

Matsudaira, P. T., and Burgess, D. R. (1979). Identification and organization of the components in the isolated microvillus cytoskeleton. *J. Cell. Biol.* 83, 667–673. doi:10.1083/jcb.83.3.667

McIntosh, B. B., and Ostap, E. M. (2016). Myosin-I molecular motors at a glance. *J. Cell. Sci.* 129, 2689–2695. doi:10.1242/jcs.186403

Montell, C., and Rubin, G. M. (1988). The *Drosophila ninaC* locus encodes two photoreceptor cell specific proteins with domains homologous to protein kinases and the myosin heavy chain head. *Cell.* 52, 757–772. doi:10.1016/0092-8674(88)90413-8

Mooseker, M. S., and Tilney, L. G. (1975). Organization of an actin filament-membrane complex. Filament polarity and membrane attachment in the microvilli of intestinal epithelial cells. *J. Cell. Biol.* 67, 725–743. doi:10.1083/jcb.67.3.725

Nachmias, V. T. (1972). Filament formation by purified *Physarum* myosin. *Proc. Natl. Acad. Sci. U. S. A.* 69, 2011–2014. doi:10.1073/pnas.69.8.2011

Odronitz, F., and Kollmar, M. (2007). Drawing the tree of eukaryotic life based on the analysis of 2,269 manually annotated myosins from 328 species. *Genome Biol.* 8, R196. doi:10.1186/gb-2007-8-9-r196

Ostap, E. M., Maupin, P., Doberstein, S. K., Baines, I. C., Korn, E. D., and Pollard, T. D. (2003). Dynamic localization of myosin-I to endocytic structures in Acanthamoeba. *Cell. Motil. Cytoskelet.* 54 (1), 29–40. doi:10.1002/cm.10081

Pernier, J., and Schauer, K. (2022). Does the actin network architecture leverage myosin-I functions? *Biology* 11, 989. doi:10.3390/biology11070989

Pollard, T. D., and Korn, E. D. (1973a). I. Isolation from Acanthamoeba castellanii of an enzyme similar to muscle myosin. *J. Biol. Chem.* 248 (13), 4682–4690. doi:10.1016/s0021-9258(19)43718-6

Pollard, T. D., and Korn, E. D. (1973b). II. Interaction with actin and with a new cofactor protein required for actin activation of Mg^{++} ATPase activity. *J. Biol. Chem.* 248 (13), 4691–4697. doi:10.1016/s0021-9258(19)43719-8

Pollard, T. D., and Ostap, E. M. (1996). The chemical mechanism of myosin-I: implications for actin-based motility and the evolution of the myosin family of motor proteins. *Cell. Struct. Funct.* 21 (5), 351–356. doi:10.1247/csf.21.351

Pollard, T. D., Shelton, E., Weihing, R. R., and Korn, E. D. (1970). Ultrastructural characterization of F-actin isolated from Acanthamoeba castellanii and identification of cytoplasmic filaments as F-actin by reaction with rabbit heavy meromyosin. *J. Mol. Biol.* 50 (1), 91–97. doi:10.1016/0022-2836(70)90106-3

Pollard, T. D., Stafford, W. F., and Porter, M. E. (1978). Characterization of a second myosin from Acanthamoeba castellanii. *J. Biol. Chem.* 253 (13), 4798–4808. doi:10.1016/s0021-9258(17)30460-x

Taylor, E. W. (2001). 1999 E.B. Wilson lecture: the cell as molecular machine. *Mol. Biol. Cell.* 12, 251–254. doi:10.1091/mbc.12.2.251

Weihing, R. R., and Korn, E. D. (1971). Acanthamoeba actin. Isolation and properties. *Biochemistry* 10, 590–600. doi:10.1021/bi00780a008

Zot, H. G., Doberstein, S. K., and Pollard, T. D. (1992). Myosin-I moves actin filaments on a phospholipid substrate: implications for membrane targeting. *J. Cell. Biol.* 116 (2), 367–376. doi:10.1083/jcb.116.2.367

frontiers | Frontiers in Physiology

TYPE Original Research
PUBLISHED 12 December 2023
DOI 10.3389/fphys.2023.1304537

OPEN ACCESS

EDITED BY
Manuel H. Taft,
Hannover Medical School, Germany

REVIEWED BY
Joseph Szule,
Texas A and M University, College Station, United States
Madhurima Saha,
University of Florida, United States
Prasad Trivedi,
Department of Pediatrics, University of Florida, in collaboration with reviewer MS

*CORRESPONDENCE
Josephine A. Carew,
josephine_carew@hms.harvard.edu

RECEIVED 29 September 2023
ACCEPTED 20 November 2023
PUBLISHED 12 December 2023

CITATION
Carew JA, Cristofaro V, Goyal RK and Sullivan MP (2023), Differential Myosin 5a splice variants in innervation of pelvic organs.
Front. Physiol. 14:1304537.
doi: 10.3389/fphys.2023.1304537

Differential Myosin 5a splice variants in innervation of pelvic organs

Josephine A. Carew[1,2,3]*, Vivian Cristofaro[1,2,4], Raj K. Goyal[1,2] and Maryrose P. Sullivan[1,2,4]

[1]Urology Research, VA Boston Healthcare System, Boston, MA, United States, [2]Harvard Medical School, Boston, MA, United States, [3]Department of Medicine, Brigham and Women's Hospital, Boston, MA, United States, [4]Department of Surgery, Brigham and Women's Hospital, Boston, MA, United States

Introduction: Myosin proteins interact with filamentous actin and translate the chemical energy generated by ATP hydrolysis into a wide variety of mechanical functions in all cell types. The classic function of conventional myosins is mediation of muscle contraction, but myosins also participate in processes as diverse as exocytosis/endocytosis, membrane remodeling, and cytokinesis. Myosin 5a (Myo5a) is an unconventional motor protein well-suited to the processive transport of diverse molecular cargo within cells and interactions with multiprotein membrane complexes that facilitate exocytosis. Myo5a includes a region consisting of six small alternative exons which can undergo differential splicing. Neurons and skin melanocytes express characteristic splice variants of Myo5a, which are specialized for transport processes unique to those cell types. But less is known about the expression of Myo5a splice variants in other tissues, their cargos and interactive partners, and their regulation.

Methods: In visceral organs, neurotransmission-induced contraction or relaxation of smooth muscle is mediated by Myo5a. Axons within urogenital organs and distal colon of rodents arise from cell bodies located in the major pelvic ganglion (MPG). However, in contrast to urogenital organs, the distal colon also contains soma of the enteric nervous system. Therefore, the rodent pelvic organs provide an opportunity to compare the expression of Myo5a splice variants, not only in different tissues innervated by the pelvic nerves, but also in different subcellular compartments of those nerves. This study examines the expression and distribution of Myo5a splice variants in the MPG, compared to the bladder, corpus cavernosum of the penis (CCP) and distal colon using immunohistochemistry and mRNA analyses.

Results/discussion: We report detection of characteristic Myo5a variants in these tissues, with bladder and CCP displaying a similar variant pattern but one which differed from that of distal colon. In all three organs, Myo5a variants were distinct compared to the MPG, implying segregation of one variant within nerve soma and its exclusion from axons. The expression of distinct Myo5a variant arrays is likely to be adaptive, and to underlie specific functions fulfilled by Myo5a in those particular locations.

KEYWORDS

protein splice variants, neurotransmission, myosin motor, peripheral nerve, pelvic organ

1 Introduction

Myosin 5a (Myo5a) is a dimeric motor protein that processively transports molecular cargos along actin filaments. The *Myo5a* gene is expressed by many secretory cell types (Desnos et al., 2003; Eichler et al., 2006; Conte et al., 2016) including the neurons/nerves of the central, enteric, and peripheral nervous systems (Prekeris and Terrian, 1997; Buttow et al., 2006; Trybus, 2008; Bridgman, 2009). The highly polarized morphology of neuronal cells, with functionally distinct extensions (dendrites and axon) protruding from the cell body (soma), each of which contains a complement of macromolecules and membranous organelles, implies the existence of mechanisms to sort and deliver the appropriate contents to each subcellular compartment. The longer-range transport of cargos within nerves depends on microtubules, which provide the tracks for cargo transport. The opposite polarity of most microtubules in dendrites and axons, which mediate interactions with different classes of motor proteins, provides one mechanism for cargo segregation. Dynein motors move cargo towards the microtubule minus-end (that is, into the dendrites) while kinesin motors move cargo towards the microtubule plus-end (into the axon) (Kardon and Vale, 2009; Hirokawa et al., 2010; Kapitein and Hoogenraad, 2011; Kneussel and Wagner, 2013). Once within the correct subcellular compartment, cargo can dissociate from dynein/kinesin motors and undergo short-range transport to its ultimate destination along actin filaments via interactions with myosin motors, including Myo5a. In addition to a transport function, Myo5a is also thought to serve as a tether that restricts the motion of cargo after it has been delivered to the correct location (Desnos et al., 2007).

The neural cargos of Myo5a are known to include organelles such as endoplasmic reticulum, multiprotein complexes including transcriptionally repressed mRNAs and ribosomes, and synaptic vesicles (Prekeris and Terrian, 1997; Wagner et al., 2011; McCaffrey and Lindsay, 2012; Calliari et al., 2014; Canclini et al., 2020). However, relatively little is known regarding regulation of the interactions between Myo5a and such diverse cargo which mediate their transportation to appropriate destinations, especially in peripheral nerves. Myo5a—cargo interactions have been primarily studied in brain and skin, the organs most obviously affected by mutation of the *Myo5a* gene (Wu et al., 1998; Wagner et al., 2011). In mice, ablation of the *Myo5a* gene expression results in the autosomal recessive dilute-lethal phenotype; that is, affected mice display both reduced pigmentation and neurological abnormalities which culminate in death by 3 weeks of age (Mercer et al., 1991). Similar lethal defects have been associated with null inheritance of the *Myo5a* gene in other species, including rat (Futaki et al., 2000; Landrock et al., 2018), dog (Christen et al., 2021) and horse (Brooks et al., 2010). Defective expression of the *MYO5a* gene in humans causes the autonomic recessive disorder, Griscelli syndrome Type I, which is characterized in affected infants by silvery grey hair color and signs of severe neurological impairment such as developmental delays, seizures, opisthotonus, and hypotonia (Griscelli et al., 1978; Griscelli and Prunieras, 1978). Interestingly, genetic changes in *Myo5a*/*MYO5a* genes that apparently affect only pigmentation have also been described in both mice and humans; these include mutation within, or even deletion of, a single exon of the Myo5a monomer (Huang et al., 1998; Menasche et al., 2003; Yilmaz et al., 2014).

Myo5a protein has a domain structure reflective of its biological functions. In the N-terminal segment, which includes the motor and lever arm, there are binding regions for ATP, actin, and the calcium-binding protein, calmodulin. The C-terminal segment contains coiled-coil regions that are required for dimerization, and a globular tail domain (GTD) which participates in cargo binding ((Trybus, 2008) and references therein). The actin binding and ATP-hydrolyzing domains of Myo5a are highly conserved to those of other myosin protein superfamily members. However, the lever arm of Myo5a is relatively long, and the presence of a coiled-coil region in the medial tail indicates dimerization of Myo5a monomers. Both of these characteristics predict that the step length of Myo5a with each cycle of ATP hydrolysis will also be relatively long, 36 nm, or one helical turn of the actin filament. Consequently, Myo5a dimers can move smoothly and efficiently along the filament surface ((Trybus, 2008) and references therein). Myo5a dimers are active, that is, capable of locomotion, only when stimulated by elevated Ca++ (Li et al., 2004) or when bound to molecular cargo (Thirumurugan et al., 2006); at other times they assume a folded conformation unable to hydrolyze ATP. Both the active and inactive forms bind to actin (Li et al.; Liu et al., 2006).

Partially overlapping with the coiled-coil domain, and just upstream of the GTD, is the Myo5a alternative exon segment. This region is comprised of six exons (sequentially termed A, B, C, D, E, and F) which can be spliced together in multiple arrangements without disturbing the reading frame (Mercer et al., 1991; Seperack et al., 1995; Huang et al.; Lambert et al., 1998a). Exons A, C and E are thought to be present in all variants, while exons B, D and F may or may not be included. In brain Myo5a, the exon arrangement ABCE predominates, while in skin and other tissues such as spleen, variants with other exon arrangements are expressed (Seperack et al., 1995). In patients with Griscelli syndrome who have abnormal pigmentation but no apparent neurological defects, alternative exon F is deleted (Menasche et al., 2003; Yilmaz et al., 2014). This exon is involved in efficient transport of pigment-containing granules (melanosomes) to the tips of skin melanocytes for their transfer to keratinocytes (Au and Huang, 2002). Binding of exon F to the accessory protein, melanophilin, bridges the interaction between Myo5a and melanosomes by concomitantly binding to Rab27a, a protein associated with melanosome membranes (Fukuda et al., 2002).

The Myo5a splice variants expressed in peripheral tissues other than skin melanocytes, have not yet been extensively characterized. We have recently identified splice variants expressed by stomach and bladder using PCR methodologies (Carew et al., 2021; Carew et al., 2022). In all stomach sections (antrum, fundus, body and pylorus), the exon arrangement identified in brain Myo5a, ABCE, was detected along with other arrangements such as ACDE, ACEF, and ACDEF. Although the latter variants were also detected in bladder, the ABCE variant was not. In the stomach, the enteric nervous system is embedded between the longitudinal and circular muscle layers (the myenteric plexus) and between the circular muscle and the mucosa (the submucosal plexus). These enteric plexuses, containing the soma and dendrites of the enteric nervous system, are inextricable from the muscle tissue penetrated by the axons. The rodent bladder, however, is innervated only by the axons

of nerves whose soma/dendrites reside at a distance, within the MPG (Drengk et al., 2000; Keast, 2006). These anatomical differences between stomach and bladder suggested that Myo5a variant mRNAs may be compartmentalized within peripheral nerves, with the ABCE variant confined to soma/dendrites while other variants are restricted to axons. Further, Myo5a mRNA was recovered from isolated bladder, which contains only the severed axons of pelvic nerves. These data confirm reports from other groups that Myo5a mRNA, as well as Myo5a protein bound to kinesins, undergoes transport into the axon (McCaffrey and Lindsay, 2012; Calliari et al., 2014; Canclini et al., 2020) and presumably can be translated within this compartment.

In rodents, the MPG innervates not only bladder, but also a number of other pelvic tissues. The work presented here analyzes the Myo5a variants present in other such tissues—the CCP, distal colon, and MPG itself, as well as the bladder. The distal colon is innervated extrinsically by the MPG, and also (like the stomach) by the enteric plexuses. Since presumably all Myo5a transcription and mRNA splicing takes place in the nucleus of the expressing cell, we hypothesized that all pelvic nerve Myo5a variants, including ABCE, would be detectable in MPG and distal colon. However, we expected that a subset of the total variant transcripts, excluding ABCE, would be detectable in CCP and bladder, since those organs contain only the axons of nerves emanating from the MPG.

2 Materials and methods

2.1 Animals

All animal procedures were approved by the Institutional Animal Care and Use Committee of the VA Boston Healthcare System. Male C57/BL6 (RRID:IMSR_JAX:000664) mice were obtained from Jackson Labs (Bar Harbor, ME, United States). Between 8 and 14 weeks of age, animals were euthanized by CO_2 asphyxiation, and organs were quickly dissected and either stabilized in RNA-Later solution (R0901, Sigma-Aldrich, St Louis, MO, United States), or embedded in OCT compound, immediately snap frozen and stored at −80°C.

2.2 Confocal Microscopy

Full thickness sections of urinary bladder, distal colon, and CCP were cut on a cryostat (12–16 µm) and fixed with cold acetone for 10 min. Whole mount preparations from dissected major pelvic ganglia were also fixed as described. After rinsing in phosphate buffered saline (PBS), tissue preparations were blocked and permeabilized with 5% donkey serum and 0.05% triton X-100 in PBS for an hour. For double labelling, tissues were incubated overnight at 4°C with rabbit primary antibody against Myo5a (Novus NBP1-92156, RRID:AB_11017070; 1:300 dilution) along with an antibody against a neuronal marker: either mouse anti-NeuN (Millipore, MAB377; RRID:AB_ 2313673), mouse anti-ßIII tubulin (Abcam, ab7751, RRID:AB_306045) or mouse anti-synaptophysin (Abcam, ab8049, RRID:AB_2198854). After extensive washing with PBS, tissues were incubated for 2 h at room temperature with an affinity-purified goat anti-rabbit secondary antibody coupled to AlexaFluor-568 (Thermo-Fisher Scientific: A21206, RRID:AB_2535792) followed by an AlexaFluor 488 conjugated donkey anti-mouse secondary antibody (Thermo-Fisher Scientific: A11031, RRID:AB_144696). In separate sections processed in parallel, the primary antibodies were omitted from the procedure to control for nonspecific binding of secondary antibodies.

Tissue sections were mounted using Fluoromount-G (0100–01, Southern Biotech, Birmingham, AL, United States) and examined by confocal microscopy (Zeiss, LSM 710) using a ×40 water objective. For image acquisition of double-labelled tissue, slides were scanned separately at each excitation wavelength to minimize emission crosstalk. Images were obtained from maximum-density projections of 8–10 optical slices.

2.3 mRNA extraction, cDNA preparation and PCR analyses

Three independent samples of each pelvic tissue (MPG, bladder, CCP, distal colon) plus one positive control (brain), were dissected from each of three animals and processed for total RNA. RNAs from MPG and brain were purified with the Qiagen RNeasy Plus Mini kit (28104); RNAs from pelvic tissues were purified using the RNeasy Fibrous Tissue Mini kit (74704). Tissues were disrupted in the kits' lysis buffer, RLT, supplemented with ß-mercaptoethanol (M3148, Sigma-Aldrich) using the Tissue Lyser II mill-bead apparatus (Qiagen, Gaithersburg, MD, United States) by two cycles of 2 minutes each at 30Hz with a 5 mm stainless steel bead (69989, Qiagen). RNA concentration and purity were determined by measurement of absorbances at 260nm and 280 nm on the Nanodrop 1000 UV-vis spectrophotometer (Thermo-Fisher Scientific) using the RNA nucleic acid quantification program. An A260/A280 ratio of ~2.0 for each sample indicated adequate purity for downstream applications.

To prepare total RNA for PCRs, 100 ng were converted to cDNA in a final volume of 20 µL using the Superscript IV VILO mastermix (11756050, Thermo-Fisher Scientific). Aliquots of the cDNA (1 µL) were used as templates for 50 µL initial PCR reactions. Initial reaction employed a forward primer upstream of Myo5a exon A (Figure 1) and reverse primer within the GTD (primer pair 1; forward, 5′ GCAGAAACTGAAGACATTGCACC 3′ and reverse, 5′ ATTCTGGCGAGACGTGTTGT 3′). Products were purified with the Qia-quick PCR-purification kit (28104, Qiagen). A 1 µL aliquot of each initial purified PCR was then used as a template for nested PCR with internal primer pair 2 (forward, 5′ GTCCTCATCTTG AGGTCGCA 3′ and reverse, 5′ATGTTGACTGGCCGGATAGG 3′). All primers were obtained from Thermo-Fisher Scientific. For both initial and nested PCR, twenty-five cycles were performed under standard conditions (denaturation at 94°C, annealing at 58°C, and extension at 72°C) in an Eppendorf thermal cycler (Hauppauge, NY, United States) using the Taq PCR mastermix (201445, Qiagen). Initial PCR reactions included a no-template control (NTC), containing full reaction mixture—buffer, TAQ polymerase, primers, dNTPs—but no cDNA as template for amplification. A 1 µL aliquot of this NTC reaction was also used as a template in the control reaction with the nested primers.

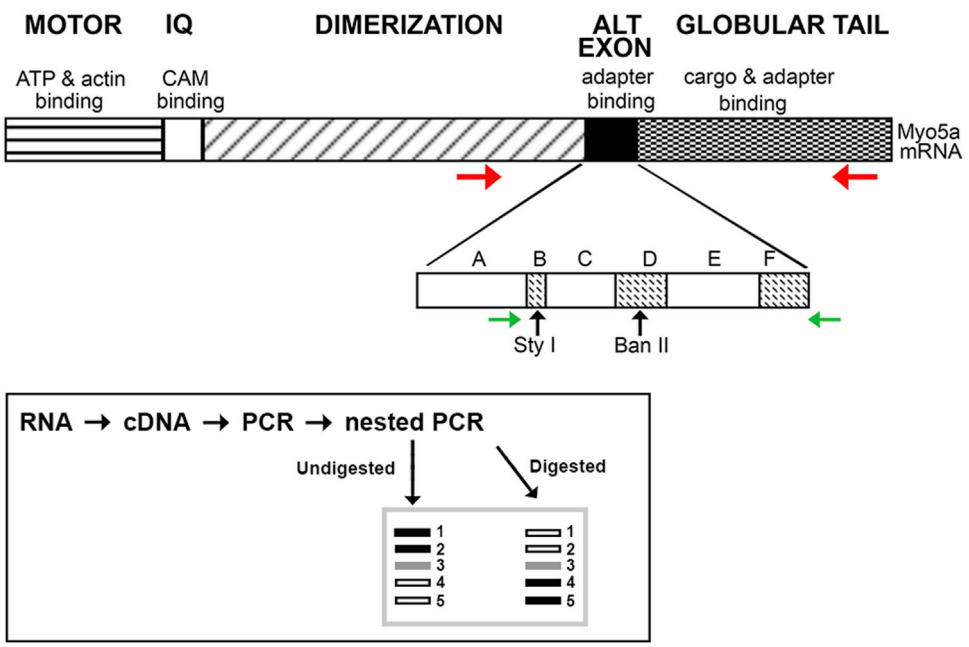

FIGURE 1
Schematic of Myo5a. The regions of Myo5a encoding the ATP binding, motor, calmodulin-binding (IQ), alternative exon and globular tail domains, and the known functions of each, are portrayed at top. The expansion depicts organization of the alternative exon domain; exons A, C and E are constitutively expressed in all variants, whereas exons B, D and F are optional. Horizontal arrows represent positions of PCR primers (red, initial reaction; green, nested reaction) while approximate positions of unique Sty I and Ban II restriction enzyme sites within exons B and D, respectively, are indicated by vertical arrows. The inset depicts the PCR and restriction enzyme methodology used to assess the presence and proportion of Myo5a splice variants.

A schematic illustrating this workflow is included in Figure 1 (inset). Except for the 5' nested primer, which is within exon A (present in all variants), all primers hybridize to sequences completely outside of the alternative exon region. In particular, the reverse primer for nested PCR described here differs from that used in our previous analyses, being located within the GTD. Since the entire region potentially carrying the alternative exons B, D, and/or F was amplified, the nested PCR products obtained represent both the configurations and the relative proportions of Myo5a variant transcripts expressed by each tissue.

Aliquots of the nested PCR products were digested with excess restriction enzyme (20–40 units of either Sty I, R3500 or Ban II, R0119) at 37°C for 2–16 h in Cut-Smart reaction buffer. All reagents were from New England Biolabs (Ipswich, MA, United States). Undigested and digested fragments were assessed in comparison to mass standards (15628019, Thermo-Fisher Scientific) by electrophoresis in Tris/acetate/EDTA buffer (9868, Ambion/Thermo-Fisher Scientific), on 2% MetaPhor agarose (50180, Lonza, Rockland, ME United States) gels. Gels were prepared just before use, according to the manufacturer's protocol, and contained the fluorescent intercalating dye, Sybr-green (S33102, Thermo-Fisher Scientific).

Gels were imaged using an Amersham Imager 600 (General Electric, Pittsburgh, PA, United States). For every lane in Figure 4, the fluorescence intensity of each band was measured and corrected for fragment size. The fluorescent signal present in each individual band was expressed as a proportion of the total fluorescence intensity, that is, the sum of all band intensities, in that lane. The proportional values for each position in the replicates from a given tissue were then averaged and plotted +/- SE. The same process was followed for analysis of restriction digestion (Figures 5, 6), except that fluorescence intensity was measured at the positions corresponding to the undigested and the digested bands, in all lanes derived from each sample. Statistical significance was determined by using the Student's t-test to compare the proportional intensity of each band under undigested *versus* digested conditions. p values below 0.05 were considered significant.

3 Results

3.1 Myo5a protein is expressed in pelvic and enteric nerves

Myo5a immunoreactivity was detected in whole mount preparations of the MPG. Double labeling with the neural marker NeuN showed that Myo5a was localized in cell bodies. Myo5a was also detected in neurites within the MPG (Figure 2A). Antibodies against Myo5a yielded abundant immunoreactivity throughout the tissues from the urinary bladder (Figure 2B), the distal colon (Figure 2C) and the CCP (Figure 2D). In double labelled preparations, Myo5a staining was extensively colocalized with immunoreactivity generated by neural markers β-III tubulin or synaptophysin.

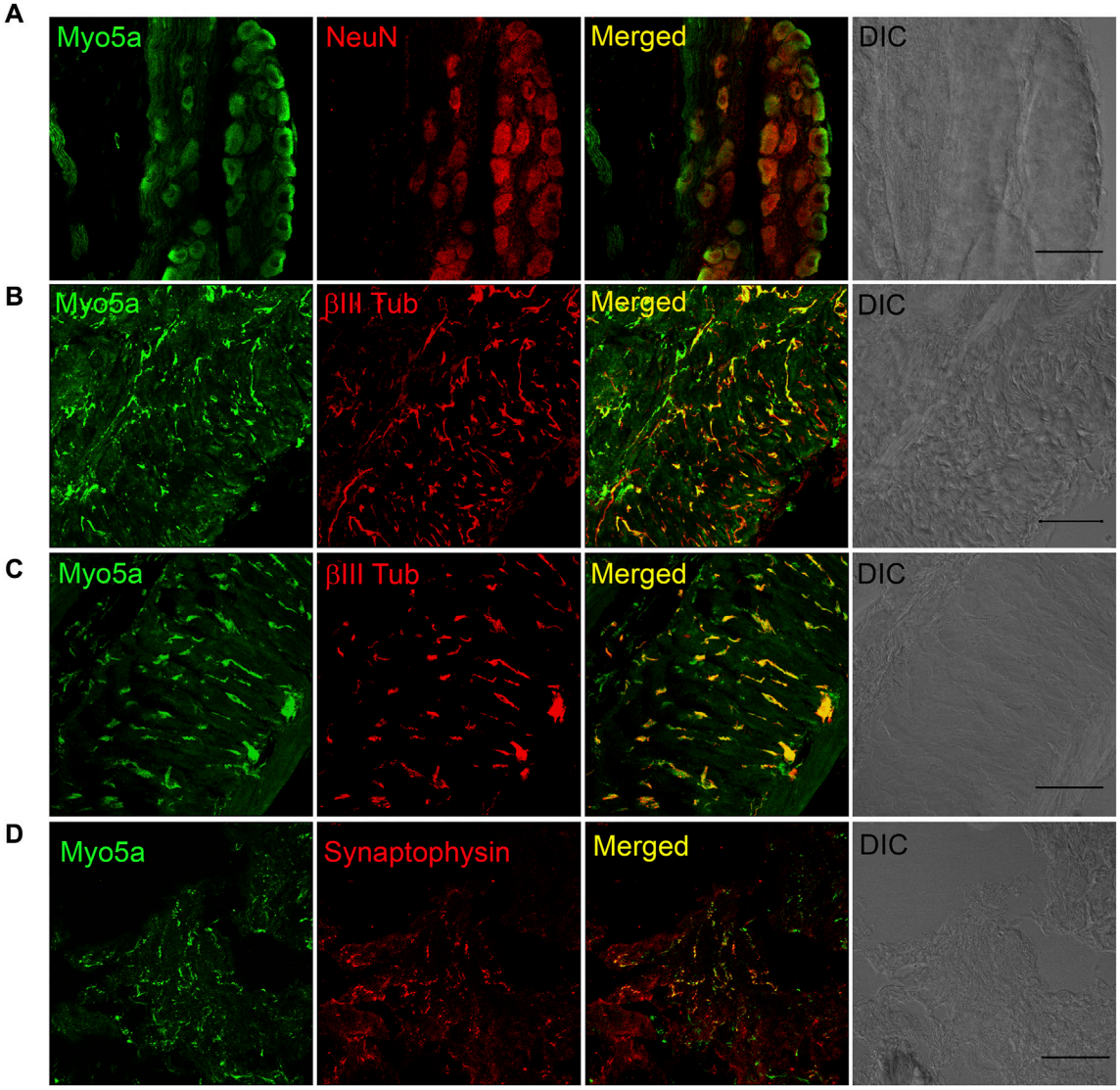

FIGURE 2
Distribution of Myosin 5a (Myo5a) in different murine organs innervated by the pelvic plexus. **(A)** Whole-mount preparation of the MPG displays abundant staining for Myo5a which was extensively co-localized with the neuronal marker NeuN. Myo5a immunoreactivity was also detectable on fibers running throughout the bladder **(B)** and the distal colon **(C)** Co-localization of Myo5a signal with β-III tubulin confirmed the neuronal nature of myo5a distribution in these tissues. **(D)** Myo5a immunoreactivity was abundantly detected and co-localized with the synaptic-vesicle marker synaptophysin in the CCP. Tissue topography was shown in the differential interference contrast (DIC) image from each preparation. Magnification ×40; scale bars = 50 μm.

3.2 Multiple splice variants of Myo5a are identified in pelvic tissues by nested PCR

Discriminating among Myo5a protein variants by Western blotting is not possible due to two factors: the lack of commercial antibodies recognizing the variant exons, and the small differences in protein mass predicted for the different Myo5a splice variants. The alternative exons B, D and F encode 3, 27 and 25 amino acids respectively relative to a protein backbone of 1828 amino acids for full-length protein lacking all three alternative exons. Therefore, the Myo5a splice variants expressed in the various pelvic tissues were identified at the mRNA level by PCR.

As shown in Figure 3, nested PCR produced three product bands separable by electrophoresis, in a representative sample from each pelvic tissue. The pattern of the distal colon included easily detectable amounts of all three product bands, and stood in strong contrast to the arrays seen for MPG (mostly the smallest band, with traces of the larger products), and for bladder and CCP (ample amounts of the two larger PCR bands with a trace of the smallest). Whether these trace bands give rise to functional Myo5a variants is not known. Further analysis was concentrated on the more abundant forms expressed in each tissue.

As mentioned above, fragments very close in size cannot be resolved by this technique alone, so each band potentially contains multiple species closely related in mass. Theoretically, eight different

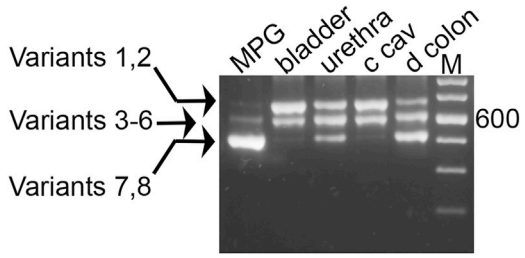

FIGURE 3
Myo5a PCR product sizes of pelvic tissues. Nested PCR was performed with a representative sample from each of four tissues, and compared by 2% agarose gel electrophoresis. An intervening lane was removed (white line). Three distinct bands were observed per sample, and in comparison to the DNA size markers (M, 100 bp ladder, with weighted 600 bp standard) they were of approximate mass 700, 600, and 500 bp. The arrows at left indicate the possible variants corresponding to each band, from Table 1.

variants, as shown in Table 1, could be generated by the nested PCR. In comparison to the mass standards in far right lane of Figure 3, the observed bands generated from the pelvic tissues are approximately 700 bp (and could be composed of variant species 1—2 from Table 1), 600 bp (variant species 3–6) and 500 bp (variant species 7–8). The uppermost band is large enough to contain sequence encoding all three variable exons: B (9 bp), D (81 bp) and F (75 bp). The central band has a mass consistent with presence of either exons B+D, D only, B+F, or F only. The smallest band might or might not include exon B, but is not large enough to include either exons D or F.

The abundance of these three product sizes were next compared in replicate undigested samples from nested PCR of the pelvic tissues. The bands were quantitated, and their relative proportions in each sample were determined and graphed, as shown in Figure 4. Although the control PCR reaction did not generate a discernable product, all nested PCR reactions run with tissue sample cDNAs gave rise to an array of product sizes characteristic of each tissue. Again, the largest product predominated in bladder and CCP, where it comprised ~50–60% of the total. This product was barely detectable (~5%) in distal colon and MPG. The central product could be easily discerned in bladder, CCP, and colon (20%–45%) but not in MPG (~5%). Finally, the smallest product was found to predominate in MPG and distal colon, but to be nearly undetectable in CCP and bladder. The product distribution of bladder was mirrored by that of CCP, but both were different from distal colon and MPG. Also, distal colon and MPG showed different distribution patterns compared to one another.

3.3 Myo5a exon B is recognized only in MPG and distal colon

To further distinguish among fragments of similar mass, the nested PCR products were digested separately with restriction enzymes Sty I and Ban II, to indicate the presence of exon B or D, respectively, as indicated in Figure 1; Table 1. The undigested and digested samples were then analyzed as described above. Quantitative comparisons for abundance of the undigested *versus* Sty I—digested bands are shown in Figure 5. By inspection of the various undigested *versus* digested counterparts in the gels of panels A and B, evidence for inclusion of exon B was found most clearly in MPG and distal colon. In MPG the Sty I digestion of the smallest PCR product appeared to be complete, indicating that exon B was present exclusively in the variant 7 arrangement described in Table 1, ABCE. However, in distal colon there was only partial Sty I digestion of this size product, suggesting that the variant 8 species, ACE, was also present along with ABCE. In addition, a Sty I digested fragment of ~550 bp was also observed in colon (see arrow in Figures 5B). Because Sty I cleavage removes 50 bp from the 5' end of a nested PCR product spanning exon B, these data indicated that the ~600 bp PCR product in distal colon included either or both variant 3, ABCDE, and variant 5, ABCEF. Aside from this, there was no suggestion of exon B in the larger PCR product pair from any tissue.

3.4 Myo5a exons D and F are identified in pelvic tissues

Digestions of the nested PCR products with restriction enzyme Ban II are shown in Figure 6; this enzyme is expected to remove 200/209 bp from the 5' end of the PCR product if exon D is included. As anticipated, Ban II did not cleave the smallest PCR product from MPG or colon. In contrast, the pair of larger PCR products from

TABLE 1 Potential splice variants of the Myo5a gene.

Species	Exons	Size (BP)	Sty I DIGEST (BP)	Ban II Digest (BP)
Variant 1	ABCDEF	677	50 and 627	209 and 468
Variant 2	A_CDEF	668	no cleavage	200 and 468
Variant 3	ABCDE_	602	50 and 552	209 and 393
Variant 4	A_CDE_	593	no cleavage	200 and 393
Variant 5	ABC_EF	596	50 and 546	no cleavage
Variant 6	A_C_EF	587	no cleavage	no cleavage
Variant 7	ABC_E_	521	50 and 471	no cleavage
Variant 8	A_C_E_	512	no cleavage	no cleavage

The predicted sizes of the undigested, Sty I digested, and Ban II digested fragments resulting from nested PCR, of each theoretically possible murine Myo5a splice variant, are shown. Each species gives a unique, identifiable signature of fragment sizes prior to and following restriction enzyme cleavage.

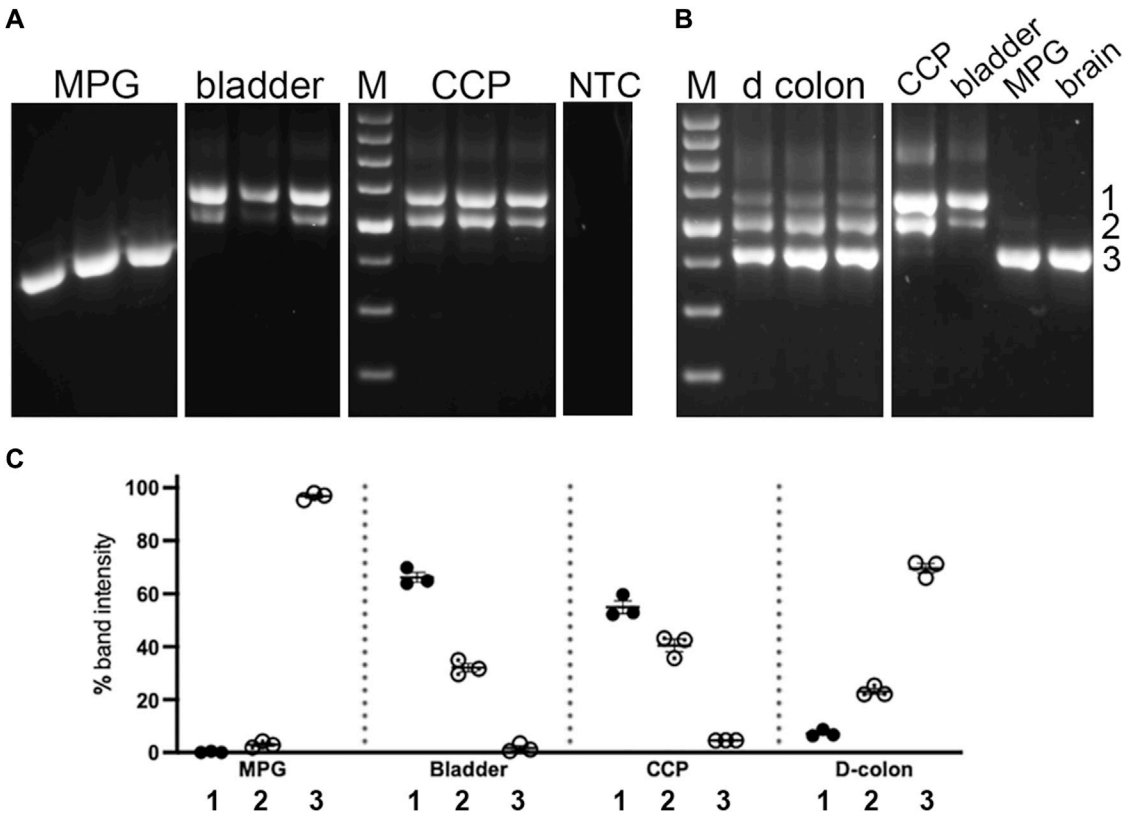

FIGURE 4
Undigested PCR products of pelvic tissues. Nested PCR was performed on three replicates of each tissue type, which were analyzed by 2% agarose gel electrophoresis, Panel **(A)** shows replicates from MPG, bladder and CCP. In parallel with experimental reactions, a control reaction which included all PCR reaction components except cDNA, was run. An aliquot of this reaction was then included as a template in a control nested PCR reaction. No PCR product was detected in this reaction (NTC). Panel **(B)** shows replicates from distal colon, as well as a single sample each from CCP, bladder, MPG and brain for comparison with the samples from panel **(A)**. For both panels, white lines indicate the removal of intervening lanes from the images. Standards differing by 100 bp increments (with weighted 600 bp standard) were run on each gel (M). Numbers 1 through 3 at the far right indicate band identities. **(C)** Relative percentages of these three PCR products were determined, then replicates were average and graphed +/- SEM. ~700 bp band 1, filled circles; ~600 bp band 2, dotted circles; ~500 bp band 3, open circles.

bladder, CCP and colon were extensively digested by Ban II, indicating that variant 2, ACDEF, (generating the 468 bp digestion product) and variant 4 arrangement described in Table 1, ACDE, (generating the 393 bp digestion product) were the major species found in bladder and CCP. The Ban II digestion pattern for distal colon, however, differed in that very little of the middle PCR product could be cleaved, suggesting that the unexpected variant 6, ACEF, and/or variant 5, ABCEF, (due to partial digestion of this sized fragment with Sty I, see above) were expressed in this tissue only.

4 Discussion

This work analyzed the Myo5a variants present at the mRNA level in several representative pelvic tissues. Accordingly, two tissues of the rodent genitourinary tract with innervation from the MPG (bladder and CCP of the penis) as well as the MPG itself, were used for PCR and restriction enzyme analysis in comparison to the distal colon, which is innervated both by the enteric nervous system and the MPG. The ABCE variant of Myo5a is so abundantly expressed in neurons of the central nervous system that it is referred to as the brain form and might be expected to be the most prevalent form in the peripheral nervous system as well. However, our previous work implied that this was not the case: the ABCE variant is detectable in stomach sections but undetectable in bladder, while variants containing the alternative exons D and F were identified in both tissues (Carew et al., 2021; Carew et al., 2022). Based on immunohistochemistry data, Myo5a protein is found predominantly in nerve trunks and extensions where it colocalizes with axonal markers such as synaptophysin and β-III-tubulin. Therefore, we expected mRNA expression of Myo5a to be limited largely to peripheral nerves in these tissues. An anatomical feature distinguishing innervation of stomach from that of bladder, is the presence of plexuses housing the soma/dendrites of enteric nerves in the stomach. Rodent bladder, in contrast, is innervated by the axons of peripheral nerves whose soma/dendrites reside in the MPG. Taken together, these data suggested that within enteric and peripheral nerves, expression of the Myo5a ABCE variant might be restricted to the soma/dendrites, while any other Myo5a variants expressed might be restricted to the axons.

The data presented here support this contention. The nested PCR product corresponding to the brain variant, ABCE, is predicted to be 521 bp and to be cleaved by the restriction enzyme Sty I to fragments of

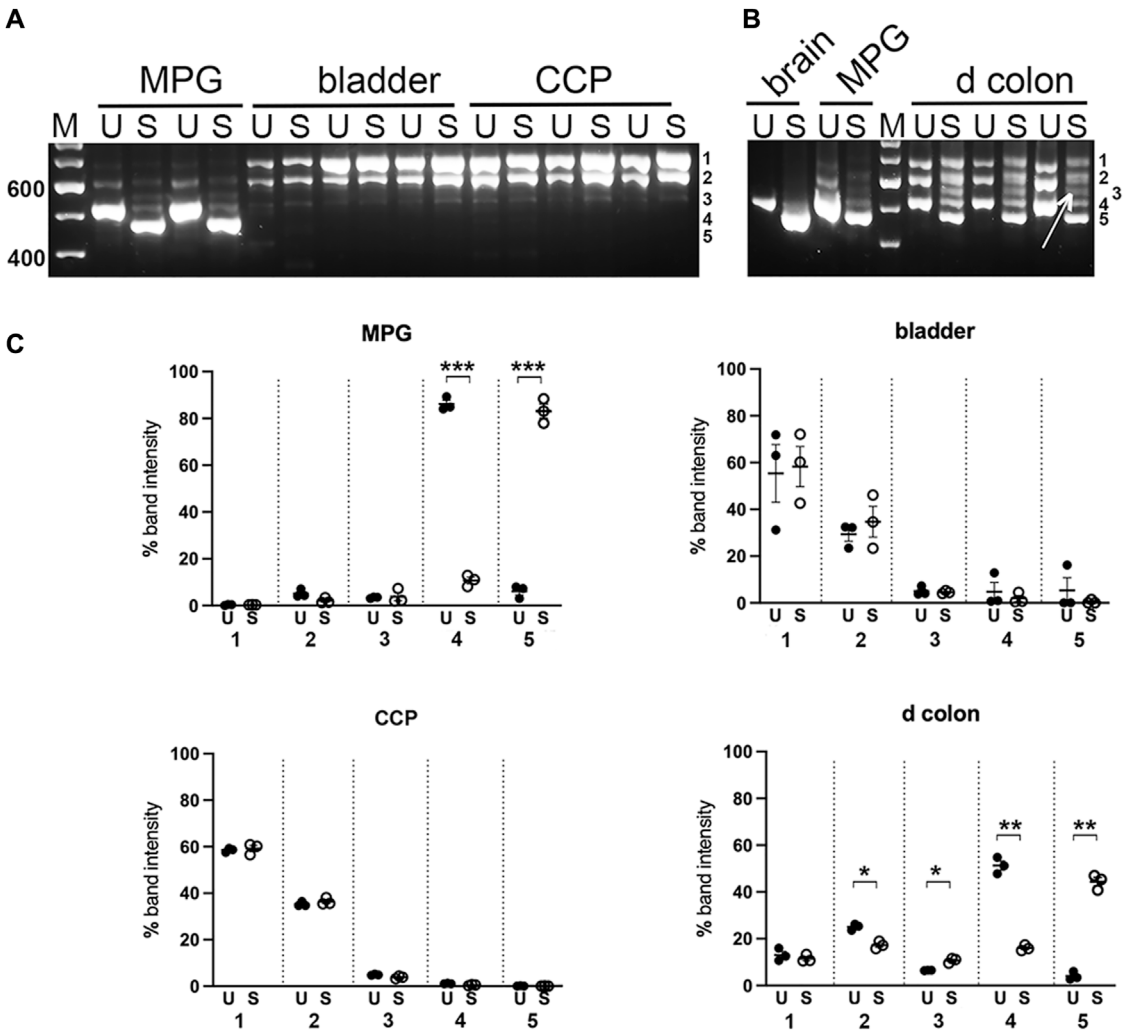

FIGURE 5
Sty I digestion of PCR products from pelvic tissues. Undigested (U) and Sty I digested (S) nested PCR pairs from replicates of MPG, bladder, CCP **(A)**, or from distal colon (d colon) and MPG, with brain for reference **(B)** were electrophoresed and analyzed as described in Methods. For mass estimation, a 100 bp DNA ladder with weighted 600 bp standard was run (M). Numbers 1 through 5 at the right of each image correspond to band identities. Bands 1, 2 and 4 correspond to the upper (~700 bp), middle (~600 bp), and lower (~500 bp) bands present in undigested samples and remaining undigested by Sty I. Band 3, indicated by arrow in panel B, represents a Sty I cleavage product of band 2; band 5 represents a cleavage product of band 4. **(C)**, Fluorescence was quantitated at each of the five band positions and converted to the percentage of total fluorescence recovered in that lane. Replicates at each band position were averaged and graphed +/- SEM, (U = undigested, closed circles; S = Sty I digestion, open circles). *n* = 3 per tissue. Significant changes in fluorescence at each band position due to Sty I digestion are indicated (*$p < 0.05$; **$p < 0.01$; ***$p < 0.001$).

471 and 50 bp. The only tissue investigated which expressed a preponderance of an ~500 bp PCR fragment completely digested by Sty I, was the isolated MPG. Aside from MPG, only the distal colon (which included the enteric plexuses) gave rise to a significant amount of an ~500 bp PCR product. Unexpectedly however, this product band was partially refractory to Sty I, suggesting that the ACE variant was included. Also surprisingly, in distal colon unlike bladder and CCP, the ~600 bp PCR product was partially cleaved by Sty I. This indicated that either or both the ABCDE/ABCEF variants were expressed in this tissue. No Sty I digestion fragments were detected in digests of either bladder or CCP PCR products, indicating these tissues were devoid of variants containing exon B.

When the PCR products were next digested with Ban II to identify variants including exon D, the largest product band (~700 bp) was fully cleaved in all tissues in which this species could be discerned (bladder, CCP, and distal colon), generating a digestion product of 468 bp. Based on the mass, resistance to Sty I, and susceptibility to Ban II, these data indicate that the ~700 bp PCR product corresponded exclusively to ACDEF. This species was the major variant of Myo5a detected in bladder and CCP. Similarly, the presence of exon D was indicated in nearly all the ~600 bp PCR product of bladder and CCP based on the degree of Ban II digestion observed, and thus corresponded to variant ACDE in these tissues. In the distal colon, however, the ~600 bp PCR product was also partially resistant to Ban II. Coupled with its partial resistance to Sty I, these data signaled expression of a mixture of variants such as ABCDE, ACDE, ABCEF and ACEF were expressed in this tissue only, among those analyzed.

Since *in situ* hybridization had indicated that Myo5a mRNA is primarily localized to nerve soma/dendrites within the myenteric plexus

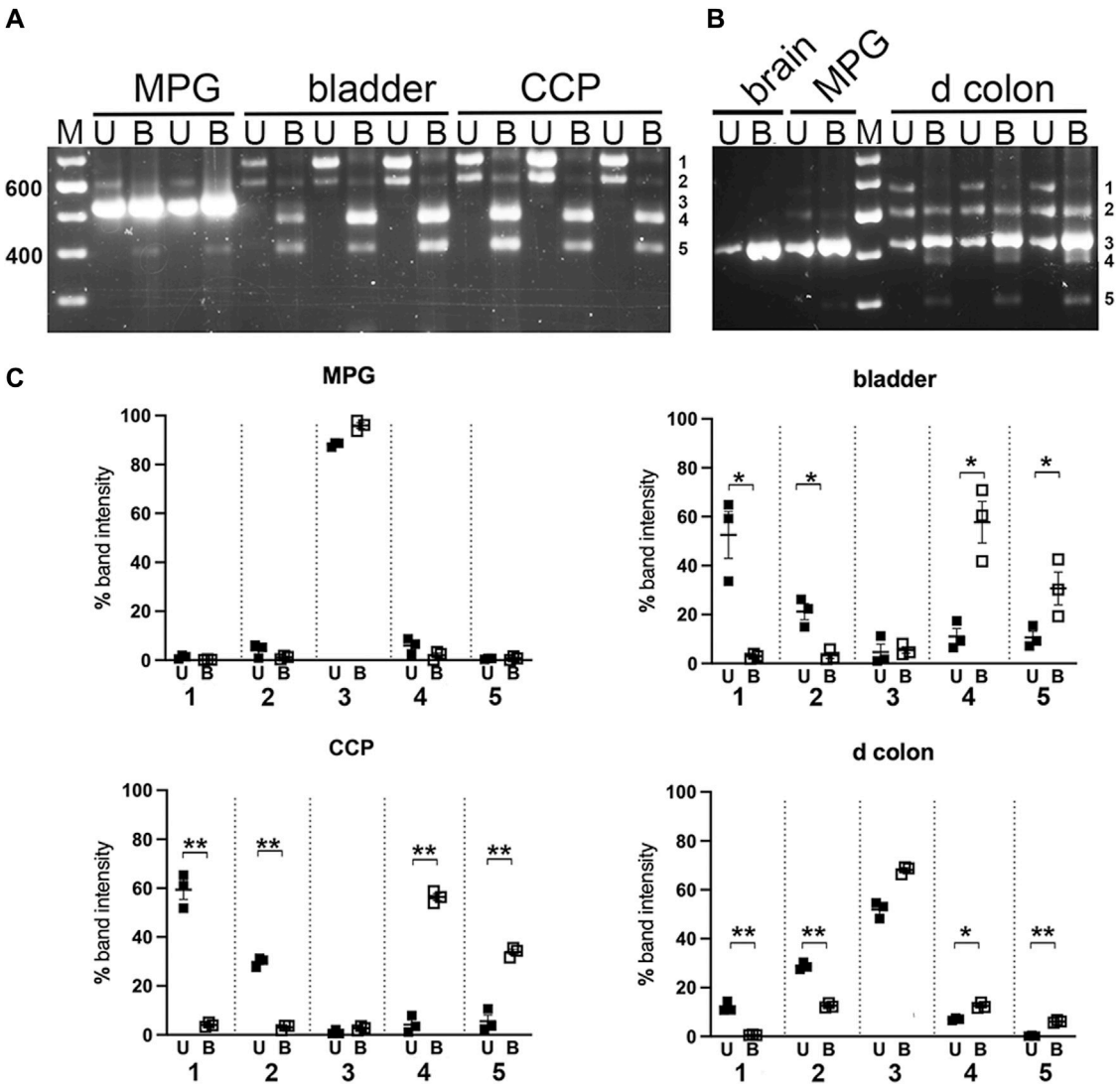

FIGURE 6
Ban II digestion of PCR products from pelvic tissues. Undigested (U) and Ban II digested **(B)** nested PCR pairs from replicates of MPG, bladder, CCP **(A)**, or from distal colon with MPG and brain for reference **(B)** were electrophoresed and analyzed as described in Methods. For mass estimation, a 100 bp DNA ladder with weighted 600 bp standard was run (M). Numbers 1 through 5 at the right of each image correspond to band identities. Bands 1, 2 and 3 correspond to the upper (~700 bp), middle (~600 bp), and lower (~500 bp) bands present in undigested samples and remaining undigested by Ban II. Band 4 represents a cleavage product of band 1; band 5 represents a cleavage product of band 2. **(C)** Fluorescence was quantitated at each of the five band positions and expressed as a percentage of total fluorescence recovered in that lane. Replicates at each band position were averaged and graphed +/- SEM. (U = undigested, closed squares; B = Ban II digestion, open squares). $n = 3$ per tissue. Significant changes in fluorescence at each band position due to Ban II digestion are indicated (*$p < 0.05$; **$p < 0.01$).

(Carew et al., 2021), and immunohistochemistry indicated extensive colocalization with neural markers (such as β-III-tubulin, synaptophysin or NeuN) (Carew et al., 2021; Carew et al., 2022), Myo5a expression in CCP, distal colon and MPG, as well as bladder, was expected to be largely restricted to nerves. But because variant-specific anti-Myo5a antibodies are unavailable, it was not possible to assign expression of a particular mRNA variant detected to a particular location by immunohistochemistry. This is a potential drawback of our study; however expression of the ABCE, or brain variant, can be confidently assigned to the soma, accounting for its detection in the distal colon as well as the MPG. The other forms detected, such as ACDEF and ACDE, which predominate in CCP and bladder, thus must be present in the axons. Interestingly, the presence of trace amounts of the larger nested PCR products in MPG might indicate the presence of these Myo5a variants in the axons within this tissue.

Previous work indicates that a complex array of Myo5a variants can be expressed even by a single cell. For example, it has been demonstrated that mRNAs corresponding to the full-length ABCDEF, the intermediate-length ABCDE and/or ABCEF and the short-length ABCE variants could be detected in cultured fibroblasts, keratinocytes, and melanocytes, as well as in mixed leukocytes isolated from blood; whereas only in melanocytes were variants ACDEF and ACE also found (Lambert et al., 1998b; Westbroek et al., 2003). In melanocytes, functional differences were noted for the different Myo5a variants. For example, the recombinant ABCE protein did not interact with melanosomes, whereas recombinant

ABCEF and ABCDEF did. While it was expected that only Myo5a variants with exon F would mediate melanosome transport (Lambert et al., 1998b; Fukuda et al., 2002) it was further shown that ABCDEF and ABCEF were not equally capable of melanosome association, despite both including exon F. Instead, the presence of exon D diminished the ability of exon F to mediate this interaction, implying that even closely-related variants may fulfill subtly different roles within a single cell type (Westbroek et al., 2003).

Our analysis indicated that variant ACEF was not abundantly expressed in pelvic tissues, although its presence can be inferred in distal colon by a degree of resistance of the ~600 bp fragment to Ban II digestion, and its presence was inferred as a minor species in bladder (Carew et al., 2022). In contrast, the ~600 bp fragment from bladder and CCP was extensively cleaved by Ban II, suggesting it was comprised mostly of ACDE in these tissues. In distal colon only, variants such as ABCDE/ABCEF, and ACE, were detected.

Interestingly, each of the nucleated cell types investigated by Lambert et al. expressed easily discernable amounts of the Myo5a brain variant, ABCE, which we detected only in tissues containing peripheral nerve soma. Taken together, these data imply that in all Myo5a—expressing secretory cells, this particular variant protein is likely to be restricted to the cell's nuclear and perinuclear regions. In our study, it was clear that the soma/dendrites of the nerves serving the bladder and CCP, which are located in the MPG, demonstrated near-exclusive expression of the ABCE variant. Only trace amounts of the larger variants could be seen in nested PCR from MPG, as might be expected if those variants were differentially sorted and rapidly exported to axons following their transcription.

The highly polarized neuron must confront an important issue: how to maintain over time the appropriate protein content of its elaborate extensions, despite their distance from the soma which contains the nucleus and is the site of gene transcription. In peripheral axons, this problem is particularly acute, since the extensive distance between the soma and the distal axon may exceed the capacity of protein transport processes to resupply macromolecular constituents critical for local functions, within a reasonable timeframe [reviewed in (Roy, 2014; Black, 2016)]. Although transport of a particular protein and of the mRNA encoding it into extensions are not mutually exclusive processes, the capacity to carry out local protein synthesis gives axons the flexibility to finely regulate the level and activity of proteins required for specialized axonal functions both spatially and temporally [reviewed in (Giuditta et al., 2008; Sahoo et al., 2018; Mofatteh, 2020)].

There is now much evidence that the mRNAs to be transported into axons initially interact with various RNA binding proteins (usually through sequence-specific interactions involving particular motifs in their untranslated regions, or UTRs). In these ribonucleoprotein complexes, or RNPs, the mRNA is held in an inactivated state (Kar et al., 2018). The RNPs undergo long-range active transport along microtubules in axons mediated by kinesin motor proteins, then short-range transport along actin filaments mediated by myosin motor proteins, in order to reach their destinations (Kalinski et al., 2015). The mRNAs themselves thus participate in the regulation of gene expression, as a consequence of their presence in the axon and their translation in response to an appropriate signal from the external milieu.

In a polarized cell such as a differentiated neuron, the transport of specific mRNAs into cellular extensions and their local translation into proteins confer a number of advantages, compared to the transport of centrally translated proteins. For example, sorting of mRNAs using sequences in their 3′UTRs or other untranslated regions is efficient, since a single RNA binding protein is capable of interaction with multiple mRNAs which may include very different coding sequences (Holt and Schuman, 2013). Further, since a single mRNA can be translated into multiple copies of its encoded protein, local control of translation permits rapid adjustment of the local proteome in response to a local stimulus (Buxbaum et al., 2015). Also, the protein translated on-demand could carry different post-translational modifications than the centrally translated protein, or be required to fulfill a unique functional role at the distal site, as is the case for ß-actin in the developing axon (Liao et al., 2015). The nascent protein, translated on-demand would also have a longer functional half-life in the axon, while its unnecessary presence in other subcellular compartments of the nerve would simultaneously be precluded.

It is not known whether locally-synthesized Myo5a fulfills specialized functions in the peripheral nerve axon, distinct from functions it might have in the other compartments. However, Myo5a is thought to play important roles in transport of synaptic vesicles within varicosities and their retention near active zones until a depolarization event, both critical functions for optimal regulation of neurotransmitter release. Our previous work characterized impairments of both inhibitory and excitatory neurotransmission in the fundus, CCP and bladder of the dilute-brown-nonagouti, or DBA, mouse, a strain carrying a defect that reduces the splicing of exon D and exons D+F in Myo5a transcripts (Chaudhury et al., 2014; Carew et al., 2021; Carew et al., 2022). It is tempting to speculate that these impairments arose from the inability of Myo5a lacking exons D and F to carry out essential neurotransmission functions in peripheral nerve axons.

Data availability statement

The original contributions presented in the study are included in the article/Supplementary Materials, further inquiries can be directed to the corresponding author.

Ethics statement

The animal study was approved by Institutional Animal Care and Use Committee of VA Boston Healthcare System. The study was conducted in accordance with the local legislation and institutional requirements.

Author contributions

JC: Conceptualization, Investigation, Methodology, Writing–original draft, Writing–review and editing. VC: Conceptualization, Investigation, Methodology, Writing–original draft, Writing–review and editing. RG: Funding acquisition,

Resources, Writing–review and editing, Conceptualization, Supervision. MS: Conceptualization, Funding acquisition, Investigation, Methodology, Project administration, Resources, Supervision, Writing–review and editing.

Funding

The author(s) declare financial support was received for the research, authorship, and/or publication of this article. This work was supported by VA Merit Review awards to MS (BX001790, BX003680) and RG (BX002806) from the United States Department of Veteran's Affairs Medical Research Service, Washington D.C, United States of America.

Conflict of interest

The authors declare that the research was conducted in the absence of any commercial or financial relationships that could be construed as a potential conflict of interest.

Publisher's note

All claims expressed in this article are solely those of the authors and do not necessarily represent those of their affiliated organizations, or those of the publisher, the editors and the reviewers. Any product that may be evaluated in this article, or claim that may be made by its manufacturer, is not guaranteed or endorsed by the publisher.

References

Au, J. S., and Huang, J. D. (2002). A tissue-specific exon of myosin Va is responsible for selective cargo binding in melanocytes. *Cell Motil. Cytoskelet.* 53 (2), 89–102. doi:10.1002/cm.10061

Black, M. M. (2016). Axonal transport: the orderly motion of axonal structures. *Methods Cell Biol.* 131, 1–19. doi:10.1016/bs.mcb.2015.06.001

Bridgman, P. C. (2009). Myosin motor proteins in the cell biology of axons and other neuronal compartments. *Results Probl. Cell Differ.* 48, 91–105. doi:10.1007/400_2009_10

Brooks, S. A., Gabreski, N., Miller, D., Brisbin, A., Brown, H. E., Streeter, C., et al. (2010). Whole-genome SNP association in the horse: identification of a deletion in myosin Va responsible for Lavender Foal Syndrome. *PLoS Genet.* 6 (4), e1000909. doi:10.1371/journal.pgen.1000909

Buttow, N. C., Espreafico, E. M., de Souza, R. R., and Romano, E. B. (2006). Immunolocalization of myosin-V in the peribronchial, intrapulmonary peritracheal plexuses of the Wistar rat. *J. Neurosci. Methods* 152 (1-2), 274–277. doi:10.1016/j.jneumeth.2005.09.012

Buxbaum, A. R., Haimovich, G., and Singer, R. H. (2015). In the right place at the right time: visualizing and understanding mRNA localization. *Nat. Rev. Mol. Cell Biol.* 16 (2), 95–109. doi:10.1038/nrm3918

Calliari, A., Farias, J., Puppo, A., Canclini, L., Mercer, J. A., Munroe, D., et al. (2014). Myosin Va associates with mRNA in ribonucleoprotein particles present in myelinated peripheral axons and in the central nervous system. *Dev. Neurobiol.* 74 (3), 382–396. doi:10.1002/dneu.22155

Canclini, L., Cal, K., Bardier, C., Ruiz, P., Mercer, J. A., and Calliari, A. (2020). Calcium triggers the dissociation of myosin-Va from ribosomes in ribonucleoprotein complexes. *FEBS Lett.* 594 (14), 2311–2321. doi:10.1002/1873-3468.13813

Carew, J. A., Cristofaro, V., Dasari, S. P., Carey, S., Goyal, R. K., and Sullivan, M. P. (2022). Myosin 5a in the urinary bladder: localization, splice variant expression, and functional role in neurotransmission. *Front. Physiol.* 13, 890102. doi:10.3389/fphys.2022.890102

Carew, J. A., Cristofaro, V., Siegelman, N. A., Goyal, R. K., and Sullivan, M. P. (2021). Expression of Myosin 5a splice variants in murine stomach. *Neurogastroenterol. Motil.* 33 (10), e14162. doi:10.1111/nmo.14162

Chaudhury, A., Cristofaro, V., Carew, J. A., Goyal, R. K., and Sullivan, M. P. (2014). Myosin Va plays a role in nitrergic smooth muscle relaxation in gastric fundus and corpora cavernosa of penis. *PloS one* 9 (2), e86778. doi:10.1371/journal.pone.0086778

Christen, M., de le Roi, M., Jagannathan, V., Becker, K., and Leeb, T. (2021). MYO5A frameshift variant in a miniature dachshund with coat color dilution and neurological defects resembling human Griscelli syndrome type 1. *Genes (Basel)* 12 (10), 1479. doi:10.3390/genes12101479

Conte, I. L., Hellen, N., Bierings, R., Mashanov, G. I., Manneville, J. B., Kiskin, N. I., et al. (2016). Interaction between MyRIP and the actin cytoskeleton regulates Weibel-Palade body trafficking and exocytosis. *J. Cell Sci.* 129 (3), 592–603. doi:10.1242/jcs.178285

Desnos, C., Huet, S., Fanget, I., Chapuis, C., Bottiger, C., Racine, V., et al. (2007). Myosin va mediates docking of secretory granules at the plasma membrane. *J. Neurosci.* 27 (39), 10636–10645. doi:10.1523/JNEUROSCI.1228-07.2007

Desnos, C., Schonn, J. S., Huet, S., Tran, V. S., El-Amraoui, A., Raposo, G., et al. (2003). Rab27A and its effector MyRIP link secretory granules to F-actin and control their motion towards release sites. *J. Cell Biol.* 163 (3), 559–570. doi:10.1083/jcb.200302157

Drengk, A. C., Kajiwara, J. K., Garcia, S. B., Carmo, V. S., Larson, R. E., Zucoloto, S., et al. (2000). Immunolocalisation of myosin-V in the enteric nervous system of the rat. *J. Auton. Nerv. Syst.* 78 (2-3), 109–112. doi:10.1016/s0165-1838(99)00073-9

Eichler, T. W., Kogel, T., Bukoreshtliev, N. V., and Gerdes, H. H. (2006). The role of myosin Va in secretory granule trafficking and exocytosis. *Biochem. Soc. Trans.* 34 (Pt 5), 671–674. doi:10.1042/BST0340671

Fukuda, M., Kuroda, T. S., and Mikoshiba, K. (2002). Slac2-a/melanophilin, the missing link between Rab27 and myosin Va: implications of a tripartite protein complex for melanosome transport. *J. Biol. Chem.* 277 (14), 12432–12436. doi:10.1074/jbc.C200005200

Futaki, S., Takagishi, Y., Hayashi, Y., Ohmori, S., Kanou, Y., Inouye, M., et al. (2000). Identification of a novel myosin-Va mutation in an ataxic mutant rat, dilute-opisthotonus. *Mamm. Genome* 11 (8), 649–655. doi:10.1007/s003350010121

Giuditta, A., Chun, J. T., Eyman, M., Cefaliello, C., Bruno, A. P., and Crispino, M. (2008). Local gene expression in axons and nerve endings: the glia-neuron unit. *Physiol. Rev.* 88 (2), 515–555. doi:10.1152/physrev.00051.2006

Griscelli, C., Durandy, A., Guy-Grand, D., Daguillard, F., Herzog, C., and Prunieras, M. (1978). A syndrome associating partial albinism and immunodeficiency. *Am. J. Med.* 65 (4), 691–702. doi:10.1016/0002-9343(78)90858-6

Griscelli, C., and Prunieras, M. (1978). Pigment dilution and immunodeficiency: a new syndrome. *Int. J. Dermatol* 17 (10), 788–791. doi:10.1111/j.1365-4362.1978.tb05980.x

Hirokawa, N., Niwa, S., and Tanaka, Y. (2010). Molecular motors in neurons: transport mechanisms and roles in brain function, development, and disease. *Neuron* 68 (4), 610–638. doi:10.1016/j.neuron.2010.09.039

Holt, C. E., and Schuman, E. M. (2013). The central dogma decentralized: new perspectives on RNA function and local translation in neurons. *Neuron* 80 (3), 648–657. doi:10.1016/j.neuron.2013.10.036

Huang, J.-D., Mermall, V., Strobel, M. C., Russell, L. B., Mooseker, M. S., Copeland, N. G., et al. (1998). Molecular genetic dissection of mouse unconventional myosin-VA: tail region mutations. *Genetics* 148, 1963–1972. doi:10.1093/genetics/148.4.1963

Kalinski, A. L., Sachdeva, R., Gomes, C., Lee, S. J., Shah, Z., Houle, J. D., et al. (2015). mRNAs and protein synthetic machinery localize into regenerating spinal cord axons when they are provided a substrate that supports growth. *J. Neurosci.* 35 (28), 10357–10370. doi:10.1523/JNEUROSCI.1249-15.2015

Kapitein, L. C., and Hoogenraad, C. C. (2011). Which way to go? Cytoskeletal organization and polarized transport in neurons. *Mol. Cell Neurosci.* 46 (1), 9–20. doi:10.1016/j.mcn.2010.08.015

Kar, A. N., Lee, S. J., and Twiss, J. L. (2018). Expanding axonal transcriptome brings new functions for axonally synthesized proteins in health and disease. *Neuroscientist* 24 (2), 111–129. doi:10.1177/1073858417712668

Kardon, J. R., and Vale, R. D. (2009). Regulators of the cytoplasmic dynein motor. *Nat. Rev. Mol. Cell Biol.* 10 (12), 854–865. doi:10.1038/nrm2804

Keast, J. R. (2006). Plasticity of pelvic autonomic ganglia and urogenital innervation. *Int. Rev. Cytol.* 248, 141–208. doi:10.1016/S0074-7696(06)48003-7

Kneussel, M., and Wagner, W. (2013). Myosin motors at neuronal synapses: drivers of membrane transport and actin dynamics. *Nat. Rev. Neurosci.* 14 (4), 233–247. doi:10.1038/nrn3445

Lambert, J., Naeyaert, J. M., Callens, T., De Paepe, A., and Messiaen, L. (1998a). Human myosin V gene produces different transcripts in a cell type-specific manner. *Biochem. Biophys. Res. Commun.* 252 (2), 329–333. doi:10.1006/bbrc.1998.9644

Lambert, J., Onderwater, J., Vander Haeghen, Y., Vancoillie, G., Koerten, H. K., Mommaas, A. M., et al. (1998b). Myosin V colocalizes with melanosomes and subcortical actin bundles not associated with stress fibers in human epidermal melanocytes. *J. Invest. Dermatol* 111 (5), 835–840. doi:10.1046/j.1523-1747.1998.00395.x

Landrock, K. K., Sullivan, P., Martini-Stoica, H., Goldstein, D. S., Graham, B. H., Yamamoto, S., et al. (2018). Pleiotropic neuropathological and biochemical alterations associated with Myo5a mutation in a rat Model. *Brain Res.* 1679, 155–170. doi:10.1016/j.brainres.2017.11.029

Li, X. D., Mabuchi, K., Ikebe, R., and Ikebe, M. (2004). Ca2+-induced activation of ATPase activity of myosin Va is accompanied with a large conformational change. *Biochem. Biophys. Res. Commun.* 315 (3), 538–545. doi:10.1016/j.bbrc.2004.01.084

Liao, G., Mingle, L., Van De Water, L., and Liu, G. (2015). Control of cell migration through mRNA localization and local translation. *Wiley Interdiscip. Rev. RNA* 6 (1), 1–15. doi:10.1002/wrna.1265

Liu, J., Taylor, D. W., Krementsova, E. B., Trybus, K. M., and Taylor, K. A. (2006). Three-dimensional structure of the myosin V inhibited state by cryoelectron tomography. *Nature* 442 (7099), 208–211. doi:10.1038/nature04719

McCaffrey, M. W., and Lindsay, A. J. (2012). Roles for myosin Va in RNA transport and turnover. *Biochem. Soc. Trans.* 40 (6), 1416–1420. doi:10.1042/BST20120172

Menasche, G., Ho, C. H., Sanal, O., Feldmann, J., Tezcan, I., Ersoy, F., et al. (2003). Griscelli syndrome restricted to hypopigmentation results from a melanophilin defect (GS3) or a MYO5A F-exon deletion (GS1). *J. Clin. Invest.* 112 (3), 450–456. doi:10.1172/JCI18264

Mercer, J. A., Seperack, P. K., Strobel, M. C., Copeland, N. G., and Jenkins, N. A. (1991). Novel myosin heavy chain encoded by murine dilute coat colour locus. *Nature* 349 (6311), 709–713. doi:10.1038/349709a0

Mofatteh, M. (2020). mRNA localization and local translation in neurons. *AIMS Neurosci.* 7 (3), 299–310. doi:10.3934/Neuroscience.2020016

Prekeris, R., and Terrian, D. M. (1997). Brain myosin V is a synaptic vesicle-associated motor protein: evidence for a Ca2+-dependent interaction with the synaptobrevin-synaptophysin complex. *J. Cell Biol.* 137 (7), 1589–1601. doi:10.1083/jcb.137.7.1589

Roy, S. (2014). Seeing the unseen: the hidden world of slow axonal transport. *Neuroscientist* 20 (1), 71–81. doi:10.1177/1073858413498306

Sahoo, P. K., Smith, D. S., Perrone-Bizzozero, N., and Twiss, J. L. (2018). Axonal mRNA transport and translation at a glance. *J. Cell Sci.* 131 (8), jcs196808. doi:10.1242/jcs.196808

Seperack, P. K., Mercer, J. A., Strobel, M. C., Copeland, N. G., and Jenkins, N. A. (1995). Retroviral sequences located within an intron of the dilute gene alter dilute expression in a tissue-specific manner. *EMBO J.* 14 (10), 2326–2332. doi:10.1002/j.1460-2075.1995.tb07227.x

Thirumurugan, K., Sakamoto, T., Hammer, J. A., 3rd, Sellers, J. R., and Knight, P. J. (2006). The cargo-binding domain regulates structure and activity of myosin 5. *Nature* 442 (7099), 212–215. doi:10.1038/nature04865

Trybus, K. M. (2008). Myosin V from head to tail. *Cell Mol. Life Sci.* 65 (9), 1378–1389. doi:10.1007/s00018-008-7507-6

Wagner, W., Brenowitz, S. D., and Hammer, J. A., 3rd (2011). Myosin-Va transports the endoplasmic reticulum into the dendritic spines of Purkinje neurons. *Nat. Cell Biol.* 13 (1), 40–48. doi:10.1038/ncb2132

Westbroek, W., Lambert, J., Bahadoran, P., Busca, R., Herteleer, M. C., Smit, N., et al. (2003). Interactions of human Myosin Va isoforms, endogenously expressed in human melanocytes, are tightly regulated by the tail domain. *J. Invest. Dermatol* 120 (3), 465–475. doi:10.1046/j.1523-1747.2003.12068.x

Wu, X., Bowers, B., Rao, K., Wei, Q., and Hammer, J. A., 3rd (1998). Visualization of melanosome dynamics within wild-type and dilute melanocytes suggests a paradigm for myosin V function *in vivo*. *J. Cell Biol.* 143 (7), 1899–1918. doi:10.1083/jcb.143.7.1899

Yilmaz, M., Cagdas, D., Grandin, V., Altintas, D. U., Tezcan, I., de Saint Basile, G., et al. (2014). Griscelli syndrome type 3-like phenotype with MYO-5A exon-F deletion. *Pediatr. Allergy Immunol.* 25 (8), 817–819. doi:10.1111/pai.12285

frontiers | Frontiers in Physiology

TYPE Review
PUBLISHED 04 January 2024
DOI 10.3389/fphys.2023.1342994

OPEN ACCESS

EDITED BY
Maria Jolanta Redowicz,
Polish Academy of Sciences, Poland

REVIEWED BY
Tomasz Prószyński,
Łukasiewicz Research Network—PORT Polish Center for Technology Development, Poland
Joseph Szule,
Texas A&M University, United States

*CORRESPONDENCE
Rüdiger Rudolf,
r.rudolf@hs-mannheim.de

RECEIVED 23 November 2023
ACCEPTED 12 December 2023
PUBLISHED 04 January 2024

CITATION
Rudolf R (2024), Myosin Va: Capturing cAMP for synaptic plasticity.
Front. Physiol. 14:1342994.
doi: 10.3389/fphys.2023.1342994

Myosin Va: Capturing cAMP for synaptic plasticity

Rüdiger Rudolf[1,2,3]*

[1]Center for Mass Spectrometry and Optical Spectroscopy (CeMOS), Mannheim University of Applied Sciences, Mannheim, Germany, [2]Interdisciplinary Center for Neurosciences, Heidelberg University, Heidelberg, Germany, [3]Mannheim Center for Translational Neurosciences, Heidelberg University, Mannheim, Germany

The plus-end directed actin-dependent motor protein, myosin Va, is of particular relevance for outward vesicular protein trafficking and for restraining specific cargo vesicles within the actin cortex. The latter is a preferred site of cAMP production, and the specificity of cAMP signaling is largely mediated through the formation of microdomains that spatially couple localized metabotropic receptor activity and cAMP production to selected effectors and downstream targets. This review summarizes the core literature on the role of myosin Va for the creation of such a cAMP microdomain at the mammalian nerve–muscle synapse that serves the activity-dependent recycling of nicotinic acetylcholine receptors (nAChRs)—a principal ligand-gated ion channel which is imperative for voluntary muscle contraction. It is discussed that i) the nerve–muscle synapse is a site with a unique actin-dependent microstructure, ii) myosin Va and protein kinase A regulatory subunit Iα as well as nAChR and its constitutive binding partner, rapsyn, colocalize in endocytic/recycling vesicles near the postsynaptic membrane, and iii) impairment of myosin Va or displacement of protein kinase A regulatory subunit Iα leads to the loss of nAChR stability. Regulation of this signaling process and underlying basic pieces of machinery were covered in previous articles, to which the present review refers.

KEYWORDS

acetylcholine receptors, AKAP, cAMP, microdomain, myosin Va, neuromuscular junction, PKA, synaptic plasticity

1 Main text

1.1 The cooperative/capture model for myosin Va

Myosin Va is an actin-dependent motor protein with particular relevance in the context of outward transport—exocytosis, and recycling—of vesicular carriers in different cell types. Along with myosin Vb and myosin Vc, myosin Va is one of three myosin V isoforms found in mammals (Reck-Peterson et al., 2000). All three are composed of a heavy chain dimer and a variable number of light chains. The heavy chains exhibit an actin-binding N-terminal motor domain, followed by a regulatory neck region containing calmodulin-binding sites, a stalk region mediating dimerization of the myosin V heavy chains, and a C-terminal cargo-binding domain (Reck-Peterson et al., 2000). Although all myosin-V isoforms are processive and plus-end-directed actin-dependent motor proteins, they appear to carry different cargo. At least partially, this is due to differential interaction with Rab-GTPases and further adaptor proteins (Wong and Weisman, 2021). Concerning myosin Va, a lack of its protein function in humans leads to Elejalde (Sanal et al., 2000) or Griscelli syndrome (Pastural et al., 1997), which is characterized by a loss of skin and hair pigmentation, immune deficiency, and

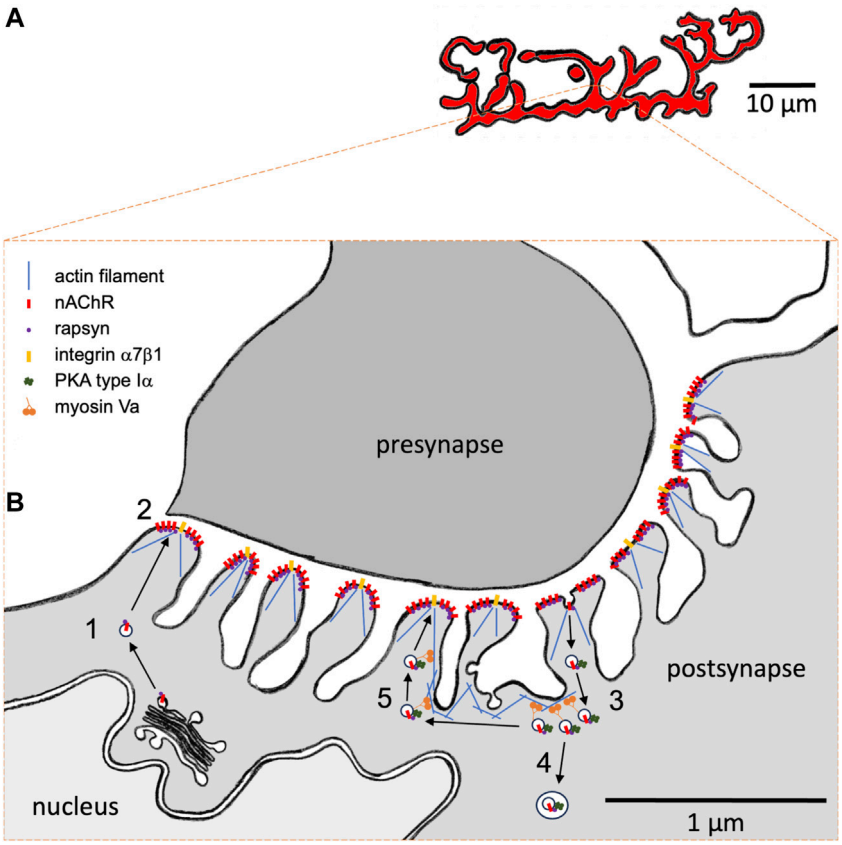

FIGURE 1
Hypothetical model of the role of myosin Va in the subsynaptic trafficking of nicotinic acetylcholine receptors (nAChR) at the mammalian neuromuscular junction (NMJ). **(A)** Representative macroscopic "pretzel"-like morphology of a healthy adult mouse NMJ. nAChRs are highly concentrated in band-like arrays with a width of 1–3 µm. NMJs usually span over a few tens of micrometers. Each muscle fiber contains one single NMJ, which usually resides roughly in the center of a muscle fiber. Motor neuron presynapse and muscle fiber postsynapse normally show a perfect match on the band-like arrays. **(B)** High-resolution view on a cross-section through an individual synaptic band. Motor neuron presynapse, top; postsynapse, bottom. The muscle fiber postsynaptic membrane shows deep junctional folds. nAChRs and integrin α7β1 are located on the crests of folds. Furthermore, dystrophin and utrophin are concentrated at the NMJ (not shown). The actin cytoskeleton is crucial for fold occurrence. Subsynaptic nuclei and secretory apparatus with ER and Golgi apparatus as well as numerous vesicular structures can be regularly observed near the postsynaptic membrane. Upon biogenesis and post-translational glycosylation, nAChRs are transported to the postsynaptic membrane in the presence of rapsyn. (1) Upon biogenesis and post-translational glycosylation, nAChRs are transported to the postsynaptic membrane in the presence of rapsyn. (2) At the membrane, agrin-dependent nAChR clustering occurs in the presence of rapsyn. (3) Endocytosis and accumulation of nAChR-containing carriers is observed next to the postsynaptic membrane. Depending on synaptic/fiber activity status, nAChRs are then either (4) degraded using autophagic processes or (5) recycled. Activity-dependent recycling of nAChRs needs myosin Va and rapsyn-mediated anchoring of PKA RIα on nAChR-recycling vesicles. Presumably, myosin Va captures these vesicles near the postsynaptic membrane in an activity-dependent cAMP microdomain and is therefore intrinsically critical for the recycling itself.

severe neurological symptoms, including seizures and muscle weakness (Griscelli et al., 1978). A very similar phenotype is observed in *dilute lethal* mice, a mutant mouse strain that carries a dominant-negative version of myosin Va (Mercer et al., 1990). Homozygous *dilute lethal* mice exhibit silvery-gray hair and die with seizures at roughly 3 weeks of age (Mercer et al., 1990).

Concerning the reasons for the pigmentation deficiency found in Griscelli patients and *dilute lethal* mice, the cooperative/capture model for the function of myosin Va was proposed in a seminal study using pigment-transporting melanocytes (Wu et al., 1998). The work described fast anterograde and retrograde microtubule-dependent transport of pigment granules (melanosomes) from the center to the periphery of melanocytes and back. In wild-type cells, most pigment granules were captured upon their arrival in the actin cortex near the cell membrane, leading to their accumulation in the cell tips. Conversely, in pigment cells from *dilute lethal* mice, melanosomes were unrestrained in the actin cortex. Therefore, they accumulated in the region with the highest microtubule density, that is, the cell center. In the absence of microtubules, the movement of melanosomes was almost null in *dilute lethal* melanocytes, whereas a motility component with a speed of 0.1–0.4 µm/s was visible in wild-type cells. The expression of a dominant-negative myosin Va C-terminal domain (MCLT) in wild-type melanocytes created a "*dilute*"-like accumulation of melanosomes in the cell center. Altogether, these data argued for the cooperation of microtubule and actin-dependent transport and for the critical role of myosin Va in capturing melanosomes in the actin-rich cell periphery.

Thus, myosin Va is critical for the trafficking and selective subcellular positioning of melanosomes. However, myosin Va

was also found to transport other organelles and subcellular structures. These include secretory granules in neuroendocrine cells (Rudolf et al., 2003), ribonucleoprotein complexes in dendrites and axons of neurons (Calliari et al., 2014), insulin-regulated glucose transporter type 4-containing recycling endosomes at postprandial states (Sun et al., 2014), exocytic and Ca^{2+}-regulated asymmetric vesicle transport during chemotactic axon growth (Wada et al., 2016), and the F-actin disassembly regulator, MICAL1 (microtubule associated monooxygenase, calponin, and LIM domain containing 1), at the midbody during cytokinesis (Niu et al., 2020). In addition, the severe neurological phenotype of Griscelli patients and *dilute lethal* mice hinted at a putative function of myosin Va in motor control or the neuromuscular apparatus.

1.2 Activity-dependent regulation of nAChR turnover in the actin-rich postsynapse

In vertebrates, neuromuscular transmission occurs at special synapses, called neuromuscular junctions (NMJs), between cholinergic lower motor neurons and skeletal muscle fibers. Their postsynaptic apparatus is characterized by a complex band-like, often "pretzel"-shaped, high-density arrangement (Figure 1A) of transmembrane nicotinic acetylcholine receptors (nAChRs), which are juxtaposed to the presynaptic membrane and are essential for neuromuscular transmission. Each band has a width of roughly 1–3 µm, and their ultrastructural analysis showed that the postsynaptic membrane of mammalian NMJs is usually deeply invaginated, forming junctional folds with a depth of a few hundred nanometers (Palade and Palay, 1954; Reger, 1955) (Figure 1B). Within a fold, nAChRs are mostly found at the crests, whereas other proteins, such as voltage-gated channels necessary for action potential generation, are located in the troughs of the folds (Flucher and Daniels, 1989).

Notably, postsynaptic nAChRs exhibit a remarkable metabolic regulation: whereas a long nAChR lifetime with a $t_{1/2}$ of 10–12 days is typical for innervated NMJs, their $t_{1/2}$ is shortened to only 1–2 days under several denervating or disease conditions (Fambrough et al., 1973; Stanley and Drachman, 1981; Ramsay et al., 1992; Strack et al., 2011; Strack et al., 2015). Similar to other transmembrane and secretory proteins, nAChR biogenesis involves co-translational import into the rough endoplasmic reticulum at subsynaptic nuclei, followed by subunit assembly, glycosylation in the Golgi apparatus, and exocytic transport to the postsynaptic membrane (for review, see Sanes and Lichtman, 1999; Tintignac et al., 2015; Li et al., 2018) (process 1 in Figure 1B). During this transport (Marchand et al., 2002) and likely during all subsequent stages (Chen et al., 2016), nAChRs are accompanied by a 43 kDa scaffold protein (Frail et al., 1988), termed rapsyn. Rapsyn is also involved in the clustering of nAChRs at the postsynaptic membrane (process 2 in Figure 1B), a process that is induced by the neuronal release of agrin (McMahan and Wallace, 1989), which activates a signal cascade *via* low-density lipoprotein receptor-related protein 4 (LRP4) (Kim et al., 2008; Zhang et al., 2008), muscle-specific kinase (MuSK) (Valenzuela et al., 1995; DeChiara et al., 1996), and downstream of tyrosine kinases-7 (Dok7) (Okada et al., 2006) proteins (for review, see Tintignac et al., 2015; Li et al., 2018). At the postsynaptic membrane, nAChRs fulfill their function as ligand-gated ion channels. *In situ* microscopy of muscles labeled with fluorescent α-bungarotoxin, which is a highly specific marker of nAChR, showed the occurrence of endocytosis of nAChR (process 3 in Figure 1B), with high amounts of nAChR-endocytic carriers under denervated/disease conditions and a low number in normal muscle (Akaaboune et al., 1999). A modification of the fluorescent α-bungarotoxin assay revealed that endocytosed nAChRs might then be either degraded (process 4 in Figure 1B) or recycled (process 5 in Figure 1B), again depending on the activity/innervation status of the synapses (Bruneau et al., 2005; Bruneau and Akaaboune, 2006; Khan et al., 2014). The clear regulatory aspect of nAChR turnover suggested the involvement of extrinsic factors that would act upon a putative endocytosis/recycling/degradation machinery.

The NMJ is a site with a particularly well-developed and organized microtubule network (Rahkila et al., 1997; Ralston et al., 1999), actin cortex (Bloch and Hall, 1983; Bloch, 1986; Cartaud et al., 2011), and intense vesicular trafficking (Fumagalli et al., 1982; Akaaboune et al., 1999; Khan et al., 2014). Already in the course of NMJ development, during which nAChR clusters are converted in the perinatal period from simple, plaque-like structures to fenestrated plaques and finally to a highly complex band-like array (pretzel-shape) (Slater, 1982; Marques et al., 2000), the actin cortex near the nAChR clusters is remodeled by several proteins, forming the so-called podosomes (Proszynski et al., 2009; for review, see Bernadzki et al., 2014). Some of these proteins link to actin and/or the dystrophin/utrophin glycoprotein complex. Both dystrophin and its sibling, utrophin, are major actin-coordinating proteins in skeletal muscle, and both are highly abundant in the NMJ (Banks et al., 2003). The lack of either of these leads to massive alterations of NMJ morphology (Deconinck et al., 1997; for review, see Dobbins et al., 2006) and a loss of junctional folds, suggesting that the actin cytoskeleton is important for fold formation and/or maintenance. Along these lines, super-resolution microscopy revealed that NMJ-specific integrin α7β1 is located, similar to nAChR, at the crest of junctional folds. However, whereas nAChRs were suggested to be localized more on the lateral crest border zones, integrins were found at the crest centers (York and Zheng, 2017) (Figure 1B). Integrins, just like dystrophin and utrophin, usually connect to the actin cytoskeleton. This further corroborates the eminent role of the actin cytoskeleton in shaping the postsynaptic apparatus with putative functional implications. Agrin-induced clustering of nAChR was also connoted with raft formation and actin cytoskeleton reorganization (Cartaud et al., 2011), a process that was mediated by the actin remodeling enzyme, coronin 6 (Chen et al., 2014).

1.3 Role of myosin Va in nAChR turnover

Using several approaches, the following condition was addressed: if the actin cytoskeleton near the NMJ would also be critical for nAChR trafficking. As outlined below, these studies included immunofluorescence, the use of myosin Va-deficient

dilute lethal mice, transient overexpression of dominant-negative versions of myosin Va (MCLT and MCST), and knockdown of myosin Va. In healthy muscle, myosin Va immunofluorescence signals were clearly enriched in the NMJ region, and the accumulation increased strongly from P1 to P16 and then stayed constant during adulthood (Röder et al., 2008). Next, a comparison of healthy and *dilute lethal* muscles showed that NMJ maturation was deficient in the diseased muscles. Whereas in the wild type, the typical transition from plaque to perforated plaque to pretzel-shape occurred during the first three postnatal weeks, the *dilute lethal* NMJs went from plaque to disintegration (Röder et al., 2008). Whereas in normal mice, the first postnatal weeks also featured a continuous increase in the half-life of nAChRs to reach its typical value of 10–12 days (Yampolsky et al., 2010b), a metabolic nAChR stabilization was completely lacking in *dilute lethal* mice (Yampolsky et al., 2010a). To investigate the putative role of myosin Va in stabilizing nAChRs in adult muscle, a sequential nAChR labeling approach was coupled to transient downregulation of myosin Va expression. This revealed that acute myosin Va knockdown in adult wild-type mouse muscle would lead to a massively decreased stability of nAChR (Röder et al., 2008). In summary, these data pointed to a specific role of myosin Va at the NMJ and, in particular, in stabilizing nAChRs in a process that was implemented during the phase of postnatal NMJ maturation from plaque to pretzel.

Next, to address the mechanism behind this putative myosin Va-dependent stabilization, three findings were of importance (Röder et al., 2008): first, in live mouse muscle, myosin Va colocalized and co-precipitated with endocytosed, α-bungarotoxin-positive nAChRs. Second, the NMJ size decreased upon overexpression of a myosin Va-dominant-negative mutant. Third, upon myosin Va-inhibition, the number of endocytic nAChR carriers was massively increased, and these puncta were not confined close to the postsynaptic membrane (as in untreated muscle) but were distributed throughout the entire fiber diameter. These findings hinted at the cooperative/capture model (see above) and suggested that myosin Va might be crucial to restraining endocytic/recycling vesicles carrying nAChRs near the plasma membrane (process 5 in Figure 1B).

1.4 A cAMP microdomain for nAChR turnover regulation

Previous reports proposed that the local production of 3′,5′-cyclic adenosine monophosphate (cAMP) upon neuronal release of the signal molecule, α-calcitonin gene-related peptide (CGRP), would enhance the stabilization of nAChR clusters at the postsynaptic membrane during embryogenesis (Lanuza et al., 2002). Furthermore, it was found that cAMP was critical for nAChR turnover regulation in the adult mouse (Shyng et al., 1991), and that a specific isoform of the regulatory subunit of protein kinase A (PKA), namely, PKA RIα, was highly enriched in a punctiform pattern next to the NMJ (Barradeau et al., 2001; Barradeau et al., 2002). In the field of signal transduction, it is a widely accepted concept that the specificity of second messenger signaling is mediated by microdomain formation, whereby essential components of a signaling pathway, that is, from transmembrane receptor over second messenger production to effector activity, are spatially restricted and segregated from neighboring microdomains (Zaccolo, 2011; Filadi and Pozzan, 2015; Omar and Scott, 2020). Consequently, whether myosin Va might be critical for nAChR stabilization by capturing endocytosed nAChRs within such a putative cAMP/PKA microdomain near the NMJ postsynaptic membrane was addressed. These studies revealed that in adult wild-type muscle, PKA type RIα, but not type RII, accumulated in numerous puncta near the NMJ. Furthermore, these puncta were also positive for endocytic nAChR and myosin Va (Röder et al., 2010). The knockdown of myosin Va massively reduced this PKA RIα enrichment, NMJ size, and nAChR stability (Röder et al., 2010). Next, treatment with CGRP led to an acute rise of cAMP in the region of PKA RIα puncta, and this effect was lost upon myosin Va knockdown (Röder et al., 2010). Altogether, these data were consistent with the existence and functional relevance of a protein complex composed of myosin Va, PKA RIα, and nAChR on endocytic/recycling vesicles. Furthermore, the studies indicated that this protein complex had to be located in a subsynaptic and active cAMP microdomain to allow recycling and a longer lifetime of nAChRs.

A-kinase anchoring proteins (AKAPs) are key to organizing such cAMP/PKA microdomains (Omar and Scott, 2020). AKAPs are characterized by at least three principal molecular features: first, special amphipathic α-helical protein domains mediate the interaction of AKAPs with PKA regulatory subunits. Second, AKAPs exhibit specific subcellular targeting domains that allow anchoring of the PKA to the site of interest. Third, to serve as scaffolding proteins, AKAPs regularly bind other signaling components involved in a given cAMP/PKA-dependent signal pathway. In the search for a potential AKAP candidate at the NMJ, evidence from previous studies pointed to rapsyn as it i) exhibits an amphipathic α-helix; ii) targets the sites of interest, that is, NMJs and nAChR; and iii) was known to exhibit multiple binding sites to further potential signal components (Ramarao et al., 2001; Lee et al., 2008; Lee et al., 2009). Fittingly, molecular modeling corroborated the rapsyn α-helical region as a potential interaction domain to PKA RIα. Furthermore, full-length rapsyn, but not rapsyn lacking the α-helix, co-precipitated with PKA RIα in culture cells (Choi et al., 2012). In addition, an *in vivo*-bimolecular fluorescence complementation assay indicated a direct interaction of rapsyn and PKA RIα in puncta exclusively near the NMJ in a punctiform pattern that was reminiscent of the distribution of PKA RIα from previous reports (Barradeau et al., 2001; Barradeau et al., 2002; Röder et al., 2010; Choi et al., 2012). Overexpression of competitive rapsyn α-helix alone or another RI anchoring disruptor peptide (RIAD) (Carlson et al., 2006) displaced PKA RIα from its normal location next to NMJ (Röder et al., 2010; Choi et al., 2012). Finally, overexpression of rapsyn α-helix or rapsyn lacking its α-helix led to NMJ fragmentation and a significantly reduced nAChR lifetime (Choi et al., 2012). Altogether, these data suggested that rapsyn serves as an AKAP that bridges PKA RIα to nAChRs in endocytic/recycling vesicles. Within this concept, tethering by myosin Va to a subsynaptic cAMP microdomain would regulate nAChR recycling to the postsynaptic membrane and the metabolic lifetime of nAChRs. This putative nAChR recycling apparatus might be tuned by intra- and extracellular signals, where its activation would presumably lead to nAChR

recycling (process 5 in Figure 1B) and its inactivation would lead to nAChR degradation (process 4 in Figure 1B) and thus affect the overall nAChR stability.

1.5 Conclusion

Until now, a series of functional or molecular factors have been found to modulate nAChR lifetime and stability (for review, see Rudolf and Straka, 2019; Martinez-Pena Y Valenzuela and Akaaboune, 2021), including muscle activity, innervation, PKC, and CaMKII. Furthermore, the basic types of machinery underlying the exocytosis, endocytosis, degradation, and recycling of nAChRs have been further characterized (for review, see Rudolf and Straka, 2019; Martinez-Pena Y Valenzuela and Akaaboune, 2021). As for other cell types and trafficking processes, dedicated small GTPases of the Rab-protein family are critical and show specific distributions at the NMJ (Wild et al., 2016; Wild et al., 2019). However, a plethora of important questions have remained unsolved. For example, how do external and internal regulatory factors tune the nAChR recycling/degradation decision, that is, which are the molecular targets that get switched? Where precisely in or close to the junctional folds do nAChR endocytosis, recycling, and degradation occur, that is, is there a spatial separation of endocytic, recycling, and degradation processes? What is the correlation between nAChR lifetime and endocytosis/recycling, that is, do nAChRs recycle multiple times?

This review proposed a concept, whereby recycling vesicles carrying postsynaptic ligand-gated ion channels are confined to the actin cytoskeleton by myosin V; furthermore, this localization is critical for regulation by second messengers. Although the evidence described here was acquired at NMJs, the general principle might not be exclusive to the peripheral nerve–muscle synapses. Indeed, the myosin Va sibling, myosin Vb, was associated with the activity-dependent recycling of AMPA receptors in hippocampal neurons (Wang et al., 2008). Although it is accepted that such recycling of AMPA receptors is under the control of Ca^{2+}, it is debated if this second messenger directly modulates myosin Vb (Wang et al., 2008) or synaptotagmin 1/7 (Sumi and Harada, 2020) to achieve activity-dependent synaptic plasticity. It will be interesting to see how these complementary fields of research will mutually stimulate each other.

Author contributions

RR: conceptualization, funding acquisition, visualization, writing–original draft, and writing–review and editing.

Funding

The author(s) declare financial support was received for the research, authorship, and/or publication of this article. RR was supported by DFG grants RU923/4-1, RU923/7-1, RU923/8-1, RU923/8-2, by grant 12056 of AFM, the Helmholtz Association, and the Hector Foundation.

Conflict of interest

The author declares that the research was conducted in the absence of any commercial or financial relationships that could be construed as a potential conflict of interest.

Publisher's note

References

Akaaboune, M., Culican, S. M., Turney, S. G., and Lichtman, J. W. (1999). Rapid and reversible effects of activity on acetylcholine receptor density at the neuromuscular junction *in vivo*. *Science* 286, 503–507. doi:10.1126/science.286.5439.503

Banks, G. B., Fuhrer, C., Adams, M. E., and Froehner, S. C. (2003). The postsynaptic submembrane machinery at the neuromuscular junction: requirement for rapsyn and the utrophin/dystrophin-associated complex. *J. Neurocytol.* 32, 709–726. doi:10.1023/B:NEUR.0000020619.24681.2b

Barradeau, S., Imaizumi-Scherrer, T., Weiss, M. C., and Faust, D. M. (2001). Muscle-regulated expression and determinants for neuromuscular junctional localization of the mouse RIalpha regulatory subunit of cAMP-dependent protein kinase. *Proc. Natl. Acad. Sci. U. S. A.* 98, 5037–5042. doi:10.1073/pnas.081393598

Barradeau, S., Imaizumi-Scherrer, T., Weiss, M. C., and Faust, D. M. (2002). Intracellular targeting of the type-I alpha regulatory subunit of cAMP-dependent protein kinase. *Trends Cardiovasc Med.* 12, 235–241. doi:10.1016/s1050-1738(02)00167-6

Bernadzki, K. M., Rojek, K. O., and Prószyński, T. J. (2014). Podosomes in muscle cells and their role in the remodeling of neuromuscular postsynaptic machinery. *Eur. J. Cell Biol.* 93, 478–485. doi:10.1016/j.ejcb.2014.06.002

Bloch, R. J. (1986). Actin at receptor-rich domains of isolated acetylcholine receptor clusters. *J. Cell Biol.* 102, 1447–1458. doi:10.1083/jcb.102.4.1447

Bloch, R. J., and Hall, Z. W. (1983). Cytoskeletal components of the vertebrate neuromuscular junction: vinculin, alpha-actinin, and filamin. *J. Cell Biol.* 97, 217–223. doi:10.1083/jcb.97.1.217

Bruneau, E., Sutter, D., Hume, R. I., and Akaaboune, M. (2005). Identification of nicotinic acetylcholine receptor recycling and its role in maintaining receptor density at the neuromuscular junction *in vivo*. *J. Neurosci.* 25, 9949–9959. doi:10.1523/JNEUROSCI.3169-05.2005

Bruneau, E. G., and Akaaboune, M. (2006). The dynamics of recycled acetylcholine receptors at the neuromuscular junction *in vivo*. *Development* 133, 4485–4493. doi:10.1242/dev.02619

Calliari, A., Farías, J., Puppo, A., Canclini, L., Mercer, J. A., Munroe, D., et al. (2014). Myosin Va associates with mRNA in ribonucleoprotein particles present in myelinated peripheral axons and in the central nervous system. *Dev. Neurobiol.* 74, 382–396. doi:10.1002/dneu.22155

Carlson, C. R., Lygren, B., Berge, T., Hoshi, N., Wong, W., Tasken, K., et al. (2006). Delineation of type I protein kinase A-selective signaling events using an RI anchoring disruptor. *J. Biol. Chem.* 281, 21535–21545. doi:10.1074/jbc.M603223200

Cartaud, A., Stetzkowski-Marden, F., Maoui, A., and Cartaud, J. (2011). Agrin triggers the clustering of raft-associated acetylcholine receptors through actin cytoskeleton reorganization. *Biol. Cell* 103, 287–301. doi:10.1042/BC20110018

Chen, P.-J., Martinez-Pena y Valenzuela, I., Aittaleb, M., and Akaaboune, M. (2016). AChRs are essential for the targeting of rapsyn to the postsynaptic membrane of NMJs in living mice. *J. Neurosci.* 36, 5680–5685. doi:10.1523/JNEUROSCI.4580-15.2016

Chen, Y., Ip, F. C. F., Shi, L., Zhang, Z., Tang, H., Ng, Y. P., et al. (2014). Coronin 6 regulates acetylcholine receptor clustering through modulating receptor anchorage to actin cytoskeleton. *J. Neurosci.* 34, 2413–2421. doi:10.1523/JNEUROSCI.3226-13.2014

Choi, K.-R. R., Berrera, M., Reischl, M., Strack, S., Albrizio, M., Roder, I. V., et al. (2012). Rapsyn mediates subsynaptic anchoring of PKA type I and stabilisation of acetylcholine receptor *in vivo*. *J. Cell Sci.* 125, 714–723. doi:10.1242/jcs.092361

DeChiara, T. M., Bowen, D. C., Valenzuela, D. M., Simmons, M. V., Poueymirou, W. T., Thomas, S., et al. (1996). The receptor tyrosine kinase MuSK is required for neuromuscular junction formation *in vivo*. *Cell* 85, 501–512. doi:10.1016/s0092-8674(00)81251-9

Deconinck, A. E., Rafael, J. A., Skinner, J. A., Brown, S. C., Potter, A. C., Metzinger, L., et al. (1997). Utrophin-dystrophin-deficient mice as a model for Duchenne muscular dystrophy. *Cell* 90, 717–727. doi:10.1016/s0092-8674(00)80532-2

Dobbins, G. C., Zhang, B., Xiong, W. C., and Mei, L. (2006). The role of the cytoskeleton in neuromuscular junction formation. *J. Mol. Neurosci.* 30, 115–118. doi:10.1385/JMN:30:1:115

Fambrough, D. M., Drachman, D. B., and Satyamurti, S. (1973). Neuromuscular junction in myasthenia gravis: decreased acetylcholine receptors. *Sci. (New York, N.Y.)* 182, 293–295. doi:10.1126/science.182.4109.293

Filadi, R., and Pozzan, T. (2015). Generation and functions of second messengers microdomains. *Cell Calcium* 58, 405–414. doi:10.1016/j.ceca.2015.03.007

Flucher, B. E., and Daniels, M. P. (1989). Distribution of Na+ channels and ankyrin in neuromuscular junctions is complementary to that of acetylcholine receptors and the 43 kd protein. *Neuron* 3, 163–175. doi:10.1016/0896-6273(89)90029-9

Frail, D. E., McLaughlin, L. L., Mudd, J., and Merlie, J. P. (1988). Identification of the mouse muscle 43,000-dalton acetylcholine receptor-associated protein (RAPsyn) by cDNA cloning. *J. Biol. Chem.* 263, 15602–15607. doi:10.1016/s0021-9258(19)37631-8

Fumagalli, G., Engel, A. G., and Lindstrom, J. (1982). Ultrastructural aspects of acetylcholine receptor turnover at the normal end-plate and in autoimmune myasthenia gravis. *J. Neuropathol. Exp. Neurol.* 41, 567–579. doi:10.1097/00005072-198211000-00001

Griscelli, C., Durandy, A., Guy-Grand, D., Daguillard, F., Herzog, C., and Prunieras, M. (1978). A syndrome associating partial albinism and immunodeficiency. *Am. J. Med.* 65, 691–702. doi:10.1016/0002-9343(78)90858-6

Khan, M. M., Strack, S., Wild, F., Hanashima, A., Gasch, A., Brohm, K., et al. (2014). Role of autophagy, SQSTM1, SH3GLB1, and TRIM63 in the turnover of nicotinic acetylcholine receptors. *Autophagy* 10, 123–136. doi:10.4161/auto.26841

Kim, N., Stiegler, A. L., Cameron, T. O., Hallock, P. T., Gomez, A. M., Huang, J. H., et al. (2008). Lrp4 is a receptor for Agrin and forms a complex with MuSK. *Cell* 135, 334–342. doi:10.1016/j.cell.2008.10.002

Lanuza, M. A., Garcia, N., Santafe, M., Gonzalez, C. M., Alonso, I., Nelson, P. G., et al. (2002). Pre- and postsynaptic maturation of the neuromuscular junction during neonatal synapse elimination depends on protein kinase C. *J. Neurosci. Res.* 67, 607–617. doi:10.1002/jnr.10122

Lee, Y., Rudell, J., and Ferns, M. (2009). Rapsyn interacts with the muscle acetylcholine receptor via alpha-helical domains in the alpha, beta, and epsilon subunit intracellular loops. *Neuroscience* 163, 222–232. doi:10.1016/j.neuroscience.2009.05.057

Lee, Y., Rudell, J., Yechikhov, S., Taylor, R., Swope, S., and Ferns, M. (2008). Rapsyn carboxyl terminal domains mediate muscle specific kinase-induced phosphorylation of the muscle acetylcholine receptor. *Neuroscience* 153, 997–1007. doi:10.1016/j.neuroscience.2008.03.009

Li, L., Xiong, W.-C., and Mei, L. (2018). Neuromuscular junction formation, aging, and disorders. *Annu. Rev. Physiology* 80, 159–188. doi:10.1146/annurev-physiol-022516-034255

Marchand, S., Devillers-Thiery, A., Pons, S., Changeux, J. P., and Cartaud, J. (2002). Rapsyn escorts the nicotinic acetylcholine receptor along the exocytic pathway via association with lipid rafts. *J. Neurosci.* 22, 8891–8901. doi:10.1523/JNEUROSCI.22-20-08891.2002

Marques, M. J., Conchello, J. A., and Lichtman, J. W. (2000). From plaque to pretzel: fold formation and acetylcholine receptor loss at the developing neuromuscular junction. *J. Neurosci.* 20, 3663–3675. doi:10.1523/JNEUROSCI.20-10-03663.2000

Martinez-Pena y Valenzuela, I., and Akaaboune, M. (2021). The metabolic stability of the nicotinic acetylcholine receptor at the neuromuscular junction. *Cells* 10, 358. doi:10.3390/cells10020358

McMahan, U. J., and Wallace, B. G. (1989). Molecules in basal lamina that direct the formation of synaptic specializations at neuromuscular junctions. *Dev. Neurosci.* 11, 227–247. doi:10.1159/000111903

Mercer, J. A., Seperack, P. K., Strobel, M. C., Copeland, N. G., and Jenkins, N. A. (1990). Novel myosin heavy chain encoded by murine dilute coat colour locus. *Nature* 352, 547. doi:10.1038/349709a0

Niu, F., Sun, K., Wei, W., Yu, C., and Wei, Z. (2020). F-actin disassembly factor MICAL1 binding to Myosin Va mediates cargo unloading during cytokinesis. *Sci. Adv.* 6, eabb1307. doi:10.1126/sciadv.abb1307

Okada, K., Inoue, A., Okada, M., Murata, Y., Kakuta, S., Jigami, T., et al. (2006). The muscle protein Dok-7 is essential for neuromuscular synaptogenesis. *Science* 312, 1802–1805. doi:10.1126/science.1127142

Omar, M. H., and Scott, J. D. (2020). AKAP signaling islands: venues for precision pharmacology. *Trends Pharmacol. Sci.* 41, 933–946. doi:10.1016/j.tips.2020.09.007

Palade, G. E., and Palay, S. L. (1954). Electron microscope observations of interneural and neuromuscular synapses. *Anat. Rec.* 118, 335.

Pastural, E., Barrat, F. J., Dufourcq-Lagelouse, R., Certain, S., Sanal, O., Jabado, N., et al. (1997). Griscelli disease maps to chromosome 15q21 and is associated with mutations in the myosin-Va gene. *Nat. Genet.* 16, 289–292. doi:10.1038/ng0797-289

Proszynski, T. J., Gingras, J., Valdez, G., Krzewski, K., and Sanes, J. R. (2009). Podosomes are present in a postsynaptic apparatus and participate in its maturation. *Proc. Natl. Acad. Sci. U. S. A.* 106, 18373–18378. doi:10.1073/pnas.0910391106

Rahkila, P., Väänänen, K., Saraste, J., and Metsikkö, K. (1997). Endoplasmic reticulum to Golgi trafficking in multinucleated skeletal muscle fibers. *Exp. Cell Res.* 234, 452–464. doi:10.1006/excr.1997.3633

Ralston, E., Lu, Z., and Ploug, T. (1999). The organization of the Golgi complex and microtubules in skeletal muscle is fiber type-dependent. *J. Neurosci.* 19, 10694–10705. doi:10.1523/JNEUROSCI.19-24-10694.1999

Ramarao, M. K., Bianchetta, M. J., Lanken, J., and Cohen, J. B. (2001). Role of rapsyn tetratricopeptide repeat and coiled-coil domains in self-association and nicotinic acetylcholine receptor clustering. *J. Biol. Chem.* 276, 7475–7483. doi:10.1074/jbc.M009888200

Ramsay, D. A., Drachman, D. B., Drachman, R. J., and Stanley, E. F. (1992). Stabilization of acetylcholine receptors at the neuromuscular synapse: the role of the nerve. *Brain Res.* 581, 198–207. doi:10.1016/0006-8993(92)90709-i

Reck-Peterson, S. L., Provance, D. W., Jr., Mooseker, M. S., and Mercer, J. A. (2000). Class V myosins. *Biochim. Biophys. Acta* 1496, 36–51. doi:10.1016/s0167-4889(00)00007-0

Reger, J. F. (1955). Electron microscopy of the motor end-plate in rat intercostal muscle. *Anatomical Rec.* 122, 1–15. doi:10.1002/ar.1091220102

Röder, I. V., Choi, K.-R. R., Reischl, M., Petersen, Y., Diefenbacher, M. E., Zaccolo, M., et al. (2010). Myosin Va cooperates with PKA RIalpha to mediate maintenance of the endplate *in vivo*. *Proc. Natl. Acad. Sci. U. S. A.* 107, 2031–2036. doi:10.1073/pnas.0914087107

Röder, I. V., Petersen, Y., Choi, K. R., Witzemann, V., Hammer, J. A., 3rd, and Rudolf, R. (2008). Role of Myosin Va in the plasticity of the vertebrate neuromuscular junction *in vivo*. *PLoS One* 3, e3871. doi:10.1371/journal.pone.0003871

Rudolf, R., Kögel, T., Kuznetsov, S. A., Salm, T., Schlicker, O., Hellwig, A., et al. (2003). Myosin Va facilitates the distribution of secretory granules in the F-actin rich cortex of PC12 cells. *J. Cell Sci.* 116, 1339–1348. doi:10.1242/jcs.00317

Rudolf, R., and Straka, T. (2019). Nicotinic acetylcholine receptor at vertebrate motor endplates: endocytosis, recycling, and degradation. *Neurosci. Lett.* 711, 134434. doi:10.1016/j.neulet.2019.134434

Sanal, O., Yel, L., Kucukali, T., Gilbert-Barnes, E., Tardieu, M., Texcan, I., et al. (2000). An allelic variant of Griscelli disease: presentation with severe hypotonia, mental-motor retardation, and hypopigmentation consistent with Elejalde syndrome (neuroectodermal melanolysosomal disorder). *J. Neurol.* 247, 570–572. doi:10.1007/s004150070162

Sanes, J. R., and Lichtman, J. W. (1999). Development of the vertebrate neuromuscular junction. *Annu. Rev. Neurosci.* 22, 389–442. doi:10.1146/annurev.neuro.22.1.389

Shyng, S. L., Xu, R., and Salpeter, M. M. (1991). Cyclic AMP stabilizes the degradation of original junctional acetylcholine receptors in denervated muscle. *Neuron* 6, 469–475. doi:10.1016/0896-6273(91)90254-w

Slater, C. R. (1982). Postnatal maturation of nerve-muscle junctions in hindlimb muscles of the mouse. *Dev. Biol.* 94, 11–22. doi:10.1016/0012-1606(82)90063-x

Stanley, E. F., and Drachman, D. B. (1981). Denervation accelerates the degradation of junctional acetylcholine receptors. *Exp. Neurol.* 73, 390–396. doi:10.1016/0014-4886(81)90274-0

Strack, S., Khan, M. M., Wild, F., Rall, A., and Rudolf, R. (2015). Turnover of acetylcholine receptors at the endplate revisited: novel insights into nerve-dependent behavior. *J. muscle Res. Cell Motil.* 36, 517–524. doi:10.1007/s10974-015-9418-0

Strack, S., Petersen, Y., Wagner, A., Röder, I. V., Albrizio, M., Reischl, M., et al. (2011). A novel labeling approach identifies three stability levels of acetylcholine receptors in the mouse neuromuscular junction *in vivo*. *PloS one* 6, e20524. doi:10.1371/journal.pone.0020524

Sumi, T., and Harada, K. (2020). Mechanism underlying hippocampal long-term potentiation and depression based on competition between endocytosis and exocytosis of AMPA receptors. *Sci. Rep.* 10, 14711. doi:10.1038/s41598-020-71528-3

Sun, Y., Chiu, T. T., Foley, K. P., Bilan, P. J., and Klip, A. (2014). Myosin Va mediates Rab8A-regulated GLUT4 vesicle exocytosis in insulin-stimulated muscle cells. *Mol. Biol. Cell* 25, 1159–1170. doi:10.1091/mbc.E13-08-0493

Tintignac, L. A., Brenner, H.-R., and Rüegg, M. A. (2015). Mechanisms regulating neuromuscular junction development and function and causes of muscle wasting. *Physiol. Rev.* 95, 809–852. doi:10.1152/physrev.00033.2014

Valenzuela, D. M., Stitt, T. N., DiStefano, P. S., Rojas, E., Mattsson, K., Compton, D. L., et al. (1995). Receptor tyrosine kinase specific for the skeletal muscle lineage: expression in embryonic muscle, at the neuromuscular junction, and after injury. *Neuron* 15, 573–584. doi:10.1016/0896-6273(95)90146-9

Wada, F., Nakata, A., Tatsu, Y., Ooashi, N., Fukuda, T., Nabetani, T., et al. (2016). Myosin Va and endoplasmic reticulum calcium channel complex regulates membrane export during axon guidance. *Cell Rep.* 15, 1329–1344. doi:10.1016/j.celrep.2016.04.021

Wang, Z., Edwards, J. G., Riley, N., Provance, D. W., Jr., Karcher, R., Li, X. D., et al. (2008). Myosin Vb mobilizes recycling endosomes and AMPA receptors for postsynaptic plasticity. *Cell* 135, 535–548. doi:10.1016/j.cell.2008.09.057

Wild, F., Khan, M. M., and Rudolf, R. (2019). Evidence for the subsynaptic zone as a preferential site for CHRN recycling at neuromuscular junctions. *Small GTPases* 10, 395–402. doi:10.1080/21541248.2017.1324939

Wild, F., Khan, M. M., Straka, T., and Rudolf, R. (2016). Progress of endocytic CHRN to autophagic degradation is regulated by RAB5-GTPase and T145 phosphorylation of SH3GLB1 at mouse neuromuscular junctions *in vivo*. *Autophagy* 12, 2300–2310. doi:10.1080/15548627.2016.1234564

Wong, S., and Weisman, L. S. (2021). Roles and regulation of myosin V interaction with cargo. *Adv. Biol. Regul.* 79, 100787. doi:10.1016/j.jbior.2021.100787

Wu, X., Bowers, B., Rao, K., Wei, Q., and Hammer, J. A., 3rd (1998). Visualization of melanosome dynamics within wild-type and dilute melanocytes suggests a paradigm for myosin V function *in vivo*. *J. Cell Biol.* 143, 1899–1918. doi:10.1083/jcb.143.7.1899

Yampolsky, P., Pacifici, P. G., Lomb, L., Giese, G., Rudolf, R., Röder, I. V., et al. (2010a). Time lapse *in vivo* visualization of developmental stabilization of synaptic receptors at neuromuscular junctions. *J. Biol. Chem.* 285, 34589–34596. doi:10.1074/jbc.M110.168880

Yampolsky, P., Pacifici, P. G., and Witzemann, V. (2010b). Differential muscle-driven synaptic remodeling in the neuromuscular junction after denervation. *Eur. J. Neurosci.* 31, 646–658. doi:10.1111/j.1460-9568.2010.07096.x

York, A. L., and Zheng, J. Q. (2017). Super-resolution microscopy reveals a nanoscale organization of acetylcholine receptors for trans-synaptic alignment at neuromuscular synapses. *eneuro* 4. doi:10.1523/ENEURO.0232-17.2017

Zaccolo, M. (2011). Spatial control of cAMP signalling in health and disease. *Curr. Opin. Pharmacol.* 11, 649–655. doi:10.1016/j.coph.2011.09.014

Zhang, B., Luo, S., Wang, Q., Suzuki, T., Xiong, W. C., and Mei, L. (2008). LRP4 serves as a coreceptor of agrin. *Neuron* 60, 285–297. doi:10.1016/j.neuron.2008.10.006

frontiers | Frontiers in Physiology

TYPE Review
PUBLISHED 18 March 2024
DOI 10.3389/fphys.2024.1374901

OPEN ACCESS

EDITED BY
Manuel H. Taft,
Hannover Medical School, Germany

REVIEWED BY
Kazuaki Homma,
Northwestern University, United States
Richard Cheney,
University of North Carolina at Chapel Hill, United States

*CORRESPONDENCE
Takushi Miyoshi,
tmiyoshi26@siumed.edu

RECEIVED 24 January 2024
ACCEPTED 21 February 2024
PUBLISHED 18 March 2024

CITATION
Miyoshi T, Belyantseva IA, Sajeevadathan M and Friedman TB (2024), Pathophysiology of human hearing loss associated with variants in myosins. *Front. Physiol.* 15:1374901.
doi: 10.3389/fphys.2024.1374901

Pathophysiology of human hearing loss associated with variants in myosins

Takushi Miyoshi[1,2]*, Inna A. Belyantseva[1], Mrudhula Sajeevadathan[2] and Thomas B. Friedman[1]

[1]Laboratory of Molecular Genetics, National Institute on Deafness and Other Communication Disorders, National Institutes of Health, Bethesda, MD, United States, [2]Division of Molecular and Integrative Physiology, Department of Biomedical Sciences, Southern Illinois University School of Medicine, Carbondale, IL, United States

Deleterious variants of more than one hundred genes are associated with hearing loss including *MYO3A*, *MYO6*, *MYO7A* and *MYO15A* and two conventional myosins *MYH9* and *MYH14*. Variants of *MYO7A* also manifest as Usher syndrome associated with dysfunction of the retina and vestibule as well as hearing loss. While the functions of MYH9 and MYH14 in the inner ear are debated, MYO3A, MYO6, MYO7A and MYO15A are expressed in inner ear hair cells along with class-I myosin MYO1C and are essential for developing and maintaining functional stereocilia on the apical surface of hair cells. Stereocilia are large, cylindrical, actin-rich protrusions functioning as biological mechanosensors to detect sound, acceleration and posture. The rigidity of stereocilia is sustained by highly crosslinked unidirectionally-oriented F-actin, which also provides a scaffold for various proteins including unconventional myosins and their cargo. Typical myosin molecules consist of an ATPase head motor domain to transmit forces to F-actin, a neck containing IQ-motifs that bind regulatory light chains and a tail region with motifs recognizing partners. Instead of long coiled-coil domains characterizing conventional myosins, the tails of unconventional myosins have various motifs to anchor or transport proteins and phospholipids along the F-actin core of a stereocilium. For these myosins, decades of studies have elucidated their biochemical properties, interacting partners in hair cells and variants associated with hearing loss. However, less is known about how myosins traffic in a stereocilium using their motor function, and how each variant correlates with a clinical condition including the severity and onset of hearing loss, mode of inheritance and presence of symptoms other than hearing loss. Here, we cover the domain structures and functions of myosins associated with hearing loss together with advances, open questions

Abbreviations: ATP, adenosine triphosphate; ADP, adenosine diphosphate; PIP2, phosphatidylinositol-4,5-bisphosphate; *DFNA*, chromosomal locus for dominantly inherited nonsyndromic deafness; *DFNB*, chromosomal locus for recessively inherited nonsyndromic deafness; ELC, essential light chain; RLC, regulatory light chain; CaM, calmodulin; IQ-motif, isoleucine-glutamine-rich motif, USH, Usher syndrome; OHC, outer hair cell; IHC, inner hair cell; RT, room temperature.

about trafficking of myosins in stereocilia and correlations between hundreds of variants in myosins annotated in ClinVar and the corresponding deafness phenotypes.

KEYWORDS

hearing, myosin, stereocilia, cargo transport, hereditary deafness

1 Introduction

Sound waves pass through the outer and middle ear providing input signals to the mechanosensory organelles on the apical surface of cochlear hair cells. These organelles represented by cylindrical protrusions called stereocilia are derived during development from microvilli and are aligned in rows of graded heights that synchronously deflect in response to sound vibrations in inner ear fluids (Schwander et al., 2010) (Figures 1A–C). Mechanical sound stimuli are converted by stereocilia into electro-chemical activities in hair cells. With the exception of the tallest row, stereocilia are equipped with mechanotransduction (MET) channels at their distal ends, which are connected to the side of adjacent longer stereocilia by tip-links that gate the MET channels (Gillespie and Muller, 2009). Open MET channels allow cations in the endolymph, specifically K^+ and Ca^{2+}, to flow into the hair cell cytoplasm. This influx causes a depolarization wave of the plasma membrane that propagates toward the base of hair cells, induces the opening of voltage-dependent Ca^{2+} channels and finally triggers Ca^{2+}-dependent fusion of glutamate-containing synaptic vesicles at the basal surface of hair cells (Corey and Hudspeth, 1979; 1983; Glowatzki and Fuchs, 2002) (Figure 1B).

Each stereocilium has a core of unidirectional F-actin tightly packed by actin cross-linkers, including ESPN, PLS1, FSCN2 and XIRP2 (Zheng et al., 2000; Shin et al., 2010; Scheffer et al., 2015; Krey et al., 2016), and connected to the underneath cuticular plate by a rootlet consisting of F-actin bundled more tightly by TRIOBP4 and TRIOBP5 (Kitajiri et al., 2010; Katsuno et al., 2019) (Figure 1C). For stereocilia, the F-actin core is a backbone to resist repeated mechanical stimuli and also a scaffold for various proteins including components of the MET machinery and motor proteins to transport or anchor these components. A similar mechanism is utilized by vestibular hair cells to detect gravity and acceleration as inputs for equilibrioception (Eatock and Lysakowski, 2006).

The myosin superfamily is one of three major families of motor proteins along with the kinesins and dyneins. Only myosins move on F-actin (Sweeney and Holzbaur, 2018). A typical myosin molecule has an ATPase head motor domain to transmit forces to F-actin, a neck containing IQ-motifs that bind regulatory light chains and a tail region to interact with specific partners. Phylogenic analyses have revealed 18 classes of myosins (Foth et al., 2006) including class-II "conventional" double-headed myosins initially discovered in skeletal muscle extracts (Kühne, 1864) and other "unconventional" myosins named after the single-headed class-I myosin discovered in *Acanthamoeba* (Pollard and Korn, 1973). While the tails of class-II myosins consist of a long coiled-coil domain to form a double-headed homodimer, those of unconventional myosins contain various motifs to recognize specific partners and usually have no or only a short coiled-coil domain (Batters and Veigel, 2016). Myosins lacking the coiled-coil domain are "unconventionally" single-headed because they cannot dimerize spontaneously. As another difference from conventional myosins, some unconventional myosins can "walk" on F-actin when dimerized by a short coiled-coil domain (e.g., class V and X) or by cargo bound to the tail (e.g., class VI and VIIA) and can transport vesicles and specific proteins as cargo (Yu et al., 2009; Sakai et al., 2011; Batters and Veigel, 2016; Liu et al., 2021). In the human genome, there are about 40 different genes encoding myosins that are grouped into 12 classes, I–III, V–VII, IX, X, XV, XVI, XVIII and XIX (Foth et al., 2006). Abnormal function of these myosins are associated with various diseases including myopathies, colitis, glomerulosclerosis, neurological defects, cancer, blindness and hearing loss (Coluccio, 2020).

In humans, variants of two genes encoding class-II conventional myosins, *MYH9* and *MYH14*, and four genes encoding class-IIIA, -VI, -VIIA and -XVA unconventional myosins, *MYO3A*, *MYO6*, *MYO7A* and *MYO15A*, are presently associated with autosomal dominant or recessive nonsyndromic sensorineural hearing loss (Table 1). Variants of *MYO7A* are also associated with autosomal recessive Usher syndrome type 1 characterized by congenital sensorineural hearing loss, vestibular dysfunction and progressive retinitis pigmentosa (Weil et al., 1995). While the functions of MYH9 and MYH14 in the inner ear are still being debated, MYO3A, MYO6, MYO7A, MYO15A and some class-I myosins (e.g., MYO1C) are expressed in inner ear hair cells and are crucial for developing and maintaining functional stereocilia by anchoring and/or transporting specific partners on the F-actin core (Table 2). Decades of studies have identified the cargo of these unconventional myosins in a stereocilium and elucidated their contribution to normal hearing including (1) formation of the MET machinery, (2) elongation of the F-actin core and (3) tethering the plasma membrane and the ankle links to the F-actin core (Friedman et al., 2020) (Figure 1D). However, less is understood about how these myosins traffic in a stereocilium using their motor function. For example, it is unknown whether or not MYO7A functions as a dimer (or perhaps as an oligomer) in a stereocilium although cargo-mediated dimerization is reported for this myosin and likely utilized in the retina (El-Amraoui et al., 2002; Sakai et al., 2011).

Variants of these myosin genes affecting the coding regions can result in sensorineural hearing loss through amino-acid sequences altered by nonsense, frameshift and missense mutations and also by in-frame deletions and insertions. Variants in noncoding regions can also result in hearing loss by damaging splicing of the primary mRNA transcript or by altering its expression levels (Anna and Monika, 2018; Walavalkar and Notani, 2020). Detecting and validating putative regulatory variants of a human gene associated with a disorder is challenging (Zhang and Lupski, 2015). One open question in the hearing research field is how a

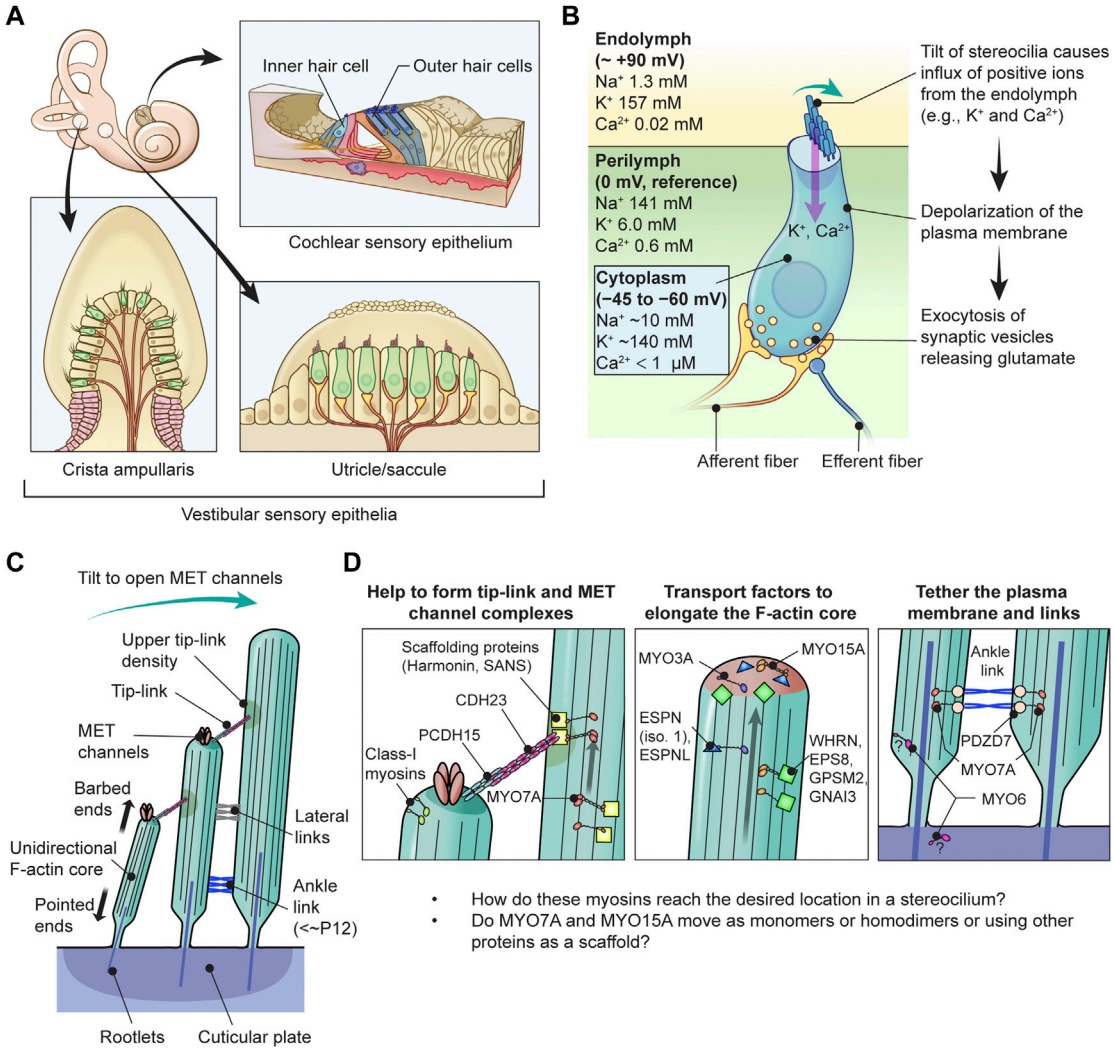

FIGURE 1
Functions of myosins in stereocilia of inner ear hair cells **(A)** Sensory epithelia in the inner ear. The cochlear sensory epithelium forms a spiral and has one row of IHCs and three rows of OHCs to detect sound stimuli (top right). Vestibular sensory epithelia are in the utricle, the saccule and three cristae ampullaris. Epithelia in the utricle and saccule detect linear acceleration in different orientations and gravity (bottom right). Epithelia in the cristae ampullaris cover angular accelerations in three-dimensional space using the fluid motion in semicircular canals perpendicular to each other (bottom left). **(B)** Inner hair cell schematically showing the mechanotransduction event during sound stimulation. Ion concentrations are previously reviewed (Wangemann, 2006; McPherson, 2018). The plasma membrane of cochlear hair cells is negatively charged between −45 mV and −60 mV against the perilymph, which have a gradient along the cochlear length (Purves, 2018), and has a steeper gradient against the positively charged endolymph, which is approximately +90 mV against the perilymph (Li et al., 2020). Deflection of stereocilia allows positive K^+ and Ca^{2+} ions in the endolymph to enter the cell body through MET channels at stereocilia tips and depolarizes the plasma membrane from the resting potential. This depolarization triggers synaptic vesicle release at the base of hair cell initiating signal transmission through the afferent fiber synapses (yellow) to the cochlear nerve. Regulatory efferent fiber endings (dark blue) are connected to the afferent nerve endings in sound transducing mature inner hair cells. **(C)** Architecture of stereocilia. The MET channels are localized at the tips of stereocilia and connected by tip-links to the side of adjacent stereocilia of the longer row, which is referred to as the upper tip-link density (UTLD) based on the high scattering of electrons in transmission electron microscopy. Each stereocilium contains a core of tightly-packed unidirectional F-actin which narrows down and is connected to the cuticular plate. Connection between the F-actin core and the cuticular plate is supported by rootlets consisting of more tightly packed F-actin. **(D)** Major functions of myosins in a stereocilium. MYO7A is localized at the UTLD and involved in localization of components of the tip-link and the MET channel (and also formation of ankle-links, right panel). Some class-I myosins are reported to play a role in adaptation during sustained sound stimulation. MYO3A and MYO15A accumulate at stereocilia tips and both transport cargo essential for elongating the F-actin core. MYO6 is thought to connect the plasma membrane to the F-actin core at stereocilia tapered base and also function in the cuticular plate.

specific variant in these myosin genes correlates with the mode of inheritance and the severity of a clinical phenotype. For example, variants of *MYO7A* are associated with both autosomal dominant (DFNA) and recessive (DFNB) nonsyndromic hearing loss as well as Usher syndrome type 1 (USH) (Weil et al., 1995; Liu et al., 1997; Weil et al., 1997). Phenotypes are different among the *MYO7A* variants associated with autosomal DFNB hearing loss in severity and threshold at each frequency and also in the age of onset (Tamagawa et al., 2002; Riazuddin et al., 2008; Schultz et al., 2011). One approach to clarify the phenotypic spectrum of variants is to use databases, such as ClinVar (https://www.ncbi.nlm.nih.gov/clinvar/), the Deafness Variation Database (https://

TABLE 1 Myosins associated (or potentially associated) with human hearing loss and their kinetic properties. Prepared based on data published in reviews (O'Connell et al., 2007; Heissler and Manstein, 2013). The italic values indicate gene names.

Gene	Locus	Duty ratio	Rate-limiting step	Velocity (μm/s) †	References
MYO1A	Refuted	0.05	Pi release	0.07–0.1 at 37°C	Collins et al. (1990), Ostap and Pollard (1996), Jontes et al. (1997), Eisenberger et al. (2014), Patton et al. (2016)
MYO1C	Disputed	0.11	Pi release	~0.06 at 37°C	Stauffer et al. (2005), Lewis et al. (2006), Lin et al. (2011), Greenberg et al. (2012), DiStefano et al. (2019)
MYO1F	Disputed	N.A.	N.A.	N.A.	DiStefano et al. (2019)
MYO3A	*DFNB30*	0.25 (0.91‡)	ADP release	0.11 at RT	Walsh et al. (2002), Komaba et al. (2003), Dose et al. (2007), Salles et al. (2009), Cirilo et al. (2021)
MYO6	*DFNA22*, *DFNB37*	0.8 (monomer)	ADP release	−0.131 (monomer), −0.307 (dimer) at 30°C§	Avraham et al. (1997), Self et al. (1999), De La Cruz et al. (2001), Melchionda et al. (2001), Ahmed et al. (2003a), Goodyear et al. (2003), Morris et al. (2003), Sakaguchi et al. (2008)
MYO7A	*DFNA11*, *DFNB2*, *USH1B*	0.9 (monomer)	ADP release	0.19 at RT	Weil et al. (1995), Liu et al. (1997), Weil et al. (1997), Udovichenko et al. (2002), Watanabe et al. (2006), Lefevre et al. (2008), Grillet et al. (2009), Dionne et al. (2018), Jaiganesh et al. (2018)
MYO15A	*DFNB3*	~0.5	ATP binding	~0.43 at 30°C	Wang et al. (1998), Beyer et al. (2000), Mogensen et al. (2007), Zampini et al. (2011), Bird et al. (2014), Jiang et al. (2020), Moreland et al. (2021)
MYH9	*DFNA17*	~0.29	Attachment to actin or Pi release¤	0.29 at 30°C	Lalwani et al. (2000), Wang et al. (2000), Yengo et al. (2012)
MYH14	*DFNA4A*	~0.34	Attachment to actin or Pi release¤	0.090 at 30°C	Donaudy et al. (2004), Heissler and Manstein (2011), Yengo et al. (2012)
(MYO5A)	*	0.7 (monomer)	ADP release	0.311 at 23°C	De La Cruz et al. (1999), Mehta et al. (1999)
(MYO10)	*	0.16, 0.6 ¶	N.A.	0.17 at 25°C€	Homma et al. (2001), Homma and Ikebe (2005), Kovacs et al. (2005)

*Listed for comparison.
†F-actin sliding assay.
‡contains the N-terminal kinase domain.
§Moves toward the pointed end of F-actin.
¤In solution as discussed in a comparative study (Yengo et al., 2012).
¶Another study supports the high duty ratio of MYO10 (Takagi et al., 2014).
€(Homma et al., 2001; Homma and Ikebe, 2005).

deafnessvariationdatabase.org/) and gnomAD (https://gnomad.broadinstitute.org/), which comprehensively curate variants with information including pathogenicity and clinical outcomes. Such databases can even point to a "hotspot" of variants in a domain whose function is not fully understood. For example, see *MYO15A* variants in Figure 6C. In this review, using ClinVar as a source of curated variants of myosin genes associated with human hearing loss, we describe the association between various myosins and hearing loss including recent advances in protein structure and function. Also discussed are open questions about trafficking of myosins in a stereocilium.

2 Domain structure and kinetic properties of myosins

A myosin monomer consists of an ATPase motor domain, a neck region that binds regulatory light chains and a tail region that interacts with specific partners. The motor domain consists of four subdomains, the N-terminal domain, the upper 50-kDa domain, the lower 50-kDa domain and the converter domain as previously reviewed (Mermall et al., 1998) (Figure 2A). The N-terminal domain of class-II and class-VI myosins have SRC Homology 3 (SH3)-like β-barrel domains (Dominguez et al., 1998; Fujita-Becker et al., 2006; Niu et al., 2024), which are also reported for class-V, -XI, -XXII and -XXIV myosins (https://www.ebi.ac.uk/interpro/entry/InterPro/IPR004009/). The SH3-like domains of class-II myosins interact with the N-terminal extension of ELC (Lowey et al., 2007) while those of class-VI myosins interact with their own tails to take on a backfolded autoinhibitory state (Niu et al., 2024). The cleft between the upper and lower 50-kDa domains acts as an interface with F-actin during a stroke and is the active site for ATP hydrolysis (Rayment et al., 1996) mediated by three highly-conserved loops, the phosphate binding loop (P-loop), Switch-1 and Switch-2 (Houdusse and Sweeney, 2016) (Figure 2B). Switch-2 undergoes a large conformational change to open and close the "back-door exit" to release the inorganic phosphate (Pi) from the cleft (Yount et al., 1995). The converter domain contains an α-helix that forms a lever arm with a long helix in the neck (Sweeney and Houdusse, 2010) and amplifies the small conformational change at the active site into a large stroke (Preller and Manstein, 2013).

10.3389/fphys.2024.1374901

TABLE 2 Presumed functions, N-terminal splicing variants and major phenotypes in mouse models.

Myosin	Presumed functions in the inner ear	N-terminal splicing variants	Major phenotypes in knockout mice	References
MYO1A	Unclear	Not found yet	Knockout mice show no overt phenotypes	Stauffer et al. (2005), Tyska et al. (2005), Solanki et al. (2021)
MYO1C	Adaptation of MET channels	Not found yet	Homozygous knockout is associated with visual impairment. Hearing loss has not been reported in peer-reviewed journals	Stauffer et al. (2005), Solanki et al. (2021)
MYO1F	Unclear	Not found yet	Knockout mice show impaired immune responses, but hearing loss is not reported	Kim et al. (2006)
MYO3A	Transports factors to elongate the F-actin core	Not found yet	Double knockout of *Myo3a* and *Myo3b* results in profound deafness and a dysmorphic staircase architecture of stereocilia	Salles et al. (2009), Lelli et al. (2016)
MYO6	Tethers plasma membrane to the F-actin core, keeps stereocilia in place and mediates vesicle transport including endocytosis	Not found yet	Loss of MYO6 function results in profound hearing loss and stereocilia bifurcated or fused with each other	Avraham et al. (1995), Avraham et al. (1997), Self et al. (1999), De La Cruz et al. (2001), Melchionda et al. (2001), Ahmed et al. (2003a), Goodyear et al. (2003), Morris et al. (2003), Sakaguchi et al. (2008)
MYO7A	Helps to form tip-link and MET channel complexes and to tether ankle links during development	MYO7A-C, MYO7A-S	Mice lacking the MYO7A function (e.g., *Shaker-1* mice) develop severely deformed stereocilia and show profound hearing loss	Weil et al. (1995), Liu et al. (1997), Weil et al. (1997), Self et al. (1998), Udovichenko et al. (2002), Watanabe et al. (2006), Lefevre et al. (2008), Grillet et al. (2009), Dionne et al. (2018), Jaiganesh et al. (2018)
MYO15A	Transport factors to elongate the F-actin core, nucleates actin monomers and maintains the length of mechanotransducing stereocilia	MYO15A-1, MYO15A-2, MYO15A-3	Mice lacking the MYO15A function (e.g., *Shaker-2* mice) show short stereocilia and profound hearing loss	Wang et al. (1998), Beyer et al. (2000), Belyantseva et al. (2003), Belyantseva et al. (2005), Mogensen et al. (2007), Zampini et al. (2011), Bird et al. (2014), Fang et al. (2015), Jiang et al. (2020), Moreland et al. (2021)
MYH9	Unclear	Not found yet	*Myh9*-null mice are embryonic lethal. Mice with mutant *Myh9* show a phenotype resembling human MYH9-related disease including platelet dysfunction and mild hearing loss	Lalwani et al. (2000), Wang et al. (2000), Mhatre et al. (2007), Yengo et al. (2012), Zhang et al. (2012)
MYH14	Unclear	Not found yet	*Myh14*-null mice are susceptible to noise-induced hearing loss	Donaudy et al. (2004), Heissler and Manstein (2011), Yengo et al. (2012), Fu et al. (2016)

To transmit force to F-actin, myosin repeats a cycle of hydrolyzing ATP to ADP + Pi accompanying the conformational change of the motor domain (Bagshaw and Trentham, 1974) (Figure 2C). In addition to the speed of the ATPase cycle, which can be roughly evaluated by the F-actin gliding assay, the duty ratio is another important parameter defined as the proportion of the ATPase cycle that the motor domain remains strongly bound to F-actin (O'Connell et al., 2007). A high duty ratio greater than ~0.5 is considered to be a necessary, but not sufficient, requirement for a myosin to show processive movements on F-actin (O'Connell et al., 2007; Pollard and Lord, 2014). The cleft in the motor domain is a mutational "hotspot" for variants associated with human hearing loss. Missense mutations in the MYO7A and MYO15A motor domains causing human and mouse hearing loss often affect the residues facing the cleft (Sellers, 2000). An additional complexity is found in class-VI myosins, which have an insertion called the "reverse gear" between the converter and lever arm. MYO6 is the only myosin that moves toward the pointed end of F-actin (Wells et al., 1999) (see Figure 2E, MYO6).

The neck region consists of a long helix connected to the α-helix in the converter domain (Sweeney and Houdusse, 2010). The length and stability of the helix is a factor determining the step size of a myosin stroke (Sakamoto et al., 2005). The neck region contains α-helical IQ motifs with a consensus sequence, [I,L,V]QXXXRGXXX[R,K] (Bahler and Rhoads, 2002), or often noted more strictly for myosins, IQXXXRGXXXR (Cheney and Mooseker, 1992). The IQ motifs interact with members of the EF-hand calcium-binding protein family including ELC, RLC and CaM (Heissler and Sellers, 2014; Jiang et al., 2020). All heavy chains of conventional class-II myosins, including MYH9 and MYH14, have two IQ motifs, IQ1 and IQ2, which interact with ELC and RLC, respectively, at high specificity (Rayment et al., 1993; Heissler and Sellers, 2014). Unconventional myosins have up to six IQ motifs depending on the class of myosins although some classes of myosins lack IQ motifs (e.g., class XIV and XVII) or have a different number of IQ motifs within the classes (e.g.,

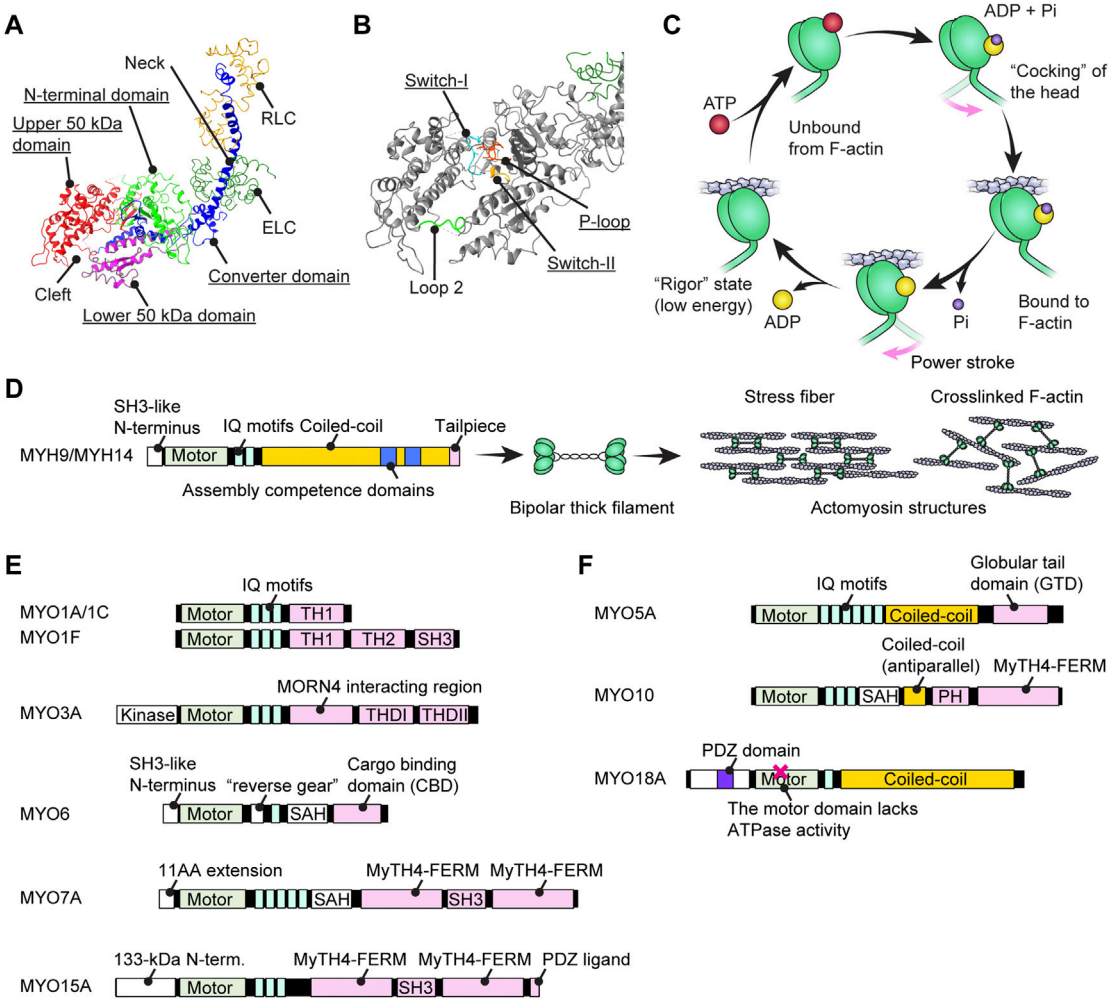

FIGURE 2
Structure of myosins and associations with human hearing loss **(A)** Four (sub)domains of the motor domain (underlined) illustrated using the structure of myosin subfragment-1 from *Gallus gallus* (PDB: 2MYS) (Rayment et al., 1993). There is a large cleft between the upper and lower 50-kDa domains. Essential and regulatory light chains are also included. **(B)** Magnified image of the motor domain in **(A)** showing three amino-acid loops crucial for ATP hydrolysis (underlined). Loop 2 connects the upper and lower 50-kDa domains. **(C)** Schematic cycle of ATP hydrolysis illustrated based on previous reviews (Houdusse and Sweeney, 2016; Sweeney and Holzbaur, 2018). Conformational changes causing F-actin binding, unbound from F-actin and a power stroke are tightly linked to each step of ATP hydrolysis. **(D)** Domain structure of conventional myosins associated with human hearing loss. MYH9 and MYH14 have a long coiled-coil to dimerize and then form actomyosin structures. The assembly competence domains are necessary for bundling in an antiparallel manner and forming a bipolar thick filament. **(E)** Domain structure of unconventional myosins associated (or potentially associated) with human hearing loss. Each myosin has unique motifs in the tail. MYO6 has a unique insertion of 53 residues called a "reverse gear" between the motor domain and the neck allowing MYO6 to move toward the pointed end of F-actin (Preller and Manstein, 2017). **(F)** Domain structure of unconventional myosins with a coiled-coil shown for comparison with **(E)**. These myosins can walk independently as a parallel dimer (MYO5A) or an antiparallel dimer (MYO10) or form a filament resembling conventional myosins (MYO18A). MYO18A has a motor domain that lacks the ATPase activity (Taft and Latham, 2020).

class I and XIII) (Minozzo and Rassier, 2013). Among the myosins related to the inner ear function, interaction with CaM (class IC, VI, III and VIIA) and ELC (class IC, VI and VIIA) are reported (Heissler and Sellers, 2014). Two of the three IQ motifs of mouse MYO15 interact with CaM, RLC and ELC but preferably with RLC and ELC (Bird et al., 2014). Some light chains can regulate the power transmission from the motor domain to the tail. For example, CaM bound to the fifth IQ of MYO7A "slide" toward the N-terminus in the presence of Ca^{2+} and reduce the rigidity between IQ5 and the adjacent single α-helix (SAH) (Li et al., 2017).

The C-terminal tail regions function as an interface for various partners including myosin itself (i.e., dimerization or multimerization) and cargo (Figures 2D–F). Class II conventional myosins MYH9 and MYH14 have a long coiled-coil tail of various lengths to dimerize with each other (Chantler et al., 2010) (Figure 2D). These heavy chain dimers can multimerize to form a bipolar thick filament as a part of contractile actomyosin structures (Craig and Woodhead, 2006; Brito and Sousa, 2020). In contrast, the tails of unconventional myosins are different between classes and even among myosins within a class and interact with different "cargo" proteins (Li and Zhang, 2020) (Figures 2E,F). Cargo of the unconventional myosins MYO7A and MYO15A include scaffolding proteins, such as harmonin, SANS and WHRN, to form a network of interactions referred to as an "interactome"

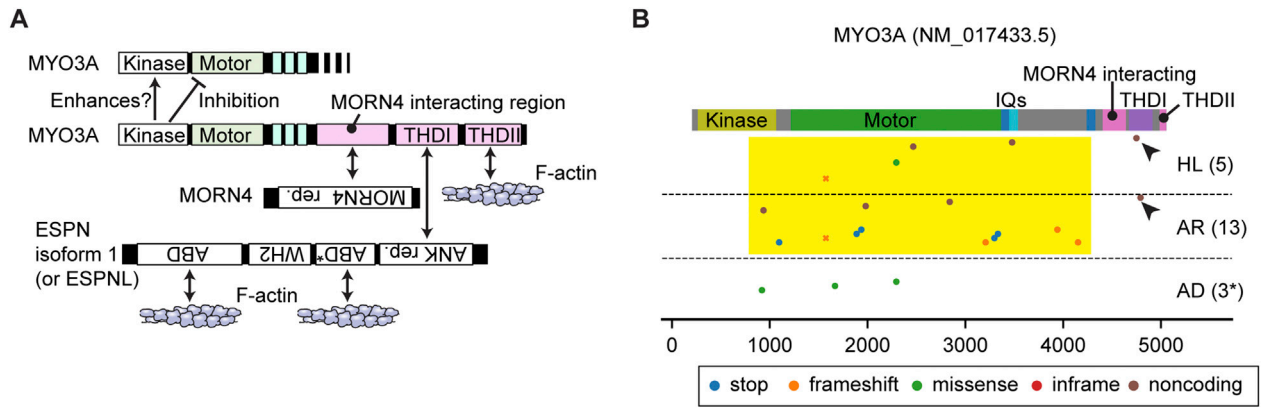

FIGURE 3
Interactome and pathogenic variants of MYO3A **(A)** Scheme showing interacting partners of MYO3A. The N-terminal kinase domain of MYO3A can phosphorylate the kinase domain and the motor domain of MYO3A (autoinhibition). The tail has region/domains that interacts with MORN4, ESPN isoform 1 (or ESPNL) and F-actin. **(B)** Pathogenic or likely pathogenic *MYO3A* variants curated by ClinVar as of 3 December 2023. Variants are plotted on the protein domains using three categories, AD: autosomal dominant nonsyndromic hearing loss, AR: autosomal recessive nonsyndromic hearing loss, HL: hearing loss with no description on the mode of inheritance. A few studies associate three variants with autosomal dominant hearing loss although the precise mechanism of the dominant inheritance is unknown (shown with asterisk). Variants in the 3′- and 5′- untranslated regions or without clinical information are not included. Most *MYO3A* variants occur in the kinase domain, the motor domain and the neck region (yellow rectangle). Two noncoding variants exist in the THDI domain that interacts with ESPN isoform 1 or ESPNL (arrowheads). Variants that belong to more than one category are plotted by crosses.

(see Figure 3A; Figure 5A; Figure 6A and the next section). Compared with conventional myosins, only a few classes of unconventional myosins have a coiled-coil domain to form a filament (class XVIII) or to walk independently as a parallel dimer (class V) or as an antiparallel dimer (class X) (Batters and Veigel, 2016) (Figure 2F). Although five unconventional myosins (class V, VI, VII, X and XVIII) encoded in the human genome have a predicted coiled-coil domain in the tail on the C-terminal side of the IQ motifs (Peckham, 2011), some of these coiled-coil domains are likely to function as a single α-helix (SAH) just to extend the lever arm (Simm et al., 2017). For example, MYO6 can dimerize through their cargo, such as Dab2, bound to the C-terminal globular domain of the tail (Yu et al., 2009) and use SAH to extend the lever arm (Mukherjea et al., 2009). MYO7A can also dimerize via MYRIP in vertebrates (via M7BP in *Drosophila*) bound to the tail and likely use SAH to extend the lever arm although SAH itself retains weak dimerization activity (Sakai et al., 2011; Liu et al., 2021). In addition, tails of some myosins can inhibit the motor function. MYO5A, MYO6 and MYO7A can take a compact backfolded conformation until cargo binds to the tail to unleash motor function (Thirumurugan et al., 2006; Spink et al., 2008; Umeki et al., 2009).

A few myosins have extensions of various length at the N-terminus of the motor domain. Among the myosins associated with human hearing loss, MYO3A has a 30-kDa kinase domain at the N-terminus. In addition, some myosins have variation at the N-terminus caused by alternative splicing of the primary mRNA transcript (Figure 5B; Figure 6B). For MYO7A, presently two isoforms have been identified, the canonical isoform with an eleven amino-acid extension at the N-terminus (MYO7A-C) and a short isoform without it (MYO7A-S) (Figure 5B). There is speculation that MYO7A-C, mainly expressed in IHCs, is responsible for positioning the MET complex (Li S. et al., 2020). MYO15A also has at least three isoforms, an isoform with a large 133-kDa N-terminal domain (MYO15A-1), a short isoform without it (MYO15A-2) and an isoform with a novel 6-kDa N-terminal domain (MYO15A-3) (Belyantseva et al., 2003; Rehman et al., 2016; Moreland and Bird, 2022) (Figure 6B). As discussed in the next section, these three isoforms have different localizations and functions in hair cells. For MYO7A and MYO15A, missense variants in the N-terminal extension are associated with hearing loss demonstrating importance of this sequence for normal hearing in humans (Figure 5C; Figure 6C). In the next section, in greater detail, we review the functions of myosins associated with hearing loss and also describe pathogenic and likely pathogenic variants documented in ClinVar and discuss correlations between variants and hearing loss.

3 Myosins and hearing loss

3.1 Loci and variants

As summarized in Table 1, two genes encoding conventional myosins, *MYH9* and *MYH14*, and four genes encoding unconventional myosins, *MYO3A*, *MYO6*, *MYO7A* and *MYO15A*, are associated with nonsyndromic hereditary hearing loss in human. The kinetic properties and functions of these myosins are different from one another. *MYO3A* and *MYO15A* are currently identified as loci of autosomal recessive nonsyndromic hearing loss, *DFNB30* and *DFNB3*, respectively (Wang et al., 1998; Walsh et al., 2002). *MYH9* and *MYH14* are identified as chromosomal loci of autosomal dominant nonsyndromic hearing loss, *DFNA17* and *DFNA4A*, respectively (Lalwani et al., 2000; Wang et al., 2000; Donaudy et al., 2004). The other two myosin genes, *MYO6* and *MYO7A*, depending on the variants, are associated with both autosomal dominant and recessive nonsyndromic hearing loss, respectively, as *DFNA22* and *DFNB37* for *MYO6* (Melchionda et al., 2001; Ahmed et al., 2003a) and *DFNA11* and *DFNB2* for *MYO7A* (Liu et al., 1997; Weil et al., 1997). Some variants of *MYO7A* are

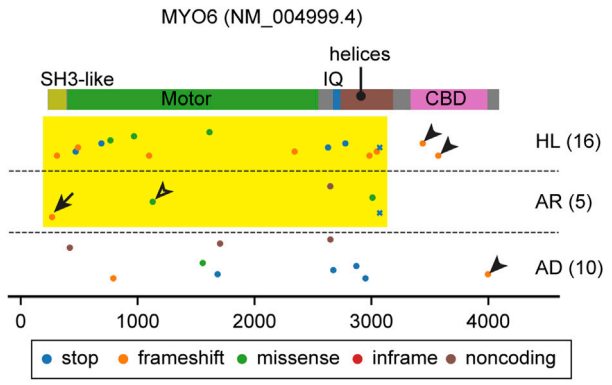

FIGURE 4
Pathogenic and likely pathogenic MYO6 variants mapped on the domain structure. Most variants affect the motor domain and the neck region (yellow rectangle) except for some frameshift variants in the CBD (arrowheads). See the text for discussion of variants indicated by an arrow (p.Thr13fs) and an open arrowhead (p.Glu299Asp). Variants are obtained and classified as described for Figure 3.

associated with Usher syndrome type 1. The locus is designated *USH1B* (Weil et al., 1995). Variants of these genes are available in databases such as ClinVar, Deafness Variation Database and gnomAD.

Correlation between variants of these myosin genes and clinical phenotypes is crucial for hearing researchers to (1) elucidate the pathophysiology of hearing loss, (2) predict the outcome of a given variant in a patient and (3) formulate therapeutic strategies for hearing loss. For clinicians, it would be best if the audiological prognosis is predictable including thresholds at each frequency in the pure tone audiogram, speech discrimination, time course in loss of hearing ability, mode of inheritance and penetrance. AlphaMissense (Cheng et al., 2023) provides *in silico* predictions for missense variants. It is also imperative to include experimental data on how each variant alters the structure or kinetics of a myosin and results in hearing loss in animal models. However, it is challenging to predict if a variant that slightly modifies the kinetics of a protein (e.g., the ATPase activity of the motor domain) will be pathogenic or not. These changes in kinetics may cause hearing loss later in life or be pathogenic only for a person with other risk alleles in their genetic background. Correlation analyses between variants and clinical outcomes may some day be complemented by aggregating environmental hazards and risks and safeguards in a patient's genetic background. Correlations between variants of myosin genes and clinical phenotypes have been reported in several studies (Tamagawa et al., 2002; Riazuddin et al., 2008; Rehman et al., 2016; Kabahuma et al., 2021). We have summarized these observations by mapping pathogenic or likely pathogenic variants available in ClinVar to the domain structures of all the myosins currently associated with human hearing loss (Figure 3B; Figure 4; Figure 5C; Figure 6C; Figure 7). In the subsections below, we examine the functions and structures of myosins necessary for normal hearing, raise questions about protein trafficking in stereocilia and further discuss the spectrum of variants in these myosin genes associated with hearing loss.

3.2 MYO3A

MYO3A has a 30-kDa kinase domain at the N-terminus and a tail that can interact with MORN4, isoform 1 of ESPN and F-actin (Figure 3A). The N-terminal kinase domain can phosphorylate two residues in the "loop 2" of the motor domain connecting the upper and lower 50-kDa domains and reduce the maximum actin-activated ATPase activity (k_{cat}) and affinity for F-actin (Quintero et al., 2010). This phosphorylation may auto-regulate the MYO3A motor activity in F-actin protrusions, such as filopodia and stereocilia (Quintero et al., 2010). The kinase domain itself has two threonine residues that can be phosphorylated, of which the C-terminal threonine has a larger impact on the kinase activity (Quintero et al., 2013). Phosphorylation of the C-terminal threonine residue in the kinase domain is mediated by another MYO3A molecule or cellular kinases, likely increasing the activity of the MYO3A kinase domain (Quintero et al., 2013). This myosin was initially considered to have a high duty ratio (~0.9) with fast phosphate release and slow ADP release (Dose et al., 2007). However, more recent analyses indicate that MYO3A has a low duty ratio (0.25) after removing the kinase domain, which enhances the ATPase activity by two-fold (Dose et al., 2008).

The MYO3A tail domain is partially unfolded but has region/domains that interact with MORN4, THDI (tail homology domain I) and THDII (tail homology domain II). MORN4 can tether its interacting partners to the plasma membrane (Li et al., 2019). THDI and THDII interact with the Ankyrin (ANK) repeat of ESPN isoform 1 or ESPNL and directly with F-actin, respectively (Les Erickson et al., 2003; Salles et al., 2009; Liu et al., 2016). Co-expression of human MYO3A lacking the kinase domain and mouse ESPN isoform 1 fragments in COS-7 cells showed elongated filopodia suggesting that constitutively active MYO3A (without regulation by the kinase domain) may recruit ESPN isoform 1 to stereocilia and boost elongation of F-actin cores (Salles et al., 2009). Concordantly, the ESPN isoform 1 knockout mouse and the jerker mouse show short, thin, immature stereocilia (Sekerkova et al., 2011; Ebrahim et al., 2016). However, a MYO3A without the kinase domain is not reported to be present in stereocilia. How the kinase domain regulates MYO3A function in stereocilia elongation, and if MYO3A with the kinase domain might be a processive motor remain to be elucidated. Interestingly, in mice, the loss of function of MYO3A is likely compensated by MYO3B. *Myo3a*$^{-/-}$ mice have normal hearing at 1 month of age while a double knockout of *Myo3a* and *Myo3b* results in profound deafness and a dysmorphic staircase architecture of hair cell stereocilia bundles (Lelli et al., 2016).

In humans, variants of *MYO3A* are associated with autosomal recessive nonsyndromic hearing loss, DFNB30 (Walsh et al., 2002). ClinVar aggregates different types of variants in this gene and associates them with autosomal recessive hearing loss or hearing loss with no description of mode of inheritance (AR and HL in Figure 3B). Most variants of *MYO3A* are nonsense mutations, frameshift mutations or mutations in the non-coding region and located in the kinase domain, the motor domain or the neck region (Figure 3B, yellow rectangle). These variants likely disrupt motor function by inserting a premature stop codon or by causing a shift in

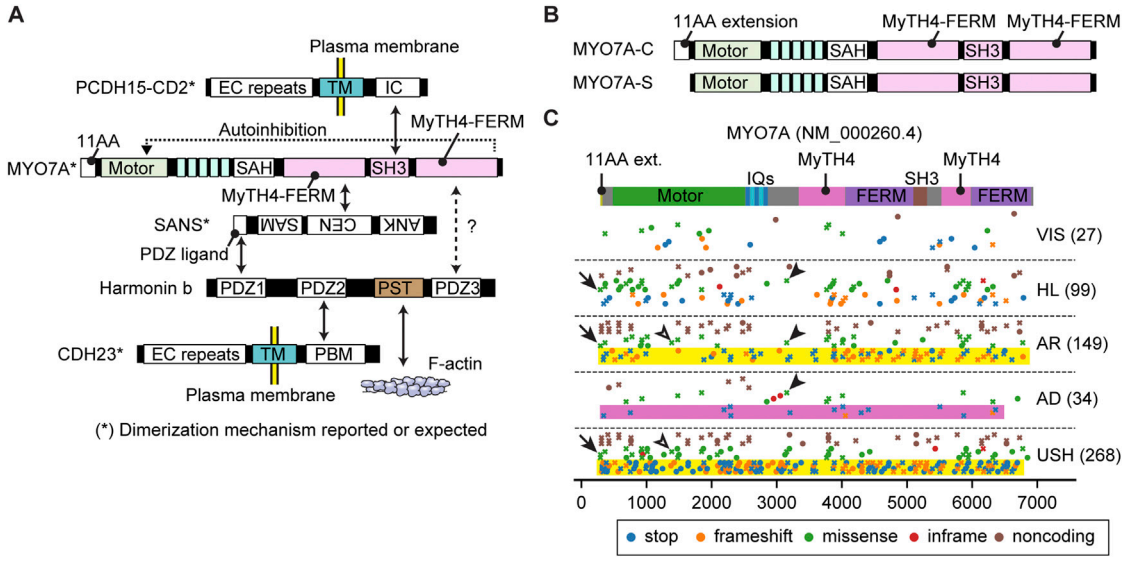

FIGURE 5
Interactome, N-terminal splicing variations and pathogenic variants of MYO7A **(A)** Interacting partners of MYO7A. SANS and harmonin isoform b (harmonin b) bridge interactions with other partners. Serine and threonine-rich (PST) sequence of harmonin b can bind to F-actin (Grillet et al., 2009). SAH domain of MYO7A has a weak dimerization activity (Sakai et al., 2011; Liu et al., 2021). SANS, PCDH15 and CDH23 can dimerize with each other (Adato et al., 2005; Dionne et al., 2018; Jaiganesh et al., 2018). The tail of MYO7A can inhibit the motor function (autoinhibition). **(B)** Different N-termini of two MYO7A isoforms. The canonical isoform has an eleven amino-acid extension at the N-terminus (MYO7A-C), while the short isoform does not (MYO7A-S). **(C)** Mapping of pathogenic and likely pathogenic MYO7A variants. Obtained and classified as described for Figure 3 adding a category, VIS, to indicate variants associated with retinal dysfunction but not with hearing loss. Nonsense and frameshift variants in *MYO7A* usually result in autosomal recessive Usher syndrome or nonsyndromic hearing loss (yellow rectangles), but some are additionally associated with autosomal dominant nonsyndromic hearing loss (pink rectangle). Overlapping phenotypic categories are observed also for missense mutations (examples shown by open and closed arrowheads). Missense variants are reported for the first methionine codon of the N-terminal extension (p.Met1Val and p. Met1Ile, arrows).

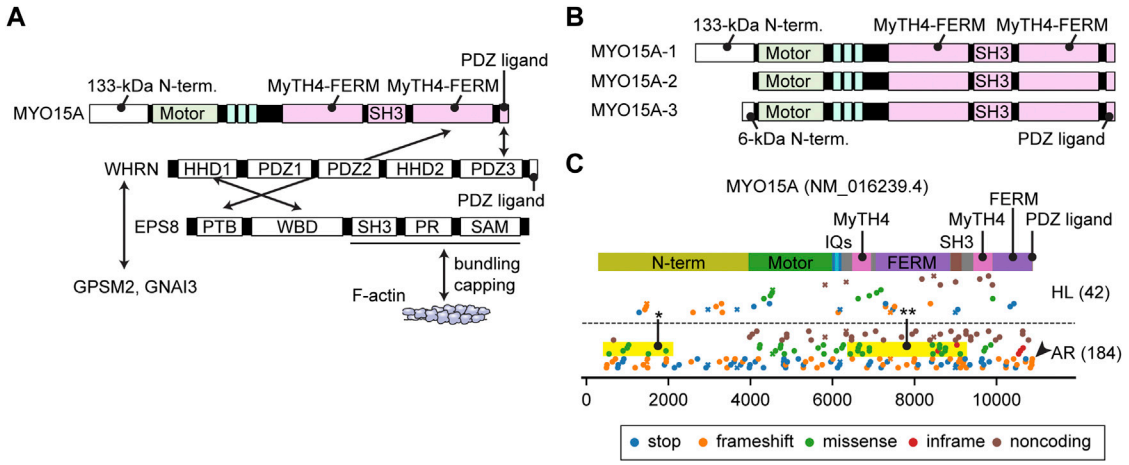

FIGURE 6
Interactome, N-terminal splicing variations and pathogenic variants of MYO15A **(A)** Known interacting partners of MYO15A. A ternary complex of MYO15A, WHRN and EPS8 interacts with each other. Another ternary of WHRN, GPSM2 and GNAI3 interacts with MYO15A. EPS8 can bundle F-actin and also cap barbed ends. Interacting partners for the first MyTH4-FERM domain and the SH3 domain of MYO15A have not been identified. **(B)** Difference in the N-termini between three MYO15A isoforms. MYO15A-1 has a large 133-kDa N-terminal domain encoded by a single exon, while a short MYO15A-2 isoform does not include this sequence. A novel MYO15A-3 isoform has a small 6-kDa N-terminal extension. **(C)** Mapping of pathogenic and likely pathogenic variants of MYO15A. Variants are obtained and classified as described for Figure 3. Nonsense and frameshift mutations distribute along the entire length of MYO15A. Some missense variants are observed in the N-terminal domain (yellow rectangle with asterisk) and in the MyTH4-FERM and SH3 domains whose binding partners are unknown (yellow rectangle with double asterisk). One variant frameshifts the C-terminal PDZ ligand (arrowhead).

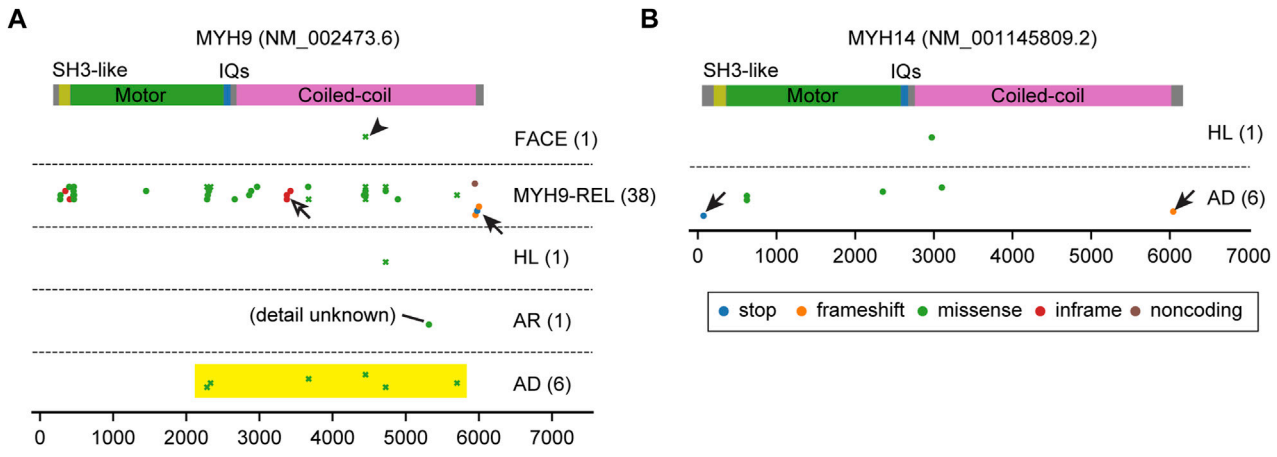

FIGURE 7
Pathogenic variants of MYH9 and MYH14. **(A, B)** Mapping of pathogenic and likely pathogenic variants in *MYH9* and *MYH14*, correspondingly. Variants are obtained and classified as described for Figure 3 with additional categories for MYH9. Nonsense or frameshift mutations are only found close to the N-terminus or the C-terminus (arrows). Almost all *MYH14* variants are associated with autosomal dominant hearing loss. In contrast, most variants of *MYH9* are associated with *MYH9*-related disorders accompanying platelet disorders and nephritis (MYH9-REL). There is one cluster of inframe mutations (p.Gln1068_Leu1074dup, p. Gln1068_Leu1074del and p. Glu1084del) in the coiled-coil domain (open arrow) for MYH9-REL. One variant is associated with a complex of symptoms including abnormal platelets and facial dysmorphology (p.Asp1424Gly, arrowhead, categorized as FACE). All *MYH9* missense variants associated with autosomal dominant hearing loss occur in the motor domain near the neck or in the neck or tail (yellow rectangle) and are associated also with *MYH9*-related disorders.

the reading frame (frameshift) of the mature mRNA. Two frameshift variants are reported in the THDI domain, which may disable the recruitment of ESPN isoform 1 or ESPNL to stereocilia (Figure 3B, arrowheads). Three missense mutations in the kinase domain (p.Leu239Pro) and in the motor domain (p.Gly488Glu and p. Leu697Trp) are each associated with autosomal dominant hearing loss (Grati et al., 2016; Dantas et al., 2018; Doll et al., 2020) (AD in Figure 3B). Although the precise mechanism of the dominant inheritance is unknown, biochemical experiments show that the two mutations in the motor domain lower the ATPase activity and alter its velocity in an F-actin sliding assay (increased by p. Gly488Glu; decreased by p. Leu697Trp) (Grati et al., 2016; Dantas et al., 2018).

A remaining question is how MYO3A traffics in a stereocilium. Currently, there is no evidence that MYO3A has a dimerization sequence, such as a coiled-coil domain, to "walk" on F-actin as a dimer or an oligomer (De La Cruz and Ostap, 2004). The low duty ratio (~0.25) of the motor domain in the absence of the kinase domain contradicts processive walking (Dose et al., 2008). To move in filopodia and stereocilia, MYO3A requires interaction with F-actin through THDII in order to perhaps cause "inchworm-like" movements (Salles et al., 2009; Raval et al., 2016). ESPN isoform 1 (or ESPNL) may assist MYO3A to move in actin protrusions considering that the tail of MYO3B, which lacks THDII to interact with F-actin, can target filopodia tips only when co-expressed with ESPN isoform 1 (Merritt et al., 2012). Increase of the duty ratio by the kinase domain could be advantageous for MYO3A to move on F-actin using its THDII domain or its cargo, ESPN isoform 1, as a scaffold although the phosphorylated motor domain also decreases its affinity for F-actin (Komaba et al., 2003; Komaba et al., 2010). It is still uncertain how class-III myosins move in F-actin protrusions including stereocilia.

3.3 MYO6

All but one myosin studied to date move on F-actin toward the barbed end. The exception is MYO6, which moves toward the pointed end of F-actin. MYO6 has an insertion called the "reverse gear" located between the converter domain and the lever arm (Wells et al., 1999; Shin et al., 2004) that is necessary for movement to the pointed end of F-actin. MYO6 also has a unique tail consisting of a single 26-kDa globular cargo binding domain (CBD) with multiple motifs to interact with a wide variety of binding partners involved in autophagy (TAX1BP, OPTN and NDP52), endocytosis (Dab2, LMTK2, TOM1/L2), mitophagy (Ubiquitin) and G-protein signaling (GIPC) (de Jonge et al., 2019) (Figure 2E). These proteins localize on the cytoplasmic side of vesicles or membrane pits, including those involved in endocytosis, and are considered to tether MYO6A to these structures (Buss and Kendrick-Jones, 2008). It is also known that MYO6 can directly interact with PIP2 in the plasma membrane through its C-terminal lipid-binding motif (Spudich et al., 2007). Some of these interacting partners, such as Dab2, OPTN and GIPC, can dimerize or oligomerize MYO6 (Phichith et al., 2009; Yu et al., 2009; Shang et al., 2017; Chatterjee et al., 2023). Despite these advances in understanding MYO6 function, MYO6 functions in the inner ear, especially in hair cells, is not fully understood. Loss of MYO6 function in Snell's waltzer mice (*Myo6*$^{sv/sv}$) results in profound hearing loss accompanying fusion of adjacent stereocilia and subsequent degeneration of the organ of Corti (Avraham et al., 1995). Bifurcated stereocilia often observed in this mouse line suggest that MYO6 anchors the plasma membrane to the F-actin core (Self et al., 1999). MYO6 also interacts with tyrosine phosphatase receptor type Q (PTPRQ), a membrane protein crucial to tether the plasma membrane to the F-actin stereocilia core (Avraham et al., 1997; Goodyear et al., 2003; Sakaguchi et al., 2008). Furthermore, it

is uncertain if MYO6 loaded with cargo traffics in a stereocilium. MYO6 ceases stepping and behaves as a molecular anchor rather than a molecular transporter when (1) under load and (2) at subsaturated ATP or in the presence of ADP (Altman et al., 2004). MYO6 may anchor stereocilia rootlets to the hair cell apical plasma membrane through PTPRQ, exerting force to help keep each stereocilium in place (Cramer, 2000).

Both autosomal dominant DFNA22 and recessive nonsyndromic hearing loss DFNB37 deafness are associated with variants of *MYO6* (Melchionda et al., 2001; Ahmed et al., 2003a). Most variants of MYO6 affect the motor domain and the neck region (Figure 4, yellow rectangle) except for some frameshift variants in the CBD (Figure 4, arrowheads). Unfortunately, many variants of *MYO6* are reported in ClinVar without information about the mode of inheritance (Figure 4). However, heterozygous $Myo6^{+/sv}$ and $Myo6^{+/-}$ mice suggest that haploinsufficiency of MYO6 function in the inner ear explains the progressive hearing loss (Karolyi et al., 2003; Seki et al., 2021). A frameshift mutation at the N-terminus (p.Thr13fs), located in annotated exon 1 of *MYO6*, is associated with autosomal recessive hearing loss, *DFNB37* (Figure 4, arrow). For this variant, perhaps the MYO6 transcript may be translated from the methionine codon at nucleotide position 18 (NM016239.4) or further downstream. A second possibility is alternative splicing that includes a "hidden" 1st exon located in highly conserved sequence in intron 1 but which in a homozygous p. Thr13fs individual is insufficient in producing enough functional MYO6 for a normal phenotype. A missense variant (p.Glu299Asp) in the motor domain is associated with autosomal recessive hearing loss, which may be the result of a slightly hypofunctional motor domain whose activity is insufficient when homozygous but sufficient when heterozygous (Figure 4, open arrowhead).

3.4 MYO7A

MYO7A has a long tail domain of approximately 1,200 residues consisting of two MyTH4-FERM domains and one SH3 domain (Figure 2E). MYO7A localizes at the upper tip-link density (UTLD) with other components of the tip-link complex, USH1C (harmonin), SANS and CDH23 (Grati and Kachar, 2011), and tethers PCDH15 at the tip of an adjacent shorter stereocilium (Kazmierczak et al., 2007) (Figure 1D). PCDH15 is mechanically connected to the MET channel complex composed of TMC1/TMC2 and accessory proteins, TMIE, CIB2 and probably LOXHD1 (Naz et al., 2002; Zhao et al., 2014; Kurima et al., 2015; Giese et al., 2017; Trouillet et al., 2021). Genes encoding the components of the tip-link complex and the MET channel complex, *USH1C*, *CDH23*, *PCDH15*, *TMIE* and *CIB2*, are associated with autosomal recessive nonsyndromic hearing loss, DFNB18, DFNB12, DFNB23, DFNB6 and DFNB48, respectively (Bork et al., 2001; Naz et al., 2002; Ahmed et al., 2003b; Riazuddin et al., 2012). Some components of the tip-link complex are also utilized in photoreceptors (Cosgrove and Zallocchi, 2014). In addition to MYO7A, four genes encoding the tip-link complex, *USH1C*, *SANS*, *CDH23* and *PCDH15*, are associated with Usher syndrome type 1 (Verpy et al., 2000; Ahmed et al., 2001; Alagramam et al., 2001; Bolz et al., 2001; Weil et al., 2003). MYO7A is also involved in transporting twinfilin-2 to stereocilia tips (Rzadzinska et al., 2009) and formation of the ankle link through interaction with a scaffolding protein PDZD7 (Grati et al., 2012; Morgan et al., 2016).

MYO7A and their interacting partners are essential components of the tip-link complex. Recent studies have elucidated an interactome among MYO7A and cargo (Figure 5A). Mouse models disabling or partially disabling the tip-link components have been useful tools to understand the formation of the tip-link complex. For example, localization of harmonin B at the UTLD is lost in mice with defective MYO7A ($Myo7a^{4626SB/4626SB}$) or SANS ($Ush1g^{js/js}$) but retained in mice with mutant CDH23 ($Cdh23^{v2J/v2J}$) or PCDH15 ($Pcdh15^{av3J/av3J}$) (Lefevre et al., 2008) suggesting that localization of harmonin B is dependent on MYO7A and SANS. The F-actin binding motif of harmonin B is essential for forming the UTLD and anchoring the tip-link to the F-actin core but not necessary for transporting the tip-link complex and harmonin B itself (Grillet et al., 2009). The eleven amino-acid extension of the canonical isoform of MYO7A (MYO7A-C in Figure 5B) may be crucial for maintaining the tip-link complex because mice lacking the MYO7A-C isoform show reduced resting open probability and slowed onset of MET currents and progressive hearing loss (Li S. et al., 2020). The tip-link components are likely replenished continuously because postnatal deletion of *Ush1c* and *Ush1g* alleles show progressive loss of tip-links and the corresponding mutant mice are profoundly deaf (Caberlotto et al., 2011). Interestingly, postnatal deletion of *Myo7a* shows progressive hearing loss and results in profound deafness in mice around P60 accompanying a decrease in MET currents without the loss of tip-links (Corns et al., 2018). Once tip-links are formed, the motor activity of MYO7A is probably not required to replenish their components.

Compared with its binding partners, less is known about how the motor activity of MYO7A is utilized in a stereocilium. Proteins in the interactome of MYO7A may provide several mechanisms for MYO7A to move in a stereocilium, (1) dimerization, (2) anchoring to the plasma membrane via CDH23 or PCDH15 (Dionne et al., 2018; Jaiganesh et al., 2018) and (3) binding to F-actin via harmonin B (Grillet et al., 2009) (Figure 5A). For dimerization, the SAH domain of MYO7A likely has a weak dimerization activity considering that a small portion of *Drosophila* myosin VIIa fragment (head + neck) can spontaneously dimerize and walk on F-actin (Liu et al., 2021) and that the SAH domain contains a motif resembling a leucine zipper (Sakai et al., 2011). In addition, SANS, PCDH15 and CDH23 can dimerize with each other and may keep multiple MYO7A molecules in close proximity (Adato et al., 2005; Dionne et al., 2018; Jaiganesh et al., 2018). Two other mechanisms may be utilized by MYO10 and MYO3A to move in F-actin protrusions. Anchoring to the plasma membrane can be used by MYO10 to form F-actin protrusions at the cell edge and then move toward the tip in the protrusion (Fitz et al., 2023). Binding to F-actin is necessary for MYO3A to move in a stereocilium or a filopodium (Salles et al., 2009; Raval et al., 2016). An open question is why MYO7A shows slow movements as a dimer, especially when compared with MYO10, which is a motor with high duty ratio functioning in filopodia (Takagi et al., 2014). MYO7A and MYO10 show similar velocities in the F-actin sliding assay, 0.19 μm/s and 0.17 μm/s, respectively (Homma and Ikebe, 2005; Watanabe et al., 2006). However, these two myosins show different

kinetics in single-molecule microscopy experiments using homodimers. Dimerized human MYO7A can only move at 11.0 ± 0.6 nm/s (Sato et al., 2017), while dimerized MYO10 can move at 578 ± 174 nm/s in filopodia (Kerber et al., 2009). Interestingly, movements of human MYO7A are slower than *Drosophila* myosin VIIa (crinkled), 72 ± 20 nm/s (Sato et al., 2017). The slow movements of MYO7A might prevent this motor protein from behaving like MYO10, which makes cellular protrusions when anchored to the plasma membrane (Fitz et al., 2023).

Variants of MYO7A are associated with hearing loss and/or retinal pathology (Figure 5C). Nonsense and frameshift variants in *MYO7A* usually result in autosomal recessive Usher syndrome type 1 or nonsyndromic hearing loss (yellow rectangles, Figure 5C). However, some nonsense and frameshift variants are also associated with autosomal dominant nonsyndromic hearing loss (pink rectangle, Figure 5C, plotted by crosses to indicate association with multiple phenotypes). Similar overlaps are observed in missense mutations (open and closed arrowheads, Figure 5C). Furthermore, 27 variants can cause only retinal symptoms (VIS in Figure 5C). Variable expressivity of *MYO7A*, and perhaps genes related to *MYO7A*, may be a reason why one variant can show different phenotypes (Zina et al., 2001). Correlation between genotypes and phenotypes, such as onset and severity of hearing loss and presence of retinal dysfunction, is complex. Currently, it is still challenging to correlate genotypes and phenotypes in Usher syndrome (Galbis-Martinez et al., 2021). Missense variants are reported in the first methionine of the N-terminal extension (p.Met1Val and p. Met1Ile) and are associated with Usher syndrome and autosomal recessive hearing loss (arrows in Figure 5C) suggesting the importance of this extension in human for intact functions of the retina and stereocilia.

3.5 MYO15A

The domain structure of the MYO15A tail is similar to MYO7A. Both have two MyTH4-FERM domains and one SH3 domain (Figure 2E). One large difference from MYO7A is a 133-kDa N-terminal domain encoded by exon 2 of MYO15A (Figure 6B). Formerly, two isoforms with and without this N-terminal extension were found and referred to as MYO15A-L and MYO15A-S. Recently, a third isoform with a small 6-kDa N-terminal extension was identified in cochlear hair cells (Rehman et al., 2016; Ranum et al., 2019) renaming the three isoforms as MYO15A-1, MYO15A-2 and MYO15A-3, respectively (Figure 6B). MYO15A-1 is localized at the tips of short stereocilia near PCDH15 and is essential for maintaining the length of the mechanotransducing stereocilia (Fang et al., 2015). MYO15A-2 lacking the N-terminal domain is crucial for elongating stereocilia to a developmentally predetermined length and can rescue abnormally short stereocilia in *Shaker-2* mice (Belyantseva et al., 2003). Although the exact function of MYO15A-3 is unknown, a previous review points to its involvement in trafficking of BAIAP2L2 (Moreland and Bird, 2022), which is an inverse BAR (I-BAR) domain proteins and interacts with phosphoinositide-rich membrane to induce plasma membrane protrusions (Zhao et al., 2011). The C-terminal PDZ ligand of MYO15A interacts with a scaffolding protein whirlin (Belyantseva et al., 2005), and MyTH4-FERM domain with an F-actin interacting protein EPS8 (Manor et al., 2011) (Figure 6A). The ternary complex of MYO15A, whirlin (WHRN) and EPS8 is essential for elongating the F-actin core. The *shaker-2*, *whirler* and *Eps8*$^{-/-}$ mice fail to elongate stereocilia to a wild-type length (Beyer et al., 2000; Mogensen et al., 2007; Zampini et al., 2011). MYO15A also has the ability to nucleate F-actin, which may contribute to the elongation of the F-actin core (Moreland et al., 2021). The ternary complex of WHRN, GPSM2 and GNAI3 is also part of the MYO15A interactome. WHRN specifies the tallest stereocilia and defines hair bundle row identity (Tadenev et al., 2019). It is unknown how MYO15A traffics in a stereocilia, but the relatively high duty ratio of its motor domain (~0.5) is consistent with processive movements as a dimer or an oligomer (Jiang et al., 2020).

Currently, variants of *MYO15A* are associated with autosomal recessive nonsyndromic hearing loss DFNB3 (Figure 6C). In addition to the nonsense and frameshift mutations distributed along the entire length of MYO15A and missense mutations in the motor domain, some missense variants are observed in the large N-terminal domain indicating the importance of this sequence (yellow rectangle with asterisk, Figure 6C). One variant truncates the C-terminal PDZ ligand as previously reported (Rehman et al., 2016) (arrowhead, Figure 6C). Interestingly, some missense mutations are reported in the first MyTH4-FERM domain and in the SH3 domain suggesting that these tail domains are sites of yet to be identified binding partners (yellow rectangle with double asterisks, Figure 6C).

3.6 Non-muscle class II myosins

Currently, variants of *MYH9* and *MYH14* genes are associated with autosomal dominant nonsyndromic hearing loss, *DFNA17* and *DFNA4A*, respectively (Lalwani et al., 2000; Wang et al., 2000; Donaudy et al., 2004). Class-II myosins contain three non-muscle myosins, NMIIA (MYH9), NMIIB (MYH10) and NMIIC (MYH14) (Heissler and Manstein, 2013). Non-muscle class-II myosins are present in every cell type (Costa and Sousa, 2020). They form contractile actomyosin structures essential for cellular organization, polarity and regulation (Vicente-Manzanares et al., 2009) (Figure 2D). Expression of non-muscle myosins are different among cell types. NMIIA and NMIIB are expressed in endothelial and epithelial cells at similar levels while NMIIB and NMIIC are abundant in nervous and lung tissue, respectively (Kawamoto and Adelstein, 1991; Golomb et al., 2004). NMIIA, NMIIB and NMIIC are expressed in mammalian cochlear epithelia and regulate extension, growth and patterning of the cochlear duct (Yamamoto et al., 2009).

The distribution of *MYH9* and *MYH14* variants are unique compared with variants of unconventional myosins (Figure 7). Nonsense or frameshift variants are only found close to the N-terminus or the C-terminus probably suggesting a dominant negative effect of truncated proteins (arrows in Figure 7). While almost all *MYH14* variants are associated with autosomal dominant hearing loss, most variants of *MYH9* are associated with other *MYH9*-related disorders including platelet disorders and nephritis (Althaus and Greinacher, 2009) (MYH9-REL in Figure 7A). Among

the variants associated with *MYH9*-related disorders, there is one cluster of inframe mutations (p.Gln1068_Leu1074dup, p. Gln1068_Leu1074del and p. Glu1084del) in the coiled-coil domain that probably does not have a destructive effect on protein folding (open arrow in Figure 7A). One variant is associated with a pleiotropic phenotype including an abnormality of platelets and facial dysmorphology (p.Asp1424Gly, arrowhead in Figure 7A). All missense variants associated with autosomal dominant hearing loss occur in the motor domain close to the neck, in the neck or in the tail and are also associated with *MYH9*-related disorders (yellow rectangle in Figure 7A and plotted by crosses to indicate association with multiple phenotypes). In patients with these variants, platelet disorders might be overlooked because of (1) bleeding is more frequently associated with variants in the motor domain than variants in the neck and the tail and (2) a tendency toward bleeding (e.g., easy bruising, epistaxis and gum bleeding) can manifest differently even between a parent and a child harboring the same variant of *MYH9* (Saposnik et al., 2014).

3.7 Disputed or refuted "deafness genes": *MYO1A*, *MYO1C* and *MYO1F*

To date, three genes encoding the class-I myosins, *MYO1A*, *MYO1C* and *MYO1F*, were initially reported as human "deafness genes" (Donaudy et al., 2003; Zadro et al., 2009). Association of variants of *MYO1A* with deafness was refuted as either the variants of *MYO1A* were identified in healthy controls or the deafness was explained by convincing variants of different genes (Eisenberger et al., 2014; Patton et al., 2016). Absence of any overt pathology in homozygous *Myo1a* knockout mice supports these findings (Tyska et al., 2005). Association of *MYO1C* and *MYO1F* variants with deafness was disputed by the ClinGen Hearing Loss Clinical Domain Working Group (CDWG) due to a lack of sufficient functional analyses (DiStefano et al., 2019). This class of myosins have a neck containing three IQ motifs and a tail with a tail homology 1 (TH1) domain (MYO1A–D, G and H) or two tail homology domains (TH1 and TH2) and one SH3 domain (MYO1E and F) (Diaz-Valencia et al., 2022) (Figure 2E). The TH1 domain has a putative pleckstrin homology (PH) motif and can interact with PIP2 in the lipid bilayer (Hokanson et al., 2006). In the inner ear, MYO1C was reported to be involved in adaptation of MET channels (i.e., rapid closing of activated MET channels) through interaction with the plasma membrane (Stauffer et al., 2005). Future studies may find additional association of class-I myosins with inner ear function.

4 Discussion

Genetic studies have identified more than one hundred genes with variants associated with hearing loss including four genes encoding unconventional myosins, *MYO3A*, *MYO6*, *MYO7A* and *MYO15A*, and two genes encoding conventional myosins, *MYH9* and *MYH14*. The four unconventional myosins and some class-I myosins are expressed in hair cells and are essential for developing and maintaining functional stereocilia. The tail domains of these unconventional myosins have motifs unique for each protein and have evolved to interact with specific protein partners and phospholipids (PIP2), which are often referred to as "cargo" transported and/or anchored on the F-actin core of a stereocilium. Major functions of cargo proteins can be largely categorized into (1) formation of the MET machinery, (2) elongation of the F-actin core and (3) tethering the plasma membrane and certain links to the F-actin core (Figure 1D) but not limited to these. For example, Twinfilin-2, which caps F-actin of stereocilia in shorter rows, is identified as cargo of MYO7A (Rzadzinska et al., 2009). In addition to elucidating the functions of cargo proteins in stereocilia development, recent topics include novel isoforms of MYO7A and MYO15A derived from previously "hidden" alternatively spliced small exons (Rehman et al., 2016; Ranum et al., 2019; Li S. et al., 2020).

Compared with the interacting partners of these myosins, less is understood about how the motor activities of these myosins are utilized and regulated in a stereocilium. For example, it is unknown how MYO7A becomes localized at the UTLD and whether or not it is dimerized. In the retina, MYO7A can be recruited to melanosomes by MYRIP which activates the MYO7A motor function through cargo-mediated dimerization (El-Amraoui et al., 2002; Sakai et al., 2011). However, there is no evidence that MYRIP is utilized in hair cell stereocilia although it is present. RNAseq in FACS-sorted hair cells shows higher expression of MYRIP in supporting cells than in hair cells (https://shield.hms.harvard.edu/viewgene.html?gene=Myrip). One scenario is that proteins in the MYO7A interactome provide mechanisms for MYO7A to move in a stereocilium as discussed in the previous section. Another possibility is that MYO7A is directly recruited to the UTLD by the proteins already there, such as CDH23, harmonin B and SANS, although another mechanism would be necessary to recruit these proteins to the UTLD in this scenario. A similar challenge can be posed to other myosins, such as MYO6 and MYO15A, for which the entire interactome in hair cells needs to be clarified. Utilization of motor activities in stereocilia may be difficult to analyze using conventional mouse models lacking functional myosins or their cargo because stereocilia in these mouse models are often severely deformed, disturbing the cargo transport system in them (Lefevre et al., 2008). To approach utilization and regulation of motor activities in a stereocilium, advances in single molecule visualization methodologies will be required to observe the *in vivo* behaviors of myosins and cargo in real time in live hair cell stereocilia.

In addition, we speculate that more detailed clinical information of patients is necessary for correlation analyses between variants and phenotypes. Large databases, such as ClinVar and gnomAD, aggregate variants with clinical symptoms. However, even from these carefully curated databases, it is difficult to obtain detailed measurements necessary for hearing research, such as thresholds at each frequency in the pure tone audiograms, speech discrimination, time course in loss of hearing ability and the clinical conditions of patients including accompanying symptoms, because these details are written in a format different for each journal, database and website. From a technical point of view, more flexible approaches, such as artificial intelligence and machine learning, may be useful to handle large and often unformatted data. Artificial intelligence has already been introduced into clinical genomics laboratories and utilized to predict the pathogenicity and phenotypic consequence of variants (Aradhya et al., 2023). With the ability to handle large data,

these novel tools may assist hearing researchers to discover correlations between variants and phenotypes and to identify variants of high priority.

Active transport by myosins are crucial for developing cell protrusions including stereocilia, microvilli and filopodia (Houdusse and Titus, 2021). Elucidating the pathophysiology of hearing loss caused by myosin variants will be useful to formulate therapeutic strategies not only for sensorineural hearing loss but also for other diseases such as cancer, virus infection and inflammatory bowel diseases.

Author contributions

TM: Conceptualization, Funding acquisition, Methodology, Project administration, Software, Validation, Visualization, Writing–original draft, Writing–review and editing. IB: Validation, Visualization, Writing–review and editing. MS: Validation, Writing–review and editing. TF: Funding acquisition, Project administration, Validation, Writing–review and editing, Supervision.

Funding

The author(s) declare that financial support was received for the research, authorship, and/or publication of this article. TM, IB, and TF were supported, in part, by NIDCD intramural research funds DC000039 to TF. TM and MS were also supported by the start-up fund from Southern Illinois University School of Medicine and the K99/R00 Pathway-to-Independence Award to TM (1K99DC019949 and 4R00DC019949).

Acknowledgments

We thank Drs. Dennis Winkler and Mhamed Grati for valuable comments and Ms. Erina He for her beautiful diagrams. Raw data and Python scripts used to draw graphs in Figures 3B, 4, 5C, 6C and 7 are available at the first author's GitHub repository (https://github.com/takushim/fpvariants).

Conflict of interest

The authors declare that the research was conducted in the absence of any commercial or financial relationships that could be construed as a potential conflict of interest.

Publisher's note

References

Adato, A., Michel, V., Kikkawa, Y., Reiners, J., Alagramam, K. N., Weil, D., et al. (2005). Interactions in the network of Usher syndrome type 1 proteins. *Hum. Mol. Genet.* 14, 347–356. doi:10.1093/hmg/ddi031

Ahmed, Z. M., Morell, R. J., Riazuddin, S., Gropman, A., Shaukat, S., Ahmad, M. M., et al. (2003a). Mutations of MYO6 are associated with recessive deafness, DFNB37. *Am. J. Hum. Genet.* 72, 1315–1322. doi:10.1086/375122

Ahmed, Z. M., Riazuddin, S., Ahmad, J., Bernstein, S. L., Guo, Y., Sabar, M. F., et al. (2003b). PCDH15 is expressed in the neurosensory epithelium of the eye and ear and mutant alleles are responsible for both USH1F and DFNB23. *Hum. Mol. Genet.* 12, 3215–3223. doi:10.1093/hmg/ddg358

Ahmed, Z. M., Riazuddin, S., Bernstein, S. L., Ahmed, Z., Khan, S., Griffith, A. J., et al. (2001). Mutations of the protocadherin gene PCDH15 cause Usher syndrome type 1F. *Am. J. Hum. Genet.* 69, 25–34. doi:10.1086/321277

Alagramam, K. N., Yuan, H., Kuehn, M. H., Murcia, C. L., Wayne, S., Srisailpathy, C. R., et al. (2001). Mutations in the novel protocadherin PCDH15 cause Usher syndrome type 1F. *Hum. Mol. Genet.* 10, 1709–1718. doi:10.1093/hmg/10.16.1709

Althaus, K., and Greinacher, A. (2009). MYH9-related platelet disorders. *Semin. Thromb. Hemost.* 35, 189–203. doi:10.1055/s-0029-1220327

Altman, D., Sweeney, H. L., and Spudich, J. A. (2004). The mechanism of myosin VI translocation and its load-induced anchoring. *Cell* 116, 737–749. doi:10.1016/s0092-8674(04)00211-9

Anna, A., and Monika, G. (2018). Splicing mutations in human genetic disorders: examples, detection, and confirmation. *J. Appl. Genet.* 59, 253–268. doi:10.1007/s13353-018-0444-7

Aradhya, S., Facio, F. M., Metz, H., Manders, T., Colavin, A., Kobayashi, Y., et al. (2023). Applications of artificial intelligence in clinical laboratory genomics. *Am. J. Med. Genet. C Semin. Med. Genet.* 193, e32057. doi:10.1002/ajmg.c.32057

Avraham, K. B., Hasson, T., Sobe, T., Balsara, B., Testa, J. R., Skvorak, A. B., et al. (1997). Characterization of unconventional MYO6, the human homologue of the gene responsible for deafness in Snell's waltzer mice. *Hum. Mol. Genet.* 6, 1225–1231. doi:10.1093/hmg/6.8.1225

Avraham, K. B., Hasson, T., Steel, K. P., Kingsley, D. M., Russell, L. B., Mooseker, M. S., et al. (1995). The mouse Snell's waltzer deafness gene encodes an unconventional myosin required for structural integrity of inner ear hair cells. *Nat. Genet.* 11, 369–375. doi:10.1038/ng1295-369

Bagshaw, C. R., and Trentham, D. R. (1974). The characterization of myosin-product complexes and of product-release steps during the magnesium ion-dependent adenosine triphosphatase reaction. *Biochem. J.* 141, 331–349. doi:10.1042/bj1410331

Bahler, M., and Rhoads, A. (2002). Calmodulin signaling via the IQ motif. *FEBS Lett.* 513, 107–113. doi:10.1016/s0014-5793(01)03239-2

Batters, C., and Veigel, C. (2016). Mechanics and activation of unconventional myosins. *Traffic* 17, 860–871. doi:10.1111/tra.12400

Belyantseva, I. A., Boger, E. T., and Friedman, T. B. (2003). Myosin XVa localizes to the tips of inner ear sensory cell stereocilia and is essential for staircase formation of the hair bundle. *Proc. Natl. Acad. Sci. U. S. A.* 100, 13958–13963. doi:10.1073/pnas.2334417100

Belyantseva, I. A., Boger, E. T., Naz, S., Frolenkov, G. I., Sellers, J. R., Ahmed, Z. M., et al. (2005). Myosin-XVa is required for tip localization of whirlin and differential elongation of hair-cell stereocilia. *Nat. Cell Biol.* 7, 148–156. doi:10.1038/ncb1219

Beyer, L. A., Odeh, H., Probst, F. J., Lambert, E. H., Dolan, D. F., Camper, S. A., et al. (2000). Hair cells in the inner ear of the pirouette and shaker 2 mutant mice. *J. Neurocytol.* 29, 227–240. doi:10.1023/a:1026515619443

Bird, J. E., Takagi, Y., Billington, N., Strub, M. P., Sellers, J. R., and Friedman, T. B. (2014). Chaperone-enhanced purification of unconventional myosin 15, a molecular motor specialized for stereocilia protein trafficking. *Proc. Natl. Acad. Sci. U. S. A.* 111, 12390–12395. doi:10.1073/pnas.1409459111

Bolz, H., Von Brederlow, B., Ramirez, A., Bryda, E. C., Kutsche, K., Nothwang, H. G., et al. (2001). Mutation of CDH23, encoding a new member of the cadherin gene family, causes Usher syndrome type 1D. *Nat. Genet.* 27, 108–112. doi:10.1038/83667

Bork, J. M., Peters, L. M., Riazuddin, S., Bernstein, S. L., Ahmed, Z. M., Ness, S. L., et al. (2001). Usher syndrome 1D and nonsyndromic autosomal recessive deafness DFNB12 are caused by allelic mutations of the novel cadherin-like gene CDH23. *Am. J. Hum. Genet.* 68, 26–37. doi:10.1086/316954

Brito, C., and Sousa, S. (2020). Non-muscle myosin 2A (NM2A): structure, regulation and function. *Cells* 9, 1590. doi:10.3390/cells9071590

Buss, F., and Kendrick-Jones, J. (2008). How are the cellular functions of myosin VI regulated within the cell? *Biochem. Biophys. Res. Commun.* 369, 165–175. doi:10.1016/j.bbrc.2007.11.150

Caberlotto, E., Michel, V., Foucher, I., Bahloul, A., Goodyear, R. J., Pepermans, E., et al. (2011). Usher type 1G protein sans is a critical component of the tip-link complex,

a structure controlling actin polymerization in stereocilia. *Proc. Natl. Acad. Sci. U. S. A.* 108, 5825–5830. doi:10.1073/pnas.1017114108

Chantler, P. D., Wylie, S. R., Wheeler-Jones, C. P., and Mcgonnell, I. M. (2010). Conventional myosins - unconventional functions. *Biophys. Rev.* 2, 67–82. doi:10.1007/s12551-010-0030-7

Chatterjee, P., Morgan, C. P., Krey, J. F., Benson, C., Goldsmith, J., Bateschell, M., et al. (2023). GIPC3 couples to MYO6 and PDZ domain proteins, and shapes the hair cell apical region. *J. Cell Sci.* 136, jcs261100. doi:10.1242/jcs.261100

Cheney, R. E., and Mooseker, M. S. (1992). Unconventional myosins. *Curr. Opin. Cell Biol.* 4, 27–35. doi:10.1016/0955-0674(92)90055-h

Cheng, J., Novati, G., Pan, J., Bycroft, C., Zemgulyte, A., Applebaum, T., et al. (2023). Accurate proteome-wide missense variant effect prediction with AlphaMissense. *Science* 381, eadg7492. doi:10.1126/science.adg7492

Cirilo, J. A., Jr., Gunther, L. K., and Yengo, C. M. (2021). Functional role of class III myosins in hair cells. *Front. Cell Dev. Biol.* 9, 643856. doi:10.3389/fcell.2021.643856

Collins, K., Sellers, J. R., and Matsudaira, P. (1990). Calmodulin dissociation regulates brush border myosin I (110-kD-calmodulin) mechanochemical activity *in vitro*. *J. Cell Biol.* 110, 1137–1147. doi:10.1083/jcb.110.4.1137

Coluccio, L. M. (2020). "Myosins and disease," in *Myosins: a superfamily of molecular motors*. Editor L. M. Coluccio (Cham: Springer International Publishing), 245–316.

Corey, D. P., and Hudspeth, A. J. (1979). Ionic basis of the receptor potential in a vertebrate hair cell. *Nature* 281, 675–677. doi:10.1038/281675a0

Corey, D. P., and Hudspeth, A. J. (1983). Kinetics of the receptor current in bullfrog saccular hair cells. *J. Neurosci.* 3, 962–976. doi:10.1523/JNEUROSCI.03-05-00962.1983

Corns, L. F., Johnson, S. L., Roberts, T., Ranatunga, K. M., Hendry, A., Ceriani, F., et al. (2018). Mechanotransduction is required for establishing and maintaining mature inner hair cells and regulating efferent innervation. *Nat. Commun.* 9, 4015. doi:10.1038/s41467-018-06307-w

Cosgrove, D., and Zallocchi, M. (2014). Usher protein functions in hair cells and photoreceptors. *Int. J. Biochem. Cell Biol.* 46, 80–89. doi:10.1016/j.biocel.2013.11.001

Costa, A. R., and Sousa, M. M. (2020). Non-muscle myosin II in axonal cell biology: from the growth cone to the axon initial segment. *Cells* 9, 1961. doi:10.3390/cells9091961

Craig, R., and Woodhead, J. L. (2006). Structure and function of myosin filaments. *Curr. Opin. Struct. Biol.* 16, 204–212. doi:10.1016/j.sbi.2006.03.006

Cramer, L. P. (2000). Myosin VI: roles for a minus end-directed actin motor in cells. *J. Cell Biol.* 150, F121–F126. doi:10.1083/jcb.150.6.f121

Dantas, V. G. L., Raval, M. H., Ballesteros, A., Cui, R., Gunther, L. K., Yamamoto, G. L., et al. (2018). Characterization of a novel MYO3A missense mutation associated with a dominant form of late onset hearing loss. *Sci. Rep.* 8, 8706. doi:10.1038/s41598-018-26818-2

De Jonge, J. J., Batters, C., O'loughlin, T., Arden, S. D., and Buss, F. (2019). The MYO6 interactome: selective motor-cargo complexes for diverse cellular processes. *FEBS Lett.* 593, 1494–1507. doi:10.1002/1873-3468.13486

De La Cruz, E. M., and Ostap, E. M. (2004). Relating biochemistry and function in the myosin superfamily. *Curr. Opin. Cell Biol.* 16, 61–67. doi:10.1016/j.ceb.2003.11.011

De La Cruz, E. M., Ostap, E. M., and Sweeney, H. L. (2001). Kinetic mechanism and regulation of myosin VI. *J. Biol. Chem.* 276, 32373–32381. doi:10.1074/jbc.M104136200

De La Cruz, E. M., Wells, A. L., Rosenfeld, S. S., Ostap, E. M., and Sweeney, H. L. (1999). The kinetic mechanism of myosin V. *Proc. Natl. Acad. Sci. U. S. A.* 96, 13726–13731. doi:10.1073/pnas.96.24.13726

Diaz-Valencia, J. D., Estrada-Abreo, L. A., Rodriguez-Cruz, L., Salgado-Aguayo, A. R., and Patino-Lopez, G. (2022). Class I Myosins, molecular motors involved in cell migration and cancer. *Cell Adh Migr.* 16, 1–12. doi:10.1080/19336918.2021.2020705

Dionne, G., Qiu, X., Rapp, M., Liang, X., Zhao, B., Peng, G., et al. (2018). Mechanotransduction by PCDH15 relies on a novel cis-dimeric architecture. *Neuron* 99, 480–492. doi:10.1016/j.neuron.2018.07.006

Distefano, M. T., Hemphill, S. E., Oza, A. M., Siegert, R. K., Grant, A. R., Hughes, M. Y., et al. (2019). ClinGen expert clinical validity curation of 164 hearing loss gene-disease pairs. *Genet. Med.* 21, 2239–2247. doi:10.1038/s41436-019-0487-0

Doll, J., Hofrichter, M. a.H., Bahena, P., Heihoff, A., Segebarth, D., Muller, T., et al. (2020). A novel missense variant in MYO3A is associated with autosomal dominant high-frequency hearing loss in a German family. *Mol. Genet. Genomic Med.* 8, e1343. doi:10.1002/mgg3.1343

Dominguez, R., Freyzon, Y., Trybus, K. M., and Cohen, C. (1998). Crystal structure of a vertebrate smooth muscle myosin motor domain and its complex with the essential light chain: visualization of the pre-power stroke state. *Cell* 94, 559–571. doi:10.1016/s0092-8674(00)81598-6

Donaudy, F., Ferrara, A., Esposito, L., Hertzano, R., Ben-David, O., Bell, R. E., et al. (2003). Multiple mutations of MYO1A, a cochlear-expressed gene, in sensorineural hearing loss. *Am. J. Hum. Genet.* 72, 1571–1577. doi:10.1086/375654

Donaudy, F., Snoeckx, R., Pfister, M., Zenner, H. P., Blin, N., Di Stazio, M., et al. (2004). Nonmuscle myosin heavy-chain gene MYH14 is expressed in cochlea and mutated in patients affected by autosomal dominant hearing impairment (DFNA4). *Am. J. Hum. Genet.* 74, 770–776. doi:10.1086/383285

Dose, A. C., Ananthanarayanan, S., Moore, J. E., Burnside, B., and Yengo, C. M. (2007). Kinetic mechanism of human myosin IIIA. *J. Biol. Chem.* 282, 216–231. doi:10.1074/jbc.M605964200

Dose, A. C., Ananthanarayanan, S., Moore, J. E., Corsa, A. C., Burnside, B., and Yengo, C. M. (2008). The kinase domain alters the kinetic properties of the myosin IIIA motor. *Biochemistry* 47, 2485–2496. doi:10.1021/bi7021574

Eatock, R. A., and Lysakowski, A. (2006). "Mammalian vestibular hair cells," in *Vertebrate hair cells*. Editors R. A. Eatock, R. R. Fay, and A. N. Popper (New York, NY: Springer New York), 348–442.

Ebrahim, S., Avenarius, M. R., Grati, M., Krey, J. F., Windsor, A. M., Sousa, A. D., et al. (2016). Stereocilia-staircase spacing is influenced by myosin III motors and their cargos espin-1 and espin-like. *Nat. Commun.* 7, 10833. doi:10.1038/ncomms10833

Eisenberger, T., Di Donato, N., Baig, S. M., Neuhaus, C., Beyer, A., Decker, E., et al. (2014). Targeted and genomewide NGS data disqualify mutations in MYO1A, the "DFNA48 gene", as a cause of deafness. *Hum. Mutat.* 35, 565–570. doi:10.1002/humu.22532

El-Amraoui, A., Schonn, J. S., Kussel-Andermann, P., Blanchard, S., Desnos, C., Henry, J. P., et al. (2002). MyRIP, a novel Rab effector, enables myosin VIIa recruitment to retinal melanosomes. *EMBO Rep.* 3, 463–470. doi:10.1093/embo-reports/kvf090

Fang, Q., Indzhykulian, A. A., Mustapha, M., Riordan, G. P., Dolan, D. F., Friedman, T. B., et al. (2015). The 133-kDa N-terminal domain enables myosin 15 to maintain mechanotransducing stereocilia and is essential for hearing. *Elife* 4, e08627. doi:10.7554/eLife.08627

Fitz, G. N., Weck, M. L., Bodnya, C., Perkins, O. L., and Tyska, M. J. (2023). Protrusion growth driven by myosin-generated force. *Dev. Cell* 58, 18–33.e6. doi:10.1016/j.devcel.2022.12.001

Foth, B. J., Goedecke, M. C., and Soldati, D. (2006). New insights into myosin evolution and classification. *Proc. Natl. Acad. Sci. U. S. A.* 103, 3681–3686. doi:10.1073/pnas.0506307103

Friedman, T. B., Belyantseva, I. A., and Frolenkov, G. I. (2020). Myosins and hearing. *Adv. Exp. Med. Biol.* 1239, 317–330. doi:10.1007/978-3-030-38062-5_13

Fu, X., Zhang, L., Jin, Y., Sun, X., Zhang, A., Wen, Z., et al. (2016). Loss of Myh14 increases susceptibility to noise-induced hearing loss in CBA/CaJ mice. *Neural Plast.* 2016, 6720420. doi:10.1155/2016/6720420

Fujita-Becker, S., Reubold, T. F., and Holmes, K. C. (2006). The actin-binding cleft: functional characterisation of myosin II with a strut mutation. *J. Muscle Res. Cell Motil.* 27, 115–123. doi:10.1007/s10974-005-9047-0

Galbis-Martinez, L., Blanco-Kelly, F., Garcia-Garcia, G., Avila-Fernandez, A., Jaijo, T., Fuster-Garcia, C., et al. (2021). Genotype-phenotype correlation in patients with Usher syndrome and pathogenic variants in MYO7A: implications for future clinical trials. *Acta Ophthalmol.* 99, 922–930. doi:10.1111/aos.14795

Giese, A. P. J., Tang, Y. Q., Sinha, G. P., Bowl, M. R., Goldring, A. C., Parker, A., et al. (2017). CIB2 interacts with TMC1 and TMC2 and is essential for mechanotransduction in auditory hair cells. *Nat. Commun.* 8, 43. doi:10.1038/s41467-017-00061-1

Gillespie, P. G., and Muller, U. (2009). Mechanotransduction by hair cells: models, molecules, and mechanisms. *Cell* 139, 33–44. doi:10.1016/j.cell.2009.09.010

Glowatzki, E., and Fuchs, P. A. (2002). Transmitter release at the hair cell ribbon synapse. *Nat. Neurosci.* 5, 147–154. doi:10.1038/nn796

Golomb, E., Ma, X., Jana, S. S., Preston, Y. A., Kawamoto, S., Shoham, N. G., et al. (2004). Identification and characterization of nonmuscle myosin II-C, a new member of the myosin II family. *J. Biol. Chem.* 279, 2800–2808. doi:10.1074/jbc.M309981200

Goodyear, R. J., Legan, P. K., Wright, M. B., Marcotti, W., Oganesian, A., Coats, S. A., et al. (2003). A receptor-like inositol lipid phosphatase is required for the maturation of developing cochlear hair bundles. *J. Neurosci.* 23, 9208–9219. doi:10.1523/JNEUROSCI.23-27-09208.2003

Grati, M., and Kachar, B. (2011). Myosin VIIa and sans localization at stereocilia upper tip-link density implicates these Usher syndrome proteins in mechanotransduction. *Proc. Natl. Acad. Sci. U. S. A.* 108, 11476–11481. doi:10.1073/pnas.1104161108

Grati, M., Shin, J. B., Weston, M. D., Green, J., Bhat, M. A., Gillespie, P. G., et al. (2012). Localization of PDZD7 to the stereocilia ankle-link associates this scaffolding protein with the Usher syndrome protein network. *J. Neurosci.* 32, 14288–14293. doi:10.1523/JNEUROSCI.3071-12.2012

Grati, M., Yan, D., Raval, M. H., Walsh, T., Ma, Q., Chakchouk, I., et al. (2016). MYO3A causes human dominant deafness and interacts with protocadherin 15-CD2 isoform. *Hum. Mutat.* 37, 481–487. doi:10.1002/humu.22961

Greenberg, M. J., Lin, T., Goldman, Y. E., Shuman, H., and Ostap, E. M. (2012). Myosin IC generates power over a range of loads via a new tension-sensing mechanism. *Proc. Natl. Acad. Sci. U. S. A.* 109, E2433–E2440. doi:10.1073/pnas.1207811109

Grillet, N., Xiong, W., Reynolds, A., Kazmierczak, P., Sato, T., Lillo, C., et al. (2009). Harmonin mutations cause mechanotransduction defects in cochlear hair cells. *Neuron* 62, 375–387. doi:10.1016/j.neuron.2009.04.006

Heissler, S. M., and Manstein, D. J. (2011). Comparative kinetic and functional characterization of the motor domains of human nonmuscle myosin-2C isoforms. *J. Biol. Chem.* 286, 21191–21202. doi:10.1074/jbc.M110.212290

Heissler, S. M., and Manstein, D. J. (2013). Nonmuscle myosin-2: mix and match. *Cell Mol. Life Sci.* 70, 1–21. doi:10.1007/s00018-012-1002-9

Heissler, S. M., and Sellers, J. R. (2014). Myosin light chains: teaching old dogs new tricks. *Bioarchitecture* 4, 169–188. doi:10.1080/19490992.2015.1054092

Hokanson, D. E., Laakso, J. M., Lin, T., Sept, D., and Ostap, E. M. (2006). Myo1c binds phosphoinositides through a putative pleckstrin homology domain. *Mol. Biol. Cell* 17, 4856–4865. doi:10.1091/mbc.e06-05-0449

Homma, K., and Ikebe, M. (2005). Myosin X is a high duty ratio motor. *J. Biol. Chem.* 280, 29381–29391. doi:10.1074/jbc.M504779200

Homma, K., Saito, J., Ikebe, R., and Ikebe, M. (2001). Motor function and regulation of myosin X. *J. Biol. Chem.* 276, 34348–34354. doi:10.1074/jbc.M104785200

Houdusse, A., and Sweeney, H. L. (2016). How myosin generates force on actin filaments. *Trends Biochem. Sci.* 41, 989–997. doi:10.1016/j.tibs.2016.09.006

Houdusse, A., and Titus, M. A. (2021). The many roles of myosins in filopodia, microvilli and stereocilia. *Curr. Biol.* 31, R586–R602. doi:10.1016/j.cub.2021.04.005

Jaiganesh, A., De-La-Torre, P., Patel, A. A., Termine, D. J., Velez-Cortes, F., Chen, C., et al. (2018). Zooming in on cadherin-23: structural diversity and potential mechanisms of inherited deafness. *Structure* 26, 1210–1225. doi:10.1016/j.str.2018.06.003

Jiang, F., Takagi, Y., Shams, A., Heissler, S. M., Friedman, T. B., Sellers, J. R., et al. (2020). The ATPase mechanism of myosin 15, the molecular motor mutated in DFNB3 human deafness. *J. Biol. Chem.* 296, 100243. doi:10.1074/jbc.RA120.014903

Jontes, J. D., Milligan, R. A., Pollard, T. D., and Ostap, E. M. (1997). Kinetic characterization of brush border myosin-I ATPase. *Proc. Natl. Acad. Sci. U. S. A.* 94, 14332–14337. doi:10.1073/pnas.94.26.14332

Kabahuma, R. I., Schubert, W. D., Labuschagne, C., Yan, D., Blanton, S. H., Pepper, M. S., et al. (2021). Spectrum of MYO7A mutations in an indigenous South African population further elucidates the nonsyndromic autosomal recessive phenotype of DFNB2 to include both homozygous and compound heterozygous mutations. *Genes (Basel)* 12, 274. doi:10.3390/genes12020274

Karolyi, I. J., Probst, F. J., Beyer, L., Odeh, H., Dootz, G., Cha, K. B., et al. (2003). Myo15 function is distinct from Myo6, Myo7a and pirouette genes in development of cochlear stereocilia. *Hum. Mol. Genet.* 12, 2797–2805. doi:10.1093/hmg/ddg308

Katsuno, T., Belyantseva, I. A., Cartagena-Rivera, A. X., Ohta, K., Crump, S. M., Petralia, R. S., et al. (2019). TRIOBP-5 sculpts stereocilia rootlets and stiffens supporting cells enabling hearing. *JCI Insight* 4, e128561. doi:10.1172/jci.insight.128561

Kawamoto, S., and Adelstein, R. S. (1991). Chicken nonmuscle myosin heavy chains: differential expression of two mRNAs and evidence for two different polypeptides. *J. Cell Biol.* 112, 915–924. doi:10.1083/jcb.112.5.915

Kazmierczak, P., Sakaguchi, H., Tokita, J., Wilson-Kubalek, E. M., Milligan, R. A., Muller, U., et al. (2007). Cadherin 23 and protocadherin 15 interact to form tip-link filaments in sensory hair cells. *Nature* 449, 87–91. doi:10.1038/nature06091

Kerber, M. L., Jacobs, D. T., Campagnola, L., Dunn, B. D., Yin, T., Sousa, A. D., et al. (2009). A novel form of motility in filopodia revealed by imaging myosin-X at the single-molecule level. *Curr. Biol.* 19, 967–973. doi:10.1016/j.cub.2009.03.067

Kim, S. V., Mehal, W. Z., Dong, X., Heinrich, V., Pypaert, M., Mellman, I., et al. (2006). Modulation of cell adhesion and motility in the immune system by Myo1f. *Science* 314, 136–139. doi:10.1126/science.1131920

Kitajiri, S., Sakamoto, T., Belyantseva, I. A., Goodyear, R. J., Stepanyan, R., Fujiwara, I., et al. (2010). Actin-bundling protein TRIOBP forms resilient rootlets of hair cell stereocilia essential for hearing. *Cell* 141, 786–798. doi:10.1016/j.cell.2010.03.049

Komaba, S., Inoue, A., Maruta, S., Hosoya, H., and Ikebe, M. (2003). Determination of human myosin III as a motor protein having a protein kinase activity. *J. Biol. Chem.* 278, 21352–21360. doi:10.1074/jbc.M300757200

Komaba, S., Watanabe, S., Umeki, N., Sato, O., and Ikebe, M. (2010). Effect of phosphorylation in the motor domain of human myosin IIIA on its ATP hydrolysis cycle. *Biochemistry* 49, 3695–3702. doi:10.1021/bi902211w

Kovacs, M., Wang, F., and Sellers, J. R. (2005). Mechanism of action of myosin X, a membrane-associated molecular motor. *J. Biol. Chem.* 280, 15071–15083. doi:10.1074/jbc.M500616200

Krey, J. F., Krystofiak, E. S., Dumont, R. A., Vijayakumar, S., Choi, D., Rivero, F., et al. (2016). Plastin 1 widens stereocilia by transforming actin filament packing from hexagonal to liquid. *J. Cell Biol.* 215, 467–482. doi:10.1083/jcb.201606036

Kühne, W. (1864). *Untersuchungen über das Protoplasma und die Contractilität*. Washington, D.C.: Biodiversity Heritage Library.

Kurima, K., Ebrahim, S., Pan, B., Sedlacek, M., Sengupta, P., Millis, B. A., et al. (2015). TMC1 and TMC2 localize at the site of mechanotransduction in mammalian inner ear hair cell stereocilia. *Cell Rep.* 12, 1606–1617. doi:10.1016/j.celrep.2015.07.058

Lalwani, A. K., Goldstein, J. A., Kelley, M. J., Luxford, W., Castelein, C. M., and Mhatre, A. N. (2000). Human nonsyndromic hereditary deafness DFNA17 is due to a mutation in nonmuscle myosin MYH9. *Am. J. Hum. Genet.* 67, 1121–1128. doi:10.1016/S0002-9297(07)62942-5

Lefevre, G., Michel, V., Weil, D., Lepelletier, L., Bizard, E., Wolfrum, U., et al. (2008). A core cochlear phenotype in USH1 mouse mutants implicates fibrous links of the hair bundle in its cohesion, orientation and differential growth. *Development* 135, 1427–1437. doi:10.1242/dev.012922

Lelli, A., Michel, V., Boutet De Monvel, J., Cortese, M., Bosch-Grau, M., Aghaie, A., et al. (2016). Class III myosins shape the auditory hair bundles by limiting microvilli and stereocilia growth. *J. Cell Biol.* 212, 231–244. doi:10.1083/jcb.201509017

Les Erickson, F., Corsa, A. C., Dose, A. C., and Burnside, B. (2003). Localization of a class III myosin to filopodia tips in transfected HeLa cells requires an actin-binding site in its tail domain. *Mol. Biol. Cell* 14, 4173–4180. doi:10.1091/mbc.e02-10-0656

Lewis, J. H., Lin, T., Hokanson, D. E., and Ostap, E. M. (2006). Temperature dependence of nucleotide association and kinetic characterization of myo1b. *Biochemistry* 45, 11589–11597. doi:10.1021/bi0611917

Li, J., Chen, Y., Deng, Y., Unarta, I. C., Lu, Q., Huang, X., et al. (2017). Ca(2+)-Induced rigidity change of the myosin VIIa IQ motif-single alpha helix lever arm extension. *Structure* 25, 579–591 e574. doi:10.1016/j.str.2017.02.002

Li, J., Liu, H., Raval, M. H., Wan, J., Yengo, C. M., Liu, W., et al. (2019). Structure of the MORN4/myo3a tail complex reveals MORN repeats as protein binding modules. *Structure* 27, 1366–1374. doi:10.1016/j.str.2019.06.004

Li, J., and Zhang, M. (2020). Cargo binding by unconventional myosins. *Adv. Exp. Med. Biol.* 1239, 21–40. doi:10.1007/978-3-030-38062-5_3

Li, S., Mecca, A., Kim, J., Caprara, G. A., Wagner, E. L., Du, T. T., et al. (2020a). Myosin-VIIa is expressed in multiple isoforms and essential for tensioning the hair cell mechanotransduction complex. *Nat. Commun.* 11, 2066. doi:10.1038/s41467-020-15936-z

Li, Y., Liu, H., Zhao, X., and He, D. Z. (2020b). Endolymphatic potential measured from developing and adult mouse inner ear. *Front. Cell Neurosci.* 14, 584928. doi:10.3389/fncel.2020.584928

Lin, T., Greenberg, M. J., Moore, J. R., and Ostap, E. M. (2011). A hearing loss-associated myo1c mutation (R156W) decreases the myosin duty ratio and force sensitivity. *Biochemistry* 50, 1831–1838. doi:10.1021/bi1016777

Liu, H., Li, J., Raval, M. H., Yao, N., Deng, X., Lu, Q., et al. (2016). Myosin III-mediated cross-linking and stimulation of actin bundling activity of Espin. *Elife* 5, e12856. doi:10.7554/eLife.12856

Liu, R., Billington, N., Yang, Y., Bond, C., Hong, A., Siththanandan, V., et al. (2021). A binding protein regulates myosin-7a dimerization and actin bundle assembly. *Nat. Commun.* 12, 563. doi:10.1038/s41467-020-20864-z

Liu, X. Z., Walsh, J., Mburu, P., Kendrick-Jones, J., Cope, M. J., Steel, K. P., et al. (1997). Mutations in the myosin VIIA gene cause non-syndromic recessive deafness. *Nat. Genet.* 16, 188–190. doi:10.1038/ng0697-188

Lowey, S., Saraswat, L. D., Liu, H., Volkmann, N., and Hanein, D. (2007). Evidence for an interaction between the SH3 domain and the N-terminal extension of the essential light chain in class II myosins. *J. Mol. Biol.* 371, 902–913. doi:10.1016/j.jmb.2007.05.080

Manor, U., Disanza, A., Grati, M., Andrade, A., Lin, H., Di Fiore, P. P., et al. (2011). Regulation of stereocilia length by myosin XVa and whirlin depends on the actin-regulatory protein Eps8. *Curr Biol.* 21 (2), 167–172. doi:10.1016/j.cub.2010.12.046

Mcpherson, D. R. (2018). Sensory hair cells: an introduction to structure and Physiology. *Integr. Comp. Biol.* 58, 282–300. doi:10.1093/icb/icy064

Mehta, A. D., Rock, R. S., Rief, M., Spudich, J. A., Mooseker, M. S., and Cheney, R. E. (1999). Myosin-V is a processive actin-based motor. *Nature* 400, 590–593. doi:10.1038/23072

Melchionda, S., Ahituv, N., Bisceglia, L., Sobe, T., Glaser, F., Rabionet, R., et al. (2001). MYO6, the human homologue of the gene responsible for deafness in Snell's waltzer mice, is mutated in autosomal dominant nonsyndromic hearing loss. *Am. J. Hum. Genet.* 69, 635–640. doi:10.1086/323156

Mermall, V., Post, P. L., and Mooseker, M. S. (1998). Unconventional myosins in cell movement, membrane traffic, and signal transduction. *Science* 279, 527–533. doi:10.1126/science.279.5350.527

Merritt, R. C., Manor, U., Salles, F. T., Grati, M., Dose, A. C., Unrath, W. C., et al. (2012). Myosin IIIB uses an actin-binding motif in its espin-1 cargo to reach the tips of actin protrusions. *Curr. Biol.* 22, 320–325. doi:10.1016/j.cub.2011.12.053

Mhatre, A. N., Li, Y., Bhatia, N., Wang, K. H., Atkin, G., and Lalwani, A. K. (2007). Generation and characterization of mice with Myh9 deficiency. *Neuromolecular Med.* 9, 205–215. doi:10.1007/s12017-007-8008-8

Minozzo, F., and Rassier, D. E. (2013). "Myosin family classification," in *Encyclopedia of biophysics*. Editor G. C. K. Roberts (Berlin, Heidelberg: Springer Berlin Heidelberg), 1658–1663.

Mogensen, M. M., Rzadzinska, A., and Steel, K. P. (2007). The deaf mouse mutant whirler suggests a role for whirlin in actin filament dynamics and stereocilia development. *Cell Motil. Cytoskelet.* 64, 496–508. doi:10.1002/cm.20199

Moreland, Z. G., and Bird, J. E. (2022). Myosin motors in sensory hair bundle assembly. *Curr. Opin. Cell Biol.* 79, 102132. doi:10.1016/j.ceb.2022.102132

Moreland, Z. G., Jiang, F., Aguilar, C., Barzik, M., Gong, R., Shams, A., et al. (2021). Myosin-driven nucleation of actin filaments drives stereocilia development critical for hearing. bioRxiv, 451618.

Morgan, C. P., Krey, J. F., Grati, M., Zhao, B., Fallen, S., Kannan-Sundhari, A., et al. (2016). PDZD7-MYO7A complex identified in enriched stereocilia membranes. *Elife* 5, e18312. doi:10.7554/eLife.18312

Morris, C. A., Wells, A. L., Yang, Z., Chen, L. Q., Baldacchino, C. V., and Sweeney, H. L. (2003). Calcium functionally uncouples the heads of myosin VI. *J. Biol. Chem.* 278, 23324–23330. doi:10.1074/jbc.M208957200

Mukherjea, M., Llinas, P., Kim, H., Travaglia, M., Safer, D., Menetrey, J., et al. (2009). Myosin VI dimerization triggers an unfolding of a three-helix bundle in order to extend its reach. *Mol. Cell* 35, 305–315. doi:10.1016/j.molcel.2009.07.010

Naz, S., Giguere, C. M., Kohrman, D. C., Mitchem, K. L., Riazuddin, S., Morell, R. J., et al. (2002). Mutations in a novel gene, TMIE, are associated with hearing loss linked to the DFNB6 locus. *Am. J. Hum. Genet.* 71, 632–636. doi:10.1086/342193

Niu, F., Li, L., Wang, L., Xiao, J., Xu, S., Liu, Y., et al. (2024). Autoinhibition and activation of myosin VI revealed by its cryo-EM structure. *Nat. Commun.* 15, 1187. doi:10.1038/s41467-024-45424-7

O'connell, C. B., Tyska, M. J., and Mooseker, M. S. (2007). Myosin at work: motor adaptations for a variety of cellular functions. *Biochim. Biophys. Acta* 1773, 615–630. doi:10.1016/j.bbamcr.2006.06.012

Ostap, E. M., and Pollard, T. D. (1996). Biochemical kinetic characterization of the Acanthamoeba myosin-I ATPase. *J. Cell Biol.* 132, 1053–1060. doi:10.1083/jcb.132.6.1053

Patton, J., Brewer, C., Chien, W., Johnston, J. J., Griffith, A. J., and Biesecker, L. G. (2016). A genotypic ascertainment approach to refute the association of MYO1A variants with non-syndromic deafness. *Eur. J. Hum. Genet.* 25, 147–149. doi:10.1038/ejhg.2016.140

Peckham, M. (2011). Coiled coils and SAH domains in cytoskeletal molecular motors. *Biochem. Soc. Trans.* 39, 1142–1148. doi:10.1042/BST0391142

Phichith, D., Travaglia, M., Yang, Z., Liu, X., Zong, A. B., Safer, D., et al. (2009). Cargo binding induces dimerization of myosin VI. *Proc. Natl. Acad. Sci. U. S. A.* 106, 17320–17324. doi:10.1073/pnas.0909748106

Pollard, L. W., and Lord, M. (2014). Getting myosin-V on the right track: tropomyosin sorts transport in yeast. *Bioarchitecture* 4, 35–38. doi:10.4161/bioa.28204

Pollard, T. D., and Korn, E. D. (1973). Acanthamoeba myosin. *J. Biol. Chem.* 248, 4682–4690. doi:10.1016/s0021-9258(19)43718-6

Preller, M., and Manstein, D. J. (2013). Myosin structure, allostery, and mechano-chemistry. *Structure* 21, 1911–1922. doi:10.1016/j.str.2013.09.015

Preller, M., and Manstein, D. J. (2017). "Myosin motors: structural aspects and functionality," in *Reference module in life sciences* (Amsterdam, Netherlands: Elsevier).

Purves, D. (2018). *Neuroscience*. New York: Oxford University Press.

Quintero, O. A., Moore, J. E., Unrath, W. C., Manor, U., Salles, F. T., Grati, M., et al. (2010). Intermolecular autophosphorylation regulates myosin IIIa activity and localization in parallel actin bundles. *J. Biol. Chem.* 285, 35770–35782. doi:10.1074/jbc.M110.144360

Quintero, O. A., Unrath, W. C., Stevens, S. M., Jr., Manor, U., Kachar, B., and Yengo, C. M. (2013). Myosin 3A kinase activity is regulated by phosphorylation of the kinase domain activation loop. *J. Biol. Chem.* 288, 37126–37137. doi:10.1074/jbc.M113.511014

Ranum, P. T., Goodwin, A. T., Yoshimura, H., Kolbe, D. L., Walls, W. D., Koh, J. Y., et al. (2019). Insights into the biology of hearing and deafness revealed by single-cell RNA sequencing. *Cell Rep.* 26, 3160–3171. doi:10.1016/j.celrep.2019.02.053

Raval, M. H., Quintero, O. A., Weck, M. L., Unrath, W. C., Gallagher, J. W., Cui, R., et al. (2016). Impact of the motor and tail domains of class III myosins on regulating the formation and elongation of actin protrusions. *J. Biol. Chem.* 291, 22781–22792. doi:10.1074/jbc.M116.733741

Rayment, I., Rypniewski, W. R., Schmidt-Base, K., Smith, R., Tomchick, D. R., Benning, M. M., et al. (1993). Three-dimensional structure of myosin subfragment-1: a molecular motor. *Science* 261, 50–58. doi:10.1126/science.8316857

Rayment, I., Smith, C., and Yount, R. G. (1996). The active site of myosin. *Annu. Rev. Physiol.* 58, 671–702. doi:10.1146/annurev.ph.58.030196.003323

Rehman, A. U., Bird, J. E., Faridi, R., Shahzad, M., Shah, S., Lee, K., et al. (2016). Mutational spectrum of MYO15A and the molecular mechanisms of DFNB3 human deafness. *Hum. Mutat.* 37, 991–1003. doi:10.1002/humu.23042

Riazuddin, S., Belyantseva, I. A., Giese, A. P., Lee, K., Indzhykulian, A. A., Nandamuri, S. P., et al. (2012). Alterations of the CIB2 calcium- and integrin-binding protein cause Usher syndrome type 1J and nonsyndromic deafness DFNB48. *Nat. Genet.* 44, 1265–1271. doi:10.1038/ng.2426

Riazuddin, S., Nazli, S., Ahmed, Z. M., Yang, Y., Zulfiqar, F., Shaikh, R. S., et al. (2008). Mutation spectrum of MYO7A and evaluation of a novel nonsyndromic deafness DFNB2 allele with residual function. *Hum. Mutat.* 29, 502–511. doi:10.1002/humu.20677

Rzadzinska, A. K., Nevalainen, E. M., Prosser, H. M., Lappalainen, P., and Steel, K. P. (2009). MyosinVIIa interacts with Twinfilin-2 at the tips of mechanosensory stereocilia in the inner ear. *PLoS One* 4, e7097. doi:10.1371/journal.pone.0007097

Sakaguchi, H., Tokita, J., Naoz, M., Bowen-Pope, D., Gov, N. S., and Kachar, B. (2008). Dynamic compartmentalization of protein tyrosine phosphatase receptor Q at the proximal end of stereocilia: implication of myosin VI-based transport. *Cell Motil. Cytoskelet.* 65, 528–538. doi:10.1002/cm.20275

Sakai, T., Umeki, N., Ikebe, R., and Ikebe, M. (2011). Cargo binding activates myosin VIIA motor function in cells. *Proc. Natl. Acad. Sci. U. S. A.* 108, 7028–7033. doi:10.1073/pnas.1009188108

Sakamoto, T., Yildez, A., Selvin, P. R., and Sellers, J. R. (2005). Step-size is determined by neck length in myosin V. *Biochemistry* 44, 16203–16210. doi:10.1021/bi0512086

Salles, F. T., Merritt, R. C., Jr., Manor, U., Dougherty, G. W., Sousa, A. D., Moore, J. E., et al. (2009). Myosin IIIa boosts elongation of stereocilia by transporting espin 1 to the plus ends of actin filaments. *Nat. Cell Biol.* 11, 443–450. doi:10.1038/ncb1851

Saposnik, B., Binard, S., Fenneteau, O., Nurden, A., Nurden, P., Hurtaud-Roux, M. F., et al. (2014). Mutation spectrum and genotype-phenotype correlations in a large French cohort of MYH9-Related Disorders. *Mol. Genet. Genomic Med.* 2, 297–312. doi:10.1002/mgg3.68

Sato, O., Komatsu, S., Sakai, T., Tsukasaki, Y., Tanaka, R., Mizutani, T., et al. (2017). Human myosin VIIa is a very slow processive motor protein on various cellular actin structures. *J. Biol. Chem.* 292, 10950–10960. doi:10.1074/jbc.M116.765966

Scheffer, D. I., Zhang, D. S., Shen, J., Indzhykulian, A., Karavitaki, K. D., Xu, Y. J., et al. (2015). XIRP2, an actin-binding protein essential for inner ear hair-cell stereocilia. *Cell Rep.* 10, 1811–1818. doi:10.1016/j.celrep.2015.02.042

Schultz, J. M., Bhatti, R., Madeo, A. C., Turriff, A., Muskett, J. A., Zalewski, C. K., et al. (2011). Allelic hierarchy of CDH23 mutations causing non-syndromic deafness DFNB12 or Usher syndrome USH1D in compound heterozygotes. *J. Med. Genet.* 48, 767–775. doi:10.1136/jmedgenet-2011-100262

Schwander, M., Kachar, B., and Muller, U. (2010). Review series: the cell biology of hearing. *J. Cell Biol.* 190, 9–20. doi:10.1083/jcb.201001138

Sekerkova, G., Richter, C. P., and Bartles, J. R. (2011). Roles of the espin actin-bundling proteins in the morphogenesis and stabilization of hair cell stereocilia revealed in CBA/CaJ congenic jerker mice. *PLoS Genet.* 7, e1002032. doi:10.1371/journal.pgen.1002032

Seki, Y., Shitara, H., Ishii, R., Ouchi, T., Yasuda, S. P., and Kikkawa, Y. (2021). Myosin VI haploinsufficiency reduced hearing ability in mice. *Neuroscience* 478, 100–111. doi:10.1016/j.neuroscience.2021.09.023

Self, T., Mahony, M., Fleming, J., Walsh, J., Brown, S. D., and Steel, K. P. (1998). Shaker-1 mutations reveal roles for myosin VIIA in both development and function of cochlear hair cells. *Development* 125, 557–566. doi:10.1242/dev.125.4.557

Self, T., Sobe, T., Copeland, N. G., Jenkins, N. A., Avraham, K. B., and Steel, K. P. (1999). Role of myosin VI in the differentiation of cochlear hair cells. *Dev. Biol.* 214, 331–341. doi:10.1006/dbio.1999.9424

Sellers, J. R. (2000). Myosins: a diverse superfamily. *Biochim. Biophys. Acta* 1496, 3–22. doi:10.1016/s0167-4889(00)00005-7

Shang, G., Brautigam, C. A., Chen, R., Lu, D., Torres-Vazquez, J., and Zhang, X. (2017). Structure analyses reveal a regulated oligomerization mechanism of the PlexinD1/GIPC/myosin VI complex. *Elife* 6, e27322. doi:10.7554/eLife.27322

Shin, C., Feng, Y., and Manley, J. L. (2004). Dephosphorylated SRp38 acts as a splicing repressor in response to heat shock. *Nature* 427, 553–558. doi:10.1038/nature02288

Shin, J. B., Longo-Guess, C. M., Gagnon, L. H., Saylor, K. W., Dumont, R. A., Spinelli, K. J., et al. (2010). The R109H variant of fascin-2, a developmentally regulated actin crosslinker in hair-cell stereocilia, underlies early-onset hearing loss of DBA/2J mice. *J. Neurosci.* 30, 9683–9694. doi:10.1523/JNEUROSCI.1541-10.2010

Simm, D., Hatje, K., and Kollmar, M. (2017). Distribution and evolution of stable single α-helices (SAH domains) in myosin motor proteins. *PLoS One* 12, e0174639. doi:10.1371/journal.pone.0174639

Solanki, A. K., Biswal, M. R., Walterhouse, S., Martin, R., Kondkar, A. A., Knolker, H. J., et al. (2021). Loss of motor protein MYO1C causes rhodopsin mislocalization and results in impaired visual function. *Cells* 10, 1322. doi:10.3390/cells10061322

Spink, B. J., Sivaramakrishnan, S., Lipfert, J., Doniach, S., and Spudich, J. A. (2008). Long single alpha-helical tail domains bridge the gap between structure and function of myosin VI. *Nat. Struct. Mol. Biol.* 15, 591–597. doi:10.1038/nsmb.1429

Spudich, G., Chibalina, M. V., Au, J. S., Arden, S. D., Buss, F., and Kendrick-Jones, J. (2007). Myosin VI targeting to clathrin-coated structures and dimerization is mediated by binding to Disabled-2 and PtdIns(4,5)P2. *Nat. Cell Biol.* 9, 176–183. doi:10.1038/ncb1531

Stauffer, E. A., Scarborough, J. D., Hirono, M., Miller, E. D., Shah, K., Mercer, J. A., et al. (2005). Fast adaptation in vestibular hair cells requires myosin-1c activity. *Neuron* 47, 541–553. doi:10.1016/j.neuron.2005.07.024

Sweeney, H. L., and Holzbaur, E. L. F. (2018). Motor proteins. *Cold Spring Harb. Perspect. Biol.* 10, a021931. doi:10.1101/cshperspect.a021931

Sweeney, H. L., and Houdusse, A. (2010). Structural and functional insights into the Myosin motor mechanism. *Annu. Rev. Biophys.* 39, 539–557. doi:10.1146/annurev.biophys.050708.133751

Tadenev, A. L. D., Akturk, A., Devanney, N., Mathur, P. D., Clark, A. M., Yang, J., et al. (2019). GPSM2-GNAI specifies the tallest stereocilia and defines hair bundle row identity. *Curr. Biol.* 29, 921–934. doi:10.1016/j.cub.2019.01.051

Taft, M. H., and Latham, S. L. (2020). "Myosin XVIII," in *Myosins: a superfamily of molecular motors*. Editor L. M. Coluccio (Cham: Springer International Publishing), 421–438.

Takagi, Y., Farrow, R. E., Billington, N., Nagy, A., Batters, C., Yang, Y., et al. (2014). Myosin-10 produces its power-stroke in two phases and moves processively along a single actin filament under low load. *Proc. Natl. Acad. Sci. U. S. A.* 111, E1833–E1842. doi:10.1073/pnas.1320122111

Tamagawa, Y., Ishikawa, K., Ishikawa, K., Ishida, T., Kitamura, K., Makino, S., et al. (2002). Phenotype of DFNA11: a nonsyndromic hearing loss caused by a myosin VIIA mutation. *Laryngoscope* 112, 292–297. doi:10.1097/00005537-200202000-00017

Thirumurugan, K., Sakamoto, T., Hammer, J. A., 3rd, Sellers, J. R., and Knight, P. J. (2006). The cargo-binding domain regulates structure and activity of myosin 5. *Nature* 442, 212–215. doi:10.1038/nature04865

Trouillet, A., Miller, K. K., George, S. S., Wang, P., Ali, N. E., Ricci, A., et al. (2021). Loxhd1 mutations cause mechanotransduction defects in cochlear hair cells. *J. Neurosci.* 41, 3331–3343. doi:10.1523/JNEUROSCI.0975-20.2021

Tyska, M. J., Mackey, A. T., Huang, J. D., Copeland, N. G., Jenkins, N. A., and Mooseker, M. S. (2005). Myosin-1a is critical for normal brush border structure and composition. *Mol. Biol. Cell* 16, 2443–2457. doi:10.1091/mbc.e04-12-1116

Udovichenko, I. P., Gibbs, D., and Williams, D. S. (2002). Actin-based motor properties of native myosin VIIa. *J. Cell Sci.* 115, 445–450. doi:10.1242/jcs.115.2.445

Umeki, N., Jung, H. S., Watanabe, S., Sakai, T., Li, X. D., Ikebe, R., et al. (2009). The tail binds to the head-neck domain, inhibiting ATPase activity of myosin VIIA. *Proc. Natl. Acad. Sci. U. S. A.* 106, 8483–8488. doi:10.1073/pnas.0812930106

Verpy, E., Leibovici, M., Zwaenepoel, I., Liu, X. Z., Gal, A., Salem, N., et al. (2000). A defect in harmonin, a PDZ domain-containing protein expressed in the inner ear sensory hair cells, underlies Usher syndrome type 1C. *Nat. Genet.* 26, 51–55. doi:10.1038/79171

Vicente-Manzanares, M., Ma, X., Adelstein, R. S., and Horwitz, A. R. (2009). Non-muscle myosin II takes centre stage in cell adhesion and migration. *Nat. Rev. Mol. Cell Biol.* 10, 778–790. doi:10.1038/nrm2786

Walavalkar, K., and Notani, D. (2020). Beyond the coding genome: non-coding mutations and cancer. *Front. Biosci. (Landmark Ed.)* 25, 1828–1838. doi:10.2741/4879

Walsh, T., Walsh, V., Vreugde, S., Hertzano, R., Shahin, H., Haika, S., et al. (2002). From flies' eyes to our ears: mutations in a human class III myosin cause progressive nonsyndromic hearing loss DFNB30. *Proc. Natl. Acad. Sci. U. S. A.* 99, 7518–7523. doi:10.1073/pnas.102091699

Wang, A., Liang, Y., Fridell, R. A., Probst, F. J., Wilcox, E. R., Touchman, J. W., et al. (1998). Association of unconventional myosin MYO15 mutations with human nonsyndromic deafness DFNB3. *Science* 280, 1447–1451. doi:10.1126/science.280.5368.1447

Wang, F., Harvey, E. V., Conti, M. A., Wei, D., and Sellers, J. R. (2000). A conserved negatively charged amino acid modulates function in human nonmuscle myosin IIA. *Biochemistry* 39, 5555–5560. doi:10.1021/bi000133x

Wangemann, P. (2006). Supporting sensory transduction: cochlear fluid homeostasis and the endocochlear potential. *J. Physiol.* 576, 11–21. doi:10.1113/jphysiol.2006.112888

Watanabe, S., Ikebe, R., and Ikebe, M. (2006). Drosophila myosin VIIA is a high duty ratio motor with a unique kinetic mechanism. *J. Biol. Chem.* 281, 7151–7160. doi:10.1074/jbc.M511592200

Weil, D., Blanchard, S., Kaplan, J., Guilford, P., Gibson, F., Walsh, J., et al. (1995). Defective myosin VIIA gene responsible for Usher syndrome type 1B. *Nature* 374, 60–61. doi:10.1038/374060a0

Weil, D., El-Amraoui, A., Masmoudi, S., Mustapha, M., Kikkawa, Y., Laine, S., et al. (2003). Usher syndrome type I G (USH1G) is caused by mutations in the gene encoding SANS, a protein that associates with the USH1C protein, harmonin. *Hum. Mol. Genet.* 12, 463–471. doi:10.1093/hmg/ddg051

Weil, D., Kussel, P., Blanchard, S., Levy, G., Levi-Acobas, F., Drira, M., et al. (1997). The autosomal recessive isolated deafness, DFNB2, and the Usher 1B syndrome are allelic defects of the myosin-VIIA gene. *Nat. Genet.* 16, 191–193. doi:10.1038/ng0697-191

Wells, A. L., Lin, A. W., Chen, L. Q., Safer, D., Cain, S. M., Hasson, T., et al. (1999). Myosin VI is an actin-based motor that moves backwards. *Nature* 401, 505–508. doi:10.1038/46835

Yamamoto, N., Okano, T., Ma, X., Adelstein, R.S., and Kelley, M.W. (2009). Myosin II regulates extension, growth and patterning in the mammalian cochlear duct. *Development* 136, 1977–1986. doi:10.1242/dev.030718

Yengo, C. M., Takagi, Y., and Sellers, J. R. (2012). Temperature dependent measurements reveal similarities between muscle and non-muscle myosin motility. *J. Muscle Res. Cell Motil.* 33, 385–394. doi:10.1007/s10974-012-9316-7

Yount, R. G., Lawson, D., and Rayment, I. (1995). Is myosin a "back door" enzyme? *Biophys. J.* 68, 44S–49S.

Yu, C., Feng, W., Wei, Z., Miyanoiri, Y., Wen, W., Zhao, Y., et al. (2009). Myosin VI undergoes cargo-mediated dimerization. *Cell* 138, 537–548. doi:10.1016/j.cell.2009.05.030

Zadro, C., Alemanno, M. S., Bellacchio, E., Ficarella, R., Donaudy, F., Melchionda, S., et al. (2009). Are MYO1C and MYO1F associated with hearing loss? *Biochim. Biophys. Acta* 1792, 27–32. doi:10.1016/j.bbadis.2008.10.017

Zampini, V., Ruttiger, L., Johnson, S. L., Franz, C., Furness, D. N., Waldhaus, J., et al. (2011). Eps8 regulates hair bundle length and functional maturation of mammalian auditory hair cells. *PLoS Biol.* 9, e1001048. doi:10.1371/journal.pbio.1001048

Zhang, F., and Lupski, J. R. (2015). Non-coding genetic variants in human disease. *Hum. Mol. Genet.* 24, R102–R110. doi:10.1093/hmg/ddv259

Zhang, Y., Conti, M. A., Malide, D., Dong, F., Wang, A., Shmist, Y. A., et al. (2012). Mouse models of MYH9-related disease: mutations in nonmuscle myosin II-A. *Blood* 119, 238–250. doi:10.1182/blood-2011-06-358853

Zhao, B., Wu, Z., Grillet, N., Yan, L., Xiong, W., Harkins-Perry, S., et al. (2014). TMIE is an essential component of the mechanotransduction machinery of cochlear hair cells. *Neuron* 84, 954–967. doi:10.1016/j.neuron.2014.10.041

Zhao, H., Pykäläinen, A., and Lappalainen, P. (2011). I-BAR domain proteins: linking actin and plasma membrane dynamics. *Curr. Opin. Cell Biol.* 23, 14–21. doi:10.1016/j.ceb.2010.10.005

Zheng, L., Sekerková, G., Vranich, K., Tilney, L. G., Mugnaini, E., and Bartles, J. R. (2000). The deaf jerker mouse has a mutation in the gene encoding the espin actin-bundling proteins of hair cell stereocilia and lacks espins. *Cell* 102, 377–385. doi:10.1016/s0092-8674(00)00042-8

Zina, Z. B., Masmoudi, S., Ayadi, H., Chaker, F., Ghorbel, A. M., Drira, M., et al. (2001). From DFNB2 to Usher syndrome: variable expressivity of the same disease. *Am. J. Med. Genet.* 101, 181–183. doi:10.1002/ajmg.1335

frontiers | Frontiers in Physiology

TYPE Original Research
PUBLISHED 28 March 2024
DOI 10.3389/fphys.2024.1394040

OPEN ACCESS

EDITED BY
Maria Jolanta Redowicz,
Polish Academy of Sciences, Poland

REVIEWED BY
William Lehman,
Boston University, United States
Mate Gyimesi,
Eötvös Loránd University, Hungary

*CORRESPONDENCE
András Kengyel,
andras.kengyel@aok.pte.hu
Dietmar J. Manstein,
manstein.dietmar@mh-hannover.de

†These authors have contributed equally to this work and share first authorship

RECEIVED 29 February 2024
ACCEPTED 20 March 2024
PUBLISHED 28 March 2024

CITATION
Kengyel A, Palarz PM, Krohn J, Marquardt A, Greve JN, Heiringhoff R, Jörns A and Manstein DJ (2024), Motor properties of Myosin 5c are modulated by tropomyosin isoforms and inhibited by pentabromopseudilin.
Front. Physiol. 15:1394040.
doi: 10.3389/fphys.2024.1394040

Motor properties of Myosin 5c are modulated by tropomyosin isoforms and inhibited by pentabromopseudilin

András Kengyel[1,2*†], Philip M. Palarz[1†], Jacqueline Krohn[1], Anja Marquardt[1], Johannes N. Greve[1], Robin Heiringhoff[1], Anne Jörns[3] and Dietmar J. Manstein[1*]

[1]Institute for Biophysical Chemistry, Hannover Medical School, Hannover, Germany, [2]Department of Biophysics, University of Pécs Medical School, Pécs, Hungary, [3]Institute of Clinical Biochemistry, Hannover Medical School, Hannover, Germany

Myosin 5c (Myo5c) is a motor protein that is produced in epithelial and glandular tissues, where it plays an important role in secretory processes. Myo5c is composed of two heavy chains, each containing a generic motor domain, an elongated neck domain consisting of a single α–helix with six IQ motifs, each of which binds to a calmodulin (CaM) or a myosin light chain from the EF–hand protein family, a coiled–coil dimer–forming region and a carboxyl–terminal globular tail domain. Although Myo5c is a low duty cycle motor, when two or more Myo5c–heavy meromyosin (HMM) molecules are linked together, they move processively along actin filaments. We describe the purification and functional characterization of human Myo5c–HMM co–produced either with CaM alone or with CaM and the essential and regulatory light chains Myl6 and Myl12b. We describe the extent to which cofilaments of actin and Tpm1.6, Tpm1.8 or Tpm3.1 alter the maximum actin–activated ATPase and motile activity of the recombinant Myo5c constructs. The small allosteric effector pentabromopseudilin (PBP), which is predicted to bind in a groove close to the actin and nucleotide binding site with a calculated ΔG of −18.44 kcal/mol, inhibits the motor function of Myo5c with a half–maximal concentration of 280 nM. Using immunohistochemical staining, we determined the distribution and exact localization of Myo5c in endothelial and endocrine cells from rat and human tissue. Particular high levels of Myo5c were observed in insulin–producing β–cells located within the pancreatic islets of Langerhans.

KEYWORDS

Myosin 5c, tropomyosin, pentabromopseudilin, molecular docking, immunohistochemistry

Abbreviations: Myo5c, myosin 5c; PBP, pentabromopseudilin; CCD, coiled–coil doman; GTD, globular tail domain; CaM, calmodulin; RLC, regulatory light chain; ELC, essential light chain; Tpm, tropomyosin; MLCK, myosin light chain kinase.

Introduction

Class V myosins belong to one of the ancient groups of the myosin superfamily, whose presence is essential from yeast to humans (Richards and Cavalier–Smith, 2005). The main function of class V myosins is to transport different cargoes such as organelles, vesicles or mRNA (Krementsova et al., 2017; Dolce et al., 2020). Class V is one of the three myosin classes, that can dimerize through the coiled–coil domain, but unlike class II myosins, members of class V do not form filaments and function exclusively as dimeric motors (Baboolal et al., 2009; Peckham, 2011).

Three isoforms of myosin V have been identified in vertebrates, which are produced and localized in different tissues (Rodriguez and Cheney, 2002). Myo5a, the most extensively studied member of this class, is highly produced in melanocytes and neurons, fulfilling a critical role in the trafficking of membranous organelles, including melanosomes in skin melanocytes and endoplasmic reticulum in Purkinje neurons (Rodriguez and Cheney, 2002; Jacobs et al., 2009; Hammer and Sellers, 2012; Gunther et al., 2014). Mutations in Myo5a lead to Griscelli syndrome, a disease characterized by hypopigmentation and neurological deficits (Rodriguez and Cheney, 2002; Gele et al., 2009; Dolce et al., 2020). Myo5b is produced in various tissues, where it functions in the recycling and transport of cytoplasmic vesicles and numerous receptors, such as the transferrin receptor or CXCR2 chemokine receptor (Takagi et al., 2008; Jacobs et al., 2009; Gunther et al., 2014). Additionally, Myo5b is produced in the intestine and its loss has been linked to microvillus atrophy and microvillus inclusion disease (Thoeni et al., 2014; Dolce et al., 2020). The third isoform of the myosin V class, myosin 5c, was discovered in 2002 through the analysis of the human EST (expressed sequence tags) database (Rodriguez and Cheney, 2002). Myo5c is widely distributed and most prominently produced in cells from intestinal and glandular tissues, including the colon, pancreas, mammary, thyroid, and different salivary glands. Myo5c is also present in various cell lines such as HeLa, HEK 293, Caco–2, or HUVEC, suggesting that Myo5c has a wide distribution among different cell types (Rodriguez and Cheney, 2002; Holthenrich et al., 2022). In endothelial cells Myo5c is involved in the transport and membrane fusion of Weibel–Palade bodies containing von Willebrand factor, an important hemostatic factor (Dolce et al., 2020; Holthenrich et al., 2022). Multi–ciliated cells possess a large number of motile cilia that beat in a coordinated and polarized manner. Myo5c was shown to control apical positioning of basal bodies in these cells that drive fluid flow in diverse tubular organs and are essential for the development and homeostasis of the vertebrate central nervous system, airway and reproductive tracts (Tu et al., 2017).

The three myosin V isoforms share a common four–domain structure. A generic motor domain binds actin in an ATP–dependent manner, an elongated neck domain providing binding sites for light chains and actin, a stiff lever arm, a coiled–coil domain (CCD) promoting the dimerization of two heavy chains, and a globular tail binding domain (GTD) that recognizes cargos or cargo adaptors (Reck–Peterson et al., 2000; Krementsov, Krementsova, and Trybus, 2004; Wang et al., 2004; Gunther et al., 2014). Adaptor proteins, such as small GTPases of the Rab family, interact with the GTD, thereby attaching class V myosins to their vesicular cargo (Zhang et al., 2018). The GTD of Myo5c interacts with Rab32, Rab38 or Rab3a resulting in attachment to secretory vesicles or melanosomes (Bultema et al., 2014; Dolce et al., 2020; Holthenrich et al., 2022).

Myo5a and Myo5b can adopt a triangular closed state structure with cargo binding and adenosine triphosphatase activity inhibited. The blocked ATPase activity and the cargo–/calcium–mediated activation of Myo5a and Myo5b is mediated through intra–and interpolypeptide chain interactions involving the motor domain, CCD and GTD of the heavy chain and CaM (Niu et al., 2022). Myo5c has an overall sequence identity of ~50% with Myo5a or Myo5b. Sequence identity is highest in the motor domain region, whereas it reaches only 20%–30% in the coiled–coil region. Moreover, it lacks the PEST domain that is present in the other isoforms (Rodriguez and Cheney, 2002; Takagi et al., 2008). A number of structural changes in the region connecting the lever arm region to the CCD suggest that Myo5c has a different hinge structure to Myo5a, which may affect how, or whether, it forms a triangular closed–state structure. Alterations include a shortened or degenerated IQ6, a missing hinge strand, and differences in the sequence linking the N–terminal portion of the CCD (Niu et al., 2022).

Kinetic analysis of Myo5c revealed significant differences compared to the other vertebrate myosin V members. Myo5c functions as a low duty ratio motor. The rate–limiting step is phosphate release (Takagi et al., 2008). Myo5c does not move processively on actin filaments and its average velocity is an order of magnitude lower than that of Myo5a or Myo5b (Takagi et al., 2008). The low duty ratio suggests that Myo5c may act as a cargo transporter in the context of ensembles only or perform other functions, such as tethering organelles or generating tension (Krendel and Mooseker, 2005; Takagi et al., 2008).

Myosin light chains are essential for the proper functioning of myosins. These light chains belong either to the CaM or CaM–related gene families and are associated with the IQ motif located in the neck region of the myosin. According to previous research, the standard view has been, that unconventional myosins bind CaM, while conventional myosins bind essential light chains (ELC) and regulatory light chains (RLC) (Heissler and Sellers, 2014). Recombinant production of functional unconventional myosins in cells that overproduce CaM has demonstrated that CaM is able to bind these myosin heavy chains. However, it remains to be shown that CaM is the only native light chain (Heissler and Sellers, 2014). Recombinant Myo5b and Myo5c were purified and produced in functional form with CaM alone (Takagi et al., 2008; Watanabe et al., 2008; Yao et al., 2016; Heissler et al., 2017). In recent years, a number of findings have lent support to the hypothesis that light chains other than CaM can bind to unconventional myosins and thereby influence their activity and stability. For example, in the case of myosin VII and myosin XV, the production of a stable holoenzyme is facilitated by the co–purification of the unconventional myosin heavy chains with light chains other than CaM (Bird et al., 2014; Holló et al., 2023). While Myo5a extracted from mouse brain was purified exclusively with CaM, Myo5a from chicken brain also contained co–purified ELC (Wang et al., 2000).

Tropomyosins (Tpm) are important actin binding proteins, that stabilize the actin filament upon binding and modulate the interaction of the filament with other actin binding proteins, e.g., with myosins (Gunning et al., 2005; Manstein et al., 2020). They are

important for a variety of actomyosin–dependent processes such as cell migration, cytokinesis, embryogenesis, and endo–or exocytosis (Curthoys et al., 2014; Kee et al., 2015; Wolfenson et al., 2016; Pathan–Chhatbar et al., 2018). The actin cofilaments with different Tpm isoforms were shown to modulate the motor properties of cytoskeletal myosins of classes I, II, and V. In addition, the N–terminal acetylation status of the Tpm isoforms was shown to contribute to the extent of modulation in an isoform–specific manner (Reindl et al., 2022). Tpm3.1 increases the sliding velocity of skeletal muscle myosin II on actin, whereas it has no effect on Myo5a (Barua et al., 2014; Barua et al., 2018). Tpm3.1 has also been shown to be involved in the regulation of organ size and cell proliferation in mice (Schevzov et al., 2015). The processive behavior of non–muscle Myo2a and Myo2b has been shown to be promoted by Tpm1.8 (Hundt et al., 2016; Pathan–Chhatbar et al., 2018). Tpm1.8 and Tpm3.1 lead to an increase in the ATPase activity of non–muscle Myo2b (Pathan–Chhatbar et al., 2018). Tpm1.6 was found in contractile stress fibers, where it is involved in their stabilization (Tojkander et al., 2011).

In this study, we show strong localization of Myo5c in human and rat pancreatic β–cells and in other glandular tissues. In addition, we report the purification and characterization of a heavy meromyosin (HMM) fragment of the Myo5c heavy chain that was either co–produced with CaM alone or with CaM, the ELC Myl6 and the RLC Myl12b. We describe the steady–state kinetics and motor function of the recombinant Myo5c constructs for the interaction with F–actin and selected cofilaments of actin with human cytoskeletal Tpm isoforms. In addition, the interaction of human Myo5c with PBP, a small allosteric effector of class V myosins, is described.

Materials and methods

Protein production and purification

The coding sequence of human Myo5c, which encodes the amino–acids 1–1108 (Uniprot–ID: Q9NQX4) (Myo5c–HMM) was fused to a C–terminal Flag affinity tag and cloned into the multiple cloning site of the pFastBac™ Dual expression vector under the control of the polyhedrin promotor (pFastBac–Myo5cHMM). pFastBac™ Dual vector containing CaM (Uniprot–ID: P0DP23) or the ELC and RLC (Myl6: Uniprot–ID: P60660 and Myl12b: Uniprot–ID: O14950) were prepared as described earlier (Reindl et al., 2022). Recombinant Myo5c–HMM was co–produced with CaM [Myo5c–HMM (CaM)] or with all three light chains: CaM, RLC and ELC [Myo5c–HMM (3LC)] in the baculovirus/*Sf9* system. Suspension cultures were harvested after 72 h and stored at −80°C.

For purification, cells were lysed in extraction buffer [10 mM MOPS–NaOH (pH 7.3), 200 mM NaCl, 15 mM $MgCl_2$, 1 mM EGTA, 0.25 mM EDTA, 5 mM ATP, 0.1 mM DTT, 0.1 mM PMSF, and protease inhibitor cocktail]. The lysate was clarified from cellular debris by centrifugation at 30,000 × *g* for 30 min, then anti–FLAG–M2 affinity resin (Sigma–Aldrich) was added to the supernatant and carefully rotated for 2 h at 4°C. The resin was collected and washed with HMM–buffer [10 mM MOPS–NaOH (pH 7.3), 5 mM $MgCl_2$, 0.1 mM EGTA, 0.1 mM DTT, 0.1 mM PMSF] completed with 500 mM NaCl and 2 mM ATP, then with low salt HMM–buffer containing 100 mM NaCl. Recombinant protein complex was eluted with 0.2 mg/mL FLAG peptide and dialyzed against HMM–buffer completed with 100 mM KCl and 1 mM DTT. The protein was used immediately or supplemented with 10% trehalose, flash–frozen in liquid nitrogen and stored at −80°C. Protein content of the final sample was proven by Western blot using Anti–Flag (F1804, Sigma–Aldrich), Anti–CaM (Abcam), Anti–Myl12b (sc–28329, Santa Cruz Biotechnology) and Anti–Myl6 (PA5–106803, Thermo Fisher Scientific) primer antibodies.

Human Tpm1.6 (NCBI Reference Sequence NP_001018004.1), Tpm1.8 (NCBI Reference Sequence NP_001288218.1) and Tpm3.1 (NCBI Reference Sequence NP_705935.1) were produced tag–free in *E. coli* strain Rosetta™ (Merck) (Pathan–Chhatbar et al., 2018; Reindl et al., 2022). After overproduction in *E. coli*, the lysate [containing 50 mM Hepes (pH 7.5), 200 mM NaCl, 5 mM $MgCl_2$, 5 mM DTT, 0.5 mg/mL lysozyme and protease inhibitor] were heated up to 80°C for 10 min and then cooled on ice. The soluble fraction was filtered, Tpm was precipitated at the appropriate pI, separated by centrifugation and resuspended in low salt buffer [20 mM Tris–HCl (pH 7.2), 100 mM NaCl, 5 mM $MgCl_2$] for anion exchange chromatography. The fractions containing Tpm was concentrated by precipitation. The protein was supplemented with 3% sucrose, flash–frozen in liquid nitrogen and stored at −80°C (Pathan–Chhatbar et al., 2018; Reindl et al., 2022). Human β–actin (Uniprot–ID: P60709) was produced in *Sf9* cells as described previously (Greve et al., 2024). α–skeletal actin (Uniprot–ID: P68139) was prepared from chicken pectoralis major muscle, as previously described for rabbit α–skeletal actin (Lehrer and Grace, 1972).

Steady–state ATPase

Steady–state kinetics were performed at 30°C with the NADH–coupled assay in a buffer containing 20 mM MOPS–NaOH (pH 7.3), 5 mM $MgCl_2$, 1 mM EGTA, 0.5 mg/mL phosphoenolpyruvate, 50 μg/mL pyruvate kinase, 20 μg/mL lactate dehydrogenase, 1 mM NADH, 2 mM ATP, 2 mM DTT. The myosin concentration was 0.15 μM. The RLC of Myo5c–HMM (3LC) was phosphorylated immediately prior to use at 25°C for 30 min 2 μM Myo5c–HMM (3LC) was incubated with recombinant human myosin light chain kinase (MLCK, Merck KGaA, Darmstadt, Germany) at a stoichiometric ratio of 20:1 in HMM–buffer containing 0.2 μM CaM, 1 mM $CaCl_2$, 1 mM ATP and 1 mM DTT. The ATPase rate was normalized to the Myo5c–HMM concentration and was plotted against the F–actin concentration. The F–actin concentration was varied between 0 and 40 μM. NADH oxidation was followed using the change in the absorption at 340 nm (ε = 6220 M^{-1} cm^{-1}) in a temperature–controlled plate reader (Multiskan FC, Thermo Fisher Scientific Inc. Waltham, MA, United States) using UV–transparent microtiter plates. The ATPase rate was normalized to the Myo5c–HMM concentration. The ATPase activity in the absence of F–actin was subtracted from the actin–activated data. ATPase rate pro motor domain was plotted against the F–actin concentration and nonlinear curve fitting was performed using Origin 2022b (OriginLab Corporation, Northampton, MA, United States) statistical program. The

parameters k_{cat}, $K_{app.actin}$, and $k_{cat}/K_{app.actin}$ were obtained by fitting the data to the Michaelis–Menten equation. $K_{0.5}$ defines $K_{app.actin}$, plateau values define k_{cat}, and $k_{cat}/K_{app.actin}$ is defined by the initial slope of the fit curve at concentrations of actin much lower than $K_{app.actin}$. To investigate the influence of Tpm, F–actin was preincubated with 1.3–fold molar excess of the different Tpm isoforms for 30 min at room temperature. To study the inhibition of Myo5c by PBP, Myo5c–HMM was preincubated for 20 min at room temperature with different concentrations of PBP (Agarwal and Knölker, 2004; Fedorov et al., 2009).

In vitro motility assay

In vitro motility assay using Atto550–phalloidin–labelled actin filaments and surface–immobilized Myo5c–HMM were performed as previously described with minor modifications (Reindl et al., 2022). Briefly, flow cells used in the *in vitro* motility assay were constructed using nitrocellulose–coated coverslips. 0.1 mg/mL Myo5c–HMM diluted in assay buffer [25 mM MOPS–NaOH (pH 7.4), 50 mM KCl, 5 mM $MgCl_2$, 10 mM DTT] was flushed into the flow cell. To prevent unspecific binding of actin to the coverslip surface, 0.5 mg/mL bovine serum albumin was flushed into the flow cell and incubated for 3 min. Next, 20 nM Atto550–phalloidin (Merck) labelled F–actin was added and incubated for 3 min. Motility was started by the addition of 4 mM ATP in assay buffer completed with 0.5% methylcellulose and an anti–photobleaching mix (5 mg/mL glucose, 100 µg/mL glucose–oxidase, 100 µg/mL catalase). Image series were recorded at an Olympus IX70 inverted fluorescence microscope (Olympus, Hamburg, Germany) equipped with a 60×/1.49 NA PlanApo oil immersion objective and an Orca Flash 4.0 CMOS camera (Hamamatsu Photonics Deutschland GmbH, Herrsching, Germany). At least three video sequences were recorded in each experiment. Sliding velocity and filament length distribution of at least 300 actin filaments were analyzed with FiJi software using the user modified wrMTrck plugin (Schindelin et al., 2012; Nussbaum–Krammer et al., 2015).

In silico modelling

A structural model of the motor domain of human Myo5c (Uniprot–ID: Q9NQX4) was generated with AlphaFold2 version 2.3.1, the fasta file was accessed on 1 November 2023 (Jumper et al., 2021). Different conformers and tautomers of PBP [2,3,4–tribromo–5–(3,5–dibromo–2–hydroxyphenyl)–1H–pyrrole] were generated with QM Conformer and Tautomer Predictor of Jaguar (Jaguar, Schrödinger, LLC, New York, NY, 2023). PBP was inserted, with Glide, into the model of human Myo5c (Glide, Schrödinger, LLC, New York, NY, 2023.). The glide grid was generated in accordance to the position of PBP in the structure of the motor domain of *Dictyostelium discoideum* myosin–2 (PDB–ID: 2JHR). The PDB–structure was accessed on 11 October 2023. Analysis of the structural models and visualization of the results was done with Maestro in the Schrödinger Suite 2023–4 (Maestro, Schrödinger, LLC, New York, NY, 2023). The structure was prepared with the Protein Preparation Workflow and the minimization was done with the Minimization tool of Maestro (Protein Preparation Wizard; Epik, Schrödinger, LLC, New York, NY, 2023) for 200 cycles with 80 steps per cycle in the VSGB solvate model (Li et al., 2011). ΔG was calculated with the Prime MM–GBSA v3.000 tool for the minimized structure (Prime, Schrödinger, LLC, New York, NY, 2023).

Immunohistochemistry

We used the following species–specific antibodies directed against epitopes in the Myo5c heavy chain. The rat polyclonal antibody PA5–65120 recognizes sequences in the C–terminal part of the coiled–coil forming region of the human Myo5c heavy chain. The rabbit polyclonal antibody PA5–103939 is directed against sequences of the rat Myo5c heavy chain that are thought to correspond to IQ6 and the adjacent hinge residues. Both antibodies were supplied by Thermo–Fisher®; they were used at a dilution of 1:400. The guinea pig polyclonal antibody IR00261–2 was obtained from Agilent Dako® and used at a dilution of 1:300. The antibody cross–reacts with high specificity with insulin from several mammalian species, including human and rat insulin. The mouse monoclonal antibody (F8/86): sc–53466, raised against von Willebrand factor protein (VWF) of human origin, was supplied by Santa Cruz Biotechnology, Inc.® and used at a dilution of 1:200. DAPI was used for nuclear counterstaining. Studies on the specificity of the primary antibodies were performed by omission of the primary or secondary antibodies labelled with different fluorescent dyes resulting in the loss of an immunostaining in the different sections. Tissue specimens were fixed in 4% paraformaldehyde in 0.15 mol/L PBS and embedded in paraffin. The human tissues of non–diabetic and type 1 diabetic subjects obtained by organ resection during surgical intervention or from organ donors have been approved by the responsible Pisa and Hannover ethics committees. Tissues of non–diabetic and diabetic rats from the human Type 1 diabetes animal model, the LEW.1AR1–iddm rat, bred in the Central Animal Facility of Hannover Medical School according to the principles of laboratory care have been approved by the Lower Saxony State Office (AZ: 2014/56).

Results

Myo5c colocalizes with insulin in pancreatic β–cells

Myo5c is abundant in the pancreas. Previous studies have shown that Myo5c appears in the exocrine part of the tissue, where it is localized to epithelial and endothelial cells (Rodriguez and Cheney, 2002; Holthenrich et al., 2022). In this study, we utilized tissue sections to investigate additional aspects of Myo5c localization. Immunostaining of human and rat pancreatic islets revealed Myo5c in insulin–producing beta cells, showing strong colocalization with insulin staining under normoglycemic and hyperglycemic conditions after autoimmune diabetes development (Figures 1A–L). In addition, strong Myo5c staining and strong colocalization with von Willebrand factor was observed

10.3389/fphys.2024.1394040

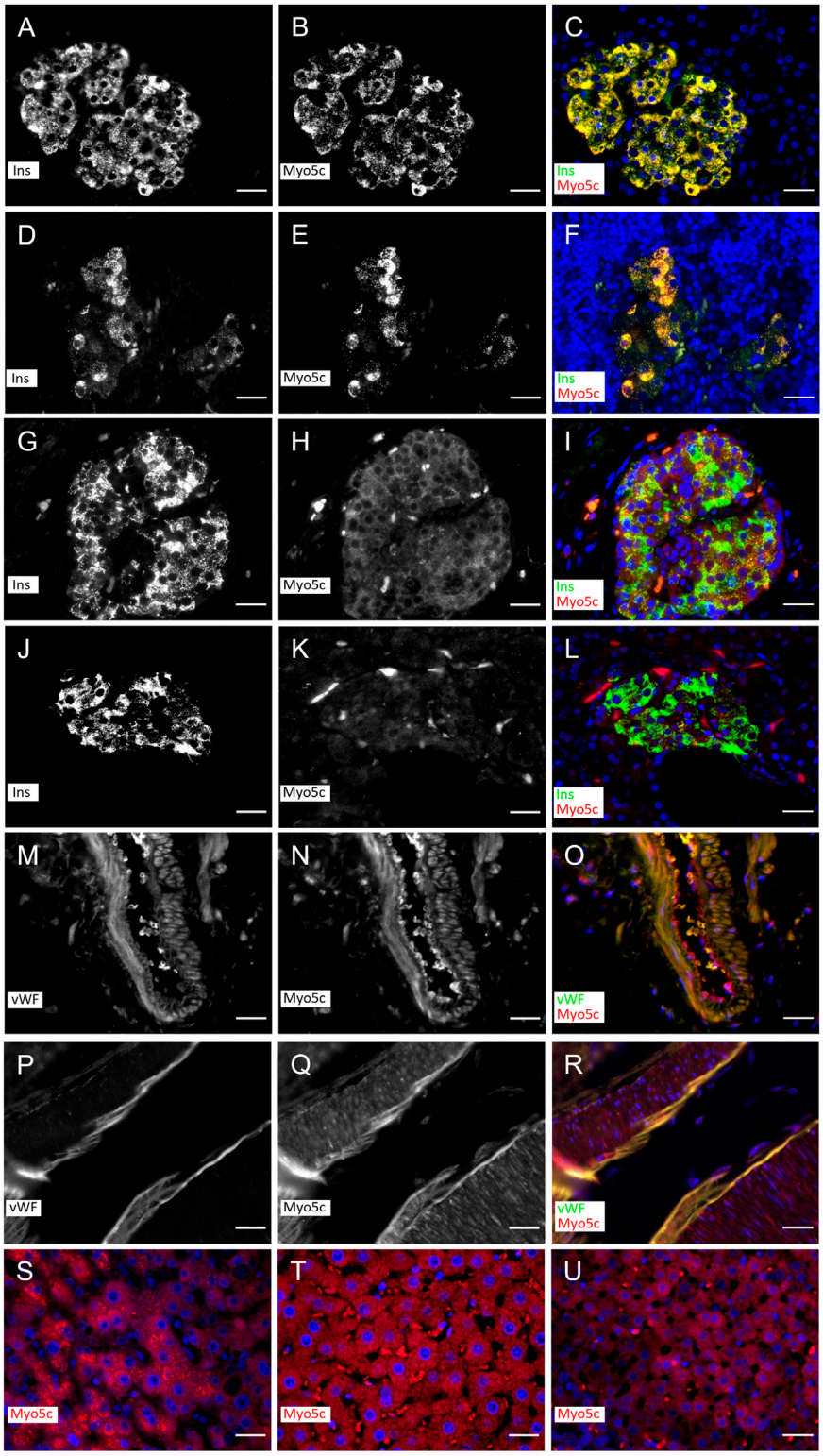

FIGURE 1
Myo5c immunostaining in β−cells in islets of rat **(A–F)** and human **(G–L)** under non−diabetic and diabetic conditions and endothelial cells of vessels of rat **(M–O)** and human **(P–R)**. Myo5c is colocalized with insulin (Ins) staining resulting in an orange−yellow overlay in the β−cells under non−diabetic **(A–C,G–I)** and diabetic **(D–F,J–L)** conditions. The endothelial layer of vessels shows a Myo5c expression in colocalization with the von Willebrand factor (vWF) **(M–O,P–R)**. A moderate protein expression of Myo5c is found also in hepatocytes of human **(S)** and rat **(T)** as well as in endocrine cells of the rat adrenal cortical region **(U)**. Nuclei are stained with DAPI. Scale Bar 25 μm.

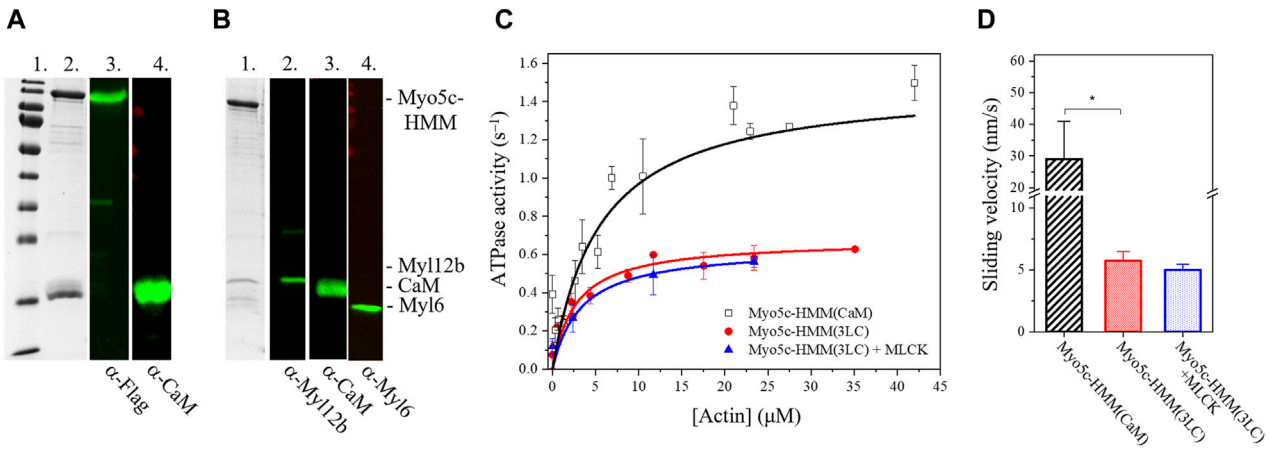

FIGURE 2
Myo5c–HMM co–produced with CaM, RLC, and ELC light chains has lower motor activity as co–produced with CaM only. **(A)** Purified Myo5c–HMM co–produced with CaM light chain. (*Lane 1*) MW marker. (*Lane 2*) Coomassie gel showing the result of purification via Flag affinity chromatography. Blot of Myo5c–HMM stained with (*Lane 3*) anti–Flag or (*Lane 4*) anti–CaM. Marker bands from highest to lowest (180, 130,100, 70, 55, 40, 35, 25, 15, 10 kDa). **(B)** Purified Myo5c–HMM co–produced with CaM, RLC, and ELC light chains. (*Lane 1*) Coomassie gel showing the result of purification via Flag affinity chromatography. Blot of Myo5c–HMM stained with (*Lane 2*) anti–Myl12b, (*Lane 3*) anti–CaM or (*Lane 4*) anti–Myl6. **(C)** Steady–state actin–activated ATPase activity of human Myo5c coproduced with CaM only (black squares) or with CaM, RLC and ELC (red circles) at various F–actin concentration ranging between 0 and 45 μM. RLC was phosphorylated by MLCK (blue triangles). **(D)** Average sliding velocity of actin over the Myo5c–HMM–coated surface, obtained from *in vitro* motility assay, was determined from at least 300 individual trajectories (mean ± SD). RLC was phosphorylated by MLCK. Asterisk marks significance $p < 0.01$.

in the endothelia of small to large pancreatic vessels in both species (Figures 1M–R). Moderate levels of Myo5c were found in human and rat hepatocytes and in the cortical region of rat adrenal glands (Figures 1S–U).

Myo5c binds RLC, ELC and CaM

The different human myosin V isoforms are commonly produced with CaM as a light chain in recombinant systems (Takagi et al., 2008; Heissler et al., 2017). We successfully produced and purified human Myo5c–HMM in the presence of CaM [Myo5c–HMM (CaM)], ~0.5 mg protein could be produced from 2 L *Sf9* cell pellet (Figure 2A). However, recent data suggests that unconventional myosins may use other possible light chains beside CaM, such as the RLCs, ELCs, or other calmodulin–like proteins (Bird et al., 2014; Holló et al., 2023). To investigate this, *Sf9* cells were coinfected with three baculovirus vectors containing the Myo5c–HMM heavy chain, CaM and the RLC/ELC (Myl12b/Myl6). Myo5c was successfully co–produced and co–purified with different light chains. Immunoblot analysis using antibodies against the different light chains demonstrated that CaM, RLC and also ELC was bound to the heavy chain (Figure 2B). The purification of Myo5c–HMM containing all three light chains [Myo5c–HMM (3LC)] from 2 L *Sf9* cell pellet resulted in ~0.5 mg protein, and less degradation was observed during and after the purification. Based on the Coomassie–stained gel, the binding ratio between the light chains and heavy chain supposed to be around 3:1 for RLC, 2:1 for CaM and 1:1 for ELC. Meanwhile, Myo5c–HMM binds six CaM, when coproduced with CaM only (Supplementary Figure S1).

Phosphorylation by MLCK has no effect on the motor function of Myo5c

RLC phosphorylation is a key regulatory mechanism of non–muscle myosin II isoforms (Garrido–Casadoet al., 2021). The motor domain is primarily activated by phosphorylation of Ser19 of the RLC by the calcium/CaM dependent MLCK. Phosphorylation enhances the ATPase activity ~25–fold (Sellers and Harvey, 1984; Vicente–Manzanares et al., 2009). In this study, we assessed whether RLC phosphorylation affects the ATPase activity of Myo5c. Before conducting the NADH–coupled ATPase assay, Myo5c–HMM was pre–incubated with MLCK and CaM for 20 min at 20°C in a Ca^{2+}–containing buffer. We observed no significant increase in ATPase activity, either in the basal or actin–activated state, suggesting that phosphorylation of Ser19 of the RLC has no effect on Myo5c–HMM activity. However, at 0.67 ± 0.01 s^{-1}, the k_{cat} measured for Myo5c–HMM (3LC) with or without phosphorylation is only about half the value measured for Myo5c–HMM (CaM) (Figure 2C).

An actin–activated ATPase activity alongside successful filament gliding confirms both the enzymatic capability and the motor function of myosin. ATPase activity indicates that myosin can bind and hydrolyze ATP, which is essential for its function as a motor protein. In addition, if performed in the presence of a range of actin concentrations, the assay provides information about the efficiency of coupling between the actin and nucleotide binding sites in the myosin motor domain. However, it doesn't necessarily prove that the motor can function correctly in terms of movement or force generation. The filament gliding assay confirms that the myosin can convert chemical energy (ATP) into mechanical work (movement) by utilizing actin as a track. Therefore, combining both assays gives a more complete assessment of

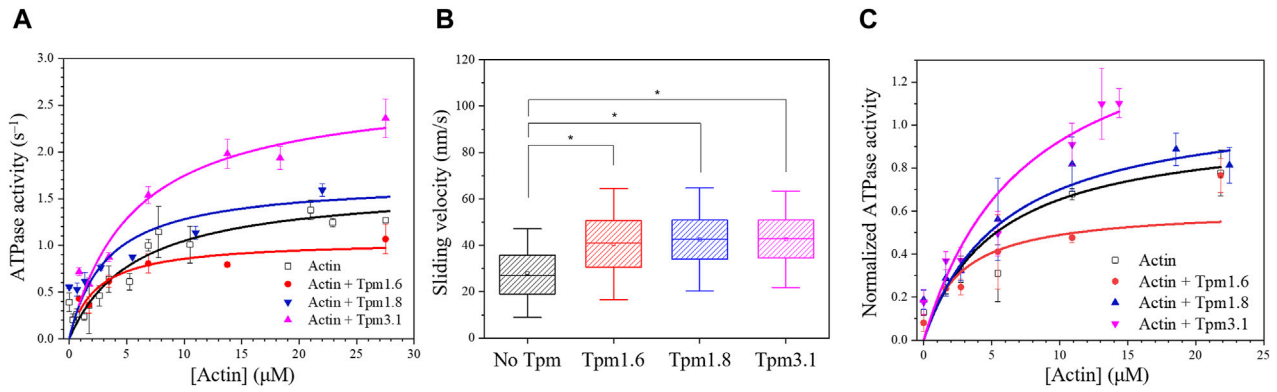

FIGURE 3
Tropomyosin isoforms affect the motor properties of Myo5c–HMM. **(A)** Steady-state actin-activated ATPase activity of human Myo5c–HMM (CaM) at various F-actin concentration ranging between 0 and 27 μM, in the presence of different Tpm isoforms. Tpm was added in a 1.3–fold molar excess, measurements were performed at 30°C (n = 2, mean ± SE). **(B)** Box chart showing the results of *in vitro* motility assay. Average sliding velocity of actin or actin–Tpm complex over the Myo5c-HMM (CaM)–coated surface was determined from at least 300 individual trajectories. 10 μM Tpm was added to all buffer solutions, assays were performed at 25°C. Box width shows percentile 25–75, whiskers represent ±SD. Asterisks mark significance $p < 0.01$. **(C)** Tpm isoforms have an impact on the motor function of Myo5c–HMM (3LC). Data were normalized to the k_{cat} of the actin–activated ATPase activity of Myo5c–HMM (3LC) in the absence of Tpm, measurements were performed at 30°C (n = 3, mean ± SE).

myosin motor function, providing complementary insights into their enzymatic activity and ability to generate force and movement.

To further test the motor function and the possible regulation of Myo5c, *in vitro* motility assay was performed, in which Myo5c–HMM was pre–phosphorylated by MLCK. The sliding velocity measured for Myo5c–HMM (3LC) was significantly lower than that of Myo5c–HMM (CaM). Phosphorylation by MLCK did not significantly change the sliding velocity of Myo5c–HMM, which is consistent with the results obtained from the ATPase assay (Figure 2D). These results indicate that phosphorylation by MLCK does not affect the motor function of Myo5c–HMM.

Tpm isoform has an impact on the motor function of Myo5c

Cytoskeletal tropomyosin isoforms play a crucial role in regulating myosin motor function (Pathan–Chhatbar et al., 2018; Reindl et al., 2022). In this study, we investigated the effect of Tpm3.1, 1.6 and 1.8 isoforms on the motor function of Myo5c–HMM (CaM) and Myo5c–HMM (3LC).

The steady–state actin–activated ATPase activity of Myo5c–HMM (CaM) was measured in the presence of either bare actin or Tpm–actin cofilaments (Figure 3A). The maximal rate of ATP hydrolysis (k_{cat}) was determined to correspond to 1.65 ± 0.14 s^{-1} in the absence of Tpm. $K_{app.actin}$, the substrate concentration required for half–maximal activity, which gives an approximation of the actin affinity of Myo5c in the presence of ATP, was found to be 5.7 ± 1.45 μM.

Measurements performed with actin–Tpm cofilaments revealed significant changes in k_{cat}, $K_{app.actin}$ or $k_{cat}/K_{app.actin}$. In the presence of Tpm3.1, we observed a 1.6–fold increase in k_{cat} from 1.65 ± 0.14 s^{-1} to 2.71 ± 0.28 s^{-1}. Cofilaments with Tpm1.6 gave a 35% reduction in k_{cat}, while cofilaments with Tpm1.8 gave a 43% reduction in K_{app} from 5.70 ± 1.45 μM to 3.24 ± 1.58 μM. The apparent second order rate constant ($k_{cat}/K_{app.actin}$), which represents the coupling efficiency between the actin and nucleotide binding sites, was increased approximately 1.5–fold for all three Tpm isoforms. The kinetic data are summarized in Table 1.

In vitro motility assays were performed to further investigate the effects of the Tpm isoforms on the motility of Myo5c. The *in vitro* sliding velocity of bare actin filaments was 29 ± 12 nm/s. The sliding velocity of fluorescently labeled and phalloidin–stabilized actin filaments on surfaces coated with Myo5c–HMM (CaM) was approximately 45% faster following preincubation of actin filaments with an excess of Tpm isoforms Tpm3.1, 1.6 or 1.8 (Figure 3B; Table 1).

The presence of Tpm1.6, 1.8 and 3.1 in cofilaments with actin induced distinct changes in Myo5c–HMM (3LC) motor function. Tpm3.1 increased the ATP turnover of Myo5c–HMM (3LC) by about 60%, while Tpm1.6 decreased it by about 40% (Figure 3C).

Myo5c motor function is inhibited by PBP

Small allosteric effectors can interfere with the mechanochemical cycle and either enhance or inhibit myosins (Manstein and Preller, 2020). The halogenated pseudilin, PBP was identified as potent inhibitors of class V myosins: the ATPase activity of *D. discoideum* Myo5b and chicken Myo5a is greatly reduced in the presence of PBP (Fedorov et al., 2009). Based on the homology within the myosin V class it is assumed that PBP is likely to be an effective inhibitor of human Myo5c. Therefore, we assessed the effect of increasing concentrations of PBP on the ATPase activity of our Myo5c–HMM construct. In the presence of 13 μM actin, the ATPase activity of Myo5c–HMM decreased in a sigmoidal manner with increasing PBP concentration (Figure 4). The half–maximal inhibitory concentration was determined to be 280 ± 60 nM, obtained from a dose–response fit for the entire data set.

TABLE 1 Impact of Tpm isoforms on the kinetic behavior of Myo5c–HMM (CaM).

Substrate	k_{cat} (s^{-1})	$K_{app\ actin}$ (μM)	$k_{cat}/K_{app\ actin}$ ($\mu M^{-1}s^{-1}$)	Sliding velocity (nm/s)
Actin	1.65 ± 0.14	5.70 ± 1.45	0.29 ± 0.09	28.68 ± 12.45
Actin + Tpm1.6	1.05 ± 0.11	2.31 ± 0.88	0.45 ± 0.13	40.53 ± 15.93
Actin + Tpm1.8	1.69 ± 0.21	3.24 ± 1.58	0.52 ± 0.13	41.42 ± 14.76
Actin + Tpm3.1	2.71 ± 0.28	5.54 ± 1.72	0.48 ± 0.16	41.71 ± 13.82

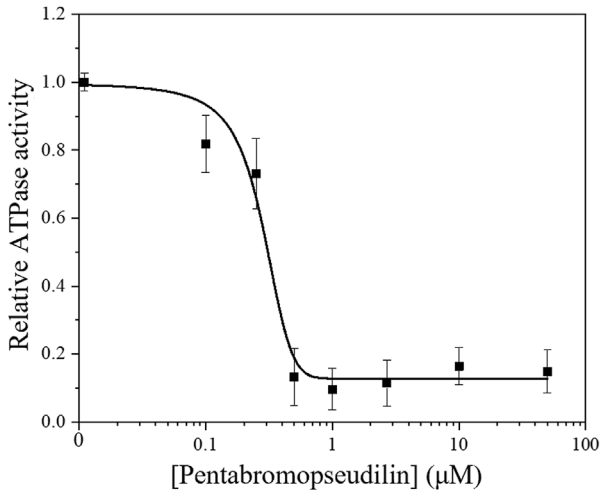

FIGURE 4
Steady–state actin–activated ATPase activity of human Myo5c–HMM at 13 μM F–actin concentration, in the presence of 0–50 μM PBP. The semilogarithmic plot shows the concentration dependence of Myo5c–HMM inhibition. The data were fitted with a dose-response model, using the equation $y = A_1 + (A_2–A_1)/\{1 + 10^{[(LOGx0–x)*P]}\}$, where the coefficient *P* is an empirical parameter reflecting the allosteric nature of the mechanism of PBP-mediated inhibition. The concentrations of PBP required for half–maximal inhibition (IC_{50}) of Myo5c–HMM was determined from the fit (n = 3, mean ± SE).

Docking model of PBP to Myo5c predicts strong binding

We prepared an AlphaFold2 model of the motor domain of human Myo5c. The model is in the pre–power stroke conformation, similar to the model of the motor domain of Myo2 from *D. discoideum*, which was crystallized in the presence of PBP and Mg^{2+}–ADP–meta–vanadate. In the *Dd* Myo2 structure, the PBP binding pocket is formed by residues from helix 13 (Lys265–Val268), helix 21 (Val411–Leu441), the strut loop (Asn588–Gln593) and loop 2 (Asp614–Thr629) (Fedorov et al., 2009; PDB–ID: 2JHR). The residues involved in PBP binding are only moderately conserved between the members of the different myosin classes, as reflected by the observed differences in the IC_{50} values for myosin isoforms from class I, II and V, and the results of molecular modeling studies probing the interactions of PBP with *Dd* Myo1E, *Sc* Myo2, *Gg* Myo5a, and *Dd* Myo5b. *Gg* Myo5a showed in these experiments the strongest inhibition by PBP of ATP binding, ATP turnover and motor activity. Consistent with these results, the number and strength of predicted interactions with PBP were greatest for *Gg* Myo5a (Fedorov et al., 2009).

We docked PBP to our AlphaFold2 model of Myo5c, using the Glide docking application of Schrödinger. We created different conformers and tautomers of PBP and selected the most chemically stable ones for docking. After minimization, we selected the PBP conformer with the strongest bonds. PBP forms several interactions in the binding groove (Figure 5A). The phenyl ring forms a pi–cation interaction with Lys627 of helix 29. The oxygen of the phenyl ring forms hydrogen bond with Asp411 of helix 21. Leu241 (β–strand connecting ß7 and helix 13) forms halogen bonds with Br3 and Br4 of the pyrrole ring. Lys244 of helix 13 forms a halogen bond with Br3 of the phenyl ring (Figures 5B, C). The calculated binding energy (ΔG) of this interaction is with −18.44 kcal/mol comparable of the binding energy reported for the interaction of PBP with *Gg* Myo5a (Fedorov et al., 2009).

Discussion

The physiological role and regulation of Myo5c, the most recently discovered member of the class V myosins, are still not fully understood. However, its abundance in the majority of the tissues (except in the neural and in some lymphatic tissues) suggests its significance. It has the highest expression level among the myosin V isoforms in epithelial and glandular tissues (Rodriguez and Cheney, 2002).

This study demonstrates that recombinant human Myo5c–HMM can be co–produced and co–purified not only with the conventionally accepted CaM, as light chain of class V myosins, but also with the RLC Myl12b and ELC Myl6. This follows a recent trend in literature where different unconventional myosins were successfully purified with light chains other than CaM, such as RLC, ELC or CALML4, which often represents a more effective purification process, resulting in a more stable protein. For example, Myo15 binds CaM, RLC (Myl12b) and ELC (Myl6) as light chains (Bird et al., 2014). Mouse Myo5a or *Drosophila* Myo7a can be purified exclusively with CaM, in contrast, Myo5a purified from chicken brain was shown to be associated with CaM and ELC and human Myo7a with CaM, RLC (Myl12b) and CALML4 (Yang et al., 2006; Heissler and Sellers, 2014; Holló et al., 2023). These findings suggest that various light chains may be physiologically relevant, but also that they may be species–specific.

When Myo5c–HMM is co–produced with CaM alone in the baculovirus/*Sf9* system, we assume that each of the six IQ motifs of Myo5c has CaM bound to it. In the presence of all three light chains, we observed light chain:heavy chain ratios of 3:1 for RLC, 2:1 for CaM and 1:1 for ELC. The enzymatic activity of Myo5c appears to be

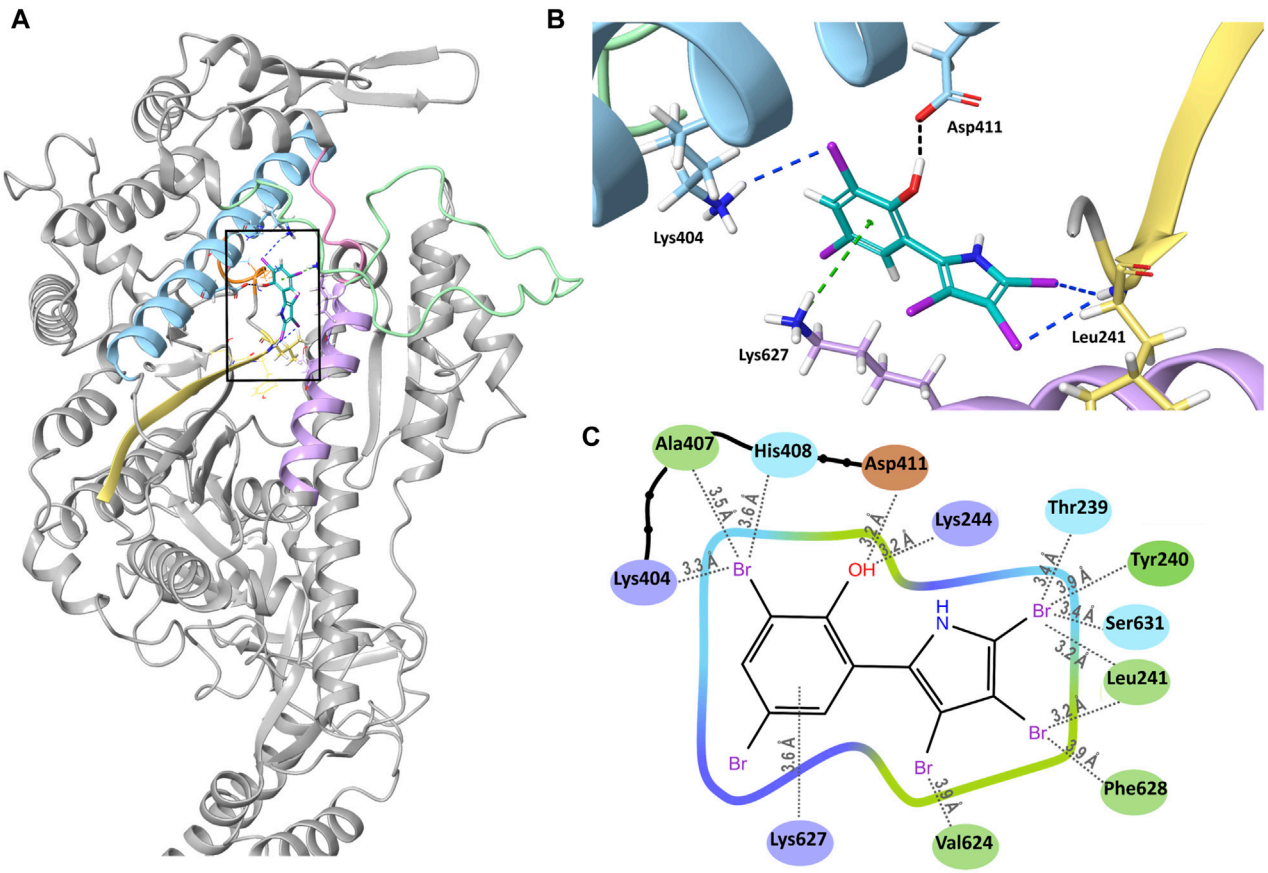

FIGURE 5
Binding of PBP to Myo5c. **(A)** Overview of PBP (cyan) bound into its binding groove (black square) in Myo5c. Helix 13 (Lys244–Val247) is shown in orange, Helix 21 (Arg391–Leu421) in blue, the strut loop (Asn566–Tyr571) in pink, loop 2 (Asn588–Thr623) in green, helix 29 (Val624–Asn640) in violet and the β–strand connecting β7 and helix 13 in yellow. **(B)** Close–up of the PBP binding site, shown from the direction of the back of the head rotated 90° to the right from the overview position. Hydrogen bond (black), halogen bonds (blue) and cation–pi interaction (green) between PBP and Myo5c are shown, structures of Myo5c in the same colors as in **(A)**. **(C)** Ligand Interaction Diagram of PBP and Myo5c residues within 4 Å. Residues are colored by their properties: negative residues in orange, positive residues in violet, hydrophobic residues in green and polar residues in blue. Distances to the nearest atom are shown with grey dotted lines.

modulated by the type of light chains bound. The maximal actin–activated ATPase activity of Myo5c–HMM (3LC) was only about half of that co–produced exclusively with CaM Myo5c–HMM (CaM) and the actin sliding velocity was also significantly lower. The activity of Myo5c has not previously been shown to be modulated by the type of light chains bound.

An important regulatory mechanism of the RLC– and ELC–containing class II myosins is the phosphorylation of the Ser19 and Thr18 amino acids of the RLC, which enhances the ATPase activity (Sellers, 1985). We tested the possible effect of phosphorylation on Myo5c when co–produced with RLC, but no difference was observed in the ATPase activity or actin sliding velocity after phosphorylating the RLC with calcium/CaM dependent MLCK. This suggests that the RLC–containing construct may not be fully active or that another regulatory mechanism is required, such as phosphorylation of the RLC on a different amino acid or by another kinase.

The regulation of unconventional myosins by different light chains is an interesting topic. For example, Myo5a exhibit kinetic differences, depending on whether it is coproduced with CaM or different ELC isoforms (La et al., 2000). Although CaM, RLC, or ELC are abundant in most tissues, there is limited knowledge about the *in vivo* exchange of light chains. The observed variations in light chain composition during myosin isolation (Wang et al., 2000), or the successful experiments using different light chains with the same myosin, suggest that unconventional myosins may be functional with different sets of light chains. However, further examination is necessary to confirm this possibility.

The motor activity of Myo5c–HMM, regardless of the type of the light chain was influenced by different Tpm isoforms. Tpm isoforms are important regulators of the actomyosin cytoskeleton, affecting the function of various myosins. Tpm3.1, for example, enhances the motor function of non–muscle Myo2a and is a more favorable track for Myo5a compared to bare actin filament (Sckolnick et al., 2016; Reindl et al., 2022). Actin filaments in complex with Tpm3.1 appear to be a more effective substrate for Myo5c–HMM both in steady–state ATPase and *in vitro* motility assays, by increasing the coupling efficiency between the actin and the nucleotide binding site on the myosin head. All the examined Tpm isoforms, including Tpm3.1, Tpm1.6, and Tpm1.8, increase the

sliding velocity of actin filaments on a Myo5c–HMM covered surface and show increased coupling efficiency. However, the long Tpm1.6 isoform decreases the maximal ATPase activity of Myo5c–HMM, while Tpm1.8 does not cause any significant change. As discussed in Reindl et al. (2022), Tpm sequences contributing to the overlap region are not the sole determinant of differences in actin affinity. Instead, global sequence differences between Tpm isoforms are of greater importance than variable exon 6 usage, which leads to the diversity in the mechanical properties of various actin–Tpm cofilaments. Furthermore, cryo-EM studies have shown that Myo2c interacts directly with Tpm3.1 through the loop 4 of the motor domain in the acto–myosin–Tpm complex (von der Ecken et al., 2015). As this region is not particularly conserved, further molecular docking simulations are required to determine the interacting structures between Myo5c and the various Tpm isoforms.

Several physiological and pharmaceutical factors can influence the motor function of a myosin. Small allosteric effectors, which alleviate certain steps of the kinetic cycle of a motor protein, are promising candidates in drug development, but also useful tools in myosin research (Manstein and Preller, 2020). PBP, a marine–derived polybrominated pseudilin was originally developed as an anti–cancer drug candidate, blocking the enzymatic activity of human lipoxygenase. Later it was found to interfere with the motor function of class I, II and V myosins. The strongest inhibition was observed for chicken acto–Myo5a, with a half–maximal dose of 1.2 ± 0.2 μM and as low as 0.4 ± 0.2 μM in the absence of actin, which was more than a magnitude lower than that for the other myosin isoforms (Fedorov et al., 2009). To examine the inhibitory effect of PBP on human Myo5c, we conducted a steady–state actin–activated ATPase assay. The inhibitory effect on acto–Myo5c–HMM was more pronounced, with an IC_{50} as low as 280 ± 60 nM. This result was supported by *in silico* analysis. Molecular docking simulations predict that PBP binds to Myo5c in a groove near the actin and nucleotide binding sites, similar to previously described models for *Dd* Myo2 and *Gg* Myo5 (Fedorov et al., 2009; Behrens et al., 2017). The binding energy of *Hs* Myo5c to PBP is ~30–times higher than that of *Dd* Myo2, which is consistent with the difference in the inhibitory effect observed in the steady–state actin–activated ATPase assay.

Our *in silico* data show that the binding energy between *Hs* Myo5c and PBP is almost the same as that between Gg Myo5a and PBP. In analogy to *Gg* Myo5a, an even more pronounced effect of PBP is expected in the absence of actin. This would result in an even lower IC_{50} for human Myo5c. Our prediction suggests a potential binding between PBP and Myo5c, however, it is important to note that this is only a prediction. To obtain more detailed information about the binding mechanism, additional molecular dynamics simulations, and crystallization experiments are required. Our results confirm previous findings that PBP is not strictly class–specific but acts preferentially on class V myosins.

A prominent localization of Myo5c was found in the pancreas. Earlier observations showed Myo5c to localize with low abundance to the apical region of the acinar cells of the exocrine pancreas in mice (Rodriguez and Cheney, 2002). Our findings, based on the use of human and rat tissues, show the presence of Myo5c in the endocrine pancreas. Specifically, we observed a strong colocalization of Myo5c with insulin in β–cells. Following the manifestation of autoimmune diabetes in the pancreas, when insulin production is severely reduced by the loss of β–cells in the pancreatic islets, Myo5c immunofluorescence was correspondingly reduced. In pancreatic β–cells, insulin–containing dense core vesicles (secretory granules) are transported from the endoplasmic reticulum to the Golgi compartment and then intracellularly to various cell domains for storage and to the cell periphery for secretion by exocytosis. This translocation is fine-tuned by the cooperative work of different motor proteins. The budding of the proinsulin containing secretory granules from the trans–Golgi network is mediated by Myo1b (Tokuo, Komaba, and Coluccio, 2021). The transport of the secretory granules occurs primarily along microtubules using kinesin motors, while closer to the cortex the vesicles are moved along actin tracks using myosin V motors (Varadi et al., 2002). Previous studies have shown that Myo5a participates in the transport of insulin secretory granules by attaching to the dense core vesicles through granulophilin–a, a Rab27a effector protein (Wang et al., 1999). Other members of the small GTPase Rab family are also involved in recruiting Myo5a to the vesicle surface. Rab3a associates specifically with synaptic vesicles and insulin secretory granules (Regazzi et al., 1996). The absence of Rab3a in mice was shown to lead to severe hyperglycemia and insulin secretory deficiencies (Varadi, Tsuboi, and Rutter, 2005). Rab3a is likely to bind to the convex region of the GTD of Myo5a and Myo5c, but not Myo5b, according to recent molecular docking data. Additionally, the myosin binding site on Rab3a differs from that of rabphilin–3a, an effector protein of Rab3a (Dolce et al., 2020). Given that Myo5c is the most prominent myosin V isoform in the pancreas and is able to bind Rab3a, it appears likely that Myo5c may act synergistically with Myo5a in insulin secretion. Furthermore, it has been demonstrated in mouse pancreatic tissue that Tpm3.1 may have a role in regulating insulin secretion. Treatment of pancreatic β–cells with TR100 or ATM1001 anti–Tpm compounds resulted in a reduction of glucose-stimulated insulin secretion, meanwhile the impact was significantly less in Tpm3.1 KO mice compared to WT (Kee et al., 2018).

The consequences of depleting Myo5c in pancreatic islets have not yet been studied. It is worth noting, that Myo5c is a non–processive motor, unlike the processive Myo5a or Myo5b, however, it can move processively in an ensemble or on actin bundles (Krementsova et al., 2017). This process may be influenced by Tpm isoforms, providing favorable or unfavorable tracks for vesicular transport. Future research will focus on how Myo5c–actin–tropomyosin complexes can be used as therapeutic targets to modulate insulin secretion.

Data availability statement

The datasets presented in this study can be found in online repositories. The names of the repository/repositories and accession number(s) can be found in the article/Supplementary Material.

Ethics statement

The studies involving humans were approved by the Ethics Committee of Hannover Medical School. The studies were conducted in accordance with the local legislation and

institutional requirements. The human samples used in this study were acquired from primarily isolated as part of our previous study for which ethical approval was obtained. Written informed consent for participation was not required from the participants or the participants' legal guardians/next of kin in accordance with the national legislation and institutional requirements. The animal study was approved by Lower Saxony State Office, District Government of Hannover (LAVES). The study was conducted in accordance with the local legislation and institutional requirements.

Author contributions

AK: Writing–review and editing, Writing–original draft, Methodology, Data curation, Conceptualization. PP: Writing–review and editing, Writing–original draft, Methodology, Data curation, Conceptualization. JK: Methodology, Writing–original draft, Data curation. AM: Methodology, Writing–original draft, Data curation. JG: Writing–original draft, Methodology, Data curation. RH: Writing–original draft, Methodology, Data curation. AJ: Writing–original draft, Methodology, Data curation. DM: Writing–review and editing, Writing–original draft, Supervision, Resources, Funding acquisition, Conceptualization.

Funding

The author(s) declare that financial support was received for the research, authorship, and/or publication of this article. Supported by grants from the Deutsche Forschungsgemeinschaft to DM (MA1081/28-1) and AJ (project-NO: 455203589). DM is a member of the European Union's Horizon 2020 research and innovation program under the EJP RD COFUND–EJP NO 825575 with support from the German Federal Ministry of Education and Research under Grant Agreement 01GM1922B. DM is a member of the Cluster of Excellence RESIST (EXC 2155; DFG–Project ID: 39087428–B11). JG is supported by the HiLF I grant for early career researcher from Medizinische Hochschule Hannover.

Acknowledgments

The authors thank Manuel H. Taft for his valuable advice during the project and Claudia Thiel for the excellent technical support. We gratefully acknowledge support provided by the Core Unit for Structural Biochemistry, the Core Unit for Laser Microscopy at MHH. Computing time was provided on supercomputers Lise and Emmy at NHR@ZIB and NHR@Göttingen, as part of the Alliance for National High Performance Computing (NHR) infrastructure. The calculations for this research were conducted with computing resources under the project ID nib00018.

Conflict of interest

The authors declare that the research was conducted in the absence of any commercial or financial relationships that could be construed as a potential conflict of interest.

Publisher's note

Supplementary material

The Supplementary Material for this article can be found online at: https://www.frontiersin.org/articles/10.3389/fphys.2024.1394040/full#supplementary-material

References

Agarwal, S., and Knölker, H.-J. (2004). A novel pyrrole synthesis. *Org. Biomol. Chem.* 2 (21), 3060–3062. doi:10.1039/B412206B

Baboolal, T. G., Sakamoto, T., Forgacs, E., White, H. D., Jackson, S. M., Takagi, Y., et al. (2009). The SAH domain extends the functional length of the myosin lever. *Proc. Natl. Acad. Sci. U. S. A.* 106 (52), 22193–22198. doi:10.1073/pnas.0909851106

Barua, B., Nagy, A., Sellers, J. R., and Hitchcock-DeGregori, S. E. (2014). Regulation of nonmuscle myosin II by tropomyosin. *Biochemistry* 53 (24), 4015–4024. doi:10.1021/bi500162z

Barua, B., Sckolnick, M., White, H. D., Trybus, K. M., and Hitchcock-DeGregori, S. E. (2018). Distinct sites in tropomyosin specify shared and isoform-specific regulation of myosins II and V. *Cytoskeleton* 75 (4), 150–163. doi:10.1002/cm.21440

Behrens, V. A., Münnich, S., Adler-Gunzelmann, G., Thiel, C., Henn, A., Latham, S. L., et al. (2017). The conserved lysine-265 allosterically modulates nucleotide- and actin-binding site coupling in myosin-2. *Sci. Rep.* 7 (1), 7650. doi:10.1038/s41598-017-07933-y

Bird, J. E., Takagi, Y., Billington, N., Strub, M.-P., Sellers, J. R., and Friedman, T. B. (2014). Chaperone-enhanced purification of unconventional myosin 15, a molecular motor specialized for stereocilia protein trafficking. *Proc. Natl. Acad. Sci.* 111 (34), 12390–12395. doi:10.1073/pnas.1409459111

Bultema, J. J., Boyle, J. A., Malenke, P. B., Martin, F. E., Dell'Angelica, E. C., Cheney, R. E., et al. (2014). Myosin vc interacts with Rab32 and Rab38 proteins and works in the biogenesis and secretion of melanosomes. *J. Biol. Chem.* 289 (48), 33513–33528. doi:10.1074/jbc.M114.578948

Curthoys, N. M., Freittag, H., Connor, A., Desouza, M., Brettle, M., Poljak, A., et al. (2014). Tropomyosins induce neuritogenesis and determine neurite branching patterns in B35 neuroblastoma cells. *Mol. Cell. Neurosci.* 58, 11–21. doi:10.1016/j.mcn.2013.10.011

Dolce, L. G., Ohbayashi, N., da Silva, D. F. C., Ferrari, A. J. R., Pirolla, R. A. S., Schwarzer, A. C. de A. P., et al. (2020). Unveiling the interaction between the molecular motor myosin vc and the small GTPase Rab3A. *J. Proteomics* 212, 103549. doi:10.1016/j.jprot.2019.103549

Fedorov, R., Böhl, M., Tsiavaliaris, G., Hartmann, F. K., Taft, M. H., Baruch, P., et al. (2009). The mechanism of pentabromopseudilin inhibition of myosin motor activity. *Nat. Struct. Mol. Biol.* 16 (1), 80–88. doi:10.1038/nsmb.1542

Garrido-Casado, M., Asensio-Juárez, G., and Vicente-Manzanares, M. (2021). Nonmuscle myosin II regulation directs its multiple roles in cell migration and division. *Annu. Rev. Cell Dev. Biol.* 37 (1), 285–310. doi:10.1146/annurev-cellbio-042721-105528

Gele, M. V., Dynoodt, P., and Lambert, J. (2009). Griscelli syndrome: a model system to study vesicular trafficking. *Pigment Cell & Melanoma Res.* 22 (3), 268–282. doi:10.1111/j.1755-148X.2009.00558.x

Greve, J. N., Marquardt, A., Heiringhoff, R., Reindl, T., Thiel, C., Di Donato, N., et al. (2024). The non-muscle actinopathy-associated mutation E334Q in cytoskeletal γ-actin perturbs interaction of actin filaments with myosin and ADF/cofilin family proteins. *ELife* 12. doi:10.7554/eLife.93013

Gunning, P. W., Schevzov, G., Kee, A. J., and Hardeman, E. C. (2005). Tropomyosin isoforms: divining rods for actin cytoskeleton function. *Trends Cell Biol.* 15 (6), 333–341. doi:10.1016/j.tcb.2005.04.007

Gunther, L. K., Furuta, K. 'ya, Bao, J., Urbanowski, M. K., Kojima, H., White, H. D., et al. (2014). Coupling of two non-processive myosin 5c dimers enables processive stepping along actin filaments. *Sci. Rep.* 4 (1), 4907. doi:10.1038/srep04907

Hammer, J. A., and Sellers, J. R. (2012). Walking to work: roles for class V myosins as cargo transporters. *Nat. Rev. Mol. Cell Biol.* 13 (1), 13–26. doi:10.1038/nrm3248

Heissler, S. M., Krishna, C., and Sellers, J. R. (2017). Kinetic signatures of myosin-5B, the motor involved in microvillus inclusion disease. *J. Biol. Chem.* 292 (44), 18372–18385. doi:10.1074/jbc.M117.801456

Heissler, S. M., and Sellers, J. R. (2014). Myosin light chains: teaching old dogs New tricks. *BioArchitecture* 4 (6), 169–188. doi:10.1080/19490992.2015.1054092

Holló, A., Billington, N., Takagi, Y., Kengyel, A., Sellers, J. R., and Liu, R. (2023). Molecular regulatory mechanism of human myosin-7a. *J. Biol. Chem.* 299 (10), 105243. doi:10.1016/j.jbc.2023.105243

Holthenrich, A., Terglane, J., Naß, J., Mietkowska, M., Kerkhoff, E., and Gerke, V. (2022). Spire1 and myosin vc promote Ca2+-evoked externalization of von Willebrand factor in endothelial cells. *Cell. Mol. Life Sci.* 79 (2), 96. doi:10.1007/s00018-021-04108-x

Hundt, N., Steffen, W., Pathan-Chhatbar, S., Taft, M. H., and Manstein, D. J. (2016). Load-dependent modulation of non-muscle myosin-2A function by tropomyosin 4.2. *Sci. Rep.* 6 (1), 20554. doi:10.1038/srep20554

Jacobs, D. T., Weigert, R., Grode, K. D., Donaldson, J. G., and Cheney, R. E. (2009). Myosin vc is a molecular motor that functions in secretory granule trafficking. *Mol. Biol. Cell* 20 (21), 4471–4488. doi:10.1091/mbc.e08-08-0865

Jumper, J., Evans, R., Pritzel, A., Green, T., Figurnov, M., Ronneberger, O., et al. (2021). Highly accurate protein structure prediction with AlphaFold. *Nature* 596 (7873), 583–589. doi:10.1038/s41586-021-03819-2

Kee, A. J., Chagan, J., Chan, J. Y., Bryce, N. S., Lucas, C. A., Zeng, J., et al. (2018). On-target action of anti-tropomyosin drugs regulates glucose metabolism. *Sci. Rep.* 8 (1), 4604. doi:10.1038/s41598-018-22946-x

Kee, A. J., Yang, L., Lucas, C. A., Greenberg, M. J., Martel, N., Leong, G. M., et al. (2015). An actin filament population defined by the tropomyosin Tpm3.1 regulates glucose uptake. *Traffic* 16 (7), 691–711. doi:10.1111/tra.12282

Krementsov, D. N., Krementsova, E. B., and Trybus, K. M. (2004). Myosin V: regulation by calcium, calmodulin, and the tail domain. *J. Cell Biol.* 164 (6), 877–886. doi:10.1083/jcb.200310065

Krementsova, E. B., Furuta, K. 'ya, Oiwa, K., Trybus, K. M., and Yusuf Ali, M. (2017). Small teams of myosin vc motors coordinate their stepping for efficient cargo transport on actin bundles. *J. Biol. Chem.* 292 (26), 10998–11008. doi:10.1074/jbc.M117.780791

Krendel, M., and Mooseker, M. S. (2005). Myosins: tails (and heads) of functional diversity. *Physiology* 20 (4), 239–251. doi:10.1152/physiol.00014.2005

La, C., Enrique, M.De, Wells, A. L., Sweeney, H. L., and Michael Ostap, E. (2000). Actin and light chain isoform dependence of myosin V kinetics. *Biochemistry* 39 (46), 14196–14202. doi:10.1021/bi001701b

Lehrer, S. S., and Grace, K. (1972). Intrinsic fluorescence of actin. *Biochemistry* 11 (7), 1211–1217. doi:10.1021/bi00757a015

Li, J., Abel, R., Zhu, K., Cao, Y., Zhao, S., and Friesner, R. A. (2011). The VSGB 2.0 model: a next generation energy model for high resolution protein structure modeling. *Proteins Struct. Funct. Bioinforma.* 79 (10), 2794–2812. doi:10.1002/prot.23106

Manstein, D. J., Meiring, J. C. M., Hardeman, E. C., and Gunning, P. W. (2020). Actin–tropomyosin distribution in non-muscle cells. *J. Muscle Res. Cell Motil.* 41 (1), 11–22. doi:10.1007/s10974-019-09514-0

Manstein, D. J., and Preller, M. (2020). Small molecule effectors of myosin function. *Adv. Exp. Med. Biol.* 1239, 61–84. doi:10.1007/978-3-030-38062-5_5

Niu, F., Liu, Y., Sun, K., Xu, S., Dong, J., Yu, C., et al. (2022). Autoinhibition and activation mechanisms revealed by the triangular-shaped structure of myosin va. *Sci. Adv.* 8 (49), eadd4187. doi:10.1126/sciadv.add4187

Nussbaum-Krammer, C. I., Neto, M. F., Brielmann, R. M., Pedersen, J. S., and Morimoto, R. I. (2015). Investigating the spreading and toxicity of prion-like proteins using the metazoan model organism *C. elegans*. *J. Vis. Exp.*, 52321. doi:10.3791/52321

Pathan-Chhatbar, S., Taft, M. H., Reindl, T., Hundt, N., Latham, S. L., and Manstein, D. J. (2018). Three mammalian tropomyosin isoforms have different regulatory effects on nonmuscle myosin-2B and filamentous β-actin *in vitro*. *J. Biol. Chem.* 293 (3), 863–875. doi:10.1074/jbc.M117.806521

Peckham, M. (2011). Coiled coils and SAH domains in cytoskeletal molecular motors. *Biochem. Soc. Trans.* 39 (5), 1142–1148. doi:10.1042/BST0391142

Reck-Peterson, S. L., William Provance, D., Mooseker, M. S., and Mercer, J. A. (2000). Class V myosins. *Biochimica Biophysica Acta (BBA) - Mol. Cell Res.* 1496 (1), 36–51. doi:10.1016/S0167-4889(00)00007-0

Regazzi, R., Ravazzola, M., Iezzi, M., Lang, J., Ahmed, Z., Andereggen, E., et al. (1996). Expression, localization and functional role of small GTPases of the Rab3 family in insulin-secreting cells. *J. Cell Sci.* 109 (9), 2265–2273. doi:10.1242/jcs.109.9.2265

Reindl, T., Giese, S., Greve, J. N., Reinke, P. Y., Chizhov, I., Latham, S. L., et al. (2022). Distinct actin–tropomyosin cofilament populations drive the functional diversification of cytoskeletal myosin motor complexes. *IScience* 25 (7), 104484. doi:10.1016/j.isci.2022.104484

Richards, T. A., and Cavalier-Smith, T. (2005). Myosin domain evolution and the primary divergence of eukaryotes. *Nature* 436 (7054), 1113–1118. doi:10.1038/nature03949

Rodriguez, O. C., and Cheney, R. E. (2002). Human myosin-vc is a novel class V myosin expressed in epithelial cells. *J. Cell Sci.* 115 (5), 991–1004. doi:10.1242/jcs.115.5.991

Schevzov, G., Kee, A. J., Wang, B., Sequeira, V. B., Hook, J., Coombes, J. D., et al. (2015). Regulation of cell proliferation by ERK and signal-dependent nuclear translocation of ERK is dependent on Tm5NM1-containing actin filaments. *Mol. Biol. Cell* 26 (13), 2475–2490. doi:10.1091/mbc.E14-10-1453

Schindelin, J., Arganda-Carreras, I., Frise, E., Kaynig, V., Longair, M., Pietzsch, T., et al. (2012). Fiji: an open-source platform for biological-image analysis. *Nat. Methods* 9 (7), 676–682. doi:10.1038/nmeth.2019

Sckolnick, M., Krementsova, E. B., Warshaw, D. M., and Trybus, K. M. (2016). Tropomyosin isoforms bias actin track selection by vertebrate myosin va. *Mol. Biol. Cell* 27 (19), 2889–2897. doi:10.1091/mbc.E15-09-0641

Sellers, J. R. (1985). Mechanism of the phosphorylation-dependent regulation of smooth muscle heavy meromyosin. *J. Biol. Chem.* 260 (29), 15815–15819. doi:10.1016/s0021-9258(17)36331-7

Sellers, J. R., and Harvey, E. V. (1984). Purification of myosin light chain kinase from limulus muscle. *Biochemistry* 23 (24), 5821–5826. doi:10.1021/bi00319a022

Takagi, Y., Yang, Yi, Fujiwara, I., Jacobs, D., Cheney, R. E., Sellers, J. R., et al. (2008). Human myosin vc is a low duty ratio, nonprocessive molecular motor. *J. Biol. Chem.* 283 (13), 8527–8537. doi:10.1074/jbc.M709150200

Thoeni, C. E., Vogel, G. F., Tancevski, I., Geley, S., Lechner, S., Pfaller, K., et al. (2014). Microvillus inclusion disease: loss of myosin vb disrupts intracellular traffic and cell polarity. *Traffic* 15 (1), 22–42. doi:10.1111/tra.12131

Tojkander, S., Gateva, G., Schevzov, G., Hotulainen, P., Naumanen, P., Martin, C., et al. (2011). A molecular pathway for myosin II recruitment to stress fibers. *Curr. Biol.* 21 (7), 539–550. doi:10.1016/j.cub.2011.03.007

Tokuo, H., Komaba, S., and Coluccio, L. M. (2021). In pancreatic β-cells myosin 1b regulates glucose-stimulated insulin secretion by modulating an early step in insulin granule trafficking from the Golgi. *Mol. Biol. Cell* 32 (12), 1210–1220. doi:10.1091/mbc.E21-03-0094

Tu, F., Sedzinski, J., Ma, Y., Marcotte, E. M., and Wallingford, J. B. (2017). Protein localization screening *in vivo* reveals novel regulators of multiciliated cell development and function. *J. Cell Sci.* 131, jcs206565. doi:10.1242/jcs.206565

Varadi, A., Ainscow, E. K., Allan, V. J., and Rutter, G. A. (2002). Involvement of conventional kinesin in glucose-stimulated secretory granule movements and exocytosis in clonal pancreatic beta-cells. *J. Cell Sci.* 115 (21), 4177–4189. doi:10.1242/jcs.00083

Varadi, A., Tsuboi, T., and Rutter, G. A. (2005). Myosin Va transports dense core secretory vesicles in pancreatic MIN6 beta-cells. *Mol. Biol. Cell* 16, 2670–2680. doi:10.1091/mbc.e04-11-1001

Vicente-Manzanares, M., Ma, X., Adelstein, R. S., and Horwitz, A. R. (2009). Non-muscle myosin II takes centre stage in cell adhesion and migration. *Nat. Rev. Mol. Cell Biol.* 10 (11), 778–790. doi:10.1038/nrm2786

von der Ecken, J., Müller, M., Lehman, W., Manstein, D. J., Penczek, P. A., and Raunser, S. (2015). Structure of the F-Actin–Tropomyosin complex. *Nature* 519 (7541), 114–117. doi:10.1038/nature14033

Wang, F., Chen, L., Arcucci, O., Harvey, E. V., Bowers, B., Xu, Y., et al. (2000). Effect of ADP and ionic strength on the kinetic and motile properties of recombinant mouse myosin V. *J. Biol. Chem.* 275 (6), 4329–4335. doi:10.1074/jbc.275.6.4329

Wang, F., Thirumurugan, K., Stafford, W. F., Hammer, J. A., Knight, P. J., and Sellers, J. R. (2004). Regulated conformation of myosin V. *J. Biol. Chem.* 279 (4), 2333–2336. doi:10.1074/jbc.C300488200

Wang, J., Takeuchi, T., Yokota, H., and Izumi, T. (1999). Novel rabphilin-3-like protein associates with insulin-containing granules in pancreatic beta cells. *J. Biol. Chem.* 274 (40), 28542–28548. doi:10.1074/jbc.274.40.28542

Watanabe, S., Watanabe, T. M., Sato, O., Awata, J., Homma, K., Umeki, N., et al. (2008). Human myosin vc is a low duty ratio nonprocessive motor. *J. Biol. Chem.* 283 (16), 10581–10592. doi:10.1074/jbc.M707657200

Wolfenson, H., Meacci, G., Liu, S., Stachowiak, M. R., Iskratsch, T., Ghassemi, S., et al. (2016). Tropomyosin controls sarcomere-like contractions for rigidity sensing and suppressing growth on soft matrices. *Nat. Cell Biol.* 18 (1), 33–42. doi:10.1038/ncb3277

Yang, Yi, Kovács, M., Sakamoto, T., Zhang, F., Kiehart, D. P., and Sellers, J. R. (2006). Dimerized *Drosophila* myosin VIIa: a processive motor. *Proc. Natl. Acad. Sci.* 103 (15), 5746–5751. doi:10.1073/pnas.0509935103

Yao, L. L., Shen, M., Lu, Z., Ikebe, M., and Xiang, D.Li (2016). Identification of the isoform-specific interactions between the tail and the head of class v myosin. *J. Biol. Chem.* 291 (15), 8241–8250. doi:10.1074/jbc.M115.693762

Zhang, N., Yao, L.-L., and Xiang-dong, Li (2018). Regulation of class V myosin. *Cell. Mol. Life Sci.* 75 (2), 261–273. doi:10.1007/s00018-017-2599-5

frontiers | Frontiers in Physiology

TYPE Original Research
PUBLISHED 10 April 2024
DOI 10.3389/fphys.2024.1368054

OPEN ACCESS

EDITED BY
Maria Jolanta Redowicz,
Polish Academy of Sciences, Poland

REVIEWED BY
James R. Sellers,
National Heart, Lung, and Blood Institute (NIH), United States
Margaret A. Titus,
University of Minnesota Twin Cities, United States

*CORRESPONDENCE
Folma Buss,
fb207@cam.ac.uk

RECEIVED 09 January 2024
ACCEPTED 22 March 2024
PUBLISHED 10 April 2024

CITATION
Behbehani R, Johnson C, Holmes AJ, Gratian MJ, Mulvihill DP and Buss F (2024), The two *C. elegans* class VI myosins, SPE-15/HUM-3 and HUM-8, share similar motor properties, but have distinct developmental and tissue expression patterns.
Front. Physiol. 15:1368054.
doi: 10.3389/fphys.2024.1368054

The two *C. elegans* class VI myosins, SPE-15/HUM-3 and HUM-8, share similar motor properties, but have distinct developmental and tissue expression patterns

Ranya Behbehani[1], Chloe Johnson[1], Alexander J. Holmes[1], Matthew J. Gratian[1], Daniel P. Mulvihill[2] and Folma Buss[1]*

[1]Cambridge Institute for Medical Research, University of Cambridge, Cambridge, United Kingdom, [2]School of Biosciences, University of Kent, Canterbury, United Kingdom

Myosins of class VI move toward the minus-end of actin filaments and play vital roles in cellular processes such as endocytosis, autophagy, protein secretion, and the regulation of actin filament dynamics. In contrast to the majority of metazoan organisms examined to date which contain a single MYO6 gene, *C. elegans*, possesses two MYO6 homologues, SPE-15/HUM-3 and HUM-8. Through a combination of *in vitro* biochemical/biophysical analysis and cellular assays, we confirmed that both SPE-15/HUM-3 and HUM-8 exhibit reverse directionality, velocities, and ATPase activity similar to human MYO6. Our characterization also revealed that unlike SPE-15/HUM-3, HUM-8 is expressed as two distinct splice isoforms, one with an additional unique 14 amino acid insert in the cargo-binding domain. While lipid and adaptor binding sites are conserved in SPE-15/HUM-3 and HUM-8, this conservation does not enable recruitment to endosomes in mammalian cells. Finally, we performed super-resolution confocal imaging on transgenic worms expressing either mNeonGreen SPE-15/HUM-3 or wrmScarlet HUM-8. Our results show a clear distinction in tissue distribution between SPE-15/HUM-3 and HUM-8. While SPE-15/HUM-3 exhibited specific expression in the gonads and neuronal tissue in the head, HUM-8 was exclusively localized in the intestinal epithelium. Overall, these findings align with the established tissue distributions and localizations of human MYO6.

KEYWORDS

MYO6, SPE-15/HUM-3, HUM-8, actin, *C. elegans*

Introduction

Unconventional myosins constitute a superfamily of motor proteins that translocate along actin filaments and play various roles in diverse cellular processes such as muscle contraction, intracellular trafficking, cell motility, endocytosis, exocytosis, and cytokinesis (Sellers, 2000; Krendel and Mooseker, 2005; Hartman and Spudich, 2012). In humans, a total of 40 myosin genes have been identified that can be grouped into 12 classes based on their distinctive domain structure and organization (Odronitz and Kollmar, 2007). Myosin motors are widely expressed across different tissues and are essential for normal cellular activities.

Caenorhabditis elegans is a species of free-living, non-parasitic nematode commonly used as a model organism, being studied extensively with respect to development and genetics, cell lineage, and in work surrounding ageing and human disease (Brenner, 1974). Its genome contains approximately 19,985 protein-coding genes, 38% of which have human orthologues (Wormbase data release WS282, 2021) (Celegans Sequencing Consortium, 1998). In the nematode, nine conventional myosins of class II and seven unconventional myosins have been identified: these include two members of class I, one class V myosin, two class VI myosins, one class VII myosin, one class IX myosin and one myosin of class XII (Baker and Titus, 1997; Johnson et al., 2022; Kollmar and Muhlhausen, 2017). Except for class XII, which is exclusive to *C. elegans*, all other myosin motors show a high degree of similarity to their human paralogues. Interestingly, unlike humans which have only a single myosin VI protein, *C. elegans* possesses two distinct myosins belonging to this class, namely, HUM-3 and HUM-8 (Baker and Titus, 1997). HUM-3 is also called SPE-15 (defective spermatogenesis-15) and so the name SPE-15/HUM-3 will be used in this study (L'Hernault et al., 1988).

In vertebrates, myosins of class VI move towards the minus-end of actin filaments, in direct contrast to all other myosins characterised to date which move in the opposite direction (Wells et al., 1999). Human myosin VI (MYO6) is involved in a range of specific cellular functions such as endocytosis, receptor trafficking, protein secretion and autophagy (Buss et al., 2001; Morris et al., 2002; Aschenbrenner et al., 2003; Warner et al., 2003; Osterweil et al., 2005; Chibalina et al., 2007; Tumbarello et al., 2012; Masters et al., 2017). Loss of these functions, as observed in MYO6-deficient Snell's waltzer mice and in humans with mutations in the MYO6 gene, contributes to various disease phenotypes, including deafness, astrogliosis, proteinuria, and hypertrophic cardiomyopathy (Avraham et al., 1995; Avraham et al., 1997; Melchionda et al., 2001; Mohiddin et al., 2004; Arden et al., 2016). Interestingly, MYO6 overexpression is commonly observed in diverse cancers, including prostate and ovarian cancer (Yoshida et al., 2004; Dunn et al., 2006).

The diverse cellular roles and phenotypic outcomes associated with MYO6 arise from its interactions with multiple cargo adaptors that play a critical role in directing the motor to its appropriate cellular location and function. These MYO6 adaptor proteins bind either to the RRL or the WWY motifs, located in distinct subdomains of the unique C-terminal cargo-binding tail (Bunn et al., 1999; Sahlender et al., 2005; Chibalina et al., 2007; Morriswood et al., 2007; Spudich et al., 2007; Finan et al., 2011). In addition, the tail contains a phosphatidylinositol 4,5-bisphosphate (PIP2) binding motif, important for recruitment of the motor to intracellular membranes, as well as two distinct ubiquitin-binding sites–a motif interacting with ubiquitin (MIU) and a MYO6 ubiquitin-binding domain (MyUb) (Penengo et al., 2006; Spudich et al., 2007; He et al., 2016). The cargo-binding tail of human MYO6 undergoes alternative splicing of two inserts: the small insert (SI, adding nine residues) and the large insert (LI, adding 31 residues). This gives rise to four splice isoforms containing the SI, LI, both, or neither. The different splice variants of MYO6 have differential interaction networks and binding partners, generating substantial potential for diversity in MYO6 function (de Jonge et al., 2019). As such, the variants can be found in different cell types and tissues. The LI isoform, for example, is specifically expressed in polarised epithelial cells containing microvilli at their apical domain, whereas the SI and no insert (NI) isoforms are expressed in cells lacking apical microvilli (Buss et al., 2001; Morris et al., 2002; Ameen and Apodaca, 2007; Wollscheid et al., 2016).

MYO6 plays a central role at several steps along the endocytic and exocytic pathways. The LI variant, for example, is involved in cell-surface receptor trafficking in epithelial cells (Buss et al., 2001; Wollsheid et al., 20,160). The role of MYO6 in clathrin-mediated endocytosis involves Dab2, an endocytic adaptor protein (Morris et al., 2002). The NI isoform, on the other hand, localises to Rab5- and APPL1-positive peripheral early endosomes, and is required for the movement of these endosomes through the actin-rich cell cortex away from the plasma membrane (Aschenbrenner et al., 2003; Chibalina et al., 2007; Masters et al., 2017). Recruitment of MYO6 to APPL1-positive endosomes involves the adaptor proteins GIPC and TOM1L1/2 (Buss et al., 1998; Tumbarello et al., 2012). The role of MYO6 in the autophagic pathway during autophagosome maturation is mediated through its cargo adaptor proteins optineurin (OPTN), TAX1 binding protein 1 (TAX1BP1), and nuclear dot protein 52 (NDP52), which also function as selective autophagy receptors (Tumbarello et al., 2012).

In contrast to the well-characterised human MYO6, the two MYO6 homologues expressed in *C. elegans*, SPE-15/HUM-3 and HUM-8, have not been extensively studied and very limited information is available regarding their function, interactome, or biophysical properties. Although there is no published literature specifically on HUM-8, it was found to localise within the mammalian midbody, a structure known to contain proteins involved in cytokinesis (Skop et al., 2004). Interestingly, MYO6 has also been shown to play a role in membrane delivery during mammalian cytokinesis, highlighting a potentially evolutionarily conserved function during cell division for HUM-8 (Arden et al., 2007).

A role for the second MYO6 homologue, SPE-15/HUM-3, has been established in spermiogenesis. In *C. elegans*, spermatogenesis leads to the formation of ameboid spermatozoa, and involves the asymmetric partitioning of cellular material. During spermatid differentiation, spermatids shed unwanted cellular material in the form of an acellular remnant, the residual body (RB), later detaching from this to become motile spermatozoa. A *SPE-15/HUM-3* null deletion mutant produces gross cytological defects in the morphology of the RB and budding spermatids, which typically fail to form spermatozoa (Kelleher et al., 2000). This is consistent with the observation that *SPE-15/HUM-3* mutant hermaphrodites are almost completely self-sterile (L'Hernault et al., 1988). In addition to this, SPE-15/HUM-3 appears to play a role in the final cytokinetic step during spermatid budding. Interestingly, this process is dependent on *C. elegans* GIPC-1 and GIPC-2, homologues of the human GIPC protein family, a group of known MYO6 adaptor proteins (Hu et al., 2019).

C. elegans is a well-established *in vivo* model system that has emerged as an important tool in pharmacological drug discovery. Myosin motors are established druggable targets and, to date, several allosteric effectors of different classes of myosins have been identified. To make potential use of *C. elegans* in a pharmacological screen for modulators of MYO6 activity, we

require a more complete understanding of the cellular, biochemical, and biophysical characteristics of the *C. elegans* MYO6 homologues. Beyond the role of SPE-15/HUM-3 in spermatogenesis, very little is known about the overall functions of SPE-15/HUM-3 and HUM-8 in different nematode tissues. Indeed, it is unclear how the roles of SPE-15/HUM-3 and HUM-8 differ, and how they compare to human MYO6 in terms of functional diversification. This study therefore sought to uncover the cellular characteristics of SPE-15/HUM-3 and HUM-8 both endogenously in *C. elegans*, and in mammalian cell systems, to provide a starting point for a detailed understanding of these MYO6 homologues.

Our findings indicate that there are no significant differences in the biophysical motor characteristics of SPE-15/HUM-3 and HUM-8 concerning their actin gliding velocity and ATPase activity. These attributes closely resemble those of human MYO6 including the reverse directionality along actin filaments, which we confirmed using a filopodia tip recruitment assay. Notably, while crucial adaptor and lipid binding sites are conserved in the cargo-binding tail domain of SPE-15/HUM-3 and HUM-8, this conservation does not facilitate recruitment to peripheral endosomes underneath the plasma membrane, where human MYO6 and the *Drosophila* homologue of MYO6, *Jaguar*, can be found. With the tail domain of human MYO6 known to be a site of alternative splicing, we also sought to uncover whether SPE-15/HUM-3 and HUM-8 undergo similar splicing patterns. Our results show that HUM-8 undergoes alternative splicing, resulting in two isoforms with one containing a unique 14 amino acid insert in the cargo binding domain, whilst SPE-15/HUM-3 is expressed as a single splice isoform. Finally, extensive super-resolution confocal imaging performed on transgenic worms highlights a distinct tissue distribution of these two MYO6 homologues in *C. elegans*. Whereas SPE-15/HUM-3 is specifically expressed in the gonads and neuronal tissue, HUM-8 can almost exclusively be found in the intestinal epithelium. Interestingly, this coincides with the known tissue distributions and localisations of MYO6 in mammalian cells.

Results

SPE-15/HUM-3 and HUM-8 have similar biophysical and structural characteristics compared to human MYO6

The cellular functions of human MYO6 are facilitated by adaptations in its protein structure, binding motifs, splice isoforms and various interaction domains. To determine the conservation of these key features across species, we performed a sequence and structural comparison of SPE-15/HUM-3 and HUM-8 with human MYO6 and *Drosophila* Jaguar. *Drosophila* was chosen here as it is another well-characterised model organism, and its MYO6 homologue has well-established functions that could be used as a reference point. A multiple sequence alignment of SPE-15/HUM-3, HUM-8, Jaguar (isoform B) and human MYO6 (isoform three containing both the LI and SI) revealed a 48% sequence identity between SPE-15/HUM-3 and human MYO6 and a 45% identity between HUM-8 and MYO6 (Supplementary Figure S1). Interestingly, Jaguar is more similar in sequence to human MYO6 (51%) than it is to either SPE-15/HUM-3 (43%) or HUM-8 (39%). The two myosins from *C. elegans* are only 63% identical, highlighting the potential for functional variation between SPE-15/HUM-3 and HUM-8. The overall level of conservation between SPE-15/HUM-3, HUM-8, human MYO6 and Jaguar confirms the evolutionary relationship between these four different myosins of class VI.

Both SPE-15/HUM-3 and HUM-8 have N-terminal extensions just prior to the start of the motor domain (8 amino acids in SPE-15/HUM-3, 73 residues in HUM-8) not found in either human MYO6 or Jaguar (Figures 1A,B). The 73 amino acid extension in HUM-8 appears in the AlphaFold model as a long extended loop without any obvious secondary structure and a very low confidence score. Within the SPE-15/HUM-3 and HUM-8 motor domain and neck region, we found conservation of sequences functionally important for myosin motors, including the characteristic GESGAGKT sequence of the ATP-binding P-loop and a single IQ calmodulin-binding motif (as in human MYO6), as well as key regions that define myosins of class VI: insert-1 (involved in regulation of nucleotide binding) and insert-2 (the 'reverse gear', responsible for reverse directionality) (Menetrey et al., 2005; Bryant et al., 2007). Predicted SPE-15/HUM-3 and HUM-8 AlphaFold structures have the same overall motor domain organisation compared to structures of human MYO6 without any indication of major structural changes (see Figure 1 A, B) (Jumper et al., 2021).

We next analysed the biophysical motor properties using *in vitro* motility assays and stopped-flow spectroscopy. The SPE-15/HUM-3 and HUM-8 motor and neck domains were co-expressed with calmodulin and purified from SF9 cells (Figure 1C). To determine the ATPase activity of SPE-15/HUM-3 and HUM-8, and to study the interaction of these myosins with F-actin, we measured the translocation speed of rhodamine-phalloidin labelled actin filaments by surface-immobilised SPE-15/HUM-3, HUM-8 or human MYO6 (Figure 1D). Our results show that SPE-15/HUM-3 and HUM-8 have similar average velocities compared to human MYO6, with gliding speeds of 52 ± 8 nm/s, 49 ± 6 nm/s and 55 ± 9 nm/s, respectively.

All myosins are united by a characteristic cyclical interaction with actin driven by ATP hydrolysis, which produces mechanical movement as a result of structural changes in the motor (Preller and Manstein, 2013). To determine if any part of the mechanochemical ATPase cycle is altered in SPE-15/HUM-3 or HUM-8 compared to human MYO6, we measured their fast reaction kinetics using stopped-flow spectroscopy. This assay measures the fluorescence of pyrene-labelled actin which is quenched when complexed to a myosin. The myosin is released from actin after ATP-binding, resulting in an increase in pyrene fluorescence. This set-up was used to measure the second order rate constant of ATP-induced dissociation of an actin.myosin complex. All three proteins follow single exponentials with no lag phase. The dependence of the observed rate constant on ATP concentration is shown in Figure 1E. The gradients of these plots were used to determine the apparent second order rate constants for ATP binding to actin.myosin, which for the three proteins were as follows; human MYO6: 5 ± 0.4 $mM^{-1}s^{-1}$, SPE-15/HUM-3: 9 ± 0.8 $mM^{-1}s^{-1}$ and HUM-8: 3 ± 0.5 $mM^{-1}s^{-1}$. Although overall very similar, the slight differences may indicate altered nucleotide affinities for the three motors. To test this further, we compared the affinity of SPE-15/HUM-3, HUM-8 or MYO6 for ADP in the presence of actin using a competition assay. In this set up, the actin.myosin complex is

10.3389/fphys.2024.1368054

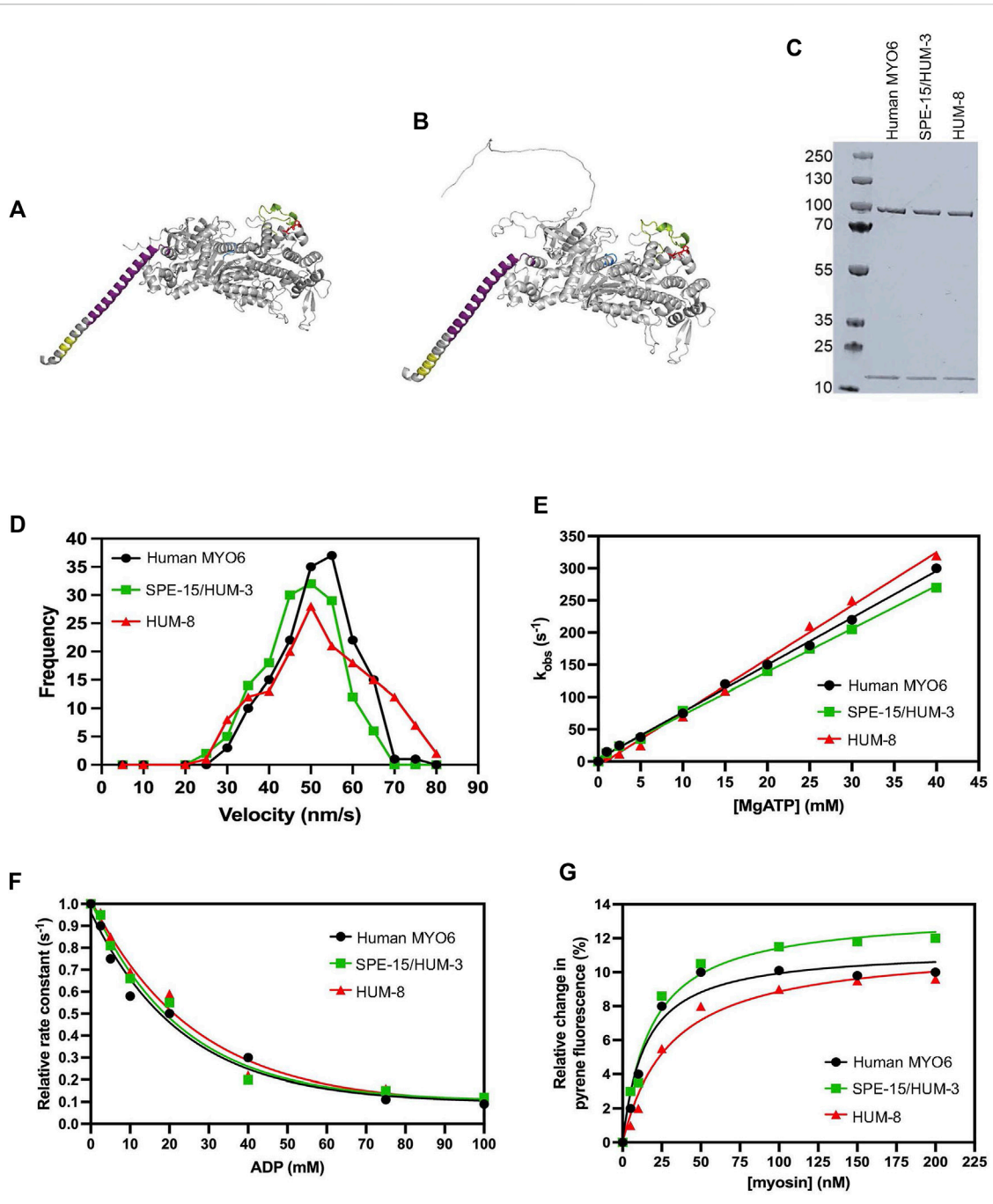

FIGURE 1
Biophysical properties of SPE-15/HUM-3 and HUM-8 compared to human MYO6. Predicted SPE-15/HUM-3 **(A)** and HUM-8 **(B)** *AlphaFold* structures of the motor and neck region. The P-loop is shown in blue, insert-1 in green, insert-2 in purple and IQ motif in yellow. **(C)** SDS-PAGE of recombinant SPE-15/HUM-3 and HUM-8 motor neck domain expressed and purified from *ExpiSF9* cells. **(D)** Actin-gliding velocity of rhodamine-phalloidin labelled actin filaments of human MYO6 (black), SPE-15/HUM-3 (green), and HUM-8 (red) motor domains as determined by *in vitro* motility assays in at least three independent experiments. The histograms show typical distributions of actin filament velocities on myosin-decorated surfaces. The mean velocity for human MYO6 was 55 ± 2.3 nm/s, 51 ± 3.3 nm/s for SPE-15/HUM-3 and 49 ± 5.6 nm/s for HUM-8 as calculated using a Gaussian fit. No statistical difference was observed between these values. **(E)** The effect of ATP concentration on the observed rate constant for ATP-induced dissociation of pyrene-actin. myosin for human MYO6 (black), SPE-15/HUM-3 (green) and HUM-8 (red). The gradient generates a second-order rate constant of ATP binding. **(F)** Plot of relative observed rate constant dependence on ADP concentration for the ATP-induced dissociation of pyrene-actin. myosin from human MYO6 (black), SPE-15/HUM-3 (green) and HUM-8 (red). **(G)** Fluorescence amplitude plotted as a function of myosin concentration can be described by a quadratic fit resulting in the affinity for actin of human MYO6 (black), SPE-15/HUM-3 (green) and HUM-8 (red).

preincubated with varying concentrations of ADP, which led to a competition in binding between the ATP and ADP. The resulting observed rate can be plotted as a function of ADP concentration, which has a hyperbolic dependence (Figure 1F). SPE-15/HUM-3 and HUM-8 have slightly weaker affinities for ADP (18 ± 4 mM and 20 ± 2 mM respectively) compared to human MYO6 (6 ±

10.3389/fphys.2024.1368054

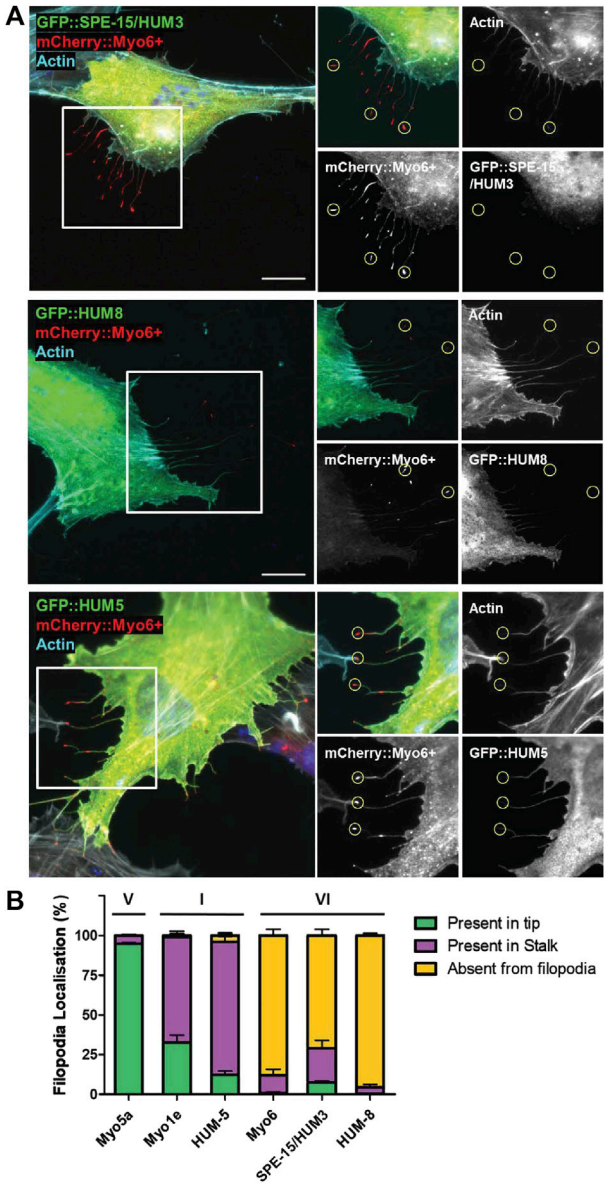

FIGURE 2
Localisation of SPE-15/HUM-3 and HUM-8 in filopodia as a measure of their directionality. **(A)** RPE cells co-transfected with GFP::SPE-15/HUM-3 (top), GFP::HUM-8 (middle) or GFP::HUM-5 (bottom) alongside mCherry:Myo6+. Actin filaments are labelled using Phalloidin-647 (cyan), Nuclei are labelled using Hoechst (blue). Yellow circles indicate examples of representative filopodia tips. Scale bar, 10 µm. **(B)** Quantification of GFP:myosin localisation in filopodia of RPE cells. 100 filopodia were counted per coverslip and assigned either 'present in tip', 'present in stalk' or 'absent from filopodia' localisation by eye from n = 3 independent experiments per condition. Error bars indicate SEM.

0.8 mM). These parameters indicate small modulations in motor activity with ATP and ADP.

Finally, to determine the affinity of SPE-15/HUM-3 and HUM-8 to actin, the ATP-induced dissociation reaction was performed with varying myosin concentrations. At higher concentrations of myosin, an increasing amount of pyrene will be quenched at the beginning of the measurement, leading to an increase in fluorescence amplitude (Figure 1G). The plotted relative amplitude as a function of myosin concentration can be described by a quadratic equation, resulting in the actin affinity. The affinities for human MYO6 and SPE-15/HUM-3 were similar, with values of 15 ± 3 and 13 ± 5 nM respectively. HUM-8 has a slightly weaker affinity value of 23 ± 5 nM, although this figure still being in the sub-nanomolar range is unlikely to impact the function of the motor. Overall, these results demonstrate that both SPE-15/HUM-3 and HUM-8 have kinetic characteristics similar to human MYO6, which are typical of a class VI myosin.

SPE-15/HUM-3 and HUM-8 do not accumulate at the plus ends of actin filaments

Both myosins, SPE-15/HUM-3 and HUM-8, contain the insert-2 in the converter region that repositions the lever arm to trigger reverse movement towards the minus-end of actin filaments (Supplementary Figure S1) (Wells et al., 1999; Menetrey et al., 2005; Bryant et al., 2007). To test whether SPE-15/HUM-3 and HUM-8 indeed share the reverse directionality with other myosins of class VI, we visualised the localisation of SPE-15/HUM-3 and HUM-8 in filopodia at the cell surface of RPE cells. To induce the formation of these filopodia, we transfected into RPE cells a mutant form of human MYO6, termed MYO6+, which is a genetically engineered plus-end directed MYO6 whose neck region, including insert-2, is replaced with the lever arm of MYO5, a plus-end tracking myosin (Masters and Buss, 2017). The mutant MYO6 induces the formation and accumulates at the tips of filopodia, thereby marking the plus-ends of actin filament bundles inside these plasma membrane protrusions. To test if SPE-15/HUM-3 and HUM-8 are indeed minus-end directed myosins, they were co-expressed together with MYO6+ in RPE cells. In addition to SPE-15/HUM-3, HUM-8 (Figure 2A) and human wild-type MYO6, we also tested the localisation of three plus-end directed myosins within filopodia: human MYO5, human MYO1E and HUM-5, the *C. elegans* homologue of a class I myosin. We subsequently quantified the localisations of the six myosins, which were either present in filopodia tips (green), along the length of the filopodia stalk (purple), or absent from filopodia altogether (yellow). The results summarized in Figure 2B indicate that the three myosins of class VI predominantly accumulate in the cytosol, and none are found in filopodia. In contrast, human MYO5A shows almost complete accumulation at the tips of filopodia, whilst the two myosins of class I are present along the length of filopodia with a modest concentration at the tips. These results may indicate that MYO5A as a processive, dimeric motor is able to maintain its position at the fast growing plus ends of actin filaments, while the slower, monomeric myosins of class I are moved away from filopodia tips *via* actin treadmilling. In summary, these experiments strongly suggest that SPE-15/HUM-3 and HUM-8 are not able to move towards the plus-end of actin filaments, confirming their classification as reverse motors.

Two splice variants of HUM-8 are expressed in *C. elegans*

Our earlier sequence alignments (Supplementary Figure S1) indicated that neither SPE-15/HUM-3 nor HUM-8 contain sequences corresponding to the human LI or SI. The alternative

10.3389/fphys.2024.1368054

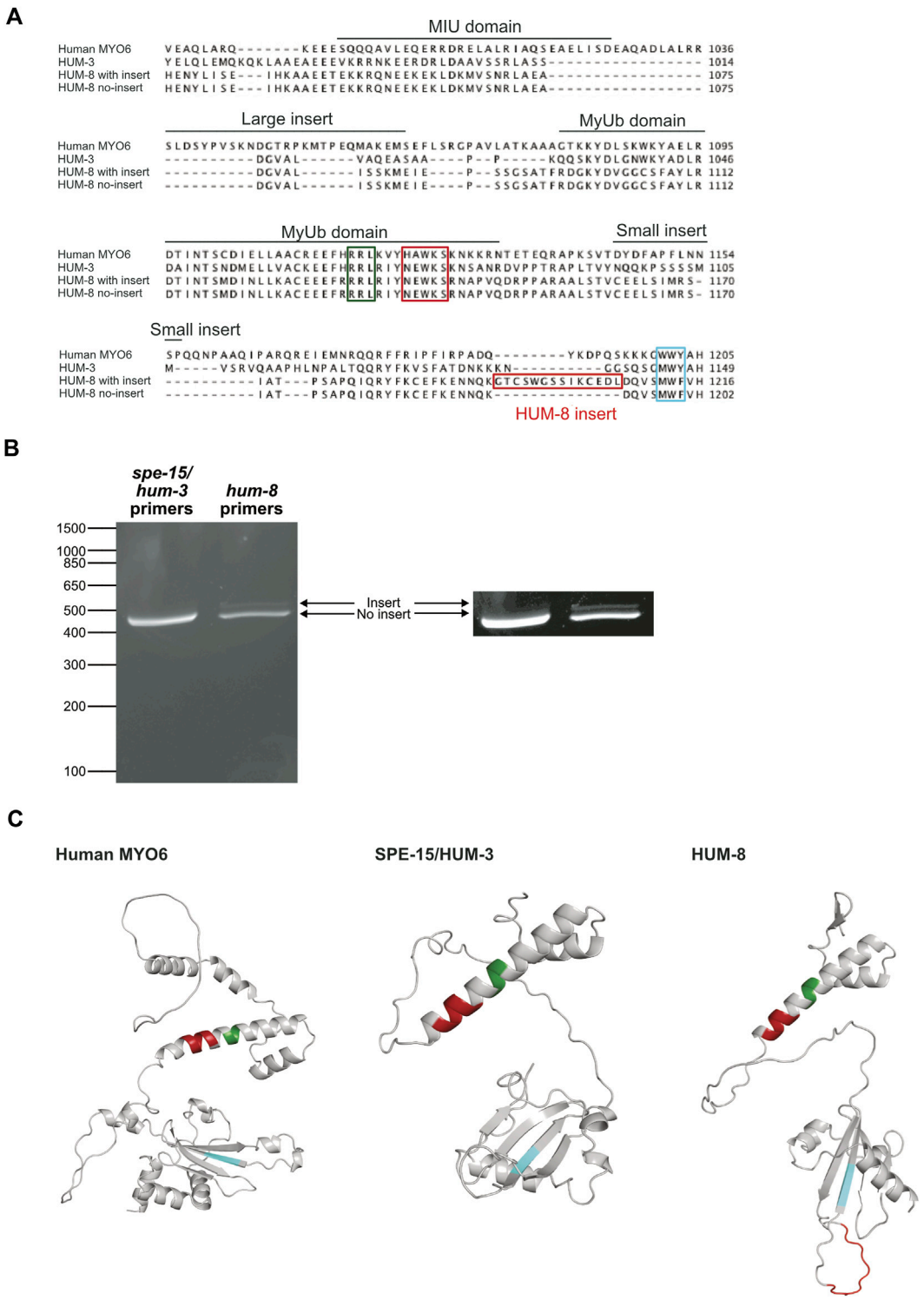

FIGURE 3
Two splice variants of HUM-8 are expressed in adult worms. **(A)** Multiple sequence alignment of the CBDs of SPE-15/HUM-3, HUM-8 and human MYO6 highlighting key regions for cargo-binding identified in MYO6 such as the RRL-motif (green), HAWKS-motif (dark red), and WWY-sequence (blue). The alignment indicates a 12 bp region in HUM-8 (HUM-8 insert, red) that is uniquely present in one HUM-8 isoform. **(B)** DNA electrophoresis gel of PCR reactions amplifying the CBDs of SPE-15/HUM-3 and HUM-8 directly from purified worm cDNA. Only a single band (468 bp) is present for SPE-15/HUM-3, indicating a single splice variant. Two bands are present in the HUM-8 lane (one at 444 bp and the other slightly larger), indicating two splice variants. The image on the right is modified for enhanced contrast to aid visualisation of the second HUM-8 band. **(C)** *AlphaFold* predicted structure of the CBDs of human MYO6 (left) alongside SPE-15/HUM-3 (middle) and HUM-8 (right), with the cargo-binding motifs outlined in **(A)** highlighted in colour. The unique HUM-8 insert, found on an extended loop, is also shown here in red.

splicing of human MYO6 gives rise to four isoforms with functional variation resulting from differences in their binding interactions with adaptor proteins. To determine whether SPE-15/HUM-3 and HUM-8 are similarly alternatively spliced, using PCR we amplified the CBD regions spanning the MIU domain and ending in the WWY motif, which in human MYO6 encompasses both the SI and the LI (highlighted in Figure 3A). The PCR products were run on a DNA agarose gel and show a single band for SPE-15/HUM-3, corresponding to a single splice variant, and two bands for HUM-8, indicating two distinct splice variants (Figure 3B). The three bands were sequenced and aligned to human MYO6, which highlighted a 42 base pair region that was present in just one of the two HUM-8 variants (amino acid sequence highlighted in red box, Figure 3A). Whilst this sequence of HUM-8 containing the additional insert has previously been computationally mapped as a potential HUM-8 isoform on UniProt, we show here that it is indeed expressed in *C. elegans*. No similar amino acid sequence was present in either SPE-15/HUM-3 or human MYO6, indicating a unique alternatively spliced region (GTCSWGSSIKCEDL) in HUM-8 only, giving rise to two potential isoforms. No homology to any known protein motifs was identified within the sequence, suggesting that if HUM-8 function is diversified through its alternative splicing, then this could possibly point to the existence of novel *C. elegans* adaptor-binding motifs.

SPE-15/HUM-3 and HUM-8 are not recruited to endosomes in mammalian cells

Cargo adaptor proteins mediate the diverse functions of human MYO6 in different cell types and tissues. From the large array of human MYO6 binding partners, only three appear to have orthologues in *C. elegans* or *Drosophila*: TOM1L2 (C07A12.7 in *C. elegans*; CG3529 in *Drosophila*), GIPC (gipc-1/gipc-2 in *C. elegans*; Kermit in *Drosophila*) and Dab2 (dab-1 in *C. elegans*; Disabled in *Drosophila*). Comparing MYO6 binding partner homologues in *C. elegans* and *Drosophila* thus yields the same repertoire of proteins, whilst most other known MYO6 binding partners do not have homologues in either of these organisms. Both *C. elegans* and *Drosophila* show significant conservation in the two cargo adaptor binding sites, the RRL and the WWY motif. Although the binding site for TOM1L2 and Dab2, the WWY motif, is changed to MWF, the second tryptophan, which has been shown to be crucial for cargo adaptor binding, is conserved (Spudich et al., 2007). In contrast, the RRL motif, the binding site for GIPC, is unchanged in SPE-15/HUM-3, HUM-8 and Jaguar.

Since GIPC interacts with APPL1 and is thus important for targeting of human MYO6 to early endosomes in the cell periphery, we next compared the localisation of SPE-15/HUM-3 and HUM-8 as well as Jaguar to human MYO6. SPE-15/HUM-3, HUM-8 (isoform with unique insert), and Jaguar were cloned into the mammalian expression vector pEGFP and, together with the NI isoform of human MYO6, expressed as GFP-fusion proteins in RPE cells. Following fixation, the cells were stained with antibodies to APPL1, the marker protein for early signalling endosomes found in the actin-rich cell cortex. Human NI GFP-MYO6 co-localises precisely with APPL1-positive endosomes in the cell periphery (Figure 4A). In contrast, whilst SPE-15/HUM-3 and HUM-8 are recruited to the plasma membrane at the leading edge of the cell, no colocalisation with APPL1 is evident for the *C. elegans* homologues (Figures 4B,C). Intriguingly, like human MYO6, the expressed *Drosophila* homologue of MYO6, Jaguar, is present on APPL1 labelled endosomes (Figure 4D).

These findings imply that the presence of a conserved RRL motif alone is not solely responsible and sufficient for recruiting these MYO6 variants to early endosomes. It is likely that additional lipid or protein binding motifs that are present in MYO6 and Jaguar but absent from SPE-15/HUM-3 and HUM-8, are required for selective targeting.

SPE-15/HUM-3 and HUM-8 vary in their developmental expression patterns

Very little is known about the specific tissue and cellular expression patterns of SPE-15/HUM-3 and HUM-8 across the worm lifespan. To gain insight into their developmental expression as a way to understand their potential functional specialisations, we utilised worms expressing fluorescently-tagged mNeonGreen:SPE-15/HUM-3 and wrmScarlet:HUM-8 (Sunybiotech). Nematodes from every larval stage (L1 to L4), as well as at days 2 and 5 of adulthood, were imaged (Figures 5A,B). Our results show that SPE-15/HUM-3 and HUM-8 are both expressed throughout all nematode developmental stages, but with varying patterns. SPE-15/HUM-3 is expressed in the head throughout the nematode lifespan (white arrows, Figure 5A). At the L4 larval stage, SPE-15/HUM-3 fluorescence is seen throughout the gonads (red arrow, Figure 5A), while at the young adult stage, this gonadal fluorescence pattern is replaced by a distinctive localisation of SPE-15/HUM-3 in each arm of the gonads (blue arrows, Figure 5A). This pattern dissipates after the young adult stage, suggesting a developmental regulation of SPE-15/HUM-3 expression, wherein SPE-15/HUM-3 is upregulated in the gonadal tissues at the L4 stage and subsequently downregulated following young adulthood. In contrast, the expression of HUM-8 is uniform throughout all developmental stages, being enriched almost exclusively in the intestinal epithelium (Figure 5B). There was no observable change in HUM-8 tissue expression at any larval stage, implying a lack of developmental regulation.

HUM-8 is expressed predominantly within the intestinal epithelium, whereas SPE-15/HUM-3 localises to neuronal tissue and the gonads

Having determined the developmental expression and distribution of both SPE-15/HUM-3 and HUM-8, we next conducted detailed localisation analysis at high-resolution to determine the tissue and cell-specific distribution of the two myosins. High-magnification tile-scan images of young adult wrmScarlet:HUM-8 worms confirmed that HUM-8 is expressed almost exclusively in the cytosol of intestinal epithelial cells (Figure 6A, dark regions seen where nuclei are excluded from fluorescence). The intestine is composed of large, cuboidal enterocytes that form pairs, each surrounding the intestinal

10.3389/fphys.2024.1368054

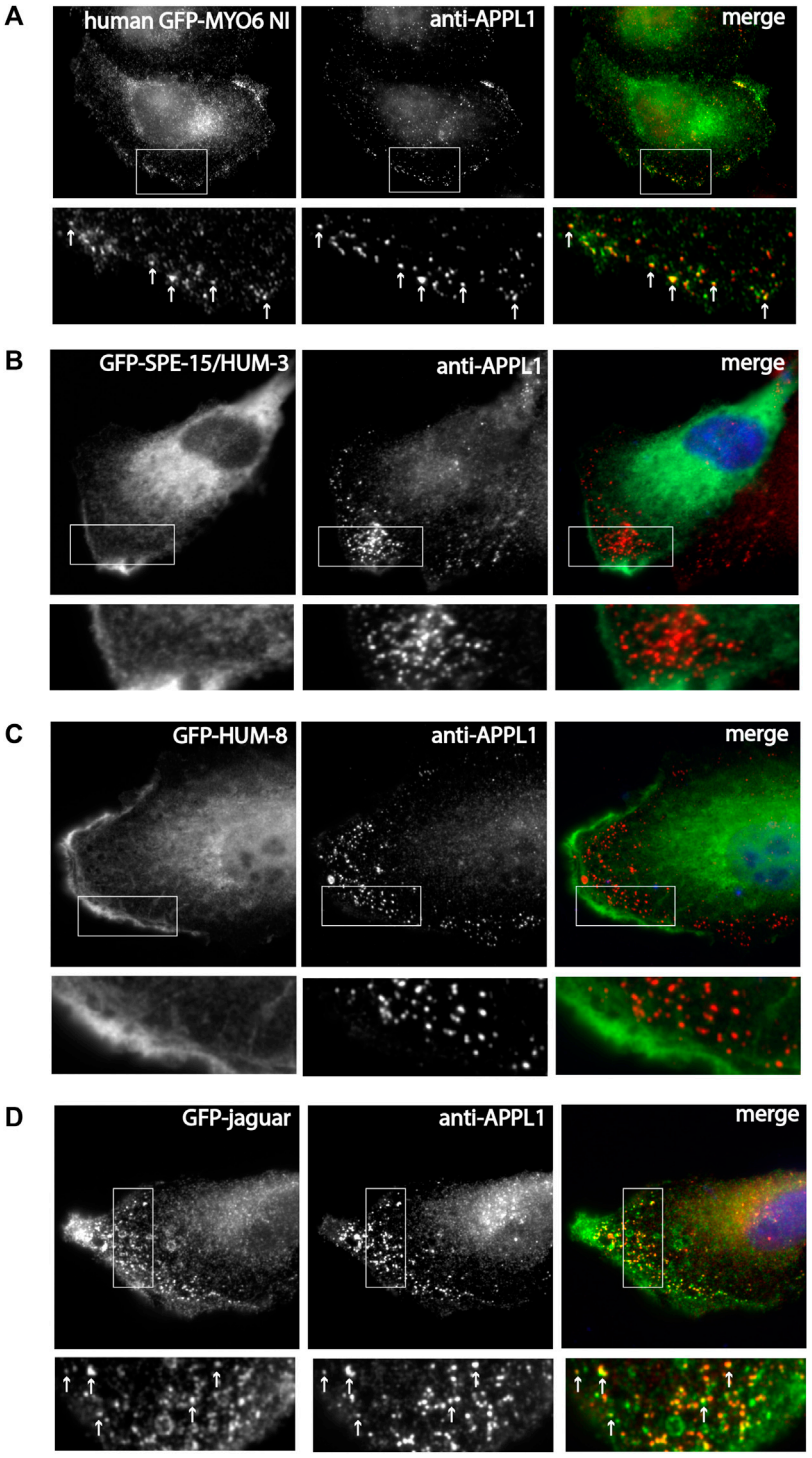

FIGURE 4
SPE-15/HUM-3 and HUM-8 are not recruited to early endosomes in mammalian cells, in contrast to the Drosophila MYO6 homologue (Jaguar). **(A)** GFP-tagged human MYO6 no insert (NI), **(B)** GFP-SPE-15/HUM-3, **(C)** GFP-HUM-8 and **(D)** GFP-jaguar were expressed in RPE cells and stained with antibodies to APPL1 to label early endosomes. Boxed area is enlarged in the panel below in A-D. White arrows in the boxed area highlight colocalization between the different myosins and APPL1-positive endosomes. While human MYO6 and Dosophila Jaguar are recruited to APPL1-positive endosomes, SPE-15/HUM-3 and HUM-8 show no colocaliation with APPL1. Scale bar, 10 μm.

lumen (Figure 6B) (Dimov and Maduro, 2019). HUM-8 is expressed at similar levels in these enterocytes. Super-resolution AiryScan images of the worm shown in Figure 6A (regions of interest highlighted in white boxes) revealed a vesicular localisation pattern of HUM-8 at higher resolution, suggesting that this myosin is localising to vesicles in intestinal cells (Figures 6C,D). Further work, however, will be required to determine the exact nature of these vesicles.

10.3389/fphys.2024.1368054

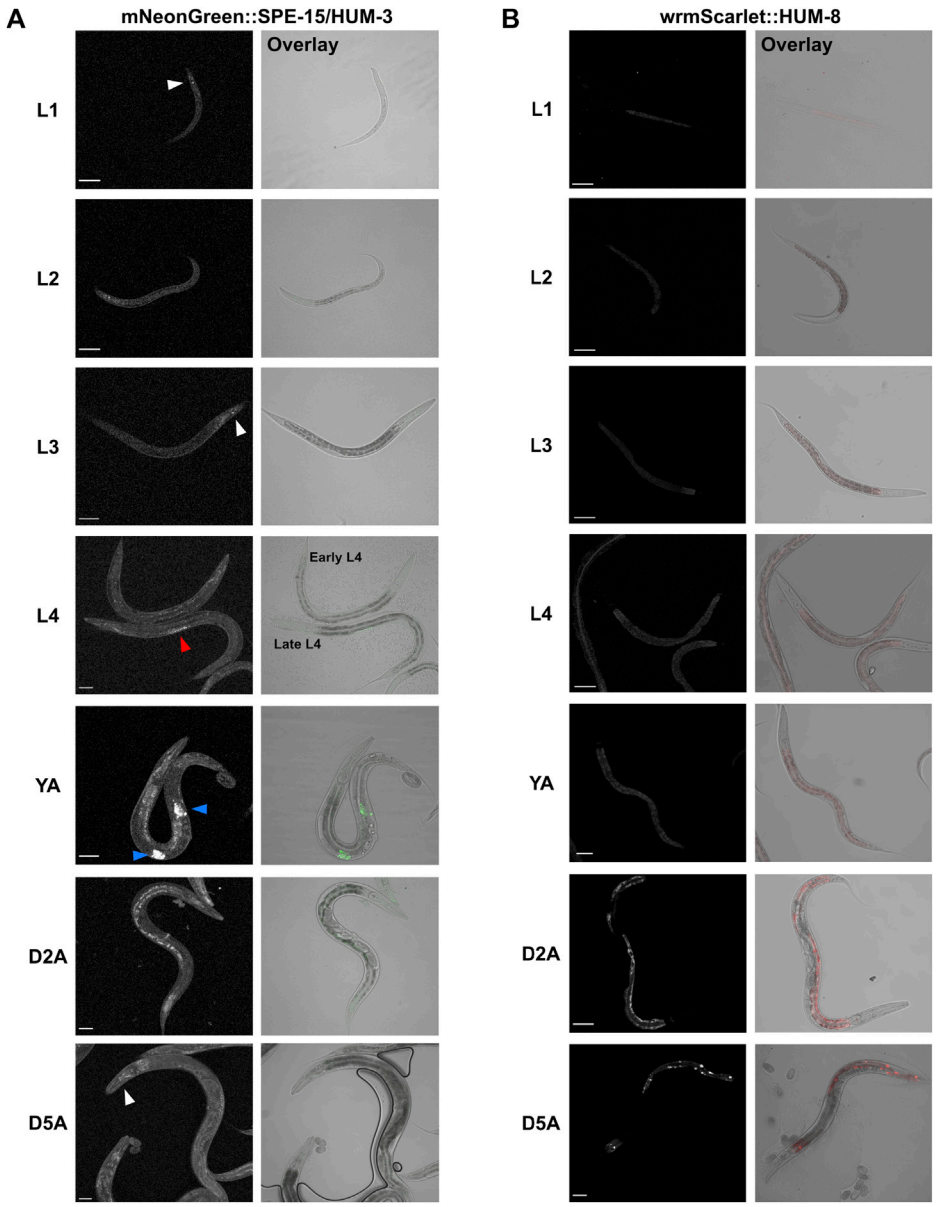

FIGURE 5
Whole-worm confocal imaging indicates differential developmental and tissue-specific expression of SPE-15/HUM-3 and HUM-8. **(A)** mNeonGreen:SPE-15/HUM-3 and **(B)** wrmScarlet:HUM-8 localisation throughout the larval stages (L1-L4) and into young adulthood (YA) and days 2 (D2A) and 5 (D5A) of adulthood. Images from three independent biological repeats (N = 8–10 animals each) were taken. For each developmental stage, a representative image is shown. White arrows point to SPE-15/HUM-3 localisation in the head, red arrows to localisation throughout the gonads, and blue arrows to a focused localization in each arm of the gonads of the nematode. All images taken at ×20 magnification. Scale bars, 50 μm.

High-magnification tile-scan images of L4 mNeonGreen:SPE-15/HUM-3 worms confirmed the localisation of SPE-15/HUM-3 to three distinct sites: cells within the nematode head, within the tail, and, most prominently, to germ cells in the gonad (white box, Figure 7A). *C. elegans* hermaphrodites exclusively undergo spermatogenesis at the L4 stage. This ceases as the worm develops into an adult, at which point oogenesis begins. A close up of the gonadal regions highlighted in Figure 7B showed SPE-15/HUM-3 expression in a very small subset of developing germ cells towards the vulva and to the proximal end of the L4 gonad. Airyscan images of this region shows that, in these cells, SPE-15/HUM-3 is concentrated in the cytoplasm around the nucleus (Figure 7B). In the young adult stage, as hermaphrodites transition from spermatogenesis to oogenesis, residual expression of SPE-15/HUM-3 is restricted to two regions either side of the vulva (two bright areas of fluorescence likely representing spermatids, Figure 7C). This change in expression from a regular extended punctate pattern (Figure 7B) to a concentrated bilateral arrangement (Figures 7C,D) likely represents the transition into the final stages of spermatogenesis as the worm develops into a young adult. Based on these developmental changes, and the localisation of the developing germ cells, it can be deduced that SPE-15/HUM-3 is expressed in spermatocytes and spermatids at the late stages of spermatogenesis, just before spermatid budding

10.3389/fphys.2024.1368054

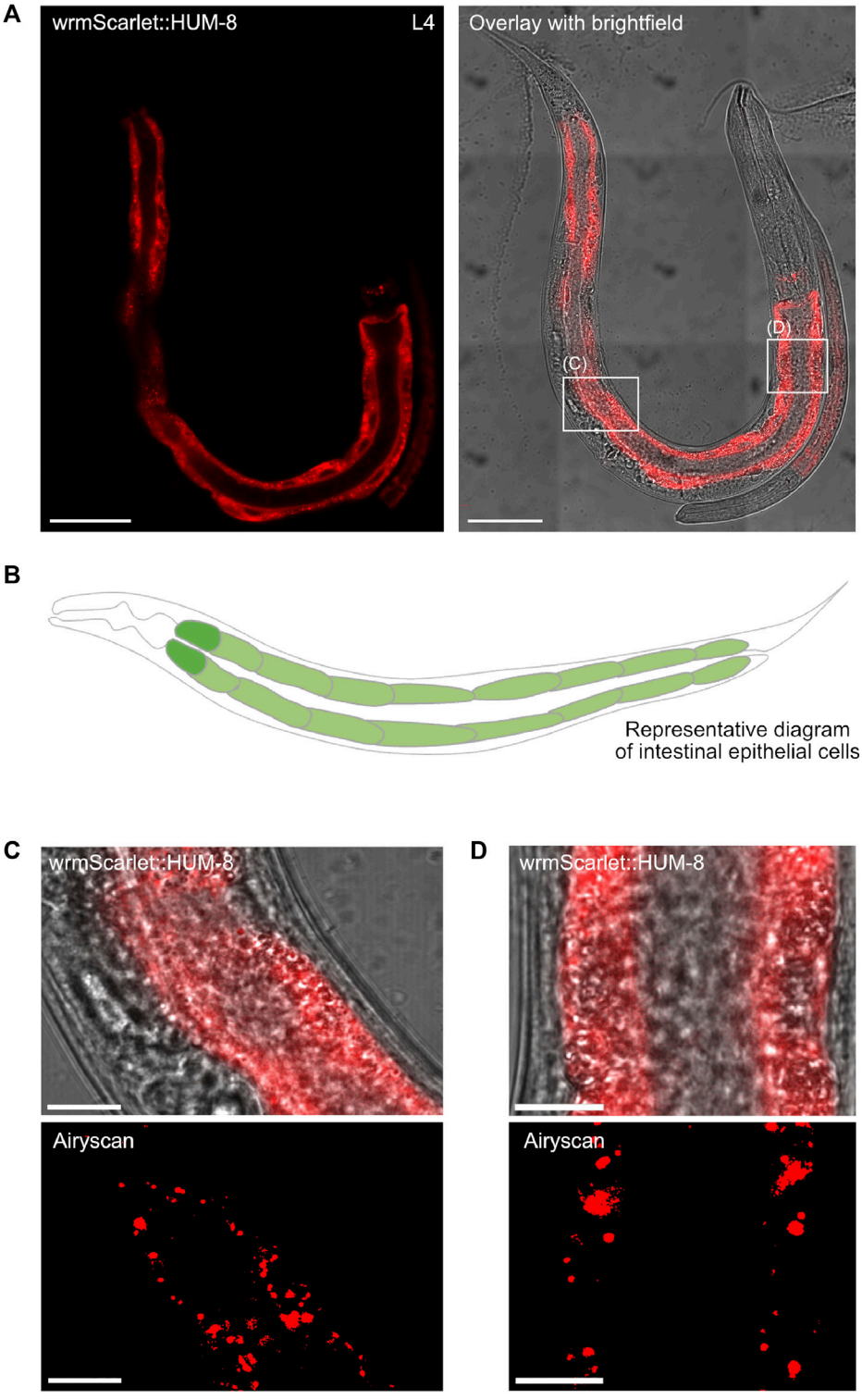

FIGURE 6
HUM-8 is expressed in the *C. elegans* intestinal epithelium. **(A)** A tile scan confocal image of a young adult worm expressing wrmScarlet:HUM-8 taken at ×63 magnification. Scale bar, 50 μm. **(B)** A representative schematic of the *C. elegans* intestine. Cells are arranged around a hollow core (the intestinal lumen). **(C)** and **(D)** are regular confocal (top) and Airyscan (bottom) images of HUM-8 within the intestinal epithelium from areas outlined in white boxes in **(A)**. Scale bar, 10 μm. **(D)**.

near the spermatheca. SPE-15/HUM-3 expression is apparently downregulated in the gonads post the young adult stage as fluorescence is not found in a spermathecal structure throughout adulthood, supporting a model wherein SPE-15/HUM-3 is here expressed solely in spermatocytes and early spermatids as spermatogenesis is occurring, but not afterwards.

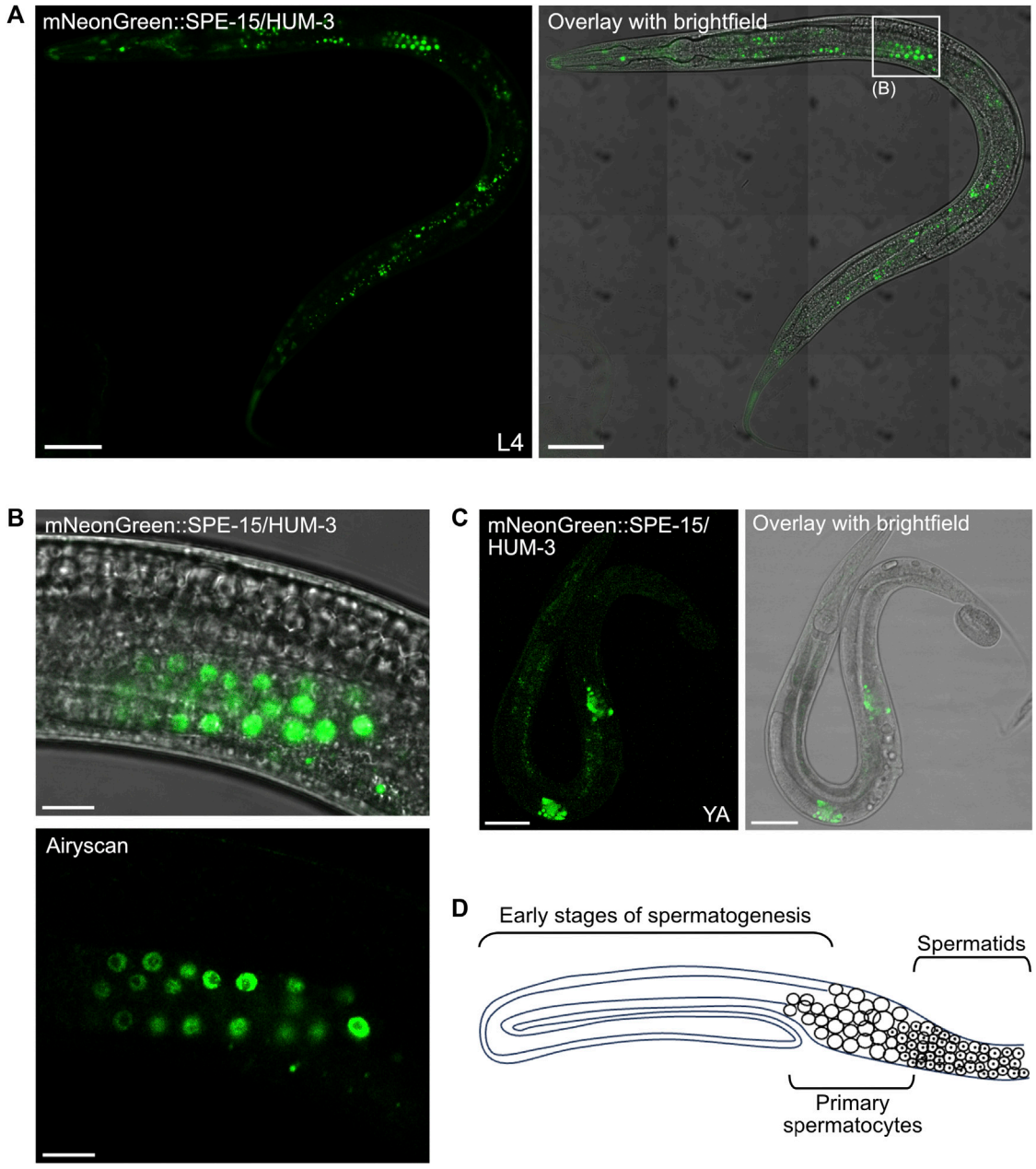

FIGURE 7
SPE-15/HUM-3 is expressed in the *C. elegans* gonads. **(A)** A tile scan confocal image of an L4 worm expressing mNeonGreen:SPE-15/HUM-3 taken at ×63 magnification. Areas outlined in white boxes are shown at a larger scale in different sections as indicated. Scale bar, 50 µm. **(B)** Regular confocal (top) and Airyscan (bottom) images of SPE-15/HUM-3 localisation in the gonads of an L4 stage worm. Scale bar, 10 µm. **(C)** Regular confocal image of a young adult mNeonGreen:SPE-15/HUM-3 worm showing SPE-15/HUM-3 within the gonads of a young adult worm. Scale bar, 50 µm. **(D)** A representative schematic of one arm of a bilaterally symmetric, two-armed, wild-type hermaphrodite gonad undergoing spermatogenesis. Distal is to the left. The diagram highlights typical organisation of the germline, showing that progression from early spermatogenesis stages into the meiotic stages occurs from distal to proximal. Primary spermatocytes have not yet undergone meiosis I. Following spermatogenesis, mature sperm are stored in a proximal spermatheca, the receptacle in which sperm are stored.

Super-resolution imaging of the head of mNeonGreen:SPE-15/HUM-3 worms shows SPE-15/HUM-3 concentrating to neuronal cell bodies around the terminal bulb of the pharynx (white arrows, Figures 8A,B, Supplementary Video). This region is occupied by neurons of the lateral and ventral ganglia (Figure 8C), which are primarily composed of interneurons and sensory neurons. SPE-15/HUM-3 is also localised to neuronal cell bodies in the retrovesicular ganglion, which is composed of both motor neurons and interneurons (red arrows, Figures 8A,B, Supplementary Video). Based on collated expression data (Wormbase data release WS282, 2021), it is most likely that SPE-15/HUM-3 localises to interneurons, which typically transmit signals between different neurons. Importantly, the expression of SPE-15/HUM-3 is not restricted to cell bodies;

10.3389/fphys.2024.1368054

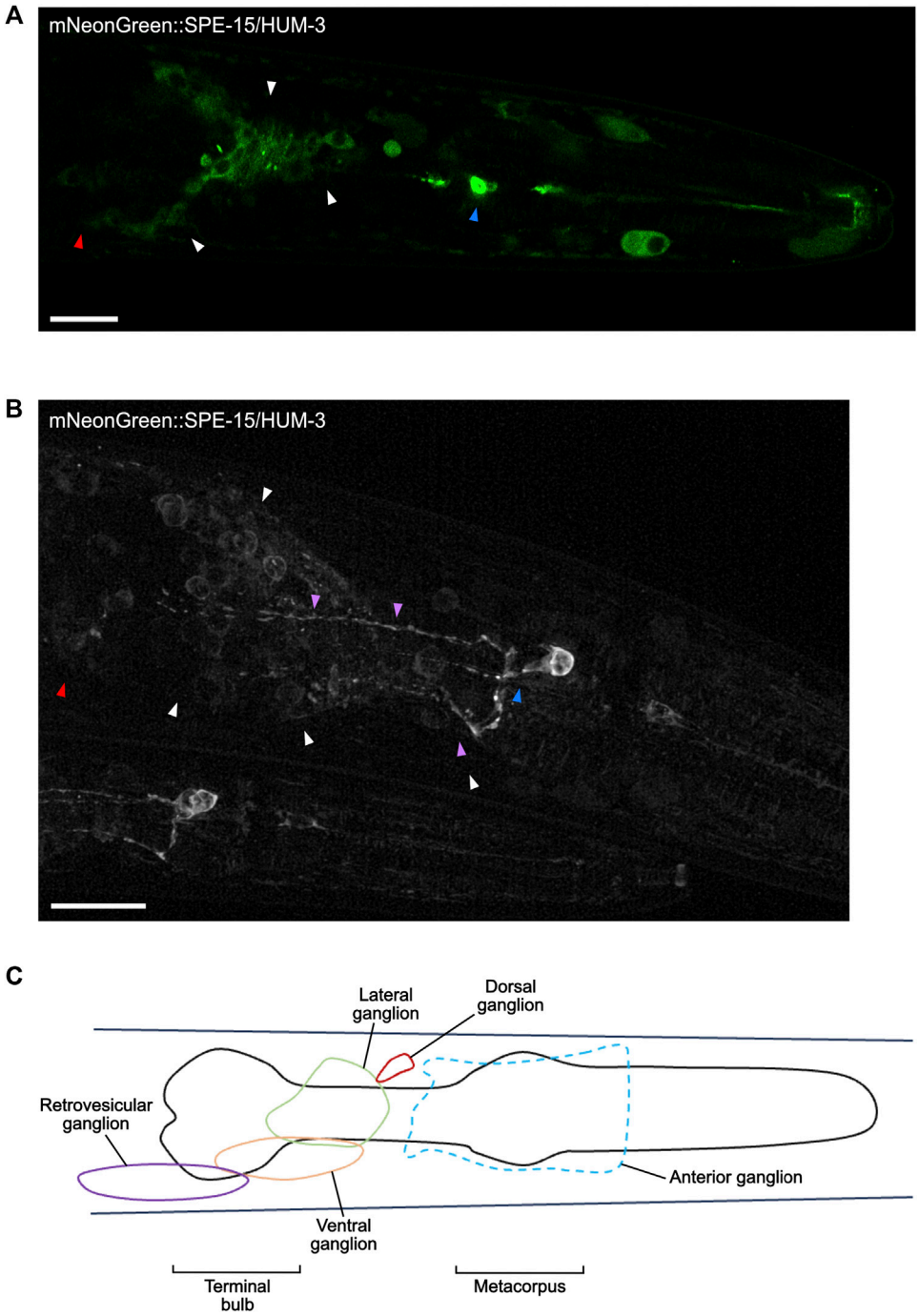

FIGURE 8
SPE-15/HUM-3 is present in cells of the nervous system within the *C. elegans* head. **(A)** An Airyscan image of SPE-15/HUM-3 expression in the head taken at ×63 magnification. **(B)** A super-resolution image of SPE-15/HUM-3 expression within a *C. elegans* head showing the same region as in **(A)**. Scale bars, 10 μm. Note that a younger worm can be found adjacent to the older, larger one. **(C)** A representative schematic highlighting the main regions, known as ganglia, containing the majority of neuronal cell bodies in the head region.

fluorescence is present in long, thin projections going across the pharynx–these projections are likely to be neuronal axons (Figure 8B). SPE-15/HUM-3 is also expressed in a prominent bulbous neuronal cell body in the metacorpus of the pharynx (blue arrows, Figures 8A,B). The WormAtlas database was used to map the identity of this neuron, which suggested it to be NSM/L (NSM indicates neuron class; "L" indicates left, position in worm), a neurosecretory-motor neuron. Interestingly, SPE-15/HUM-3 further localises to an axon with a "dashed" pattern that terminates at the terminal bulb (purple arrows, Figures 8A,B). It is unclear which neuron the process is associated with, but it could possibly be that of NSM/L, whose processes are known to periodically swell, forming structures containing vesicles to which SPE-15/HUM-3 could possibly be localising (Axang et al., 2008).

In summary, our extensive imaging analysis has identified distinct developmental and tissue expression patterns for the MYO6 homologues SPE-15/HUM-3 and HUM-8 in *C. elegans*, supporting the conclusion that both of these myosins of class VI function uniquely and specifically within their respective tissues.

Discussion

Despite the extensive cellular and biophysical characterisation of human MYO6, the biophysical properties, tissue distribution and function of the two *C. elegans* MYO6 homologues, SPE-15/HUM-3 and HUM-8, are largely unknown. In this study, we confirm that SPE-15/HUM-3 and HUM-8 are indeed minus-end-directed myosins of class VI. These myosins have comparable biophysical and structural characteristics to human MYO6. However, they also possess distinctive structural and sequence-specific elements that set them apart from other myosins of class VI. Through our imaging analysis we provide, for the first time, visualisation of the unique developmental and tissue expression patterns of both myosins endogenously within the nematode. This sheds new light on the potential diversification of MYO6 function in *C. elegans*.

Our sequence and predicted structural analysis of SPE-15/HUM-3 and HUM-8 classifies both motors as myosins of class VI with a high degree of sequence similarity to human MYO6. Key myosin class VI-defining elements, including insert-1, which has been suggested to modulate nucleotide binding, and insert-2 ('reverse gear'), responsible for the reverse directionality of MYO6, are conserved in SPE-15/HUM-3 and HUM-8. Interestingly, in contrast to human MYO6 both SPE-15/HUM-3 and HUM-8 have N-terminal extensions at their motor domains, which potentially provide additional protein-protein interaction motifs or functional domains. Such examples of myosins include myosins of class III that contain an N-terminal kinase domain (Dose and Burnside, 2000) and MYO16, which contains a 400 amino acid N-terminal extension with several protein interaction motifs. These motifs facilitate binding to other myosin motors. In addition, the extension includes phosphorylation sites and ankyrin repeats which play a role in modifying the ATPase activity (Kengyel et al., 2015). Moreover, studies on class I myosins have demonstrated that the N-terminal region plays a crucial role in refining motor functions, as it helps stabilize the post-power-stroke conformation. This region is a vital structural component in the force sensing capabilities of myosin and indicates a method for creating functional diversity among different myosin isoforms (Greenberg et al., 2015).

Our analysis of the biophysical motor properties of SPE-15/HUM-3 and HUM-8 confirmed them as class VI myosins. *In vitro* motility assays and stopped-flow spectroscopy indicated that SPE-15/HUM-3 and HUM-8 move with similar velocities and display similar ATPase kinetics to human MYO6. Our findings suggest that SPE-15/HUM-3 and HUM-8 share comparable motor properties with human MYO6, emphasising their classification as myosins of class VI. The marginal differences in nucleotide affinities and ADP binding suggest subtle modulations in motor activity but reinforce the overall resemblance to human MYO6.

One key feature of SPE-15/HUM-3 and HUM-8 is the presence of insert-2 in the converter region. This insert repositions the lever arm, which plays a crucial role in determining the direction of myosin movement along actin filaments. We determined the direction of movement of SPE-15/HUM-3 and HUM-8 using a cellular assay whereby each myosin was expressed in RPE cells alongside MYO6+, an engineered plus-end-directed MYO6 that induces the formation of filopodia in cells and accumulates at the tips of such protrusions. We found that neither SPE-15/HUM-3 nor HUM-8 localise to filopodia tips, suggesting that they are not plus-end-directed. While our filopodia tip recruitment assay does not provide direct proof that SPE-15/HUM-3 and HUM-8 move towards the minus end of actin filaments, their almost complete absence from filopodia strongly suggests that SPE-15/HUM-3 and HUM-8, along with human MYO6, are not capable of moving towards the plus end of actin filaments. This supports their classification as reverse motors, and their presumed movement towards the minus ends of actin filaments highlights their unique role in cellular processes. Interestingly, different classes of plus-end directed myosins show differential localisation along filopodia. While the highly processive dimeric MYO5A almost exclusively accumulates at the tips, slower monomeric myosins of class I, MYO1E and HUM-5, reach the tip but are also found along the length of the filopodia. This might reflect the slower velocity of MYO1E and HUM-5 compared to MYO5A, which leads to retrograde movement powered by actin treadmilling. In addition, these myosins of class I are also recruited into filopodia through their lipid binding tail domains. In conclusion, while our cellular assay does not directly prove minus-end-directed movement, the minimal localisation of SPE-15/HUM-3 and HUM-8 in filopodia strongly suggests that these two myosins, like human MYO6, have reverse motor characteristics.

While there is considerable conservation in the motor domain between SPE-15/HUM-3 and HUM-8 and human MYO6 and Jaguar, the tail domains of SPE-15/HUM-3 and HUM-8 exhibit significant sequence divergence, with the exception of a few key binding motifs, such as the MyUb ubiquitin-binding domain, the RRL and the WWY/MWY adaptor binding motif (Berg et al., 2001). This suggests that, although SPE-15/HUM-3 and HUM-8 are assumed to perform similar functions to their mammalian counterpart, notable distinctions in known adaptor-binding regions suggest potential interactions with *C. elegans*-specific binding partners. Orthologues for only three of the known MYO6 adaptor proteins have been identified in worms, providing further evidence for the functional divergence between SPE-15/HUM-3/HUM-8 and human MYO6.

PCR analysis of *C. elegans* cDNA revealed that HUM-8, but not SPE-15/HUM-3, is alternatively spliced. SPE-15/HUM-3 is expressed as a single splice isoform, whereas HUM-8 is expressed as two distinct splice isoforms. The second variant of HUM-8 is alternatively spliced in the CBD and has an additional 14 amino acids inserted just upstream of the MWF motif. In human cells, MYO6 is alternatively spliced in its tail domain to produce four distinct isoforms that are differentially expressed in different cell types. Alternative splicing in the CBD is known to modulate the intracellular targeting and function of human MYO6. The SI isoform of human MYO6 contains a c-Src kinase phosphorylation motif (DYD) required for its function (Tomatis

et al., 2013). The LI isoform, on the other hand, produces an additional secondary structure, the regulatory helix (α2-linker), that can sterically alter the interaction of MYO6 with its adaptors. This forms a novel clathrin-binding domain in addition to masking the RRL binding motif, preventing interactions with RRL binding partners (Wollscheid et al., 2016). In contrast, there is currently no information regarding the differential expression or function of HUM-8 isoforms in *C. elegans*. The contribution of the 14 amino acid insert to the potential divergence in cellular functions between the two HUM-8 variants remains uncertain. It is yet to be determined whether this region adds functionally significant secondary structural elements or regulatory phosphorylation motifs. The GTCSWGSS sequence found within the unique HUM-8 insert contains four phosphorylatable sites, three serines and a threonine. Currently, databases lack information about potential phosphorylation sites for SPE-15/HUM-3 and HUM-8. Mapping HUM-8 phosphorylation motifs using phosphoproteomics could therefore provide a starting point in understanding the function of this unique insert. In summary, although alternative splicing does occur in at least one of the *C. elegans* MYO6 orthologues, the site of alternative splicing observed in HUM-8 differs from the pattern observed in human MYO6.

Cargo adaptor proteins play a crucial role in orchestrating the diverse functions of human MYO6 in different cellular pathways. Interestingly, from the numerous binding partners of human MYO6 the same orthologues are expressed in *C. elegans* and *Drosophila*, TOM1L2, GIPC and Dab2. Dab2 facilitates recruitment of human MYO6 to clathrin-coated pits/vesicles at the apical domain in polarized epithelial cells, a role that overlaps with the specific expression of HUM-8 in intestinal epithelial cells. Further work will be required to test whether the *C. elegans* orthologue of Dab2 indeed functions with SPE-15/HUM-3 in enterocytes. The other two potential adaptor proteins expressed in *C. elegans* as well as in *Drosophila* are orthologues of Tom1/L2 and GIPC highlighting a conserved function of SPE-15/HUM-3/8 and Jaguar on early endosomes. Interestingly, when expressing GFP-SPE-15/HUM-3, GFP-HUM-8 or the *Drosophila* Jaguar in mammalian cells, the *Drosophila* orthologue, similarly to human MYO6, was recruited to APPL1-positive early endosomes in the cell periphery, whilst both SPE-15/HUM-3 and HUM-8 were predominantly present as diffuse cytosolic pools and neither was associated with any obvious vesicles or organelles.

Imaging of *C. elegans* strains carrying *mNeonGreen::SPE-15/HUM-3* and *wrmScarlet::hum-8* using confocal microscopy indicated that SPE-15/HUM-3 was developmentally regulated during spermatogenesis in the gonads, but expressed throughout the worm lifespan elsewhere, whereas HUM-8 does not undergo any developmental regulation. Super-resolution microscopy revealed distinct tissue expression patterns of SPE-15/HUM-3 and HUM-8. While the latter is concentrated in intestinal cells of the gut, SPE-15/HUM-3 is enriched in several types of neurons in the head, as well as within the gonads. In the head region, SPE-15/HUM-3 localises to the cell bodies and axons of interneurons in the lateral and retrovesicular ganglia. The *C. elegans* connectome consists of about 87 interneurons, with those in the lateral and ventral ganglia near the terminal bulb belonging to neuron classes AV and AI.

The role of MYO6 in neurons has been investigated in various organisms. In mice, MYO6 is highly expressed throughout the brain and within synapses. It forms a complex with its adaptor SAP97, regulating the trafficking of AMPA receptors to and from the plasma membrane (Wu et al., 2002; Osterweil et al., 2005). Loss of MYO6 leads to impaired synaptic transmission in mice (Yano et al., 2006). Interestingly, AV-type interneurons, known for expressing several AMPA receptor subunits, do not express the SAP97 homologue, DLG-1, highlighting the importance of searching for novel MYO6 adaptors (Firestein and Rongo, 2001). Furthermore, in *Drosophila*, the absence of functional Jaguar results in locomotor defects due to improper synaptic vesicle localisation and disruptions in synaptic transmission at neuromuscular junctions (Kisiel et al., 2011). AV interneurons, specifically involved in initiating both forward and backward movements, play a crucial role in locomotion (Piggott et al., 2011). Another significant neuron, NSM/L, where SPE-15/HUM-3 is localised, is also involved in locomotion (Altun et al., 2021). The consistent enrichment of SPE-15/HUM-3 in these interneurons suggests a conserved role of MYO6 in locomotion in *C. elegans*. The localisation of SPE-15/HUM-3 in neuronal cell bodies and axons strongly implies its potential involvement in neuronal endocytosis and mediation of synaptic transmission.

SPE-15/HUM-3 also localises to late spermatocytes in the gonad during spermatogenesis throughout the L4 and early young adult stages. This is in accordance with the established function of SPE-15/HUM-3 in the segregation of cellular components, and the mediation of membrane constriction, during spermatid budding in secondary spermatocytes (Kelleher et al., 2000; Hu et al., 2019). GIPC, the worm homologue of human GIPC-1/-2, has recently been shown to be expressed exclusively in sperm throughout *C. elegans* development, where it appears to function solely in the segregation of cellular components (Kim et al., 2021). The observation of SPE-15/HUM-3 in the gonads here confirms the importance of MYO6 during spermatogenesis in *C. elegans*. It will be crucial to demonstrate a direct interaction between GIPC and SPE-15/HUM-3 to further underscore the importance of this interaction network.

HUM-8 expression, on the other hand, was observed almost exclusively in intestinal epithelial enterocytes. The role of MYO6 in polarised epithelial cells containing apical microvilli is well-established. In polarised Caco-2 cells derived from the human small intestine, the LI isoform of MYO6 concentrates at the apical domain, colocalising with clathrin-coated pits and vesicles (Buss et al., 2001). In mice, the lack of functional MYO6 causes defects in endocytosis from the apical plasma membrane in enterocytes, leading to a loss of brush border cell structure and integetry (Ameen and Apodaca, 2007; Hegan et al., 2012). Considering that we have observed a vesicular expression pattern of HUM-8 in enterocytes, and the prediction of HUM-8 binding to clathrin light and heavy chains (STRING interaction database), this suggests a potential conservation of the endocytic function of MYO6 in *C. elegans*.

The results from this study support SPE-15/HUM-3 and HUM-8 as reverse-directed class VI myosins with similar biophysical characteristics to human MYO6. As observed for human MYO6, HUM-8 undergoes differential alternative splicing generating two distinct splice isoforms. Importantly, SPE-15/HUM-3 and HUM-8 show distinct developmental expression patterns and localisations in

C. elegans, highlighting functional specialisations of these two myosins of class VI in nematodes. Although key sequence motifs important for cargo adaptor binding are conserved between human MYO6 and the *C. elegans* orthologues, SPE-15/HUM-3 and HUM-8 are, in contrast to *Drosophila* Jaguar, not recruited to APPL1 endosomes in human cells. Interestingly, however, most of the *C. elegans* tissues in which SPE-15/HUM-3 and HUM-8 are enriched, and the pathways in which they are predicted to be involved in, correlate with those in which human MYO6 functions. Although SPE-15/HUM-3 and HUM-8 show distinctive properties pointing to their evolutionary diversification within *C. elegans*, some of the work presented here also suggests conservation of endogenous localisations, and potentially functions, between the *C. elegans* and human MYO6s.

Material and methods

Bioinformatics

Protein sequences for SPE-15/HUM-3 (SPE-15, accession Q9TZI9), HUM-8 (accession U4PBY2), human MYO6 (accession Q9UM54), and *Drosophila* Jaguar (accession A0A0B4KGX1) were retrieved from UniProtKB. Genomic and cDNA sequences were retrieved from NCBI (*spe-15* ID 171712, *hum-8* ID 176872, *MYO6* ID 4646). MYO6 isoform three and Jaguar isoform B sequences were used.

The AlphaFold2 database was used for structural predictions of full-length SPE-15/HUM-3, HUM-8, and human MYO6 (Jumper et al., 2021). The structures were modeled in PyMOL (Schrodinger and DeLane, 2020). Multiple sequence alignments were generated using Clustal Omega at EMBL-EBI (Sievers et al., 2011). Alignments were visualised and exported using Jalview (Waterhouse et al., 2009).

Transgenic C.elegans strains

Fluorescently tagged *C. elegans* strains were generated using CRISPR/Cas9 by SunyBiotech. A 924 base pair insertion of mNeonGreen and 3Xflag was added to the N-terminus of the F47G6.4a.1 gene to generate the SPE-15/HUM-3 strain PHX5136 (spe-15 (syb5136) [*mNeonGreen::3xFLAG::spe-15*]). The Hum-8 strain PHX5091 included a 759 base pair insertion of a wrmScarlet and 3Xflag at the N-terminus of the Y66H1A.6a.1 gene (hum-8 (syb5091)[*wrmScarlet::3xFLAG::hum-8*]). Both strains allow expression of SPE-15/HUM-3 and HUM-8 at endogenous levels.

Nematode maintenance and age synchronisation

C. elegans worms were maintained at 20°C on NGM (nematode growth medium) plates seeded with OP50 (in LB). To synchronise worm developmental stage, the nematodes were washed off the plates using M9 buffer (0.3% KH_2PO_4, 0.6% Na_2HPO_4, 0.5% NaCl, 1 mM $MgSO_4$). Worms were centrifuged at 1,000 rpm for 3 min at 4°C, the supernatant aspirated, and the pellet washed with 10 mL of M9 buffer. This was repeated until the supernatant was clear (typically 3 times). Bleach solution (20% NaOCl, 0.5 M KOH) was added to the pellet, and the tube vortexed for 10 s at 2 min intervals for 10 min. The eggs were centrifuged at 1,000 rpm for 30 s. The supernatant was aspirated, and this step was repeated twice. The egg solution in M9 was then pipetted onto an NGM plate.

RNA purification from N2 worms and conversion to cDNA

N2 worms grown on 3 × 90 mm NGM plates were washed 3 times with M9 buffer, generating an ~ 100 µL packed worm pellet. The pellet was resuspended with 1 mL of TRIzol reagent (Invitrogen) and vortexed at 2000 rpm at room temperature in a ThermoMixer F1.5 (Eppendorf). 200 µL of chloroform was added, and the mixture incubated for 15 min at room temperature with occasional vortexing. The mixture was centrifuged at 14,000 rpm for 15 min at 4°C. The supernatant was then transferred to a new microcentrifuge tube, an equal volume of isopropanol added, and the sample incubated for 10 min at room temperature. The sample was then centrifuged at 14,000 rpm for 20 min at 4°C. The pellet was washed with 1 mL of ice-cold 75% ethanol, and centrifuged again at 14,000 rpm for 5 min at 4°C. The supernatant was removed, and the RNA pellet allowed to air dry before being dissolved in 40 µL of RNase-free dH_2O and incubated at 65°C for 5 min cDNA was produced from purified *C. elegans* RNA using the ProtoScript II First Strand cDNA Synthesis kit (NEB). Reaction mixtures were prepared according to manufacturer's protocol using Random Primer Mix.

Molecular biology

All constructs used throughout this study are detailed in Table 1. The human calmodulin used in this study was in a pFastBac1 vector and was a gift from Dr J Sellers, NIH, Washington, United States. Sequences were amplified from the cDNA of unsynchronised N2 worms and subsequently cloned into the appropriate expression vector unless otherwise specified (pFastBac1 for expression in insect cells, all others for expression in mammalian cells).

Filopodia localisation assay

RPE cells were grown at 37°C in Dulbecco's Modified Eagle Medium F-12 Nutrient Mixture (DMEM/F-12 (1:1) (Gibco) supplemented with 10% fetal bovine serum and 1% penicillin-streptomycin solution (Pen-Strep, Sigma-Aldrich). Cells were plated onto glass coverslips and transfected with mCherry-MYO6+ and GFP-myosin constructs using FuGene six according to manufacturer's protocol. After 24 h, cells were fixed in 4% PFA, permeabilised using 0.2% Triton X-100, and blocked for 1 h in 1% BSA prior to antibody staining. Primary antibodies: anti-GFP (AB_221569,

TABLE 1 List of constructs used throughout this study.

Plasmid name	Uniprot accession	Source of template	Primers used (5′-3′)	Encoded protein	References
GFP_SPE-15/HUM-3_pEGFP C1	Q9TZI9	*C. elegans* N2 cDNA	5′-ATATCCGGAATGGATAGTAGCACACATAGTACC-3′ 5′-TATGGGCCCCTATGGAGTCCACTCTTGAATTGG3′	GFP-SPE-15/HUM-3	This study
GFP_HUM-5_pEGFP C1	G5ECZ0	*C. elegans* N2 cDNA	5′-AGAGTCGACATGTCGTATGGTGGACACGAC-3′ 5′-ATAGGTACCTCAAGCAACTTGAGCAGTCAACTG-3′	GFP-HUM-5	This study
GFP_HUM-8_pEGFP C1	U4PBY2	*C. elegans* N2 cDNA	5′-ATAGTCGACATGCTACGAACGTTGAAC-3′ 5′-TATGGTACCCTAATTCAAGCATCCCAATTTCCAATG-3′	GFP-HUM-8	This study
MYO1E_pEGFP C1	Q12965	Human cDNA		GFP-MYO1E	Buss lab
MYO5A_pEGFP C1	Q9Y4I1	Human cDNA		GFP-MYO5A	Buss lab
6xH_SPE-15/HUM-3_1-841_GSG linker C-tag_pFastBac1	Q9TZI9	*C. elegans* N2 cDNA	5′-AAATTTGCGCGCATGCACCATCACCATCACCATGATAGTAGCACACATAGTACC-3′ 5′-AAATTTTCTAGACTACACCCAGGTGTCGATGGAGCCCCTGCCGCTGCCCACCCAGGTGTCGATGGAGCCCCT-3′	6His-SPE-15/HUM-3motor-C-tag	This study
6xH_HUM-8_61-904_GSG-linker C-tag pFastBac1	U4PBY2	*C. elegans* N2 cDNA	5′- AAATTTGTCGACATGCACCATCACCATCACCATATGATAAATGTGTCTCAG-3′ 5′- AAATTTAAGCTTCTACACCCAGGTGTCGATGGAGCCCCTGCCGCTGCCAGCAATTTGTCGTGAGAACCG-3′	6His-HUM-8motor-C-tag	This study
MYO6+_ mCherry C1					Masters and Buss (2017)

10.3389/fphys.2024.1368054

Molecular Probes) and anti-RFP (AB_2336064, ChromoTek). Secondary antibodies: anti-rabbit AlexaFluor® 488 and anti-rat AlexaFluor® 568 (Thermo Fisher Scientific). Additional stains: Phalloidin-647 (Molecular Probes) and Hoechst. Images were taken on Zeiss Axio Imager. Z2 using a Plan-Aprochromat 100x/1.40 M27 oil-immersion objective lens and processed using ImageJ. To quantify myosin localisation, 100 filopodia were counted per coverslip in three independent experiments (n = 3) for each condition.

Protein purification

ExpiSf9 cells were grown at 2 × 10^6 cells/mL at 37°C in ExpiSF CD Medium (Gibco) supplemented with 0.4% Normocin (Invivogen). Baculoviral particles and proteins were generated using the ExpiSF expression system (Gibco) according to manufacturer's instructions. To generate baculovirus particles, 12.5 µg *Bacmid* DNA was mixed with *ExpiFectamine* (Gibco), added to 62.5 × 10^6 cells, and incubated at 27°C for 72 h. The supernatant containing the viral particles was subsequently harvested and used directly to scale-up expression. 1 mL of baculovirus containing the myosin motor domain and 0.1 mL of baculovirus containing calmodulin (gifted from Dr. J. Sellers, NIH, Washington, USA) were simultaneously added to 200 mL of cells and incubated until cell viability dropped below 60% (approximately 4 days). Cells were pelleted at 500x RCF for 5 min and frozen. For protein purification the cell pellets were resuspended in 10 mL of myosin extraction buffer (10 mM MOPS pH 7.4, 500 mM NaCl, 5 mM MgCl2, 1 mM EGTA, 1 mM DTT) and sonicated for 2 min in 20 s bursts. Extract was centrifuged at 35,000 RPM for 30 min at 4°C. The supernatant was combined with 1 mL of Ni-NTA resin (ThermoFisher) and incubated for 60 min at 4°C. Resin was washed 2x in myosin extraction buffer and 2x with low salt buffer (10 mM MOPS pH 7.4, 0.1 mM EGTA, 100 mM NaCl). Protein was eluted with 4 mL of low salt buffer containing 150 mM imidazole. Fractions were aliquoted and snap frozen in liquid N_2. Actin was prepared from rabbit muscle as described previously (Spudich and Watt, 1971). The actin was labelled with pyrene at Cys-374. When used at sub-micromolar concentrations, the actin was stabilised by incubation in a 1:1 mixture with phalloidin to prevent depolymerisation.

Stopped-flow spectroscopy

Stopped-flow experiments were performed as described previously (Walklate et al., 2016) using a HiTech Scientific SF-61DX2 stopped flow spectrometer. Rabbit muscle actin was prepared as previously described (Pardee and Spudich, 1982) and was labelled with pyrene (Sigma) at Cys-374 following the protocol by Criddle et al., 1985. All measurements were performed at 20°C in 20 mM MOPS pH 7.0, 25 mM KCl, 5 mM MgCl2, 1 mM DTT. Fluorescence transients were measured using intrinsic S1 tryptophan fluorescence (excitation at 295 nm, emission through a WG320 filter) or pyrene-labelled actin (excitation 365, emission through a KV389 filter). Data was acquired and analysed in the Kinetic Studio software.

Motility assays

To measure the velocity of myosin along actin filaments, an *in vitro* motility assay was performed as described in (Aksel et al., 2015; Adhikari et al., 2016). Rabbit muscle actin was prepared as previously described (Pardee and Spudich, 1982). Fluorescent labelling of actin was carried out at a concentration of 50–70 µM G-actin in 5 mM HEPES (pH 7.5), 2 mM $MgCl_2$ and 0.1 mM $CaCl_2$ with overnight incubation at 0°C in the dark in the presence of 1 M equivalent of phalloidin (Sigma) and 3 M equivalents of tetramethylrhodamine (Molecular Probes). All reagents were dissolved in assay buffer (AB) (25 mM $MgCl_2$, 1 mM EGTA, 1 mM dithiothreitol and 25 mM imidazole, pH 7.4) containing 0.1 mg/mL bovine serum albumin (ABBSA), unless otherwise stated. Glass coverslips were coated with 0.2% nitrocellulose and air-dried before use. Reagents were sequentially flowed through the channels in the following order: 50 µL of 4 µM SNAP-PDZ18 (affinity tag), 100 µL of ABBSA to block the surface from nonspecific attachments, 50 µL of 100 nM 8-residue (RGSIDTWV)-tagged myosin, 100 µL of ABBSA to wash any unattached proteins; 50 µL of 30 nM rhodamine-phalloidin-labelled rabbit actin, 100 µL of an oxygen-scavenging system consisting of 5 mg/mL glucose, 0.1 mg/mL glucose oxydase and 0.02 mg/mL catalase and 50 µL 2 mM ATP. All motility experiments were performed at 20°C. Actin filaments were detected using a Zeiss Axio-observer microscope at ×100 magnification. The gliding velocity of filaments was analysed using the Fiji MtrackJ plugin.

Insert detection

cDNA was amplified using KOD Hot Start DNA polymerase kit (Merck) with the following primers: 5′-GTGAAACGTCGTAACAAGGAA-3′ and 5′-ATACCACATTCCAGATTGAGA-3′ for SPE-15/HUM-3 insert detection, and 5′-GAAAAGAAACGGCAAAATGAA-3′ and 5′-GAACCACATACTAACTTGATCTTT-3'. PCR products were subsequently run on a 1.5% agarose gel. Bands were excised and purified using Qiagen Gel Purification Kit. The DNA was subsequently cloned into a TOPO vector using the Zero Blunt PCR cloning Kit (Invitrogen) for sequencing.

C. elegans microscopy

For live microscopy, nematodes were mounted on a 2% agarose pad and anestheised using 50 mM sodium azide. Confocal images of whole-worms were taken using the Zeiss LSM780 laser scanning microscope with a plan-apochromatic 20x/0.8 M27 objective. Images were acquired in two channels using a plane scan mode: mNeonGreen was excited at 488 nm with a master gain of 837 AU and a pinhole size of 37 µm; wrmScarlet was excited at 561 nm with a master gain of 755AU and a pinhole size of 38 µm. Images were taken using differential interference contrast (DIC) optics. Higher-magnification images of worms were taken using the Zeiss LSM880 laser scanning microscope with a plan-apochromatic 63x/1.40 M27 oil-immersion objective. Images were acquired in two channels, using a plane scan mode: mNeonGreen were excited at 488 nm with a master gain of 837 AU and a pinhole size of 266 µm; wrmScarlet was excited at 561 nm with a master gain of

755 AU and a pinhole size of 300 µm. Airyscan images were acquired using a fixed zoom of 1.8 and a pinhole size of 108 µm. Super-resolution images were taken using the Zeiss Elyra 7 with lattice SIM2. All images were processed with Fiji software.

Data availability statement

The original contributions presented in the study are included in the article/Supplementary Material, further inquiries can be directed to the corresponding author.

Ethics statement

The manuscript presents research on animals that do not require ethical approval for their study.

Author contributions

RB: Data curation, Formal Analysis, Investigation, Validation, Visualization, Writing–original draft. CJ: Data curation, Formal Analysis, Investigation, Supervision, Writing–review and editing. AH: Data curation, Formal Analysis, Investigation, Writing–review and editing. MG: Data curation, Formal Analysis, Investigation, Writing–review and editing. DM: Conceptualization, Methodology, Resources, Writing–review and editing. FB: Conceptualization, Data curation, Funding acquisition, Investigation, Project administration, Supervision, Writing–original draft.

Funding

The author(s) declare financial support was received for the research, authorship, and/or publication of this article. This work was supported by a Trinity College Krishnan-Ang Studentship to RB, an MRC-funded PhD studentship to AJH (MC00076), and a Henry Wellcome Fellowship to CAJ. Work in the DM lab is supported by funding from the Biotechnology and Biological Sciences Research Council (BB/S005544/1 & BB/X007448/1) and in the FB lab through a program grant from the Medical Research Council (MR/S007776/1). CIMR is supported by the Wellcome Trust with an equipment grant (108415).

Acknowledgments

We thank Sue Arden for help and advise and for many helpful discussions.

Conflict of interest

The authors declare that the research was conducted in the absence of any commercial or financial relationships that could be construed as a potential conflict of interest.

Publisher's note

Supplementary material

The Supplementary Material for this article can be found online at: https://www.frontiersin.org/articles/10.3389/fphys.2024.1368054/full#supplementary-material

References

Adhikari, A. S., Kooiker, K. B., Sarkar, S. S., Liu, C., Bernstein, D., Spudich, J. A., et al. (2016). Early-onset hypertrophic cardiomyopathy mutations significantly increase the velocity, force, and actin-activated ATPase activity of human β-cardiac myosin. *Cell Rep.* 17 (11), 2857–2864. doi:10.1016/j.celrep.2016.11.040

Aksel, T., Choe Yu, E., Sutton, S., Ruppel, K. M., and Spudich, J. A. (2015). Ensemble force changes that result from human cardiac myosin mutations and a small-molecule effector. *Cell Rep.* 11 (6), 910–920. doi:10.1016/j.celrep.2015.04.006

Altun, Z. F., Herndon, L. A., Wolkow, C. A., Crocker, C., Lints, R., and Hall, D. H. (2021). WormAtlas. Available at: http://www.wormatlas.org.

Ameen, N., and Apodaca, G. (2007). Defective CFTR apical endocytosis and enterocyte brush border in myosin VI-deficient mice. *Traffic* 8 (8), 998–1006. doi:10.1111/j.1600-0854.2007.00587.x

Arden, S. D., Puri, C., Au, J. S., Kendrick-Jones, J., and Buss, F. (2007). Myosin VI is required for targeted membrane transport during cytokinesis. *Mol. Biol. Cell* 18 (12), 4750–4761. doi:10.1091/mbc.e07-02-0127

Arden, S. D., Tumbarello, D. A., Butt, T., Kendrick-Jones, J., and Buss, F. (2016). Loss of cargo binding in the human myosin VI deafness mutant (R1166X) leads to increased actin filament binding. *Biochem. J.* 473 (19), 3307–3319. doi:10.1042/BCJ20160571

Aschenbrenner, L., Lee, T., and Hasson, T. (2003). Myo6 facilitates the translocation of endocytic vesicles from cell peripheries. *Mol. Biol. Cell* 14 (7), 2728–2743. doi:10.1091/mbc.e02-11-0767

Avraham, K. B., Hasson, T., Sobe, T., Balsara, B., Testa, J. R., Skvorak, A. B., et al. (1997). Characterization of unconventional MYO6, the human homologue of the gene responsible for deafness in Snell's waltzer mice. *Hum. Mol. Genet.* 6 (8), 1225–1231. doi:10.1093/hmg/6.8.1225

Avraham, K. B., Hasson, T., Steel, K. P., Kingsley, D. M., Russell, L. B., Mooseker, M. S., et al. (1995). The mouse Snell's waltzer deafness gene encodes an unconventional myosin required for structural integrity of inner ear hair cells. *Nat. Genet.* 11 (4), 369–375. doi:10.1038/ng1295-369

Axang, C., Rauthan, M., Hall, D. H., and Pilon, M. (2008). Developmental genetics of the *C. elegans* pharyngeal neurons NSML and NSMR. *BMC Dev. Biol.* 8, 38. doi:10.1186/1471-213X-8-38

Baker, J. P., and Titus, M. A. (1997). A family of unconventional myosins from the nematode *Caenorhabditis elegans*. *J. Mol. Biol.* 272 (4), 523–535. doi:10.1006/jmbi.1997.1232

Berg, J. S., Powell, B. C., and Cheney, R. E. (2001). A millennial myosin census. *Mol. Biol. Cell* 12 (4), 780–794. doi:10.1091/mbc.12.4.780

Brenner, S. (1974). The genetics of *Caenorhabditis elegans*. *Genetics* 77 (1), 71–94. doi:10.1093/genetics/77.1.71

Bryant, Z., Altman, D., and Spudich, J. A. (2007). The power stroke of myosin VI and the basis of reverse directionality. *Proc. Natl. Acad. Sci. U. S. A.* 104 (3), 772–777. doi:10.1073/pnas.0610144104

Bunn, R. C., Jensen, M. A., and Reed, B. C. (1999). Protein interactions with the glucose transporter binding protein GLUT1CBP that provide a link between GLUT1 and the cytoskeleton. *Mol. Biol. Cell* 10 (4), 819–832. doi:10.1091/mbc.10.4.819

Buss, F., Arden, S. D., Lindsay, M., Luzio, J. P., and Kendrick-Jones, J. (2001). Myosin VI isoform localized to clathrin-coated vesicles with a role in clathrin-mediated endocytosis. *EMBO J.* 20 (14), 3676–3684. doi:10.1093/emboj/20.14.3676

Buss, F., Kendrick-Jones, J., Lionne, C., Knight, A. E., Côté, G. P., and Paul Luzio, J. (1998). The localization of myosin VI at the golgi complex and leading edge of fibroblasts and its phosphorylation and recruitment into membrane ruffles of A431 cells after growth factor stimulation. *J. Cell Biol.* 143 (6), 1535–1545. doi:10.1083/jcb.143.6.1535

Celegans Sequencing Consortium (1998). Genome sequence of the nematode *C. elegans*: a platform for investigating biology. *Science* 282 (5396), 2012–2018. doi:10.1126/science.282.5396.2012

Chibalina, M. V., Seaman, M. N., Miller, C. C., Kendrick-Jones, J., and Buss, F. (2007). Myosin VI and its interacting protein LMTK2 regulate tubule formation and transport to the endocytic recycling compartment. *J. Cell Sci.* 120 (Pt 24), 4278–4288. doi:10.1242/jcs.014217

Criddle, A. H., Geeves, M. A., and Jeffries, T. (1985). The use of actin labelled with N-(1-pyrenyl)iodoacetamide to study the interaction of actin with myosin subfragments and troponin/tropomyosin. *Biochem. J.* 232 (2), 343–349. doi:10.1042/bj2320343

de Jonge, J. J., Batters, C., O'Loughlin, T., Arden, S. D., and Buss, F. (2019). The MYO6 interactome: selective motor-cargo complexes for diverse cellular processes. *FEBS Lett.* 593 (13), 1494–1507. doi:10.1002/1873-3468.13486

Dimov, I., and Maduro, M. F. (2019). The *C. elegans* intestine: organogenesis, digestion, and physiology. *Cell tissue Res.* 377 (3), 383–396. doi:10.1007/s00441-019-03036-4

Dose, A. C., and Burnside, B. (2000). Cloning and chromosomal localization of a human class III myosin. *Genomics* 67 (3), 333–342. doi:10.1006/geno.2000.6256

Dunn, T. A., Chen, S., Faith, D. A., Hicks, J. L., Platz, E. A., Chen, Y., et al. (2006). A novel role of myosin VI in human prostate cancer. *Am. J. pathology* 169 (5), 1843–1854. doi:10.2353/ajpath.2006.060316

Finan, D., Hartman, M. A., and Spudich, J. A. (2011). Proteomics approach to study the functions of Drosophila myosin VI through identification of multiple cargo-binding proteins. *Proc. Natl. Acad. Sci. U. S. A.* 108 (14), 5566–5571. doi:10.1073/pnas.1101415108

Firestein, B. L., and Rongo, C. (2001). DLG-1 is a MAGUK similar to SAP97 and is required for adherens junction formation. *Mol. Biol. Cell* 12 (11), 3465–3475. doi:10.1091/mbc.12.11.3465

Greenberg, M. J., Lin, T., Shuman, H., and Ostap, E. M. (2015). "Mechanochemical tuning of myosin-I by the N-terminal region," in Proceedings of the National Academy of Sciences of the United States of America 112 (26), E3337–E3344.

Hartman, M. A., and Spudich, J. A. (2012). The myosin superfamily at a glance. *J. Cell Sci.* 125 (Pt 7), 1627–1632. doi:10.1242/jcs.094300

He, F., Wollscheid, H. P., Nowicka, U., Biancospino, M., Valentini, E., Ehlinger, A., et al. (2016). Myosin VI contains a compact structural motif that binds to ubiquitin chains. *Cell Rep.* 14 (11), 2683–2694. doi:10.1016/j.celrep.2016.01.079

Hegan, P. S., Giral, H., Levi, M., and Mooseker, M. S. (2012). Myosin VI is required for maintenance of brush border structure, composition, and membrane trafficking functions in the intestinal epithelial cell. *Cytoskeleton* 69 (4), 235–251. doi:10.1002/cm.21018

Hu, J., Cheng, S., Wang, H., Li, X., Liu, S., Wu, M., et al. (2019). Distinct roles of two myosins in *C. elegans* spermatid differentiation. *PLoS Biol.* 17 (4), e3000211. doi:10.1371/journal.pbio.3000211

Johnson, C. A., Behbehani, R., and Buss, F. (2022). Unconventional myosins from *Caenorhabditis elegans* as a probe to study human orthologues. *Biomolecules* 12 (12), 1889. doi:10.3390/biom12121889

Jumper, J., Evans, R., Pritzel, A., Green, T., Figurnov, M., Ronneberger, O., et al. (2021). Highly accurate protein structure prediction with AlphaFold. *Nature* 596 (7873), 583–589. doi:10.1038/s41586-021-03819-2

Kelleher, J. F., Mandell, M. A., Moulder, G., Hill, K. L., L'Hernault, S. W., Barstead, R., et al. (2000). Myosin VI is required for asymmetric segregation of cellular components during *C. elegans* spermatogenesis. *elegans Spermatogenes. Curr. biology:CB* 10 (23), 1489–1496. doi:10.1016/s0960-9822(00)00828-9

Kengyel, A., Bécsi, B., Kónya, Z., Sellers, J. R., Erdődi, F., and Nyitrai, M. (2015). Ankyrin domain of myosin 16 influences motor function and decreases protein phosphatase catalytic activity. *Eur. biophysics J. EBJ* 44 (4), 207–218. doi:10.1007/s00249-015-1015-z

Kim, J., Min, H., Ko, S., and Shim, Y. H. (2021). Depletion of gipc-1 and gipc-2 causes infertility in *Caenorhabditis elegans* by reducing sperm motility. *Biochem. biophysical Res. Commun.* 534, 219–225. doi:10.1016/j.bbrc.2020.11.108

Kisiel, M., Majumdar, D., Campbell, S., and Stewart, B. A. (2011). Myosin VI contributes to synaptic transmission and development at the Drosophila neuromuscular junction. *BMC Neurosci.* 12, 65. doi:10.1186/1471-2202-12-65

Krendel, M., and Mooseker, M. S. (2005). Myosins: tails (and heads) of functional diversity. *Physiol. Bethesda, Md* 20, 239–251. doi:10.1152/physiol.00014.2005

L'Hernault, S. W., Shakes, D. C., and Ward, S. (1988). Developmental genetics of chromosome I spermatogenesis-defective mutants in the nematode *Caenorhabditis elegans*. *Genetics* 120 (2), 435–452. doi:10.1093/genetics/120.2.435

Masters, T. A., and Buss, F. (2017). Filopodia formation and endosome clustering induced by mutant plus-end-directed myosin VI. *Proc. Natl. Acad. Sci. U. S. A.* 114 (7), 1595–1600. doi:10.1073/pnas.1616941114

Masters, T. A., Tumbarello, D. A., Chibalina, M. V., and Buss, F. (2017). MYO6 regulates spatial organization of signaling endosomes driving AKT activation and actin dynamics. *Cell Rep.* 19 (10), 2088–2101. doi:10.1016/j.celrep.2017.05.048

Melchionda, S., Ahituv, N., Bisceglia, L., Sobe, T., Glaser, F., Rabionet, R., et al. (2001). MYO6, the human homologue of the gene responsible for deafness in Snell's waltzer mice, is mutated in autosomal dominant nonsyndromic hearing loss. *Am. J. Hum. Genet.* 69 (3), 635–640. doi:10.1086/323156

Menetrey, J., Bahloul, A., Wells, A. L., Yengo, C. M., Morris, C. A., Sweeney, H. L., et al. (2005). The structure of the myosin VI motor reveals the mechanism of directionality reversal. *Nature* 435 (7043), 779–785. doi:10.1038/nature03592

Mohiddin, S. A., Ahmed, Z. M., Griffith, A. J., Tripodi, D., Friedman, T. B., Fananapazir, L., et al. (2004). Novel association of hypertrophic cardiomyopathy, sensorineural deafness, and a mutation in unconventional myosin VI (MYO6). *J. Med. Genet.* 41 (4), 309–314. doi:10.1136/jmg.2003.011973

Morris, S. M., Arden, S. D., Roberts, R. C., Kendrick-Jones, J., Cooper, J. A., Luzio, J. P., et al. (2002). Myosin VI binds to and localises with Dab2, potentially linking receptor-mediated endocytosis and the actin cytoskeleton. *Traffic* 3 (5), 331–341. doi:10.1034/j.1600-0854.2002.30503.x

Morriswood, B., Ryzhakov, G., Puri, C., Arden, S. D., Roberts, R., Dendrou, C., et al. (2007). T6BP and NDP52 are myosin VI binding partners with potential roles in cytokine signalling and cell adhesion. *J. Cell Sci.* 120 (Pt 15), 2574–2585. doi:10.1242/jcs.007005

Odronitz, F., and Kollmar, M. (2007). Drawing the tree of eukaryotic life based on the analysis of 2,269 manually annotated myosins from 328 species. *Genome Biol.* 8 (9), R196. doi:10.1186/gb-2007-8-9-r196

Osterweil, E., Wells, D. G., and Mooseker, M. S. (2005). A role for myosin VI in postsynaptic structure and glutamate receptor endocytosis. *J. Cell Biol.* 168 (2), 329–338. doi:10.1083/jcb.200410091

Pardee, J. D., and Spudich, J. A. (1982). Purification of muscle actin. *Methods Enzym.* 85 Pt B, 164–181. doi:10.1016/0076-6879(82)85020-9

Penengo, L., Mapelli, M., Murachelli, A. G., Confalonieri, S., Magri, L., Musacchio, A., et al. (2006). Crystal structure of the ubiquitin binding domains of rabex-5 reveals two modes of interaction with ubiquitin. *Cell* 124 (6), 1183–1195. doi:10.1016/j.cell.2006.02.020

Piggott, B. J., Liu, J., Feng, Z., Wescott, S. A., and Xu, X. Z. (2011). The neural circuits and synaptic mechanisms underlying motor initiation in *C. elegans*. *Cell* 147 (4), 922–933. doi:10.1016/j.cell.2011.08.053

Preller, M., and Manstein, D. J. (2013). Myosin structure, allostery, and mechano-chemistry. *Struct. Lond. Engl. 1993* 21 (11), 1911–1922. doi:10.1016/j.str.2013.09.015

Sahlender, D. A., Roberts, R. C., Arden, S. D., Spudich, G., Taylor, M. J., Luzio, J. P., et al. (2005). Optineurin links myosin VI to the Golgi complex and is involved in Golgi organization and exocytosis. *J. Cell Biol.* 169 (2), 285–295. doi:10.1083/jcb.200501162

Schrodinger, L., and DeLano, W. (2020). The PyMOL molecular graphic system. version 1.2r3pre. Available at: http://www.pymol.org/pymol.

Sellers, J. R. (2000). Myosins: a diverse superfamily. *Biochimica biophysica acta* 1496 (1), 3–22. doi:10.1016/s0167-4889(00)00005-7

Sievers, F., Wilm, A., Dineen, D., Gibson, T. J., Karplus, K., Li, W., et al. (2011). Fast, scalable generation of high-quality protein multiple sequence alignments using Clustal Omega. *Mol. Syst. Biol.* 7, 539. doi:10.1038/msb.2011.75

Skop, A. R., Liu, H., Yates, J., Meyer, B. J., and Heald, R. (2004). Dissection of the mammalian midbody proteome reveals conserved cytokinesis mechanisms. *Science* 305 (5680), 61–66. doi:10.1126/science.1097931

Spudich, G., Chibalina, M. V., Au, J. S., Arden, S. D., Buss, F., and Kendrick-Jones, J. (2007). Myosin VI targeting to clathrin-coated structures and dimerization is mediated by binding to Disabled-2 and PtdIns(4,5)P2. *Nat. Cell Biol.* 9 (2), 176–183. doi:10.1038/ncb1531

Spudich, J. A., and Watt, S. (1971). The regulation of rabbit skeletal muscle contraction. *J. Biol. Chem.* 246 (15), 4866–4871. doi:10.1016/s0021-9258(18)62016-2

Tomatis, V. M., Papadopulos, A., Malintan, N. T., Martin, S., Wallis, T., Gormal, R. S., et al. (2013). Myosin VI small insert isoform maintains exocytosis by tethering secretory granules to the cortical actin. *J. Cell Biol.* 200 (3), 301–320. doi:10.1083/jcb.201204092

Tumbarello, D. A., Waxse, B. J., Arden, S. D., Bright, N. A., Kendrick-Jones, J., and Buss, F. (2012). Autophagy receptors link myosin VI to autophagosomes to mediate

Tom1-dependent autophagosome maturation and fusion with the lysosome. *Nat. Cell Biol.* 14 (10), 1024–1035. doi:10.1038/ncb2589

Walklate, J., Ujfalusi, Z., and Geeves, M. A. (2016). Myosin isoforms and the mechanochemical cross-bridge cycle. *J. Exp. Biol.* 219 (Pt 2), 168–174. doi:10.1242/jeb.124594

Warner, C. L., Stewart, A., Luzio, J. P., Steel, K. P., Libby, R. T., Kendrick-Jones, J., et al. (2003). Loss of myosin VI reduces secretion and the size of the Golgi in fibroblasts from Snell's waltzer mice. *EMBO J.* 22 (3), 569–579. doi:10.1093/emboj/cdg055

Waterhouse, A. M., Procter, J. B., Martin, D. M. A., Clamp, M., and Barton, G. J. (2009). Jalview Version 2--a multiple sequence alignment editor and analysis workbench. *Bioinformatics* 25, 1189–1191. doi:10.1093/bioinformatics/btp033

Wells, A. L., Lin, A. W., Chen, L. Q., Safer, D., Cain, S. M., Hasson, T., et al. (1999). Myosin VI is an actin-based motor that moves backwards. *Nature* 401 (6752), 505–508. doi:10.1038/46835

Wollscheid, H. P., Biancospino, M., He, F., Magistrati, E., Molteni, E., Lupia, M., et al. (2016). Diverse functions of myosin VI elucidated by an isoform-specific α-helix domain. *Nat. Struct. Mol. Biol.* 23 (4), 300–308. doi:10.1038/nsmb.3187

Wu, H., Nash, J. E., Zamorano, P., and Garner, C. C. (2002). Interaction of SAP97 with minus-end-directed actin motor myosin VI. Implications for AMPA receptor trafficking. *J. Biol. Chem.* 277 (34), 30928–30934. doi:10.1074/jbc.M203735200

Yano, H., Ninan, I., Zhang, H., Milner, T. A., Arancio, O., and Chao, M. V. (2006). BDNF-mediated neurotransmission relies upon a myosin VI motor complex. *Nat. Neurosci.* 9 (8), 1009–1018. doi:10.1038/nn1730

Yoshida, H., Cheng, W., Hung, J., Montell, D., Geisbrecht, E., Rosen, D., et al. (2004). Lessons from border cell migration in the Drosophila ovary: a role for myosin VI in dissemination of human ovarian cancer. *Proc. Natl. Acad. Sci. U. S. A.* 101 (21), 8144–8149. doi:10.1073/pnas.0400400101

frontiers | Frontiers in Physiology

TYPE Original Research
PUBLISHED 07 May 2024
DOI 10.3389/fphys.2024.1368416

OPEN ACCESS

EDITED BY
Shoichiro Ono,
Emory University, United States

REVIEWED BY
Primal De Lanerolle,
University of Illinois Chicago, United States
Vivek Peche,
Washington University in St. Louis, United States

*CORRESPONDENCE
Maria Jolanta Rędowicz,
j.redowicz@nencki.edu.pl

RECEIVED 10 January 2024
ACCEPTED 01 April 2024
PUBLISHED 07 May 2024

CITATION
Nowak J, Lenartowski R, Kalita K, Lehka L, Karatsai O, Lenartowska M and Rędowicz MJ (2024), Myosin VI in the nucleolus of neurosecretory PC12 cells: its involvement in the maintenance of nucleolar structure and ribosome organization.
Front. Physiol. 15:1368416.
doi: 10.3389/fphys.2024.1368416

Myosin VI in the nucleolus of neurosecretory PC12 cells: its involvement in the maintenance of nucleolar structure and ribosome organization

Jolanta Nowak [1], Robert Lenartowski [2,3], Katarzyna Kalita [4], Lilya Lehka [1], Olena Karatsai [1], Marta Lenartowska [2,3] and Maria Jolanta Rędowicz [1]*

[1]Laboratory of Molecular Basis of Cell Motility, Nencki Institute of Experimental Biology, Polish Academy of Sciences, Warsaw, Poland, [2]Faculty of Biological and Veterinary Sciences, Nicolaus Copernicus University in Torun, Torun, Poland, [3]Centre for Modern Interdisciplinary Technologies, Nicolaus Copernicus University in Torun, Torun, Poland, [4]Laboratory of Neurobiology, Nencki-EMBL Partnership for Neural Plasticity and Brain Disorders—BRAINCITY, Nencki Institute of Experimental Biology, Polish Academy of Sciences, Warsaw, Poland

We have previously shown that unconventional myosin VI (MVI), a unique actin-based motor protein, shuttles between the cytoplasm and nucleus in neurosecretory PC12 cells in a stimulation-dependent manner and interacts with numerous proteins involved in nuclear processes. Among the identified potential MVI partners was nucleolin, a major nucleolar protein implicated in rRNA processing and ribosome assembly. Several other nucleolar proteins such as fibrillarin, UBF (upstream binding factor), and B23 (also termed nucleophosmin) have been shown to interact with MVI. A bioinformatics tool predicted the presence of the nucleolar localization signal (NoLS) within the MVI globular tail domain, and immunostaining confirmed the presence of MVI within the nucleolus. Depletion of MVI, previously shown to impair PC12 cell proliferation and motility, caused disorganization of the nucleolus and rough endoplasmic reticulum (rER). However, lack of MVI does not affect nucleolar transcription. In light of these data, we propose that MVI is important for nucleolar and ribosome maintenance but not for RNA polymerase 1-related transcription.

KEYWORDS

actinomycin D, B23, fibrillarin, myosin VI, nucleolin, nucleolus, nucleolar stress, PC12 cells

1 Introduction

Myosins are actin-based ATP-dependent molecular motors involved in a panoply of cellular processes associated with motile and contractile processes. They are classified into over 30 families (classes) based on differences in a primary sequence of the ATP- and actin-binding motor domain, engaged in force generation (Odronitz and Kollmar, 2007). The best characterized and most abundant of myosins are muscle myosins, which together with the so-called non-muscle isoforms (resembling classical muscle counterparts) form class II, also termed as conventional myosins. All other myosins, very diverse in their structure and function, are termed as unconventional ones. Myosins are mainly known to function in the

cytoplasm; however, it has been shown that several unconventional myosins are present in the nucleus, where they play important roles in numerous nuclear processes (de Lanerolle, 2012; Belin and Mullins, 2013; Sarshad and Percipalle, 2014). Among them are nuclear myosin IC (NMIC, isoforms b and c), myosins VA and VB, myosin VI, myosin XVIB, and myosins XVIIIA and XVIIIB. In the nucleus, these myosins are believed to interact with nuclear actin and participate in intra-nuclear trafficking, DNA replication and repair, as well as transcription (Shahid-Fuente and Toseland, 2023; Cook and Toseland, 2021; Cook et al., 2020; Caridi et al., 2018). It is noteworthy that three isoforms, nuclear myosin IC (NMI), myosin VA, and myosin VB, have been found in the nucleolus (Lindsay and McCaffrey, 2009; Philimonenko et al., 2004; Pranchevicius et al., 2008). However, molecular mechanisms of involvement of these myosins in nucleolar processes still remain poorly understood.

Myosin VI (MVI), present in the nucleus, is the only known myosin moving toward the minus (pointed) end of actin filaments (Wells et al., 1999; Sweeney and Houdusse, 2010). Similar to other myosins, MVI heavy chain (MW ~140 kDa) contains the N-terminal motor domain, a neck region, and the C-terminal tail domain involved in cargo binding (Avraham et al., 1995; de Jonge et al., 2019; Li et al., 2016) (Figure 1A).

In the cytoplasm, it acts as a transporting motor or an anchor linking vesicles and/or plasma membrane proteins to the actin cytoskeleton (Sweeney and Houdusse, 2007; 2010; Chibalina et al., 2009; Li et al., 2016). It plays important roles in endocytosis, cell motility, and adhesion, as well as in the maintenance of membranous compartments such as the Golgi apparatus and endoplasmic reticulum (ER) (Chibalina et al., 2009; Warner et al., 2003; Karolczak et al., 2015; Zakrzewski et al., 2021). It has been shown that in mice and humans, loss or point mutations within the MVI gene (*MYO6*) lead to deafness as well as mild defects in several organs, including the brain, heart, kidney, intestines, testis, and skeletal muscles (Avraham et al., 1997; Osterweil et al., 2005; Mohhidin et al., 2004; Hegan et al., 2015; Karatsai et al., 2023; Gotoh et al., 2010; Ameen and Apodaca 2007; Zakrzewski et al., 2021; Lehka et al., 2022). In addition, a significant increase in its synthesis was detected in highly malignant cancers, suggesting its important role in cell proliferation (Yoshida et al., 2004; Dunn et al., 2006; Zhan et al., 2023).

In the nuclei of numerous cancer cell lines, MVI was found to localize to chromatin-free regions, where it was associated with the RNA polymerase II (Pol2) transcription machinery (Jung et al., 2006; Vreugde et al., 2006; Majewski et al., 2018). It was shown that in the nucleus of HeLa cells, MVI acts as the molecular anchor that holds Pol2 in high-density clusters, and perturbation of MVI leads to the disruption of Pol2 localization and chromatin organization (Hari-Gupta et al., 2022). These changes subsequently lead to a decrease in gene expression, suggesting that MVI plays a crucial role in the spatial regulation of gene expression (Hari-Gupta et al., 2022). Moreover, the same group showed that a direct binding of MVI to DNA is important for its interaction with Pol2 (Fili et al., 2017). In addition, several other reports demonstrated the involvement of MVI not only in gene transcription but also in gene pairing (Cho and Chen 2010; Loikkanen et al., 2009; Zorca et al., 2015).

In line with the aforementioned observations, our previous data demonstrate that in neurosecretory PC12 cells, MVI translocates, in a stimulation-dependent manner, to the nucleus, where it localizes to numerous nuclear compartments, including the nucleolus. It also interacts with a variety of proteins involved in nuclear (and nucleolar) functions, including nucleolin and ribosomal protein S6 (Majewski et al., 2018). In the present study, we addressed for the first time the functional significance of the presence of MVI within the nucleolus. Our data demonstrate that besides nucleolin, MVI interacts with several nucleolar proteins involved in rRNA synthesis and processing, including UBF (upstream binding factor), fibrillarin, and B23 (also termed nucleophosmin, NPM1). We show that MVI is involved in the maintenance of nucleolar integrity and ribosome localization at the ER membranes. However, contrary to NMIC (Philimonenko et al., 2004), MVI does not seem to be involved in pre-rRNA synthesis.

2 Materials and methods

2.1 Plasmids

Plasmids for the expression of the recombinant globular tail domain of MVI fused with GST (glutathione S-transferase) in *E. coli* was constructed by subcloning a fragment of the rat MVI nucleotide sequence (Majewski et al., 2012) (gene ID D4A5I9) corresponding to the MVI globular tail (aa 1046-1285) into the pGEX-4T1 vector (from GE Healthcare, Cat. No 28-9545-49). Glutathione Sepharose 4B was also obtained from GE Healthcare (Cat. No 17-0756-01).

2.2 Antibodies and fluorescent markers

The antibodies were used as follows: rabbit polyclonal antibody to MVI (Proteus, Cat. No 25-6791), mouse monoclonal antibody to β-actin (Sigma-Aldrich, Cat. No A3854), mouse monoclonal antibody to B23 (Abcam, Cat. No ab 10530), rabbit polyclonal antibody to GRP78 (Abcam, Cat. No 21685), mouse monoclonal antibody to fibrillarin (Thermo Fisher Scientific, Cat. No MA3-16771), mouse monoclonal antibody to glyceraldehyde-3-phosphate dehydrogenase (GAPDH, Millipore, Cat. No MAB 274), mouse monoclonal antibody to RPA 194 (Pol1) (Santa Cruz Biotechnology, Cat. No sc-48385), mouse monoclonal antibody to UBF (Santa Cruz Biotechnology, Cat. No sc-13125), goat polyclonal antibody to lamin B (Santa Cruz Biotechnology, Cat. No sc-6217), mouse monoclonal antibody to p-S6 (Cell Signaling, Cat. No 62016), mouse monoclonal antibody to S6 (Cell Signaling, Cat. No 2317), rabbit monoclonal antibody to p-p70S6K (Cell Signaling, Cat. No 9234), rabbit monoclonal antibody to p70S6K (Cell Signaling, Cat. No 2708), goat anti-mouse IgG antibody, HRP conjugate (Millipore, Cat. No AP308P), goat anti-rabbit IgG antibody, HRP conjugate (Millipore, Cat. No AP307P), and donkey anti-goat IgG antibody, HRP conjugate (Santa Cruz Biotechnology, Cat. No sc-2020).

VECTASHIELD PLUS Antifade Mounting Medium with DAPI was obtained from Vector Laboratories (Cat. No H2000). For immunofluorescence studies, the following secondary antibodies were used: goat anti-rabbit IgG labeled with Alexa Fluor 488 (Invitrogen, Cat. No A11008) and goat anti-mouse IgG labeled with Alexa Fluor 546 (Invitrogen, Cat. No A11003).

The *in situ* proximity ligation assay (PLA) kit was purchased from Sigma-Aldrich (kit components: Duolink In Situ PLA Probe Anti-Mouse MINUS, Cat. No DUO 92004; Duolink In Situ PLA

Probe Anti-Rabbit PLUS, Cat. No DUO 92002; Duolink In Situ Detection Reagents Red, Cat. No DUO 92008; Duolink In Situ Wash Buffers, Cat. No DUO 82049; and Duolink In Situ Mounting Medium with DAPI, Cat. No DUO 92006).

2.3 Cell culture

The non-adherent variant of PC12 cells (American Type Cell Culture Collection, ATCC, Cat. No CRL-1721) was cultured in RPMI media (Gibco, Cat. No 52400025) containing 2 mM L-glutamine, 4.5 g/L glucose supplemented with 10% heat-inactivated horse serum (Gibco, Cat. No 26050088), 5% heat-inactivated fetal bovine serum (Gibco, Cat. No 10270106), and antibiotics: 1% penicillin/streptomycin (Gibco, Cat. No 15140-122) at 37°C in humidified air containing 5% CO_2.

In addition, stable MVI knockdown (MVI-KD) and a control scrambled cell lines (control), both obtained earlier by Dr. Ł. Majewski (Majewski et al., 2011), were used. These lines were prepared using a plasmid encoding *sh*RNA directed against the MVI mRNA and a plasmid encoding a control *sh*RNA not recognizing any known mammalian mRNA sequences (Majewski et al., 2011). MVI-KD and control PC12 cells were cultured in F12K (Kaighn's Modification of Ham's F-12) (ATCC, Cat. No 30-2004) containing 2 mM L-glutamine, 1.5 g/L sodium bicarbonate supplemented with 2.5% heat-inactivated fetal bovine serum (Gibco, Cat. No 10270106), 15% heat-inactivated horse serum (Gibco, Cat. No 26050088), antibiotics: 1% penicillin/streptomycin (Gibco, Cat. No 15140-122), and hygromycin B as a selective antibiotic (250 ng/mL) at 37°C in humidified air containing 5% CO_2.

Cells were lysed in an ice-cold buffer that contained 50 mM Tris–HCl pH 7.5 (Sigma-Aldrich, Cat. No T6687), 150 mM NaCl (Chempure, Cat. No 117941206), 0.1% Triton X-100 (Sigma-Aldrich, Cat. No SLCJ7494), 2 mM EGTA (Sigma-Aldrich, Cat. No E3889), 1 mM DTT (Sigma-Aldrich, Cat. No 10197777001), 1 mM PMSF (Sigma-Aldrich, Cat. No P7626), cOmplete™ Protease Inhibitor Cocktail (Roche, Cat. No 04693132001), and phosphatase inhibitor PhosSTOP™ (Roche, Cat. No 4906845001).

2.4 Subcellular fractionation

To obtain the cytoplasmic, nuclear, and nucleolar fractions, PC12 cells were subjected to fractionation according to the Hacot protocol (Hacot et al., 2010) with several modifications. Briefly, cells were washed with PBS, harvested, and centrifuged at 200 *g* for 3 min at RT. The pellet was resuspended in a hypotonic buffer consisting of 10 mM HEPES, pH 7.9, 10 mM KCl, 1.5 mM $MgCl_2$, and 0.5 mM DTT and kept on ice for 15 min to induce osmotic shock, causing cell membrane disruption. The suspension was homogenized using a Dounce-type glass tissue homogenizer and centrifuged at 1,200 *g* for 5 min at 4°C. The resultant supernatant contained the cytoplasmic protein fraction, while the pellet contained both cell debris and cell nuclei. The pellet was then subjected to centrifugation in the sucrose gradient: it was resuspended in S1 buffer (0.25 M sucrose and 10 mM $MgCl_2$), and the suspension was placed in centrifuge tubes containing S2 buffer (0.88 M sucrose and 0.5 mM $MgCl_2$) and centrifuged at 1,200 *g* for 5 min at 4°C. The supernatant was discarded, and the pellet at the bottom of the tube (representing the purified fraction of cell nuclei) was resuspended in buffer S3 (0.35 M sucrose and 0.5 mM $MgCl_2$). Next, the nucleolus fraction was obtained by sonication of the purified nuclei fraction using a S-250D sonicator (Branson Ultrasonic S.A.) with a 1/8" (3.2 mm) microtip at 30% power of the device in three cycles/sequences (10-s sonication and 10-s pause). The suspension that resulted upon sonication was applied to the surface of the S2 buffer and centrifuged at 2,000 *g* for 20 min at 4°C. The supernatant contained the nucleoplasmic fraction, and the pellet contained the nucleolar fraction, which was suspended in S3 buffer. All the obtained fractions were subjected to SDS-PAGE, followed by immunoblotting analysis for the presence of MVI and other marker proteins (GAPDH for the cytoplasm, and fibrillarin for the nucleoplasm and nucleolus) used as the internal loading control and indicators of fraction purity. The protein concentration was determined using the standard Bradford method.

2.5 Cell stimulation

To induce secretion, PC12 cells were cultured as described above and stimulated essentially according to Vitale et al. (1992) and Trifaró and Lee (1980). Treatment with 56 mM KCl is generally accepted as a method for *in vitro* PC12 cell stimulation as high concentrations of external KCl cause PC12 cell plasma membrane depolarization and evoke catecholamine release. Briefly, cells were washed with Locke's solution containing 2.6 mM KCl, 154 mM NaCl, 2.2 mM $CaCl_2$, 0.5 mM KH_2PO_4, 1.25 mM K_2HPO_4, 1.2 mM $MgCl_2$, and 10 mM glucose. Then, they were incubated in Locke's solution with elevated K^+ concentration (56 mM KCl, 103.6 mM NaCl, 2.2 mM $CaCl_2$, 0.5 mM KH_2PO_4, 1.25 mM K_2HPO_4, 1.2 mM $MgCl_2$, and 10 mM glucose) to stimulate secretion or in calcium-free Locke's solution (2.6 mM KCl, 154 mM NaCl, 0.5 mM KH_2PO_4, 1.25 mM K_2HPO_4, 1.2 mM $MgCl_2$, and 10 mM glucose) to block the secretion. Cells were further processed for post-embedding immunogold MVI localization.

2.6 Actinomycin D treatment

To induce nucleolar stress, PC12 cells were treated with the Pol1 transcription inhibitor, actinomycin D (ActD) (Sigma-Aldrich, Cat. No A1410). Briefly, examined cells were incubated at 37°C for 3 h in the culture medium in the presence or absence of 0.05 μg/mL ActD and subjected to further analyses.

2.7 Immunoblot analysis

PC12 cell lysates and subcellular fractions were separated using 10% polyacrylamide SDS gels and then transferred to a nitrocellulose membrane (Bio-Rad, Cat. No 1620115). After the transfer, the membrane was blocked for 1 h at room temperature in TBS containing 5% non-fat milk powder or 5% BSA (Sigma-Aldrich, Cat. No A7906-150G) and 0.2% Triton X-100 followed by overnight

incubation with appropriate dilutions (from 1:100 to 1:5,000) of different primary antibodies. The primary antibodies were detected using 1:10,000 dilutions of anti-rabbit (Millipore, Cat. No AP307P), anti-mouse (Millipore, Cat. No AP308P), or anti-donkey (Cat. No sc-2020, Santa Cruz Biotechnology) secondary antibodies conjugated with horse radish peroxidase. The reaction was developed using the ECL detection kit (Pierce, Cat. No 34095 and Millipore, Cat. No P90720). Usually, 10–20 µg of protein was loaded onto the gel. Band densitometry quantification was performed using the Fiji distribution of ImageJ 1.52a software (National Institutes of Health and the University of Wisconsin, Madison, WI, United States).

2.8 Immunolocalization studies

The distribution of MVI and other examined proteins in PC12 cells was evaluated by indirect immunocytochemistry. Cells on coverslips were fixed in 4% paraformaldehyde for 15 min, washed three times with phosphate-buffered saline (PBS) for 5 min, and blocked in a solution that contained 2% horse serum and 0.02% Triton X-100 in PBS for 1 h at room temperature. Coverslips were then incubated overnight at 4°C with rabbit polyclonal antibody to MVI, mouse monoclonal antibody to B23, rabbit polyclonal antibody to GRP78, mouse monoclonal antibody to fibrillarin, mouse monoclonal antibody to RPA 194 (Pol1), mouse monoclonal antibody to UBF, or mouse monoclonal antibody to S6 in a blocking solution and washed three times in PBS with 0.02% Triton X-100. This was followed by incubation with Alexa Fluor 488-conjugated anti-rabbit secondary antibody or Alexa Fluor 546-conjugated secondary anti-mouse antibody in a blocking solution for 60 min.

Finally, cells were washed three times in PBS with 0.02% Triton X-100 and mounted using VECTASHIELD PLUS Antifade Mounting Medium with DAPI. The specimens were visualized using a Zeiss LSM780 spectral confocal microscope equipped with a Plan-Apochromat 63x/1.40 Oil DIC M27 lens. In double immunostaining, special care was taken to control for any possible cross-reactivity (cross-bleeding) of the detection systems. We carefully adjusted the spectral ranges of detectors and always scanned the images sequentially. For negative controls, the primary antibody was omitted.

2.9 Confocal endoplasmic reticulum visualization

ER was visualized by staining with the ER-specific dye, ER Tracker™ Blue/White DPX (Thermo Fisher Scientific, Cat. No E12353), which is retained within the ER lumen, thus labeling the ER tubular network, according to the manufacturer's instructions. Briefly, cells were seeded on glass coverslips and cultured for 24 h and then incubated for 30 min at 37°C and 5% CO_2 with 1 µM ER tracker diluted in the culture medium. Then, the stained cells were fixed with 4% formaldehyde for 10 min, washed in PBS, and mounted using VECTASHIELD PLUS Antifade Mounting Medium without DAPI. Images were collected with the Zeiss LSM780, inverted Axio Observer Z.1 equipped with the 63x/1.4 Oil Plan-Apochromat DIC objective. A diode laser of 405 nm was used to excite fluorescence. Optical sections (2048 pixels × 2048 pixels × 8 Bit/pixel) were collected. The images were processed using ZEN Blue 2.1 software.

2.10 Ultrastructure of PC12 cells—transmission electron microscopy

PC12 cells were cultured on Thermanox™ coverslips (Electron Microscopy Sciences, Cat. No 72274) coated with poly-L-lysine (PLL, Electron Microscopy Sciences, Cat. No 19320) in RPMI-1640 medium supplemented with 10% HS, 5% FBS, and antibiotics: 1% penicillin/streptomycin or F12K medium supplemented with 2.5% FBS, 15% HS, and antibiotics: 1% penicillin/streptomycin, depending on the cell type. Cells were washed three times for 30 s each in PBS and fixed with 2% glutaraldehyde (GA) solution in PBS for 1 h at room temperature. Next, the fixed cells were washed three times for 10 min each in PBS, followed by post-fixation in 1% osmium tetroxide (OsO_4) for 30 min at room temperature (OsO_4 not only fixes but also provides contrast to lipid membranes). Sections were then rinsed twice for 10 min in PBS and twice for 5 min in deionized water, followed by dehydration in ethanol solutions of increasing concentrations in a so-called dehydration series, starting with 50% alcohol, followed by 70%, 80%, 90%, 96%, (5 min each) and anhydrous (99.8% absolute), twice for 15 min each, and then embedded in Spurr resin (Sigma-Aldrich, Cat. No EM0300) according to the standard protocol. The resin-submerged sections were cut into ultra-thin sections (60–70 nm thick) by using a diamond knife (Micro Star Technologies) and a Leica UTC ultramicrotome and collected on copper microscope grids (Electron Microscopy Sciences, Cat. No EMS400CU). The sections were stained with 2.5% uranyl acetate and 0.4% lead citrate and then examined by using a Joel EM 100 transmission electron microscope.

2.11 Post-embedding immunogold MVI localization

PC12 cells were grown on Thermanox™ coverslips, as described earlier. The cells were gently rinsed with PBS and fixed with 4% (v/v) formaldehyde and 0.25% (v/v) GA in the same PBS buffer for 1 h at room temperature. Fixed cells were washed three times with PBS, dehydrated in graded ethanol concentrations, and embedded in LR White resin (Electron Microscopy Sciences, Cat. No 14380) according to the standard protocol. Ultrathin sections were cut by using a diamond knife (Micro Star Technologies) and a Leica UTC ultramicrotome and collected on Formvar film-coated nickel grids (Electron Microscopy Sciences, Cat. No FCF400-Ni). The sections were then pretreated with 50 mM glycine in PBS for 10 min and incubated with a blocking solution containing 3% (w/v) bovine serum albumin (BSA) in PBS for 5 min at room temperature. Next, sections were placed in 1:50 dilution of a primary MVI antibody in

10.3389/fphys.2024.1368416

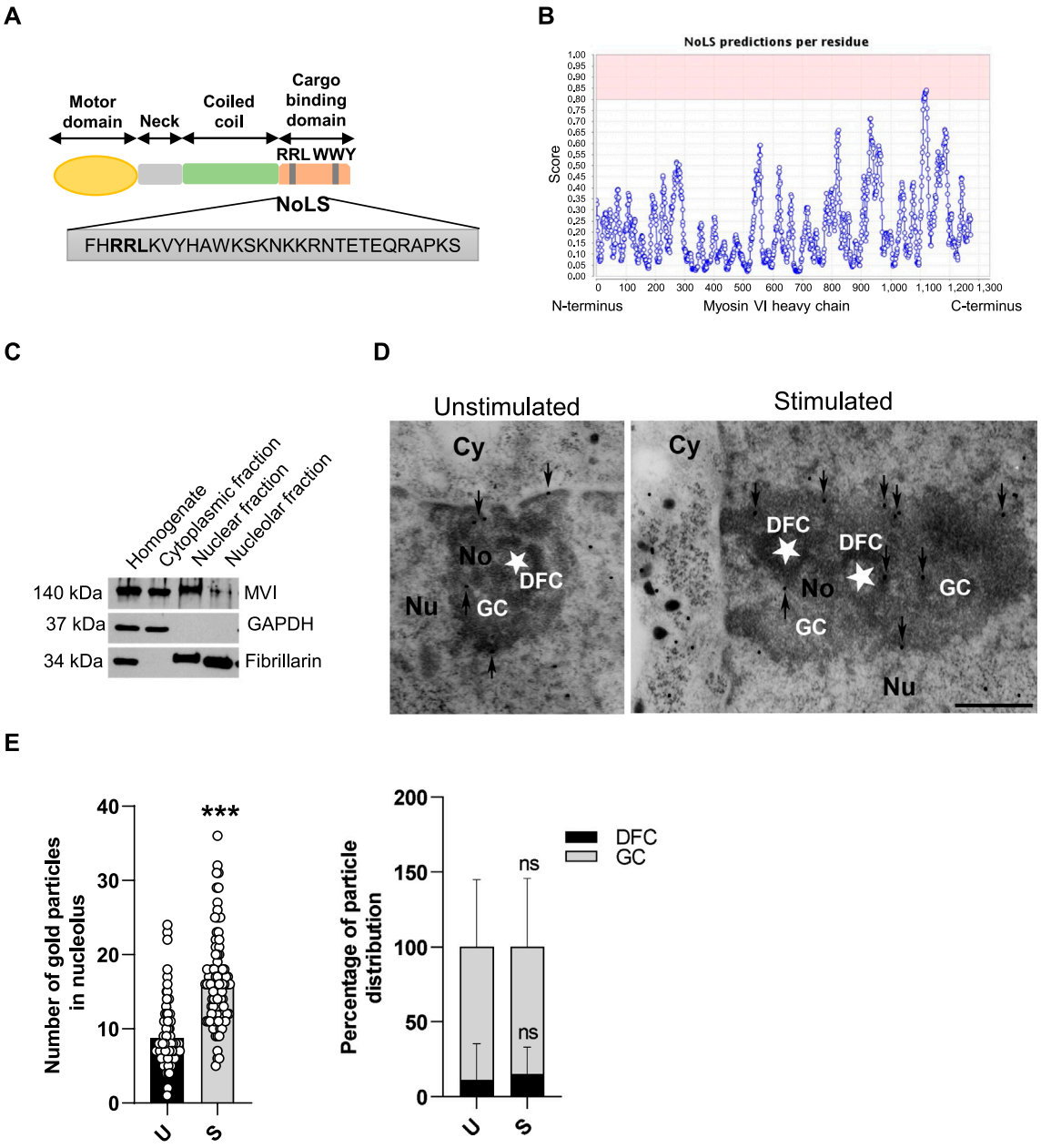

FIGURE 1
MVI is present within the nucleolus of PC12 cells. **(A)** Schematic diagram of the organization of the MVI heavy chain with depiction of the putative NoLS (nucleolar localization sequence) predicted by the NoD detector; detailed explanation is provided in the text. **(B)** Schematic diagram presenting NoD analysis with localization of a putative NoLS (a region with a score > 0.8; shown in pink) within the MVI heavy chain globular tail domain. The numbers on the *x*-axis correspond to amino acid positions of the MVI heavy chains. **(C)** Subcellular fractionation of PC12 cells. MVI is detectable in the nucleolar fraction. GAPDH, cytoplasmic protein marker, was detected only in the cytoplasmic fraction, but not in the nuclear and nucleolar fractions. Fibrillarin, nucleolar protein marker, was detected in both in the nuclear and nucleolar fractions. **(D)** Assessment of the sub-nucleolar distribution of MVI by means of immunogold electron microscopy in unstimulated and stimulated cells. Labeling was concentrated in the dense fibrillar component (DFC) surrounding the fibrillar center (asterisk) and in the granular component (GC) of the nucleolus. Cy, cytoplasm; Nu, nucleus; No, nucleolus. Bars, 1 μm. **(E)** Quantification of the gold particles in the nucleoli of PC12 cells before (U) and after stimulation with 56 mM KCl (S); ***, $p < 0.001$ (left graph). Quantification of distribution of the gold particles within DFC and GC subdomains (right graph). ns, not statistically significant. 100% corresponds to all the particles spotted in the nucleoli at given conditions. Quantitative analyses were based on ~100 images of nucleoli of unstimulated and stimulated cells from three different cell cultures. For quantification of distribution of MVI in nucleolar subdomains, the analyses were carried out for 20 nucleoli of two experimental conditions.

PBS supplemented with 0.3% BSA for 2 h, followed by incubation with a gold-conjugated anti-rabbit IgG 15-nm secondary antibody (BB International, Cat. No R14003) at 1:100 dilution in PBS with 0.1% BSA for 30 min. Both incubations were carried out at room temperature. For the negative control, the primary antibody was omitted. Finally, the sections were stained with 2.5% uranyl acetate

10.3389/fphys.2024.1368416

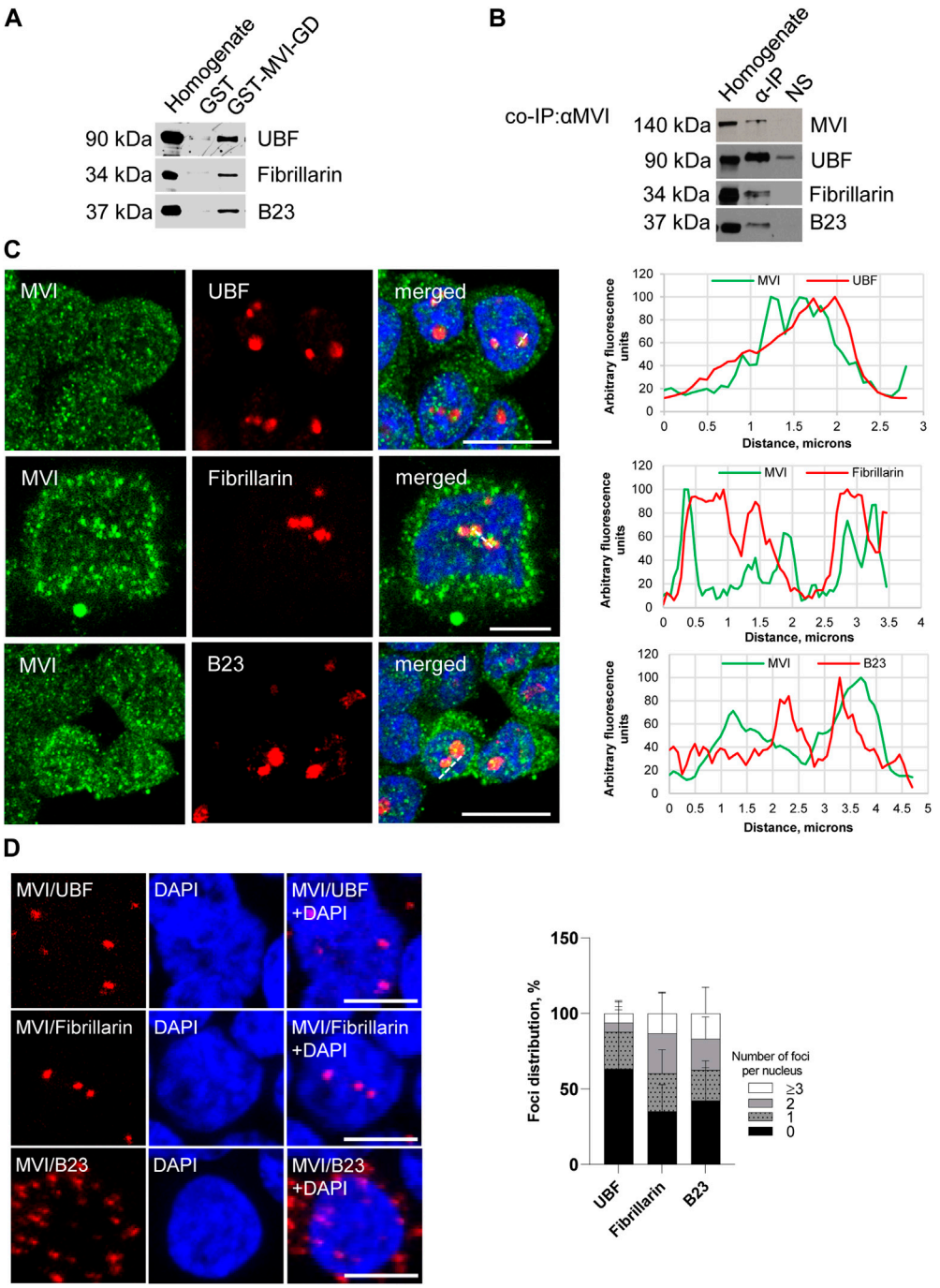

FIGURE 2
Assessment of the interaction of MVI with nucleolar proteins. **(A)** Immunoblot analysis of pull-down fractions. Homogenate, PC12 cell homogenate before loading onto Glutathione Sepharose; GST-MVI-GD, a fraction eluted from the resin with an attached MVI globular tail fused with GST, and GST, a fraction eluted from the GST-attached resin. The fractions were probed with antibodies against UBF, fibrillarin, and B23. **(B)** Co-immunoprecipitation of MVI/UBF, MVI/fibrillarin, and MVI/B23 with the anti-MVI antibody. Cell homogenates (homogenate), samples precipitated with anti-MVI antibody (α-IP) or with a non-immune serum (NS), were probed with anti-UBF, anti-fibrillarin, and anti-B23 antibodies, as marked on the figure. **(C)** Co-localization of MVI (in green) with UBF, fibrillarin, and B23 (in red). In blue, nuclei stained with DAPI. Images of the cell central sections (z = 0.3 μm) were obtained with a Zeiss LSM 780 confocal microscope. Bars, 10 μm. Left panels in C, fluorescence image profile and co-localization analyses; graphs represent fluorescence intensity profiles calculated on images obtained from samples co-immunostained for MVI and nucleolar proteins, as marked on the images with a dashed line. **(D)** PLA assay probing MVI/UBF, MVI/fibrillarin, and MVI/B23 interactions (in red) in PC12 cells. In blue, nuclei stained with DAPI. Images of the cell central sections (z = 0.3 μm) were obtained with a Zeiss LSM 780 confocal microscope. Bars, 10 μm. Graph in right, evaluation of PLA-positive foci, corresponding to the interaction of MVI with UBF, fibrillarin, and B23 per nucleus. 100% corresponds to all the examined nuclei (N = 64 for UBF, N = 59 for fibrillarin, and N = 87 for B23); detailed information is given in Supplementary Figure S2B).

and examined on a JEOL JEM 1010 transmission electron microscope.

2.12 GST pull-down assay

The fusion proteins composed of GST and MVI C-terminal globular tail domain (GST-MVI-GD) as well as GST alone were purified, as described by Majewski et al. (2012). For the lysate, cells were lysed in an ice-cold buffer that contained 50 mM Tris (pH 7.5), 150 mM NaCl, 0.1% Triton X-100, 1 mM DTT, 2 mM EGTA, 50 mM NaF, 1 mM Na_3VO_4, and 1 mM PMSF and supplemented with the cOmplete™ Protease Inhibitor Cocktail and phosphatase inhibitor PhosSTOP™. The assay was performed as described by Majewski et al. (2012). Briefly, the lysates were precleared with GST-bound Glutathione Sepharose 4B beads for 2 h at 4°C to remove proteins non-specifically binding to Glutathione Sepharose 4B and/or GST and subsequently incubated with Glutathione Sepharose 4B beads bound to GST-MVI-GD or GST alone for 4 h at 4°C. The beads were exhaustively washed in the ice-cold lysate buffer, described above, and subjected to SDS–PAGE electrophoresis followed by immunoblotting.

2.13 Proximity ligation assay (PLA)

PC12 cells after fixation were blocked in the Duolink blocking solution in a humidity chamber for 30 min at 37°C and incubated with the following primary antibodies: rabbit polyclonal anti-MVI and mouse monoclonal antibodies anti-B23, anti-fibrillarin, anti-UBF, anti-Pol1, anti-p-S6, and anti-S6, diluted in Duolink Antibody diluent solution for 3 h at 37°C. Cells were next washed two times in a wash buffer for 5 min at room temperature. Next, secondary antibodies conjugated with oligonucleotides, PLA probe anti-mouse MINUS, and PLA probe anti-rabbit PLUS were applied in the Duolink antibody diluent solution for 1 h at 37°C and then washed twice for 5 min. The Duolink assay was further performed strictly according to the manufacturer's instructions. For negative controls, the primary antibodies were omitted.

2.14 Co-immunoprecipitation

To perform co-immunoprecipitation, PC12 cells (CRL-1721) were lysed in a buffer containing 50 mM Tris (pH 7.5), 150 mM NaCl, 2 mM EGTA, 0.1% Triton X-100, 2 mM $MgCl_2$, 2 mM MgATP, 50 mM NaF, and 1 mM Na_3VO_4, supplemented with the cOmplete™ Protease Inhibitor Cocktail and phosphatase inhibitor PhosSTOP™. The lysates were pre-cleared with A/G agarose beads (Santa Cruz Biotechnology, Cat. No sc-2003) for 30 min at 4°C and subsequently incubated for 4 h at 4°C with 10 µg of the anti-MVI antibody (Proteus, Cat. No 25-6791) or non-immunized rabbit IgG (Santa Cruz Biotechnology, Cat. No sc-2027) as a control, followed by overnight incubation with the aforementioned agarose beads. Next, the beads were washed with the lysis buffer and then subjected to SDS–PAGE electrophoresis followed by immunoblotting with antibodies of interest to detect the co-immunoprecipitated complexes.

2.15 Quantitative real-time polymerase chain reaction (qRT-PCR)

RNA was isolated from 5×10^6 PC12 cells (scrambled and MVI-KD) using the RNeasy Plus Universal Mini Kit (Qiagen, Cat. No 73404) according to the manufacturer's instructions. DNA contamination from RNA samples was removed through treatment with RNase-Free DNase I (Qiagen, Cat. No 79254). First-strand cDNA synthesis was performed using 1 µg of RNA and the SuperScript™ III Reverse Transcriptase Kit (Thermo Fisher Scientific, Cat. No 18080-093) with random hexamers. Quantitative PCR was performed using the Fast SYBR Green Master Mix (Applied Biosystems, Cat. No 4385612) with an Applied Biosystems 7900HT Fast Real-Time PCR System. The oligonucleotide primer sequence used for rRNA analysis included 45S pre-rRNA—forward: 5′-TGGGGCAGCTTTATGACAAC-3′; 45S pre-rRNA—reverse: 5′-TAGCACCAAACGGGAAAACC-3′;

18S rRNA—forward: 5′GTTGGTTTTCGGAACTGAGGC3';

18S rRNA—reverse: 5′GTCGGCATCGTTTATGGTCG3'.

Pre-rRNA and 18S rRNA levels were quantified using the ΔΔ CT method ($2^{-\Delta\Delta CT}$). Expression values were obtained from four independent experiments run in triplicates of each cDNA sample: 45S pre-rRNA relative to 18S rRNA (from the same cDNA preparations) (Kalita et al., 2008).

2.16 Identification of nucleolar localization signals in MVI

To identify a nucleolar localization signal (NoLS) within the MVI heavy chain, the NoD webserver was used (http://www.compbio.dundee.ac.uk/nod) (Scott et al., 2011).

2.17 Statistical analyses

All experiments were performed at least three times in two–three technical replicates. The results were expressed as means ± SD (standard deviation). If the data were normally distributed, we performed parametric two-tailed Student's t-test or one-way ANOVA using GraphPad Prism 8.4.3 software (San Diego, CA, United States). Data that were non-normally distributed were analyzed with a nonparametric Mann–Whitney U-test to determine the significance. Statistical significance was defined as * for $p < 0.05$, ** for $p < 0.01$, *** for $p < 0.001$, and ns for no statistical significance ($p > 0.05$).

3 Results

We have previously shown that nucleolin and ribosomal protein S6, both involved in pre-rRNA transcription and ribosome assembly, are potential MVI binding partners in neurosecretory PC12 (Majewski et al., 2018). These observations prompted us to investigate the role of MVI in nucleolar and ribosomal functions.

3.1 Myosin VI is present within the nucleolus

We started the examination with identification of structural grounds for the presence of MVI in the nucleolus. For this, we performed an analysis using a nucleolar localization sequence detector, NoD, created on the basis of the data of 46 human-confirmed nucleolar localization signals (NoLS) (Scott et al., 2011). The analysis predicted the presence of one NoLS within the MVI heavy chain with the following sequence: FHRRLKVYHAWKSKNKKRNTETEQRAPKS (Figures 1A and B). This positively charged region with the pi value of 10.99 (calculated with a protein isoelectric point calculator, http://isoelectric.org) spans residues 1114 and 1142, situated within the MVI cargo-binding domain. Furthermore, it overlaps the bipartite nuclear localization signal (NLS) and contains both the RRL motif, involved in electrostatic interaction with MVI partners, and the positively charged region (WKSKNKKRN), involved in PIP_2 binding (Tumbarello et al., 2013; Spudich et al., 2007).

PC12 cell fractionation and immunogold staining showed that MVI is present in the nucleolar fraction (Figures 1C–E). Furthermore, analysis of immunogold staining revealed that the presence of MVI within the nucleolus is increased upon cell stimulation with 56 mM KCl (Figures 1D and E). Quantification of MVI-associated gold particles revealed that MVI localizes mainly to the granular component (GC) and dense fibrillar component (DFC), but the majority was present within the GC. This distribution does not depend on stimulation, as the same fraction of MVI is visible in both sub-compartments regardless of stimulation (Figure 1E).

3.2 Interaction of MVI with protein markers of sub-nucleolar compartments

To show whether MVI can interact with markers of nucleolar compartments, namely, UBF (upstream binding factor, marker of FC), fibrillarin (marker of DFC), and B23 (marker of GC), we performed a series of experiments using the immunoprecipitation (IP) as well as pull-down techniques, immunofluorescence staining, and proximity ligation assay (PLA) (Figure 2; Supplementary Figures S1, S2).

The pull-down assay with the MVI cargo-binding domain (GST-MVI-GD) as a bait, followed by immunoblotting, revealed that the selected marker proteins were present in the fractions precipitated with the MVI fragment and not with GST alone (Figure 2A). In addition, the analysis of the fractions co-IPed with the anti-MVI antibody (see Figure 2B) demonstrated the presence of the above-mentioned nucleolar proteins and MVI in the precipitates obtained upon incubation of cell lysates with the antibody but not with the control non-immune serum. It should be noted that the low yield of IP and pull-down assays for fibrillarin suggests that these interactions may be weak and/or transient.

Double immunostaining for MVI and the aforementioned nucleolar proteins showed their co-localization, further confirming their interaction with MVI (Figure 2C; Supplementary Figure S1).

To check whether these interactions also exist *in cellulo*, we employed the proximity ligation assay (PLA), designed for *in situ* detection of two proteins existing within close intracellular proximity (within the 20–40 nm range) (Soderberg et al., 2006). As shown in Figure 2D and Supplementary Figure S2A, red dots representing positive PLA signals indicative of the close proximity of two examined proteins were observed within the nucleus for UBF, fibrillarin, and B23. Thus, these data confirm the interaction of MVI with these proteins *in situ*. Positive signals in the perinuclear region were also detected for B23. Quantification of the number of PLA foci per nucleus revealed that the interaction does not take place in all the nuclei and varies between the examined proteins (Figure 2D; Supplementary Figure S2B). The highest fraction of "foci-positive" nuclei was observed for fibrillarin (~65%), and the lowest for UBF (~36%). As for B23, the fraction of "foci-positive" nuclei constitutes ~57%, but in case of these interactions, we observed the highest fraction of the nuclei, which contained ≥3 foci (~17%).

3.3 Effects of MVI depletion on the organization of the nucleolus

Since MVI is known to be involved in the organization of cytoskeletal compartments, and in PC12 cells (Majewski et al., 2011), we tested whether and how depletion (by ~90%) of this molecular motor (Figure 3A) affects the organization of the nucleolus. For this, we employed transmission electron microscopy, which showed different phenotypes, with more or less defective nucleoli in MVI-depleted cells (Figure 3B; Supplementary Figure S3). In the presented examples, the nucleoli are disorganized, with structural defects in both the DFC and GC subdomains. Furthermore, in some of the images, identification of these nucleolar compartments was not possible at all.

3.4 Effects of MVI depletion on localization of nucleolar proteins

Since depletion of MVI causes disorganization of the nucleolus, we checked whether its presence is required for preserving the association of the examined nucleolar proteins with their locations. For this, we performed immunostaining for UBF, fibrillarin, and B23 in MVI-KD cells (Figure 4; Supplementary Figures S4–S6). Furthermore, the morphological changes observed in the nucleoli of MVI-KD cells suggest that MVI depletion may evoke conditions resembling nucleolar stress to some extent.

Therefore, we incubated MVI-KD cells with the Pol1 inhibitor, ActD, at the concentration of 0.05 μg/mL, known to inhibit the activity of this polymerase only (Reich et al., 1961). Since there is no information on the effect of ActD on the nucleoli of PC12 cells, we visualized the effects of this Pol1 inhibitor using transmission electron microscopy on the nucleoli of the examined cells (Supplementary Figure S7). As expected, the ActD treatment caused a collapse of the nucleoli with a segregation of its fibrillar and granular components (Yang et al., 2018; Lafita-Navarro and Conacci-Sorrell, 2023). In addition, we showed that ActD at this concentration does not affect the content of MVI in the cytoplasm and nuclear fractions of control cells (Supplementary Figure S8).

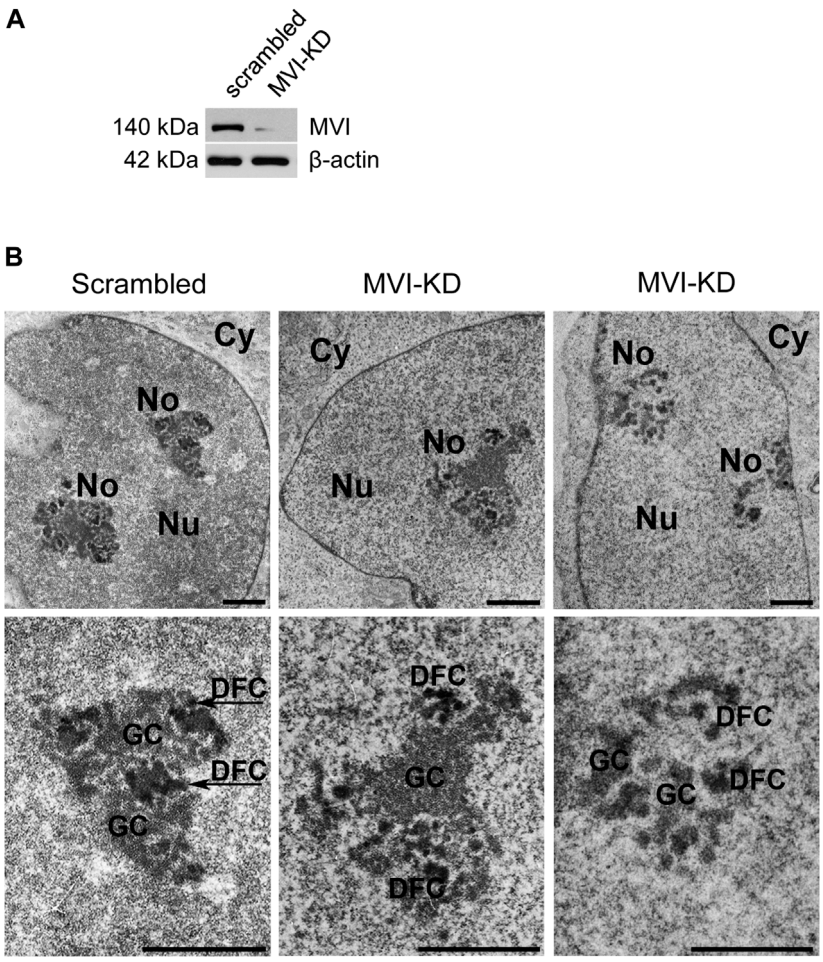

FIGURE 3
Effect of MVI depletion on morphology of nucleoli. **(A)** Immunoblot analysis of MVI in scrambled and MVI-KD PC12 cells. **(B)** Electron microscopy images of the nucleoli of scrambled and MVI-KD cells. Lower panels, ~×2.5 magnification of the areas marked in the corresponding upper panels. Nu, nucleus; No, nucleolus; FC, fibrillar center; DFC, dense fibrillar component; GC, granular component. Bars, 1 μm.

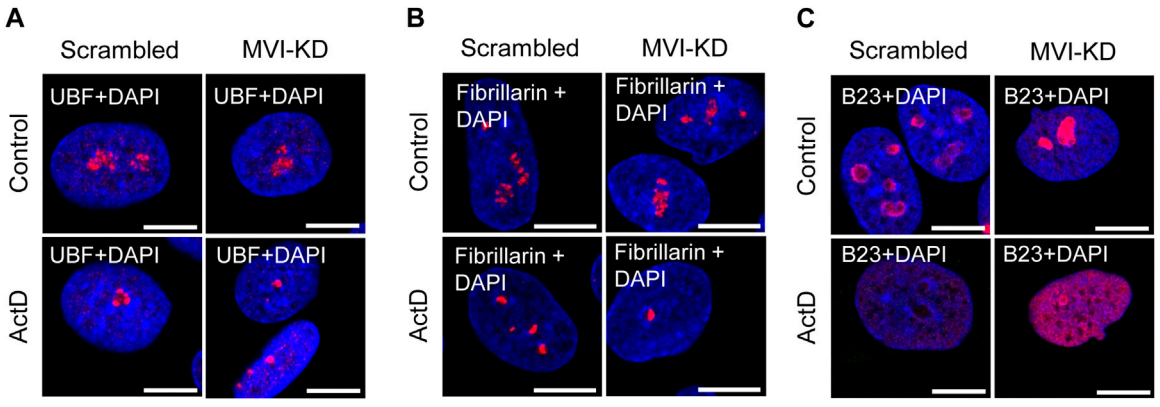

FIGURE 4
Effect of MVI depletion and actinomycin D on the localization of nucleolar proteins. **(A)** Localization of UBF (in red) in scrambled and MVI-KD cells after 3-h treatment with (ActD) and without (control) actinomycin D at the 0.05 μg/mL concentration. **(B)** Nucleolar localization of fibrillarin (in red) in scrambled and MVI-KD cells after 3-h treatment with (ActD) and without (control) actinomycin D at the 0.05 μg/mL concentration. **(C)** Redistribution of nucleolar protein B23 (in red) in scrambled and MVI-KD cells after 3-h treatment with (ActD) and without (control) actinomycin D at the 0.05 μg/mL concentration. In blue, nuclei stained with DAPI. Images of the cell central sections (z = 0.3 μm) were obtained with a Zeiss LSM 780 confocal microscope. Bars, 10 μm.

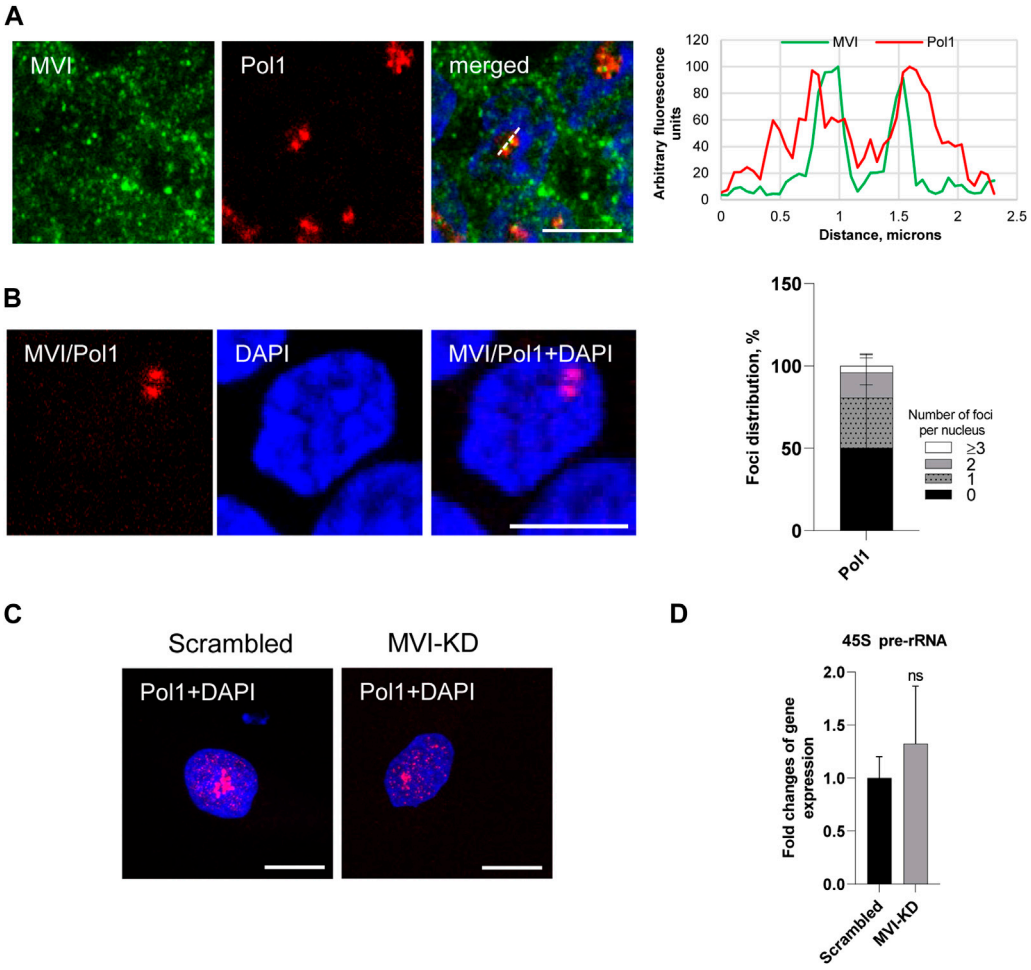

FIGURE 5
Effect of MVI depletion on Pol1 activity. **(A)** Co localization of MVI (in green) with Pol1 (in red). In blue, nuclei stained with DAPI. Right panel in B, fluorescence image profile and co localization profiles calculated on images obtained from samples co-immunostained for MVI and Pol1, as marked on the image with a dashed line. **(B)** PLA assay probing the MVI/Pol1 interaction (in red) in PC12 cells. In blue, nuclei stained with DAPI. Graph in right, evaluation of PLA-positive foci, corresponding to the interaction of MVI with Pol1 per nucleus. 100% corresponds to all the examined nuclei (N = 40, detailed information is given in Supplementary Figure S10. **(C)** Immunostaining for Pol1 (in red) in scrambled and MVI-KD cells. Nuclei were stained with DAPI (in blue). Images in B and C of the cell central sections (*z* = 0.3 μm) were obtained with a Zeiss LSM 780 confocal microscope. Bars, 10 μm. **(D)** Levels of 45S pre-rRNA in scrambled and MVI-KD cells were determined by quantitative real-time PCR and normalized against the levels of 18S rRNA. ns, not statistically significant. A quantitative analysis was based on assays performed in triplicates on four different cell cultures.

As presented in Figure 4A and Supplementary Figure S4, depletion of MVI did not affect the localization of UBF, as in both scrambled and MVI-KD cells, this protein was dispersed within the nucleolus. In control cells treated with ActD, UBF localized to the nucleolar caps shaped around the nucleolar remnants (Yang et al., 2018). Localization of this protein in the ActD-treated MVI-KD cells did not substantially differ from that in the control counterparts. A similar observation was made for fibrillarin (Figure 4B; Supplementary Figure S5). Thus, depletion of MVI in the presence or absence of ActD does not affect the localization of UBF and fibrillarin. Furthermore, MVI knockdown does not affect the overall level of these two proteins (Supplementary Figure S9).

However, the examination of localization of B23 revealed the evident difference between the two tested conditions (Figure 4C; Supplementary Figure S6). While in scrambled cells, this protein mostly localized to the nucleolar periphery, in MVI-KD cells, it was present within the entire nucleolus. Treatment of both cell types with ActD caused delocalization of B23 to the nucleoplasm, but in MVI-depleted cells, incubated with the inhibitor, the nucleoplasmic staining for B23 was more prominent, and the protein was still present at the edges of the nucleolar remnants (Figure 4C; Supplementary Figure S6). Immunoblotting analysis did not reveal statistically significant changes in the level of B23 in MVI-KD lysates (Supplementary Figure S9).

3.5 Examination of involvement of MVI in Pol1 activity

Next, we decided to test whether depletion of MVI could affect Pol1-based transcription (see Figure 5; Supplementary Figures S10 and S11).

As shown in Figures 5A and B and Supplementary Figure 10, Pol1 co-localizes with MVI and interacts with this motor protein *in situ*, as revealed by the immunofluorescence and PLA assays.

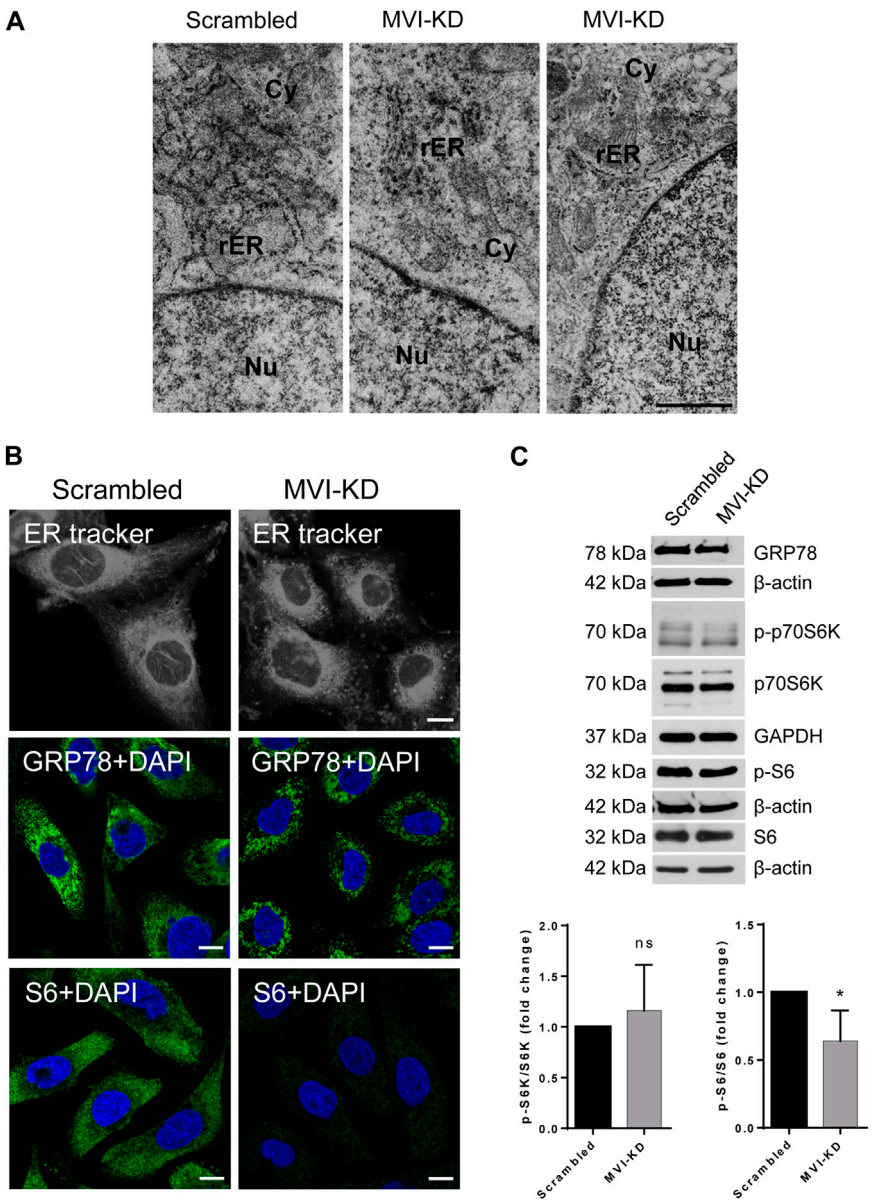

FIGURE 6
Effect of MVI depletion on endoplasmic reticulum organization (ER). **(A)** Electron microscopy visualization of the ER of scrambled and MVI-KD cells. Bars, 2 μm. **(B)** Visualization of the ER with fluorescent microscopy. Upper panels, the ER in scrambled and MVI-KD cell lines visualized by staining with the ER-specific dye, ER Tracker™ Blue/White DPX. Middle panels, immunostaining for GRP78 in scrambled and MVI-KD cells. GRP78 was visualized with anti-GRP78 antibody (in green) and nuclei with DAPI (in blue). Bottom panels, immunostaining for S6 in scrambled and MVI-KD cells. S6 was visualized with the anti-S6 antibody (in green) and nuclei with DAPI (in blue). Images in B of the central cell section (z = 0.3 μm) were obtained with a Zeiss LSM 780 confocal microscope. Bars, 10 μm. **(C)** Immunoblotting analysis of GRP78, p-S6, and S6 as well as of p-p70S6K and p70S6K in scrambled and MVI-KD PC12 cells. β-actin and GAPDH served as protein loading controls. Graphs, ratio of p-p70S6K to p70S6K levels (on the left) and p-S6 to S6 levels (on the right). 1, the levels of the examined proteins in scrambled cells. *, $p < 0.05$; ns, not statistically significant.

Quantification of the number of PLA foci per nucleus revealed that the Pol1–MVI interaction takes place in about 50% nuclei (Figure 5B).

In addition, the depletion of MVI did not have an evident effect on Pol1 distribution (Figure 5C; Supplementary Figure 11).

To test whether MVI could be involved in Pol1-based transcription, we used the q-RT-PCR technique to examine whether the depletion of MVI affects the synthesis of 45S pre-rRNA transcript (Kalita et al., 2008). As shown in Figure 5D, there is no significant change in the amount of the transcript in MVI-KD cells with respect to control cells, suggesting that MVI does not play a significant role in Pol1 activity.

3.6 Involvement of MVI in ribosome organization

Our previous results indicate that in PC12 cells, MVI not only localizes to the endoplasmic reticulum (ER) membranes but also

interacts with ribosomal protein S6 (Majewski et al., 2018), which suggests that this molecular motor might be involved in the ribosome and/or ER organization. Furthermore, our current observation that MVI is important for the maintenance of the nucleolar organization makes this suggestion plausible.

The analysis of the TEM images revealed that in MVI-KD cells, the ER membranes are not only inflated but also less decorated with the ribosomes with respect to control scrambled cells (Figure 6A). In addition, live staining for the ER membranes with the ER Tracker showed profound changes in the ER organization in MVI-KD cells (Figure 6B, upper panels).

Immunostaining for GRP78, a key protein involved in protein folding and quality control in the ER (Kleizen and Braakman 2004), confirmed the disorganization/fragmentation of this membranous compartment in MVI-KD cells (Figure 6B, middle panels). Immunostaining for S6 (Figure 6B, bottom panels) revealed a very weak signal in MVI-KD cells. This is in contrast to our observation that the overall level of S6, similarly to GRP78, was not affected by MVI depletion (Figure 6C). This could be explained in terms that depletion of MVI might impair the availability of an S6 epitope *in cellulo*. We also examined the level of p70S6K (and its active, phosphorylated form, p-p70S6K), a kinase involved in regulation of S6 activity. As presented in Figure 6C, the ratio of p-p70S6K to p70S6K level is not affected by MVI depletion, but the ratio of p-S6 to S6 is decreased, indicating that the activity of S6 is associated with MVI.

4 Discussion

Our study demonstrates for the first time that in neurosecretory PC12 cells, MVI interacts with several nucleolar proteins and seems to play a role in nucleolus and ribosome maintenance, though it seems not to be crucial for Pol1-dependent transcription.

MVI translocates to the nucleus due to the presence of several nuclear localization signals (NLS) within its heavy chain (Majewski et al., 2018; Vreugde et al., 2006, Hari-Gupta el al., 2022). Here, we show that MVI also contains one putative nucleolar localization signal (NoLS), situated within the MVI cargo-binding domain, overlapping the bipartite NLS and containing motifs involved in the interaction with MVI partners and phospholipids (Figure 1A) (Majewski et al., 2018; Spudich et al., 2007; Tumbarello et al., 2013). It is plausible that this region may be involved in the MVI presence in the nucleolus, though the specificity of this putative NoLS is not clear yet. It is noteworthy that the presence of two functional NoLS regions was confirmed within myosin IC heavy chain (also termed as NMIC) that are necessary for its nucleolar presence, specifically for isoform B of NMIC (Schwab et al., 2013). Of note, there are three NMIC posttranslational forms A, B, and C, and two of them, B and C, localize to the nucleus (Ihnatovych et al., 2012). One NoLS is located within the N-terminal positively charged peptide specific for this NMIC isoform, and the second is present upstream of the neck region within the head domain (Schwab et al., 2013). The authors postulate that this is a mechanistic explanation for the observed functional differences between the NMIC isoforms. Interestingly, a different mechanism is behind the nuclear/nucleolar translocation of myosin VA (MVA), one of the three myosin isoforms reported to be located in the nucleolus. It has been shown in neurons that while phosphorylation of Ser1650 of MVB by CaMKII is crucial for its presence in the nucleus (where it localizes within the speckles), inhibition of transcription causes its redistribution to the nucleolus (Pranchevicius et al., 2008). Though there is no report on how myosin VB (MVB) translocates to the nucleus/nucleolus, it is plausible that the same mechanism is employed as the region corresponding to the amino acid sequence of MVB reveals a high degree of similarity to the MVA isoform (Rodriquez and Cheney 2002).

Localization of MVI to the nucleolar subdomains as well as its newly revealed interaction with proteins specific to these regions, UBF, fibrillarin, and B23 suggest the involvement of MVI in ribosome biogenesis taking place in this nuclear compartment. However, based on these analyses, we cannot state whether or not MVI directly interacts with these nucleolar proteins or is simply a part of a complex containing one or all of them. In addition, our earlier observation on the interaction of MVI with nucleolin seems to strengthen this suggestion (Majewski et al., 2018). Furthermore, a shift in the localization of B23 in MVI-depleted cells, especially under nucleolar stress conditions, additionally confirms our suggestion regarding the important role of this molecular motor in nucleolar functions. In addition, data showing that depletion of MVI affects the nucleolar structure and ER organization, particularly the decrease in ribosome decoration, further confirm this suggestion. Notably, disorganization of the ER was also observed in MVI-depleted myoblasts (Karolczak et al., 2015).

However, despite co-localization of MVI with Pol1, its depletion does not seem to affect this polymerase activity. So far, two unconventional myosins, MVB and NMIC, have been found to be associated with Pol1 complexes (Lindsay and McCaffrey 2009; Philimonenko et al., 2004). While for MVB, the mechanisms of its involvement in nucleolar transcription have not yet been elucidated, much more is known about the involvement of NMIC. It has been shown that it plays a role in both the maturation and export of competent pre-ribosomal subunits to the nuclear pore complex (Obrldik et al., 2010). Furthermore, the presence of NMIC also facilitates the modification of histone H3 at Lys9 (H3AcK9) that is required to activate rRNA gene transcription and cell cycle progression (Sarshad et al., 2013). In line with this is our recent observation that in the nuclei of PC12 cells MVI co-localizes with the same modification of histone 3 (Majewski et al., 2018). In addition, in our cell model, MVI interacts with several proteins such as hnRNPs and SC35 (Majewski et al., 2018) as well as the above-mentioned nucleolin, UBF, fibrillarin, and B23, all involved in maturation and processing of the products of the Pol1 and/or Pol2 transcription. We hypothesize that interactions with these newly identified nucleolar partners could be responsible for engagement of MVI in processes taking place in the nucleolus.

Thus, the question arises about the mechanism(s) behind the observed effects of MVI depletion on the organization of the nucleolus and ribosome-containing ER membranes. Based on our and other groups' data, it is known that MVI interacts with numerous partners specific not only for the cell/tissue type but also for the MVI isoform present in a given cell/cellular compartment (Majewski et al., 2018; Wollscheid et al., 2016; Tumbarello et al., 2013; Dos Santos et al., 2022). Recently, we showed that in PC12 cells, the dominant one is the isoform without the large insert, which is able to shuttle between the cytoplasm and the nucleus in a stimulation-dependent manner (Majewski et al., 2018). The data presented herein, showing that the number of MVI-positive particles is elevated upon stimulation, indicate that upon cell stimulation, MVI can

also translocate to the nucleolus (either from the nucleoplasm and/or directly from the cytoplasm), where it can interact with nucleolar proteins and, thus, be involved in nucleolar processes. Its presence is important for the maintenance of the nucleolus morphology, indicating that it may act here as the crosslinker stabilizing the structure *via* the interaction between the nuclear/nucleolar actin pool(s) and nucleolar proteins (Ulferts et al., 2021). Interestingly, similar effects on nucleolar morphology have been demonstrated for fascin, an actin filament-bundling protein primarily known for its involvement in the promotion of cell migration (Lamb and Tootle, 2020). The other possibility is that depletion of MVI impairs the import of the nucleolar components from the cytoplasm as MVI can act as a transporting motor as well (Cook et al., 2020). In addition, the lack of MVI may affect the export of the products of the nucleolar processes, and this could be responsible for the observed disorganization of the ER membranes and the reduced ribosome load. Involvement of MVI in ribosome biogenesis/assembly could also result from its interaction with ribosomal protein S6 and, in particular, with its active phosphorylated form (p-S6), which is a downstream effector of mTOR kinase (Majewski et al., 2018; Meyuhas 2015). Of note, MVI–S6 interactions have been also shown for skeletal muscle and myogenic cells [Lehka et al., unpublished]. It is noteworthy that an ATP-dependent spatial association of S6-containing small ribosomal subunits (SSUs) with NMIC and actin within the nuclear compartments and at the nuclear pores has been shown in HeLa cells (Cisterna et al., 2006; Cisterna et al., 2009). The authors' suggestion that NMIC is involved in the actin-dependent export of SSUs to the cytoplasm supports our hypothesis that MVI could be engaged in transporting ribosome components to and from the nucleus/nucleolus. The MVI–S6 interaction has not yet been characterized at the molecular level, but our staining for S6 in MVI-depleted cells seems to indicate that loss of MVI could affect the conformation of this 29-kDa protein of the 40S ribosomal subunit, as it was revealed upon RNA binding, indicating a direct interaction (Draper and Reynaldo 1999).

In summary, our study indicates for the first time that MVI is involved in nucleolar processes and ribosome biogenesis through its interaction(s) with the proteins involved in nucleolar and ribosome functions. However, further studies are needed to characterize these interactions at the molecular level.

Data availability statement

The original contributions presented in the study are included in the article/Supplementary Material; further inquiries can be directed to the corresponding author.

Ethics statement

Ethical approval was not required for the studies on animals in accordance with the local legislation and institutional requirements because only commercially available established cell lines were used.

Author contributions

JN: data curation, investigation, methodology, software, validation, visualization, writing–original draft, and writing–review and editing. RL: data curation, investigation, methodology, visualization, and writing–review and editing. KK: investigation, methodology, validation, writing–original draft, and writing–review and editing. LL: investigation, methodology, validation, and writing–review and editing. ML: conceptualization, data curation, investigation, methodology, supervision, writing–original draft, and writing–review and editing. OL: data curation, investigation, visualization, writing-review and editing. MR: conceptualization, funding acquisition, project administration, supervision, validation, writing–original draft, and writing–review and editing.

Funding

The author(s) declare that financial support was received for the research, authorship, and/or publication of this article. This work has been supported by the statutory funds to the Nencki Institute from Polish Ministry of Science and Higher Education.

Acknowledgments

The authors would like to thank Dr. Lukasz Majewski and Dr. Magdalena Sobczak for their invaluable input in the initiation of the project.

Conflict of interest

The authors declare that the research was conducted in the absence of any commercial or financial relationships that could be construed as a potential conflict of interest.

The author(s) declared that they were an editorial board member of Frontiers, at the time of submission. This had no impact on the peer review process and the final decision.

Publisher's note

Supplementary material

The Supplementary Material for this article can be found online at: https://www.frontiersin.org/articles/10.3389/fphys.2024.1368416/full#supplementary-material

References

Ameen, N., and Apodaca, G. (2007). Defective CFTR apical endocytosis and enterocyte brush border in myosin VI-deficient mice. *Traffic* 8 (8), 998–1006. doi:10.1111/j.1600-0854.2007.00587.x

Avraham, K. B., Hasson, T., Sobe, T., Balsara, B., Testa, J. R., Skvorak, A. B., et al. (1997). Characterization of unconventional MYO6, the human homologue of the gene responsible for deafness in Snell's waltzer mice. *Hum. Mol. Genet.* 6 (8), 1225–1231. doi:10.1093/hmg/6.8.1225

Avraham, K. B., Hasson, T., Steel, K. P., Kingsley, D. M., Russell, L. B., Mooseker, M. S., et al. (1995). The mouse Snell's waltzer deafness gene encodes an unconventional myosin required for structural integrity of inner ear hair cells. *Nat. Genet. Dec* 11 (4), 369–375. doi:10.1038/ng1295-369

Belin, B. J., and Mullins, R. D. (2013). What we talk about when we talk about nuclear actin. *Nucleus* 4 (4), 291–297. doi:10.4161/nucl.25960

Caridi, C. P., D'Agostino, C., Ryu, T., Zapotoczny, G., Delabaere, L., Li, X., et al. (2018). Nuclear F-actin and myosins drive relocalization of heterochromatic breaks. *Nature* 559 (7712), 54–60. doi:10.1038/s41586-018-0242-8

Chibalina, M. V., Puri, C., Kendrick-Jones, J., and Buss, F. (2009). Potential roles of myosin VI in cell motility. *Biochem. Soc. Trans.* 37 (Pt 5), 966–970. doi:10.1042/BST0370966

Cho, S. J., and Chen, X. (2010). Myosin VI is differentially regulated by DNA damage in p53-and cell type-dependent manners. *J. Biol. Chem.* 285 (35), 27159–27166. doi:10.1074/jbc.M110.142117

Cisterna, B., Malatesta, M., Dieker, J., Muller, S., Prosperi, E., and Biggiogera, M. (2009). An active mechanism flanks and modulates the export of the small ribosomal subunits. *Histochem Cell. Biol.* 131 (6), 743–753. doi:10.1007/s00418-009-0583-3

Cisterna, B., Necchi, D., Prosperi, E., and Biggiogera, M. (2006). Small ribosomal subunits associate with nuclear myosin and actin in transit to the nuclear pores. *FASEB J.* 20 (11), 1901–1903. doi:10.1096/fj.05-5278fje

Cook, A. W., Gough, R. E., and Toseland, C. P. (2020). Nuclear myosins - roles for molecular transporters and anchors. *J. Cell. Sci.* 133 (11), jcs242420. doi:10.1242/jcs.242420

Cook, A. W., and Toseland, C. P. (2021). The roles of nuclear myosin in the DNA damage response. *J. Biochem.* 169 (3), 265–271. doi:10.1093/jb/mvaa113

de Jonge, J. J., Batters, C., O'Loughlin, T., Arden, S. D., and Buss, F. (2019). The MYO6 interactome: selective motor-cargo complexes for diverse cellular processes. *FEBS Lett.* 593 (13), 1494–1507. doi:10.1002/1873-3468.13486

de Lanerolle, P. (2012). Nuclear actin and myosins at a glance. *J. Cell. Sci.* 125 (Pt 21), 4945–4949. doi:10.1242/jcs.099754

Dos Santos, Á. N., Hari-Gupta, Y., Gough, R. E., Wang, L., Martin-Fernandez, M., Aaron, J., et al. (2022). Binding partners regulate unfolding of myosin VI to activate the molecular motor. *Biochem. J.* 479 (13), 1409–1428. doi:10.1042/BCJ20220025

Draper, D. E., and Reynaldo, L. P. (1999). RNA binding strategies of ribosomal proteins. *Nucleic Acids Res.* 27 (2), 381–388. doi:10.1093/nar/27.2.381

Dunn, T. A., Chen, S., Faith, D. A., Hicks, J. L., Platz, E. A., Chen, Y., et al. (2006). A novel role of myosin VI in human prostate cancer. *Am. J. Pathol. 169 Am. J. Pathol.* 169 (5), 1843–1854. doi:10.2353/ajpath.2006.060316

Fili, N., Hari-Gupta, Y., Dos Santos, Á., Cook, A., Poland, S., Ameer-Beg, S. M., et al. (2017). NDP52 activates nuclear myosin VI to enhance RNA polymerase II transcription. *Nat. Commun.* 8 (1), 1871. doi:10.1038/s41467-017-02050-w

Gotoh, N., Yan, Q., Du, Z., Biemesderfer, D., Kashgarian, M., Mooseker, M. S., et al. (2010). Altered renal proximal tubular endocytosis and histology in mice lacking myosin-VI. *Cytoskeleton* 67 (3), 178–192. doi:10.1002/cm.20435

Hacot, S., Coute, Y., Belin, S., Albaret, M. A., Mertani, H. C., Sanchez, J. C., et al. (2010). Isolation of nucleoli. *Curr. Protoc. Cell. Biol.* Chapter 3, Unit3.36. doi:10.1002/0471143030.cb0336s47

Hari-Gupta, Y., Fili, N., Dos Santos, Á., Cook, A. W., Gough, R. E., Reed, H. C. W., et al. (2022). Myosin VI regulates the spatial organisation of mammalian transcription initiation. *Nat. Commun.* 13 (1), 1346. doi:10.1038/s41467-022-28962-w

Hegan, P. S., Lanahan, A. A., Simons, M., and Mooseker, M. S. (2015). Myosin VI and cardiomyopathy: left ventricular hypertrophy, fibrosis, and both cardiac and pulmonary vascular endothelial cell defects in the Snell's waltzer mouse. *Cytoskelet. Hob.* 72 (8), 373–387. doi:10.1002/cm.21236

Ihnatovych, I., Migocka-Patrzalek, M., Dukh, M., and Hofmann, W. A. (2012). Identification and characterization of a novel myosin Ic isoform that localizes to the nucleus. *Cytoskelet. Hob.* 69, 555–565. doi:10.1002/cm.21040

Jung, E. J., Liu, G., Zhou, W., and Chen, X. (2006). Myosin VI is a mediator of the p53-dependent cell survival pathway. *Mol. Cell. Biol.* 26 (6), 2175–2186. doi:10.1128/MCB.26.6.2175-2186.2006

Kalita, K., Makonchuk, D., Gomes, C., Zheng, J. J., and Hetman, M. (2008). Inhibition of nucleolar transcription as a trigger for neuronal apoptosis. *J. Neurochem.* 105 (6), 2286–2299. doi:10.1111/j.1471-4159.2008.05316.x

Karatsai, O., Lehka, L., Wojton, D., Grabowska, A. I., Duda, M. K., Lenartowski, R., et al. (2023). Unconventional myosin VI in the heart: involvement in cardiac dysfunction progressing with age. *Biochim. Biophys. Acta Mol. Basis Dis.* 1869 (6), 166748. doi:10.1016/j.bbadis.2023.166748

Karolczak, J., Pavlyk, I., Majewski, Ł., Sobczak, M., Niewiadomski, P., Rzhepetskyy, Y., et al. (2015). Involvement of unconventional myosin VI in myoblast function and myotube formation. *Histochem Cell. Biol.* 144 (1), 21–38. doi:10.1007/s00418-015-1322-6

Kleizen, B., and Braakman, I. (2004). Protein folding and quality control in the endoplasmic reticulum. *Curr. Opin. Cell. Biol.* 16 (4), 343–349. doi:10.1016/j.ceb.2004.06.012

Lafita-Navarro, M. C., and Conacci-Sorrell, M. (2023). Nucleolar stress: from development to cancer. *Semin. Cell. Dev. Biol.* 136, 64–74. doi:10.1016/j.semcdb.2022.04.001

Lamb, M. C., and Tootle, T. L. (2020). Fascin in cell migration: more than an actin bundling protein. *Biol. (Basel).* 9 (11), 403. doi:10.3390/biology9110403

Lehka, L., Wojton, D., Topolewska, M., Chumak, V., Majewski, Ł., and Rędowicz, M. J. (2022). Loss of unconventional myosin VI affects cAMP/PKA signaling in hindlimb skeletal muscle in an age-dependent manner. *Front. Physiol.* 13, 933963. doi:10.3389/fphys.2022.933963

Li, J., Lu, Q., and Zhang, M. (2016). Structural basis of cargo recognition by unconventional myosins in cellular trafficking. *Traffic* 17 (8), 822–838. doi:10.1111/tra.12383

Lindsay, A. J., and McCaffrey, M. W. (2009). Myosin Vb localises to nucleoli and associates with the RNA polymerase I transcription complex. *Cell. Motil. Cytoskelet.* 66 (12), 1057–1072. doi:10.1002/cm.20408

Loikkanen, I., Toljamo, K., Hirvikoski, P., Väisänen, T., Paavonen, T. K., and Vaarala, M. H. (2009). Myosin VI is a modulator of androgen-dependent gene expression. *Oncol. Rep.* 22 (5), 991–995. doi:10.3892/or_00000526

Majewski, L., Nowak, J., Sobczak, M., Karatsai, O., Havrylov, S., Lenartowski, R., et al. (2018). Myosin VI in the nucleus of neurosecretory PC12 cells: stimulation-dependent nuclear translocation and interaction with nuclear proteins. *Nucleus* 9 (1), 125–141. doi:10.1080/19491034.2017.1421881

Majewski, L., Sobczak, M., Havrylov, S., Jozwiak, J., and Redowicz, M. J. (2012). Dock7: a GEF for Rho-family GTPases and a novel myosin VI-binding partner in neuronal PC12 cells. *Biochem. Cell. Biol.* 90 (4), 565–574. doi:10.1139/o2012-009

Majewski, L., Sobczak, M., Wasik, A., Skowronek, K., and Redowicz, M. J. (2011). Myosin VI in PC12 cells plays important roles in cell migration and proliferation but not in catecholamine secretion. *J. Muscle Res. Cell. Motil.* 32 (4-5), 291–302. doi:10.1007/s10974-011-9279-0

Meyuhas, O. (2015). Ribosomal protein S6 phosphorylation: four decades of research. *Int. Rev. Cell. Mol. Biol.* 320, 41–73. doi:10.1016/bs.ircmb.2015.07.006

Mohiddin, S. A., Ahmed, Z. M., Griffith, A. J., Tripodi, D., Friedman, T. B., Fananapazir, L., et al. (2004). Novel association of hypertrophic cardiomyopathy, sensorineural deafness, and a mutation in unconventional myosin VI (MYO6). *J. Med. Genet.* 41 (4), 309–314. doi:10.1136/jmg.2003.011973

Obrdlik, A., Louvet, E., Kukalev, A., Naschekin, D., Kiseleva, E., Fahrenkrog, B., et al. (2010). Nuclear myosin 1 is in complex with mature rRNA transcripts and associates with the nuclear pore basket. *FASEB J.* 24 (1), 146–157. doi:10.1096/fj.09-135863

Odronitz, F., and Kollmar, M. (2007). Drawing the tree of eukaryotic life based on the analysis of 2,269 manually annotated myosins from 328 species. *Genome Biol.* 8 (9), R196. doi:10.1186/gb-2007-8-9-r196

Osterweil, E., Wells, D. G., and Mooseker, M. S. (2005). A role for myosin VI in postsynaptic structure and glutamate receptor endocytosis. *J. Cell. Biol.* 168 (2), 329–338. doi:10.1083/jcb.200410091

Philimonenko, V. V., Zhao, J., Iben, S., Dingová, H., Kyselá, K., Kahle, M., et al. (2004). Nuclear actin and myosin I are required for RNA polymerase I transcription. *Nat. Cell. Biol.* 6 (12), 1165–1172. doi:10.1038/ncb1190

Pranchevicius, M. C., Baqui, M. M., Ishikawa-Ankerhold, H. C., Lourenço, E. V., Leão, R. M., Banzi, S. R., et al. (2008). Myosin Va phosphorylated on Ser1650 is found in nuclear speckles and redistributes to nucleoli upon inhibition of transcription. *Cell. Motil. Cytoskelet.* 65 (6), 441–456. doi:10.1002/cm.20269

Reich, E., Franklin, R. M., Shatkin, A. J., and Tatum, E. L. (1961). Effect of Actinomycin D on cellular nucleic acid synthesis and virus production. *Science* 134 (3478), 556–557. doi:10.1126/science.134.3478.556

Rodriguez, O. C., and Cheney, R. E. (2002). Human myosin-Vc is a novel class V myosin expressed in epithelial cells. *J. Cell. Sci.* 115 (Pt 5), 991–1004. doi:10.1242/jcs.115.5.991

Sarshad, A., Sadeghifar, F., Louvet, E., Mori, R., Böhm, S., Al-Muzzaini, B., et al. (2013). Nuclear myosin 1c facilitates the chromatin modifications required to activate rRNA gene transcription and cell cycle progression. *PLoS Genet.* 9 (3), e1003397. doi:10.1371/journal.pgen.1003397

Sarshad, A. A., and Percipalle, P. (2014). New insight into role of myosin motors for activation of RNA polymerases. *Int. Rev. Cell. Mol. Biol.* 311, 183–230. doi:10.1016/B978-0-12-800179-0.00004-0

Schwab, R. S., Ihnatovych, I., Yunus, S. Z., Domaradzki, T., and Hofmann, W. A. (2013). Identification of signals that facilitate isoform specific nucleolar localization of myosin IC. *Exp. Cell. Res.* 319 (8), 1111–1123. doi:10.1016/j.yexcr.2013.02.008

Scott, M. S., Troshin, P. V., and Barton, G. J. (2011). NoD: a nucleolar localization sequence detector for eukaryotic and viral proteins. *BMC Bioinforma.* 12, 317. doi:10.1186/1471-2105-12-317

Shahid-Fuente, I. W., and Toseland, C. P. (2023). Myosin in chromosome organisation and gene expression. *Biochem. Soc. Trans.* 51 (3), 1023–1034. doi:10.1042/BST20220939

Soderberg, O., Gullberg, M., Jarvius, M., Ridderstråle, K., Leuchowius, K. J., Jarvius, J., et al. (2006). Direct observation of individual endogenous protein complexes *in situ* by proximity ligation. *Nat. Methods* 3 (12), 995–1000. doi:10.1038/nmeth947

Spudich, G., Chibalina, M. V., Au, J. S., Arden, S. D., Buss, F., and Kendrick-Jones, J. (2007). Myosin VI targeting to clathrin-coated structures and dimerization is mediated by binding to Disabled-2 and PtdIns(4,5)P2. *Nat. Cell. Biol.* 9 (2), 176–183. doi:10.1038/ncb1531

Sweeney, H. L., and Houdusse, A. (2007). What can myosin VI do in cells? Curr. *Opin. Cell. Biol.* 19 (1), 57–66. doi:10.1016/j.ceb.2006.12.005

Sweeney, H. L., and Houdusse, A. (2010). Myosin VI rewrites the rules for myosin motors. *Cell.* 141 (4), 573–582. doi:10.1016/j.cell.2010.04.028

Trifaró, J. M., and Lee, R. W. (1980). Morphological characteristics and stimulus-secretion coupling in bovine adcrenal chromaffin cell cultures. *Neuroscience* 5 (9), 1533–1546. doi:10.1016/0306-4522(80)90018-4

Tumbarello, D. A., Kendrick-Jones, J., and Buss, F. (2013). Myosin VI and its cargo adaptors - linking endocytosis and autophagy. *J. Cell. Sci.* 126 (Pt 12), 2561–2570. doi:10.1242/jcs.095554

Ulferts, S., Prajapati, B., Grosse, R., and Vartiainen, M. K. (2021). Emerging properties and functions of actin and actin filaments inside the nucleus. *Cold Spring Harb. Perspect. Biol.* 13 (3), a040121. doi:10.1101/cshperspect.a040121

Vitale, M. L., Rodríguez Del Castillo, A., and Trifaro, J. M. (1992). Loss and Ca^{2+}-dependent retention of scinderin in digitonin-permeabilized chromaffin cells: correlation with Ca^{2+}-evoked catecholamine release. *J. Neurochem.* 59 (5), 1717–1728. doi:10.1111/j.1471-4159.1992.tb11003.x

Vreugde, S., Ferrai, C., Miluzio, A., Hauben, E., Marchisio, P. C., Crippa, M. P., et al. (2006). Nuclear myosin VI enhances RNA polymerase II-dependent transcription. *Mol. Cell.* 23 (5), 749–755. doi:10.1016/j.molcel.2006.07.005

Warner, C. L., Stewart, A., Luzio, J. P., Steel, K. P., Libby, R. T., Kendrick-Jones, J., et al. (2003). Loss of myosin VI reduces secretion and the size of the Golgi in fibroblasts from Snell's waltzer mice. *EMBO J.* 22 (3), 569–579. doi:10.1093/emboj/cdg055

Wells, A. L., Lin, A. W., Chen, L. Q., Safer, D., Cain, S. M., Hasson, T., et al. (1999). Myosin VI is an actin-based motor that moves backwards. *Nature* 401 (6752), 505–508. doi:10.1038/46835

Wollscheid, H. P., Biancospino, M., He, F., Magistrati, E., Molteni, E., Lupia, M., et al. (2016). Diverse functions of myosin VI elucidated by an isoform-specific α-helix domain. *Nat. Struct. Mol. Biol.* 23 (4), 300–308. doi:10.1038/nsmb.3187

Yang, K., Yang, J., and Yi, J. (2018). Nucleolar Stress: hallmarks, sensing mechanism and diseases. *Cell. Stress* 2 (6), 125–140. doi:10.15698/cst2018.06.139

Yoshida, H., Cheng, W., Hung, J., Montell, D., Geisbrecht, E., Rosen, D., et al. (2004). Lessons from border cell migration in the Drosophila ovary: a role for myosin VI in dissemination of human ovarian cancer. *Proc. Natl. Acad. Sci. U. S. A.* 101 (21), 8144–8149. doi:10.1073/pnas.0400400101

Zakrzewski, P., Lenartowska, M., and Buss, F. (2021). Diverse functions of myosin VI in spermiogenesis. *Histochem Cell. Biol.* 155 (3), 323–340. doi:10.1007/s00418-020-01954-x

Zhan, X. J., Wang, R., Kuang, X. R., Zhou, J. Y., and Hu, X. L. (2023). Elevated expression of myosin VI contributes to breast cancer progression via MAPK/ERK signaling pathway. *Cell. Signal* 106, 110633. doi:10.1016/j.cellsig.2023.110633

Zorca, C. E., Kim, L. K., Kim, Y. J., Krause, M. R., Zenklusen, D., Spilianakis, C. G., et al. (2015). Myosin VI regulates gene pairing and transcriptional pause release in T cells. *Proc. Natl. Acad. Sci. U. S. A.* 112 (13), E1587–E1593. doi:10.1073/pnas.1502461112

frontiers | Frontiers in Physiology

TYPE Review
PUBLISHED 09 May 2024
DOI 10.3389/fphys.2024.1401717

OPEN ACCESS

EDITED BY
Manuel H. Taft,
Hannover Medical School, Germany

REVIEWED BY
Anne Houdusse,
Institut Curie, France
James R. Sellers,
National Heart, Lung, and Blood Institute (NIH), United States

*CORRESPONDENCE
Peter J. Hanley,
peter.hanley@health-and-medical-university.de

RECEIVED 15 March 2024
ACCEPTED 22 April 2024
PUBLISHED 09 May 2024

CITATION
Horsthemke M, Arnaud C-A and Hanley PJ (2024), Are the class 18 myosins Myo18A and Myo18B specialist sarcomeric proteins? *Front. Physiol.* 15:1401717.
doi: 10.3389/fphys.2024.1401717

Are the class 18 myosins Myo18A and Myo18B specialist sarcomeric proteins?

Markus Horsthemke[1], Charles-Adrien Arnaud[1,2] and Peter J. Hanley[1]*

[1]IMM Institute for Molecular Medicine, HMU Health and Medical University Potsdam, Potsdam, Germany, [2]Department of Medicine, Science Faculty, MSB Medical School Berlin, Berlin, Germany

Initially, the two members of class 18 myosins, Myo18A and Myo18B, appeared to exhibit highly divergent functions, complicating the assignment of class-specific functions. However, the identification of a striated muscle-specific isoform of Myo18A, Myo18Aγ, suggests that class 18 myosins may have evolved to complement the functions of conventional class 2 myosins in sarcomeres. Indeed, both genes, *Myo18a* and *Myo18b*, are predominantly expressed in the heart and somites, precursors of skeletal muscle, of developing mouse embryos. Genetic deletion of either gene in mice is embryonic lethal and is associated with the disorganization of cardiac sarcomeres. Moreover, Myo18Aγ and Myo18B localize to sarcomeric A-bands, albeit the motor (head) domains of these unconventional myosins have been both deduced and biochemically demonstrated to exhibit negligible ATPase activity, a hallmark of motor proteins. Instead, Myo18Aγ and Myo18B presumably coassemble with thick filaments and provide structural integrity and/or internal resistance through interactions with F-actin and/or other proteins. In addition, Myo18Aγ and Myo18B may play distinct roles in the assembly of myofibrils, which may arise from actin stress fibers containing the α-isoform of Myo18A, Myo18Aα. The β-isoform of Myo18A, Myo18Aβ, is similar to Myo18Aα, except that it lacks the N-terminal extension, and may serve as a negative regulator through heterodimerization with either Myo18Aα or Myo18Aγ. In this review, we contend that Myo18Aγ and Myo18B are essential for myofibril structure and function in striated muscle cells, while α- and β-isoforms of Myo18A play diverse roles in nonmuscle cells.

KEYWORDS

unconventional myosins, MYO18A, MYO18B, sarcomere, stress fibers, knockout (KO) mice

Introduction

In mouse and human, the myosin superfamily of motor proteins is divided into 12 classes. Conventional class 2 myosins have long coiled-coil domains which mediate dimerization and assembly into bipolar (thick) filaments, whereas the other 11 classes are collectively referred to as unconventional myosins and serve various specific roles (Kalhammer and Bähler, 2000; Sellers, 2000; Hartman et al., 2011; Maravillas-Montero and Santos-Argumedo, 2012; Batters and Veigel, 2016; Coluccio, 2020). All myosins contain a conserved head (motor) domain which typically exhibits ATPase activity and binds to filamentous actin (F-actin), enabling the chemical energy from ATP hydrolysis to be

converted to force production (Mermall et al., 1998; Sellers, 2000). Class 18 myosins are encoded by two genes: *Myo18a* and *Myo18b* in mice, and *MYO18A* and *MYO18B* in humans (Bruford et al., 2020). Extensive biochemical analyses of purified myosin 18A (Myo18A) and myosin 18B (Myo18B) proteins or protein fragments have revealed, surprisingly, that these myosins exhibit negligible ATPase activity (Guzik-Lendrum et al., 2013; Taft et al., 2013; Latham et al., 2020; Taft and Latham, 2020), perhaps barely sufficient to justify membership in the myosin superfamily. Nevertheless, class 18 myosins have strong phylogenetic roots and show localization to actin-based structures, such as actin stress fibers and sarcomeres (Salamon et al., 2003; Mori et al., 2005; Ajima et al., 2008; Billington et al., 2015; Horsthemke et al., 2019; Latham et al., 2020; Taft and Latham, 2020; Ouyang et al., 2021). Whether Myo18A and Myo18B exhibit ATPase activity in their natural environment remains to be clarified. Alternatively, these proteins may act as scaffold proteins or inhibitors (brakes) to actin translation by bipolar myosin two filaments, among other functions. In this review, we contend that Myo18B and the gamma-isoform of Myo18A, Myo18Aγ, have evolved as indispensible structural elements or regulators of sarcomeres. We also discuss the diverse functions ascribed to the PDZ-containing alpha-isoform of Myo18A, Myo18Aα, and we briefly speculate on the roles of the beta-isoform, Myo18Aβ.

Myosin 18A

Myo18A was first identified over two decades ago (Furusawa et al., 2000). In 2000, Furusawa et al. (Furusawa et al., 2000) cloned a novel myosin, which was initially denoted MysPDZ (myosin containing PDZ) since it harbors an N-terminal extension containing a PDZ domain in addition to a KE (lysine and glutamic acid)-rich sequence. Northern blot analysis revealed that MysPDZ (7.5 kb transcript), now known as Myo18Aα, is widely expressed in mouse tissues, whereas a 7.0 kb transcript is additionally expressed in hematopoietic cells and a 10.5 kb transcript is expressed in heart and skeletal muscle. In further work, Mori et al. (Mori et al., 2003) showed that the 7.0 kb transcript corresponds to an isoform lacking the PDZ-containing N-terminal extension, which was denoted MysPDZβ, as distinct from MysPDZα (MysPDZ), and is now denoted Myo18Aβ. Fluorescence imaging of either Myo18A labeled with antibodies against the coiled-coil domain or expressed YFP-tagged Myo18A constructs revealed that MysPDZα (Myo18Aα) localizes to the perinuclear region, possibly corresponding to the endoplasmic reticulum and Golgi apparatus, and the actin cytoskeleton, whereas MysPDZβ (Myo18Aβ) localizes diffusely in the cytoplasm. Truncation mutants fused to YFP or a Myc tag (also known as c-Myc tag) indicated that the KE-rich sequence was required for localization to F-actin, whereas the PDZ domain mediated localization to the plasma membrane (Mori et al., 2005).

The physiological roles of the widely expressed PDZ-containing myosin Myo18Aα have not yet been conclusively established. PDZ domains typically function as scaffolding modules (molecular glue), mediating protein-protein interactions and often localizing proteins to specific subcellular locations (Bezprozvanny and Maximov, 2001; Liu and Fuentes, 2019). These domains recognize short peptide motifs at the C-terminus of their target proteins, which include membrane-bound receptors and ion channels. Using anti-surfactant protein A receptor 210 antibodies, affinity chromatography, and mass spectrometry, Yang et al. (Yang et al., 2005) deduced that Myo18A is the molecular correlate of surfactant protein A receptor 210, which mediates the clearance of pathogens opsonized with surfactant protein A, a collectin secreted by alveolar epithelial type II cells (Casals et al., 2018; King and Chen, 2020). The authors identified a putative transmembrane α-helix in the head domain of Myo18A, suggesting that it is a single-pass membrane protein. Moreover, antibodies targeted to the neck domain of Myo18A blocked the binding of surfactant protein A to macrophages, implying that the N-terminus is on the cytosolic side of the plasma membrane. The apparent minimal ATPase activity of Myo18A (Guzik-Lendrum et al., 2013; Taft et al., 2013) would support a potential role of Myo18A as a membrane-bound receptor. Macrophages predominantly express Myo18Aβ (Horsthemke et al., 2019) which would be expected to bind surfactant protein A without further action, whereas expression of Myo18Aα, which occurs, for example, following activation of macrophages with leukemia inhibitory factor (Mori et al., 2003), is probably required to recruit proteins via its cytosolic PDZ domain and initiate phagocytosis. More recently, macrophages isolated from myeloid-restricted *Myo18a* conditional knockout mice were shown to exhibit normal motility, chemotaxis, and phagocytosis, but, unfortunately, surfactant protein A binding or phagocytosis mediated by surfactant protein A opsonization were not investigated (Horsthemke et al., 2019). However, RAW 264.7 cells (macrophage cell line) stably transfected with a dominantly negative truncated Myo18Aα mutant exhibited markedly impaired uptake of surfactant protein A-opsonized *Staphylococcus aureus* (Sever-Chroneos et al., 2011). On the contrary, the diffuse cytosolic localization of N-terminally YFP-tagged Myo18Aβ (Mori et al., 2003), which corresponds to the short variant of surfactant protein A receptor 210 (Yang et al., 2005), argues against a role for Myo18A isoforms as plasma membrane receptors. Lack of membrane localization of YFP-Myo18Aβ cannot be explained by an inhibitory effect of the fluorescent protein tag since N-terminally YFP-tagged Myo18Aα localizes to the plasma membrane (Mori et al., 2003). Further investigations are necessary to confirm whether Myo18A is indeed a transmembrane protein which binds surfactant protein A-opsonized particles. However, it is most unlikely that the Myo18A head domain spans the plasma membrane since this would require extensive unfolding of this highly conserved structure.

In 2009, Dippold et al. (2009) reported that Myo18A, identified by co-immunoprecipitation and mass spectrometry, is a binding partner of GOLPH3 (Golgi phosphoprotein 3). When Myo18A was knocked down in HeLa cells using siRNA, it mimicked the effects of GOLPH3 knockdown by inducing a more condensed (less stretched) Golgi structure and reducing vesicle budding. Expression of GFP-tagged mouse Myo18A, predicted to be resistant to the siRNA used to target human Myo18A, rescued the Golgi morphology phenotype, whereas a motor mutant (lacking ATPase activity) failed to rescue the phenotype. These data implied a model in which Myo18A is linked to Golgi via GOLPH3 and binds to actin filaments to exert force (actomyosin-ATPase activity) and produce a flattened stack of cisternae, the characteristic morphology

of the Golgi apparatus. At variance with this model, two independent groups showed that Myo18A binds weakly to F-actin, but only exhibits negligible ATPase activity, even in the presence of GOLPH3 (Guzik-Lendrum et al., 2013; Taft et al., 2013; Bruun et al., 2017). Indeed, *in vitro* gliding assays revealed that Myo18A inhibits the translocation of actin filaments by class 2 myosin (Guzik-Lendrum et al., 2013). However, Taft et al. (2013) showed that GOLPH3 interacts with the PDZ domain of Myo18A and increases its affinity for actin. One possibility to explain the incongruent findings is that mixed bipolar filaments containing both nonmuscle myosin 2 and Myo18Aα (Billington et al., 2015) could provide a means for stretching Golgi cisternae. In this scenario, nonmuscle myosin 2 exerts force and Myo18Aα binds to GOLPH3 and acts as an F-actin tethering protein (Guzik-Lendrum et al., 2013; Taft et al., 2013), along the lines schematically illustrated by Billington et al. (2015). Bruun et al. (2017) re-investigated the role of Myo18A in Golgi morphology and found using two different anti-Myo18A C-terminus antibodies that endogenous Myo18A, as well as GFP-tagged Myo18Aα, did not localize to Golgi. The authors also showed that knockdown of Myo18A using shRNA did not affect Golgi morphology. Similarly, Horsthemke et al. (2019) observed no differences in the Golgi morphology of resident peritoneal macrophages isolated from wild-type and myeloid-restricted *Myo18a* conditional knockout mice. Thus, although Myo18A interacts with Golgi proteins, the extent and functional importance of Myo18A localization to Golgi remains to be clarified.

Various studies have implicated Myo18A in cell motility. Tan et al. (2008) deduced that Myo18A is part of a tripartite protein complex essential for cell motility. This complex, which also includes LRAP35a (leucine repeat adapter protein 35a), encoded by *LURAP1* and also known as leucine rich adaptor protein 1, and MRCK (myotonic dystrophy kinase-related Cdc42-binding kinase), encoded by *CDC42BPA* and also known as CDC42-binding protein kinase alpha, promotes nonmuscle myosin 2-dependent actomyosin assembly and retrograde actomyosin flow. The authors stressed that the Myo18A-containing tripartite protein complex localizes to retrograde moving actomyosin bundles in the lamella, which consist of nonmuscle myosin 2-rich actin arcs and dorsal stress fibers (Burnette et al., 2014), but not actin stress fibers, also known as ventral stress fibers or subnuclear actin stress fibers, which contain nonmuscle myosin 2 and are anchored to the substrate at each end by focal adhesions. siRNA-mediated knockdown of Myo18A led to loss of actomyosin structures in the lamella. Moreover, MRCK localization to the lamella was decreased by either knockdown of Myo18A or introduction of a motor mutant (lacking ATPase activity) of Myo18A. Using U2OS cells (human epithelial cell line derived from an osteosarcoma) and wound-healing assays, Tan et al. (2008) also showed that microinjection of a dominant-negative construct of Myo18A inhibited cell migration. These data suggest that Myo18A is required for the formation and/or maintenance of nonmuscle myosin 2-containing actin arcs and dorsal stress fibers. In accord with Tan et al. (2008), Billington et al. (2015) clearly showed using confocal microscopy that GFP-tagged Myo18Aα and GFP-tagged Myo18Aβ colocalized with tdTomato-tagged nonmuscle myosin 2A in lamellar protrusions of U2OS cells, but GFP-tagged Myo18Aα additionally localized to subnuclear actin stress fibers. The authors also showed by co-sedimentation and electron microscopy that polymerization of nonmuscle myosin 2A with Myo18Aβ produced mixed bipolar filaments. Indeed, mixed bipolar filaments containing nonmuscle myosin 2A together with Myo18Aα or Myo18Aβ could be resolved in cells using superresolution imaging, obtained by TIRF-SIM (combined total internal reflection fluorescence (TIRF) and structured illumination microscopy (SIM)). Thus, imaging by various independent groups strongly supports the notion that Myo18Aα associates with nonmuscle myosin 2-containing stress fibers, but there are conflicting results in relation to Myo18Aβ (Mori et al., 2005; Billington et al., 2015). We assume that the N-terminal extension of Myo18Aα, lacking in Myo18Aβ, is required for localization to actin stress structures. The role of Myo18Aβ remains unclear, although it has been shown to form antiparallel dimers in high-salt buffer (Billington et al., 2015) and may heterodimerize with Myo18Aα. Further work is required to clarify the subcellular localization and function of Myo18Aβ.

Myo18A was also implicated in regulating actin cytoskeletal dynamics and cell motility by Hsu et al. (2010), who identified Myo18A as an interaction partner of PAK2 (p21-activated kinase 2) by co-immunoprecipitation and mass spectrometry. PAKs are a family (PAK1–PAK6) of serine/threonine kinases which interact with and are thought to be important downstream targets of the p21 Rho GTPases Rac1 and Cdc42, each of which induce actin polymerization and membrane protrusions and are key mediators of cell motility and chemotactic navigation (Lawson and Ridley, 2018). The authors deduced that PAK2 binds to Myo18A via the βPIX/GIT1 (β-PAK-interacting exchange factor and G protein-coupled receptor kinases interactor 1) complex. βPIX, encoded by *ARHGEF7* (Rho guanine nucleotide exchange factor 7), interacts with group I PAKs (PAK1–PAK3) though its N-terminal SH3 (Src homology 3) domain. This interaction leads to the activation of Rac and Cdc42 via the Dbl-homology (DH) domain of βPIX, which serves as a selective GEF (guanine nucleotide exchange factor) for Rac and Cdc42. Following guanine nucleotide exchange, Rac-GTP and Cdc42-GTP activate group I PAKs, which in turn inhibit cofilin via LIM kinases, among other functions. Thus, βPIX not only activates Rac and Cdc42 but also serves as a link to their downstream targets (PAK1–PAK3). Hsu et al. (2010) showed that knockdown of Myo18A did not impair the formation of PAK/βPIX/GIT1 complexes, but induced morphological changes, including marked cell spreading and a reduction in dorsal ruffles, as well as decreased cell migration in wound healing assays. Truncation mutant analysis indicated that the C-terminus of Myo18Aα, also present in Myo18Aβ, interacts with βPIX. In complementary work, Hsu et al. (2014) showed that deletion of the C-terminal extension impairs cellular localization of βPIX in A431 cells and decreases cell motility. Consistent with these findings, Myo18Aα was shown to target the Rac-/Cdc42-GEF βPIX to the dendritic spines of cultured Purkinje neurons, whereas knockdown of Myo18Aα or deletion of the C-terminal Myo18Aα-binding site of βPIX markedly decreased βPIX enrichment in spines, which was associated with loss of F-actin and nonmuscle myosin 2 in these structures (Alexander et al., 2021). Thus, Myo18Aα and possibly also Myo18Aβ localize to nonmuscle myosin 2-containing stress fibers and interact with proteins that regulate actin dynamics. To gain further insight, phenotypic analysis of mice selectively lacking both Myo18A isoforms would be most helpful, especially if homozygous mutants prove to be viable.

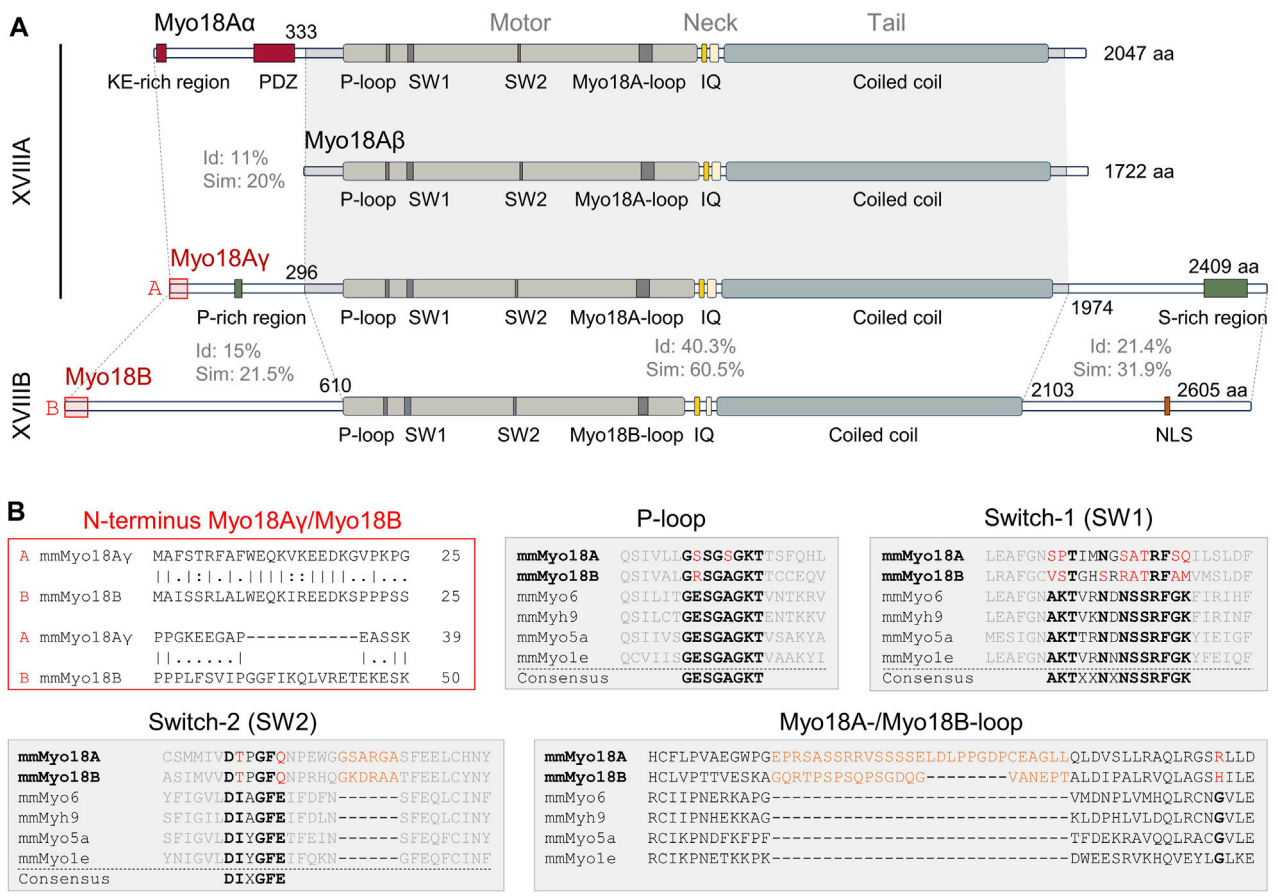

FIGURE 1
Domain structures and sequence alignments of Myo18A and Myo18B. **(A)**, Domain structures of mouse (*Mus musculus*) Myo18Aα, Myo18Aβ, Myo18Aγ, and Myo18B. Sequence identity (Id) and similarity (Sim) are indicated for various regions. Abbreviations: KE-rich, lysine (K) and glutamic acid (E)-rich; PDZ, post-synaptic density (PSD) protein, *Drosophila* discs-large (Dlg) tumor suppressor protein, and zonula occludens (ZO) protein; P-loop, phosphate-binding loop; SW1, switch-1; SW2, switch-2; IQ, IQ (isoleucine (I) and glutamine (Q)) calmodulin-binding motif; aa, amino acids; P-rich, proline (P)-rich; S-rich, serine (S)-rich; NLS, nuclear localization signal. **(B)**, Alignment of the extreme N-terminal ends of Myo18Aγ and Myo18B (marked by red boxes in panel **(A)**, highlighting high identity and similarity. In the aligned sequences, vertical lines ("|") indicate positions of identity (amino acids are identical), colons (":") indicate positions of similarity (amino acids have similar side chain properties), single dots (".") indicate mismatch of amino acids, and dashes ("–") indicate gaps in a sequence relative to its counterpart. The gray filled boxes show alignment of *Mus musculus* (*Ms*) Myo18A and *Ms* Myo18B P-loop, switch-1, and switch-2 sequences with those of *Ms* Myo6, *Ms* Myh9 (nonmuscle myosin IIA), *Ms* Myo5a, and *Ms* Myo1e. Conserved sequence motifs are highlighted in bold black, while deviations in Myo18A and Myo18B are shown in red. Inserts specific for Myo18A and Myo18B are shown in orange.

In developing zebrafish embryos, *myo18a* genes, *myo18aa* and *myo18ab*, were observed to be expressed in the somites (Cao et al., 2014). Knockdown of either gene resulted in mildly irregular localization of dystrophin and α-dystroglycan, two key proteins involved in linking F-actin to the extracellular matrix. This irregularity manifested as unsharp somite demarcations and was associated with disrupted myofibers (skeletal muscle cells), identified using anti-slow myosin heavy chain antibodies. Simultaneous knockdown of both genes or overexpression of the PDZ-containing N-terminal extension resulted in a more pronounced phenotype. Further work by Cao et al. (2016) showed that Myo18A is required for adhesion of cultured zebrafish embryo myoblasts to laminin-coated substrates. Together with other findings, including interaction of Myo18A with the Golgi protein Golgin45, Cao et al. (2016) deduced that the N-terminal extension of Myo18A acts as a scaffold to bind various signaling molecules, link Golgi to F-actin, and stabilize myoblast adhesion to the extracellular matrix.

Deletion of *Myo18a* in mouse is embryonic lethal at around embryonic day 12.5, but surprisingly lacZ (X-Gal) staining indicated that *Myo18a* is highly expressed in the developing heart, as well as in somites (Horsthemke et al., 2019). Cardiac myocyte-restricted deletion of *Myo18a* in mice was similarly embryonic lethal and electron microscopy revealed disorganized cardiac sarcomeres in embryos carrying homozygous *Myo18a* mutations. More surprisingly, a novel isoform of Myo18A, denoted Myo18Aγ, was detected in the heart which was larger than Myo18Aα and contained alternative N- and C-terminal extensions (Horsthemke et al., 2019). Notably, the N-terminal extension of Myo18Aγ does not contain either a KE-rich sequence or PDZ domain, but instead contains a polyproline helix (Figure 1A). Myo18Aγ-GFP expressed in neonatal rat ventricular myocytes clearly showed localization to the sarcomeric A-band. All of these findings are reminiscent of

Myo18B, discussed in the next section, and suggest that each class 18 myosin gene encodes a protein required for sarcomere function.

Most recently, Myo18Aα was shown to immunoprecipitate with GIPC3 (GIPC PDZ domain containing family, member 3) and the authors showed that the PDZ domain of GIPC3 interacts with the C-terminus of Myo18Aα, which is shared by Myo18Aβ (Chatterjee et al., 2023). GIPC3 localizes to the cuticular plate of inner and outer hair cells of the cochlea during postnatal development. Each stereocilium of the hair cells inserts into the cuticular plate, a dense network of filamentous actin. SIM imaging of immunolabeled Myo18Aα showed that it localizes immediately below the actin-rich cuticular plate. Mutations of various unconventional myosin genes are associated with deafness (Friedman et al., 1999; Moreland and Bird, 2022), including *Myo6* (Avraham et al., 1995), *Myo7a* (Gibson et al., 1995; Weil et al., 1995), and *Myo15a* (Wakabayashi et al., 1998; Liang et al., 1999; Belyantseva et al., 2003). Whether mutations or deletion of *Myo18a* in hair cells causes significant abnormalities in the morphology and function of hair cells remains to be determined.

Myosin 18B

In a human squamous cell lung carcinoma cell line, Lu24, a homozygous deletion on chromosome 22q12.1 suggested the presence of a tumor suppressor gene within the deletion, ultimately leading to the identification of a novel myosin gene, denoted *MYO18B*, which is structurally related to *MYO18A* (Nishioka et al., 2002). Consistent with a potential role as a tumor suppressor gene, *MYO18B* is inactivated by deletions, mutations, or methylation in about 50% of lung carcinomas (Yokota et al., 2003). Further studies have shown that MYO18B expression is reduced in various cancers, including primary ovarian and colorectal carcinoma, and restoration of MYO18B expression in pleural mesothelioma cell lines decreased tumor growth and metastatic potential. In contrast, high MYO18B expression was correlated with poor prognosis in hepatocellular carcinoma and knockdown of *MYO18B* in HepG2 cells (human hepatocellular carcinoma cell line) decreased cell proliferation and invasiveness. Thus, MYO18B has been associated with either tumor suppression or progression and the role of MYO18B presumably varies depending on the specific cancer type and the cellular context. Interestingly, among prostate cancer cell lines, *MYO18A* expression was shown to be higher in a cell line with higher metastatic potential, and the authors inferred, based on knockdown studies, that effects of MYO18A on actin organization and motility could contribute to metastasis (Makowska et al., 2015).

Nishioka et al. (2002) also investigated the expression of *MYO18B* across various human tissues. Northern blot analysis revealed that MYO18B transcripts (~8 kb) were expressed in heart and skeletal muscle, but not in other tissues. Using real-time quantitative PCR, which is much more sensitive than Northern blot, *MYO18B* expression was detected in a broader range of tissues, including bone marrow, thymus, and testis. Phylogenetic analysis highlighted that MYO18A genes are expressed in both vertebrates and invertebrates, whereas human and mouse Myo18B genes appear to have arisen from a duplication in vertebrates. Using human and mouse tissues, Salamon et al. (2003) similarly could only detect MYO18B mRNA in heart and skeletal muscle using Northern blotting, with higher levels in the heart. RT-PCR corroborated these findings, but expression of MYO18B mRNA could be detected in other tissues, albeit after a high number of PCR cycles. The authors showed that *Myo18b* expression is weak in C2C12 cells (mouse myoblast cell line), but it increases following induction of myogenesis (myogenic differentiation), reaching a peak and leveling off at around day 3 after induction. When cells were stably transfected with Myo18B-Myc, the tagged protein was found to be localized to the cytoplasm, but following myogenesis, Myc-tagged Myo18B localized to some of the nuclei. Localization of endogenous Myo18B to the nucleus was observed in a subset of cultured rat ventricular myocytes, but Myo18B also localized to bands (A-bands) between Z-disks, labeled with anti-α-actinin-2 antibodies, in myofibrils. Notably, Myo18B did not appear to localize to the nucleus in ventricular myocytes exhibiting a prominent banding pattern.

Using anti-human MYO18B-N-terminus and anti-human MYO18B-C-terminus antibodies, Ajima et al. (2008) showed that Myo18B localized to actin stress fibers in differentiated C2C12 cells, but localization to the nucleus was not observed. Exogenously expressed MYO18B-GFP, but not GFP-tagged MYO18B lacking the N-terminal extension, similarly localized to actin fibers. Furthermore, the N-terminus alone was sufficient for localization to stress fibers. However, in frozen sections of mouse cardiac and skeletal muscle, immunofluorescence imaging indicated that Myo18B (green signal) localizes to Z-lines, labeled with anti-α-actinin antibodies (red signal). These findings contradict those of Salamon et al. (2003), who found that Myo18B localizes to the A-band, and we presume that the anti-Myo18B antibodies used by Ajima et al. exhibited poor specificity, at least in cardiac myocytes. The authors also generated *Myo18b* reporter knockout mice, but homozygous mutants died around embryonic day 10.5. LacZ (X-Gal) staining of heterozygous mutant embryos revealed that *Myo18b* is highly expressed in the heart, and also clearly in somites. Electron microscopy of embryonic day 10.5 hearts showed developing sarcomeres in wild-type hearts, whereas sarcomeric thick and thin filaments appeared less organized in homozygous mutant hearts, especially in cross-sections of developing myofibrils. Thus, Myo18B appears to localize to sarcomeres and may be critical for the formation and/or maintenance of myofibrils.

Consistent with a role in the heart, mutations of *MYO18B* have been associated with cardiomyopathies (Alazami et al., 2015; Malfatti et al., 2015; Mihaylova et al., 2020). The pathophysiology of the cardiomyopathies is unclear, although loss-of-function mutations of *myo18b* in zebrafish were reported to severely impair myofibrillogenesis in fast-twitch skeletal muscle cells (Berger et al., 2017; Gurung et al., 2017), suggesting that it may be explained by impaired formation and/or maintenance of myofibrils, as speculated by Ajima et al. (2008). Latham et al. (2020) provided insight into the function of Myo18B by showing that it initially localizes to nuclei during cardiac differentiation and then to actin stress fibers before incorporating into sarcomeres. Moreover, recombinant Myo18B heavy meromyosin exhibited negligible ATPase activity and failed to translocate F-actin filaments in *in vitro* gliding assays. These data suggest that Myo18B may be involved in sarcomere assembly in accord with

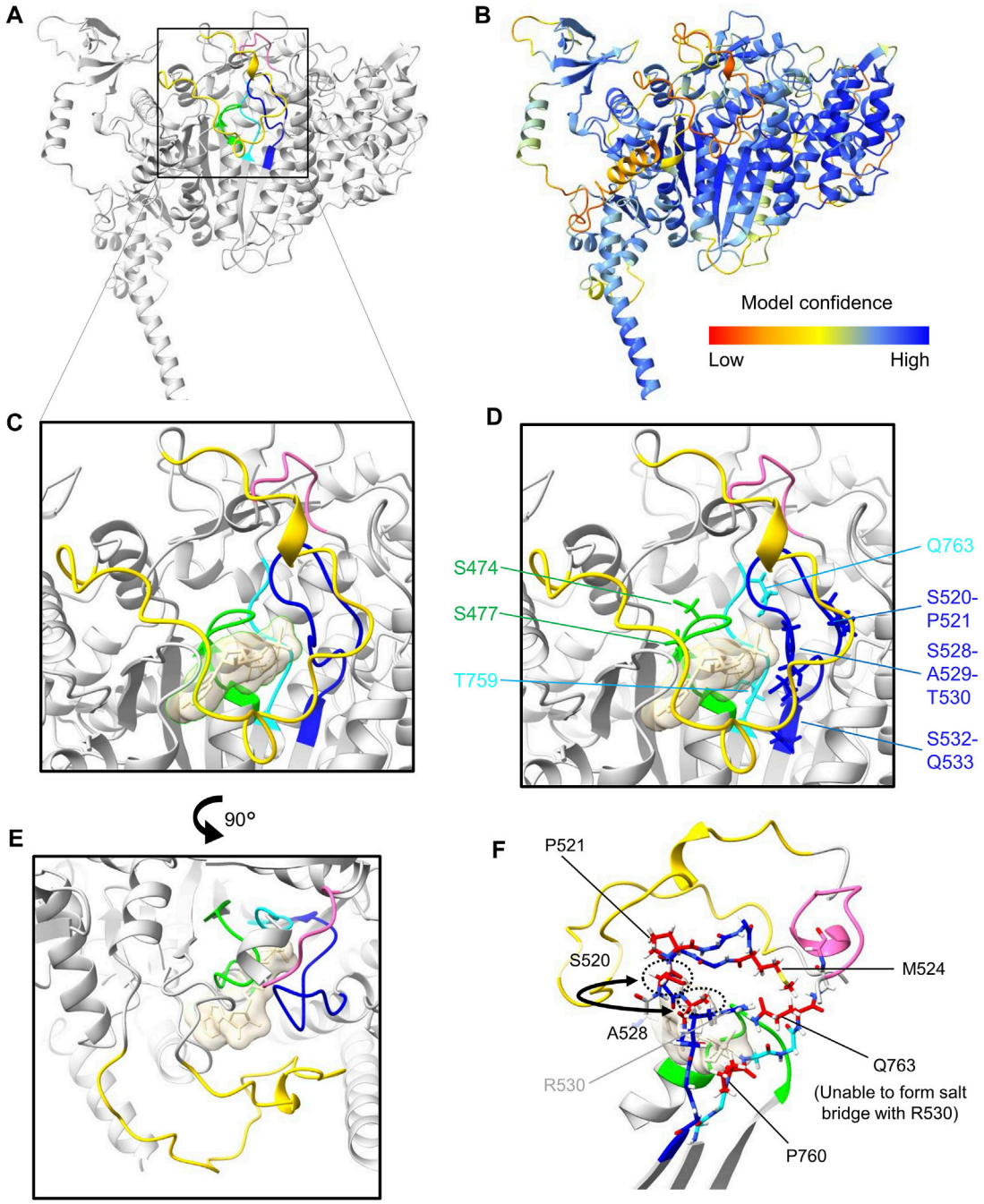

FIGURE 2
Protein structure prediction of (*Mus musculus*) Myo18Aγ. **(A)**, AlphaFold v2.3.2 was used to perform structure predictions via a Jupyter Notebook hosted on GitHub. Due to computational power constraints, predictions were restricted to amino acid residues 1 to 1400, encompassing the N-terminal extension, as well as the head domain. Visual representation of the structure was generated using ChimeraX. For clarity, only the head domain is represented (residues 281–1200). The ribbon representation of the head domain is shaded in gray, except for features forming and surrounding the nucleotide-binding pocket: the P-loop (G473–T480) is colored green, SW-1 (S520–Q533) is blue, and SW-2 (D758–Q763) is cyan. In addition, a small loop extension following SW-2 (G769–A774) is highlighted pink and the moderately large Myo18A-loop (E1024–L1052) is yellow. **(B)**, Ribbon representation of the head domain color-coded for the confidence score (pLDDT, predicted local distance difference test) of the model generated by AlphaFold. **(C)**, Close-up view of the nucleotide-binding pocket, albeit including the synthetic substrate ADP-AlF_4 (transparent sand colored surface), incorporated by overlaying the structure 1MND from the PDB. **(D)**, Side chains of residues which deviate from censensus sequences are shown as sticks (see also Figure 1B). **(E)**, Rotated view (90° rotation relative to panels **(C, D)** highlighting the proximity of the moderately long Myo18A-loop (yellow) to the nucleotide-binding site. **(F)**, View optimized to show the side chains of residues within SW-1 and SW-2 which deviate (colored red) from the consensus sequences.

the transition model in which myofibrils arise from actin stress fibers, which serve as premyofibrils and initially contain nonmuscle myosin IIB (Sanger et al., 2005; Sanger et al., 2010). Immunolabeling of Myo18B in cardiac myocytes, derived from human embryonic stem cells, together with anti-β-cardiac myosin (encoded by *MYH7*) or anti-α-actinin antibodies clearly showed that Myo18B localizes to sarcomeric A-bands, as distinct from Z-lines. The authors also confirmed that Myo18B binds actin filaments and proposed a model in which Myo18B tethers the thick filament to the thin (actin) filament and provides internal resistance to sarcomere length changes. Superresolution imaging by another group (Jiu et al., 2019) using U2OS cells suggested another function for Myo18B, which may also apply to sarcomeres, in which Myo18B mediates lateral stacking of nonmuscle myosin IIB-containing actin stress fibers, which notably are thought to be precursors of sarcomeres. Zhao et al. (2020) confirmed that Myo18B acts as "glue" for nonmuscle myosin two stacks. U2OS cells lacking Myo18B exhibited a paucity of thick ventral stress fibers and focal adhesions, as well as lower traction forces, when plated on a hard surface (glass), compared to control cells. Moreover, *MYO18B* knockout cells exhibited decreased migration velocity and directionality.

Sequence alignments and predicted structure

Sequence alignments reveal moderate sequence identity and similarity between the shared motor, neck, and tail domains of Myo18A isoforms compared to Myo18B (Figure 1A). In contrast, the N- and C-termini are highly variable and exhibit low identity and similarity. One notable exception is the extreme N-terminus, particularly the first 19 amino acids, which exhibit high identity and similarity between Myo18Aγ and Myo18B (Figure 1B). The N-terminal extensions of Myo18Aα, Myo18Aγ, and Myo18B are distinctive features of class 18 myosins, and they are likely sufficient for localization to actin stress fibers in the case of Myo18Aα, or sarcomeric A-bands in the case of Myo18Aγ and Myo18B.

Guzik-Lendrum et al. (2013) previously highlighted significant deviations of Myo18A from conserved structural motifs of the nucleotide-binding pocket in the head domain of myosins, which include the P-loop (phosphate-binding loop), switch-1 (SW-1), and switch-2 (SW-2). Similar deviations can also be observed for Myo18B, as highlighted by Taft and Latham (2020) and depicted in Figures 1B, 2D. A model of the head domain of *Mus musculus* Myo18Aγ predicted using AlphaFold v2.3.2 (Jumper et al., 2021) is depicted in Figures 2A, B, including magnified views of the nucleotide-binding pocket (Figures 2C–F; PDB file available upon request). Note that a model of *Mus musculus* Myo18Aα was previously predicted and deposited on the beta version of the AlphaFold Protein Structure Database (accession number Q9JMH9). As expected, the prediction of the structure of the head domain of Myo18Aγ is very close to that of Myo18Aα (rmsd 0.557).

P-loops are recognized for their ability to bind both the phosphates of nucleotides and Mg^{2+} ions. Within myosins, the P-loop contains a highly conserved consensus sequence motif (GESGAGKT) (Ruppel and Spudich, 1996) (Figure 1B). Changes from this consensus sequence, such as substituting the negatively charged amino acid glutamic acid (E) with the uncharged polar amino acid serine (S) in Myo18A or the positively charged amino acid arginine (R) in Myo18B, may have a significant impact on ATP binding and hydrolysis.

Switch-1 is also a critical region in myosin proteins that undergoes considerable conformational changes upon nucleotide binding and hydrolysis (Smith and Rayment, 1996; Fujii and Namba, 2017; Kato et al., 2018). This was previously demonstrated through alanine scanning, which identified residues in switch-1 required for nucleotide binding and ATPase activity (Shimada et al., 1997). Both Myo18A and Myo18B harbor numerous deviations from the consensus sequence motif of switch-1 (Taft and Latham, 2020) (Figure 1B). Mapping of these deviations in our predicted model (Figure 2F) shows that hydrophobic residues replace charged and polar residues: (i) M524 replaces a positively charged residue typically seen in the variable position in other myosin sequences and (ii) A528 has effectively exchanged positions with S520, resulting in a deviation of the consensus sequence from (A520, S528) to (S520, A528). This swap, illustrated by the semicircular arrow (Figure 2F), positions A528 closer to the binding pocket.

Switch-2 is another important structural motif which has been deduced to stabilize the closed conformation of the nucleotide-binding pocket and thereby promote ATP hydrolysis (Furch et al., 1999; Trivedi et al., 2012). In both Myo18A and Myo18B, the position typically occupied by the hydrophobic amino acid isoleucine (I) in the switch-2 consensus sequence DIXGFE, where X denotes any residue, is instead filled by threonine (T). However, what is perhaps more remarkable, the presence of glutamine (Q763 in Figure 2F) instead of negatively charged glutamic acid at the end of the motif (DIXGFE → DTXGFQ) is expected to prevent formation of a salt bridge with a conserved arginine (R530 in Figure 2F) on switch-1 (Furch et al., 1999; Guzik-Lendrum et al., 2013), demonstrated to be critical for ATP hydrolysis and actin affinity (Onishi et al., 1997; Friedman et al., 1998; Onishi et al., 1998; Furch et al., 1999).

Other notable deviations from the consensus sequence in Myo18A are the presence of prolines (P) in switch-1 (P521) and switch-2 (P760) (Figures 2D, F), as well as the loop extensions E1024–L1052 (yellow in Figure 2), denoted the Myo18A-loop, and G769–A774 (pink in Figure 2). Myo18B also contains a proline in switch-2 (Figure 1B). These prolines may impair conformational flexibility of the loops required for catalysis. Loop extensions have previously been pointed out (Guzik-Lendrum et al., 2013). The large Myo18A-/Myo18B-loop (sequences shown in Figure 1B) is not predicted with high confidence, but as depicted in Figure 2E, the Myo18A-loop (colored yellow) is likely to hinder nucleotide access to the binding site. The small loop extension (colored pink) at the C-terminal end of switch-2 is predicted with high confidence and causes the whole loop to fold in a different conformation compared to known structures, such as myosin S1 fragments of *Dictyostelium discoideum* and *Bos taurus* (Protein Data Bank (PDB) identification codes 1MND and 8QYU, respectively).

Conclusion

The genes encoding class 18 myosins, *Myo18a* and *Myo18b*, are highly expressed in the developing heart and somites, as well as in

adult striated muscle, and deletion of either gene is embryonic lethal around embryonic day 11.5, notably at a time when the need for blood pumping function becomes vital for growth. Myo18B and specific isoforms of Myo18A may be involved in myogenesis, potentially playing roles in the transition of premyofibrils, nonmuscle myosin 2-containing stress fibers, to sarcomeres. In differentiated cardiac myocytes, both Myo18B and the gamma-isoform of Myo18A localize to the A-bands of sarcomeres, presumably via their respective N-terminal extensions (Figure 1A). Myo18Aγ and Myo18B most likely coassemble with class 2 myosins at low stoichiometric ratios to form mixed-class bipolar myosin filaments. They may function as scaffold proteins, potentially extending to the thin filaments to provide stability and internal resistance. These putative functions align with the apparent lack of ATPase activity in the head domains of class 18 myosins, although it remains to be established whether this holds true *in vivo*. Whether Myo18Aγ and Myo18B also regulate sarcomere function, for example, by acting as sarcomere length-dependent molecular brakes, remains to be explored.

Ultimately, Myo18Aγ and Myo18B are localized somewhere in the A-bands of highly organized sarcomeres, which have just been resolved at unprecedented resolution using cryo-electron microscopy by the groups of Roger Craig (Dutta et al., 2023) and Stefan Raunser (Tamborrini et al., 2023). Thus, there is a good chance that the precise arrangements and interaction partners of Myo18Aγ and Myo18B will soon be determined using such state-of-the-art structural data sets.

Assuming that class 18 myosins have evolved to become indispensible components of sarcomeres, the relative importance of PDZ-containing Myo18Aα remains to be clarified. Myo18Aα has been implicated in diverse functions, including Golgi structure and function and surfactant protein A binding, whereas the shorter PDZ-less isoform Myo18Aβ may act as a negative regulator via heterodimerization. One approach to assess the relative importance of the various Myo18A isoforms would be to genetically inhibit the expression of Myo18Aα in mice and screen for phenotypes. Subsequently, if no significant abnormalities manifest, the α-isoform-specific knockout mouse model could be further modified to additionally inhibit expression of the β-isoform, while retaining the expression of Myo18Aγ. That is, phenotypic analysis of Myo18A isoform-specific knockout mouse models may help to resolve the specific functions of the various isoforms.

Author contributions

MH: Formal Analysis, Visualization, Writing–review and editing, Conceptualization. C-AA: Conceptualization, Formal Analysis, Visualization, Writing–review and editing. PH: Writing–original draft, Conceptualization.

Funding

The author(s) declare that financial support was received for the research, authorship, and/or publication of this article. This work is funded by the Deutsche Forschungsgemeinschaft (DFG, German Research Foundation)–project number 512106520 (HA 3271/12-1).

Conflict of interest

The authors declare that the research was conducted in the absence of any commercial or financial relationships that could be construed as a potential conflict of interest.

Publisher's note

References

Ajima, R., Akazawa, H., Kodama, M., Takeshita, F., Otsuka, A., Kohno, T., et al. (2008). Deficiency of Myo18B in mice results in embryonic lethality with cardiac myofibrillar aberrations. *Genes cells.* 13, 987–999. doi:10.1111/j.1365-2443.2008.01226.x

Alazami, A. M., Kentab, A. Y., Faqeih, E., Mohamed, J. Y., Alkhalidi, H., Hijazi, H., et al. (2015). A novel syndrome of Klippel-Feil anomaly, myopathy, and characteristic facies is linked to a null mutation in MYO18B. *J. Med. Genet.* 52, 400–404. doi:10.1136/jmedgenet-2014-102964

Alexander, C. J., Barzik, M., Fujiwara, I., Remmert, K., Wang, Y. X., Petralia, R. S., et al. (2021). Myosin 18Aα targets the guanine nucleotide exchange factor β-Pix to the dendritic spines of cerebellar Purkinje neurons and promotes spine maturation. *Faseb J.* 35, e21092. doi:10.1096/fj.202001449R

Avraham, K. B., Hasson, T., Steel, K. P., Kingsley, D. M., Russell, L. B., Mooseker, M. S., et al. (1995). The mouse Snell's waltzer deafness gene encodes an unconventional myosin required for structural integrity of inner ear hair cells. *Nat. Genet.* 11, 369–375. doi:10.1038/ng1295-369

Batters, C., and Veigel, C. (2016). Mechanics and activation of unconventional myosins. *Traffic* 17, 860–871. doi:10.1111/tra.12400

Belyantseva, I. A., Boger, E. T., and Friedman, T. B. (2003). Myosin XVa localizes to the tips of inner ear sensory cell stereocilia and is essential for staircase formation of the hair bundle. *Proc. Natl. Acad. Sci. U. S. A.* 100, 13958–13963. doi:10.1073/pnas.2334417100

Berger, J., Berger, S., Li, M., and Currie, P. D. (2017). Myo18b is essential for sarcomere assembly in fast skeletal muscle. *Hum. Mol. Genet.* 26, 1146–1156. doi:10.1093/hmg/ddx025

Bezprozvanny, I., and Maximov, A. (2001). PDZ domains: more than just a glue. *Proc. Natl. Acad. Sci. U. S. A.* 98, 787–789. doi:10.1073/pnas.98.3.787

Billington, N., Beach, J. R., Heissler, S. M., Remmert, K., Guzik-Lendrum, S., Nagy, A., et al. (2015). Myosin 18A coassembles with nonmuscle myosin 2 to form mixed bipolar filaments. *Curr. Biol.* 25, 942–948. doi:10.1016/j.cub.2015.02.012

Bruford, E. A., Braschi, B., Denny, P., Jones, T. E. M., Seal, R. L., and Tweedie, S. (2020). Guidelines for human gene nomenclature. *Nat. Genet.* 52, 754–758. doi:10.1038/s41588-020-0669-3

Bruun, K., Beach, J. R., Heissler, S. M., Remmert, K., Sellers, J. R., and Hammer, J. A. (2017). Re-evaluating the roles of myosin 18Aα and F-actin in determining Golgi morphology. *Cytoskelet. Hob.* 74, 205–218. doi:10.1002/cm.21364

Burnette, D. T., Shao, L., Ott, C., Pasapera, A. M., Fischer, R. S., Baird, M. A., et al. (2014). A contractile and counterbalancing adhesion system controls the 3D shape of crawling cells. *J. Cell Biol.* 205, 83–96. doi:10.1083/jcb.201311104

Cao, J., Li, S., Shao, M., Cheng, X., Xu, Z., and Shi, D. (2014). The PDZ-containing unconventional myosin XVIIIA regulates embryonic muscle integrity in zebrafish. *J. Genet. Genomics* 41, 417–428. doi:10.1016/j.jgg.2014.06.008

Cao, J. M., Cheng, X. N., Li, S. Q., Heller, S., Xu, Z. G., and Shi, D. L. (2016). Identification of novel MYO18A interaction partners required for myoblast adhesion and muscle integrity. *Sci. Rep.* 6, 36768. doi:10.1038/srep36768

Casals, C., Campanero-Rhodes, M. A., García-Fojeda, B., and Solís, D. (2018). The role of collectins and galectins in lung innate immune defense. *Front. Immunol.* 9, 1998. doi:10.3389/fimmu.2018.01998

Chatterjee, P., Morgan, C. P., Krey, J. F., Benson, C., Goldsmith, J., Bateschell, M., et al. (2023). GIPC3 couples to MYO6 and PDZ domain proteins, and shapes the hair cell apical region. *J. Cell Sci.* 136, jcs261100. doi:10.1242/jcs.261100

Coluccio, L. M. (2020). Myosins and disease. *Adv. Exp. Med. Biol.* 1239, 245–316. doi:10.1007/978-3-030-38062-5_12

Dippold, H. C., Ng, M. M., Farber-Katz, S. E., Lee, S. K., Kerr, M. L., Peterman, M. C., et al. (2009). GOLPH3 bridges phosphatidylinositol-4- phosphate and actomyosin to stretch and shape the Golgi to promote budding. *Cell* 139, 337–351. doi:10.1016/j.cell.2009.07.052

Dutta, D., Nguyen, V., Campbell, K. S., Padrón, R., and Craig, R. (2023). Cryo-EM structure of the human cardiac myosin filament. *Nature* 623, 853–862. doi:10.1038/s41586-023-06691-4

Friedman, A. L., Geeves, M. A., Manstein, D. J., and Spudich, J. A. (1998). Kinetic characterization of myosin head fragments with long-lived myosin.ATP states. *Biochemistry* 37, 9679–9687. doi:10.1021/bi973143f

Friedman, T. B., Sellers, J. R., and Avraham, K. B. (1999). Unconventional myosins and the genetics of hearing loss. *Am. J. Med. Genet.* 89, 147–157. doi:10.1002/(sici)1096-8628(19990924)89:3<147::aid-ajmg5>3.0.co;2-6

Fujii, T., and Namba, K. (2017). Structure of actomyosin rigour complex at 5.2 Å resolution and insights into the ATPase cycle mechanism. *Nat. Commun.* 8, 13969. doi:10.1038/ncomms13969

Furch, M., Fujita-Becker, S., Geeves, M. A., Holmes, K. C., and Manstein, D. J. (1999). Role of the salt-bridge between switch-1 and switch-2 of Dictyostelium myosin. *J. Mol. Biol.* 290, 797–809. doi:10.1006/jmbi.1999.2921

Furusawa, T., Ikawa, S., Yanai, N., and Obinata, M. (2000). Isolation of a novel PDZ-containing myosin from hematopoietic supportive bone marrow stromal cell lines. *Biochem. Biophys. Res. Commun.* 270, 67–75. doi:10.1006/bbrc.2000.2377

Gibson, F., Walsh, J., Mburu, P., Varela, A., Brown, K. A., Antonio, M., et al. (1995). A type VII myosin encoded by the mouse deafness gene shaker-1. *Nature* 374, 62–64. doi:10.1038/374062a0

Gurung, R., Ono, Y., Baxendale, S., Lee, S. L., Moore, S., Calvert, M., et al. (2017). A zebrafish model for a human myopathy associated with mutation of the unconventional myosin MYO18B. *Genetics* 205, 725–735. doi:10.1534/genetics.116.192864

Guzik-Lendrum, S., Heissler, S. M., Billington, N., Takagi, Y., Yang, Y., Knight, P. J., et al. (2013). Mammalian myosin-18A, a highly divergent myosin. *J. Biol. Chem.* 288, 9532–9548. doi:10.1074/jbc.M112.441238

Hartman, M. A., Finan, D., Sivaramakrishnan, S., and Spudich, J. A. (2011). Principles of unconventional myosin function and targeting. *Annu. Rev. Cell Dev. Biol.* 27, 133–155. doi:10.1146/annurev-cellbio-100809-151502

Horsthemke, M., Nutter, L. M. J., Bachg, A. C., Skryabin, B. V., Honnert, U., Zobel, T., et al. (2019). A novel isoform of myosin 18A (Myo18Aγ) is an essential sarcomeric protein in mouse heart. *J. Biol. Chem.* 294, 7202–7218. doi:10.1074/jbc.RA118.004560

Hsu, R. M., Hsieh, Y. J., Yang, T. H., Chiang, Y. C., Kan, C. Y., Lin, Y. T., et al. (2014). Binding of the extreme carboxyl-terminus of PAK-interacting exchange factor β (βPIX) to myosin 18A (MYO18A) is required for epithelial cell migration. *Biochim. Biophys. Acta* 1843, 2513–2527. doi:10.1016/j.bbamcr.2014.06.023

Hsu, R. M., Tsai, M. H., Hsieh, Y. J., Lyu, P. C., and Yu, J. S. (2010). Identification of MYO18A as a novel interacting partner of the PAK2/betaPIX/GIT1 complex and its potential function in modulating epithelial cell migration. *Mol. Biol. Cell* 21, 287–301. doi:10.1091/mbc.e09-03-0232

Jiu, Y., Kumari, R., Fenix, A. M., Schaible, N., Liu, X., Varjosalo, M., et al. (2019). Myosin-18B promotes the assembly of myosin II stacks for maturation of contractile actomyosin bundles. *Curr. Biol.* 29, 81–92. doi:10.1016/j.cub.2018.11.045

Jumper, J., Evans, R., Pritzel, A., Green, T., Figurnov, M., Ronneberger, O., et al. (2021). Highly accurate protein structure prediction with AlphaFold. *Nature* 596, 583–589. doi:10.1038/s41586-021-03819-2

Kalhammer, G., and Bähler, M. (2000). Unconventional myosins. *Essays Biochem.* 35, 33–42. doi:10.1042/bse0350033

Kato, Y., Miyakawa, T., and Tanokura, M. (2018). Overview of the mechanism of cytoskeletal motors based on structure. *Biophys. Rev.* 10, 571–581. doi:10.1007/s12551-017-0368-1

King, S. D., and Chen, S. Y. (2020). Recent progress on surfactant protein A: cellular function in lung and kidney disease development. *Am. J. Physiol. Cell Physiol.* 319, C316–c320. doi:10.1152/ajpcell.00195.2020

Latham, S. L., Weiß, N., Schwanke, K., Thiel, C., Croucher, D. R., Zweigerdt, R., et al. (2020). Myosin-18B regulates higher-order organization of the cardiac sarcomere through thin filament cross-linking and thick filament dynamics. *Cell Rep.* 32, 108090. doi:10.1016/j.celrep.2020.108090

Lawson, C. D., and Ridley, A. J. (2018). Rho GTPase signaling complexes in cell migration and invasion. *J. Cell Biol.* 217, 447–457. doi:10.1083/jcb.201612069

Liang, Y., Wang, A., Belyantseva, I. A., Anderson, D. W., Probst, F. J., Barber, T. D., et al. (1999). Characterization of the human and mouse unconventional myosin XV genes responsible for hereditary deafness DFNB3 and shaker 2. *Genomics* 61, 243–258. doi:10.1006/geno.1999.5976

Liu, X., and Fuentes, E. J. (2019). Emerging themes in PDZ domain signaling: structure, function, and inhibition. *Int. Rev. Cell Mol. Biol.* 343, 129–218. doi:10.1016/bs.ircmb.2018.05.013

Makowska, K. A., Hughes, R. E., White, K. J., Wells, C. M., and Peckham, M. (2015). Specific myosins control actin organization, cell morphology, and migration in prostate cancer cells. *Cell Rep.* 13, 2118–2125. doi:10.1016/j.celrep.2015.11.012

Malfatti, E., Böhm, J., Lacène, E., Beuvin, M., Romero, N. B., and Laporte, J. (2015). A premature stop codon in MYO18B is associated with severe nemaline myopathy with cardiomyopathy. *J. Neuromuscul. Dis.* 2, 219–227. doi:10.3233/JND-150085

Maravillas-Montero, J. L., and Santos-Argumedo, L. (2012). The myosin family: unconventional roles of actin-dependent molecular motors in immune cells. *J. Leukoc. Biol.* 91, 35–46. doi:10.1189/jlb.0711335

Mermall, V., Post, P. L., and Mooseker, M. S. (1998). Unconventional myosins in cell movement, membrane traffic, and signal transduction. *Science* 279, 527–533. doi:10.1126/science.279.5350.527

Mihaylova, V., Chablais, F., Herenger, Y., Spiegel, R., and Heinrich Jung, H. (2020). Novel truncating mutations of MYO18B causing congenital myopathy in a Swiss patient. *Neurol. Genet.* 6, e458. doi:10.1212/NXG.0000000000000458

Moreland, Z. G., and Bird, J. E. (2022). Myosin motors in sensory hair bundle assembly. *Curr. Opin. Cell Biol.* 79, 102132. doi:10.1016/j.ceb.2022.102132

Mori, K., Furusawa, T., Okubo, T., Inoue, T., Ikawa, S., Yanai, N., et al. (2003). Genome structure and differential expression of two isoforms of a novel PDZ-containing myosin (MysPDZ) (Myo18A). *J. Biochem.* 133, 405–413. doi:10.1093/jb/mvg053

Mori, K., Matsuda, K., Furusawa, T., Kawata, M., Inoue, T., and Obinata, M. (2005). Subcellular localization and dynamics of MysPDZ (Myo18A) in live mammalian cells. *Biochem. Biophys. Res. Commun.* 326, 491–498. doi:10.1016/j.bbrc.2004.11.058

Nishioka, M., Kohno, T., Tani, M., Yanaihara, N., Tomizawa, Y., Otsuka, A., et al. (2002). MYO18B, a candidate tumor suppressor gene at chromosome 22q12.1, deleted, mutated, and methylated in human lung cancer. *Proc. Natl. Acad. Sci. U. S. A.* 99, 12269–12274. doi:10.1073/pnas.192445899

Onishi, H., Morales, M. F., Kojima, S., Katoh, K., and Fujiwara, K. (1997). Functional transitions in myosin: role of highly conserved Gly and Glu residues in the active site. *Biochemistry* 36, 3767–3772. doi:10.1021/bi9630772

Onishi, H., Morales, M. F., Kojima, S., Katoh, K., and Fujiwara, K. (1998). Smooth muscle myosin. Amino acid residues responsible for the hydrolysis of ATP. *Adv. Exp. Med. Biol.* 453, 99–104.

Ouyang, Z., Zhao, S., Yao, S., Wang, J., Cui, Y., Wei, K., et al. (2021). Multifaceted function of myosin-18, an unconventional class of the myosin superfamily. *Front. Cell Dev. Biol.* 9, 632445. doi:10.3389/fcell.2021.632445

Ruppel, K. M., and Spudich, J. A. (1996). Structure-function analysis of the motor domain of myosin. *Annu. Rev. Cell Dev. Biol.* 12, 543–573. doi:10.1146/annurev.cellbio.12.1.543

Salamon, M., Millino, C., Raffaello, A., Mongillo, M., Sandri, C., Bean, C., et al. (2003). Human MYO18B, a novel unconventional myosin heavy chain expressed in striated muscles moves into the myonuclei upon differentiation. *J. Mol. Biol.* 326, 137–149. doi:10.1016/s0022-2836(02)01335-9

Sanger, J. W., Kang, S., Siebrands, C. C., Freeman, N., Du, A., Wang, J., et al. (2005). How to build a myofibril. *J. Muscle Res. Cell Motil.* 26, 343–354. doi:10.1007/s10974-005-9016-7

Sanger, J. W., Wang, J., Fan, Y., White, J., and Sanger, J. M. (2010). Assembly and dynamics of myofibrils. *J. Biomed. Biotechnol.* 2010, 858606. doi:10.1155/2010/858606

Sellers, J. R. (2000). Myosins: a diverse superfamily. *Biochim. Biophys. Acta* 1496, 3–22. doi:10.1016/s0167-4889(00)00005-7

Sever-Chroneos, Z., Krupa, A., Davis, J., Hasan, M., Yang, C. H., Szeliga, J., et al. (2011). Surfactant protein A (SP-A)-mediated clearance of *Staphylococcus aureus* involves binding of SP-A to the staphylococcal adhesin eap and the macrophage receptors SP-A receptor 210 and scavenger receptor class A. *J. Biol. Chem.* 286, 4854–4870. doi:10.1074/jbc.M110.125567

Shimada, T., Sasaki, N., Ohkura, R., and Sutoh, K. (1997). Alanine scanning mutagenesis of the switch I region in the ATPase site of *Dictyostelium discoideum* myosin II. *Biochemistry* 36, 14037–14043. doi:10.1021/bi971837i

Smith, C. A., and Rayment, I. (1996). Active site comparisons highlight structural similarities between myosin and other P-loop proteins. *Biophys. J.* 70, 1590–1602. doi:10.1016/S0006-3495(96)79745-X

Taft, M. H., Behrmann, E., Munske-Weidemann, L. C., Thiel, C., Raunser, S., and Manstein, D. J. (2013). Functional characterization of human myosin-18A and its interaction with F-actin and GOLPH3. *J. Biol. Chem.* 288, 30029–30041. doi:10.1074/jbc.M113.497180

Taft, M. H., and Latham, S. L. (2020). Myosin XVIII. *Adv. Exp. Med. Biol.* 1239, 421–438. doi:10.1007/978-3-030-38062-5_19

Tamborrini, D., Wang, Z., Wagner, T., Tacke, S., Stabrin, M., Grange, M., et al. (2023). Structure of the native myosin filament in the relaxed cardiac sarcomere. *Nature* 623, 863–871. doi:10.1038/s41586-023-06690-5

Tan, I., Yong, J., Dong, J. M., Lim, L., and Leung, T. (2008). A tripartite complex containing MRCK modulates lamellar actomyosin retrograde flow. *Cell* 135, 123–136. doi:10.1016/j.cell.2008.09.018

Trivedi, D. V., David, C., Jacobs, D. J., and Yengo, C. M. (2012). Switch II mutants reveal coupling between the nucleotide- and actin-binding regions in myosin V. *Biophys. J.* 102, 2545–2555. doi:10.1016/j.bpj.2012.04.025

Wakabayashi, Y., Takahashi, Y., Kikkawa, Y., Okano, H., Mishima, Y., Ushiki, T., et al. (1998). A novel type of myosin encoded by the mouse deafness gene shaker-2. *Biochem. Biophys. Res. Commun.* 248, 655–659. doi:10.1006/bbrc.1998.8976

Weil, D., Blanchard, S., Kaplan, J., Guilford, P., Gibson, F., Walsh, J., et al. (1995). Defective myosin VIIA gene responsible for Usher syndrome type 1B. *Nature* 374, 60–61. doi:10.1038/374060a0

Yang, C. H., Szeliga, J., Jordan, J., Faske, S., Sever-Chroneos, Z., Dorsett, B., et al. (2005). Identification of the surfactant protein A receptor 210 as the unconventional myosin 18A. *J. Biol. Chem.* 280, 34447–34457. doi:10.1074/jbc.M505229200

Yokota, J., Nishioka, M., Tani, M., and Kohno, T. (2003). Genetic alterations responsible for metastatic phenotypes of lung cancer cells. *Clin. Exp. Metastasis* 20, 189–193. doi:10.1023/a:1022978932215

Zhao, S., Shi, X., Zhang, Y., Wen, Z., Cai, J., Gao, W., et al. (2020). Myosin-18B promotes mechanosensitive CaMKK2-AMPK-VASP regulation of contractile actin stress fibers. *iScience* 23, 100975. doi:10.1016/j.isci.2020.100975

frontiers | Frontiers in Physiology

TYPE Review
PUBLISHED 17 May 2024
DOI 10.3389/fphys.2024.1390186

OPEN ACCESS

EDITED BY
Maria Jolanta Redowicz,
Polish Academy of Sciences, Poland

REVIEWED BY
Manuel H. Taft,
Hannover Medical School, Germany
James R. Sellers,
National Heart, Lung, and Blood Institute (NIH), United States
Thomas Pollard,
Yale University, United States

*CORRESPONDENCE
James A. Spudich,
jspudich@stanford.edu

RECEIVED 22 February 2024
ACCEPTED 01 April 2024
PUBLISHED 17 May 2024

CITATION
Spudich JA (2024), One must reconstitute the functions of interest from purified proteins. *Front. Physiol.* 15:1390186. doi: 10.3389/fphys.2024.1390186

One must reconstitute the functions of interest from purified proteins

James A. Spudich*

Department of Biochemistry, Stanford University School of Medicine, Stanford, CA, United States

I am often asked by students and younger colleagues and now by the editors of this issue to tell the history of the development of the *in vitro* motility assay and the dual-beam single-molecule laser trap assay for myosin-driven actin filament movement, used widely as key assays for understanding how both muscle and nonmuscle myosin molecular motors work. As for all discoveries, the history of the development of the myosin assays involves many people who are not authors of the final publications, but without whom the assays would not have been developed as they are. Also, early experiences shape how one develops ideas and experiments, and influence future discoveries in major ways. I am pleased here to trace my own path and acknowledge the many individuals involved and my early science experiences that led to the work I and my students, postdoctoral fellows, and sabbatical visitors did to develop these assays. Mentors are too often overlooked in historical descriptions of discoveries, and my story starts with those who mentored me.

KEYWORDS

myosin, actin, *Dictyostelium*, motility assay, single molecule assay, interdisciplinary research

Mentors are important players in all of our lives

My own story could start as a boy fascinated with chemistry, but I will fast forward to my experiences in the Physiology Course in Woods Hole, during the summers of 1962 and 1963, where I learned the importance of interdisciplinary approaches for elucidating questions about a biological system. The interdisciplinary approach, widely used in laboratories now, was not common in an individual laboratory or even in a department then. The Physiology Course in 1962 and 1963 was headed up by my first mentor, John Woodland Hastings, known as "Woody," with whom I worked on bioluminescence as an undergraduate chemistry major at the University of Illinois, Urbana-Champaign. Woody was ahead of his time assembling an interdisciplinary group of stellar course instructors covering biochemistry, physics, genetics, developmental biology, and cell biology. Instructors came from far and wide. Ken van Holde was a physical biochemist at the University of Illinois, who together with Robert "Buzz" Baldwin, developed a method for rapid approach to sedimentation equilibrium and its use to analyze the size and shape of protein molecules. Ken van Holde also designed improvements in light scattering and circular dichroism. In the course, he taught about basic chemical and physical properties of proteins in relation to their bioIogical specificity and function. The laboratory studies included investigations of the physical properties of protein molecules which are sensitive to their molecular configuration, weight, and shape. Phil Hartman was a Johns Hopkins Biologist and pioneer in microbial genetics and mutagenesis. Ed Adelberg, from Yale, was a

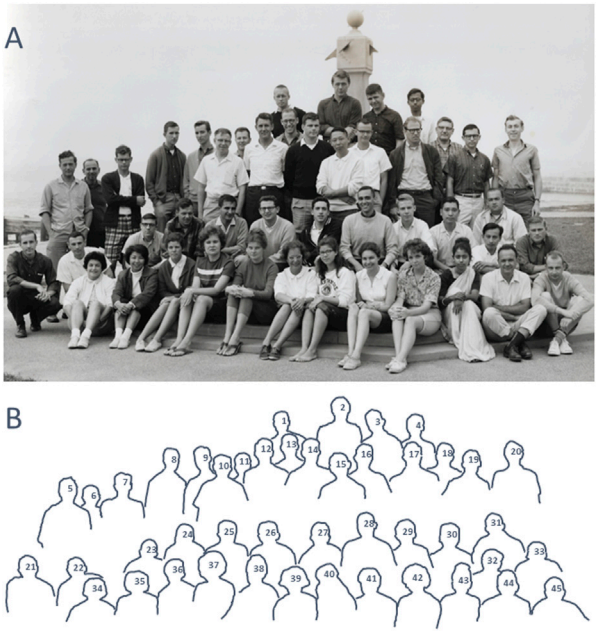

FIGURE 1
Participants in the Woods Hole 1963 summer Physiology Course. **(A)** Photograph of participants. Not all participants are in the photo. **(B)** Pen outline of the individuals in the photo, numbered to coincide with the numbers in parentheses below. A complete list of course participants is: *Course Director and Instructor*–J. Woodland Hastings (12). Instructors–Alex Keynan (6), Harlyn Halvorson (10), Shinya Inoue (15), Fred Karush (18), Ken van Holde (24), Ed Adelberg, Philip Hartman. Assistant Instructors–with Hastings, Jim Spudich (9), Jorge Churchich (25), Margarita Churchich; with van Holde, William Deal (11), Lawrence Cohen, S. Y. Sun; with Halvorson, Roger Bretthauer (33); with Inoue, Hidemi Sato (30), Jonathan Hardy (2); with Hartman and Adelberg, M. Levin (22), Riyo Kunisawa (35), Frank Vasington; with Karush, Sayaka Utsumi (32). *Course Assistants*–Carolyn Veeder (40), John Spudich (8), Randy Sweeney. *Consultants, Guest lecturers*–Merkel Jacobs, Arthur Parpart, Albert Szent-Gyorgyi, William McElroy, Martin Pollock (5?), Herman Kalckar (5?). *Students*–Robert Barlow, Jr (1), Kunal Saha (4), Jon Jacklett (7), Jay Mittenthal (13), Joel Shaper (13), Raymond Stephens (16), William Hahn (17), Ben Leichtling (19), Deric Bownds (21), Allen Phillips (23), Robert Trivus (26), Steve Harrison (27), Joseph Fratantoni (28), Robert Grey (29), Marshall Elzinga (31), Laura Ponticorvo (34), Dorothy Nauman (36), Shirley Hilden (37), Mary-Jane Tunis (38), Linda Garrick (39), Yvonne Connelly (41), Pam Stoddard (42), Annamma Cownan (43), Felix Madrid (44), Richard Humphrey (45), Julian Haynes, Eugene Jacobson, Ronald Sederoff, Willie Curry, Richard DeSa, Richard Muesing. Source: Reproduced from Marine Biological Laboratory Archives, licensed under CCBY 4.0 International.

founder of microbial genetics. One of his long-term investigations involved the genetic regulation of amino acid biosynthesis in *E. coli*. In the course, Phil Hartman and Ed Adelberg taught microbial genetics and physiology. The lab involved isolation of bacterial mutants, analysis of growth factor requirements, and genetic analysis through transduction tests as well as by conjugation. Alex Keynan was an Israeli microbiologist who studied germination of *Bacillus subtilis* spores and quorum sensing in bacterial populations. Harlyn Halvorson, who later served as Director of the Marine Biological Laboratory, was a microbiologist who also studied bacterial sporulation. Two of my favorite instructors were the biochemist Andrew Szent-Györgyi, who introduced me to muscle research, and the cell biologist Shinya Inoue, who was developing his latest innovations in light microscopy for studying spindle dynamics during mitosis. Their influence on the specifics of my future scientific contributions was pivotal. Imagine as a young scientist in training, just completing his B.S. degree, being exposed to such an intense course with a diverse array of approaches to biological problems. I had published three manuscripts from my undergraduate work with Woody, combining my organic chemistry expertise with biochemistry and photometry. Those were exciting times for me, and the Woods Hole Physiology Course then and now changes the scientific lives of many students who experience it (Figure 1).

Leaving Woods Hole in 1963, I began my graduate training in the Department of Biochemistry at Stanford, established by Arthur Kornberg. I was in a class of three new graduate students and was one of the earliest students in the Department, which was founded just 4 years earlier. The ratio of students to faculty at that time was close to 1:1. One of the many remarkable aspects of the department was that, although Arthur was my thesis advisor, all the faculty members, Paul Berg, Bob Lehman, Dale Kaiser, Buzz Baldwin, Dave Hogness, and the new assistant professors Lubert Stryer and George Stark, were all my mentors. The Department was heavily focused on hard-core biochemistry–you ground up cells, made an extract, which was then fractionated by conventional biochemical approaches, following the activity of the enzyme you were trying to purify. *"You will never understand how a system works if you cannot reconstitute the functions of interest from purified proteins!"* was drilled into us graduate students–this was the Department of Biochemistry's creed. The Department was so focused on protein purification from cell extracts that there was not even a microscope available when I started. To visualize *B. subtilis* cells, which I was happily grinding up in pursuit of the origin of proteins in the developmental transition from a vegetative cell to a spore, I had to borrow a microscope from the Department of Genetics. Shinya Inoue would have been amused.

Those years of hard-core biochemistry focus and training were invaluable throughout my career and taught me many fundamental facts and principles that I would not have learned otherwise. Arthur was interested in starting a program on understanding the developmental transition of a *B. subtilis* vegetative cell into a spore. I knew a lot about that subject from my Woods Hole experience and was delighted to help launch that new program in his lab. Early on in my thesis research, I purified *B. subtilis* adenylate kinase from vegetative cells and spores to compare their properties. After purifying over multiple columns, I had activity in a very low protein concentration fraction, but in the next step I lost all activity! This could have been due to the loss of a critical co-factor, as Tom Pollard and Ed Korn describe in an accompanying paper in this issue (Pollard and Korn, 2023). But in my case, it was another key lesson that all biochemists learn–placing a protein in a glass or plastic tube immediately results in the protein adhering to the surface of the vessel as a monolayer. In a very dilute solution of protein at a near final purification step, one can lose all your enzyme stuck onto the tube surface, which is what happened to my laboriously purified adenylate kinase. A lesson hard learned–one must rinse glass- and plastic-ware with a bovine serum albumin (BSA) solution to saturate the surface with protein to avoid losing your precious purified enzyme. A nascent glass or plastic surface tightly binds a monolayer of the first protein presented to it. I would use this hard-earned knowledge, 5 years later in my laboratory, to

great eventual benefit, as a beginning Assistant Professor in the new Department of Biochemistry and Biophysics at UCSF chaired by Bill Rutter.

When in 1968, it was time to start post-doctoral work, my intuition derived from my Woods Hole experience led me in a very different direction from the common practice of graduate students at the time. The usual practice was a 1-yr postdoctoral experience working on a very similar area of research as a graduate student, but in Europe to get the "European experience," and then assume an assistant professorship back in the US continuing research on the same problem using the same familiar biochemical approaches. I was, however, determined to obtain first-hand exposure to both genetics and structural biology, and therefore planned two consecutive postdocs, totaling 3 years of postdoctoral research, nearly unheard of in those days. Arthur said I would be an old man before starting creative research on my own, but my instincts to get firsthand experiences in genetics and structural biology proved to be a decision that would serve me well in my research career.

I arranged to spend the year of 1968 with Charley Yanofsky in the Department of Biology at Stanford using genetic approaches, working to understand recombination near the tryptophan operon in *E. coli*. That year, working with another giant of a scientist, using purely genetic approaches, had an enormous impact on my research going forward. We published an interesting paper regarding DNA recombination in the Journal of Molecular Biology from those studies.

My next step was to learn techniques of structural biology. In those days there was only one place to consider going to learn structural biology, the Laboratory of Molecular Biology (LMB) at the Medical Research Council (MRC) in Cambridge, England. This powerhouse of Nobel laureates was an inspiring place, several miles outside of Cambridge center. Being isolated, a restaurant with long rectangular tables was established on the sixth floor of the building where lunch was served as well as afternoon tea. This is where an enormous amount of scientific exchange occurred between various laboratories, and new ideas emerged daily. That sixth floor restaurant was essential for the dynamic cross-fertilization that was so impressive there, and I was to incorporate this into an initiative that I became involved in 30 years later at Stanford called Bio-X (https://biox.stanford.edu/; for early history, see Supplementary Information).

At the LMB, Aaron Klug was at an early stage of carrying out reconstructions from electron micrographs to obtain the 3D structure of virus particles. Working with John Finch and David DeRosier, Aaron showed that in cases like tobacco mosaic virus, being a long cylindrical, helical structure, one can use helical diffraction theory to solve its structure, where single views of the virus contain all the information needed to obtain the 3D structure (De Rosier and Klug, 1968). Think of a barber pole–from one view from one direction you can understand the 3D structure of the barber pole pattern. Rather than apply directly to Aaron's lab for a postdoc position, my interests in muscle contraction, peaked by interactions with Andrew Szent-Györgyi in Woods Hole, led me to join the laboratory of Hugh Huxley, the leader in the field of muscle structure and function. Peter Moore, Hugh Huxley and David DeRosier were just publishing a helical reconstruction of actin with myosin heads bound when I arrived in Cambridge in 1969 (Moore et al., 1970). It was also the year that Hugh was submitting for publication his pivotal *Science* paper on the swinging crossbridge model of muscle contraction (Huxley, 1969), a draft of which he gave me to read upon my arrival. My previous training was so focused on biochemistry and genetics that I remember being captivated by the power of the structural approaches Hugh used, both electron microscopy of fixed muscle and isolated proteins and low angle X-ray scattering of live muscle tissue, to reveal important concepts of how muscle works. From the perspective of my background, however, I was surprised that there was no biochemical *in vitro* reconstitution of the primary functions of interest, which in this case are *movement and force production.* Furthermore, genetic approaches were largely missing. Both became focuses of my own laboratory after I left the LMB for my first faculty position at UCSF.

As a postdoctoral fellow at the LMB, I was keen to contribute something new to Hugh's lab and to the field. At the time, it was clear that the tropomyosin-troponin complex was important for calcium regulation of muscle contraction, but the biochemical mechanism and structural aspects of the system were not worked out. My postdoctoral work at LMB necessarily began with purification of the proteins involved, actin and tropomyosin-troponin, so I could study their interaction. Actin preparations at that time were heavily contaminated with tropomyosin-troponin, and because of my description in my first paper from this work of how to obtain highly purified actin, it became one of my most frequently cited papers (Spudich and Watt, 1971). The actin purification method overshadowed the important biochemical titrations described in that paper that proved that tropomyosin-troponin regulates the actin-myosin interaction by complexing with actin, and in a 1:7 M ratio of tropomyosin-troponin:actin. A key associate of Hugh's at the LMB-MRC was Alan Weeds who taught me about the biochemistry of myosin and its sub-fragments, which I used in my studies. I was fortunate in those 2 years to combine biochemistry with helical reconstructions from electron micrographs that led us to hypothesize the steric blocking mechanism for tropomyosin-troponin function (Spudich et al., 1972), a hypothesis extended by low angle X-ray diffraction studies of muscle by Hugh (Huxley, 1972) and by Parry and Squire (Parry and Squire, 1973). The steric blocking model gained more and more experimental support as higher-resolution structures were solved (Lehman, 2016; von der Ecken et al., 2015; Tobacman, 2021). My training in structural biology at the LMB-MRC was pivotal for what I accomplished over the next 5 decades. Those 2 years in Cambridge at the LMB with Hugh provided me the structural biology tools to add to the interdisciplinary approach that was to define my entire career.

With training in chemistry, physics, biochemistry, genetics, and structural biology, what's next?

From Cambridge, I accepted a position as Assistant Professor of the new Department of Biochemistry and Biophysics at UCSF, chaired by Bill Rutter. It was 1971 and I had multiple ideas about important biological problems to apply my interdisciplinary training to, including the interesting developmental biology project that I had worked on earlier–what's involved in the conversion of a bacterial vegetative

cell into a dormant spore, and then back again to a vegetative cell when the correct environment is present. Whatever I decided to work on, the objective was to design experiments that would provide definitive answers to the pivotal questions at hand, regardless how difficult. Throughout my career, I have told my students and postdoctoral fellows to go for the decisive experiment, do not be afraid to fail, dream about your work, and be grateful for the privilege of carrying out creative research.

I wrote an NIH grant for the sporulation project while still in Cambridge, which was funded. By the time I arrived for my position at UCSF, however, my intuition led me to study two other fundamental unanswered questions in cell biology at the time: how the chemical energy of ATP hydrolysis brings about mechanical movement of muscle contraction, and what roles does a myosin-like motor have in nonmuscle cells. I called my NIH grants officer and explained that I had decided to work on something totally different. He asked me to send a one-page description of what I was doing to put in his file, and I used the funds awarded to study bacterial sporulation to study myosin instead–gone are those days!

Given the dictum *"You will never understand how a system works until you can reconstitute the functions of interest from purified proteins,"* where the primary myosin-driven functions of interest for muscle and nonmuscle cells are movement and force production, my key first goal was to develop a quantitative *in vitro* motility assay for movement of muscle actin driven by the molecular motor myosin. From my earlier experience I knew one could add myosin to a clean slide and form a monolayer of the motor protein on which actin filaments might move, but how does one visualize the actin filaments, which as individual filaments are too thin to be seen by conventional light microscopy. The first possible solution derived from my studies of actin from the cellular slime mold *Dictyostelium discoideum*, as described below.

My second goal was to develop a model organism to unravel the molecular basis of the myriad nonmuscle-cell movements that are clearly visible by light microscopy. In the late 1960s, Sadashi Hatano and Tazawa in Japan (Hatano and Tazawa, 1968), and Mark Adelman and Ed Taylor in the United States (Adelman and Taylor, 1969a; Adelman and Taylor, 1969b), had shown that actin and myosin are present in the acellular slime mold *Physarum polycephalum*. And as they recall in this issue (Pollard and Korn, 2023), Tom Pollard and Ed Korn found an entirely new type of myosin that changed the field in a dramatic way (Pollard and Korn, 1973a; Pollard and Korn, 1973b). Pollard and Korn were the initiators of what became an explosion of interest in unconventional myosins. Also in 1969 (Ishikawa et al., 1969), microfilaments associated with cell membranes were shown to be actin, by decorating them with the heavy meromyosin (HMM) fragment of myosin to give the characteristic arrowhead appearance that Hugh Huxley had shown for the muscle proteins in 1963 (Huxley, 1963). Non-muscle cell motility was on the verge of an explosion of activity.

At UCSF my laboratory explored *Neurospora crassa, Saccharomyces cerevisiae, Physarum polycephalum, Dictyostelium discoideum, Nitella axillaris, Strongylocentrotus purpuratus* and chick embryo fibroblasts (CEFs), none of which I had worked on in my previous training. The giant cells of the alga *Nitella* were particularly intriguing because of their striking intracellular cytoplasmic streaming that was visible under a simple light microscope, which was one of the first items I purchased for my own laboratory. Although not suitable for biochemistry or genetics, *Nitella* would assume an important role in my lab a decade later.

Our attempts to explore CEFs as a biochemical system led to an interesting finding. These cells were being worked on by Warren Levinson at UCSF. When we lysed the CEF cells growing on plates with the detergent Triton X-100, and viewed the plate by light microscopy, we noticed that a 'ghost' of each cell was still present, with its nucleus still apparent, somehow being held in its original position. Further electron microscopy revealed an extensive actin bundled network forming what we called a 'cytoskeleton' (Brown et al., 1976), a term I thought we coined, but Tom Pollard, a master of cell biology literature and a reviewer of this manuscript, pointed out that the term 'cytoskeleton' was developed in the 19th and early 20th centuries (Pollard, 1976; Frixione, 2000).

The slime mold *Dictyostelium* proved to be best for biochemical studies. Margaret Clarke, one of my first postdoctoral fellows, identified a myosin in *Dictyostelium* with properties similar to conventional muscle myosin (Clarke and Spudich, 1974), unlike the lower molecular weight *Acanthamoeba* myosin, named myosin-I, described by Tom Pollard and Ed Korn the year before (Pollard and Korn, 1973a; Pollard and Korn, 1973b). The conventional muscle myosin became known as myosin-II, and the *Dictyostelium discoideum* (D. d.) myosin that Margaret discovered was a myosin-II type. Later, Margaret (Meg) Titus (Titus et al., 1989; Titus et al., 1993) and John Hammer (Wessels et al., 1991; Urrutia et al., 1993; Hammer and Jung, 1996) identified multiple other forms of myosin in *Dictyostelium*.

Reconstitution of functions of interest from purified proteins often requires expression of the proteins of interest in an appropriate cell system

In 1977, I joined the new Department of Structural Biology at Stanford, where we continued to expand on our work on D. d. myosin II. Modern biochemistry commonly includes using molecular genetics to express and purify proteins of interest in an appropriate cell system. Unfortunately, no myosin type has ever been able to be expressed in a functional form using bacteria as an expression system. We hoped we might be able to use *Dictyostelium* for this purpose, though *Dictyostelium* had not been used as an expression system before. In attempts to express a truncated form of D. d. myosin II in *Dictyostelium* cells, Arturo de Lozanne discovered unexpectedly that one can very efficiently target genes in *Dictyostelium* by homologous recombination (De Lozanne and Spudich, 1987). He disrupted the single copy D. d. myosin II gene and provided the first genetic proof that myosin II is required for cytokinesis. Dietmar Manstein, Meg Titus and Arturo then used a linear plasmid to knock out the D. d. myosin II gene (Manstein et al., 1989). *Dictyostelium* cells in suspension undergo normal cell division associated with the mitotic cycle. The D. d. myosin II knockout cells fail to divide in suspension and become large and multinucleated. On a surface, however, the knockout cells divide by a process we named *traction-mediated cytofission*, which is not associated with the mitotic cycle and might

be how eukaryotic cells divided in early evolution. Importantly, the knockout cells were able to form pseudopodia and move along a surface, disproving the prevailing hypothesis that myosin II was needed for this process. Looking for an alternative force for driving cells forward, it soon became apparent that actin polymerization was the driving force (Theriot, 2000; Pollard and Cooper, 2009). While the D. d. Myosin II is not needed for general cell movement, it is required for directed cell movement, as occurs during *Dictyostelium* chemotaxis. *Dictyostelium* cells accumulate myosin II at their rear, inhibiting pseudopodia formation in that region, providing a force to detach the rear of the cell from the surface that the cell is moving on as the cell moves forward, and giving the cell the polarity it needs for directed cell motility (Liang et al., 2002).

Sometimes in research you are dealt a spectacular hand that you were not expecting. Suddenly, we had a eukaryotic cell that was entirely devoid of myosin II, and we could keep these cells alive by growing them on a surface where they underwent traction-mediated cytofission. We soon showed that we could rescue cytokinesis in suspension by replacing the myosin gene by introducing a copy of the D. d. myosin gene on a plasmid (Egelhoff et al., 1990). This was followed by rescuing cytokinesis with a GFP-tagged D. d. myosin II, which allowed us to quantify the movements of the myosin during various stages of the cell cycle and watch its accumulation in the pre-furrow region during mitosis (Moores et al., 1996). We also used the power of combining this cellular system with biochemical studies of purified proteins to understand the regulation of myosin thick filament formation by phosphorylation of the C-terminal portion of the myosin tail (Egelhoff et al., 1993; Sabry et al., 1997; Liang et al., 1999; Liang et al., 2002).

Another example of the power of combining biochemistry and cell biology is seen in the work of my graduate student William Shih. William took on the daunting task of creating a form of D. d. Myosin II to be used to carry out time resolved fluorescence energy transfer measurements on the myosin in various nucleotide states. This required removing existing cysteine residues from the myosin head domain and placing cysteine residues, which could be tagged with donor and acceptor fluorescent probes, at appropriate positions that would reflect the orientation of the so-called lever arm of the myosin head. But how would he know that the modifications he made left the myosin in a functional form? The answer is that he could express his altered myosin in the myosin null cell and make sure it could rescue cytokinesis. His studies were the first to demonstrate dynamically that the lever arm exists in different orientations depending on the nucleotide state in the active site (Shih et al., 2000).

Another stellar graduate student, Kathy Ruppel, used random mutagenesis to create 21 point mutations in the motor domain of D. d. myosin II to dissect structure/function relationships. She classified them into three distinct groups based on the ability to complement myosin null cell phenotypes: wild type, intermediate, and null. Biochemical analysis of the mutated myosins also revealed three classes of mutants that correlated well with the phenotypic classification (Ruppel and Spudich, 1996). Such an extensive mutational analysis of myosin function could only begin to be done by others later when myosins began to be expressed in Sf9 and mammalian expression systems. Kathy's work coincided with the publication of the myosin head structure by Ivan Rayment and his colleagues (Rayment et al., 1993a; Rayment et al., 1993b; Schroder et al., 1993), which allowed her to also place the mutations in the context of the 3D structure of the myosin. This was a tour de force made possible because of the properties *Dictyostelium* and, of course, the exceptional talents of Kathy Ruppel.

Young investigators looking for a model eukaryotic cell to explore their chosen biological process of interest should consider adopting *Dictyostelium* (Egelhoff et al., 1991; Egelhoff and Spudich, 1991). I know of no other cell that has many of the properties of mammalian cells, can be easily grown in large quantities for expressing proteins for biochemistry, and offers the opportunity to meld biochemical results with cellular behaviors utilizing homologous recombination. *Dictyostelium* could be the organism of choice for modern biochemists and biologists, comparable to *Escherichia coli*, which served the biochemistry community so well in earlier decades.

In the early days of my UCSF laboratory, I worked on identifying actin in *Dictyostelium* and showed that it is associated with the cell membrane. *Dictyostelium* is a highly phagocytic organism and readily engulfs polystyrene beads, turning the cell membrane inside out (Figure 2A). Actin filaments are polar, and this polarity can be visualized by decorating the actin filaments with myosin, which gives rise to an arrowheaded appearance every 36 nm along the filament. Thus, the actin filament has a barbed end and a pointed end. In muscle, myosin molecules move along each actin filament toward its barbed end (Huxley, 1963), which is anchored to the muscle Z-lines. Assuming actin filaments were similarly anchored to cell membranes at their barbed-ends, the phagocytized beads should have tufts of actin filaments emanating from them, which should move along a myosin-coated glass surface (Figure 2A). Thus, I enriched the phagocytized beads from cell lysates on a sucrose gradient and showed that they did indeed have actin filaments attached (Spudich and Clarke, 1974) (Figure 2B). When added to the myosin-coated slide, I observed some saltatory particle movements, meaning some phagocytic vesicles moved directionally over short distances! But these were rare and not quantifiable in a convincing way. The results, however, encouraged me to believe that it would be possible to observe actin moving along a myosin-coated surface when we understood more about the system, and when we found a good way to visualize the actin filaments.

In 1977 I was recruited to be the first faculty member to join the newly formed Department of Structural Biology at Stanford, headed by Lubert Stryer. In the next years we extensively characterized the actin-myosin system in *Dictyostelium*. Interestingly, inconsistent with Hugh Huxley's swinging cross bridge proposal (Huxley, 1969), Toshio Yanagida (Yanagida, 1981), using polarized fluorescence microscopy to measure the angles of fluorescent nucleotides bound to myosin heads during muscle contraction, and the laboratories of Roger Cooke and Dave Thomas, using labeling of a sulfhydryl group in the myosin head domain with electron paramagnetic resonance (EPR) probes (Cooke et al., 1982; Cooke et al., 1984; Cooke, 1986), showed that the entire head domain does not change orientation during the power stroke of the contractile interaction between myosin and actin. It was more imperative than ever to develop a quantitative *in vitro* motility system to test the various models under consideration. In new experiments, we created actin filament coated beads, reminiscent of the *Dictyostelium* phagocytized beads I explored earlier, by nucleating actin filament growth off polylysine-coated polystyrene

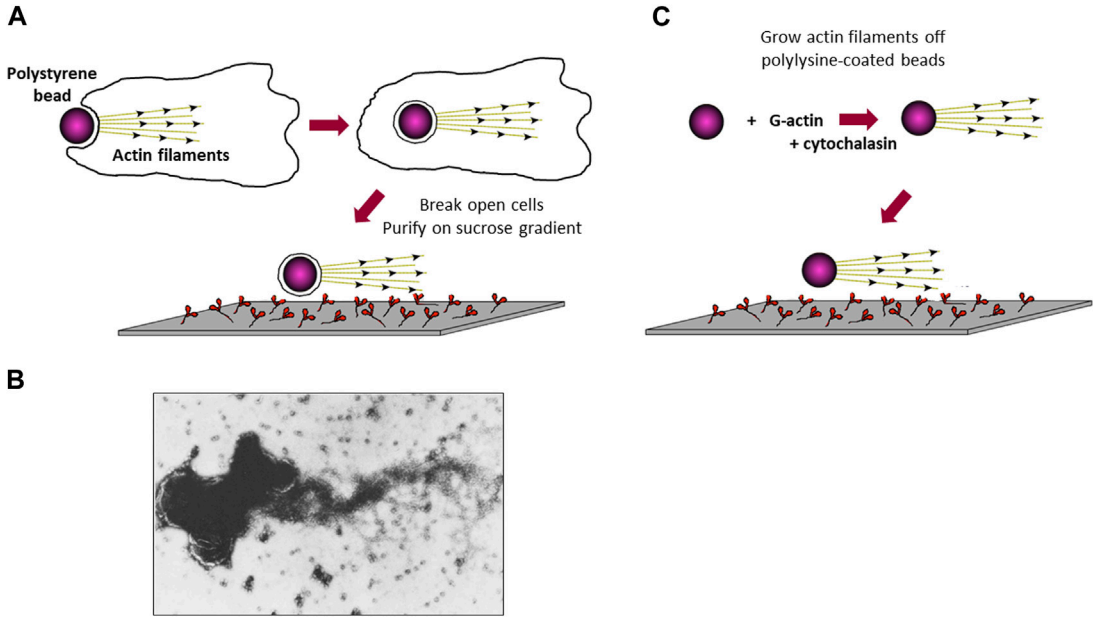

FIGURE 2
Attempts to visualize *in vitro* movement of actin-coated polystyrene beads along a myosin-coated glass slide. **(A)** Schematic drawing of a polystyrene bead being phagocytized by a *Dictyostelium* cell, followed by cell lysis and purification of the actin-coated polystyrene beads to test for movement on a myosin-coated slide. **(B)** Electron microscope image of a cluster of beads with a tuft of actin filaments projecting off its surface. The major protein in these preparations was shown biochemically to be actin (Spudich and Clarke, 1974). **(C)** Schematic drawing of actin grown off the surface of a polylysine-coated polystyrene bead, followed by testing for movement on a myosin-coated slide.

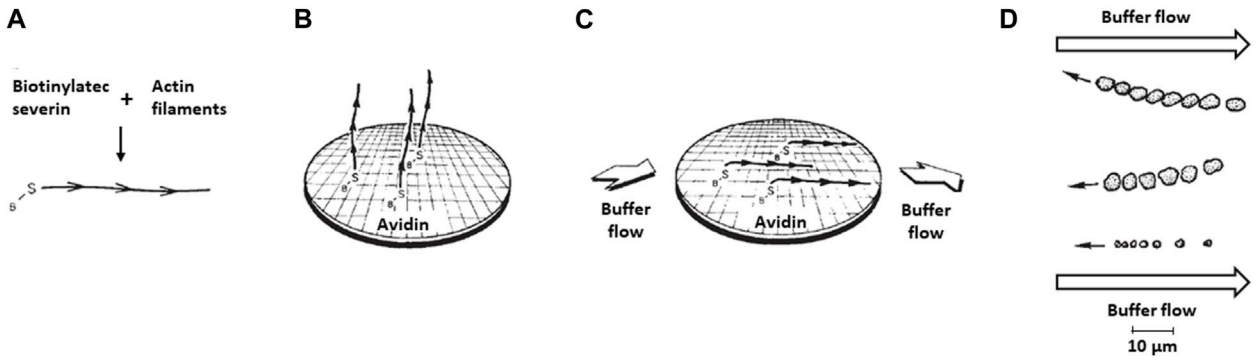

FIGURE 3
Movement of myosin-coated polystyrene beads on oriented actin filaments on a surface. **(A)** Biotinylated-severin is attached to the barbed-end of actin filaments. **(B)** The biotinylated severin bound actin filaments are attached to an avidin-bound surface. Depicted is a schematic drawing of an electron microscope grid placed on the glass slide before avidin coating to allow eventual examination by electron microscopy of the quality of the actin filament orientation after buffer flow across the slide. **(C)** Buffer flow across the slide orients the actin filaments. **(D)** Actual upstream movement observed of three different-sized clumps of myosin-coated beads along oriented actin filaments. The two larger bead aggregates were coated with D. d. myosin II and their positions are shown every 10 s, corresponding to a rate of movement of ~0.5 µm s^{-1}. The smaller bead aggregate was coated with skeletal muscle myosin and its position is shown every 2 s, corresponding to a rate of movement of ~2 µm s^{-1}. Figure adapted from (Spudich et al., 1985).

beads (Brown and Spudich, 1979). In the presence of cytochalasin D, which binds to the barbed-end of filaments and blocks actin monomer addition, actin filaments grow with their barbed-ends at the bead surface and pointed-ends projecting outward (Figure 2C). Unfortunately, these still did not show robust and convincing directed motion on myosin-coated surfaces.

So, we reversed the components and attempted to watch myosin-coated beads move along oriented actin filaments attached to a glass slide. In 1981, Susan Brown and Keichi Yamamoto, postdoctoral fellows in my laboratory, had identified and purified *Dictyostelium* severin (Brown et al., 1982; Yamamoto et al., 1982), a protein that severs actin filaments, but more importantly, tightly binds the barbed-ends of actin filaments and can be tagged with a small molecule, as shown by Rona Giffard and Alan Weeds in my lab (Giffard et al., 1984). The idea was to use biotinylated severin to attach actin filaments by their barbed ends to an avidin-coated slide (Figures 3A, B). *Remember, the first protein put*

down onto a clean glass surface will form a monolayer, in this case avidin, and so the actin filaments will not bind nonspecifically and only bind through the avidin-biotin link. Hence, biotinylated-severin bound to the barbed-end of actin filaments attach the actin filaments to the surface *via* their barbed-ends (Figure 3B), with the filaments being free to be oriented by buffer flow over the slide (Figure 3C). The actin filaments should then orient with the pointed-ends of the filaments downstream, and the myosin-coated beads should move upstream against the flow of the buffer. When we placed the myosin-coated beads on these actin-coated slides and added ATP we were disappointed to not see convincing robust directional movements. In retrospect, we did not have sufficient alignment of the actin filaments–we were not monitoring filament alignment at that time by electron microscopy, as we did later.

Then in 1982, Mike Sheetz joined my laboratory as a sabbatical visitor and was interested in improving the myosin-coated bead movement along severin-bound actin filaments oriented on a surface. It still was not working. This is when *Nitella* re-entered my lab. Since the early 1970s when we first explored *Nitella*, Yolanda Kersey, who was a student in Tom Pollard's laboratory interested in myosin in plants, came to Norm Wessells' laboratory in the Department of Biological Sciences at Stanford as a postdoctoral fellow to study the basis for motility in *Nitella*. Kersey and Wessels showed that actin cables in *Nitella* are well organized and continuous along the cytoplasmic face of organized chloroplast rows (Kersey and Wessells, 1976). Yolanda contacted me to get advice about using myosin to decorate the actin filaments to visualize their orientation. I happily supplied her with the myosin fragment HMM and advised her on the best conditions to use it to decorate the actin. Using HMM binding, Yolanda showed that the actin cables (filaments) are oriented in the direction consistent with the observed direction of movement of presumed myosin-coated vesicular elements (cytoplasmic streaming), the direction expected if a conventional myosin was involved (Kersey et al., 1976). Yolanda's experiments were pivotal for what happened next in my laboratory.

At one late-night session at the laboratory with Mike, I suggested that we get some *Nitella*, the cylindrical cells of which can be a centimeter long and sufficiently wide to cut open longitudinally with iridectomy scissors. The cut open cell could then be pinned down by its four corners so that the oriented actin cables would be exposed. Furthermore, the right person to show us how to do this was a fellow faculty member in the Department of Structural Biology, Peter Sargent. Peter is a neurobiologist who was performing such surgical operations on similar-sized nerve axons. Peter showed Mike how to cut open the *Nitella*, Mike added the myosin-coated beads, and they moved steadily and unidirectionally along chloroplast rows in the very first experiment (Sheetz and Spudich, 1983)! The myosin coating the beads prevented the beads from binding other proteins, such as the actin cables themselves, and so they were free to move along the oriented actin filaments without a load. Peter Sargent's help with *Nitella* was a key step in this pivotal experiment.

Mike then left my laboratory for Woods Hole with Eric Shooter's graduate student Ron Vale to see if they could see myosin-coated beads move along tracks in squid axons. Together with Bruce Schnapp and Tom Reese, Ron and Mike found that myosin was not involved in this movement, as they originally assumed, and discovered and purified a new microtubule-based molecular motor which Ron named kinesin (Vale et al., 1985a; Vale et al., 1985b). Their discoveries depended on the principle that the first protein that a glass slide or polystyrene bead encounters forms a monolayer of that protein on the surface, which then keeps the surface from non-specifically binding to other proteins. Their discovery of kinesin energized the field and opened years of exciting work from their laboratories and many others.

Meanwhile, at Stanford I was working to eliminate the vagaries of the complex *Nitella* substratum and establish a totally-defined *in vitro* motility assay for myosin moving on actin–one must reconstitute the functions of interest from purified proteins. The *Nitella* experiment showed that the myosin-coated beads were functional and the actin filament orientation in our severin-based assay was undoubtedly the problem. I returned to the severin-based assay to try to get better orientation of the actin filaments, now using the electron microscope to judge orientation, and the expected upstream movement could now be clearly seen (Figure 3D).

Then, in January 1984, Steve Kron joined my laboratory as a graduate student, and his first task was to optimize this assay. With Steve's prior bioengineering expertise in fluid mechanics and viscometry, we got good movement of myosin-coated beads on oriented actin filaments (Spudich et al., 1985), the first myosin movement assay with purified proteins. Importantly, this assay established that one can achieve several $\mu m\ s^{-1}$ velocity, approaching the velocity of contraction of unloaded muscle contraction, with nothing more than purified actin, myosin, and ATP. The assay, however, was too complicated to be used widely.

A pivotal observation by Toshio Yanagida led Steve Kron to develop the assay that became standard in the field

In 1984, Toshio Yanagida and his students reported the seminal finding that one can visualize individual actin filaments labeled with rhodamine-phalloidin by fluorescence microscopy (Yanagida et al., 1984). This was fantastic because it allowed us to return to the myosin-coated surface concept that we had tried earlier, but now we could see the actin filaments directly by fluorescence microscopy! In Toshio's 1984 paper (Yanagida et al., 1984), he and his students demonstrated effects on the Brownian motion of actin filaments in solution when myosin and ATP were added, an assay for monitoring actin-myosin interactions, but not an assay for making velocity measurements.

Determined to find an assay that was easier than the myosin-coated bead assay, Steve Kron coated a glass slide with purified skeletal myosin thick filaments and then rinsed the slide with BSA to make sure any remaining nascent surface area was saturated with protein. He then added fluorescently labeled actin filaments and ATP. The experiment worked the first time (Kron and Spudich, 1986) (Figures 4A, B), and the rest is history. Since the surface was covered with myosin plus BSA, the actin was free to move along the myosin-coated surface without showing non-specific binding to the surface. The Kron assay is so simple and so robust, that it has naturally assumed a prominent position in actin-myosin biology and muscle contraction work throughout the world. Steve's experiment has been said to be transformative in the field of muscle and actin-myosin-based nonmuscle motility (Rall, 2014), the type of accolade every PhD student and scientific advisor welcomes.

The power of having developed a quantitative assay with purified proteins for the function of interest, movement in this

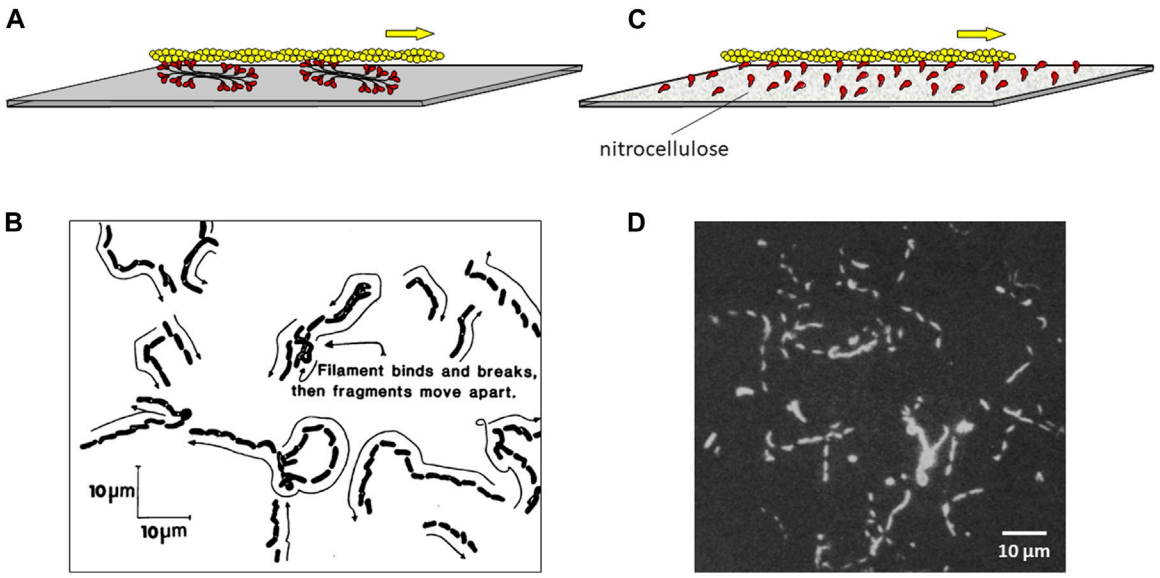

FIGURE 4
Movement of fluorescent actin filaments on a myosin-coated surface. **(A)** Schematic drawing of an actin filament (yellow) moving across a lawn of myosin bipolar thick filaments (red) coating a microscope slide. **(B)** Actual trajectories of actin filaments moving on myosin filaments as diagrammed in **(A)**. Skeletal muscle actin filaments moved on skeletal muscle myosin attached to the slide over 38 s. Their positions are indicated at successive short intervals as they appeared on the video monitor. The average rate of movement in multiple experiments was ~3 μm s^{-1}. Figure reproduced from (Kron and Spudich, 1986). **(C)** Schematic drawing of an actin filament (yellow) moving across a lawn of purified S1 myosin heads (red) coating a microscope slide, which was pretreated with nitrocellulose. **(D)** Stroboscopic photograph of movement of fluorescent actin filaments moving on papain derived skeletal muscle S1. A photographic shutter was used to illuminate the filaments for 1 s every 4 s for a total of 12 s. The scale bar is 10 μm. Thus the average rate of movement was ~1–2 μm s^{-1}. Figure reproduced from (Toyoshima et al., 1987).

case, was made immediately obvious by my postdoctoral fellow Yoko Toyoshima, who together with Steve Kron, Elizabeth McNally, and others in my laboratory showed that the globular head, or subfragment 1 (S1), of myosin is the motor domain (Toyoshima et al., 1987). In these experiments, Yoko tried saturating the slide surface with a variety of reagents before adding the S1 because adding the S1 directly to the clean slide did not work well, presumably because the S1 bound to the clean glass in an orientation that was not favorable for actin interaction. This was not a problem for the myosin thick filaments bound to the slide, because the structure of the thick filament assures there is always an array of myosin heads oriented away from the slide and able to interact with actin (Figure 4A). Nitrocellulose solved the S1 problem (Figures 4C,D). Something about adding the S1 to a nitrocellulose-coated slide allowed a sufficient number of S1 molecules to be oriented properly to drive actin filament movement smoothly across the surface for prolonged periods. This result eliminated competing theories to the swinging cross-bridge hypothesis and focused research on the S1 head to understand how the myosin family of molecular motors works. Almost 2 decades of work finally led us to the early goals I had set for my lab in the early 1970s.

But what about force, the other function of interest that needed to be reconstituted from purified proteins?

With the Kron assay solving the need for a robust and simple *in vitro* assay for measuring the velocity of movement of myosin along actin, the next step was to find a way to measure the force that myosin molecules produce when they interact with actin in a totally reconstituted purified protein system. This was first accomplished in 1988 by Toshio Yanagida and his students, who developed a technique for manipulating a single actin filament using a fine glass needle to measure and exert force on it by a small number of myosin molecules (Kishino and Yanagida, 1988). They extended this technique and measured displacements and forces with nanometer and piconewton resolutions in the millisecond time range (Ishijima et al., 1991). Details of this glass needle approach was described in 1996 (Ishijima et al., 1996). However, it was imperative to clearly visualize what a single myosin molecule does when it interacts with actin because of disagreements at the time about how far myosin moves along actin upon hydrolyzing one ATP molecule (the step size). Experiments from Toshio's laboratory reported the step size to be > 40 nm (Yanagida et al., 1993; Saito et al., 1994). This number would rule out the conventional swinging cross bridge model of muscle contraction, whereas our experiments had suggested a smaller step size of about 10 nm, which was compatible with the swinging cross bridge model (Toyoshima et al., 1990; Uyeda et al., 1990; Uyeda et al., 1991). Toshio and I debated about these results at scientific meetings and in published papers for more than a decade during the years 1980–1995, while maintaining a close friendship and respect for one another. In the early 1990s we agreed, over a glass of wine, that what was needed was to watch what a single myosin molecule does when it interacts with a single actin filament. Steve Kron played an important role in the next step for my laboratory.

My colleague Gil Chu, in the Department of Biochemistry, imagined that Steve Kron in my lab might be interested in

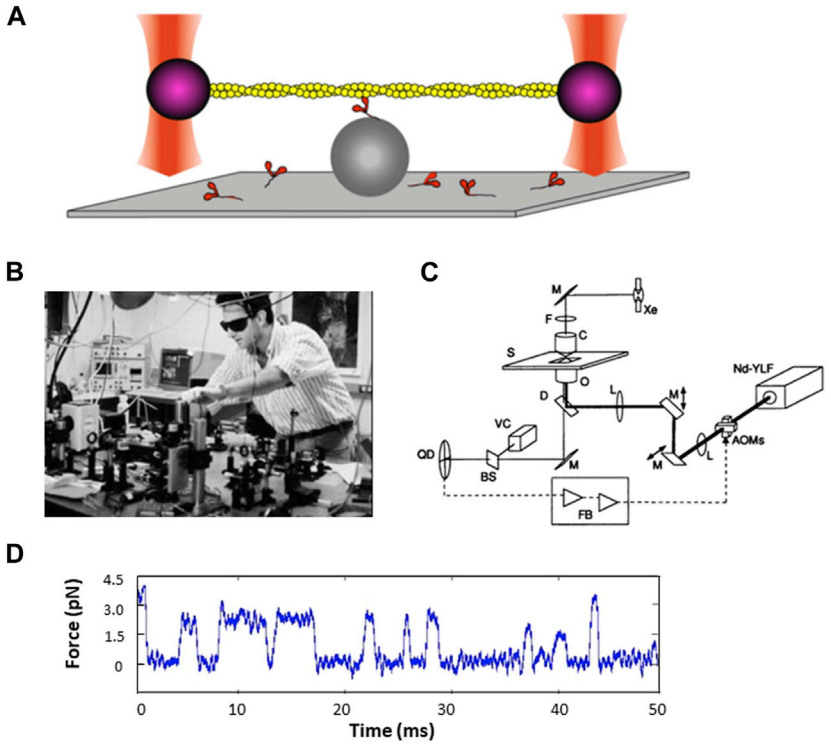

FIGURE 5
Force measurements using the dual beam laser trap. **(A)** Schematic drawing of a single fluorescent actin filament (yellow) with a 1-μm polystyrene bead (purple) attached at each end of the actin filament, with each bead being held by an independently controlled laser trap (red). The filament is lowered onto another polystyrene bead (grey) fixed to a microscope slide, with a single myosin molecule on top. **(B)** Photograph of Jeff Finer building the dual beam laser trap in the Beckman building basement. Reproduced by permission. **(C)** Schematic diagram of the feedback-enhanced laser trap system. The thick solid line represents the laser beam path; the thin solid line represents the imaging path. Brightfield illumination from a xenon arc lamp (Xe) is used for visualizing the sample with a video camera (VC) and used to project an image of a trapped bead in the specimen plane (S) onto a quadrant photodetector (QD). Two orthogonal acousto-optic modulators (AOMs) are used for rapidly deflecting the laser beam before it enters the back aperture of the microscope objective (0). Additional optics include lenses (L), mirrors (M), dichroic filter (D), interference filter (F), beamsplitter (BS), and microscope condenser (C). The second trapping beam and fluorescence imaging pathways are not shown for simplicity. The quadrant detector output (dashed line) can be processed by feedback electronics (FB) and used to drive the acousto-optic modulators. Figure reproduced from (Finer et al., 1995).[1] **(D)** Sample trace of force transients as a function of time.

helping his brother, Steve Chu, who hoped to exploit optical traps to manipulate biological molecules. Steve Chu had recently arrived at Stanford from Bell Labs where he completed his work on cooling and trapping atoms for which he later received the Nobel Prize. He was excited to take on new challenges. Steve Kron and Steve Chu found time to work together in the evenings and learned to image single DNA molecules held in flow by optically trapping beads tethered to the ends. This was Steve Chu's entree to molecular biology and his initial connection to my laboratory.

A new graduate student in my lab, Jeff Finer, and a sabbatical visitor, Bob Simmons, a well-known British investigator with extensive experience in developing specialized equipment with feedback systems for measuring force transients in muscle fibers, wanted to adapt the Kron *in vitro* motility assay to the single molecule level. Jeff, Bob, and I wanted to develop a laser trap for trapping a single bead attached to the barbed-end of an actin filament and have the filament be acted upon by a single myosin molecule on a surface, a modification of the Kron motility assay. Jeff and Bob tried several different geometries with different ways to raise myosin molecules above the surface, such as engineered surfaces with ridges, but nothing was working. Then one night Jeff had a dream in which a dumbbell consisting of a single actin filament with a polystyrene bead attached at each end, each bead being trapped by its own laser beam, was lowered onto a single myosin molecule raised off the glass slide by another bead fixed to the surface (Figure 5A).

With Steve Chu's help, Jeff and Bob built the first dual beam laser trap in Steve's space in the Department of Physics in the Varian building, using a Zeiss microscope as its base. They started with a single-beam gradient optical trap with a high-resolution photodiode position detector to show that an optical trap can be used to make quantitative measurements of nanometer displacements and piconewton forces with millisecond resolution (Simmons et al., 1993; Simmons et al., 1996). For the dual beam trap, they started with a quadrant detector (QD) to look for possible myosin-driven movement of actin attached to a bead at each end, and then, at Steve Chu's suggestion, they added acousto-optic modulators (AOMs) to bring feedback into the system. They also added motors to move one

1 This article was published in Biophys. J., Vol. 68 (4 Suppl. I), Finer, J. T., Mehta, A. D., and Spudich, J. A., Characterization of single actinmyosin interactions, 291S–297S, Copyright Elsevier (1995).

of the beams to eliminate having to move knobs for the mirrors and the stage. But that trap was on an upper floor of the Varian building and there was too much vibrational noise for the measurements we wanted to make with our actin-myosin system, so Jeff built another dual-beam trap in the basement of the Beckman building, on solid ground and just downstairs from my laboratory. Bob had returned to England but continued to help from afar. Jeff made several pivotal changes to the new dual-beam trap in Beckman, including getting rid of a microscope base and switching to a custom-made open optics system where he had better control over all the parts, and adding more motors to control the traps and the stage, which dramatically increased the efficiency of catching actin filaments (Figures 5B, C). He also improved nearly every other component including a laser that did not need a lot of water cooling. Even so, there was still too much noise to pick up the step size or force measurements produced by a single myosin molecule.

An obvious issue was the airflow in the room, and one day I suggested to Jeff that he buy enough posterboard to cut and tape together to cover all the optics to isolate the path of the laser beam from the general room airflow. This worked! The twenty dollars' worth of posterboard added to the $100,000 instrument Jeff had built allowed us to see individual force and step size transients generated by a single myosin molecule interacting with a single actin filament. That trap gave us the first convincing step size and force traces that allowed us to conclude that a single myosin molecule produces force in the single digit pN range and displaces an actin filament by about 10 nm for each interaction (Finer et al., 1994) (Figure 5D). Justin Molloy was an early important contributor in this area and described an analysis method that suggested a somewhat shorter step size of about 4 nm (Molloy et al., 1995). Together with Claudia Veigel, as well as independently, Justin and Claudia have made numerous important contributions toward developing single molecule laser trap methodology and understanding how myosin motors work (for reviews, see (Knight et al., 2001; Ruegg et al., 2002; Ruegg et al., 2002; Molloy and Veigel, 2003; Veigel and Schmidt, 2011; Batters and Veigel, 2016)).

This was the time that Amit Mehta, a graduate student in the Physics Department, joined my laboratory. Over the years, I have hosted several Physics graduate students in my laboratory. They carried out their PhD work in my lab and got their degrees from the Department of Physics. Amit, like all the others, was an outstanding student, brought his strong physics background to our effort, and helped us understand the strengths and limitations of our trap measurements (Mehta et al., 1998a; Mehta et al., 1998b). He also contributed new insights such as the ability to detect single-molecule interactions using correlated thermal diffusion (Mehta et al., 1997).

Meanwhile, Steve Chu's students were carrying out single molecule analyses of fluorescently labeled DNA (Perkins et al., 1994a; Perkins et al. 1994b; Perkins et al., 1995; Smith et al., 1995; Perkins et al., 1997). Just as Jeff Finer and Bob Simmons from my lab spent months working in Steve Chu's lab to build the first dual beam trap, four of Steve's physics students spent more than a year working in space in my lab in Beckman generally soaking up biochemistry and molecular biology principles and specifically learning how to prepare DNA, ligate λ-phage DNA molecules together to make sufficiently long DNA molecules for their biophysical studies, and biotinylate one end of the DNA molecule and attach it to a streptavidin-coated polystyrene sphere to be manipulated in an optical trap. These students included Steve Quake, Tom Perkins, and Doug Smith, all of whom went on to establish careers interfacing physics and biology. What made my collaboration with Steve Chu so powerful was that our students spent considerable time in each other's environments, and this led to the interdisciplinary program in biosciences, bioengineering, and biomedicine at Stanford called Bio-X (https://biox.stanford.edu/; for early history, see Supplementary Information).

Another key founder of single molecule measurements was my former postdoctoral fellow Steve Block (note there are many Steves in this story!). After contributing importantly to domains of myosin involved in force production in my lab (Hynes et al., 1987), in 1987 Steve left for his first independent position as a staff scientist at the Rowland Institute in Cambridge, MA and a Lecturer at Harvard. There he began developing a single beam laser trap for measuring the step size of the processive kinesin molecule (Block et al., 1990). Mike Sheetz and Scot Kuo at Duke University also developed a single beam laser trap and reported force measurements by a single kinesin molecule (Kuo and Sheetz, 1993). The trap that Steve Block and his colleagues described in their 1993 Svoboda et al. paper (Svoboda et al., 1993) was groundbreaking, with precise and accurate measurements of 8-nm steps of kinesin along a microtubule. Later, at Stanford, Steve and his colleagues took single molecule mechanics to an incredibly high level of resolution and precision and applied it not only to kinesin but to RNA polymerase as well (Shaevitz et al., 2003; Abbondanzieri et al., 2005; Greenleaf and Block, 2006; Block, 2007; Guydosh and Block, 2007; Herbert et al., 2008; Clancy et al., 2011; Andreasson et al., 2015).

In 2015, Jongmin Sung along with others in my lab developed the technique of harmonic force spectroscopy (HFS) using the dual beam trap (Sung et al., 2015; Sung et al., 2017). This method measures the force dependence of myosin interactions with actin by oscillating the stage during their attachment. HFS has the advantage that the force is applied to the myosin rapidly and no feedback loops are required. This approach has proved very useful. For example, Chao Liu in my lab led experiments using HFS to measure the detachment rate of single molecules of human β-cardiac myosin and its load dependence, and showed that both can be modulated by small-molecule compounds and cardiomyopathy-causing mutations (Liu et al., 2018).

In summary, Steve Block's single beam rendition of laser traps and our dual beam trap approach for single molecule analyses have been adopted worldwide, and a new field of single molecule analysis has flourished and contributed to many new discoveries. We and others have used the dual-beam laser trap to study multiple myosin motors (for reviews, see, for example, (Mehta et al., 1999a; Rocket al. 2000; Warshaw, 2004; Dantzig et al., 2006; Sun and Goldman, 2011; Karagiannis et al., 2014; Greenberg et al., 2017). It was using the dual beam laser trap that allowed us, for example, to show that myosin V and myosin VI are processive motors (Mehta et al., 1999b; Rief et al., 2000; Rock et al., 2001) and to examine details of how they step along actin (Purcell et al., 2002; Liao et al., 2009; Dunn et al., 2010; Elting et al., 2011). Taro Uyeda, Alex Dunn, and Zev Bryant were key postdoctoral fellows who used the Kron *in vitro* motility assay, the dual beam laser trap, and other single molecule approaches to provide conclusive evidence for the swinging lever arm mechanism for myosin-based movement (Uyeda et al., 1996; Bryant et al., 2007; Dunn and Spudich, 2007).

Particularly powerful is combining the *in vitro* motility assay with laser-trap measurements to reveal mechanisms of myosin stepping. An

example is Myosin VI, which was the biggest challenge to the lever-arm hypothesis. This unusual myosin takes very long (~36-nm) steps (Yanagida and Iwane, 2000; Rock et al., 2001) despite having a very short light-chain-binding domain which in other myosins almost certainly acts as a lever arm to amplify mechanical movement. By mapping the step sizes using the laser trap and the velocities and direction of movement of four different constructs of myosin VI (Bryant et al., 2007) onto the known poststroke structure of the motor (Menetrey et al., 2005), it became clear that myosin VI does indeed conform to the swinging lever arm hypothesis. In this case, the lever arm strokes through an angle of ~180° to give rise to a large mechanical stroke of ~20 nm. The remaining ~16 nm derives from diffusion of the free head in search of an appropriate actin-binding site. These results drove home the power of the *in vitro* motility assay and single-molecule analysis to reveal detailed structural information about functionally important mechanical transitions in proteins and solidified the swinging-lever-arm hypothesis as a general mechanism used by the myosin family.

The *in vitro* motility and dual beam laser trap assays also proved fundamental for understanding the molecular basis of hypercontractility in individuals having hypertrophic cardiomyopathy (HCM), a genetic disease often caused by mutations in human β-cardiac myosin, the molecular motor that drives systolic heart contraction. A key collaborator in my laboratory in these studies is Kathy Ruppel, and Suman Nag, Darshan Trivedi, and Masataka Kawana have played major roles (Nag et al., 2017; Trivedi et al., 2018; Trivedi et al. 2020; Trivedi et al. 2020; Kawana et al., 2022). Other key collaborators in our HCM studies are Leslie Leinwand, University of Colorado, Anne Houdusse, the Curie Institute, and Dan Bernstein and Euan Ashley, Stanford University School of Medicine. HCM hypercontractility primarily derives from a mutation-induced increase in the number of myosin heads accessible for interaction with actin (Spudich, 2015). This understanding led to the development of a first-in-class drug, mavacamten, which is an inhibitor of human β-cardiac myosin (Anderson et al., 2018; Rohde et al., 2018). Mavacamten normalizes the power output of HCM patients by reducing the number of myosin heads accessible for interaction with actin, simply reversing the effect of the HCM mutations.

Conclusion

The *in vitro* motility and dual beam laser trap assays, as well as other related techniques (Churchman et al., 2005; Churchman et al., 2006; Dunn and Spudich, 2007; Mortensen et al., 2015), which were developed by talented students, postdoctoral fellows, and sabbatical visitors in my laboratory over the years, were based on the 'mantra' drilled into me in my graduate student days, "*one must reconstitute the functions of interest from purified proteins.*" These assays have been fundamental to the work on myosin molecular motors from my laboratory and many others in the field. As emphasized in this article, all discoveries depend on a cast of individuals over a long period of time. Such is the nature of scientific discoveries, as well as of other areas of creative endeavors. I thank the editors for giving me the chance to acknowledge those who played important roles in prominent discoveries that came from my laboratory in the latter part of the 20th and early part of the 21st centuries.

Author contributions

JS: Writing–original draft, Writing–review and editing.

Funding

The author(s) declare financial support was received for the research, authorship, and/or publication of this article. This work was funded by grant NIH R01GM33289 (JS).

Acknowledgments

Discoveries in science are a community enterprise involving scores of investigators making pivotal contributions along the way. I apologize to those who contributed to the breakthroughs we made on the workings of molecular motors but are not mentioned due to the limitations of the length of this brief review. I thank all the members of my laboratory over these many years, with whom I have shared the joys of discovery. I also thank Steve Kron, Steve Quake, Jeff Finer, and Amit Mehta for discussions and suggested edits, as well as the reviewers for helpful suggestions, especially my biochemistry of the cytoskeleton comrade of the last 50 years Tom Pollard, who has always known the importance of reconstitution of the functions of interest from purified proteins. Thanks also to Ray Stephens for enormous help in tracking down the names of the professors, assistants, and students in the 1963 photo of the participants in the 1963 Woods Hole Physiology Course. And special thanks to Annamma (Anna) Spudich (formerly Annamma Cownan, see Figure 1) for her extensive editing and important contributions and support at many levels throughout the decades of research encompassed in this article.

Conflict of interest

JS is a co-founder and consultant for Cytokinetics Inc and owns stock in the company, which has a focus on therapeutic treatments for cardiomyopathies and other muscle diseases.

Publisher's note

Supplementary material

The Supplementary Material for this article can be found online at: https://www.frontiersin.org/articles/10.3389/fphys.2024.1390186/full#supplementary-material

References

Abbondanzieri, E. A., Greenleaf, W. J., Shaevitz, J. W., Landick, R., and Block, S. M. (2005). Direct observation of base-pair stepping by RNA polymerase. *Nature* 438 (7067), 460–465. doi:10.1038/nature04268

Adelman, M. R., and Taylor, E. W. (1969a). Isolation of an actomyosin-like protein complex from slime mold plasmodium and the separation of the complex into actin- and myosin-like fractions. *Biochemistry* 8 (12), 4964–4975. doi:10.1021/bi00840a046

Adelman, M. R., and Taylor, E. W. (1969b). Further purification and characterization of slime mold myosin and slime mold actin. *Biochemistry* 8 (12), 4976–4988. doi:10.1021/bi00840a047

Anderson, R. L., Trivedi, D. V., Sarkar, S. S., Henze, M., Ma, W., Gong, H., et al. (2018). Deciphering the super relaxed state of human β-cardiac myosin and the mode of action of mavacamten from myosin molecules to muscle fibers. *Proc. Natl. Acad. Sci. U. S. A.* 115 (35), E8143–E8152. doi:10.1073/pnas.1809540115

Andreasson, J. O., Shastry, S., Hancock, W. O., and Block, S. M. (2015). The mechanochemical cycle of mammalian kinesin-2 KIF3A/B under load. *Curr. Biol.* 25 (9), 1166–1175. doi:10.1016/j.cub.2015.03.013

Batters, C., and Veigel, C. (2016). Mechanics and activation of unconventional myosins. *Traffic* 17 (8), 860–871. doi:10.1111/tra.12400

Block, S. M. (2007). Kinesin motor mechanics: binding, stepping, tracking, gating, and limping. *Biophys. J.* 92 (9), 2986–2995. doi:10.1529/biophysj.106.100677

Block, S. M., Goldstein, L. S., and Schnapp, B. J. (1990). Bead movement by single kinesin molecules studied with optical tweezers. *Nature* 348 (6299), 348–352. doi:10.1038/348348a0

Brown, S., Levinson, W., and Spudich, J. A. (1976). Cytoskeletal elements of chick embryo fibroblasts revealed by detergent extraction. *J. Supramol. Struct.* 5 (2), 119–130. doi:10.1002/jss.400050203

Brown, S. S., and Spudich, J. A. (1979). Nucleation of polar actin filament assembly by a positively charged surface. *J. Cell Biol.* 80 (2), 499–504. doi:10.1083/jcb.80.2.499

Brown, S. S., Yamamoto, K., and Spudich, J. A. (1982). A 40,000-dalton protein from *Dictyostelium discoideum* affects assembly properties of actin in a Ca2+-dependent manner. *J. Cell Biol.* 93 (1), 205–210. doi:10.1083/jcb.93.1.205

Bryant, Z., Altman, D., and Spudich, J. A. (2007). The power stroke of myosin VI and the basis of reverse directionality. *Proc. Natl. Acad. Sci. U. S. A.* 104 (3), 772–777. doi:10.1073/pnas.0610144104

Churchman, L. S., Flyvbjerg, H., and Spudich, J. A. (2006). A non-Gaussian distribution quantifies distances measured with fluorescence localization techniques. *Biophys. J.* 90 (2), 668–671. doi:10.1529/biophysj.105.065599

Churchman, L. S., Okten, Z., Rock, R. S., Dawson, J. F., and Spudich, J. A. (2005). Single molecule high-resolution colocalization of Cy3 and Cy5 attached to macromolecules measures intramolecular distances through time. *Proc. Natl. Acad. Sci. U. S. A.* 102 (5), 1419–1423. doi:10.1073/pnas.0409487102

Clancy, B. E., Behnke-Parks, W. M., Andreasson, J. O., Rosenfeld, S. S., and Block, S. M. (2011). A universal pathway for kinesin stepping. *Nat. Struct. Mol. Biol.* 18 (9), 1020–1027. doi:10.1038/nsmb.2104

Clarke, M., and Spudich, J. A. (1974). Biochemical and structural studies of actomyosin-like proteins from non-muscle cells. Isolation and characterization of myosin from amoebae of *Dictyostelium discoideum*. *J. Mol. Biol.* 86 (2), 209–222. doi:10.1016/0022-2836(74)90013-8

Cooke, R. (1986). The mechanism of muscle contraction. *CRC Crit. Rev. Biochem.* 21 (1), 53–118. doi:10.3109/10409238609113609

Cooke, R., Crowder, M. S., and Thomas, D. D. (1982). Orientation of spin labels attached to cross-bridges in contracting muscle fibres. *Nature* 300 (5894), 776–778. doi:10.1038/300776a0

Cooke, R., Crowder, M. S., Wendt, C. H., Barnett, V. A., and Thomas, D. D. (1984). Muscle cross-bridges: do they rotate? *Adv. Exp. Med. Biol.* 170, 413–427. doi:10.1007/978-1-4684-4703-3_37

Dantzig, J. A., Liu, T. Y., and Goldman, Y. E. (2006). Functional studies of individual myosin molecules. *Ann. N. Y. Acad. Sci.* 1080, 1–18. doi:10.1196/annals.1380.002

De Lozanne, A., and Spudich, J. A. (1987). Disruption of the Dictyostelium myosin heavy chain gene by homologous recombination. *Science* 236 (4805), 1086–1091. doi:10.1126/science.3576222

De Rosier, D. J., and Klug, A. (1968). Reconstruction of three dimensional structures from electron micrographs. *Nature* 217 (5124), 130–134. doi:10.1038/217130a0

Dunn, A. R., Chuan, P., Bryant, Z., and Spudich, J. A. (2010). Contribution of the myosin VI tail domain to processive stepping and intramolecular tension sensing. *Proc. Natl. Acad. Sci. U. S. A.* 107 (17), 7746–7750. doi:10.1073/pnas.1002430107

Dunn, A. R., and Spudich, J. A. (2007). Dynamics of the unbound head during myosin V processive translocation. *Nat. Struct. Mol. Biol.* 14 (3), 246–248. doi:10.1038/nsmb1206

Egelhoff, T. T., Lee, R. J., and Spudich, J. A. (1993). Dictyostelium myosin heavy chain phosphorylation sites regulate myosin filament assembly and localization *in vivo*. *Cell* 75 (2), 363–371. doi:10.1016/0092-8674(93)80077-r

Egelhoff, T. T., Manstein, D. J., and Spudich, J. A. (1990). Complementation of myosin null mutants in *Dictyostelium discoideum* by direct functional selection. *Dev. Biol.* 137 (2), 359–367. doi:10.1016/0012-1606(90)90260-p

Egelhoff, T. T., and Spudich, J. A. (1991). Molecular genetics of cell migration: Dictyostelium as a model system. *Trends Genet.* 7 (5), 161–166. doi:10.1016/0168-9525(91)90380-9

Egelhoff, T. T., Titus, M. A., Manstein, D. J., Ruppel, K. M., and Spudich, J. A. (1991). Molecular genetic tools for study of the cytoskeleton in Dictyostelium. *Methods Enzymol.* 196, 319–334. doi:10.1016/0076-6879(91)96029-q

Elting, M. W., Bryant, Z., Liao, J. C., and Spudich, J. A. (2011). Detailed tuning of structure and intramolecular communication are dispensable for processive motion of myosin VI. *Biophys. J.* 100 (2), 430–439. doi:10.1016/j.bpj.2010.11.045

Finer, J. T., Mehta, A. D., and Spudich, J. A. (1995). Characterization of single actin-myosin interactions. *Biophys. J.* 68 (4 Suppl. l), 291S–297S.

Finer, J. T., Simmons, R. M., and Spudich, J. A. (1994). Single myosin molecule mechanics: piconewton forces and nanometre steps. *Nature* 368 (6467), 113–119. doi:10.1038/368113a0

Frixione, E. (2000). Recurring views on the structure and function of the cytoskeleton: a 300-year epic. *Cell Motil. Cytoskelet.* 46 (2), 73–94. doi:10.1002/1097-0169(200006)46:2<73::AID-CM1>3.0.CO;2-0

Giffard, R. G., Weeds, A. G., and Spudich, J. A. (1984). Ca2+-dependent binding of severin to actin: a one-to-one complex is formed. *J. Cell Biol.* 98 (5), 1796–1803. doi:10.1083/jcb.98.5.1796

Greenberg, M. J., Shuman, H., and Ostap, E. M. (2017). Measuring the kinetic and mechanical properties of non-processive myosins using optical tweezers. *Methods Mol. Biol.* 1486, 483–509. doi:10.1007/978-1-4939-6421-5_19

Greenleaf, W. J., and Block, S. M. (2006). Single-molecule, motion-based DNA sequencing using RNA polymerase. *Science* 313 (5788), 801. doi:10.1126/science.1130105

Guydosh, N. R., and Block, S. M. (2007). Not so lame after all: kinesin still walks with a hobbled head. *J. Gen. Physiol.* 130 (5), 441–444. doi:10.1085/jgp.200709902

Hammer, J. A., and Jung, G. (1996). The sequence of the dictyostelium myo J heavy chain gene predicts a novel, dimeric, unconventional myosin with a heavy chain molecular mass of 258 kDa. *J. Biol. Chem.* 271 (12), 7120–7127. doi:10.1074/jbc.271.12.7120

Hatano, S., and Tazawa, M. (1968). Isolation, purification and characterization of byosin B from myxomycete plasmodium. *Biochim. Biophys. Acta* 154 (3), 507–519. doi:10.1016/0005-2795(68)90011-1

Herbert, K. M., Greenleaf, W. J., and Block, S. M. (2008). Single-molecule studies of RNA polymerase: motoring along. *Annu. Rev. Biochem.* 77, 149–176. doi:10.1146/annurev.biochem.77.073106.100741

Huxley, H. E. (1963). Electron microscope studies on the structure of natural and synthetic protein filaments from striated muscle. *J. Mol. Biol.* 7, 281–308. doi:10.1016/s0022-2836(63)80008-x

Huxley, H. E. (1969). The mechanism of muscular contraction. *Science* 164 (3886), 1356–1365. doi:10.1126/science.164.3886.1356

Huxley, H. E. (1972). Structural changes in the actin- and myosin-eontaining filaments during contraction. *Cold Spring Harb. Symp. Quant. Biol.* 37, 361–376. doi:10.1101/sqb.1973.037.01.046

Hynes, T. R., Block, S. M., White, B. T., and Spudich, J. A. (1987). Movement of myosin fragments *in vitro*: domains involved in force production. *Cell* 48 (6), 953–963. doi:10.1016/0092-8674(87)90704-5

Ishijima, A., Doi, T., Sakurada, K., and Yanagida, T. (1991). Sub-piconewton force fluctuations of actomyosin *in vitro*. *Nature* 352 (6333), 301–306. doi:10.1038/352301a0

Ishijima, A., Kojima, H., Higuchi, H., Harada, Y., Funatsu, T., and Yanagida, T. (1996). Multiple- and single-molecule analysis of the actomyosin motor by nanometer-piconewton manipulation with a microneedle: unitary steps and forces. *Biophys. J.* 70 (1), 383–400. doi:10.1016/S0006-3495(96)79582-6

Ishikawa, H., Bischoff, R., and Holtzer, H. (1969). Formation of arrowhead complexes with heavy meromyosin in a variety of cell types. *J. Cell Biol.* 43 (2), 312–328. doi:10.1083/jcb.43.2.312

Karagiannis, P., Ishii, Y., and Yanagida, T. (2014). Molecular machines like myosin use randomness to behave predictably. *Chem. Rev.* 114 (6), 3318–3334. doi:10.1021/cr400344n

Kawana, M., Spudich, J. A., and Ruppel, K. M. (2022). Hypertrophic cardiomyopathy: mutations to mechanisms to therapies. *Front. Physiol.* 13, 975076. doi:10.3389/fphys.2022.975076

Kersey, Y. M., Hepler, P. K., Palevitz, B. A., and Wessells, N. K. (1976). Polarity of actin filaments in Characean algae. *Proc. Natl. Acad. Sci. U. S. A.* 73 (1), 165–167. doi:10.1073/pnas.73.1.165

Kersey, Y. M., and Wessells, N. K. (1976). Localization of actin filaments in internodal cells of characean algae. A scanning and transmission electron microscope study. *J. Cell Biol.* 68 (2), 264–275. doi:10.1083/jcb.68.2.264

Kishino, A., and Yanagida, T. (1988). Force measurements by micromanipulation of a single actin filament by glass needles. *Nature* 334 (6177), 74–76. doi:10.1038/334074a0

Knight, A. E., Veigel, C., Chambers, C., and Molloy, J. E. (2001). Analysis of single-molecule mechanical recordings: application to acto-myosin interactions. *Prog. Biophys. Mol. Biol.* 77 (1), 45–72. doi:10.1016/s0079-6107(01)00010-4

Kron, S. J., and Spudich, J. A. (1986). Fluorescent actin filaments move on myosin fixed to a glass surface. *Proc. Natl. Acad. Sci. U. S. A.* 83 (17), 6272–6276. doi:10.1073/pnas.83.17.6272

Kuo, S. C., and Sheetz, M. P. (1993). Force of single kinesin molecules measured with optical tweezers. *Science* 260 (5105), 232–234. doi:10.1126/science.8469975

Lehman, W. (2016). Thin filament structure and the steric blocking model. *Compr. Physiol.* 6 (2), 1043–1069. doi:10.1002/cphy.c150030

Liang, W., Licate, L., Warrick, H., Spudich, J., and Egelhoff, T. (2002). Differential localization in cells of myosin II heavy chain kinases during cytokinesis and polarized migration. *BMC Cell Biol.* 3, 19. doi:10.1186/1471-2121-3-19

Liang, W., Warrick, H. M., and Spudich, J. A. (1999). A structural model for phosphorylation control of Dictyostelium myosin II thick filament assembly. *J. Cell Biol.* 147 (5), 1039–1048. doi:10.1083/jcb.147.5.1039

Liao, J. C., Elting, M. W., Delp, S. L., Spudich, J. A., and Bryant, Z. (2009). Engineered myosin VI motors reveal minimal structural determinants of directionality and processivity. *J. Mol. Biol.* 392 (4), 862–867. doi:10.1016/j.jmb.2009.07.046

Liu, C., Kawana, M., Song, D., Ruppel, K. M., and Spudich, J. A. (2018). Controlling load-dependent kinetics of β-cardiac myosin at the single-molecule level. *Nat. Struct. Mol. Biol.* 25 (6), 505–514. doi:10.1038/s41594-018-0069-x

Manstein, D. J., Titus, M. A., De Lozanne, A., and Spudich, J. A. (1989). Gene replacement in Dictyostelium: generation of myosin null mutants. *EMBO J.* 8 (3), 923–932. doi:10.1002/j.1460-2075.1989.tb03453.x

Mehta, A. D., Finer, J. T., and Spudich, J. A. (1997). Detection of single-molecule interactions using correlated thermal diffusion. *Proc. Natl. Acad. Sci. U. S. A.* 94 (15), 7927–7931. doi:10.1073/pnas.94.15.7927

Mehta, A. D., Finer, J. T., and Spudich, J. A. (1998a). Use of optical traps in single-molecule study of nonprocessive biological motors. *Methods Enzymol.* 298, 436–459. doi:10.1016/s0076-6879(98)98039-9

Mehta, A. D., Finer, J. T., and Spudich, J. A. (1998b). Reflections of a lucid dreamer: optical trap design considerations. *Methods Cell Biol.* 55, 47–69. doi:10.1016/s0091-679x(08)60402-1

Mehta, A. D., Rief, M., Spudich, J. A., Smith, D. A., and Simmons, R. M. (1999a). Single-molecule biomechanics with optical methods. *Science* 283 (5408), 1689–1695. doi:10.1126/science.283.5408.1689

Mehta, A. D., Rock, R. S., Rief, M., Spudich, J. A., Mooseker, M. S., and Cheney, R. E. (1999b). Myosin-V is a processive actin-based motor. *Nature* 400 (6744), 590–593. doi:10.1038/23072

Menetrey, J., Bahloul, A., Wells, A. L., Yengo, C. M., Morris, C. A., Sweeney, H. L., et al. (2005). The structure of the myosin VI motor reveals the mechanism of directionality reversal. *Nature* 435 (7043), 779–785. doi:10.1038/nature03592

Molloy, J. E., Burns, J. E., Kendrick-Jones, J., Tregear, R. T., and White, D. C. (1995). Movement and force produced by a single myosin head. *Nature* 378 (6553), 209–212. doi:10.1038/378209a0

Molloy, J. E., and Veigel, C. (2003). Biophysics. Myosin motors walk the walk. *Science* 300 (5628), 2045–2046. doi:10.1126/science.1087148

Moore, P. B., Huxley, H. E., and DeRosier, D. J. (1970). Three-dimensional reconstruction of F-actin, thin filaments and decorated thin filaments. *J. Mol. Biol.* 50 (2), 279–295. doi:10.1016/0022-2836(70)90192-0

Moores, S. L., Sabry, J. H., and Spudich, J. A. (1996). Myosin dynamics in live Dictyostelium cells. *Proc. Natl. Acad. Sci. U. S. A.* 93 (1), 443–446. doi:10.1073/pnas.93.1.443

Mortensen, K. I., Sung, J., Flyvbjerg, H., and Spudich, J. A. (2015). Optimized measurements of separations and angles between intra-molecular fluorescent markers. *Nat. Commun.* 6, 8621. doi:10.1038/ncomms9621

Nag, S., Trivedi, D. V., Sarkar, S. S., Adhikari, A. S., Sunitha, M. S., Sutton, S., et al. (2017). The myosin mesa and the basis of hypercontractility caused by hypertrophic cardiomyopathy mutations. *Nat. Struct. Mol. Biol.* 24 (6), 525–533. doi:10.1038/nsmb.3408

Parry, D. A., and Squire, J. M. (1973). Structural role of tropomyosin in muscle regulation: analysis of the x-ray diffraction patterns from relaxed and contracting muscles. *J. Mol. Biol.* 75 (1), 33–55. doi:10.1016/0022-2836(73)90527-5

Perkins, T. T., Quake, S. R., Smith, D. E., and Chu, S. (1994a). Relaxation of a single DNA molecule observed by optical microscopy. *Science* 264 (5160), 822–826. doi:10.1126/science.8171336

Perkins, T. T., Smith, D. E., and Chu, S. (1994b). Direct observation of tube-like motion of a single polymer chain. *Science* 264 (5160), 819–822. doi:10.1126/science.8171335

Perkins, T. T., Smith, D. E., and Chu, S. (1997). Single polymer dynamics in an elongational flow. *Science* 276 (5321), 2016–2021. doi:10.1126/science.276.5321.2016

Perkins, T. T., Smith, D. E., Larson, R. G., and Chu, S. (1995). Stretching of a single tethered polymer in a uniform flow. *Science* 268 (5207), 83–87. doi:10.1126/science.7701345

Pollard, T. D. (1976). Cytoskeletal functions of cytoplasmic contractile proteins. *J. Supramol. Struct.* 5 (3), 317–334. doi:10.1002/jss.400050306

Pollard, T. D., and Cooper, J. A. (2009). Actin, a central player in cell shape and movement. *Science* 326 (5957), 1208–1212. doi:10.1126/science.1175862

Pollard, T. D., and Korn, E. D. (1973a). Acanthamoeba myosin. *J. Biol. Chem.* 248 (13), 4682–4690. doi:10.1016/s0021-9258(19)43718-6

Pollard, T. D., and Korn, E. D. (1973b). Acanthamoeba myosin. II. Interaction with actin and with a new cofactor protein required for actin activation of Mg 2+ adenosine triphosphatase activity. *J. Biol. Chem.* 248 (13), 4691–4697. doi:10.1016/s0021-9258(19)43719-8

Pollard, T. D., and Korn, E. D. (2023). Discovery of the first unconventional myosin: Acanthamoeba myosin-I. *Front. Physiol.* 14, 1324623. doi:10.3389/fphys.2023.1324623

Purcell, T. J., Morris, C., Spudich, J. A., and Sweeney, H. L. (2002). Role of the lever arm in the processive stepping of myosin V. *Proc. Natl. Acad. Sci. U. S. A.* 99 (22), 14159–14164. doi:10.1073/pnas.182539599

Rall, J. A. (2014). *Mechanism of muscular contraction*. Springer.

Rayment, I., Holden, H. M., Whittaker, M., Yohn, C. B., Lorenz, M., Holmes, K. C., et al. (1993a). Structure of the actin-myosin complex and its implications for muscle contraction. *Science* 261 (5117), 58–65. doi:10.1126/science.8316858

Rayment, I., Rypniewski, W. R., Schmidt-Base, K., Smith, R., Tomchick, D. R., Benning, M. M., et al. (1993b). Three-dimensional structure of myosin subfragment-1: a molecular motor. *Science* 261 (5117), 50–58. doi:10.1126/science.8316857

Rief, M., Rock, R. S., Mehta, A. D., Mooseker, M. S., Cheney, R. E., and Spudich, J. A. (2000). Myosin-V stepping kinetics: a molecular model for processivity. *Proc. Natl. Acad. Sci. U. S. A.* 97 (17), 9482–9486. doi:10.1073/pnas.97.17.9482

Rock, R. S., Rice, S. E., Wells, A. L., Purcell, T. J., Spudich, J. A., and Sweeney, H. L. (2001). Myosin VI is a processive motor with a large step size. *Proc. Natl. Acad. Sci. U. S. A.* 98 (24), 13655–13659. doi:10.1073/pnas.191512398

Rock, R. S., Rief, M., Mehta, A. D., and Spudich, J. A. (2000). *In vitro* assays of processive myosin motors. *Methods* 22 (4), 373–381. doi:10.1006/meth.2000.1089

Rohde, J. A., Roopnarine, O., Thomas, D. D., and Muretta, J. M. (2018). Mavacamten stabilizes an autoinhibited state of two-headed cardiac myosin. *Proc. Natl. Acad. Sci. U. S. A.* 115 (32), E7486–E7494. doi:10.1073/pnas.1720342115

Ruegg, C., Veigel, C., Molloy, J. E., Schmitz, S., Sparrow, J. C., and Fink, R. H. (2002). Molecular motors: force and movement generated by single myosin II molecules. *News Physiol. Sci.* 17, 213–218. doi:10.1152/nips.01389.2002

Ruppel, K. M., and Spudich, J. A. (1996). Structure-function studies of the myosin motor domain: importance of the 50-kDa cleft. *Mol. Biol. Cell* 7 (7), 1123–1136. doi:10.1091/mbc.7.7.1123

Sabry, J. H., Moores, S. L., Ryan, S., Zang, J. H., and Spudich, J. A. (1997). Myosin heavy chain phosphorylation sites regulate myosin localization during cytokinesis in live cells. *Mol. Biol. Cell* 8 (12), 2605–2615. doi:10.1091/mbc.8.12.2605

Saito, K., Aoki, T., Aoki, T., and Yanagida, T. (1994). Movement of single myosin filaments and myosin step size on an actin filament suspended in solution by a laser trap. *Biophys. J.* 66 (3 Pt 1), 769–777. doi:10.1016/s0006-3495(94)80853-7

Schroder, R. R., Manstein, D. J., Jahn, W., Holden, H., Rayment, I., Holmes, K. C., et al. (1993). Three-dimensional atomic model of F-actin decorated with Dictyostelium myosin S1. *Nature* 364 (6433), 171–174. doi:10.1038/364171a0

Shaevitz, J. W., Abbondanzieri, E. A., Landick, R., and Block, S. M. (2003). Backtracking by single RNA polymerase molecules observed at near-base-pair resolution. *Nature* 426 (6967), 684–687. doi:10.1038/nature02191

Sheetz, M. P., and Spudich, J. A. (1983). Movement of myosin-coated fluorescent beads on actin cables *in vitro*. *Nature* 303 (5912), 31–35. doi:10.1038/303031a0

Shih, W. M., Gryczynski, Z., Lakowicz, J. R., and Spudich, J. A. (2000). A FRET-based sensor reveals large ATP hydrolysis-induced conformational changes and three distinct states of the molecular motor myosin. *Cell* 102 (5), 683–694. doi:10.1016/s0092-8674(00)00090-8

Simmons, R. M., Finer, J. T., Chu, S., and Spudich, J. A. (1996). Quantitative measurements of force and displacement using an optical trap. *Biophys. J.* 70 (4), 1813–1822. doi:10.1016/S0006-3495(96)79746-1

Simmons, R. M., Finer, J. T., Warrick, H. M., Kralik, B., Chu, S., and Spudich, J. A. (1993). Force on single actin filaments in a motility assay measured with an optical trap. *Adv. Exp. Med. Biol.* 332, 331–336. ; discussion 336-337. doi:10.1007/978-1-4615-2872-2_32

Smith, D. E., Perkins, T. T., and Chu, S. (1995). Self-diffusion of an entangled DNA molecule by reptation. *Phys. Rev. Lett.* 75 (22), 4146–4149. doi:10.1103/PhysRevLett.75.4146

Spudich, J. A. (2015). The myosin mesa and a possible unifying hypothesis for the molecular basis of human hypertrophic cardiomyopathy. *Biochem. Soc. Trans.* 43 (1), 64–72. doi:10.1042/BST20140324

Spudich, J. A., and Clarke, M. (1974). The contractile proteins of *Dictyostelium discoideum*. *J. Supramol. Struct.* 2 (2-4), 150–162. doi:10.1002/jss.400020209

Spudich, J. A., Huxley, H. E., and Finch, J. T. (1972). Regulation of skeletal muscle contraction. II. Structural studies of the interaction of the tropomyosin-troponin complex with actin. *J. Mol. Biol.* 72 (3), 619–632. doi:10.1016/0022-2836(72)90180-5

Spudich, J. A., Kron, S. J., and Sheetz, M. P. (1985). Movement of myosin-coated beads on oriented filaments reconstituted from purified actin. *Nature* 315 (6020), 584–586. doi:10.1038/315584a0

Spudich, J. A., and Watt, S. (1971). The regulation of rabbit skeletal muscle contraction. I. Biochemical studies of the interaction of the tropomyosin-troponin complex with actin and the proteolytic fragments of myosin. *J. Biol. Chem.* 246 (15), 4866–4871. doi:10.1016/s0021-9258(18)62016-2

Sun, Y., and Goldman, Y. E. (2011). Lever-arm mechanics of processive myosins. *Biophys. J.* 101 (1), 1–11. doi:10.1016/j.bpj.2011.05.026

Sung, J., Mortensen, K. I., Spudich, J. A., and Flyvbjerg, H. (2017). How to measure load-dependent kinetics of individual motor molecules without a force-clamp. *Methods Enzymol.* 582, 1–29. doi:10.1016/bs.mie.2016.08.002

Sung, J., Nag, S., Mortensen, K. I., Vestergaard, C. L., Sutton, S., Ruppel, K., et al. (2015). Harmonic force spectroscopy measures load-dependent kinetics of individual human β-cardiac myosin molecules. *Nat. Commun.* 6, 7931. doi:10.1038/ncomms8931

Svoboda, K., Schmidt, C. F., Schnapp, B. J., and Block, S. M. (1993). Direct observation of kinesin stepping by optical trapping interferometry. *Nature* 365 (6448), 721–727. doi:10.1038/365721a0

Theriot, J. A. (2000). The polymerization motor. *Traffic* 1 (1), 19–28. doi:10.1034/j.1600-0854.2000.010104.x

Titus, M. A., Warrick, H. M., and Spudich, J. A. (1989). Multiple actin-based motor genes in Dictyostelium. *Cell Regul.* 1 (1), 55–63. doi:10.1091/mbc.1.1.55

Titus, M. A., Wessels, D., Spudich, J. A., and Soll, D. (1993). The unconventional myosin encoded by the myoA gene plays a role in Dictyostelium motility. *Mol. Biol. Cell* 4 (2), 233–246. doi:10.1091/mbc.4.2.233

Tobacman, L. S. (2021). Troponin revealed: uncovering the structure of the thin filament on-off switch in striated muscle. *Biophys. J.* 120 (1), 1–9. doi:10.1016/j.bpj.2020.11.014

Toyoshima, Y. Y., Kron, S. J., McNally, E. M., Niebling, K. R., Toyoshima, C., and Spudich, J. A. (1987). Myosin subfragment-1 is sufficient to move actin filaments *in vitro*. *Nature* 328 (6130), 536–539. doi:10.1038/328536a0

Toyoshima, Y. Y., Kron, S. J., and Spudich, J. A. (1990). The myosin step size: measurement of the unit displacement per ATP hydrolyzed in an *in vitro* assay. *Proc. Natl. Acad. Sci. U. S. A.* 87 (18), 7130–7134. doi:10.1073/pnas.87.18.7130

Trivedi, D. V., Adhikari, A. S., Sarkar, S. S., Ruppel, K. M., and Spudich, J. A. (2018). Hypertrophic cardiomyopathy and the myosin mesa: viewing an old disease in a new light. *Biophys. Rev.* 10 (1), 27–48. doi:10.1007/s12551-017-0274-6

Trivedi, D. V., Nag, S., Spudich, A., Ruppel, K. M., and Spudich, J. A. (2020). The myosin family of mechanoenzymes: from mechanisms to therapeutic approaches. *Annu. Rev. Biochem.* 89, 667–693. doi:10.1146/annurev-biochem-011520-105234

Urrutia, R. A., Jung, G., and Hammer, J. A., 3rd (1993). The Dictyostelium myosin IE heavy chain gene encodes a truncated isoform that lacks sequences corresponding to the actin binding site in the tail. *Biochim. Biophys. Acta* 1173 (2), 225–229. doi:10.1016/0167-4781(93)90185-g

Uyeda, T. Q., Abramson, P. D., and Spudich, J. A. (1996). The neck region of the myosin motor domain acts as a lever arm to generate movement. *Proc. Natl. Acad. Sci. U. S. A.* 93 (9), 4459–4464. doi:10.1073/pnas.93.9.4459

Uyeda, T. Q., Kron, S. J., and Spudich, J. A. (1990). Myosin step size. Estimation from slow sliding movement of actin over low densities of heavy meromyosin. *J. Mol. Biol.* 214 (3), 699–710. doi:10.1016/0022-2836(90)90287-V

Uyeda, T. Q., Warrick, H. M., Kron, S. J., and Spudich, J. A. (1991). Quantized velocities at low myosin densities in an *in vitro* motility assay. *Nature* 352 (6333), 307–311. doi:10.1038/352307a0

Vale, R. D., Reese, T. S., and Sheetz, M. P. (1985a). Identification of a novel force-generating protein, kinesin, involved in microtubule-based motility. *Cell* 42 (1), 39–50. doi:10.1016/s0092-8674(85)80099-4

Vale, R. D., Schnapp, B. J., Reese, T. S., and Sheetz, M. P. (1985b). Organelle, bead, and microtubule translocations promoted by soluble factors from the squid giant axon. *Cell* 40 (3), 559–569. doi:10.1016/0092-8674(85)90204-1

Veigel, C., and Schmidt, C. F. (2011). Moving into the cell: single-molecule studies of molecular motors in complex environments. *Nat. Rev. Mol. Cell Biol.* 12 (3), 163–176. doi:10.1038/nrm3062

von der Ecken, J., Muller, M., Lehman, W., Manstein, D. J., Penczek, P. A., and Raunser, S. (2015). Structure of the F-actin-tropomyosin complex. *Nature* 519 (7541), 114–117. doi:10.1038/nature14033

Warshaw, D. M. (2004). Lever arms and necks: a common mechanistic theme across the myosin superfamily. *J. Muscle Res. Cell Motil.* 25 (6), 467–474. doi:10.1007/s10974-004-1767-z

Wessels, D., Murray, J., Jung, G., Hammer, J. A., 3rd, and Soll, D. R. (1991). Myosin IB null mutants of Dictyostelium exhibit abnormalities in motility. *Cell Motil. Cytoskelet.* 20 (4), 301–315. doi:10.1002/cm.970200406

Yamamoto, K., Pardee, J. D., Reidler, J., Stryer, L., and Spudich, J. A. (1982). Mechanism of interaction of Dictyostelium severin with actin filaments. *J. Cell Biol.* 95 (3), 711–719. doi:10.1083/jcb.95.3.711

Yanagida, T. (1981). Angles of nucleotides bound to cross-bridges in glycerinated muscle fiber at various concentrations of ε-ATP, ε-ADP and ε-AMPPNP detected by polarized fluorescence. *J. Mol. Biol.* 146, 539–560. doi:10.1016/0022-2836(81)90046-2

Yanagida, T., Ishijima, A., Saito, K., and Harada, Y. (1993). Coupling between ATPase and force-generating attachment-detachment cycles of actomyosin *in vitro*. *Adv. Exp. Med. Biol.* 332, 339–347. doi:10.1007/978-1-4615-2872-2_33

Yanagida, T., and Iwane, A. H. (2000). A large step for myosin. *Proc. Natl. Acad. Sci. U. S. A.* 97 (17), 9357–9359. doi:10.1073/pnas.97.17.9357

Yanagida, T., Nakase, M., Nishiyama, K., and Oosawa, F. (1984). Direct observation of motion of single F-actin filaments in the presence of myosin. *Nature* 307 (5946), 58–60. doi:10.1038/307058a0

frontiers | Frontiers in Physiology

TYPE Original Research
PUBLISHED 03 June 2024
DOI 10.3389/fphys.2024.1393952

OPEN ACCESS

EDITED BY
Maria Jolanta Redowicz,
Polish Academy of Sciences, Poland

REVIEWED BY
Michael Ostap,
University of Pennsylvania, United States
Matthew J. Gage,
University of Massachusetts Lowell, United States

*CORRESPONDENCE
Georgios Tsiavaliaris,
tsiavaliaris.georgios@mh-hannover.de

RECEIVED 01 March 2024
ACCEPTED 02 May 2024
PUBLISHED 03 June 2024

CITATION
Diensthuber RP, Hartmann FK, Kathmann D, Franz P and Tsiavaliaris G (2024), Switch-2 determines Mg^{2+}ADP-release kinetics and fine-tunes the duty ratio of *Dictyostelium* class-1 myosins.
Front. Physiol. 15:1393952.
doi: 10.3389/fphys.2024.1393952

Switch-2 determines Mg^{2+}ADP-release kinetics and fine-tunes the duty ratio of *Dictyostelium* class-1 myosins

Ralph P. Diensthuber, Falk K. Hartmann, Daniela Kathmann, Peter Franz and Georgios Tsiavaliaris*

Institute for Biophysical Chemistry, OE 4350, Hannover Medical School, Hannover, Germany

Though myosins share a structurally conserved motor domain, single amino acid variations of active site elements, including the P-loop, switch-1 and switch-2, which act as nucleotide sensors, can substantially determine the kinetic signature of a myosin, *i.e.*, to either perform fast movement or enable long-range transport and tension generation. Switch-2 essentially contributes to the ATP hydrolysis reaction and determines product release. With few exceptions, class-1 myosin harbor a tyrosine in the switch-2 consensus sequence DIYGFE, at a position where class-2 myosins and a selection of myosins from other classes have a substitution. Here, we addressed the role of the tyrosine in switch-2 of class-1 myosins as potential determinant of the duty ratio. We generated constitutively active motor domain constructs of two class-1 myosins from the social amoeba *Dictyostelium discoideum*, namely, Myo1E, a high duty ratio myosin and Myo1B, a low duty ratio myosin. In Myo1E we introduced mutation Y388F and in Myo1B mutation F387Y. The detailed functional characterization by steady-state and transient kinetic experiments, combined with *in vitro* motility and landing assays revealed an almost reciprocal relationship of a number of critical kinetic parameters and equilibrium constants between wild-type and mutants that dictate the lifetime of the strongly actin-attached states of myosin. The Y-to-F mutation increased the duty ratio of Moy1B by almost one order of magnitude, while the introduction of the phenylalanine in switch-2 of Myo1E transformed the myosin into a low duty ratio motor. These data together with structural considerations propose a role of switch-2 in fine-tuning ADP release through a mechanism, where the class-specific tyrosine together with surrounding residues contributes to the coordination of Mg^{2+} and ADP. Our results highlight the importance of conserved switch-2 residues in class-1 myosins for efficient chemo-mechanical coupling, revealing that switch-2 is important to adjust the duty ratio of the amoeboid class-1 myosins for performing movement, transport or gating functions.

KEYWORDS

myosin, myosin-1, actin, duty ratio, kinetics

1 Introduction

Class-1 myosins act primarily at the interface between the actin cytoskeleton and membrane systems, where they provide the mechanical forces and tension to drive membrane rearrangements, coordinate actin remodeling, and accomplish intracellular transport functions (McConnell and Tyska, 2010; McIntosh and Ostap, 2016; Barger

et al., 2019; Manenschijn et al., 2019; Lutton et al., 2023). Apart from a modular tail that contains domains and motifs for cargo binding and membrane association (Adams and Pollard, 1989), the class-1 myosins share a globular head through which they interact with actin and hydrolyze ATP to perform fast movement, transport or gating functions (Mezgueldi et al., 2002; Laakso et al., 2008; Lin et al., 2011). A critical parameter of the myosin kinetic cycle is the duty ratio, which defines the fraction of time a myosin spends in the strongly attached actin states relative to its total ATPase cycle time. Low duty ratio myosins are generally fast movers (Johnson et al., 2019) due to a fast release of the hydrolysis products and short-lived strongly-actin bound states (Bloemink and Geeves, 2011), whereas high duty ratio myosins are characterized by a rate limiting ADP release, which prolongs the occupation of states of strong actin interactions (De La Cruz et al., 1999; Amrute-Nayak et al., 2019) and which is considered as prerequisite for the generation of tension and processive movement (Armstrong et al., 2012).

The myosin motor domain contains surface exposed actin-binding loops and harbors in the inner core a conserved nucleotide-binding pocket formed by three structural motifs, termed P-loop, switch-1, and switch-2 that act as nucleotide sensors (Wittinghofer and Geeves, 2016). Their reversible switching between open and closed conformations enables ATP hydrolysis and couples actin-cleft closure to the bending of the relay helix followed by a rotational rigid-body movement of the converter domain that drives the power-stroke concomitant with product release (Preller and Holmes, 2013; Franz et al., 2021). Mutagenic studies have shown that conserved residues within switch-2 are critical for efficient ATP hydrolysis and activation of ATPase activity (Furch et al., 1999; Málnási-Csizmadia et al., 2005; Nagy et al., 2010). Through hydrogen bond formation and Mg^{2+}-coordination, switch-2 serves as important regulator of ATP-hydrolysis and product release. A tyrosine residue is found in the switch-2 consensus sequence DIYGFE of various myosins at a position were fast skeletal muscle myosin-2 and a selection of myosins from other classes have an alanine, serine or phenylalanine (Odronitz and Kollmar 2007). Recently, we have shown that physiological changes in the concentration of free Mg^{2+}-ions can modulate the kinetic and motor properties of the high duty ratio amoeboid class-1 myosins Myo1E and Myo1D, which contain a tyrosine residue at this position (Fujita-Becker et al., 2005; Dürrwang et al., 2006), but not of the low duty ratio Myo1B with a phenylalanine substitution (Tsiavaliaris et al., 2008). To dissect a potential contribution of this variant residue on the duty ratio of the myosins, we generated mutant constructs, in which the amino acid was replaced by a tyrosine (construct $Myo1B^{F387Y}$) or a phenylalanine (construct $Myo1E^{Y388F}$). In the case of Myo1B, the F387Y mutation sensitized the myosin to modulate its kinetics by free Mg^{2+}-ions. The F-to-Y substitution decelerated ADP release and increased the ADP affinity of the actin bound states, affecting duty ratio and motor activity. For Myo1E the Y-to-F substitution produced the opposite effects resulting in loss of Mg^{2+}-sensitivity and low duty ratio. Structural models propose a role of this tyrosine residue in mediating interactions between switch-2, Mg^{2+}, and the nucleotide important to fine-tune Mg^{2+}ADP release and consequently the duty ratio of the myosins.

2 Materials and methods

2.1 Reagents

Standard chemicals, anti-His antibody, and TRITC-phalloidin were purchased from Sigma; restriction enzymes, polymerases and DNA-modifying enzymes were purchased from MBI-Fermentas and Roche Applied Sciences. The 2'-(3'-)-O-(N′-Methylanthraniloyl) derivatives of ATP (mantATP) and ADP (mantADP) were purchased from Jena Bioscience.

2.2 Plasmid construction and protein purification

Expression plasmids pDXA-MyoB-S332E-F387Y-2R and pDXA-MyoE-S336E-Y388F-2R, which encode the constitutively active motor domain constructs of *Dd* myosion-1B and *Dd* myosion-1E harboring mutations F387Y and Y388F, respectively, fused to an artificial lever arm (2R) and a C-terminal His_8-tag, were generated by PCR using mutagenesis primers 5′-GATTTCAAA ACCATAAATATCTAAAATACC-3′ for introducing mutation F387Y in the motor domain of myosin-1B and 5′-CTCAAAACC AAAGATATCAAG-3′ for introducing mutation Y388F in the motor domain of myosin-1E. *E. coli* strain XL1Blue (Stratagene, Heidelberg) was used for amplification of the plasmids. Myosin constructs were confirmed by sequencing. Wild-type and mutant constructs were produced in *Dictyostelium discoideum* and purified as described (Fujita-Becker et al., 2005; Dürrwang et al., 2006; Tsiavaliaris et al., 2008). Chicken skeletal actin was purified as described (Pardee and Aspudich, 1982). Pyrene-labeled actin was prepared from skeletal actin as described (Criddle et al., 1985).

2.3 Steady-state and transient kinetic experiments, *in vitro* motility and landing assays

Steady-state ATPase activity measurements were performed at 25°C in buffer containing 25 mM 2-(4-(2-Hydroxyethyl)-1-piperazinyl)-ethansulfonsäure (HEPES) pH = 7.3, 25 mM KCl, 5 mM $MgCl_2$, 1 mM Dithiothreitol and 1 mM ATP using the NADH-coupled assay (Diensthuber et al., 2015). Unless otherwise stated, transient kinetic measurements were performed at 20°C in experimental buffer containing 20 mM 3-(N-morpholino) propanesulfonic acid (MOPS) pH = 7.0, 100 mM KCl, 5 mM $MgCl_2$ and 1 mM DTT using a Hi-tech Scientific SF-61DX double-mixing stopped-flow system (TgK Scientific Limited, Bradford on Avon, U.K.). Data were analyzed according to the procedures and kinetic models described (Bagshaw et al., 1974; Millar and Geeves, 1983; Cremo and Geeves, 1998; Batra et al., 1999; Furch et al., 1999). Data for wild-type myosins were depicted from Dürrwang et al., 2006; Tsiavaliaris et al., 2008, respectively, and are listed in the tables as assigned, if not otherwise stated. *In vitro* motility assays were performed at 30 °C using an Olympus IX81 inverted fluorescence microscope as described (Taft et al., 2008). Penta·His Antibody (Qiagen) was used for the specific attachment of wild-type and mutant myosin constructs on nitrocellulose coated coverslips. Actin

filament tracking was performed using DiaTrack 3.05 software. Average actin sliding velocities were obtained from Gaussian fits to the velocity distributions using Origin 2022b software (OriginLab, Northampton, MA, USA). Landing assays were performed as described (Taft et al., 2008).

2.4 Molecular dynamics simulations and homology modelling

Mutation Y388F was introduced in the X-ray crystal structure of the Myo1E motor domain (pdb: 1LKX) using the Schrödinger Suite (Schrödinger Inc.), selecting the rotamers with the lowest sterical hindrance, and energy-minimization of the entire model was performed with MacroModel (Schrödinger Inc.), CNSsolve 1.2 (Brunger, 2007), and the OPLS3 force field. Molecular dynamics simulation of Myo1E^{Y388F} was carried out with Gromacs 4.0 (Hess et al., 2008) and OPLS (Optimized Potentials for Liquid Simulations) all-atom force field. The myosin was solvated with the TIP3P explicit water model and neutralized by addition of sodium counter ions as described (Preller et al., 2011). MD simulations were performed in a NpT ensemble (300 K, 1 bar) using Berendsen temperature coupling and Parrinello-Rahman pressure coupling. The particle-mesh Ewald method (Darden et al., 1993) was used for long-range electrostatic interactions. Short-range van der Waals and coulomb forces were treated with 12 Å cutoffs. A 2 fs time step was used during the production runs, and all bond lengths were constrained with the LINCS algorithm (Hess et al., 1997). The coordinates were optimized with the conjugate gradient algorithm to a final force of <10 kJ·mol^{-1}·nm^{-1} after energy minimization with the steepest descent algorithm to a force of 1,000 kJ·mol^{-1}·nm^{-1}. The solvent molecules were equilibrated for 100 ps. A 4 ns equilibration of the entire system was performed to reach a plateau of the root mean square deviation of the backbone atoms. Production runs were performed for 100 ns? Myo1B homology models were generated with Modeller (Šali and Blundell, 1993) using the crystal structure of Myo1E motor domain (pdb: 1LKX) as template. Best models were selected according to the Modeller objective function and the discrete optimized protein energy score (DOPE). Images were generated with Pymol (DeLano scientific).

2.5 Equations

$$L(\rho) = Z \cdot \left(1 - e^{-\frac{\rho}{\rho_0}}\right)^n \quad (1)$$

$$duty\ ratio = \frac{\tau_{strong}}{\tau_{total}} \approx \frac{\frac{1}{k_{-AD}}}{\frac{1}{k_{cat}}} \quad (2)$$

3 Results and discussion

3.1 Switch-2 mutations do not impair steady-state ATP turnover

The ATPase activities of the wild-type myosin motor domain constructs Myo1B^{wt} and Myo1E^{wt} and the corresponding switch-2 mutants Myo1B^{F387Y}, Myo1E^{Y388F}, all carrying the S-to-E mutation at the TEDS site, which mimics the phosphorylation state and transforms the myosins into active, ATPase competent motors (Fujita-Becker et al., 2005; Dürrwang et al., 2006) were examined in the absence and presence of F-actin. Data for wild-type myosins were depicted from (Dürrwang et al., 2006; Tsiavaliaris et al., 2008) if not otherwise stated. Hyperbolic fit of the actin-dependence of the rate of ATP turnover according to Michaelis-Menten (Figure 1) yielded the basal ATPase activity (k_{basal}), the apparent equilibrium constant of half-maximal activation of maximum ATP turnover ($\mathbf{K_{app}}$), and actin-activated ATPase activity for saturating actin concentrations ($\boldsymbol{k_{cat}}$). The steady-state parameters are summarized in Table 1. The mutants displayed reduced k_{basal} rates compared to the wild-types, while $\mathbf{K_{app}}$ remained largely unaffected. In the case of Myo1B^{F387Y}, the actin-activated ATPase activity increased almost linear, which allows only rough estimates of the apparent equilibrium constant ($\mathbf{K_{app}}$) and the maximum ATP turnover rate ($\boldsymbol{k_{cat}}$). Myo1B^{F387Y} shows a 3-fold reduction in both, $\boldsymbol{k_{cat}}$ and the catalytic efficiency $\boldsymbol{k_{cat}/K_{app}}$. Latter is a measure of how effectively actin activates the ATPase reaction as defined by the 2nd order rate constant of actin binding in the presence of ATP. These parameters were unaffected in Myo1E^{Y388F}. Since we observed different impact of the mutations on the catalytic activity of the myosins, we extended the analysis to transient kinetic experiments and focused our investigations on those steps of the ATPase cycle that determine the occupation and lifetime of the strongly vs. weakly actin-bound states of the myosins.

3.2 Switch-2 mutations produce inverse effects on ADP dissociation, actin affinity, and weak-to-strong actin interactions

First, we studied nucleotide interactions according to Figure 2 applying the kinetic models as described (Geeves et al., 1984; Taylor, 1991; Franz et al., 2021). Nucleotide binding in the absence of actin was mainly unaffected by the mutations (Table 2). However, both mutants displayed accelerated ADP release rates (k_{-D}, Figure 3) and two to three-fold weaker affinities for ADP than the corresponding wild-types (K_D; Table 2). The Y-to-F mutation in Myo1E^{Y388F} accelerated both rates of the two-step ADP release (Dürrwang et al., 2006) by up to four-fold, whereas mutant and wild-type Myo1B displayed single-step ADP release kinetics that differed by approx. two-fold. We interpret the accelerated ADP release as the major contributor of the reduced ADP affinity. In the presence of actin, equilibrium and rate constants of the interaction with ATP, defined by $\mathbf{K_1}$ and $\boldsymbol{k_{+2}}$ (Figure 2), were differently affected in the mutants (Table 2). Myo1B^{F387Y} displayed five-fold slower ATP-binding ($\mathbf{K_1 k_{+2}}$) and three-fold lower ATP affinity of the A·M state. Myo1E^{Y388F} showed wild-type like ATP-binding behavior and a higher ATP-affinity of the A·M state than the wild-type. The tyrosine appears to disturb high affinity ATP binding by affecting the isomerization of the A·M·T state to the A-M*·T state. Pronounced changes were also observed for the ADP affinity of the A·M state ($\mathbf{K_{AD}}$) determined from the inhibition of the ATP-induced dissociation of the actomyosin complex with increasing ADP concentrations (Figure 4). Here, it is important to highlight the monophasic (Figures 4A, D) vs. biphasic actomyosin dissociation kinetics (Figures 4B, C) between wild-type and mutants. Monophasic dissociation kinetics are typical for myosins with a low affinity for ADP (Tsiavaliaris et al., 2002). A biphasic actomyosin

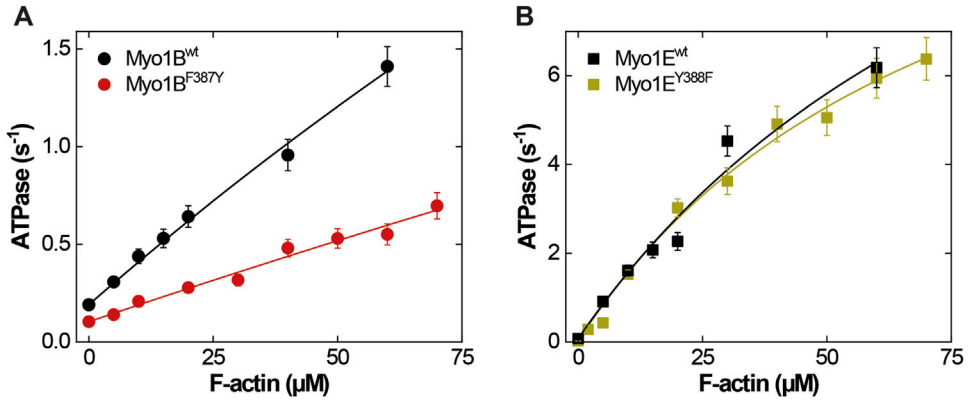

FIGURE 1
Steady-state ATPase activities of wild-type and mutant myosins. **(A)** Actin-activated ATPase of Myo1B^{wt} (black circles) and Myo1B^{F387Y} (red circles). **(B)** Actin-activated ATPase of Myo1E^{wt} (black squares) and Myo1B^{F387Y} (green squares). Michaelis-Menten parameters are summarized in Table 1.

TABLE 1 Actin-activated ATPase activities.

		Myo1B^{wta}	Myo1B^{F387Y}	Myo1E^{wta}	Myo1E^{Y388F}
Basale ATPase	k_{basal} (s^{-1})	0.16 ± 0.02	0.08 ± 0.01	0.08 ± 0.01	0.02 ± 0.01
Michaelis-Menten parameters	$\boldsymbol{k_{cat}}$ (s^{-1})	3.1 ± 0.4	>1	15.4 ± 3	13.4 ± 2
	$\mathbf{K_{app}}$ (μM)	96 ± 20	>100	91 ± 30	77 ± 17
	$\boldsymbol{k_{cat}/K_{app}}$ ($\mu M^{-1}s^{-1}$)	0.032 ± 0.008	>0.01	0.17 ± 0.06	0.17 ± 0.05

[a]Depicted from Dürrwang et al., 2006 or Tsiavaliaris et al., 2008.

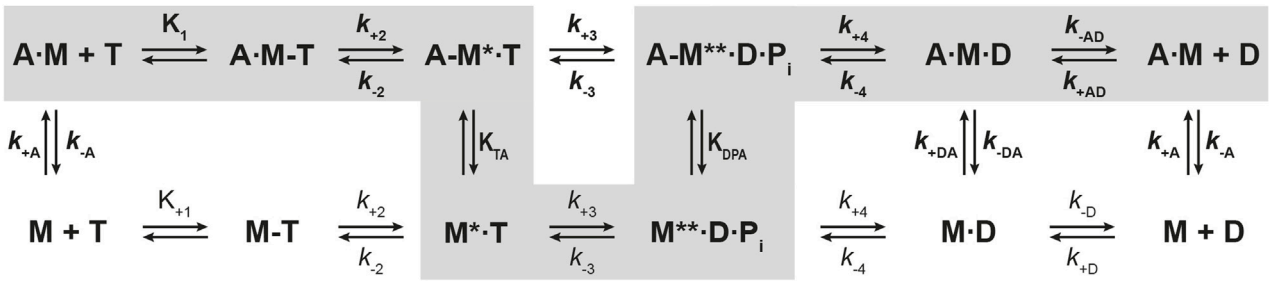

FIGURE 2
Kinetic scheme of the actomyosin ATPase cycle. Shown are the biochemical pathways of myosin during the interaction with nucleotides in the presence of actin (upper pathway) and absence of actin (lower pathway). Highlighted in grey is the force generating pathway. The biochemical states are defined in terms of the interacting proteins and nucleotides, where A = actin, M = myosin, T = ATP, D = ADP, P_i = phosphate. Equilibrium constants and rate constants associated with actin are shown in bold (**K**, ***k***), all others in regular fonts (K, *k*). In the force producing pathway, strongly actin-bound states of myosin are assigned as A·M, A·M-T, A·M·D, weakly actin-bound states as A-M*·T, A-M**·D·P_i, and actin-detached states as M, M-T, M*·T and M**·D·P_i. A dash defines a weak interaction, a dot a strong interaction. States assigned with asterisk (*) are fluorescence sensitive conformational transition and isomerisation states. $\boldsymbol{k_{-AD}}$ = rate constant of ADP dissociation from actomyosin; $\boldsymbol{k_{+AD}}$ = rate constant of ADP binding to actomyosin; k_{-D} = rate constant of ADP release from myosin; k_{+D} = rate constant of ADP binding to myosin; $\boldsymbol{k_{+A}}$ = rate constant of actin binding to myosin; $\boldsymbol{k_{-A}}$ = rate constant of actin dissociation from myosin. $\mathbf{K_{TA}}$: equilibrium constant of the actin interaction of myosin with bound ATP. $\mathbf{K_{DPA}}$: equilibrium constant of the actin interaction of myosin in the ADP-P_i state. $\mathbf{K_A}$: equilibrium constant of actin binding to myosin. $\mathbf{K_{AD}}$: equilibrium constant of actin binding to myosin with bound ADP.

dissociation reaction, in which the amplitude of the fast phase decreases and the amplitude of the slow phase increases with excess ADP, is indicative for a highly favorable A·M·D state, where ADP and ATP compete for the same binding site (Batra et al., 1999; Dürrwang et al., 2006). For both single and biphasic dissociation reactions, the ADP dependence of the rate (Figures 4A, D) and amplitude (Figures 4B, C) could be described by hyperbolic functions yielding $\mathbf{K_{AD}}$ values listed in Table 2. Myo1B^{F387Y} displayed a five-fold higher affinity for ADP than Myo1B^{wt}, whereas the ADP affinity of the actin-bound state of Myo1E^{Y388F} (A·M·D) was more than 6-fold decreased compared to wild-type. Thus, the F-to-Y substitution in Myo1B^{F387Y} appears to strengthen

10.3389/fphys.2024.1393952

TABLE 2 Rate and equilibrium constants of nucleotide interactions in the presence and absence of actin.

Nucleotide	Constant	Myo1B^{wtc}	Myo1B^{F387Y}	Myo1E^{wtc}	Myo1E^{Y388F}
Nucleotide binding to myosin					
ATP	K_1k_{+2} ($\mu M^{-1}s^{-1}$)	1.97 ± 0.01	weak signal	0.96 ± 0.03	1.1 ± 0.02
	k_{+2} (s^{-1})	>1,000	n.a.	900 ± 215	750 ± 190
	$1/K_1$	350 ± 25	n.a.	940 ± 45	680 ± 32
mantATP	K_1k_{+2} ($\mu M^{-1}s^{-1}$)	1.3 ± 0.02	1.54 ± 0.1	0.91 ± 0.01	1.08 ± 0.1
ADP	k_{+D} ($\mu M^{-1}s^{-1}$)[a]	1.2 ± 0.3	1.4 ± 0.3	0.34 ± 0.02	0.69 ± 0.1
	k_{-D1} (s^{-1})	0.7 ± 0.003	1.26 ± 0.06	6.39 ± 0.51[d]	26.4 ± 1.9
	k_{-D2} (s^{-1})	n.a.	n.a.	1.77 ± 0.24[d]	5.17 ± 0.52
	K_D (μM)	0.4 ± 0.10	1.13 ± 0.23	7.1 ± 0.4[d]	25.8 ± 2.1
Nucleotide binding to actomyosin					
ATP	$\mathbf{K_1k_{+2}}$ ($\mu M^{-1}s^{-1}$)	1.11 ± 0.03	0.22 ± 0.01	0.4 ± 0.01	0.41 ± 0.04
	$\mathbf{k_{+2}}$ (s^{-1})	>1,000	790 ± 62	750 ± 54	393 ± 18
	$\mathbf{1/K_1}$ (μM)	>900	3050 ± 276	1875 ± 152	975 ± 101
ADP	$\mathbf{k_{+AD}}$ ($\mu M^{-1}s^{-1}$)	4.95 ± 0.5	15 ± 2	2.5 ± 0.5	0.97 ± 0.1
	$\mathbf{k_{-AD}}$ (s^{-1})	233 ± 20[d]	150 ± 13	28 ± 4	180 ± 18
	$\mathbf{K_{AD}}$ (μM)	47 ± 5[d]	10 ± 1	12 ± 2	81 ± 17
	$\mathbf{K_{AD}}/K_D$	118 ± 32	9 ± 2	1.7 ± 0.3	3.1 ± 0.7
	$\mathbf{k_{-AD}}/k_{-D1}$	333 ± 29	115 ± 11	4.4 ± 0.7	6.8 ± 0.84
	$\mathbf{k_{-AD}}/k_{-D1}$	n.a.	n.a.	15.8 ± 3.1	34.8 ± 4.9
	K_i $[Mg^{2+}]_{free}$	n.a.	400 ± 45	800 ± 145	n.a.
Duty ratio[b]		0.01 ± 0.002	>0.01	0.55 ± 0.13	0.07 ± 0.01

[a]$k_{+D} = k_{-D}/K_D$.
[b]Calculated from Eq. 2.
[c]Depicted from Dürrwang et al., 2006 or Tsiavaliaris et al., 2008.
[d]data from this study.

ADP binding and concomitantly prolong the strongly actin-bound states of the motor, while the Y-to-F substitution in Myo1E^{Y388F} induces the opposite effects. This altered ADP affinity is also reflected in the ADP release kinetics ($\mathbf{k_{-AD}}$, Figure 5), which were almost 2-fold decelerated for Myo1B^{F387Y} and more than six-fold accelerated for Myo1E^{Y388F} compared to the wild-types (Table 2). The mutations also displayed an inverse effect of the actin affinity of the ADP-bound states. Myo1B^{F387Y} displayed a more than 30-fold higher actin affinity in complex with ADP ($\mathbf{K_{DA}}$) compared to the wild-type, whereas Myo1E^{Y388F} showed a more than six-fold reduced actin affinity (Table 3). These prominent changes suggest an important role of the tyrosine for the mechano-chemical coupling mechanism of the class-1 myosins, which we investigated further.

3.3 Switch-2 mutations alter ADP release kinetics in a Mg^{2+}-controlled manner

It is well known that $\mathbf{k_{-AD}}$ is the major determining parameter of the duty ratio (Mikhailenko et al., 2008; Taft et al., 2008; Diensthuber et al., 2015). In case that $\mathbf{k_{-AD}}$ is of similar order as $\mathbf{k_{cat}}$, the ADP release can limit the overall ATPase, which is a discernible characteristic of processive motors and motors made for tension, such as *Mm*myosin-5a, *Dd*myosin-5b, *Dd*myosin-1E, *Hs*myosin-7a, or *Nt*myosin-11 (Dürrwang et al., 2006; Watanabe et al., 2006; Sakamoto et al., 2008; Taft et al., 2008; Diensthuber et al., 2015). Contrary, the rate-limiting step of low duty ratio myosins is commonly the actin-accelerated P_i-release, which precedes the fast dissociation of Mg^{2+}ADP (Takagi et al., 2004). Previously, we and others have reported the existence of an equilibrium between magnesium free (A·M·D) and magnesium bound actomyosin-ADP (A·M·Mg^{2+}D) states in high-duty ratio myosins (De La Cruz et al., 2000; Hannemann et al., 2005; Rosenfeld et al., 2005; Taft et al., 2008; Jacobs et al., 2011) through which product dissociation can occur either sequentially, where Mg^{2+} is released prior to ADP (Rosenfeld et al., 2005) or together with ADP (Chizhov et al., 2013). The preference for either path depends on free Mg^{2+}-ions, which shift the equilibrium towards the simultaneous release of Mg^{2+} and ADP (Chizhov et al., 2013). Therefore, the fraction of time the myosin remains strongly attached to actin can be affected by free Mg^{2+}-ions. For high duty ratio myosins we have shown that elevated, physiologically relevant free Mg^{2+} concentrations can inhibit the ADP release to such an extent that Mg^{2+}ADP dissociation from the actin-bound states becomes

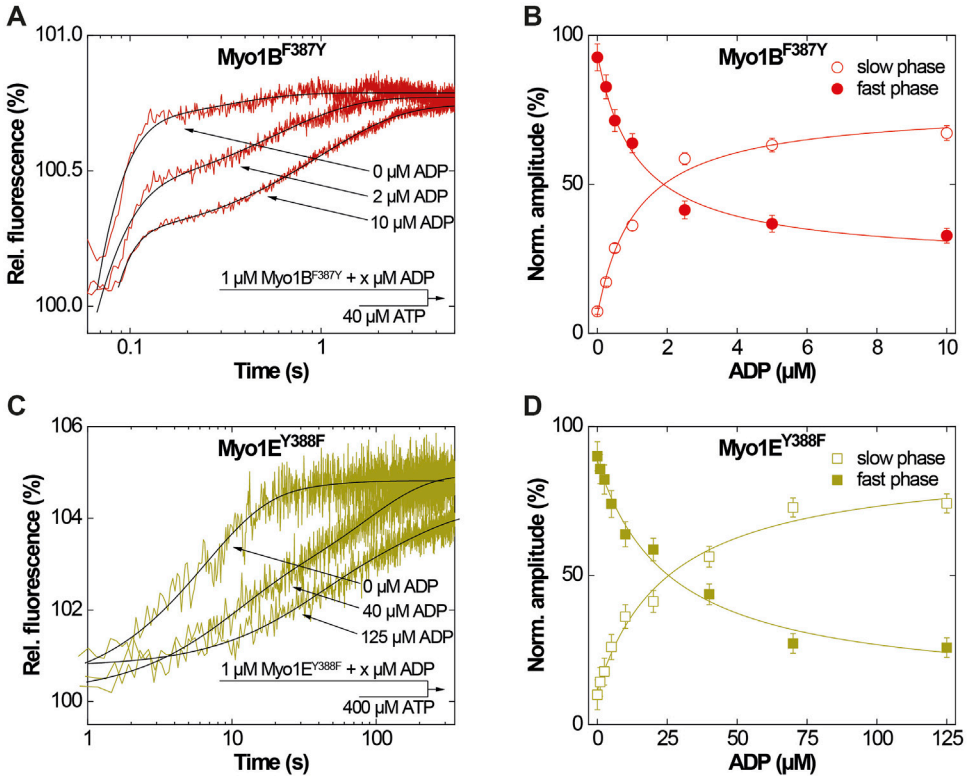

FIGURE 3
ADP-interactions of Myo1B^{F387Y} and Myo1E^{Y388F} in the absence of actin. **(A)** Single fluorescence transients as monitored upon mixing 1 µM Myo1B^{F387Y} pre-incubated with 0, 2 or 10 µM ADP with excess ATP. **(B)** Normalized amplitudes of the slow phase (open circles) and fast phase (filled circles) as obtained from biexponential fits to the transients observed upon mixing 1 µM Myo1B^{F387Y} pre-incubated with increasing concentrations ADP with excess ATP. **(C)** Single fluorescence transients as monitored upon mixing 1 µM Myo1E^{Y388F} pre-incubated with 0, 40 or 125 µM ADP with excess ATP. **(D)** Normalized amplitudes of the slow phase (open circles) and fast phase (filled circles) as obtained from biexponential fits to the transients observed upon mixing 1 µM Myo1E^{Y388F} pre-incubated with increasing concentrations ADP with excess ATP.

the rate-limiting step, strongly influencing the motile properties and the duty ratio of these motors (Fujita-Becker et al., 2005; Dürrwang et al., 2006; Taft et al., 2008; Nagy et al., 2010; Diensthuber et al., 2015; Amrute-Nayak et al., 2019). The low duty ratio myosin Myo1B^{wt} (Tsiavaliaris et al., 2008) or skeletal class-2 myosin isoforms do not display such Mg^{2+}-dependence of the ADP-release kinetics and motor activity (Taft et al., 2008). To examine whether the myosin isoform-specific sensitivity towards free Mg^{2+}-ions was affected by the mutation, we measured the rate of ADP release from the actin-bound states using the fluorescent analogue mantADP. By displacing the bound mantADP with excess ADP in the presence of increasing concentrations of free Mg^{2+}-ions at constant ionic strength (Figure 5), we obtained the rates of ADP release from single exponential fits of the fluorescence decays (Figures 5A, C). Interestingly, Myo1B^{F387Y} displayed ADP release rates (k_{-AD}) that were dependent on free Mg^{2+}, contrary to the wild-type, which did not show such a behavior (Figure 5B). The rates declined hyperbolically from initially 400 ± 25 s^{-1} (at 0.05 mM free Mg^{2+}) to 120 ± 25 s^{-1} (at 10 mM free Mg^{2+}) with an apparent inhibition constant K_i^{Mg} of 0.45 ± 0.3 mM. The Myo1E constructs displayed exactly the opposite behavior: Myo1E^{wt} showed a Mg^{2+}-dependence of $\boldsymbol{k_{-AD}}$ as previously published (Dürrwang et al., 2006), whereas Myo1E^{Y388F} displayed ADP release rates that were independent of free Mg^{2+}-ions (Figure 5D) yielding values comparable to those of Myo1B^{wt} (Figure 5B). All other experimentally determined kinetic parameters listed in the tables showed no or only minor changes. We therefore omitted graphical representation of the data. In summary, the tyrosine in switch-2 of class-1 myosins appears to play a determining role for Mg^{2+}ADP release, which could also affect the motile properties and duty ratio of the myosins.

3.4 Switch-2 mutations inversely affect duty ratio and motor activity as a consequence of altered thermodynamic and kinetic coupling

To investigate this, we generated motor domain constructs with artificial lever arms and performed *in vitro* motility assays as previously described (Taft et al., 2008). The experiments were performed under constant ionic strength and revealed an inhibitory effect of free Mg^{2+} on the actin sliding velocity of Myo1E^{wt} and Myo1B^{F387Y} but not on that of Myo1B^{wt} and Myo1E^{Y388F} (Figures 6A, C). We note that for Myo1E^{wt}, the rate constant for ADP release ($\boldsymbol{k_{-AD}}$) at excess free Mg^{2+}-concentrations is similar to $\boldsymbol{k_{cat}}$ and thus the rate-limiting parameter of the ATPase. For the mutant Myo1E^{Y388F}, the ADP release is not a rate limiting factor of the ATPase cycle, since it proceeds by more than one order of magnitude faster than the steady-state ATP turnover ($\boldsymbol{k_{cat}}$). This hints for a low duty ratio. This kinetic data reveal that the tyrosine is an important residue in switch-2 that controls Mg^{2+}ADP release and potentially the weak-to-strong actin binding interactions. The thermodynamic coupling

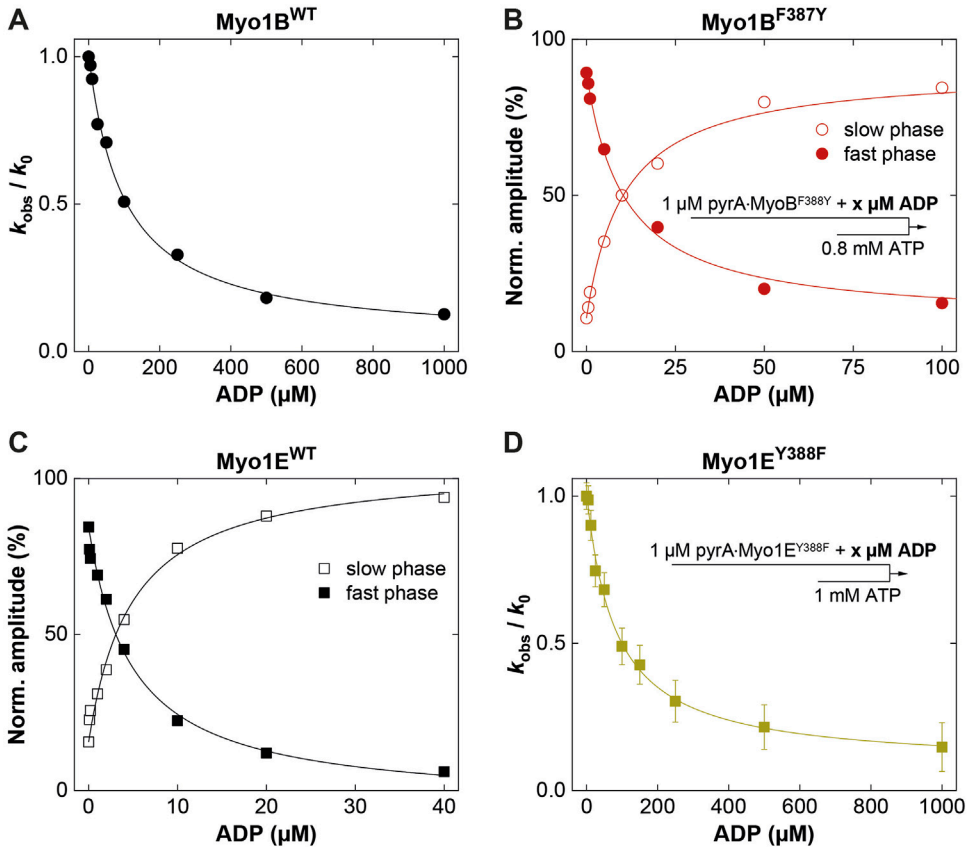

FIGURE 4
ADP-interactions of wild-type and mutant myosins in the presence of actin. **(A)** Plot of the relative change of the observed rate constant (k_{obs}/k_0) as obtained from single exponential fits to the fluorescence transients observed upon mixing pyrA·Myo1B^{wt} in the presence of increasing ADP concentrations with excess ATP. **(B)** Normalized amplitudes of the slow phase (open circles) and fast phase (filled circles) as obtained from biexponentional fits to the fluorescence transients observed upon mixing 1 μM pyrA·Myo1B^{F387Y} in the presence of increasing ADP concentrations with excess ATP. **(C)** Normalized amplitudes of the slow phase (open squares) and fast phase (filled squares) as obtained from biexponentional fits to the fluorescence transients observed upon mixing pyrA·Myo1E^{wt} in the presence of increasing ADP concentrations with excess ATP. **(D)** Plot of the relative change of the observed rate constant (k_{obs}/k_0) as obtained from single exponential fits to the fluorescence transients observed upon mixing 1 μM pyrA·Myo1E^{F388Y} in the presence of increasing ADP concentrations with excess ATP.

constants ($\mathbf{K_{AD}}/K_D$; $\mathbf{K_{DA}}/\mathbf{K_A}$) and the kinetic coupling constant ($\boldsymbol{k}_{-\mathbf{AD}}/k_{-D}$) of nucleotide and actin binding are valuable parameters related to weak-to-strong actin binding transitions (Bloemink and Geeves, 2011). They report how effectively actin can displace ADP, providing predictions of the duty ratio of a myosin. High duty ratio myosins display low coupling constants that tend to approximate unity or acquire values below 1, since the displacement of ADP from myosin by actin is slowed down, often rate limiting the ATPase cycle, which contributes to prolonged population of the strongly actin bound states. Myo1E^{wt} displays typical coupling constants ($\mathbf{K_{AD}}/\mathbf{K_D}$ = 1.7 ± 0.3; $\mathbf{K_{DA}}/\mathbf{K_A}$ = 2.0 ± 0.6; $\boldsymbol{k}_{-\mathbf{AD}}/k_{-D1}$ = 4.4 ± 0.7; $\boldsymbol{k}_{-\mathbf{AD}}/k_{-D2}$ = 15.8 ± 3.1; Table 2, 3) of a high duty ratio motor, whereas the coupling constants of Myo1B^{wt} ($\mathbf{K_{AD}}/\mathbf{K_D}$ = 118 ± 32; $\mathbf{K_{DA}}/\mathbf{K_A}$ = 126 ± 36; $\boldsymbol{k}_{-\mathbf{AD}}/k_{-D}$ = 333 ± 29; Table 2, 3) resemble those of fast motors with a low duty ratio characterized by an effective actin-stimulated ADP release (Bloemink and Geeves, 2011). Notably, the mutations almost reversed the coupling parameters. The Y-to-F substitution in Myo1E^{Y388F} led to an increase of the coupling constants by two- to seven-fold ($\mathbf{K_{AD}}/\mathbf{K_D}$ = 3.1 ± 0.7; $\mathbf{K_{DA}}/\mathbf{K_A}$ = 15.3 ± 5.0; $\boldsymbol{k}_{-\mathbf{AD}}/k_{-D1}$ = 6.8 ± 0.8; $\boldsymbol{k}_{-\mathbf{AD}}/k_{-D2}$ = 34.8 ± 4.9; Table 2, 3), which indicates a decrease of the duty ratio. The F-to-Y substitution in Myo1B^{F387Y} caused a decrease of all coupling constants ($\mathbf{K_{AD}}/\mathbf{K_D}$ = 9 ± 2; $\mathbf{K_{DA}}/\mathbf{K_A}$ = 8 ± 3; $\boldsymbol{k}_{-\mathbf{AD}}/k_{-D}$ = 115 ± 11; Table 2, 3), indicating that the duty ratio is also affected. Using Eq. 2 (Watanabe et al., 2006; Ito et al., 2007), we calculated the duty ratios (Table 2) revealing for the mutant Myo1E^{Y388F} indeed a lower duty ratio (0.07 ± 0.01) compared to Myo1E^{wt} (0.55 ± 0.13). For Myo1B^{wt} we obtained a low duty ratio (0.01 ± 0.01), while the calculation of the duty ratio of Myo1B^{F387Y} predicts a value > 0.01.

Although the duty ratios calculated from the kinetic data correlate well with the coupling parameters, the values appear to be underestimated, particularly for the Myo1B constructs. This is due to the high uncertainty in determining $\boldsymbol{k}_{\mathbf{cat}}$. To experimentally validate the effect of the mutations on the duty ratio, we performed landing assays at two boundary conditions (0.25 mM and 5 mM free Mg^{2+} concentrations) to account for the Mg^{2+}-effect observed in the kinetics and motility assays (Figure 5; Figures 6A, C). The number of motile landing events decreased with decreasing motor densities (Figures 6B, D). The dependency of the landing rates on motor density was best fit by Eq. 1 as described (Hancock and Howard, 1998). From the reciprocal of n, the duty ratio could be calculated (Sumiyoshi et al., 2007), revealing that the duty ratio of Myo1E^{wt} increased from 0.38 ± 0.11 at 0.25 mM free Mg^{2+} to 0.91 ± 0.07 at 5 mM

10.3389/fphys.2024.1393952

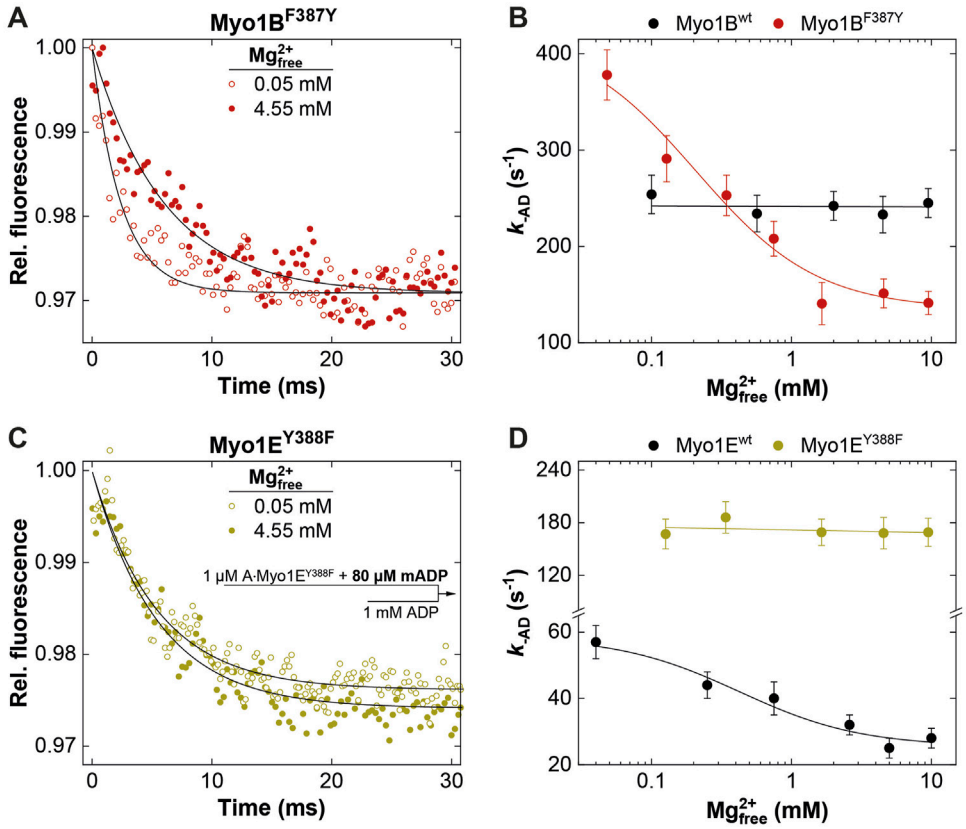

FIGURE 5
Effect of $[Mg^{2+}]_{free}$ on ADP release from actomyosin. Relative mantADP-fluorescence time traces as observed upon mixing 1 µM A·Myo1B^{F387Y} **(A)** or 1 µM A·Myo1E^{Y388F} **(C)** pre-equilibrated with 80 µM mADP at 0.05 mM and 4.55 mM free Mg^{2+}-concentrations, with excess ADP. Rate of ADP release (k_{-AD}) from A·Myo1B^{wt} and A·Myo1B^{F388Y} **(B)** and related Myo1E constructs **(D)** as a function of the free Mg^{2+}-concentration as obtained from single exponential fits to the mantADP-fluorescence time traces.

TABLE 3 Rate and equilibrium constants of actin interactions.

Constant	Myo1B^{wt*}	Myo1B^{F387Y}	Myo1E^{wt*}	Myo1E^{Y388F}
Myosin binding to actin				
k_{+A} ($\mu M^{-1}s^{-1}$)	1.1 ± 0.2	0.9 ± 0.08	2.9 ± 0.2	4.2 ± 0.3
k_{-A} (s^{-1})	0.005 ± 0.001	0.002 ± 0.0005	0.0015 ± 0.0003	0.0015 ± 0.0004
K_A (nM)	4.5 ± 1.0	2.2 ± 0.6	0.5 ± 0.1	0.4 ± 0.1
Myosin binding to actin in the presence of ADP				
k_{+DA} ($\mu M^{-1}s^{-1}$)	0.03 ± 0.004[a]	0.29 ± 0.04[a]	6.0 ± 0.8[a]	4.1 ± 0.6[a]
k_{-DA} (s^{-1})	0.017 ± 0.002	0.005 ± 0.001	0.005 ± 0.001	0.0007 ± 0.0001
K_{DA} (nM)	567 ± 100	17 ± 4	1.0 ± 0.2	6.1 ± 1.3 0.2
K_{DA}/K_A	126 ± 36	8 ± 3	2.0 ± 0.6	15.3 ± 5.0

[a]Calculated.

free Mg^{2+}, whereas the duty ratio of Myo1E^{Y388F} dropped to 0.14 ± 0.02 at 0.25 mM free Mg^{2+} and 0.2 ± 0.04 at 5 mM free Mg^{2+}, respectively. This demonstrates the loss of the Mg^{2+}-sensitivity of the motor (Table 4) consistent with Mg^{2+}-insensitive ADP-release kinetics (Figure 5) and Mg^{2+}-insensitive motor activity (Figures 6A, C). Myo1B^{wt} was significantly more difficult to handle in the landing assays. At densities below 5000 motor molecules μm^{-2}, we observed almost no landing events, which speaks for a low duty ratio of the motor. Therefore, there are no data available for Myo1B^{wt}. Myo1B^{F387Y} displayed landing events that were dependent on both, free Mg^{2+}-ions and motor density, yielding duty ratios of 0.14 ± 0.02 at 0.25 mM Mg^{2+} and 0.5 ± 0.1 at 5 mM free Mg^{2+}. The estimation of the duty ratio for

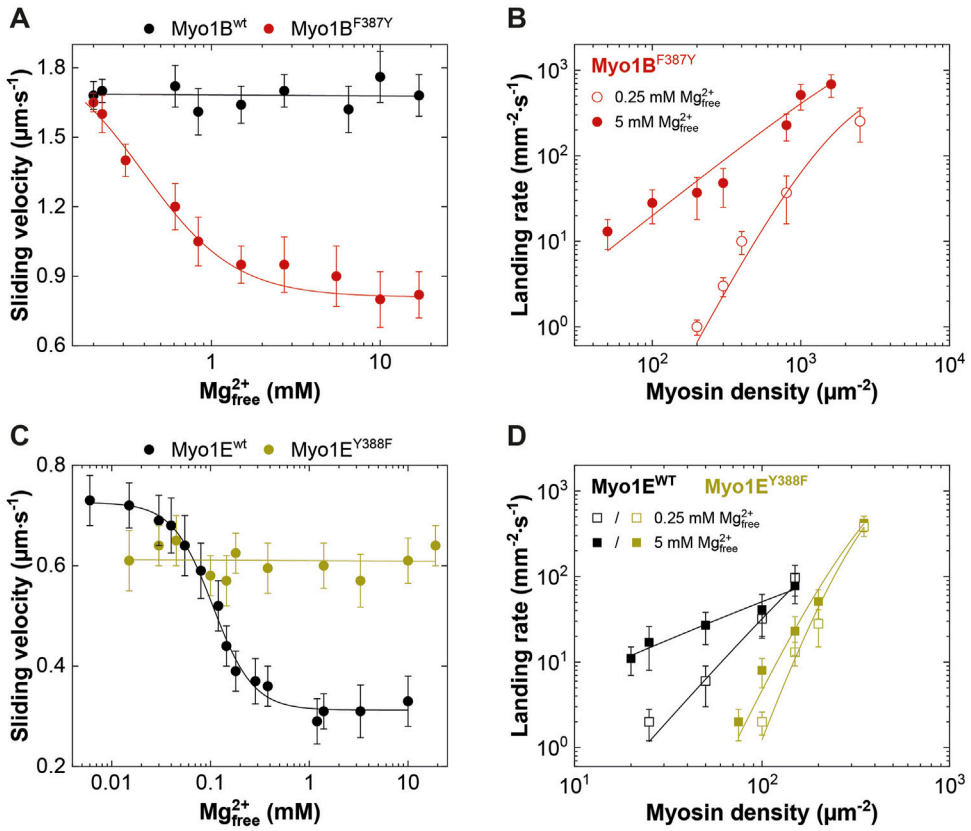

FIGURE 6
Effect of $[Mg^{2+}]_{free}$ on myosin motor activity and landing rate. **(A,C)** Average actin sliding velocities of wild-type and mutant myosins at increasing free Mg^{2+}-concentrations. Myo1B^{wt} and Myo1E^{Y388F} display no Mg^{2+} sensitivity. **(B)** Landing rate as a function of Myo1B^{F387Y} motor density. **(D)** Landing rate as a function of Myo1E^{wt} and Myo1E^{Y388F} motor density. The landing assays were performed at 5 mM (filled symbols) and 0.25 mM (open symbols) free Mg^{2+} concentrations.

Myo1B^{F387Y} should be taken with care, since the number of moving actin filaments at low motor densities became increasingly less. However, the data clearly demonstrate that the introduction of the tyrosine in Myo1B significantly increases the duty ratio of the myosin.

3.5 Switch-2 mutations influence Mg^{2+}ADP release through altered interactions of active site elements

Finally, we used the available X-ray structure of Myo1E (pdb: 1LKX) (Kollmar et al., 2002) and generated energy minimized homology models of Myo1E^{Y388F}, which we applied to molecular dynamics simulations to obtain insights into potential conformational changes induced by the mutation (Figure 7). The superimposed structures in complex with ADP-VO_4 show Y388 in switch-2 of wild-type Myo1E^{wt} to form a 2.9 Å hydrogen bond with the β7-sheet residue L183 of the transducer (Figure 7A). This conformation appears to stabilize the Mg^{2+}-ion in the binding pocket of the wild-type myosin. The structural model of Myo1E^{Y388F} predicts the loss of this hydrogen bond (Figure 7B). As a consequence switch-2 is slightly shifted, which enables residue D386 to strengthen the hydrogen bond with P-loop residue T108. This in turn weakens the T108-mediated coordination of the Mg^{2+}-ion. This conformational shift of switch-2 appears to additionally affect the Mg^{2+}-coordination mediated via switch-1 residue S158. Consequently, these small conformational rearrangements of switch-2 appear to disrupt the coordination sphere of Mg^{2+}, which is apparently associated with an accelerated Mg^{2+}-ADP release and the inability of the Myo1E^{Y388F} to sense free Mg^{2+}-ions. For Myo1B we generated energy-minimized homology models (Figure 7B) to show that a hydrogen bond between Y387 in the mutant and L183 can be formed like in Myo1E^{wt}, which is absent in the wild-type (Figure 7B, blue residues). This tyrosine-mediated hydrogen bond may be critical for stabilizing Mg^{2+} and ADP, which could explain the Mg^{2+}-dependent suppression of the ADP-release from acto·Myo1B^{F387Y} and the prolonged strongly actin-bound states responsible for the higher duty ratio. These structural considerations are supported by X-ray and cryoEM structures of Myo5, revealing that the tyrosine in switch-2 is important for stabilizing the rigor conformation in high duty ratio motors via the interaction with leucine in the ß7 sheet (Coureux et al., 2004; Pospich et al., 2021). Mechanistically, the effect of free Mg^{2+} can be interpreted as previously described for Myo5b (Rosenfeld et al., 2005; Chizhov et al., 2013). The dissociation of the Mg^{2+} can occur prior or in complex with ADP. Thus, increased concentrations of free Mg^{2+}-ions can slow down the release of the nucleotide. Our structural models attribute this to the altered switch-2 conformation induced by the mutations affecting the ADP affinity of the

TABLE 4 Regulation of myosin motor activity and duty ratio.

Parameter	Myo1B^{wta}		Myo1B^{F387Ya}		Myo1E^{wta}		Myo1E^{Y388Fa}	
*In vitro*motility assays								
v_{max} (μm s^{-1})	1.76 ± 0.11		1.68 ± 0.06		0.73 ± 0.05		0.64 ± 0.06	
v_{min} (μm s^{-1})	1.61 ± 0.09		0.82 ± 0.1		0.31 ± 0.05		0.58 ± 0.05	
K_i (mM)	n.a.		0.19 ± 0.03		0.13 ± 0.02		n.a.	
Hill coefficient (n)	n.a.		1.96 ± 0.17		2.11 ± 0.21		n.a.	
Landing assays								
	$[Mg^{2+}]_{free}$		$[Mg^{2+}]_{free}$		$[Mg^{2+}]_{free}$		$[Mg^{2+}]_{free}$	
	250 μM	5 mM	250 μM	5 mM	250 μM	5 mM	250 μM	5 mM
Landing rate order	n.a.		7.2 ± 1.5	2 ± 1	2.6 ± 0.8	1.1 ± 0.1	7 ± 1.1	5.1 ± 0.9
Duty ratio (n^{-1})	n.a.		0.14 ± 0.02	0.5 ± 0.1	0.38 ± 0.11	0.91 ± 0.07	0.14 ± 0.02	0.2 ± 0.04

[a]Data of this study.

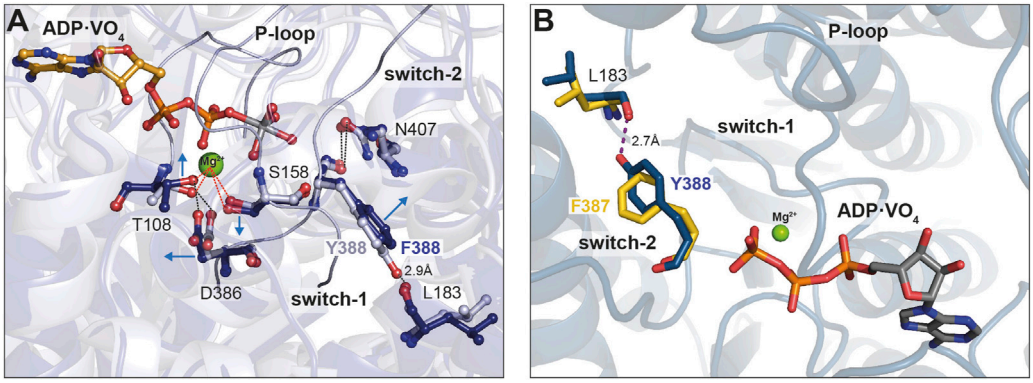

FIGURE 7
Close up view of the switch-2 region of the motor domain of Myo1B and Myo1E. **(A)** Superposition of structural models showing the influence of the Y-to-F mutation in Myo1E on Mg^{2+} and ADP coordination. The introduction of mutation Y388F prevents the formation of a hydrogen bond with L183, which stabilizes the nucleotide coordination sphere in the wild-type. The arrows indicate the positional shift of switch-2 residues induced by the mutation. The altered conformation of D386 (switch-2) strengthens the hydrogen bond with T108 (P-loop) and weakens the T108-mediated coordination of the Mg^{2+}. **(B)** Superimposed structural models showing the influence of the F-to-Y substitution in Myo1B. The Tyr in Myo1B^{F387Y} can adopt a conformation that allows the formation of a hydrogen bond with residue L183, in a similar manner as in Myo1E^{wt}. The hydrogen bond is assumed to stabilize the conformation of switch-2 enhancing the coordination capacity for Mg^{2+} and nucleotide. The images were created using the "Pymol" program.

actomyosin complex. The tyrosine stabilizes the Mg^{2+}·ADP state, while the phenylalanine causes accelerated release rates. However, the F-to-Y mutation in MyoB^{F387Y} did not alter the ADP dissociation from the acto-MyoB^{F387Y} complex to rate-limit the overall ATPase cycle time, as in the case of MyoBF387Y. Obviously, other structural elements including switch-1, loop-1, W-helix, and loop-2, all of which have been related to product release (Bobkov et al., 1996; Sweeney et al., 1998; Murphy and Spudich, 1999; Clark et al., 2005; Bloemink et al., 2014; Franz et al., 2021), contribute additionally in fine-tuning the ADP release kinetics. With respect to switch-2, our data suggest the tyrosine in class-1 myosins suppresses the actin-induced acceleration of ADP release by strengthening the coordination of Mg^{2+} and ADP through the stabilization of the conformation of the surrounding active site elements.

3.6 Conclusions

The presence of the tyrosine in the switch-2 consensus sequence of myosins is not strictly indicative for a high duty ratio. For example, mammalian class-I myosins contain a tyrosine and display under unloaded conditions characteristics of a low duty ratio motor (Greenberg and Ostap, 2013), whereas under tension (Greenberg et al., 2012; Pyrpassopoulos et al., 2016) and/or Ca^{2+}-dependent binding of calmodulin to the neck region (Lewis et al., 2012), they exhibit altered rates and equilibrium constants of the transitions in the ATPase cycle, which can increase the duty ratio (Laakso et al., 2008). Interestingly, the class-VI myosin members are high duty ratio motors, although they possess an alanine at the Y388-equivalent position (De la Cruz et al., 2001). Furthermore, the exchange of the tyrosine in switch-2 of mammalian

myosin-5a by an alanine resulted in an increased processive behaviour of the motor and strengthened the free Mg^{2+}-dependent suppression of ADP release from actomyosin, however, at reduced speed (Nagy et al., 2010). These findings suggest that natural variations of structural elements besides switch-2, including those mediating actin interactions, such as loop-2, loop-4, the CM-loop, activation loop, helix-loop-helix (Goodson et al., 1999; Onishi et al., 2006; Diensthuber et al., 2015) have a dominant role in the regulation of the duty ratio, since they couple actin-interactions to product release as exemplary shown for class-V and class-I (Yengo and Sweeney, 2004; Lieto-Trivedi et al., 2007).

Here, we provide kinetic and molecular insights into the product release mechanisms of two functionally distinct class-1 myosins and reveal that switch-2 dictates the duty ratio of the motors and their ability to perform rapid movement, processive motion, or gating function. The Mg^{2+}-sensitivity of the class-1 myosins appears to be an important feature in cellular processes that require a switching between fast contractility and slow tension bearing, such as during endocytosis, where the myosins act as motorized cross-linkers between the membrane and actin cytoskeleton systems to provide the contractile forces to accomplish actin and membrane remodelling (Manenschijn et al., 2019). Additionally, class-1 myosins can act as tension-sensitive tethers or even transporters (McIntosh and Ostap, 2016). Thus, it would be interesting to analyse how switch-2 in conjunction with other structural elements implicated in regulating Mg^{2+}ADP release define the duty ratio of individual myosin-1 isoforms to perform distinct and multiple types of molecular functions.

Data availability statement

The original contributions presented in the study are included in the article/supplementary material, further inquiries can be directed to the corresponding author.

Author contributions

RD: Formal Analysis, Investigation, Methodology, Validation, Writing–review and editing, Visualization. FH: Formal Analysis, Investigation, Methodology, Validation, Writing–review and editing, Visualization. DK: Formal Analysis, Investigation, Methodology, Validation, Writing–review and editing, Visualization. PF: Formal Analysis, Validation, Writing–review and editing, Visualization. GT: Conceptualization, Data curation, Formal Analysis, Funding acquisition, Investigation, Methodology, Project administration, Resources, Software, Supervision, Validation, Visualization, Writing–original draft, Writing–review and editing.

Funding

The author(s) declare that financial support was received for the research, authorship, and/or publication of this article. This research work was funded by the Deutsche Forschungsgemeinschaft (DFG), grant number TS169/3-1 and TS169/5-1 (GT).

Acknowledgments

We thank Matthias Preller (Department of Natural Sciences, University of Applied Sciences Bonn-Rhein-Sieg, Germany) for providing Figure 7B.

Conflict of interest

The authors declare that the research was conducted in the absence of any commercial or financial relationships that could be construed as a potential conflict of interest.

Publisher's note

References

Adams, R. J., and Pollard, T. D. (1989). Binding of myosin I to membrane lipids. *Nature* 340 (6234), 565–568. doi:10.1038/340565A0

Amrute-Nayak, M., Nayak, A., Steffen, W., Tsiavaliaris, G., Scholz, T., and Brenner, B. (2019). Transformation of the nonprocessive fast skeletal myosin II into a processive motor. *Small* 15 (7), e1804313. doi:10.1002/smll.201804313

Armstrong, J. M., Krementsova, E., Michalek, A. J., Heaslip, A. T., Nelson, S. R., Trybus, K. M., et al. (2012). Full-length myosin Va exhibits altered gating during processive movement on actin. *Proc. Natl. Acad. Sci. U. S. A.* 109 (5), E218–E224. doi:10.1073/pnas.1109709109

Bagshaw, C. R., Eccleston, J. F., Eckstein, F., Goody, R. S., Gutfreund, H., and Trentham, D. R. (1974). The magnesium ion-dependent adenosine triphosphatase of myosin. Two-step processes of adenosine triphosphate association and adenosine diphosphate dissociation. *Biochem. J.* 141 (2), 351–364. doi:10.1042/bj1410351

Barger, S. R., Reilly, N. S., Shutova, M. S., Li, Q., Maiuri, P., Heddleston, J. M., et al. (2019). Membrane-cytoskeletal crosstalk mediated by myosin-I regulates adhesion turnover during phagocytosis. *Nat. Commun.* 10 (1), 1249. doi:10.1038/s41467-019-09104-1

Batra, R., Geeves, M. A., and Manstein, D. J. (1999). Kinetic analysis of *Dictyostelium discoideum* myosin motor domains with glycine-to-alanine mutations in the reactive thiol region. *Biochemistry* 38 (19), 6126–6134. doi:10.1021/bi982251e

Bloemink, M., Deacon, J., Langer, S., Vera, C., Combs, A., Leinwand, L., et al. (2014). The hypertrophic cardiomyopathy myosin mutation R453C alters ATP binding and hydrolysis of human cardiac β-myosin. *J. Biol. Chem.* 289 (8), 5158–5167. doi:10.1074/jbc.M113.511204

Bloemink, M. J., and Geeves, M. A. (2011). Shaking the myosin family tree: biochemical kinetics defines four types of myosin motor. *Seminars Cell and Dev. Biol.* 22 (9), 961–967. doi:10.1016/j.semcdb.2011.09.015

Bobkov, A. A., Bobkova, E. A., Lin, S. H., and Reisler, E. (1996). The role of surface loops (residues 204-216 and 627-646) in the motor function of the myosin head. *Proc. Natl. Acad. Sci. U. S. A.* 93 (6), 2285–2289. doi:10.1073/pnas.93.6.2285

Brunger, A. T. (2007). Version 1.2 of the crystallography and nmr system. *Nat. Protoc.* 2 (11), 2728–2733. doi:10.1038/nprot.2007.406

Chizhov, I., Hartmann, F. K., Hundt, N., and Tsiavaliaris, G. (2013). Global fit analysis of myosin-5b motility reveals thermodynamics of Mg2+-sensitive acto-myosin-ADP states. *PLoS ONE* 8 (5), e64797. doi:10.1371/journal.pone.0064797

Clark, R., Ansari, M. A., Dash, S., Geeves, M. A., and Coluccio, L. M. (2005). Loop 1 of transducer region in mammalian class I myosin, Myo1b, modulates actin affinity, ATPase activity, and nucleotide access. *J. Biol. Chem.* 280 (35), 30935–30942. doi:10.1074/jbc.M504698200

Coureux, P. D., Sweeney, H. L., and Houdusse, A. (2004). Three myosin V structures delineate essential features of chemo-mechanical transduction. *EMBO J.* 23 (23), 4527–4537. doi:10.1038/sj.emboj.7600458

Cremo, C. R., and Geeves, M. A. (1998). Interaction of actin and ADP with the head domain of smooth muscle myosin: implications for strain-dependent ADP release in smooth muscle. *Biochemistry* 37 (7), 1969–1978. doi:10.1021/bi9722406

Criddle, A. H., Geeves, M. A., and Jeffries, T. (1985). The use of actin labelled with N-(1-pyrenyl)iodoacetamide to study the interaction of actin with myosin subfragments and troponin/tropomyosin. *Biochem. J.* 232 (2), 343–349. doi:10.1042/bj2320343

Darden, T., York, D., and Pedersen, L. (1993). Particle mesh Ewald: an N·log(N) method for Ewald sums in large systems. *J. Chem. Phys.* 98 (12), 10089–10092. doi:10.1063/1.464397

De la Cruz, E. M., Ostap, E. M., and Sweeney, H. L. (2001). Kinetic mechanism and regulation of myosin VI. *J. Biol. Chem.* 276 (34), 32373–32381. doi:10.1074/jbc.M104136200

De La Cruz, E. M., Sweeney, H. L., and Ostap, E. M. (2000). ADP inhibition of myosin V ATPase activity. *Biophysical J.* 79 (3), 1524–1529. doi:10.1016/S0006-3495(00)76403-4

De La Cruz, E. M., Wells, A. L., Rosenfeld, S. S., Ostap, E. M., and Sweeney, H. L. (1999). The kinetic mechanism of myosin V. *Proc. Natl. Acad. Sci. U. S. A.* 96 (24), 13726–13731. doi:10.1073/pnas.96.24.13726

Diensthuber, R. P., Tominaga, M., Preller, M., Hartmann, F. K., Orii, H., Chizhov, I., et al. (2015). Kinetic mechanism of Nicotiana tabacum myosin-11 defines a new type of a processive motor. *FASEB J.* 29 (1), 81–94. doi:10.1096/fj.14-254763

Dürrwang, U., Fujita-Becker, S., Erent, M., Kull, F. J., Tsiavaliaris, G., Geeves, M. A., et al. (2006). Dictyostelium myosin-IE is a fast molecular motor involved in phagocytosis. *J. Cell Sci.* 119 (3), 550–558. doi:10.1242/jcs.02774

Franz, P., Ewert, W., Preller, M., and Tsiavaliaris, G. (2021). Unraveling a force-generating allosteric pathway of actomyosin communication associated with adp and pi release. *Int. J. Mol. Sci.* 22 (1), 104–119. doi:10.3390/ijms22010104

Fujita-Becker, S., Dürrwang, U., Erent, M., Clark, R. J., Geeves, M. A., and Manstein, D. J. (2005). Changes in Mg2+ ion concentration and heavy chain phosphorylation regulate the motor activity of a class I myosin. *J. Biol. Chem.* 280 (7), 6064–6071. doi:10.1074/jbc.M412473200

Furch, M., Fujita-Becker, S., Geeves, M. A., Holmes, K. C., and Manstein, D. J. (1999). Role of the salt-bridge between switch-1 and switch-2 of Dictyostelium myosin. *J. Mol. Biol.* 290 (3), 797–809. doi:10.1006/jmbi.1999.2921

Geeves, M. A., Goody, R. S., and Gutfreund, H. (1984). Kinetics of acto-S1 interaction as a guide to a model for the crossbridge cycle. *J. Muscle Res. Cell Motil.* 5 (4), 351–361. doi:10.1007/BF00818255

Goodson, H. V., Warrick, H. M., and Spudich, J. A. (1999). Specialized conservation of surface loops of myosin: evidence that loops are involved in determining functional characteristics. *J. Mol. Biol.* 287 (1), 173–185. doi:10.1006/jmbi.1999.2565

Greenberg, M. J., Lin, T., Goldman, Y. E., Shuman, H., and Ostap, E. M. (2012). Myosin IC generates power over a range of loads via a new tension-sensing mechanism. *Proc. Natl. Acad. Sci. U. S. A.* 109 (37), E2433–E2440. doi:10.1073/pnas.1207811109

Greenberg, M. J., and Ostap, E. M. (2013). Regulation and control of myosin-I by the motor and light chain-binding domains. *Trends Cell Biol.* 23 (2), 81–89. doi:10.1016/j.tcb.2012.10.008

Hancock, W. O., and Howard, J. (1998). Processivity of the motor protein kinesin requires two heads. *J. Cell Biol.* 140 (6), 1395–1405. doi:10.1083/jcb.140.6.1395

Hannemann, D. E., Cao, W., Olivares, A. O., Robblee, J. P., and De La Cruz, E. M. (2005). Magnesium, ADP, and actin binding linkage of myosin V: evidence for multiple myosin V-ADP and actomyosin V-ADP states. *Biochemistry* 44 (24), 8826–8840. doi:10.1021/bi0473509

Hess, B., Bekker, H., Berendsen, H. J. C., and Fraaije, J. G. E. M. (1997). LINCS: a linear constraint solver for molecular simulations. *J. Comput. Chem.* 18, 1463–1472. doi:10.1002/(sici)1096-987x(199709)18:12<1463::aid-jcc4>3.3.co;2-l

Hess, B., Kutzner, C., Van Der Spoel, D., and Lindahl, E. (2008). GROMACS 4: algorithms for highly efficient, load-balanced, and scalable molecular simulation. *J. Chem. theory Comput.* 4 (3), 435–447. doi:10.1021/ct700301q

Ito, K., Ikebe, M., Kashiyama, T., Mogami, T., Kon, T., and Yamamoto, K. (2007). Kinetic mechanism of the fastest motor protein, Chara myosin. *J. Biol. Chem.* 282 (27), 19534–19545. doi:10.1074/jbc.M611802200

Jacobs, D. J., Trivedi, D., David, C., and Yengo, C. M. (2011). Kinetics and thermodynamics of the rate-limiting conformational change in the actomyosin V mechanochemical cycle. *J. Mol. Biol.* 407 (5), 716–730. doi:10.1016/j.jmb.2011.02.001

Johnson, C. A., Walklate, J., Svicevic, M., Mijailovich, S. M., Vera, C., Karabina, A., et al. (2019). The ATPase cycle of human muscle myosin II isoforms: adaptation of a single mechanochemical cycle for different physiological roles. *J. Biol. Chem.* 294 (39), 14267–14278. doi:10.1074/jbc.RA119.009825

Kollmar, M., Dürrwang, U., Kliche, W., Manstein, D. J., and Kull, F. J. (2002). Crystal structure of the motor domain of a class-I myosin. *EMBO J.* 21 (11), 2517–2525. doi:10.1093/emboj/21.11.2517

Laakso, J. M., Lewis, J. H., Shuman, H., and Ostap, E. M. (2008). Myosin I can act as a molecular force sensor. *Science* 321 (5885), 133–136. doi:10.1126/science.1159419

Lewis, J. H., Greenberg, M. J., Laakso, J. M., Shuman, H., and Ostap, E. M. (2012). Calcium regulation of myosin-I tension sensing. *Biophysical J.* 102 (12), 2799–2807. doi:10.1016/j.bpj.2012.05.014

Lieto-Trivedi, A., Dash, S., and Coluccio, L. M. (2007). Myosin surface loop 4 modulates inhibition of actomyosin 1b ATPase activity by tropomyosin. *Biochemistry* 46 (10), 2779–2786. doi:10.1021/bi602439f

Lin, T., Greenberg, M. J., Moore, J. R., and Ostap, E. M. (2011). A hearing loss-associated myo1c mutation (R156W) decreases the myosin duty ratio and force sensitivity. *Biochemistry* 50 (11), 1831–1838. doi:10.1021/bi1016777

Lutton, J. E., Coker, H. L. E., Paschke, P., Munn, C. J., King, J. S., Bretschneider, T., et al. (2023). Formation and closure of macropinocytic cups in Dictyostelium. *Curr. Biol.* 33 (15), 3083–3096.e6. doi:10.1016/j.cub.2023.06.017

Málnási-Csizmadia, A., Dickens, J. L., Zeng, W., and Bagshaw, C. R. (2005). Switch movements and the myosin crossbridge stroke. *J. Muscle Res. Cell Motil.* 26 (1), 31–37. doi:10.1007/s10974-005-9004-y

Manenschijn, H. E., Picco, A., Mund, M., Rivier-Cordey, A. S., Ries, J., and Kaksonen, M. (2019). Type-I myosins promote actin polymerization to drive membrane bending in endocytosis. *eLife* 8, e44215. doi:10.7554/eLife.44215

McConnell, R. E., and Tyska, M. J. (2010). Leveraging the membrane - cytoskeleton interface with myosin-1. *Trends Cell Biol.* 20 (7), 418–426. doi:10.1016/j.tcb.2010.04.004

McIntosh, B. B., and Ostap, E. M. (2016). Myosin-I molecular motors at a glance. *J. Cell Sci.* 129 (14), 2689–2695. doi:10.1242/jcs.186403

Mezgueldi, M. E., Tang, N., Rosenfeld, S. S., and Ostap, E. M. (2002). The kinetic mechanism of myo1e (human myosin-IC). *J. Biol. Chem.* 277 (24), 21514–21521. doi:10.1074/jbc.M200713200

Mikhailenko, S. V., Oguchi, Y., Ohki, T., Shimozawa, T., Olivares, A. O., De La Cruz, E. M., et al. (2008). How the load and the nucleotide state affect the actin filament binding mode of the molecular motor myosin V. *J. Korean Phys. Soc.* 53 (3), 1726–1730. doi:10.3938/jkps.53.1726

Millar, N. C., and Geeves, M. A. (1983). The limiting rate of the ATP-mediated dissociation of actin from rabbit skeletal muscle myosin subfragment 1. *FEBS Lett.* 160 (1–2), 141–148. doi:10.1016/0014-5793(83)80954-5

Murphy, C. T., and Spudich, J. A. (1999). The sequence of the myosin 50-20K loop affects myosin's affinity for actin throughout the actin-myosin ATPase cycle and its maximum ATPase activity. *Biochemistry* 38 (12), 3785–3792. doi:10.1021/bi9826815

Nagy, N. T., Sakamoto, T., Takács, B., Gyimesi, M., Hazai, E., Bikádi, Z., et al. (2010). Functional adaptation of the switch-2 nucleotide sensor enables rapid processive translocation by myosin-5. *FASEB J.* 24 (11), 4480–4490. doi:10.1096/fj.10-163998

Odronitz, F., and Kollmar, M. (2007). Drawing the tree of eukaryotic life based on the analysis of 2,269 manually annotated myosins from 328 species. *Genome Biol.* 8 (9), R196. doi:10.1186/gb-2007-8-9-r196

Onishi, H., Mikhailenko, S. V., and Morales, M. F. (2006). Toward understanding actin activation of myosin ATPase: the role of myosin surface loops. *Proc. Natl. Acad. Sci. U. S. A.* 103 (16), 6136–6141. doi:10.1073/pnas.0601595103

Pardee, J. D., and Aspudich, J. (1982). Purification of muscle actin. *Methods Enzym.* 85, 164–181. doi:10.1016/0076-6879(82)85020-9

Pospich, S., Sweeney, H. L., Houdusse, A., and Raunser, S. (2021). High-resolution structures of the actomyosin-v complex in three nucleotide states provide insights into the force generation mechanism. *eLife* 10, e73724. doi:10.7554/eLife.73724

Preller, M., Bauer, S., Adamek, N., Fujita-Becker, S., Fedorov, R., Geeves, M. A., et al. (2011). Structural basis for the allosteric interference of myosin function by reactive thiol region mutations G680A and G680V. *J. Biol. Chem.* 286 (40), 35051–35060. doi:10.1074/jbc.M111.265298

Preller, M., and Holmes, K. C. (2013). The myosin start-of-power stroke state and how actin binding drives the power stroke. *Cytoskelet. Hob.(N.J.)* 70 (10), 651–660. doi:10.1002/cm.21125

Pyrpassopoulos, S., Arpağ, G., Feeser, E. A., Shuman, H., Tüzel, E., and Ostap, E. M. (2016). Force generation by membrane-associated myosin-I. *Sci. Rep.* 6, 25524. doi:10.1038/srep25524

Rosenfeld, S. S., Houdusse, A., and Sweeney, H. L. (2005). Magnesium regulates ADP dissociation from myosin V. *J. Biol. Chem.* 280 (7), 6072–6079. doi:10.1074/jbc.M412717200

Sakamoto, T., Webb, M. R., Forgacs, E., White, H. D., and Sellers, J. R. (2008). Direct observation of the mechanochemical coupling in myosin Va during processive movement. *Nature* 455 (7209), 128–132. doi:10.1038/nature07188

Šali, A., and Blundell, T. L. (1993). Comparative protein modelling by satisfaction of spatial restraints. *J. Mol. Biol.* 234 (3), 779–815. doi:10.1006/JMBI.1993.1626

Sweeney, H. L., Rosenfeld, S. S., Brown, F., Faust, L., Smith, J., Xing, J., et al. (1998). Kinetic tuning of myosin via a flexible loop adjacent to the nucleotide binding pocket. *J. Biol. Chem.* 273 (11), 6262–6270. doi:10.1074/jbc.273.11.6262

Sumiyoshi, H., Ooguchi, M., Ooi, A., Okagaki, T., and Higashi-Fujime, S. (2007). Insight into the mechanism of fast movement of myosin from Chara coralline. *Cell Motil. Cytoskeleton.* 64 (2), 131–142. doi:10.1002/cm.20171

Taft, M. H., Hartmann, F. K., Rump, A., Keller, H., Chizhov, I., Manstein, D. J., et al. (2008). Dictyostelium myosin-5b is a conditional processive motor. *J. Biol. Chem.* 283 (40), 26902–26910. doi:10.1074/jbc.M802957200

Takagi, Y., Shuman, H., and Goldman, Y. E. (2004). Coupling between phosphate release and force generation in muscle actomyosin. *Philosophical Trans. R. Soc. Lond. Ser. B, Biol. Sci.* 359 (1452), 1913–1920. doi:10.1098/rstb.2004.1561

Taylor, E. W. (1991). Kinetic studies on the association and dissociation of myosin subfragment 1 and actin. *J. Biol. Chem.* 266 (1), 294–302. doi:10.1016/s0021-9258(18)52434-0

Tsiavaliaris, G., Fujita-Becker, S., Batra, R., Levitsky, D. I., Kill, F. J., Geeves, M. A., et al. (2002). Mutations in the relay loop region result in dominant-negative inhibition of myosin II function in Dictyostelium. *EMBO Rep.* 3 (11), 1099–1105. doi:10.1093/embo-reports/kvf214

Tsiavaliaris, G., Fujita-Becker, S., Dürrwang, U., Diensthuber, R. P., Geeves, M. A., and Manstein, D. J. (2008). Mechanism, regulation, and functional properties of Dictyostelium myosin-1B. *J. Biol. Chem.* 283 (8), 4520–4527. doi:10.1074/jbc.M708113200

Watanabe, S., Ikebe, R., and Ikebe, M. (2006). Drosophila myosin VIIA is a high duty ratio motor with a unique kinetic mechanism. *J. Biol. Chem.* 281 (11), 7151–7160. doi:10.1074/jbc.M511592200

Wittinghofer, A., and Geeves, M. A. (2016). Review: the ATPase mechanism of myosin and actomyosin. *Biopolymers* 105 (8), 483–491. doi:10.1002/bip.22853

Yengo, C. M., and Sweeney, H. L. (2004). Functional role of loop 2 in myosin V. *Biochemistry* 43 (9), 2605–2612. doi:10.1021/bi035510v

Frontiers in Physiology

Understanding how an organism's components work together to maintain a healthy state

The second most-cited physiology journal, promoting a multidisciplinary approach to the physiology of living systems - from the subcellular and molecular domains to the intact organism and its interaction with the environment.

Discover the latest Research Topics

See more →

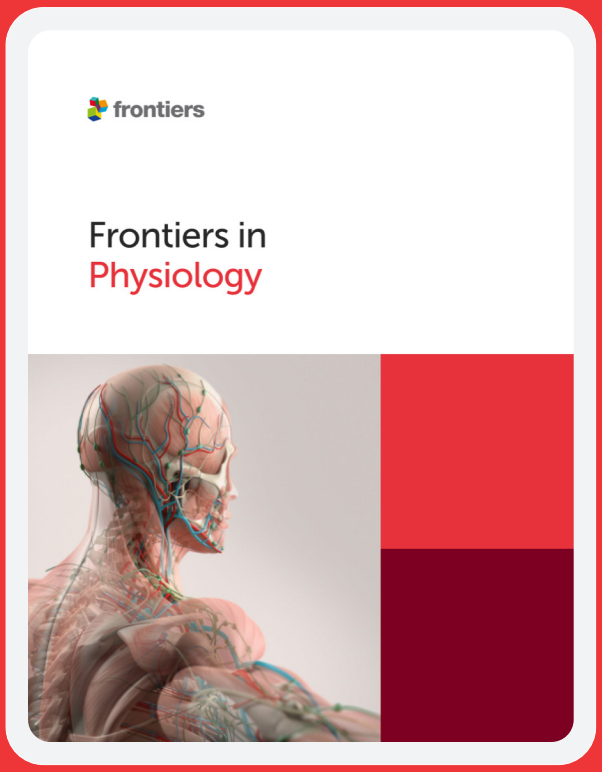

Frontiers

Avenue du Tribunal-Fédéral 34
1005 Lausanne, Switzerland
frontiersin.org

Contact us

+41 (0)21 510 17 00
frontiersin.org/about/contact